Performance-Based Seismic Design Concepts and Implementation

Proceedings of an International Workshop

Bled, Slovenia   •   June 28 – July 1, 2004

Edited by

Peter Fajfar
University of Ljubljana

and

Helmut Krawinkler
Stanford University

PERFORMANCE-BASED SEISMIC DESIGN
CONCEPTS AND IMPLEMENTATION

PROCEEDINGS OF THE INTERNATIONAL WORKSHOP
BLED, SLOVENIA, 28 JUNE – 1 JULY 2004

Edited by

Peter Fajfar
University of Ljubljana, Slovenia

and

Helmut Krawinkler
Stanford University, California

CONTENTS

iii

iv

PREFACE

The workshop on "Seismic Design Methodologies for the Next Generation of Codes," held in Bled, Slovenia, in 1997, initiated considerable progress worldwide to establish basic concepts and methods for performance-based earthquake engineering. An increasing acceptance of PBEE concepts by practicing engineers, together with extensive research, has led to implementation in the design and upgrade of buildings, bridges, and other man-made structures.

Encouraged by the success of the 1997 workshop, we decided to organize an international forum aimed at continuing dialog on the implementation worldwide of new ideas. The International Workshop on Performance-Based Seismic Design — Concepts and Implementation, was held in Bled, June 28 – July 1, 2004.

Much of the past research in performance-based earthquake engineering has focused on rigorous approaches to performance assessment and on metrics for communicating performance (in probabilistic terms) to stakeholders. In the design process (design of new structures and upgrading of existing ones), the challenge is to create a system that will deliver desired performance in a cost-effective way. The objective of the international workshop was to assess the states of knowledge and practice related to this challenge so that progress in research and implementation in engineering practice can be accelerated, with a common foundation established on which to base the various approaches advocated in different countries.

At the workshop, 45 invited participants and 12 observers from 14 countries addressed the following topics: loss estimation, fragility and vulnerability, and impact on risk management; implementation in engineering practice; performance-based design concepts; and integration of experimental and analytical simulations.

Forty-three papers, which were submitted before the workshop and posted on the workshop website, were presented during the first two days of the workshop. The last two days were devoted to discussions organized in the form of working group sessions, and a final plenary session. The workshop provided a valuable forum for the exchange of research results and ideas on issues important for advancement of performance-based earthquake engineering methodologies.

These proceedings contain the workshop resolutions, conclusions, and recommendations, as well as a compendium of the invited papers. The proceedings are intended to assess the state of the art and state of the practice in performance-based seismic design, to define future directions for the development of performance-based earthquake engineering, and to identify important research needs.

We are deeply indebted to the authors who accepted the invitation to attend the workshop, wrote original and thoughtful papers, presented them at the workshop, chaired the sessions, and participated in the lively discussions. The invaluable help of the advisory committee consisting of Professors Jack P. Moehle (chair), Gregory G.

Peter Fajfar
Professor of Structural Earthquake Engineering
University of Ljubljana
Slovenia

Helmut Krawinkler
John A. Blume Professor of Engineering
Stanford University
California, U.S.A.

Bled, July 2004

LIST OF PARTICIPANTS

Sergio M. Alcocer, National University of Mexico, Mexico D.F., Mexico
Mark Aschheim, Santa Clara University, California, U.S.A.
Nuray Aydinoğlu, Boğaziçi University, Istanbul, Turkey
Robert E. Bachman, Robert E. Bachman S.E., Sacramento, California, U.S.A.
Julian J. Bommer, Imperial College London, U.K.
Patricio Bonelli, Technical University Federico Santa Maria, Valparaiso, Chile
Edmund Booth, Edmund Booth Consulting Engineer, London, U.K.
Anil K. Chopra, University of California, Berkeley, California, U.S.A.
Craig D. Comartin, C.D. Comartin, Inc., Oakland, California, U.S.A.
C. Allin Cornell, Stanford University, California, U.S.A.
Edoardo Cosenza, University of Naples Federico II, Italy
Gregory G. Deierlein, PEER, University of California, Berkeley, U.S.A.
Amr S. Elnashai, University of Illinois, Urbana, U.S.A.
Peter Fajfar, University of Ljubljana, Slovenia
Michael N. Fardis, University of Patras, Greece
Matej Fischinger, University of Ljubljana, Slovenia
Ahmed Ghobarah, McMaster University, Hamilton, Ontario, Canada
Ronald O. Hamburger, Simpson Gumpertz & Heger, San Francisco, California, U.S.A.
Tara C. Hutchinson, University of California, Irvine, U.S.A.
Toshimi Kabeyasawa, University of Tokyo, Japan
Kazuhiko Kawashima, Tokyo Institute of Technology, Japan
Mervyn J. Kowalsky, North Carolina State University, Raleigh, U.S.A.
Helmut Krawinkler, Stanford University, California, U.S.A.
Sashi K. Kunnath, University of California, Davis, U.S.A.
Laura N. Lowes, University of Washington, Seattle, U.S.A.
Gaetano Manfredi, University of Naples Federico II, Italy
Eduardo Miranda, Stanford University, California, U.S.A.
Masayoshi Nakashima, Kyoto University, Japan
Paolo Negro, Joint Research Centre, E.C., Ispra (VA), Italy
Shunsuke Otani, Chiba University, Japan
Rui Pinho, ROSE School, Pavia, Italy
Artur V. Pinto, Joint Research Centre, E.C., Ispra (VA), Italy
Paolo E. Pinto, University of Rome "La Sapienza," Italy
Keith Porter, California Institute of Technology, Pasadena, U.S.A.
Andrei M. Reinhorn, University at Buffalo, State University of New York, U.S.A.
Avigdor V. Rutenberg, Technion, Haifa, Israel
Hitoshi Shiohara, University of Tokyo, Japan
Sri Sritharan, Iowa State University, Ames, U.S.A.
Boža Stojadinović, University of California, Berkeley, U.S.A.

Haluk Sucuoğlu, Middle East Technical University, Ankara, Turkey

Keh-Chyuan Tsai, National Center for Research on Earthquake Engineering, Taipei, Taiwan

Wai Keung Tso, McMaster University, Hamilton, Ontario, Canada

Andrew S. Whittaker, University at Buffalo, State University of New York, U.S.A.

Miha Tomaževič, Slovenian National Building and Civil Engineering Institute, Ljubljana, Slovenia

Roko Žarnić, University of Ljubljana, Slovenia

Matjaz Dolšek, University of Ljubljana, Slovenia

Bruno Dujič, University of Ljubljana, Slovenia

Paolo Franchin, University of Rome "La Sapienza," Italy

Iunio Iervolino, University of Naples Federico II, Italy

Tatjana Isaković, University of Ljubljana, Slovenia

Peter Kante, University of Ljubljana, Slovenia

Miha Kramar, University of Ljubljana, Slovenia

Damjan Marušić, University of Ljubljana, Slovenia

Iztok Peruš, University of Ljubljana, Slovenia

Karmen Poljanšek, University of Ljubljana, Slovenia

Vladimir Sigmund, University J.J. Strossmayer, Osijek, Croatia

Jaka Zevnik, University of Ljubljana, Slovenia

RESOLUTIONS

The International Workshop on Performance-Based Seismic Design — Concepts and Implementation was held in Bled, Slovenia, 28 June – 1 July, 2004. The main sponsors of the workshop were the Pacific Earthquake Engineering Research Center of the University of California, Berkeley, and the Ministry of Education, Science and Sport of Slovenia. Workshop attendees included representatives from 14 countries from Asia, Europe, and North and South America.

The workshop provided a valuable forum to exchange research results and design practice ideas on issues important for seismic risk reduction and the development of performance-based earthquake engineering concepts. The theme of the workshop was to assess the states of knowledge and practice related to performance-based design and its implementation, and to identify challenges that need to be addressed so that progress in research and implementation in engineering practice can be accelerated, with a common foundation established on which to base the various approaches advocated in different countries.

The participants agreed:

(1) that the workshop has led to a greater understanding of many of the issues involved in performance-based design, and that much progress has been made in the development of concepts and procedures suitable for implementation in engineering practice. Nevertheless, many issues remain unresolved and additional research and studies are needed to implement rigorous performance-based design with confidence.

(2) that performance-based design concepts provide a suitable framework for future seismic code development.

(3) that common interests exist among researchers and practitioners of the countries represented at the workshop. Progress in research and implementation in engineering practice can be accelerated by the international dialog on the implementation worldwide of new ideas. Cooperative research on issues of common interest should be encouraged. The participants recognize that performance-based design has many facets and may take on very different meaning and approaches depending on prevailing economic and societal priorities. Nevertheless, by continuing the international dialog, a common foundation can be established on which to base the various approaches advocated in different countries.

(4) that an urgent need exists for worldwide sharing of data obtained from experimental and analytical studies and from field measurements taken during earthquakes. A protocol for international data sharing should be developed and efforts should be initiated for the creation of a worldwide data repository.

(5) that in order to accelerate the transfer of knowledge from researchers to engineering practice, a need exists for incorporating performance-based design concepts and reliability theory into educational curricula.

(6) that recognizing the benefits of the exchange of ideas that occurred at the workshop, international gatherings should be held on a periodic basis to share information on the development of performance-based design.

CONCLUSIONS AND RECOMMENDATIONS

The workshop focused on issues important to the development of performance-based seismic design methodologies that can form the basis for practical guidelines, standards, and code implementation. The emphasis was on general concepts rather than issues specific to design and construction practices, and on code approaches in various countries. The workshop participants recognize that issues specific to different materials, innovative structural systems, existing versus new construction, and regions of different seismicity have not been addressed.

The following recommendations and conclusions have been developed by four working groups and are based on extensive discussions of the presentations given during the first two days of the workshop.

Working Group on Loss Estimation, Fragilities and Vulnerability, and Impact on Risk Management

Co-Chairs: Comartin and Whittaker
Recorder: Miranda
Working Group Members: Bachman, Cornell, Elnashai, Hutchinson, Lowes, Manfredi, Kawashima, Porter, Reinhorn, Nakashima, Pinho, Pinto P., Sucuoĝlu, Franchin, Iervolino, Kante, Kramar

Conclusions and Recommendations

(1) There is an urgent need to install dense arrays of instruments in selected buildings, bridges, and other structures to collect performance (loss) data. The structures and sites should be selected so that the likelihood of recording a comprehensive set of data for important types of structures within a short time frame is maximized, i.e., the emphasis should be on instrumentation of structures in urban areas of high seismicity. This will necessitate the development of plans and protocols for damage and loss (performance) data collection, and the documentation of comprehensive information on properties of the structures before the occurrence of an earthquake.

(2) It is recommended to develop an expert system, essentially a "virtual contractor," to aid in aggregation of capital losses for different damage scenarios, i.e., to enable the calculation of capital losses for specified distributions of engineering demand parameters. The development of the expert system knowledge base will require the systematic collection and synthesis of both loss data from past earthquakes and information from expert contractors. The expert system shell should be common to all countries and regions but the knowledge base will vary by region and country.

(3) An international web-based repository should be developed and maintained for performance data and information of interest in the context of performance-based earthquake engineering, including a stakeholder encyclopedia (describing and defining performance in a manner meaningful to the stakeholders) and fragility data for structural, nonstructural, and content components and systems. As part of this effort, protocols should be developed for testing and documentation of experimental results.

Working Group on Implementation of PBEE in Engineering Practice

Co-Chairs: Hamburger and Kabeyasawa
Recorder: Bommer
Working Group Members: Alcocer, Aschheim, Aydinoĝlu, Bonelli, Booth, Chopra, Cosenza, Deierlein, Fajfar, Fardis, Fischinger, Ghobarah, Kowalsky, Krawinkler, Kunnath, Negro, Otani, Pinto A., Rutenberg, Shiohara, Sritharan, Tsai, Tso, Dolšek, Marušić, Peruš, Poljanšek, Sigmund, Zevnik

Conclusions and Recommendations

(1) Performance-based seismic design can be viewed as a process of system conception followed by an assessment procedure in which the performance of the structural system is evaluated and improved as needed to satisfy stated performance objectives. Design tools should be developed, particularly for new structures, to assist in the conception of an effective structural system in order to provide a good starting point for subsequent assessment. Direct design, without subsequent assessment, is a feasible option for simple structures.

(2) The foundation of PBSD procedures should be reliability based. For implementation in engineering practice, the reliability concepts may be incorporated implicitly through appropriate demand and capacity factors, while explicit incorporation of reliability concepts is an option to be considered primarily for major facilities with special performance requirements. Reliability concepts should also be considered to improve and transition existing code-based design methods and to improve the calibration of prescriptive rules in existing codes. They may also be partially introduced into codes to aid the transition to full use of PBSD.

(3) PBSD concepts should be incorporated into codes on a worldwide basis, but with due consideration to the need for simplicity and for sound engineering judgment, and with due consideration of economic and societal priorities.

(4) Opportunities should be sought out to demonstrate the feasibility and advantages of PBSD approaches compared to presently employed prescriptive approaches.

(5) Future guidelines and codes must be clear regarding the limitations in the use of the different analytical procedures (linear static, nonlinear static, linear dynamic,

nonlinear dynamic) and when they should not be used. Emphasis in research should be on the development of nonlinear analysis procedures. For nonlinear static (pushover) analysis, additional research is needed on extension to irregular structures (particularly unsymmetrical) and structures with significant higher mode effects. Nonlinear dynamic procedures need improvement of large displacement predictions and of element hysteretic models.

(6) More work needs to be done in defining appropriate performance measures, with an emphasis on providing protection against life-safety hazards and excessive economic losses.

Working Group on Performance-Based Design Concepts

Co-Chairs: Deierlein and Fardis
Recorder: Aschheim
Working Group Members: Aydinoĝlu, Bachman, Bommer, Bonelli, Booth, Chopra, Comartin, Cornell, Fajfar, Fischinger, Ghobarah, Hamburger, Hutchinson, Kabeyasawa, Kawashima, Kowalsky, Krawinkler, Manfredi, Miranda, Otani, Pinho, Pinto P., Porter, Rutenberg, Shiohara, Sucuoĝlu, Tso, Whittaker, Dolšek, Franchin, Iervolino, Poljanšek, Sigmund, Zevnik

Conclusions and Recommendations

(1) The goal of performance based seismic design (PBSD) is to assist in the engineering of cost-effective facilities, whose safety and resistance to damage from earthquakes meet the needs and expectations of key stakeholders and society at large more effectively and reliably than can be achieved with codes using prescriptive design rules. Key incentives for the use of PBSD include:

   (a) Reduction in the initial capital costs of facilities designed to have comparable performance to that implied by existing standards based on prescriptive rules.

   (b) Ability to design higher-performance structures that have improved safety and lower life-cycle costs associated with seismic risk.

(2) The most immediate need for and benefit from PBSD are for existing structures and new facilities with special features that are not adequately addressed by existing codes (e.g., innovative new structural systems, bridges on liquefiable soils, and industrial plants with complex geometries).

(3) Efforts should be continued to demonstrate the benefits that PBSD will provide to key stakeholders and, thereby, to the engineering professionals who embrace PBSD in design practice. This should include pilot applications to both special facilities that cannot be reliably designed using current codes and standards, and to more conventional facilities.

(4) More attention should be given to bridges, industrial facilities, and other important infrastructure facilities and systems.

(5) Research efforts toward improving capabilities for prediction of collapse should be emphasized. Structural collapse is defined as the state in which a structural component (for local collapse) or the structural system (for global collapse) is no longer capable of resisting its tributary gravity load. Criteria for local collapse need to be established and elaborated. The extent to which local collapse propagates and conceivably leads to system collapse depends on the configuration and redundancy of the system and its ability to redistribute gravity loads from the failed component(s) to the neighboring ones. Much more experimental data on component deterioration and system collapse are needed in order to calibrate analytical models being developed for collapse prediction.

(6) A transition from presently employed prescriptive design requirements to performance-based design requirements should be gradual in order to calibrate the consequences of performance-based design and provide safeguards against its misuse. Overriding issues are societal concerns with loss of life and excessive financial losses that may have a regional impact.

(7) Research efforts toward improving analysis capabilities for structure-soil-foundation systems should be intensified, and collaboration between structural and geotechnical engineers should be emphasized.

Working Group on Harmonization of Experimental and Analytical Simulations

Co-Chairs: Elnashai and Nakashima
Recorders: A. Pinto and Ghobarah
Working Group Members: Alcocer, Cosenza, Kunnath, Lowes, Negro, Otani, Reinhorn, Sritharan, Tsai, Žarnić, Kante, Kramar, Marušić, Peruš

Advanced experimental facilities have become available worldwide; for example, NEES, E-Defense, JRC, and NCREE. Experiments on complex structural systems at larger scales become more practicable; they provide great opportunities for more accurate characterization of various limit states of structures and ultimately for accelerated acceptance of PBEE. New experimental facilities, techniques, and devices require new approaches to research and development. The following specific recommendations are along these lines.

Conclusions and Recommendations

(1) Testing procedures. Experimentation should cover the full range of behavior from damage initiation to collapse. Test structures should contain nonstructural and content systems to the extent feasible. In simplified test configurations, much attention needs to be paid to simulation of boundary conditions. Field testing should be encouraged to provide realistic performance data. A great need

exists to develop testing protocols, including interaction between testing and analysis, peer review of procedures, careful selection of input motion, and specialized protocols for testing of nonstructural components and for material testing. Advanced instrumentation should be developed (including high-resolution image processing) for comprehensive documentation of damage data. All experimental data should be documented, archived, and shared publicly after verification, taking into account intellectual rights.

(2) ***Analytical prediction of behavior until collapse***. Improved approaches need to be developed to simulate collapse and behavior of nonstructural systems, and for constitutive modeling of new and existing materials. Computer analysis programs should emphasize user-friendliness and should be developed through partnerships of researchers and practicing engineers with software companies.

(3) ***Distributed simulations.*** The benefits obtained from geographically distributed simulation should be clearly advocated, including the identification of systems that necessitate distributed simulation and cannot be dealt with otherwise. To raise public awareness, news media should be utilized to inform the general public, including the technical community and policy makers, of major distributed simulation efforts and to encourage tele-observation of experimental activities.

A EUROPEAN PERSPECTIVE TO PERFORMANCE-BASED SEISMIC DESIGN, ASSESSMENT AND RETROFITTING

Michael N. FARDIS[1]

ABSTRACT

Performance-based features of the recent first European Standard for seismic design of buildings (EN1998-1:2004) and of the final draft European Standard for seismic assessment and retrofitting of buildings (prEN1998-3, May 2004) are reviewed, with emphasis on concrete buildings. EN1998-1:2004 includes two performance levels: (a) local collapse endangering lives and (b) limitation of damage in structural and non-structural elements. They are meant to be checked under a rare and an occasional earthquake, respectively, with the definition of the associated seismic hazard levels left to the country. Buildings designed for energy dissipation are protected from global collapse under a very rare (but unspecified) earthquake across-the-board application of capacity design to control the inelastic mechanism. The link between the behavior factor q that reduces elastic lateral forces of the (local-) collapse prevention earthquake and member detailing against member collapse is derived. prEN1998-3 provides for 3 performance levels: near collapse, significant damage and limited damage. The country will decide which ones will be checked and may leave the associated hazard level to be chosen by owners. Verification of ductile members is fully deformation-based. The tools for verification of existing, new or retrofitted members are given as expressions for their limit deformations.

Keywords: Earthquake-resistant design; Eurocode 8; Performance-based seismic design; Seismic assessment; Seismic design; Seismic retrofitting.

1. PERFORMANCE-BASED DESIGN IN EC8 AND ITS BACKGROUND

Since the early 90's, the activity of the European Earthquake Engineering community has been centered around, and motivated by, the drive towards European codification, namely the development of a European Standard for seismic design: Eurocode 8, or "EN1998: Design of structures for earthquake resistance". Recent fruits of this effort are the two parts of Eurocode 8 positively voted in March 2004 (CEN 2004a):

- EN1998-1:2004, "Part 1: General rules, seismic actions, rules for buildings",
- EN1998-5:2004, "Part 5: Foundations, retaining structures, geotechnical aspects"

and the very recent draft (CEN 2004b):

- prEN1998-3, "Part 3: Assessment and retrofitting of buildings,"

---

[1] *Department of Civil Engineering, University of Patras, GR26500, Greece, fardis@upatras.gr*

to be sent soon to the 28 members of the European Committee for Standardisation (CEN) for voting. Concepts and approaches for Performance-based seismic design, assessment and retrofitting have deeply penetrated these three standards. So, they will soon find their way into everyday engineering practice, as within 2007 the about 60 Eurocode Parts will be put in parallel use with existing national codes and by year 2010 they will be the exclusive structural design standards in Europe.

Although the philosophy is the same as in the US, several aspects of the performance-based approach in Eurocode 8 have developed independently and bear a strong European flavor. Due to the importance of these recent developments for Europe, Parts 1 and 3 of Eurocode 8 have a central place in the paper. The emphasis is on concrete buildings, where the author's expertise and technical contribution lie.

In Europe Performance Levels are associated to, or identified with, Limit States. The Limit State concept appeared in Europe in the '60s, to define states of unfitness of the structure for its intended purpose (CEB 1970). They are termed Ultimate Limit States if they concern the safety of people or structures, or Serviceability Limit States if they concern the normal function and use of the structure, the comfort of occupants, or damage to property (mainly to non-structural elements and finishes). According to the Eurocode on the basis of structural design (CEN 2002) the Limit States approach is the backbone of structural design for any type of loads, including seismic.

The CEB Model Code for seismic design of concrete structures (CEB, 1985) introduced two Limit States: (a) Structural Safety (no-collapse) and (b) Serviceability. Design for both was for a single hazard level of unspecified mean return period. The European Prestandard (ENV) for the seismic design of new buildings (CEN 1994) differs from the 1985 CEB seismic Model Code in that its scope covers practically all materials and types of structures, and in the requirement to check two Limit States at distinct Hazard Levels: (a) the Ultimate Limit State against Life-threatening Collapse and (b) the Serviceability Limit State against damage and loss of use. For ordinary structures the first Limit State is associated with the 475-year (10%/50yr) earthquake and checked by as in the 1985 CEB seismic Model Code, except the interstory drift limitations. The second Limit State is checked only in buildings, where interstory drifts under 40% to 50% of the 475-year earthquake are limited to values that depend on the brittleness of non-structural partitions. As in the CEB seismic Model Code, alternative levels of ductility for concrete buildings — termed "Ductility Classes" — are three. The performance-based requirements of the 1994 ENV (CEN 1994) were retained and expanded in the 2004 EN (CEN 2004a), described in the sequel.

The European Prestandard (ENV) for repair and seismic strengthening of existing buildings (CEN 1996) does not present any conceptual advances over its 1994 counterpart for new buildings. Except that the interstory drift limits for the Serviceability earthquake are not checked, the evaluation criteria for the existing building are limited to full conformity with the requirements of one of the three "Ductility Classes" of the ENV for new buildings (CEN 1994), under a seismic action reduced due to the shorter remaining lifetime of the building. Retrofitting is also to full conformity with the rules of the ENV for new buildings.

2. PERFORMANCE-BASED ASPECTS OF PART 1 OF EUROCODE 8 FOR THE DESIGN OF NEW BUILDINGS

2.1 Performance Objectives and Their implications for Design

EC8-Part 1 specifies a two-level seismic design with explicit performance objectives:
1. Protection of life under a rare seismic action, by preventing collapse of the structure or parts of it and ensuring structural integrity and residual load capacity.
2. Limited property loss in a frequent earthquake, via limitation of structural and non-structural damage.

Performance level 1 is achieved by proportioning and detailing structural elements for a combination of strength and ductility that provides a safety factor between 1.5 and 2 against substantial loss of lateral load resistance. The damage limitation performance level is pursued by limiting the overall deformations (lateral displacements) of the building to levels acceptable for the integrity of all its parts (including non-structural ones) and through non-engineered measures for the integrity of (masonry) infills.

The three Ductility Classes (DCs) were essentially reduced to two: DC Medium (M) and High (H). The third class (DC L or Low), amounting to design essentially for strength (with q=1.5 due to overstrength) without engineered ductility, is limited to low seismicity (design PGA not more than 0.1g). For the other two DCs a third — but not explicitly stated — performance objective is prevention of global collapse under an extremely strong earthquake, like the "Maximum Considered Earthquake" (MCE) of US codes. It is recognized, though, that repair after that earthquake may be unfeasible or economically prohibitive and that the damaged structure may collapse in a strong aftershock. This performance objective is pursued by control of the inelastic response mechanism through systematic and across-the-board application of capacity design.

The Eurocodes have adopted a policy of letting National Authorities control the safety and cost-effectiveness provided by structures in their territory, by choosing the values of certain key parameters (termed Nationally Determined Parameters or NDPs) that control safety and economy. Within this policy, the hazard levels corresponding to the two performance levels are left for the countries to determine. Eurocode 8 recommends though the following, for structures of ordinary importance:
i.   A seismic action for (local) collapse prevention — termed "design" seismic action — with 10% exceedance probability in 50 yrs (return period: 475 yrs).
ii. A 10% in 10 yrs "serviceability" earthquake for damage limitation (mean return period: 95 yrs).

Enhanced performance of essential or large occupancy facilities is achieved not by upgrading the performance level for given earthquake level, as in US codes, but by modifying the hazard level for which the performance level is pursued. For essential or large occupancy structures the seismic action at both performance levels should be increased so that its exceedance probability in 50 or 10 years, respectively, is less than 10%. At the collapse prevention level the recommended value of the NDP-importance

factor γ_I is 1.4 or 1.2 for essential or large occupancy buildings, respectively. A γ_I-value of 0.8 is recommended for buildings of reduced importance for public safety.

The same spectral shape is used for the seismic action for both performance levels, with a single multiplicative factor reflecting the difference in hazard level. The value of this factor should express national choice regarding protection of property, but also the local seismotectonic environment. A value of 0.4 or 0.5 is recommended for this NDP-conversion factor, giving at the end about the same property protection in ordinary or large-occupancy buildings, less property protection for buildings of low importance (by 15–20% at the level of the seismic action) and higher property protection for essential facilities (by 15–20% at the level of the seismic action), possibly allowing them to operate during or immediately after a frequent event.

The drift limit under the 10% in 10 years "serviceability" earthquake is 0.5% if non-structural elements are brittle and attached to the framing, 0.75% if they are ductile, and 1% if they are not forced to follow structural deformations or do not exist. The 1% drift limit is to protect also structural members from significant inelastic deformations under the "serviceability" earthquake. Drift demands are calculated on the basis of the equal-displacement rule (and in concrete buildings for 50% of the uncracked gross section stiffness). As the National Annex will set the level of "serviceability" earthquake, it will also determine to which extent these limits will control member dimensions. With the EC8-recommended values of 0.5x0.8=0.4 to 0.4x1.4=0.56 for the ratio of the "serviceability" to the "design" seismic action, these limits are 2 to 3 times stricter than in current US codes and control member sizes in concrete moment frames (and in steel and composite as well).

The standard design procedure for the (local-)collapse prevention level is force-based design on the basis of the results of linear analysis for the 5%-damped elastic spectrum reduced by the "behavior factor" q. In DC M (Medium M) and H (High H) buildings the global energy dissipation and ductility capacity needed for q-factor values (well) above the value of 1.5 attributed to overstrength is ensured via:

- measures to control the inelastic response mechanism, so that concentration of inelastic deformation in a small part of the structure (mainly a soft story mechanism) and brittle failure modes are avoided;
- detailing of the plastic hinge regions for the inelastic deformations expected to develop there under the design seismic action.

Concentration of inelastic deformations and soft story mechanisms are avoided by configuring and proportioning the lateral-force resisting system so that vertical members remain practically straight — i.e., elastic — above the base. Concrete wall or dual systems are promoted and are capacity-designed for yielding to take place only at base of their walls. In concrete moment frames columns are capacity-designed to be stronger than the beams, with an overstrength factor of 1.3 on beam design flexural capacities in their comparison with those of columns. All concrete beams, columns and walls are capacity-designed against (brittle) shear failure.

DC M and H represent two different balances of strength and ductility, more or less equivalent in terms of total material requirements and performance at the local

collapse prevention level (Panagiotakos and Fardis, 2004a, 2004b). DC M is slightly easier to design for and achieve at the site and may provide better performance in moderate earthquakes. DC H may give better performance under motions (much) stronger than the design seismic action. Unlike US codes, EC8 does not link selection of the ductility class to seismicity or to the importance and occupancy of the building, nor puts any limit to their application. The choice is left to the National Annex, which may in turn leave it to the designer depending on the particular project.

Unless the Country objects through its National Annex to Eurocode 8, it is allowed to design without employing the q-factor, but directly on the basis of nonlinear analysis (pushover or time-history analysis). In that case ductile members verified by comparing directly deformation supplies to demands. The definition of acceptable member deformation limits is left to the National Annexes. To ensure a minimum global and local ductility in buildings designed on the basis of nonlinear analysis, Eurocode 8 requires that they meet all DC M rules (for member detailing, strong columns-weak beams in frames, capacity design in shear, etc.). By allowing design directly through nonlinear analysis with member verification on the basis of deformations, the 1st generation of Eurocode 8 paves the way for fully displacement- and deformation-based design in the 2nd generation.

2.2 Member Detailing for Deformation Demands Derived from the Behavior Factor

2.2.1 Required Curvature Ductility Factor μ_ϕ at the End Section of Plastic Hinges

In buildings designed with the common forced-based approach that employs the q-factor for the reduction of elastic forces, the value of q is taken to be related to the global displacement ductility factor, μ, through the Vidic et al. (1994) q-μ-T relation:

$$\mu_\delta=q, \text{ if } T_1 \geq T_C, \ \mu_\delta=1+(q-1)T_C/T_1, \text{ if } T_1 < T_C \tag{1}$$

where T_1 = building fundamental period and T_C = period at the upper limit of the constant acceleration spectral region. The q-factor does not assume district values for the two ductility classes, but continuous ones proportional to a system overstrength ratio, α_u/α_1, which is equal to the ratio of the base shear that turns the structure into a mechanism to the base shear at first plastic hinge formation in the system. Default values are given for this ratio, to avoid computing it through pushover analysis. Continuous values are obtained then from Eq. (1) for μ_δ, to be converted then to local inelastic deformation demands in concrete members (expressed in terms of the local curvature ductility factor, μ_ϕ) through the following approximation:

$$\mu_\phi=2\mu_\delta-1 \tag{2}$$

derived as follows:

The available value of the chord-rotation ductility factor at the end of a concrete member, μ_θ, is taken to relate to that of μ_ϕ at the end section via an expression similar to Eq. (2), in which μ_θ replaces μ_δ. This expression derives from:

i.   The well-known relation μ_θ - μ_ϕ that employs the plastic hinge length, L_{pl};
ii. An empirical relation for L_{pl}, fitted to hundreds of cyclic test results on members with flexure-controlled failure, for ultimate curvatures computed assuming: (a) a steel ultimate strain, ε_{su}, equal to the minimum values of 2.5% and 5% given in Eurocode 2 for steel Classes A or B and to $\varepsilon_{su} = 6\%$ for steel Class C, and (b) the ultimate strain of confined concrete given by the Eurocode 2 relation:

$$\varepsilon_{cu,c} = 0.0035 + 0.1\alpha\omega_w \tag{3}$$

where $\omega_w = \rho_w f_{yw}/f_c$ is the volumetric mechanical ratio of confining steel with respect to the confined concrete core and α the confinement effectiveness ratio:

$$\alpha = \left(1 - \frac{s_h}{2b_o}\right)\left(1 - \frac{s_h}{2h_o}\right)\left(1 - \frac{\sum b_i^2}{6h_o b_o}\right) \tag{4}$$

In Eq. (4) b_o and h_o are the dimensions of the confined core to the hoop centerline and b_i the spacing of laterally restrained longitudinal bars on the perimeter;
iii. Rounding-up the values of L_{pl} resulting from (ii) above for the range of member parameters common in buildings into a single one: $L_{pl} = 0.185L_s$, where L_s is the shear span at the member end. Then Eq.(2), with μ_θ replacing μ_δ, gives a safety factor on μ_ϕ for given μ_θ, which is on average equal to 1.65 for columns, 1.35 for beams or 1.1 for walls, within the range of possible values of q for DC M and H buildings and for the usual range of L_{pl} for the 3 types of concrete members.

Once a beam-sway plastic mechanism is ensured, the demand value of μ_θ at those member ends where plastic hinges may form (at beam ends and the base of columns and walls) is about equal to the global displacement ductility factor, μ_δ. Hence Eq.(2).

Members are detailed to provide the value of $\mu_\phi = \phi_u/\phi_y$ from Eq.(2). This is achieved on the basis of the definition of ϕ_u as $\phi_u = \varepsilon_{cu}/\xi_{cu}d$, with ξ_{cu} computed as:

$$\xi_{cu} = \frac{(1-\delta_1)(\nu + \omega_1 - \omega_2) + (1+\delta_1)\omega_v}{(1-\delta_1)\left(1 - \dfrac{\varepsilon_c}{3\varepsilon_{cu}}\right) + 2\omega_v} \tag{5}$$

where ω_1, ω_2, ω_v are mechanical ratios of tension and compression reinforcement and of the (web) vertical bars between them, $\nu = N/bdf_c$ is the axial load ratio, $\delta_1 = d_1/d$ the distance of the tension or compression reinforcement from the corresponding extreme fibers, normalized to d, $\varepsilon_c = 0.002$ the strain of concrete at f_c and ε_{cu} its ultimate strain.

2.2.2 Maximum Tension Reinforcement Ratio at the Ends of DC M or H Beams

Taking $\phi_y = 1.5f_y/E_s d$, as derived from beams tests at yielding, $\omega_v = 0$, $\nu = 0$ and $\varepsilon_{cu} = 0.0035$ at the unconfined extreme compression fibers, the upper limit of the beam tension reinforcement ratio, ρ_1, is derived. Using the design values, $f_{cd} = f_{ck}/\gamma_c$,

$f_{yd}=f_{yk}/\gamma_s$, of the concrete and steel strengths and the value $\varepsilon_{yd}=f_{yd}/E_s$ of $\varepsilon_y=f_y/E_s$ and rounding up a coefficient, the following condition for DC M or H beams is derived:

$$\rho_{1,max} = \rho_2 + \frac{0.0018}{\varepsilon_{yd}\mu_\phi} \frac{f_{cd}}{f_{yd}} \tag{6}$$

where ρ_2 is the compression reinforcement ratio and both ρ_1 and ρ_2 are normalized to the width b of the compression zone. With this rounding, the safety factor of 1.35 on μ_ϕ from Eq.(2) mentioned in (iii) above increases to 1.6 if the values $\gamma_c=1.5$, $\gamma_s=1.15$ recommended in Eurocode 2 for the persistent and transient design situation are adopted, and to 1.4 if the values $\gamma_c=1$, $\gamma_s=1$ are used instead, as recommended in Eurocode 2 for the accidental design situation ($1.6/1.4\approx\gamma_s=1.15$). This "theoretical" safety factor can be compared to the ratio of: (a) the real value of (ρ_1-ρ_2) in beams cyclically tested to flexural failure, to (b) the value obtained from Eqs. (6) and (2) for the value of $\mu_\theta=\mu_\delta$ at beam ultimate deflection. The median value of the ratio in 52 beam tests is 0.725 for $\gamma_c=1$, $\gamma_s=1$, or 0.825 for $\gamma_c=1.5$, $\gamma_s=1.15$. Being less than 1.0, these values suggest that Eq.(6) is unsafe. Nonetheless, if the value of $\mu_\theta=\mu_\delta$ is determined as the ratio of beam ultimate drift not to the experimental drift at yielding, but to the value $M_yL_s/3(0.5EI)$ that corresponds to the effective elastic stiffness of 0.5EI assumed in Eurocode 8, the median ratio in the 52 tests becomes 2.5 for $\gamma_c=1$, $\gamma_s=1$, or 2.85 for $\gamma_c=1.5$, $\gamma_s=1.15$, above the "theoretical" safety factors of 1.4 or 1.6.

2.2.3 Confining Reinforcement at the Base of DC M or H Columns or Walls

Similar is the derivation of the confining reinforcement required by Eurocode 8 at the base of columns or walls (in the boundary elements). Setting: $\phi_u=\varepsilon_{cu,c}/\xi_{cu}h$ and $\phi_y=\lambda\varepsilon_y/h$ with $\lambda = 1.85$ for columns and $\lambda = 1.45$ for walls, as derived from test results, using again Eq.(5) but this time for the confined core after spalling of the concrete cover ($\delta_1\approx0$) and with all variables in both sides of Eq.(5) normalized to h instead of d, using Eq.(3) for the ultimate strain of confined concrete, rounding-up coefficients and using the design strengths of materials, we obtain the Eurocode 8 requirement for confining reinforcement of symmetrically reinforced ($\omega_1=\omega_2$) columns or walls:

$$\alpha\omega_{wd} = 30\mu_\phi\varepsilon_{yd}(\nu_d + \omega_{vd})\frac{b_c}{b_o} - 0.035 \tag{7}$$

where b_c is the width of the compression flange and b_o the corresponding width of the confined core. In columns Eurocode 8 neglects ω_{vd} in the parenthesis, compared to ν_d. With the rounding-up, the safety factor of 1.65 in columns or 1.1 in walls on the value of μ_ϕ from Eq.(2) — as mentioned in (iii) above — becomes nearly 2.65 for columns or 2.25 for walls. This "theoretical" safety factor can be compared to the ratio of: (a) the value of $\alpha\omega_{wd}+0.035$ required from Eqs. (7) and (2) in columns or walls cyclically tested to flexural failure for the value of μ_θ at member ultimate deflection, to (b) the real value of $\alpha\omega_{wd}+0.035$ (proportional to the available value of μ_ϕ according to Eq.(7)) in the test. The median value of the ratio in 626 cyclic tests of columns with non-zero ν_d is 0.88 for $\gamma_c=1$, $\gamma_s=1$, or 0.92 for $\gamma_c=1.5$, $\gamma_s=1.15$. The corresponding median values in 49 cyclic wall tests is 0.93 for $\gamma_c=1$, $\gamma_s=1$, or 0.96 for $\gamma_c=1.5$,

γ_s=1.15. Values less than 1.0 mean that Eq.(7) may be unsafe. If μ_θ is determined as the ratio of the member ultimate drift not to the experimental yield drift, but to the value $M_yL_s/3(0.5EI)$ corresponding to the effective elastic stiffness of 0.5EI assumed in Eurocode 8, the median ratio becomes 2.08 for γ_c=1, γ_s=1, or 2.26 for γ_c=1.5, γ_s=1.15 in the 626 column tests, and 2.69 for γ_c=1, γ_s=1 or 3.13 for γ_c=1.5, γ_s=1.15 in the 49 wall tests (not far from the "theoretical" values of 2.25 and 2.65 quoted above).

Table 1. Compliance criteria for assessment or retrofitting of concrete members

Members	Limited Damage (LD)	Significant Damage (SD)	Near Collapse (NC)	
			Linear analysis	Non-linear analysis
Ductile primary	$\theta_E \le \theta_y$[1]	$\theta_E \le 0.75\theta_{u,m-\sigma}$[2]	$\theta_E \le \theta_{u,m-\sigma}$[2]	
Ductile secondary		$\theta_E \le 0.75\theta_{u,m}$[3]	$\theta_E \le \theta_{u,m}$[3]	
Brittle primary	Checked only if NC is not checked. Then criteria of NC apply with $V_{E,max}$ from analysis, or with $V_{E,CD}$ for linear analysis in SD Limit State	$V_{E,CD}$[4]$\le V_{Rd,EC2}$[5], $V_{Rd,EC8}/1.15$[6]	$V_{E,max} \le V_{Rd,EC2}$[5], $V_{Rd,EC8}/1.15$[6]	
Brittle secondary		$V_{E,CD}$[4]$\le V_{Rm,EC2}$[7], $V_{Rm,EC8}$[8]	$V_{E,max} \le V_{Rm,EC2}$[7], $V_{Rm,EC8}$[8]	

(1) θ_E: chord-rotation demand from the analysis; θ_y: chord-rotation at yielding, Eqs.(8)–(11).
(2) $\theta_{u,m-\sigma}$: mean-minus-stand. deviation chord-rotation supply, equal to $\theta_{u,m}/1.5$ if $\theta_{u,m}$ is computed via Eq. (12), or to $\theta_y+\theta^{pl}_{u,m}/1.8$, if Eq. (13) is used.
(3) $\theta_{u,m}$: mean chord-rotation supply from Eq. (12), or $\theta_{u,m}=\theta_y+\theta^{pl}_{u,m}$ from Eq. (13).
(4) $V_{E,CD}$: shear force computed from equilibrium as in capacity-design.
(5) $V_{Rd,EC2}$: shear resistance before flexural yielding, as given for monotonic loading in Eurocode 2, using mean material strengths divided by partial factors of materials and by a "confidence factor" that depends on the amount and reliability of available information.
(6) $V_{Rd,EC8}$: shear resistance for shear failure in cyclic loading after flexural yielding, given by Eqs. (14)–(16) as applicable, with mean material strengths divided by partial factors for materials and the "confidence factor" depending on the available information.
(7) As in [5, 6] above, respectively, but using mean material strengths.

3. THE FULLY PERFORMANCE-BASED PART 3 OF EUROCODE 8, FOR THE ASSESSMENT AND RETROFITTING OF OLDER BUILDINGS

3.1 Performance Objectives for Assessment and Retrofitting

Part 3 of Eurocode 8 (CEN 2004b) adopts a fully performance-based approach for existing buildings. Three performance levels (termed "Limit States") are defined:

- "Near Collapse" (NC), similar to "Collapse prevention" in the U.S. In the verifications, a member may approach its ultimate force or deformation capacity.
- "Significant Damage" (SD), corresponding to "Life safety" in the US and to the local-collapse prevention level for which new buildings are designed in

EC8-Part 1. The verifications should provide a margin against member ultimate capacity.

- "Damage Limitation" (DL), corresponding to "Immediate Occupancy" in the US. Members should be verified to remain elastic.

The "Seismic Hazard" levels for which the three Limit States are required will be decided nationally as NDPs, or by the owner, if the National Annex does not choose. The Eurocode itself gives no recommendation, but mentions that the performance objective recommended as suitable to ordinary new buildings is a 225yr earthquake (20% in 50 years), a 475yr event (10% in 50 years), or a 2475yr one (2% in 50 years), for the DL, the SD or the NC "Limit State", respectively. National Authorities will decide too whether all three Limit States will need to be verified, or whether checking one or two Limit States at the corresponding seismic hazard level will suffice. It is hoped that National Authorities will set the performance requirements for existing buildings in their territory so that the chance that owners will retrofit their property increases and the population of buildings to be retrofitted is acceptable for the society and the national economy. The same spectral shape holds for all hazard levels.

3.2 Compliance Criteria for Concrete Buildings

Informative Annex A in (CEN 2004b) specifies for members of concrete buildings the performance requirements mentioned already with the definition of the three Limit States, as shown in Table 1. Flexure is always considered as a ductile mechanism and checked in terms of deformations - in this case in terms of chord-rotations at member ends. Shear is considered as a brittle mechanism and checked in terms of forces.

The mean value of the chord rotation at yielding, θ_y, or ultimate, $\theta_{u,m}$ (total or plastic part) is given as (Biskinis and Fardis 2004, Fardis and Biskinis 2003):

for beams, rectangular columns: $\theta_y = \phi_y \dfrac{L_s + a_V z}{3} + 0.0013\left(1 + 1.5\dfrac{h}{L_s}\right) + \dfrac{0.13\phi_y d_b f_y}{\sqrt{f_c}}$ (8)

for walls, rectangular, bar-belled: $\theta_y = \phi_y \dfrac{L_s + a_V z}{3} + 0.002\left(1 - 0.125\dfrac{L_s}{h}\right) + \dfrac{0.13\phi_y d_b f_y}{\sqrt{f_c}}$ (9)

$$\theta_{um} = 0.016\left(1 - \frac{3}{8}a_w\right)(0.3^\nu)\left[\frac{\max(0.01; \omega_2)}{\max(0.01; \omega_1)}f_c\right]^{0.225}\left(\frac{L_s}{h}\right)^{0.35} 25^{\left(\alpha\rho_{sx}\frac{f_{yw}}{f_c}\right)}(1.25^{100\rho_d})$$ (10)

$$\theta_{um}^{pl} = \theta_{um} - \theta_y = 0.0145(1 - 0.4a_w)(0.25^\nu)\left[\frac{\max(0.01; \omega_2)}{\max(0.01; \omega_1)}\right]^{0.3} f_c^{0.2}\left(\frac{L_s}{h}\right)^{0.35} 25^{\left(\alpha\rho_{sx}\frac{f_{yw}}{f_c}\right)}(1.275^{100\rho_d})$$ (11)

The new variables in Eqs.(8)–(11) are: a_V=1 if the shear force at flexural yielding, M_y/L_s, exceeds the shear at diagonal cracking, or 0 otherwise; z: internal lever arm = 0.9d in beams or columns, $0.8l_w$ in walls; d_b: diameter of longitudinal bars; a_w=1 for walls, 0 otherwise; ρ_{sx}: confining reinforcement ratio in the direction of bending; ρ_d: diagonal reinforcement ratio. All other variables have been defined

before (factor α in Eq.(4)). Material strengths, f_y, f_c, are in MPa. In members not detailed for earthquake resistance, the right-hand-side of Eqs.(10), (11) is multiplied times 0.85.

The shear resistance under cyclic loading after flexural yielding is also given, to supplement the shear design rules in Eurocode 2 that address only monotonic loading and do not reflect the decrease in shear resistance with the plastic part of the chord-rotation ductility demand, $\mu^{pl}_\theta = \mu_\theta - 1$. In units MN, m (Biskinis et al. 2004):

Shear resistance (diagonal tension) of beams, columns or walls with rectangular web:

$$V_R = \frac{h-x}{2L_s} \min(N, 0.55 A_c f_c) + \left(1 - 0.05 \min(5, \mu^{pl}_\theta)\right) \left[0.16 \max(0.5, 100\rho_{tot}) \left(1 - 0.16 \min\left(5, \frac{L_s}{h}\right)\right) \sqrt{f_c} \, A_c + V_w \right]$$

(12)

Shear resistance of walls with rectangular web due to 45° compression in the web:

$$V_R = 0.85 \left(1 - 0.06 \min(5, \mu^{pl}_\theta)\right) \left(1 + 1.8 \min\left(0.15, \frac{N}{A_c f_c}\right)\right) \left(1 + 0.25 \max(1.75, 100\rho_{tot})\right) \left(1 - 0.2 \min\left(2, \frac{L_s}{h}\right)\right) \sqrt{\min(f_c, 100)} \, b_w z$$

(13)

Shear resistance of squat columns ($L_s/h \leq 2$) due to crushing along the diagonal:

$$V_R = \frac{4}{7} \left(1 - 0.02 \min(5, \mu^{pl}_\theta)\right) \left(1 + 1.35 \frac{N}{A_c f_c}\right) \left(1 + 0.45 \cdot 100\rho_{tot}\right) \sqrt{\min(f_c, 40)} \, b_w z \sin 2\theta \qquad (14)$$

New variables in Eqs.(12)–(14) are: x: compression zone depth; $A_c = b_w d$; ρ_{tot}: total longitudinal reinforcement ratio; V_w: contribution of transverse reinforcement to shear resistance: $V_w = \rho_w b_w z f_{yw}$ (ρ_w: transverse reinforcement ratio); θ: angle between the diagonal and the axis of the column ($\tan\theta = h/2L_s$).

Eqs.(8)–(14) and the calculation of the yield moment, M_y, are modified for:

- members with lap-splicing of longitudinal bars (ribbed bars, or smooth ones with hooked ends) starting at the yielding end (Biskinis and Fardis 2004);
- members, with or without lapping of longitudinal bars, retrofitted with a jacket of FRP, concrete, or steel (*fib* 2002, Biskinis and Fardis 2004).

For example, for spliced ribbed bars: (a) calculations should be based on twice the value of the compression reinforcement ratio; (b) if the lap length l_o is $l_o < l_{o,min} = 0.3 d_b f_y / \sqrt{f_c}$, in the calculations of yield properties the yield stress, f_y, should be multiplied by $l_o/l_{o,min}$, and (c) if $l_o < 40 d_b$, θ^{pl}_{um} from Eq.(11) should be multiplied times $(l_o - 10 d_b)/30 d_b$. For wrapping with FRP, the exponent of the confinement term (the power of 25) in Eqs.(10), (11) may be taken equal to: $\alpha \rho_f \min(f_{u,f}, \varepsilon_{u,f} E_f)(1 - 0.7 \min(f_{u,f}, \varepsilon_{u,f} E_f) \rho_f / f_c)$, where f indexes the FRP, the confinement effectiveness ratio depends on the radius R of the rounded corners of the section as: $\alpha = 1 - [(b-2R)^2 + (h-2R)^2]/3bh$, the FRP ratio ρ_f is: $\rho_f = 2 t_f / b_w$ and the limit strain $\varepsilon_{u,f}$ is equal to 0.011 for CFRP and to 0.027 for GFRP.

4. ANALYSIS METHODS FOR PERFORMANCE-BASED DESIGN, ASSESSMENT OR RETROFITTING OF BUILDINGS

Part 1 of Eurocode 8 (CEN 2004a) includes the following analysis options for the design of buildings or the assessment of their performance:

- Linear static (termed "lateral force" method).
- Linear modal response spectrum analysis.
- Nonlinear static analysis ("pushover").
- Nonlinear dynamic (response time-history).

Linear modal response spectrum analysis is the standard procedure for design, applicable to all types of new buildings. Countries are allowed to limit the use of nonlinear analysis methods for the design of new buildings via their National Annex.

Pushover analyses should be performed under two lateral load patterns: one for uniform lateral accelerations and another similar to the lateral forces used in linear static (lateral force) analysis, if applicable, or are derived from a modal response spectrum one, if it isn't. The target displacement is derived via the well-known N2 procedure (Fajfar, 2000), which is given in an informative annex and employs Eq. (1).

Part 3 of Eurocode 8 (CEN 2004c) adopts a fully displacement-based approach. So the main objective of the seismic analysis is the estimation of deformation demands in structural members. The four analysis options of Part 1 are available. In all of them the seismic action is given by the 5%-damped elastic spectrum or the quantities of interest derived from it: the target displacement for non-linear static analysis, the acceleration time-histories for nonlinear dynamic analysis. The spectrum is anchored to the PGA corresponding to the hazard level chosen for the Limit State for which analysis results will be used, with multiplication by the "importance factor" of the building (the same as in Part 1). All analyses, except nonlinear dynamic ones, essentially use the equal-displacement rule: at the level of member deformations, e.g., chord-rotation demands, for the first two types of analysis, or of the displacement of an equivalent SDOF system for pushover analysis (as modified by Eq.(1)).

For linear analysis to be applicable, ductility demands should be fairly uniformly distributed in the entire structure. Taking the ratio D/C of bending moment at a member end from elastic analysis, D, to the corresponding capacity, C, as a measure of the local ductility demand (D/C is roughly equal to the demand value of the chord-rotation ductility ratio), the maximum of the D/C-ratio in all primary elements should not exceed its minimum value over all primary elements with D/C>1 by more than a NDP-factor between 2 to 3 with a recommended value of 2.5. The D/C ratio is taken equal to 1 (elastic) at sections around beam-column joints where plastic hinges will not form on the basis of the sum of beam flexural capacities compared to that of columns. No limit is set to the ductility demands on "ductile" elements.

If linear analysis is applied, internal forces in "brittle" mechanisms of behavior are estimated as in capacity-design: from equilibrium, assuming that "ductile" locations delivering force to the "brittle" mechanisms develop their force capacity, or

the force demand from the analysis, whichever is less. Force capacities are estimated from expected values of material strengths, times a "confidence factor" greater than 1 that depends on the amount and reliability of information on the as-built structure.

Applicability criteria of linear static analysis, instead of a modal one, are as in Part 1 (CEN 2004a): no significant heightwise irregularity in geometry, mass, lateral stiffness or story strength, and $T_1 \leq 2s$, $T_1 \leq 4T_C$ (T_1, T_C as for Eq.(1)). If $T_1 > 2s$ or $T_1 > 4T_C$, the nonlinear analysis should be dynamic or of the "modal-pushover" type.

The models used in analysis of existing or retrofitted buildings should follow the rules in Part 1 (CEN 2004a) for new buildings. According to them, the elastic stiffness should be the secant stiffness at incipient yielding, which Part 1 allows taking equal to 50% of the uncracked stiffness of the concrete section. The Part 1 rule provides safe-sided force demands in force-based design but underestimates member effective secant-to-yield rigidity and gives unconservative estimates of chord rotation demands for verification in the displacement-based assessment and retrofitting of Part 3. To avoid this, the secant-to-yield rigidity of concrete members may be computed from the yield moment and the chord rotation at yielding (Eqs.(8), (9)) as:

$$EI_{eff} = M_y L_s / 3\theta_y \qquad (15)$$

REFERENCES

Biskinis, D., G. Roupakias, and M. N. Fardis. (2004). Degradation of shear strength of RC members with inelastic cyclic displacements, *ACI Struct. Journal* 101 (in print).

Biskinis, D. E., and M. N. Fardis. (2004). Cyclic strength and deformation capacity of RC members, including members retrofitted for earthquake resistance, *Proceedings 5th International Ph.D Symposium in Civil Engineering*, Delft, Balkema.

CEB. (1970). CEB-FIP *International Recommendations for design and construction of concrete structures*. Bulletin No. 72. Comité Euro-international du Bêton, Paris.

CEB. (1985). *CEB Model Code for seismic design of concrete structures*. Bulletin No. 165. Comité Euro-international du Bêton, Lausanne.

CEN. (1994). European prestandard ENV 1998-1:1994: Eurocode 8: Design provisions for earthquake resistance of structures. Brussels.

CEN. (1996). European prestandard ENV 1998-1-4: 1996: Eurocode 8: *Design provisions for earthquake resistance of structures. Part 1–4: Strengthening and repair of buildings*. Comité Européen de Normalisation. Brussels.

CEN. (2002). European Standard EN 1990: Eurocode: *Basis of structural design*. Comité Européen de Normalisation. Brussels.

CEN. (2004a). European Standard EN 1998-1: Eurocode 8: *Design of structures for earthquake resistance. Part 1: General rules, seismic actions and rules for buildings*. Comité Européen de Normalisation. Brussels.

CEN. (2004c). Draft European Standard prEN 1998-3: Eurocode 8: *Design of*

structures for earthquake resistance. Part 3: Assessment and retrofitting of buildings. Final draft (No. 7) for translations. Comité Européen de Normalisation. Brussels.

Fajfar, P. (2000). A non-linear analysis method for performance-based seismic design. *Earthquake Spectra*. 16(3): 573–593.

Fardis, M. N., and D. Biskinis. (2003). Deformation capacity of RC members as controlled by flexure or shear, *Intern. Symp. on Performance-based Engineering for Earthquake Resistant Structures Honouring Prof. S. Otani*, Univ. of Tokyo, 511–530.

Fib. (2002). *Seismic Assessment and Retrofit of RC Buildings*. Bulletin No.24. Fédération Internationale du Bêton, Lausanne.

Panagiotakos, T. B., and M. N. Fardis. (2004a). Performance of RC frame buildings designed for alternative Ductility Classes according to Eurocode 8 (Final version, 2003), *Proc. 5th US-Japan Workshop on Performance-based Earthquake Engineering Methodology for Reinforced Concrete Building Structures*, 63–76.

Panagiotakos, T. B., and M. N. Fardis. (2004b). Seismic performance of RC frames designed to Eurocode 8 or to the Greek Codes 2000. *Bulletin of Earthquake Engineering*. 2(2), Kluwer Academic Publishers (in print).

Vidic, T., P. Fajfar, and M. Fischinger. (1994). Consistent inelastic design spectra: strength and displacement. *Earthquake Engineering and Structural Dynamics*. 23: 502–521.

OVERVIEW OF A COMPREHENSIVE FRAMEWORK FOR EARTHQUAKE PERFORMANCE ASSESSMENT

Gregory G. DEIERLEIN[1]

ABSTRACT

The Pacific Earthquake Engineering Research (PEER) Center is developing a comprehensive performance-based methodology to provide a framework for the next generation of seismic design codes and criteria. The performance assessment process follows a logical progression of steps, beginning with seismic hazard characterization, and continuing through simulation of structural response, damage modeling and assessment, and loss modeling. The outcomes of each process are articulated through four generalized variables, termed the earthquake Intensity Measure (IM), Engineering Demand Parameters (EDP), Damage Measures (DM), and Decision Variables (DV). A rigorous probabilistic framework permits consistent characterization of the inherent uncertainties throughout the process. Through its modular architecture, the framework facilitates a systems approach to organize the multidisciplinary research necessary to develop the models, criteria, and tools necessary for its implementation. The proposed methodology can be implemented directly for performance assessment, or can be used as the basis for establishing simpler performance criteria and provisions for performance-based design.

Keywords: Performance based design; Earthquake engineering; Probabilistic.

1. INTRODUCTION

Performance-based earthquake engineering (PBEE) seeks to improve seismic risk decision-making through assessment and design methods that have a strong scientific basis and that express options in terms that enable stakeholders to make informed decisions. Publication of the first generation of PBEE procedures in the United States (FEMA-273 1997 and ATC-40 1996) marked a major advancement to formalize concepts that had been envisioned by the earthquake engineering profession for many years (Krawinkler and Miranda, 2004). The basic concept of these procedures is shown in Figure 1, where a building is being loaded by earthquake-induced lateral forces that result in nonlinear response and damage. Relations are then established between structural response indices (interstory drifts, inelastic component deformations, and member forces) and performance-oriented descriptions such as Immediate Occupancy, Life Safety and Collapse Prevention.

---

[1] *Professor, John A. Blume Earthquake Engrg. Center, Stanford University, e-mail: ggd@stanford.edu*
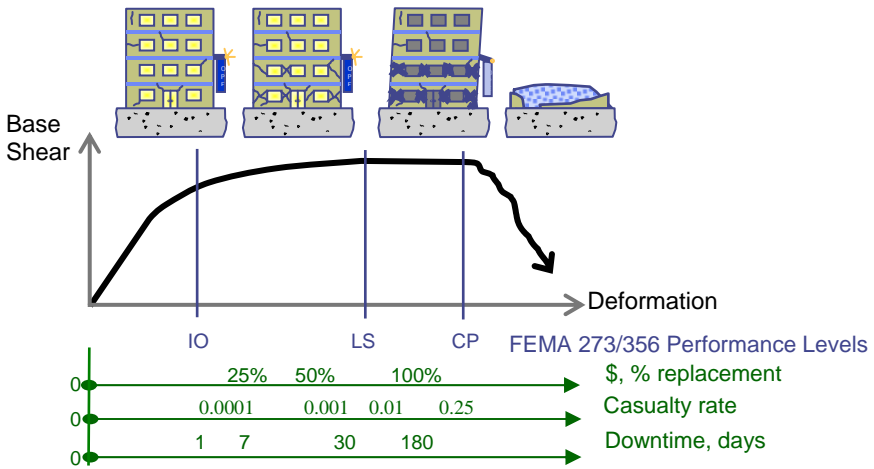
Figure 1. Schematic of PBEE assessment process and performance metrics.

As with the introduction of any new technologies, there are limitations in the first-generation PBEE procedures that warrant further development. Among these are the following: (1) Engineering demands and the calibrations between demands and component performance are based on simplified analysis techniques, which are not amenable to the use of more realistic inelastic time-history simulation technologies; (2) Associations between engineering demands and component performance are based somewhat inconsistently on relations between laboratory tests, analytical models, and engineering judgment; (3) Relationships between building system performance and component limit states (e.g., definition of "Life Safety" performance based on a single component deformation) are tenuous; and (4) Except for the probabilistic definition of the seismic hazard, the methods are largely deterministic and do not rigorously account for the uncertainties in performance prediction.

One of the key improvements of the PBEE approach under development by PEER is to provide a more explicit and transparent evaluation of system performance metrics, that are more informative to stakeholders. Referring to the lower axes in Figure 1, these metrics provide quantitative measures of economic loss, life safety risks (casualties), and downtime. Metrics of this sort are common in regional seismic loss assessment. In this sense, the proposed framework will help unify detailed building-specific engineering provisions with more empirically based regional loss assessment methods, such HAZUS (Kircher et al. 1997a,b).

2. PERFORMANCE ASSESSMENT FRAMEWORK

As outlined in Table 1, the proposed assessment methodology is articulated by four processes, which are roughly distinguished along disciplinary lines. Associated with each process is an output variable, which provides for a systematic transfer of information from one process to another. The assessment begins with definition of a

ground motion *Intensity Measure (IM)*, which describes in a probabilistic sense the salient features of the ground motion hazard that affect structural response. The next step involves structural analysis to calculate *Engineering Demand Parameters (EDP)*, which quantify in an engineering sense the response of the structure the input ground motions. The *EDPs* are then related to *Damage Measures* (*DM*), which describe the physical condition of the structure and its components resulting from the imposed demands. Finally, the process culminates with the calculation of *Decision Variables (DV)*, which are represented by the performance metrics of the type shown at the bottom of Figure 1. Underlying the methodology is a probabilistic framework for propagating the aleatory and epistemic uncertainties throughout the process.

2.1 Earthquake *Intensity Measure (IM)*

The earthquake *IM* is the primary parameter by which the earthquake hazard is defined. Traditional *IMs,* such as peak ground motions or spectral parameters are widely available through conventional probabilistic seismic hazard analyses. For example, the common $IM = Sa_{T1}$ can be described through a seismic hazard curve as the mean annual frequency of exceedance, $\lambda[IM]$, for a specific site and vibration period of the building. In addition to quantifying *IM*, the hazard characterization includes the selection of appropriate ground motion input records for response history analyses. PEER's research on hazard analysis involves close coordination with the

Table 1. Components of PBEE assessment framework

Process	Output Variable	Disciplines	Key Parameters
Seismic Hazard Analysis **Site →IM**	**IM: Intensity Measure** • $S_a(T_1)$ • PGA, PGV • Aires intensity • Inelastic spectra	Seismology; geotechnical engineering	• fault location & type • location & length of rupture (M-R) • site & soil conditions
Structural Analysis **IM →EDP**	**EDP: Engrg. Demand Parameter** • peak & residual interstory drift • floor accelerations • component forces & deformations	structural & geotechnical engineering	• foundation & structural system properties • model parameters • gravity loads
Damage Assessment **EDP→DM**	**DM: Damage Measure** • component damage and repair states • hazards (falling, egress, chemical release, etc.) • collapse	structural & construction engineering; architecture; loss modeling	• structural & components • HVAC & plumbing systems • cladding & partition details • contents
Loss & Risk Analysis **DM→DV**	**DV: Decision Variable** • casualties • closure issues (post EQ safety) • direct $ losses • repair duration	construction cost estimating; loss modeling; risk mgmt.	• occupancy • time of earthquake • post-eq recovery resources

earth science and engineering seismology communities to improve the accuracy of conventional *IM*s and to investigate alternative seismic intensity measures (potentially vector ***IMs***) that correlate best with earthquake-induced damage (e.g., Stewart et al. 2001, Baker and Cornell 2004, Cornell 2004).

One of the important questions in choosing an *IM* relates to how well it represents the damaging effects of earthquake ground motions on structures. To illustrate this issue, consider the results from multiple inelastic time history analyses, shown in Figure 2, which were conducted as part of a trial application of the PBEE methodology for a non-ductile reinforced concrete building (Krawinkler 2004). Each curve in this figure represents a so-called Incremented Dynamic Analysis (IDA, see Vamvatsikos and Cornell 2002), where each point on the curve corresponds to the peak response (in this case the maximum interstory drift ratio) obtained through an inelastic time history analyses for an input ground motion that has been scaled to a specified spectral acceleration (*Sa*), defined at a period equal to the elastic first-mode period of the structure, Sa_{T1}. Results are shown for fifteen different ground motions scaled up to hazard intensities with a 2% mean annual frequency of exceedence in 50 years (2/50). The solid dots at the end of each curve correspond to the spectral intensity and drift ratio where collapse was detected — often below the 2/50 level for this seismically deficient existing building.

The large scatter in response is due so-called record-to-record variability, resulting from the fact that $IM = Sa_{T1}$ does not fully capture all the "damaging features" of the earthquake records. As described later, the proposed PBEE framework can account for this variability; though, it would be advantageous to identify alternative *IMs* that would reduce the variability and capture significant features of the seismic hazard at the site. Some promising examples of improved *IMs* include pairs of spectral ordinates and inelastic spectral displacement, among others (e.g., Cornell 2004, Baker et al. 2004, Cordova et al. 2001). Apart from reducing variability, to the extent that improved *IM* capture better the damaging features of a record and the site hazard, criteria for selecting input ground motions for inelastic time-history analyses become less important.
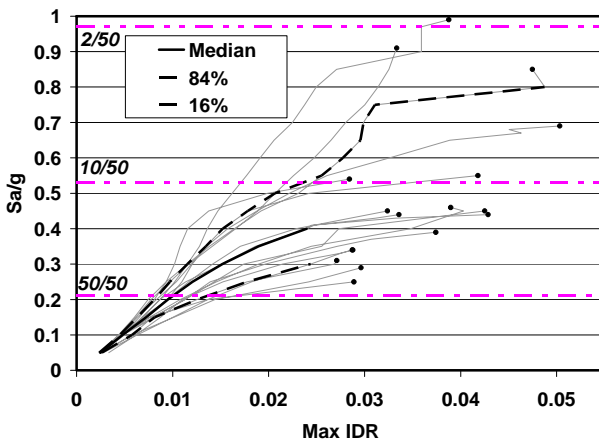

Figure 2. Incremental dynamic analysis (IDA) of non-ductile 7-story RC building subjected to 15 scaled ground motions (Krawinkler 2004).

2.2   Simulation of *Engineering Demand Parameters (EDP)*

For buildings, the most common *EDP*s are interstory drift ratios, inelastic component deformations (e.g., plastic hinge rotations), and floor accelerations. Both peak and residual deformations are of interest, as the latter impact the post-earthquake repair and safety. Selection of *EDPs* is largely driven by one's ability to reliably calculate the *EDPs*, coupled with how well they correlate with relevant damage predictions. Inelastic time history analyses are emphasized for accurate *EDP* response predictions over the full range of behavior, up through collapse. However, it is envisioned that static inelastic pushover analysis methods will continue to be a viable option for design. Any type of inelastic simulation should be as realistic as possible, where appropriate, taking into account soil-foundation-structure interaction and participation of "non-structural" components (cladding, masonry partitions, etc.).

Prospects for accurate computation of the *EDP* relations vary with the target *EDP*. For example, procedures for calculation of nonlinear dynamic response of ductile frames are increasingly becoming routine with validated analytical models and computational procedures. Simulation of structural collapse, especially for less ductile systems, remains problematic because of the lack of validated models to track the response of softening systems with large deformations. Nevertheless, progress is being made — evident, for example, in the collapse predictions in Figure 2.

To accelerate the development and implementation of robust numerical models to simulate inelastic structural response, PEER has embarked on the development of an open-source, object-oriented software framework. *OpenSees* (Open System for Earthquake Engineering Simulation; http://opensees.berkeley.edu) is a collection of modules to facilitate the implementation of models and simulation procedures for structural and geotechnical earthquake engineering. An emphasis within this effort is the development, implementation, and validation of models to simulate collapse of existing non-ductile reinforced-concrete buildings, which due to inadequate seismic design, may experience severe strength and stiffness degradation under large earthquakes (e.g., Elwood and Moehle 2003, Kaul 2004, Ibarra and Krawinkler 2004).

Approaches, such as the IDA technique described previously, permit one to systematically characterize relationships between the *EDP* response quantities and the ground motion *IM*. Mathematically, these relationships can be described by a conditional probability, *P(EDP/IM)*, which captures the variability in the prediction of response. In the example of Figure 2, the probability distribution, *P(EDP/IM)*, would describe the peak interstory drift ratios, conditioned on hazard intensity, *Sa*, where the variability is solely the result of the ground motion characteristics (so-called "record-to-record variability"). While the ground motion and hazard characterization are known to be a primary source of uncertainties, the simulations and resulting probability distributions should account for other significant uncertainties in the structural model itself, e.g., variation of material properties, modeling uncertainties associated with the strength and deformation characteristics of structural components, variations in dead loads and seismic mass, etc.

2.3 Evaluation of Component *Damage Measures (DM)*

The *DM*s provide explicit descriptions of damage to structural elements, non-structural elements, and contents. These descriptions must be relevant and in sufficient detail to enable subsequent quantification of the necessary repairs, disruption of function, and safety hazards (e.g., falling hazards, release of hazardous substances, etc.). As with the *IM-EDP* relationships, the associations between *EDP* and *DM* should account for uncertainty in the damage predictions.

Shown in Figure 3 are examples of conditional fragility relations for nonstructural partition walls, describing the probability of being in a given damage state as a function of the interstory drift ratio demand. In this case, the three damage states are predicated on the nature of the repairs to restore the wall to its undamaged state, i.e., DM1 requires patching cracks and repainting, DM 2 requires replacement of the wall boards, and DM3 requires replacement of the entire partition, wallboards plus stud framing. The curves shown in Figure 3a are conditional probabilities of the damage exceeding each damage state, P*(DM>dm$_i$|IDR)*, whereas the curves in Figure 3b are the conditional probabilities of being in any one damage state, *P(DM=dm$_i$|IDR)*. The latter form is required for subsequent loss calculations.

Using data from previously published tests, new tests, and post-earthquake reconnaissance, PEER researchers have compiled a number of damage fragility curves for structural and nonstructural building components and building contents (e.g., Taghavi and Miranda 2003, Aslani and Miranda 2003, Krawinkler 2004, Pagni and Lowes 2004, Hutchinson and Chaudhuri 2004, Eberhard et al. 2001). Assembling these fragility curves is often a major challenge, particularly since much of the prior testing has emphasized strength and ductility capacity of components, with insufficient attention to damage measures such as residual crack width, spalling, permanent displacement, etc. The hope is that this situation will improve through the establishment standards and documented examples for data reporting and formatting in a manner that supports modeling needs of the PBEE framework.

In many cases the component damage measures are primarily focused on
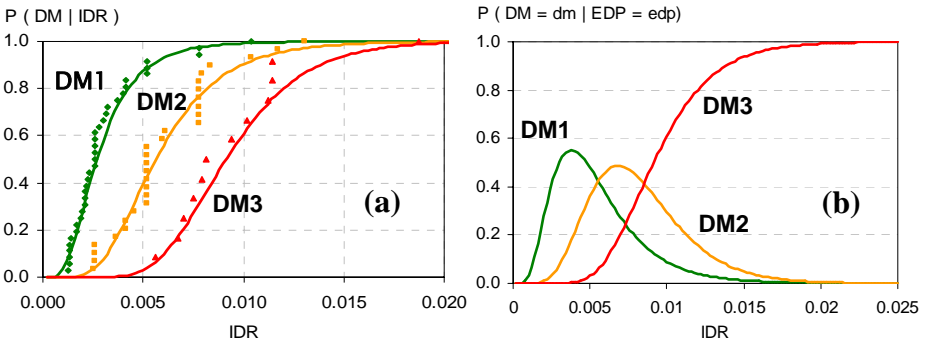
Figure 3. Fragility relationships for drywall partitions for three damage states conditioned on interstory drift (Krawinkler & Miranda, 2004).

describing the economic losses associated with replacement or repair costs and implications on continued functionality. However, in some cases, the damage measures correspond to structural collapse hazards, which are not modeled explicitly in the analysis. One example of this are fragility models that relate interstory drift to the loss of vertical load carrying capacity of reinforced concrete slab to column connections (Aslani and Miranda 2003). Such connections are usually considered part of the gravity load system, and, as such their resistance to lateral earthquake forces is ignored and they are often not included in the structural analysis model. Event in cases where their lateral resistance is modeled, the slab-column analysis model is rarely configured to simulate vertical collapse. As described later, loss processing of the *DM* information will depend on consequences of the component damage and whether or not significant stability related effects are captured in the structural analysis simulation.

2.4 Loss Modeling and *Decision Variables (DV)*

The final step in the assessment is to calculate *DVs* in terms that are meaningful for decision makers, e.g., direct dollar losses, continued functionality and downtime (or restoration time), and life safety risks. In a similar manner as was done for the other variables, the *DV*s are expressed through probabilities of *DV* conditioned on *DM*, *P(DV|DM)*. Shown in Figure 4 is an example of a loss function for drywall partitions, where the normalized losses (ratio of repair cost to initial construction cost) are associated with the three damage states described previously (Figure 3). Often the repair costs will exceed the initial construction costs, due to the construction staging operations and the inter-relationship of various building components. For example, DM3 (full replacement of the wall partition) may require work on electrical and mechanical components that are undamaged but inside the damaged wall.

When computing losses, it is important keep track of the inter-relationships between damage and losses for various components. The electrical and mechanical repair costs associated with DM3 in the drywall partitions is one example of how damage to one component may lead to repairs in another. A related example is repairs to architectural finishes, which could either be considered as a cost associated with the repair of structural elements lying behind the finishes or of damage to the finishes themselves. In cases such as this, there is a danger to double count the repairs, and hence, over-estimate the repair costs. Depending on the occupancy, damage to building contents represents another important source of

$P (L_i | DM_i)$

Figure 4. Normalized Loss Function for Drywall Partitions (Krawinkler and Miranda 2004).

economic and functional loss that should not be overlooked (Comerio 2003, 2004).

Evaluation of the other two main decision variables, downtime and casualty risks, are more complicated and not as far advanced as modeling of repair costs. Repair durations are an obvious contributor to downtime predictions, though experience suggests that other factors may be more significant, including post-earthquake safety of the structure and its impact on accessibility to the building, availability of financial and other necessary resources for repairs, plus a host of even less predictable issues, such as the influence of external management or socio-political factors. Research is currently under way in PEER to provide a framework to clearly articulate the downtime issues and suggest approaches for decision making on a case-by-case basis.

The prediction of casualty rates is another problematic area, due in large part to the lack of verifiable data. Available models and data, developed by PEER and other agencies, suggest occupancy fatality rates on the order of 1% to 1.5% for partially collapsed buildings and 10% to 20% for fully collapsed buildings (Krawinkler 2004). These rates are based on the actual building occupancy. For mean annual frequency predictions, these should be adjusted for the likely occupancy.

3. PROBABILISTIC BASIS AND EQUATIONS FOR THE FRAMEWORK

The probabilistic expressions of the PBEE methodology components (*IM, EDP, DM*, and *DV*) can be integrated by the total probability theorem, expressed conceptually as:

$$\lambda(\mathbf{DV}) = \iiint G\langle \mathbf{DV}|\mathbf{DM}\rangle \,|\, dG\langle \mathbf{DM}|\mathbf{EDP}\rangle \,|\, dG\langle \mathbf{EDP}|\mathbf{IM}\rangle \,|\, d\lambda(\mathbf{IM}) \qquad (1)$$

where λ*(IM)* represents the mean annual frequencies of exceedence (MAF) for *IM*, the intermediate terms $G\langle A/B\rangle$ are conditional probabilities for the methodology components *EDP*, *DM*, and *DV*, and λ*(DV)* is the probabilistic (MAF) description of the performance metrics, e.g., the mean annual frequency, Y, that the direct economic loss will exceed X percent of the building replacement cost, i.e., Y = λ *(Loss > X% replacement cost)*. The bold font reminds us that most of the terms in (1) are vectors. Implied by (1) is that the assessment can be modeled as a Markov process, where the conditional probabilities are independent and can each be evaluated as such.

While conceptually straightforward, there are many details associated with the implementation of the framework that are fairly complex. A few implementation details are elaborated on in the next two sections; for further explanations the reader is referred to Krawinkler and Miranda (2004), Krawinkler (2004), Miranda and Aslani (2003, 2004), Baker and Cornell (2003) Comerio (2004), Ibarra and Krawinkler (2004), Miranda et al. (2004), Porter et al. (2001).

3.1 Collapse Prediction

It is useful to distinguish collapse mechanisms between ones that occur primarily through global sidesway instability versus a local gravity load collapse. In concept, either of these modes can be simulated by inelastic time history analyses, though in

practice the localized gravity load collapse mechanisms are often handled through component fragility functions $P(DM/EDP)$, such as the functions for slab-column connection punching failure mentioned previously (Aslani and Miranda, 2003).

Where collapse is simulated directly, such as indicated by the end points of the IDA curves for the reinforced-concrete building in Figure 2, the MAF of collapse can be calculated by integrating the first two terms of (1) as follows:

$$\lambda(Collapse) = \int_{IM} P\langle Collapse | \mathbf{IM} = im_i \rangle \, | \, d\lambda(\mathbf{IM}) \qquad (2)$$

The graphical interpretation of this is shown schematically in Figure 5, where the *IM* hazard and median IDA curves are plotted together with a common *IM (= Sa_{T1})* vertical axis. The median EDP-IDA curve and associated probability distributions are statistical representations of the IDA data (e.g., Figure 2). The calculation of $\lambda(Collapse)$ by (2), is simply the integration of the vertically plotted distribution of *P[Collapse|Sa],* shown in Figure 5, with the $\lambda(IM)$ hazard curve.

When localized collapse (or a global collapse triggered by a local failure) is detected indirectly through a damage function, the integration takes the form:

$$\lambda(Collapse) = \iint_{IM,EDP} \max\left[P\langle LC | \mathbf{EDP} = edp_j \rangle \right] \left| P\langle \mathbf{EDP} > edp_j | \mathbf{IM} = im_i \rangle d\lambda(\mathbf{IM}) \qquad (3)$$

The first integral can be visualized by the integration of the $\lambda(Sa)$ hazard curve with the horizontal distribution of *P[IDR/Sa],* shown in Figure 5. The result of this integration is a mean annual frequency exceedence curve for *EDP*, $\lambda(EDP>Y)$. This curve is plotted on the left side of Figure 6, alongside a set of component damage probability curves, $P[DM = dm_i / IDR = idr_i]$, with the two graphs associated by their common vertical EDP axis. The component damage curves of Figure 6 are similar to the ones shown previously in Figure 4b, only in this case they pertain to structural components where the final damage state, e.g., DM_3, corresponds to a local collapse (*LC*) condition. The second integration in (3) is performed over the full range of EDP for every structural component that has a DM associated with collapse. Assuming that the failure of any one such component is severe enough to be deemed "collapse," the resulting MAF of collapse is determined by the maximum likelihood of collapse in any one element — hence, the "*max*" notation in (3).
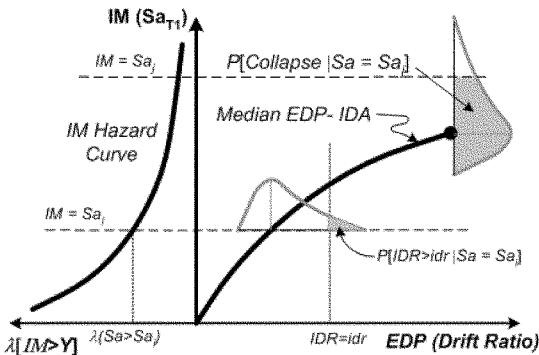
Figure 5. Integration of IM hazard with EDP response.

23

3.2   Loss Assessment

The assessment of direct losses (e.g., dollar losses associated with repair and replacement costs) is essentially an extension of (3) to first determine the mean annual frequency of *DMs* for all the damage states (Figure 6) and then integrate these with their associated loss functions (e.g., Figure 4). However, since this requires integration of damage and losses over many components, there is an added complication of accounting for correlations in the maximum EDPs, which multiple components in the building are subjected to, and correlations among the EDP-DM and DM-DV (damage and loss) distributions for common families of components. These correlations were not an issue for collapse prediction, since collapse is assumed to be either simulated directly through the IDA (Figure 2) or triggered by a single component.

Figure 6.   Integration of EDP exceedence with component damage.

Aslani and Miranda (2004) and Miranda et al. (2004) outline an efficient approach to resolve these issues and determine the MAF of loss, $\lambda(IM)$. Briefly, their approach begins with calculated of an expected annual loss, which is the sum of expected annual component losses for the non-collapse case and the expected annual loss from collapse. Both of these are straightforward to calculate given the MAFs of damage, $\lambda(DM)$, and collapse, $\lambda(Collapse)$. Next, they calculate the dispersion on the expected loss by combining the dispersion for those components that contribute significantly to the loss, taking into account correlations among the components. Their preliminary findings show this to be a viable and effective method; and their data confirm that the MAF of the loss can be quite sensitive to the assumed correlations between component losses.

4. RELATIONSHIP OF PBEE TO DECISION MAKING AND DESIGN

While there are a multitude of opinions on seismic risk decision making, a commonly agreed upon view is that PBEE should provide stakeholders with information to make better informed decisions. Further, in addition to providing data, PBEE approaches will need to foster a change in mindset from the status quo where seismic risk decisions are generally avoided due to reliance on minimum building code requirements. In a report on organizational and societal considerations regarding risk decision making, May (2003) dispels the notion of defining performance in terms of an "acceptable risk" and, instead, promotes an approach that supports decision making based on tradeoffs. How these tradeoffs are decided, and what the priorities are, can differ dramatically depending on the circumstances, as seen, for example, in two recently completed testbed exercises (Krawinkler 2004, Comerio 2004).
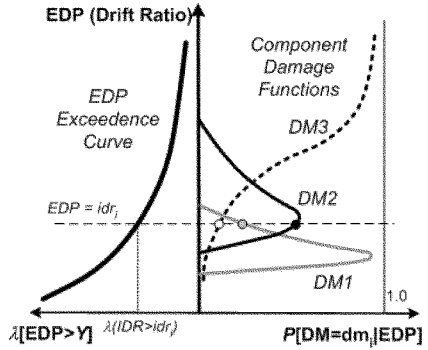
Whereas financial and insurance organizations are comfortable dealing with mean annual expected losses or mean annual frequencies of exceedence on loss (which fit into their business planning models), other stakeholders prefer more "intuitive" measures, such as likely losses or downtimes from one or more earthquake scenarios. In some cases, stakeholders may evaluate earthquake hazard mitigation through structural retrofit as one alternative among other strategies (such as insurance) to manage their risk. In other cases, PBEE may assist in quantifying trade-offs between the cost-benefits of earthquake mitigation compared to other business or societal needs and priorities. A practical implication of this is that the PBEE methodology should permit alternative descriptions of the performance metrics. Thus, while cast in terms of a rigorous probabilistic framework, the intent is that the final expression of the PBEE decision variables can be translated into different formats.

Thinking in broader terms about PBEE and the proposed methodology, two goals are envisioned. The first is to create a performance engine to be applied in full detail to the seismic performance assessment of important or critical facilities, where such efforts are warranted. The second is to provide the means of calibrating simplified procedures that might be used for advancement of future building codes. It is in this application that the methodology is likely to have its largest potential impact.

ACKNOWLEDGEMENTS

REFERENCES

ATC-40. (1996). *Seismic Evaluation and Retrofit of existing concrete buildings, Report No. ATC-40*, Applied Technology Council, Redwood City, CA.

Aslani, H., E. Miranda. (2003). "Fragility Assessment of Reinforced Concrete Interior Slab Column Connections," *J. Struct. Engrg.,* ASCE, submitted for publication.

Aslani, H., E. Miranda. (2004). "Component-Level and System-Level Sensitivity Study for Earthquake Loss Estimation," Paper No. 1070, Proc. 13WCEE, Vancouver, B.C.

Baker, J. W., C. A. Cornell. (2004). "Choice of a Vector of Ground Motion Intensity Measures for Seismic Demand Hazard Analysis," Paper No. 3384, Proc. 13WCEE, Vancouver, B.C.

Baker, J., C. A. Cornell. (2003). *Uncertainty Specification and Propagation for Loss Estimation Using FOSM Method, PEER Report 2003-07,* http:/peer.berkeley.edu.

Comerio, M., J. C. Stallmeyer, W. Holmes, P. Morris, S. Lau. (2002). *Nonstructural Loss Estimation: The UC Berkeley Case Study, PEER 2002-01,* http:/peer.berkeley.edu.

Comerio, M. (ed.). (2004). *PEER Testbed Study on a Laboratory Building: Exercising Seismic Performance Assessment, PEER Report 2004/#,* (in press). http:/peer.berkeley.edu.

Cordova, P. P., G. G. Deierlein, S. S. F. Mehanny, C. A. Cornell. "Development of a Two-Parameter Seismic Intensity Measure and Probabilistic Assessment Procedure," *PEER Report 2000/10, 2nd US-Japan Workshop on PBEE for RC Building Structs.*, pg. 195-214.

Cornell, C. A. (2004). "Hazard, Ground Motions, and Probabilistic Assessments for PBSD," *PBSD Concepts and Impl., PEER Report 2004/# (in press).* http:/peer.berkeley.edu.

Eberhard, M. O., A. Mookerjee, and M. Parrish. (2001). *Uncertainties in Performance Estimates for RC Columns*, PEER Center, Richmond, CA, http://ce.washington.edu/~peera1.

Elwood, K. J., J. P. Moehle. (2003). *Shake Table Tests and Analytical Studies on the Gravity Load Collapse of RC Frames, PEER Report 2003/01,* http:/peer.berkeley.edu.

FEMA-273. (1997). *NEHRP guidelines for the seismic rehabilitation of buildings, Report No. FEMA-273,* Federal Emergency Management Agency, Washington, D.C.

FEMA-356. (2000). *Prestandard and commentary for the seismic rehabilitation of buildings, Report No. FEMA-356,* Federal Emergency Management Agency, Washington, D.C.

Hutchinson, T., R. Chaudhuri. (2004). "Seismic Fragility of Small Equipment and Contents," *PBSD Concepts and Impl., PEER Report 2004/# (in press),* http:/peer.berkeley.edu.

Ibarra, L. F., H. Krawinkler. (2004). "Global Collapse of Deteriorating MDOF Systems," Paper No. 116, Proc. of 13WCEE, Vancouver, B.C.

Kaul, R. (2004). *Object Oriented Development of Strength and Stiffness Degrading Models for Reinforced Concrete Structures*, Ph.D. Thesis., CEE Dept. Stanford Univ., Stanford, CA.

Kircher, C. A., A. A. Nassar, K. Onder, W. T. Holmes. (1997). "Development of Building Damage Functions for Earthquake Loss Estimation," *Earthquake Spectra,* 13(4), pp. 663-682

Kircher, C. A., R. K. Reitherman, R. V. Whitman, C. Arnold. (1997)."Estimation of Earthquake Losses to Buildings, *Earthquake Spectra*, 13(4), pp. 703-720.

Krawinkler, H. [ed.] (2004), *Van Nuys Hotel Building Testbed Report: Exercising Seismic Performance Assessment, PEER Report 2004/#*, (in press), http:/peer.berkeley.edu.

Krawinkler, H., E. Miranda. (2004). "Chapter 9 - Performance-Based Earthquake Engineering," *Earthquake Engineering,* Y. Bozorgnia, V. V. Bertero, eds. CRC Press.

Lowes, L., N. Mitra, A. Altoontash. (2003). *A Beam-Column Joint Model for Simulating the Earthquake Response of RC Frames, PEER Report 2003/10,* http:/peer.berkeley.edu.

May, P. J. (2001). *Organizational and Societal Considerations for Performance-Based Earthquake Engineering, PEER Report. 2001-04,* http:/peer.berkeley.edu.

Miranda, E., H. Aslani, S. Taghavi. (2004). "Assessment of Seismic Performance in Terms of Economic Losses," *PBSD Concepts and Impl., PEER Report 2004/# (in press).*

Miranda, E., H. Aslani. (2003). *Probabilistic Response Assessment for Building-Specific Loss Estimation, PEER 2000/03*, http:/peer.berkeley.edu.

Pagni, C. A., L. N. Lowes. (2004). "Tools to Enable Prediction of the Economic Impact of Earthquake Damage in Older RC Beam-Column Joints," *PBSD Concepts and Impl., PEER Report 2004/# (in press),* http:/peer.berkeley.edu.

Porter, K., A. S. Kiremidjian, S. LeGrue. (2001). "Assembly-Based Vulnerability of Buildings and Its Use in Performance Evaluation," *Earthquake Spectra,* EERI, 17(2), pgs. 291-312.

Stewart, J. P., S. J. Chiou, J. Bray, R. W. Graves, P. G. Somerville, N. A. Abrahamson. (2001). *Ground Motion Evaluation Procedures for PBD, PEER 2001/09,* http:/peer.berkeley.edu.

Taghavi, S., E. Miranda. (2003). *Response Assessment of Nonstructural Building Elements, PEER Report 2003/05,* http:/peer.berkeley.edu.

Vamvatsikos, D., and C. A. Cornell. (2002). *Incremental Dynamic Analysis.* Earthquake Engineering and Structural Dynamics, 31(3): p. 491-514.

AN OUTLINE OF AIJ GUIDELINES FOR PERFORMANCE EVALUATION OF EARTHQUAKE RESISTANT REINFORCED CONCRETE BUILDINGS

Toshimi KABEYASAWA*

ABSTRACT

This paper outlines AIJ guidelines for seismic performance evaluation published in January 2004 as a draft. The guidelines provides deterministic and probabilistic methods of evaluating seismic performance level of a reinforced concrete building which has been designed in detail based on an appropriate design guidelines. The limit states of the structures are selected on the inelastic load-deformation curve by estimating the post-earthquake damage levels of members corresponding to the performance objectives as: (1) serviceability, (2) minor repair, (3) major repair, and (4) safety. The deterministic procedure evaluates the basic seismic capacity index for each limit state, which is defined as the amplitude ratio of the capacity earthquake to the standard earthquake, where the capacity earthquake is to induce the response equal to the limit state. The probabilistic evaluation method is provided as an additional procedure, where the performance level is expressed using the probability of exceeding the limit state by site-specific earthquakes during design service life.

Keywords: Limit states; Seismic performance evaluation; Serviceability; Reparability; Safety.

1. INTRODUCTION

The Architectural Institute of Japan has proposed a series of seismic design guidelines for reinforced concrete buildings[1][2], where calculation methods and detailing of reinforced concrete members are presented to assure ductile overall mechanism. The evaluation methods, especially for ultimate strength and deformability of members, proposed in these guidelines, have not only promoted research as a model code but also have been used in advanced practical design.

On the other hand, the Building Standard Law of Japan was revised in 2001, where design earthquake response spectrum was explicitly specified at the bedrock and the design method of comparing the inelastic response with the limit states was introduced as the design criteria, called as *"limit strength design method."* Although, the basic concepts for defining the limit states were specified, the detailed and general calculation methods were not specified.

Earthquake Research Institute, University of Tokyo
Address: 1-1-1 Yayoi, Bunkyo-ku, Tokyo 113-0032, Japan, E-mail: kabe@eri.u-tokyo.ac.jp

A subcommittee on performance evaluation and limit states in the reinforced concrete steering committee of the Architectural Institute of Japan (AIJ) published a new guidelines as a draft[3] in January 2004, which proposed new concepts on seismic performance evaluation of reinforced concrete buildings as well as detailed evaluation methods on member performances, especially, on the limit state deformations, based on recent research backgrounds. This paper outlines *the new AIJ Guidelines 2004*.

2. REVIEW OF AIJ GUIDELINES FOR SEISMIC DESIGN OF REINFORCED CONCRETE BUILDINGS

The Architectural Institute of Japan has published a series of design guidelines on structural design or earthquake resistant design of reinforced concrete buildings. The design guidelines based on ultimate strength concept[1] was first published in 1988 as a draft, the first edition in 1990, and English version in 1994. The guidelines specified a method of ensuring the overall beam-yielding collapse mechanism based on so-called "capacity design philosophy." The hinge regions and the non-hinge regions are clearly selected and the design actions for non-hinge regions are factored considering possible variations. Also the guidelines presents new design methods such as for (1) shear to ensure target ductility, (2) bond, (3) beam-column joints, (4) detailing against high axial load, (5) non-structural components.

AIJ published the second design guidelines based on inelastic displacement concept[2], in 1997 as a draft, and the first edition in 1999. The guidelines was originally planned as a revised version of above first guidelines, although it was published in a new style of performance-based verification, including inelastic limit deformation demands and new methods of calculating deformation capacity of reinforced concrete members. The guidelines has introduced or presented (1) criteria or limit states clearly defined using inelastic deformations, (2) performance verification format, (3) various analytical tools, (4) design against bi-directional motions, (5) potential hinge regions, (6) new design equation for shear and bond, (7) design formula for deformability, (8) quantitative design for confinement, and (9) design example. These two guidelines gave a method of evaluating structural and member capacities in practice, although they basically followed the structural demand levels for the ultimate lateral load carrying capacity prescribed in the former Building Standard Law(BSL) of Japan until 2001.

The new AIJ guidelines 2004[3] for seismic performance evaluation introduced the following basic concepts or new methods in practice:
(1) definition of seismic performance, both in deterministic and probabilistic ways,
(2) specification of earthquakes for performance evaluation,
(3) simple and practical formula for estimating soil amplification,
(4) analytical methods for estimating inelastic response of the building,
(5) limit states defined with deformation based on member damage levels,
(6) reparable limit states derived from post-earthquake residual damage, and

28

(7) a method of performance evaluation based probability of exceeding limit states.
The guidelines consist of the following three volumes in Japanese:
(i) Level 1 documents: Evaluation concept
(ii) Level 2 documents: Evaluation methods in practice
(iii) Level 3 documents: Evaluation example
The full provisions and most of the commentaries are being translated into English towards publication in the near future.

3. PERFORMANCE OBJECTIVES

Serviceability and safety are the two basic performance objectives, as commonly adopted in performance-based design codes for buildings in the world.

Serviceability is the performance objective so as to keep functional use without repair normally under moderate earthquakes. Therefore, the serviceability limit state shall be corresponded to the so-called slight or no damage levels. In the BSL of Japan, the allowable stress design is to deal with this, although the relationship between the criteria and the damage level is not clear. A procedure is presented in *the Guidelines* for verifying that the residual crack width is sufficiently small.

Safety is the performance objective so as to protect human life, and corresponds to the ultimate limit state or the safety limit state. Therefore, the design objective may be selected so that the structure can bear gravity loads and would not collapse. In terms of structural damage, the state may be just before collapse at the loss of gravity-load carrying capacity or P-δ deformation limits. In *the Guidelines*, the ultimate limit state of members is to be evaluated similarly by past AIJ guidelines[1][2], where the so-called inelastic deformability (ductility) limit is defined, while the deformability is defined as the point where the lateral resisting forces starts to decrease. For structures designed by the inelastic displacement concept possess a large margin up to the actual limit of collapse. However, a general method of evaluating the collapse limit is not yet established and the response with strength deterioration is not clear.

In addition to these two performance objectives, restorability or reparability are identified in *the new Guidelines.* This might not be a basic performance objective conceptually, because most of the damage less than near collapse may be regarded as "anyhow restorable." However, it has often been pointed out after the experiences of recent major earthquake disasters in urban areas such as Northridge and Kobe, that the reparability, which means whether economically reparable or not, could also be one of the most explicitly important performances for the owners and often be critical performance objective for the designers.

Ideally, the criteria should be established by quantifying the damage level of structural and nonstructural members such that economically allowable repair is possible, i.e., by taking into account estimated cost for restoration after earthquakes, where the diminished basic performance of safety and serviceability caused by the earthquake shall be restored to the required levels. In *the Guidelines,* the reparability limit state is mainly defined based on the residual crack widths instead of repair cost.

Also, since the reparable damage ranges widely from slight to major, *the Guidelines* considers two levels, i.e., the reparability limit states I and II. The first is the level of damage such that "slight repair might be needed but successive use will be possible," and in terms of damage classification as minor and nearly minor-to-moderate. The latter is such that "although successive use might not be available, economical restoration is quite possible by repair or strengthening to some extent," and damage level of moderate and nearly moderate-to-severe damage. There still left an enough margin to the actual safety limit deformation from these two limit states.

The seismic performance of a building shall be evaluated independently on the three principal directions of the structure for each of above performance objectives.

4. PERFORMANCE INDEX AND EARTHQUAKES

The seismic performance level is expressed as a continuous value using *the seismic performance index.* The value of the seismic performance index calculated in deterministic form as (1) below is the basic expression in *the Guidelines*, although (2), in probability form, may be used together with (1).

(1) The index in terms of the intensity of the earthquake ground motion at bedrock when the building response attains to the limit states (i.e., serviceability, reparability or ultimate limit states), i.e., the intensity of *the capacity earthquake*, defined as the ratio to the intensity of *the standard earthquake*:

$$\text{Seismic performance index} = \frac{\text{Intensity of the capacity earthquake}}{\text{Intensity of the standard earthquake}} \tag{1}$$

(2) The index in terms of the probability of the building response to exceed the limit states, due to the earthquake ground motion that may occur on the site during the service life of the building, i.e., *the site earthquake motion*.

Particularly in the evaluation by the second probability form, many assumptions are included in the models, because the state of knowledge on these fields is limited. Many would have to be revised as results from future research. Thus in the meantime, the method in *the Guidelines* is to be used for measuring the probabilistic significance relatively and as interpretation on the deterministic index.

In accordance with above two definitions, the expected earthquake ground motions are also discriminated in two ways: *the standard earthquake motion and the site earthquake motion.*

The standard earthquake motion is defined at the engineering bedrock in terms of the elastic acceleration response spectrum with 5 percent of critical damping corresponding to the same level as the design earthquake specified by the Building Standard Law of Japan, namely as:

$$
\begin{aligned}
&\text{Sa}(T, h = 0.05) = 320 + 3000T &&\text{if } T \le 0.16 \\
&\text{Sa}(T, h = 0.05) = 800 &&\text{if } 0.16 \le T < 0.64 \\
&\text{Sa}(T, h = 0.05) = 512 / T &&\text{if } 0.64 \le T < 5.0
\end{aligned} \tag{2}
$$

where, T: natural period of structure(sec.), Sa: acceleration response spectrum at engineering bedrock without surface soil, h: damping coefficient. The earthquake ground motion is used as the standard for evaluating the seismic performance capacity of a structure, which includes the site amplification through the surface soil from the bedrock. A new and simple method of calculating the site amplification from the bedrock is presented in *the Guidelines*. *The standard earthquake motion* is basically the same as defined in the BSL and does not have an explicit conception of exceeding probability and regional hazard.

On the other hand, *the site earthquake motion* is the earthquake motion used for evaluating the seismic performance risk of a structure at the construction site. The level and the characteristics are to be calculated based on the site-specific ground characteristics as well as the regional seismic activity.

5. ESTIMATION OF RESPONSES

A variety of analytical methods are supposed to be used for estimating responses of the structures, from equivalent linearization to time-history response analysis with detailed structural models. The principles for the structural and response analyses are prescribed in *the Guidelines*.

The response evaluation procedures covered in *the Guidelines* may be roughly classified as (a)-(d) below:

(a) Static nonlinear (pushover) analysis and response estimation based on reduced SDOF system (equivalent linearization),

(a) Pushover analysis and reduced SDOF time-history response analysis,

(b) (a) and time history response analysis of multiple lumped-mass systems,

(c) (a) and nonlinear time history response analysis at the member level,

(d) Nonlinear time history response analysis at the member level.

The method (a), which is a de facto standard procedure in *the Guidelines*, may be described more in detail as follows:

(1) Static nonlinear analysis of the structure with fixed foundation under an assumed load distribution (pushover analysis) is performed to obtain the equivalent load-displacement relationship of the reduced SDOF system, and the relationships between the equivalent displacement and the inter-story drift angle, member deformation angle (ductility factor) and member force.

(2) The limit deformations on the relations corresponding to the limit states (serviceability, reparability I/II, safety) are calculated from damage rates based on member deformations. The detailed evaluation methods are given in the level 2 documents. Also possible errors in the analysis due to higher modes, material strength, shall be taken into account.

(3) The earthquake response spectrum at the base of the building is evaluated from the standard earthquake at the engineering bedrock taking into account the soil amplification.

(4) The inelastic responses of the reduced SDF are related to the amplification factors of the spectrum by the equivalent linearization method, modified capacity spectrum method (CSM), and identify the level of *the capacity earthquake*, the deterministic performance index, defined as the factor when the response attains to the limit states. The inelastic responses by CSM can be calculated numerically or graphically, as shown in Figure 1, but also it should be noted that the estimated response can explicitly be formulated by simple equations base on the poly-linear relations of the spectrum. The CSM for estimation may be modified so

Figure 1. Capacity spectrum method (CSM) for estimation of inelastic response of SDF.

that the equivalent period can be made optimum (shorter) instead of the secant stiffness to the peak as adopted in the new BSL. A factor of 0.82 for the equivalent period is recommended, and this can simply be considered by shifting the earthquake spectrum to the longer side by the factor as shown in Figure 2.
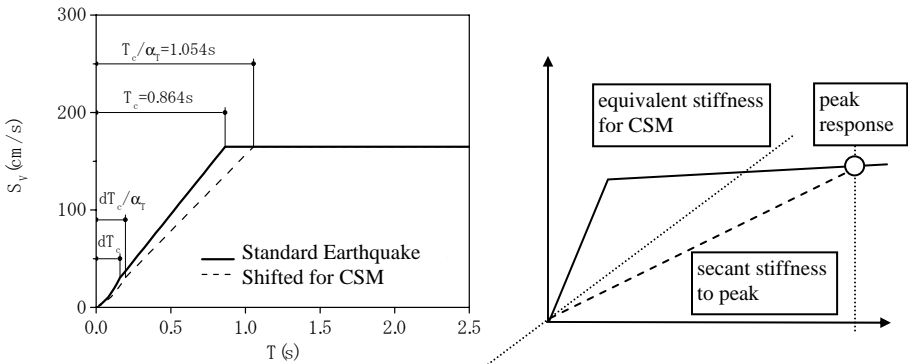
Figure 2. Shift of velocity spectrum of the standard earthquake taking optimum equivalent stiffness for CSM instead of secant stiffness to peak displacement.

6. DAMAGE AND LIMIT DEFORMATIONS

The structural limit deformation is defined for each limit state in each horizontal direction as the corresponding equivalent SDF lateral deformation, when any of the inter-story deformations first attained to its story limit deformation. The story limit deformations shall be evaluated based on the damage level of the members, which shall be classified into the following four levels with the corresponding limit states: (1) Level I: serviceability limit, (2) Level II: reparability limit I, (3) Level III: reparability limit II, and (4) Level IV: safety limit. These limit states shall be evaluated based on the residual damage states as:

(1) Serviceability limit state: the residual crack width shall be less than 0.2mm and the reinforcing bar shall remain elastic at maximum.

(2) Reparability limit state I: the residual crack width shall be less than 0.5mm to 1.0mm and the reinforcing bar shall remain within small inelastic strain at maximum. Slight damage to concrete may occur.

(3) Reparability limit state II: the residual crack width shall be less than 1.0mm to 2.0mm and the reinforcing bar may be with large inelastic strain but without buckling. Falling-off of cover concrete may occur but no damage to core concrete.

(4) Safety limit state: deformability limit without significant decay of seismic resistance (not less than 80% of maximum strength), which may be caused by crushing of concrete, buckling or rupture of reinforcing bars, shear failure or bond failure.

The above limit states are expressed on the skeleton of typical hysteretic relations of ductile member, such as flexural yielding beam, as shown in Figure 3. Practical methods of evaluating the limit deformations in terms of member end rotation angles are shown in the level 2 documents of the *Guidelines,* separately for each member, such as beam, column, wall, beam-column joint, and non-structural element. As for evaluation of the serviceability and the safety limit states, past AIJ guidelines may also be available, while the method of evaluating reparability, especially maximum and residual crack widths, are based on the following concept and models, which are newly introduced into the *Guidelines*.

Ductile inelastic deformations of reinforced concrete members are caused mostly by the tensile deformation, or widening of cracks. It has been pointed out from many past experimental research that total sum of crack widths along the member could easily be related to the overall deformation of the members by a simple deformation model, each for decomposed deformation modes, such as flexural, shear or axial deformations. Based on recent experimental data and observation, maximum crack widths can be related to the member deformations, assuming a simple deformation model with cracks of equal spacing, which are dependent on the reinforcement ratio across the cracks, as shown in Figure 4. Then the maximum crack widths are formulated using the number of cracks and the averaged crack widths. The residual crack widths are derived from the maximum widths at the peak proportionally to the maximum and unloading deformation points based on the unloading rules of typical

hysteresis model (Takeda model), as shown in Figure 5. The reparable limit deformations are also calculated from compressive extreme fiber strains of covering concrete and the smaller values should be adopted.

The calculated and observed crack widths are compared as shown in Figure 6. The assumptions in the evaluation methods are verified through several recent test data, mostly two-thirds or larger model, although general verification through other various tests, are still needed, especially, on scale effects and dynamic loading effects, and so on. The economical feature, the cost for repair and strengthening, should also be investigated and incorporated further.
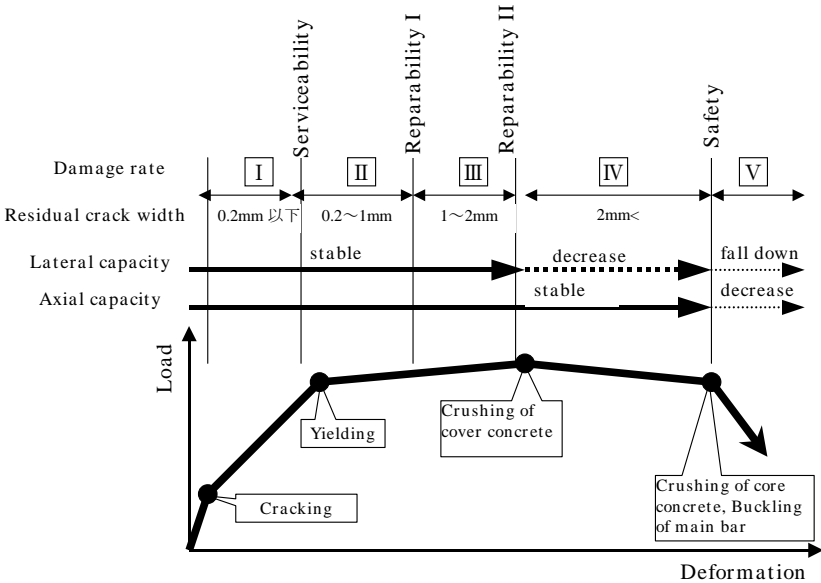
Figure 3. Member damage ratios on the hysteresis relations.
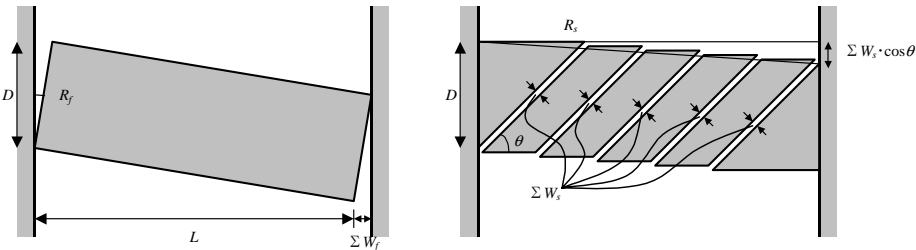
Figure 4. Models for evaluation of flexural and shear crack widths.

The limit inter-story deformations are defined as above, corresponding to the critical damage rate of the members, also considering the ratios of classified damage rates of all the members in the story.
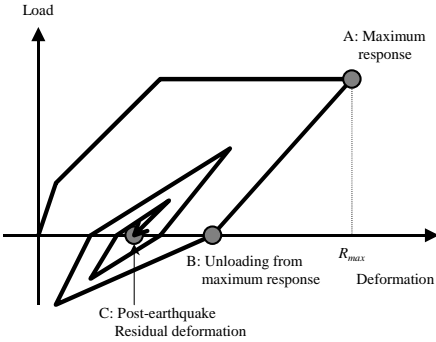
Figure 5. Relations between maximum deformation and residual deformation.
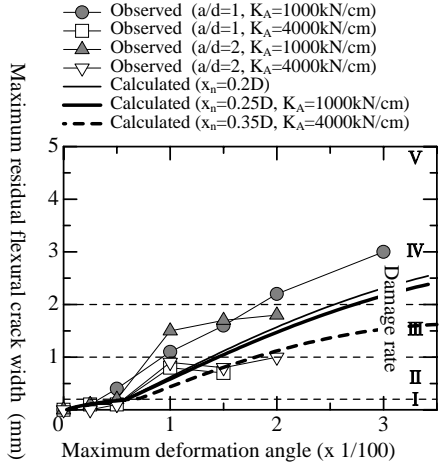
Figure 6. Observed and calculated residual crack widths after unloading from maximum deformations.
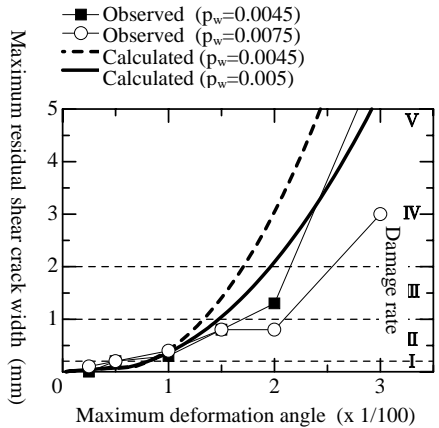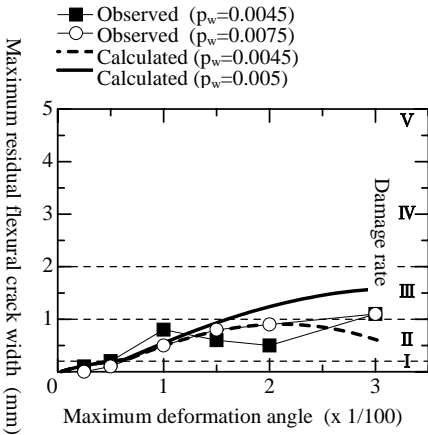
Figure 6—*continued*.

7. SEISMIC PERFORMANCE RISK

Because the deterministic performance index expresses only performance relative to the standard earthquake, the level should ideally be expressed in probabilistic form, namely, using the absolute values of probability of exceeding the limit states. However, it is difficult by our present state of knowledge to predict accurately the probabilistic density of seismic activity and the deviations in site-specific ground characteristics. Also still large deviations and errors exist in evaluation of capacity and response. Therefore, in the *Guidelines*, the probability formula is introduced additionally with concept of *the site earthquake* for evaluation. *The site earthquakes* shall be evaluated based on site-specific parameters including seismic activity, ground amplification, source characteristics, propagation path and so on, also reflecting the future research development in engineering seismology.

A new method of evaluating the probability of exceeding the limit states is explained in the level 2 documents, where inelastic displacement responses are formulated by the modified CSM and poly-linear spectrum of *the site earthquakes.* The seismic hazard model is based on a recent research paper. The hazard maps are being developed in national research institutes, although preconditions in the development should be revised further from future research. The probabilities of exceedance calculated for an evaluation example are shown in the next section.

8. EVALUATION EXAMPLE

In the third level document, *Evaluation example*, a calculation procedure of evaluation is shown for an example building. The building is 12-story reinforced concrete structure, which is a design example in the past AIJ guidelines[2]. The limit state deformations, the seismic capacity index, the probability of exceeding the limit states are calculated for the building numerically in detail. The structure is a regular-shaped, open-frame in X-direction and wall-frame in Y-direction. In accordance with the past guidelines, the building has been designed more carefully than by BSL with design factors, so that the ductile overall mechanism is ensured. Deformability of members are ensured up to the deformation angles of 1/50, 1/67 and 1/100 for beam, column and wall, respectively, although the lateral ultimate lateral load-carrying capacities are made almost equal to the required strength in the BSL, that are determined from the structural characteristics coefficients, Ds=0.3 for open frame in X-dir, and Ds=0.4 for wall-frame in Y-dir.

The calculated overall and story limit deformations are shown in Table 1. The seismic capacity indices, the ratios of the capacity earthquakes to the standard earthquake are also shown in the right column of the table. These estimates by the pushover analysis and CSM are almost equal to the responses calculated from additional time-history analysis. The seismic performance indices, namely the amplification factors of the earthquakes are around 1.0 for the reparable limit I, 1.5 for the reparable limit II, and higher than 2.0 for the safety limit.

Table 1. Limit deformations and seismic capacity indices.

Direction	Limit state	Base shear coefficient	Overall limit deformation	Inter-story limit deformation	Seismic capacity index
X-direction	Serviceability	0.160	1/412	1/355 (5F)	0.30
	Reparability I	0.245	1/151	1/117 (4F)	1.05
	Reparability II	0.255	1/98	1/75 (4F)	1.54
	Safety	0.265	1/57	1/45 (4F)	2.35
Y-direction	Serviceability	0.192	1/823	1/631 (9F)	0.26
	Reparability I	0.378	1/183	1/146 (9F)	1.00
	Reparability II	0.395	1/120	1/120 (9F)	1.74
	Safety	0.408	1/76	1/67 (9F)	2.75
Skewed direction(60°)	Safety	-	1/57	-	3.23

Therefore, the ultimate capacity would have enough margin of deformability up to the safety limit, in case of the design with the statically required capacity and the standard design spectrum in the BSL. In other words, the *"limit strength design method"* allows the design such that the required lateral strengths may be less than required conventionally, if the deformability up to the safety limit is ensured. However, it is not recommended in the *Guidelines* to make these margins less by selecting less capacity, but to designate these higher performance levels for proper description in the market. It should be noted that this is the result in case of ideally regular type of building with ensured overall mechanism, when the error of estimation might probably be minimum. The factored design of wall and columns based on the capacity design philosophy should be reemphasized. There still need further investigation both on demand and capacity, such as, extreme ground motion, inelastic responses of irregular structures, nonlinear soil-structure interaction and so on.

The risk analysis was carried out for this example with design service life of 50 years: at first, the probabilities of exceeding *the capacity earthquake* were evaluated in X and Y directions, respectively, as 12% and 7.6% for reparability I, 1.5% and 0.18% for reparability II, 0.21% and 0.13% for safety limit sates. This is the case when the soil amplification is evaluated in detail and reduction of velocity spectrum, i.e., the constant displacement spectrum is assumed over certain period. This could be underestimation, therefore, the constant velocity was assumed over the peak and evaluated alternatively then: 18% and 7.6% for reparability I, 6.5% and 2.0% for reparability II, 0.92% and 0.41% for safety limit sates. Because data were available only for the reliability of safety limit evaluation, the model was applied: the probability of exceeding the safety limit in Y direction was evaluated as 3.6% and 1.4% for the first and the latter assumptions in the spectrum shape. The accuracy in evaluating the limit states must and the earthquake hazard must be made higher in the future. It is expected that the proposed method will be made use of in practice, such as setting rates of earthquake disaster insurance or life-cycle cost analysis.

9. CONCLUSION

The new *AIJ Guidelines* is outlined, which provides deterministic and probabilistic methods of evaluating the actual seismic performance level of a designed reinforced concrete building. The limit states of the structures are defined based on the residual damage rates of members corresponding to the performance objectives as: (1) serviceability, (2) minor repair, (3) major repair, and (4) safety. The deterministic procedure evaluates the basic seismic capacity index for each limit state, which is defined as the amplitude ratio of the capacity earthquake to the standard earthquake, where the capacity earthquake is to induce the response equal to the limit state. The probabilistic evaluation method is provided as an additional procedure, where the performance level is expressed using the probability of exceeding the limit state by site-specific earthquakes during design service life.

The *Guidelines* is being translated into English and the English version is to be published from AIJ in the near future. We hope the *Guidelines* will be referred widely as research and technical documents as well as model code of practice for seismic performance evaluation. It is expected that more sophisticated alternative methods will be proposed based on reliable verification through intensive research in the future.

ACKNOWLEDGEMENT

REFERENCES

[1] Architectural Institute of Japan. (1990). *Design Guidelines for Earthquake-Resistant Reinforced Concrete Buildings Based on Ultimate Strength Concept 1988(draft),* 1990 (the first edition in Japanese), 1994 (in English version), AIJ, Tokyo.

[2] Architectural Institute of Japan. (1999). *Design Guidelines for Earthquake-Resistant Reinforced Concrete Buildings Based on Inelastic Displacement Concept 1997 (draft),* 1999 (the first edition in Japanese), AIJ, Tokyo.

[3] Architectural Institute of Japan. (2004). *Guidelines for Seismic Performance Evaluation of Reinforced Concrete Buildings,* 2004 (draft), AIJ, Tokyo.

HAZARD, GROUND MOTIONS AND PROBABILISTIC ASSESSMENTS FOR PBSD

Allin CORNELL[1]

ABSTRACT

Performance-based seismic design (PBSD) requires an integration of the response and behavior of the structure itself with a representation of the seismic threat to the site and a representation of the ground motions that will excite the structure. Further PBSD should assess the likelihoods of possible limit states and of the range of future losses, reflecting the randomness and uncertainty in all the steps in the process from the seismicity through structural response to loss estimation. This paper addresses all these issues but emphasizes the subject of representation of the ground motion for PBSD, starting from the perspective of what the structural analysis objectives are. This subject includes a focus on the interface between the work of the seismologist and that of the structural engineer.

   Keywords: Seismic hazard; Ground motions; Uncertainty analysis.

1. INTRODUCTION

Following, for example, the vision of the Pacific Earthquake Engineering Research (PEER) Center (e.g., Deierlein, 2004; Krawinkler, 2004, Miranda (2004)) it is presumed here that the ultimate objective of seismic performance assessment of structures (whether existing or designs for proposed structures) is the determination of decision metrics such as the mean annual loss (in economic and/or life safety terms) and/or mean annual frequency (or probability) of certain limit states, such as global instability collapse or maximum interstory drift ratio (MIDR) greater than 5%. Further, looking to current advanced and future practice, it is assumed here that the basis for these assessments will by non-linear "time history" structural analysis. As commissioned by the workshop convenors this paper will address two general areas, first, the "front end" input to such assessments and, second, the global subject of probabilistic analysis in performance-based seismic assessments (PBSA). The paper addresses the workshop theme of performance-based seismic design (PBSD) indirectly in that it is assumed that such an detailed assessment is a step, perhaps only a near-final confirmatory step, in PBSD.

---

[1] *Dept. of Civil and Environmental Engineering, Stanford University, Stanford, CA, 94305-4020, USA*

The first area, hazard and ground motions, will be addressed not from the perspective of the seismologist from whom we engineers traditionally get this information, but rather from the perspective of what PBEA objectives, needs and resources. The second subject, probabilistic assessments, will in the space available be limited to a rather formal overview of the issues and solutions, and an illustrative example.

2. SEISMIC HAZARD AND GROUND MOTIONS

2.1 Current Practice and PBEA Objective

Advanced U. S. practice today would find an engineering seismologist responsible for providing input to an engineer who has set out to do a nonlinear dynamic assessment of a design. The seismologist would provide (1) a probabilistic seismic hazard analysis (PSHA) (site-specific or downloaded from a USGS web site), (2) for one or more mean annual frequency (or annual probability) levels, a uniform hazard (response) spectrum (UHS), and (3) for each such level, a suite of n accelerograms for use in nonlinear dynamic analyses. Typically the seismograms have been selected to reflect the likely magnitudes, distances, and other earthquake parameters thought to dominate the hazard at the site (perhaps in some particular frequency range); this choice is guided by study of the "disaggregated" hazard. The seismograms might be recordings, "UHS spectrum-matched" recordings, or various forms of synthetic accelerograms. The engineer will subsequently run time history analyses for each of the n accelerograms in the suite of accelerograms associate with annual frequency, p, and observe for each a variety of outputs. Consider, for example, one useful parameter, MIDR. If the average of MIDR of the n records exceeds 7% (in a steel moment resisting frame) he may conclude that frame failure is likely given that such ground motions; in fact he may conclude that the annual frequency of failure is about p, but few if any current structural norms would require him to state his conclusions in such explicit terms.

In contrast it is presumed here that PBSA will require that the engineer confirm in direct or indirect terms that the annual frequency of important limit states, denoted, C, such as global structural collapse or economic loss greater than 10% of replacement cost, are less than prescribed or recommended values. More generally, he will seek the annual frequency, λ_C, of one or more "limit state" events, C. To be concrete we shall refer here to structural response limit states such as global instability collapse, MIDR greater than x%, etc.

Given the PBSA objective of estimating λ_C, we observe first that the problem naturally subdivides itself into characterizing the seismicity surrounding the site and assessing the behavior of the structure given a particular earthquake event occurs, or in formal terms into $\lambda(X)$ and $P[C|X]$, in which $\lambda(X)$ is the mean annual exceedance frequency of earthquake events in the region with the vector X of parameters (such as magnitude, distance from the site, faulting style, etc.), i.e., the mean annual frequency

of events with [X1>x_1, X$_2$>x_2, …] and *P[C|X]*, is the conditional probability of *C* given an event with parameters **X**. With this information the "total probability theorem" states that $\lambda_C = \int P[C \mid \mathbf{X}] \mid d\lambda(\mathbf{X}) \mid$. The differential $\mid d\lambda(\mathbf{X}) \mid$ is the mean annual frequency density (or absolute value of the partial derivative of $\lambda(\mathbf{X})$) times $dx_1 dx_2$.… In the following sections we seek various ways to estimate *P[C|X]* under the assumption that the seismologist has sole responsibility for $\lambda(\mathbf{X})$ and that this a well studied and commonly practiced problem of engineering seismology. For simplicity and concreteness we shall assume below that **X** = *[M, R]*, the magnitude and distance of the earthquake.

2.2   Option A: Direct Estimation of *P[C|X=x]* and λ_C

Estimating *P[C|X]* is a joint responsibility of the seismologist and structural engineer. A direct way of estimating *P[C|X]* is for the seismologist to prepare a sample of *n'* (more strictly, a random sample of equally likely) accelerograms. The structural engineer must then analyze his structure for each record and count the number of observations, *r*, of the event *C*, e.g., collapse. His estimate of *P[C|X]* is then simply *r/n'*. This process must be repeated for *m* well selected sets of the parameters, X_i, i = 1, …*m*, for a total of *n* = *n'm* records. Then the estimate of λ_C is $\lambda_C \approx \sum P[C \mid X_i] \Delta\lambda(X_i)$ in which $\Delta\lambda(X_i)$ is approximately the annual frequency of events with characteristics X_i. (The set of *m* sets of characteristics should be effectively exhaustive and exclusive.)

   In practice one must have a sample size *n'* large enough to estimate each of the *m* *P[C|X]*'s adequately. For comparative purposes suppose that this condition can be satisfied by estimating the median MIDR to within a standard error of 10%. Then the necessary sample size is about $(0.8/0.1)^2$, or more than 50, given that the coefficient of variation (COV) of the MIDR of a typical frame in near failure regime is at least 0.8. (This is conservative as, given only {M, R}, the standard deviation of the natural log of the peak response of a simple linear oscillator is 0.7 or more.) Assuming that *m* = 10 to 20 in order to cover adequately the range of say **X** = {M,R}, the total required sample size is of order 1000. In advanced application this number can be reduced by a factor of 2 or more by using "smart" Monte Carlo, or by, for example, a response surface analysis[2] or regression of MIDR on **X**. Of course once these analyses have been completed they can be used to find λ_C for many different events, C, such as other failure modes or other values of MIDR or economic losses. Examples of U. S. researchers using such methods include Ang, Wen, and Beck and their co-workers.

---

[2] Note that this would be in effect a structure-specific MIDR "attenuation law".

2.3 Option B: Estimation of $P[C|IM, X]$ and λ_C

With the objective of reducing the number of nonlinear analyses it can be helpful to introduce the notion of an "intensity measure", or IM. Familiar scalar examples include PGA and spectral acceleration, S_a. We shall restrict our attention here to scalar IM's. An IM is scalar property of an accelerograms that can be found simply and cheaply (at most be integration of the equation of motion of a simple oscillator.) With the introduction of this variable and the total probability theorem we may write $\lambda_C = \iint P[C|IM, \mathbf{X}]\, f(IM \mid \mathbf{X})\,|\,d\lambda(\mathbf{X})|$ in which $f(IM|X)$ is the conditional probability density function of the IM given X, which is customarily available as an "attenuation law" in engineering seismology. The estimation of $P[C|IM,X]$ would proceed as above except that the records selected in each X "bin" (e.g., each {M,R} pair) should also have a specified IM level (e.g., a given PGA value) usually obtained by simply scaling the record to that level. For each of several levels of IM the set of records is analyzed and the probability for that IM level and X bin, $P[C|IM,X]$ is estimated as above as the ratio r/n'. Upon repetition over the set of X bins, $\lambda_C \approx \sum\sum P[C \mid IM_j, \mathbf{X}_i]\,\Delta f(IM_j \mid \mathbf{X}_i)\,\Delta\lambda(\mathbf{X}_i)$. The advantage of introducing the IM as that the dispersion (defined here as the standard deviation of the natural log (or approximately the COV) of say the MIDR given IM and X is only about 0.3 to 0.4 for a nonlinear MDOF frame at large ductility levels, implying, using the rule above, that only some $(0.35/0.1)^2$ or order 10 records are necessary in for each first factor in the summation. However, assuming some 4 to 6 IM levels[3] and 10-20 X pairs the total required sample size is still in the range of 500. Again clever sampling or response-surface/regression modeling can potentially reduce this number substantially. Indeed one result of performing regressions such as MIDR on IM and X is that observation that one or more of the variables in X, such as R the distance to the fault, are statistically insignificant once IM is included in the equation. This implies one can reduce by a factor root (10-20) or 4, say, the number of cases and hence the sample size necessary. In fact if the IM is well chosen experience shows that *all* the variables in X may be found to be statistically insignificant, or at least practically so, i.e., the response (given IM) is no longer importantly sensitive to, say, M and R. This is not unexpected; in the limiting case of IM equal S_a at period T, the maximum response of a simple linear SDOF oscillator with natural period T is totally insensitive to X once the IM is known. And it is common practice to assume both that the equal displacement rule holds for moderate-period, moderate-ductility nonlinear oscillators and that the maximum roof drift of a low to moderate-height frame is proportional to the response of a nonlinear oscillator. This insensitivity is exploited in the next section.

---

[3] In fact if only a single event C is targeted, e.g., MIDR > 7%, this number of levels may be reduced to as few as 1 or 2, Jalayer (2003).

2.4 Option C: Sufficient IMs: Estimation of P[C|IM] and λ_C

In this section we introduce the notion of a "sufficient" IM and demonstrate the advantages it brings to PBSA. An IM is sufficient if $P[C \mid IM, \mathbf{X}] = P[C \mid IM]$, that is if the probability of the event given *IM* and *X* does not in fact depend on *X* at all. In this case $\lambda_C = \iint P[C \mid IM, \mathbf{X}] \, f(IM \mid \mathbf{X}) \mid d\lambda(\mathbf{X}) \mid = \int P[C \mid IM] \mid d\lambda_{IM}(IM) \mid$ in which λ_{IM} is simply the "hazard curve" of the *IM*, i.e., $\lambda_{IM}(u)$ is the mean annual frequency that the IM exceeds a specific value u. Formally $\lambda_{IM} = \int G(IM \mid \mathbf{X}) \mid d\lambda(\mathbf{X}) \mid$. This can be obtained by conventional hazard analysis and can be left to solely to the seismologist, provided the engineer has specified which *IM* he believes is appropriate for his particular structure. This may be as simple as specifying that he wants the IM to be the spectral acceleration at a period in the general vicinity of the (low strain) natural period of his structure. Estimation of λ_C reduces to selecting a set of accelerograms, scaling them to each of a set of IM levels, estimating as above the probability P[C|IM] and then summing: $\lambda_C \approx \sum P[C \mid IM] \, \Delta\lambda_{IM}(IM)$. Assuming that the dispersion of for example MIDR given a value of IM is about 0.3 to 0.4, each level will take order 10 samples and there need to be 4 to 6 levels then the total number of runs is only about 50. As discussed above this number can be reduced in special cases and by tools such as regression. Incremental dynamic analysis is one scheme that may be employed in one or more ways (Jalayer, 2003), especially when one wants to use the same runs for analyses of different *C*'s for which different *IM*'s may be most effective, e.g., S_a for MIDR and PGA for peak floor accelerations. Applications of Option C are now numerous; it has been widely used in the PEER Center, where S_a at a period near that of the natural period has been the *IM* of choice. The author's students have accumulated many cases; see www.stanford.edu/groups/RMS for theses and paper manuscripts. The introduction of the sufficient IM raises the question of how to establish sufficiency of a candidate IM and how to select the best from a collection of sufficient IM's. These questions will be addressed below. In Luco et al. (2002) all three options A, B, and C are used and compared.

2.5 Record Selection for PBEA

Whenever assessment through nonlinear dynamic analysis is anticipated the question of appropriate record selection always arises. The source of records for consideration ranges from empirical recordings, through artificially "spectrum-matched" accelerograms derived from recordings, to various forms of synthetics, including colored Gaussian noise and geophysically based rupture simulations. Consider first the choice from among a catalog of recorded accelerograms. The question of record selection is not unrelated to the discussions above. Under Options A and B above the records must be selected appropriate to each of the several *X* bins (e.g., by magnitude, distance levels). In contrast, under Option C, because sufficiency (independence) with

respect to X has presumably been established, in principle one may select records from *any* values of X (Iervolino, 2004). In practice even in this case it is prudent to use records from the general magnitude regime of interest. In deciding which record characteristics to mirror in the selection it is helpful to think in terms, primarily, of any systematic effects on spectral shape. Systematic spectral shape deviation from the appropriate range can effect linear response of MDOF systems and nonlinear response of even SDOF systems. Hence, for example, it is prudent to avoid selecting records from soft soil sites or from records that may include directivity effects. If the site *should* include such effects special efforts are necessary.

Recent efforts (Baker, 2004b) have demonstrated that one such systematic effect is that of "epsilon". Epsilon is the deviation of a record's S_a (at the structure's first-mode period, say) from that expected for the record's specific values of X; in short it is the deviation or "residual" from the S_a attenuation law (normalized by the "sigma" or standard error of the law.) High epsilon values are associated with peaks in the record's spectrum, and hence (for a fixed S_a or IM level) with more benign nonlinear behavior. (As the effective period of the structure lengthens it "falls off the peak" and into a less energetic portion of the frequency content.) But rare, high IM levels (or low λ_{IM} levels) that contribute most directly to rare MIDR levels are in turn associated with high values of epsilon (as evidenced in PSHA disaggregations for epsilon). Therefore when selecting records for analyses at these high IM levels one should consider choosing them from among records that have comparable epsilon levels (e.g., 1 to 2), in order that they *do* have the right, *non*-smooth shape near the period of interest. This is one reason why selecting records with shapes close to that of the UHS (or artificially matching a record's spectrum to the UHS) may bias the response conservatively.

Spectrum-matched or "spectrum-compatible" records have the advantage of reducing the dispersion in the response and hence of reducing the required sample size. There is also evidence that they are unconservatively biased for large ductility levels (Carballo, 2000).

Geophysically sound synthetics may be the only way we can obtain appropriate records for certain infrequently recorded cases, such as very near the source of large magnitude events. The various empirically based schemes of record simulation (e.g., from simple to evolutionary power spectral models, ARMA-based procedures, etc.) have the merit that one can produce from them large samples of nominally similar "earthquakes". Care should be exercised to insure that their spectra are "rough enough" for accurate nonlinear analysis.

2.6 Seeking Better IMs: Sufficiency and Efficiency

The benefits of sufficient IMs are clearly a reduction in difficulty and reduction in the number of nonlinear analyses. The observation raises the subject of seeking still better IMs, i.e., ones that might prove sufficient over a broader range of seismic conditions (i.e., regions of X) and ones that might reduce the dispersion in response

predictions and hence required sample sizes even further. This subject has been the object of previous studies and recent PEER investigations.

The candidates for improved IMs include both scalars and vectors. The scalars are developed as functionals of several variables shown to carry information about the response of a particular structure, e.g., a function (1) of S_a and magnitude, M, if studies show that S_a is not sufficient with respect to magnitude for a particular structure (e.g., a tall long period structure), or (2) of the two S_a's at both the first and second mode periods, or (3) of the S_a's of the first-mode S_a and the S_a at some longer period. Both of the latter examples are designed to capture spectral shape information in the period ranges of interest to a specific structure, second mode in the first case and that of an effective-period-lengthened nonlinear structure in the second. Luco (2002) proposes a scalar that is a SSRS-like combination (employing modal participation factors) of the inelastic displacement of an elasto-plastic oscillator (with yield displacement equal that derived from a static push-over analysis of the MDOF structure) and the second-mode elastic spectral displacement. The vectors may include similar such variables (e.g., Bazzurro (2002), Baker (2004b)).

As discussed above the sufficiency is typically demonstrated by showing the lack of dependence of the response on certain *X* variables given the *IM* level. For example, Figure 1a shows that for this structure the S_a is sufficient with respect to magnitude as the residuals from a regression of MIDR on S_a show no significant dependence on M. In contrast when seeking a better IM one looks for additional variables (beyond S_a, say) that demonstrate additional explanatory power. Figure 1b shows that epsilon does this for this structure.
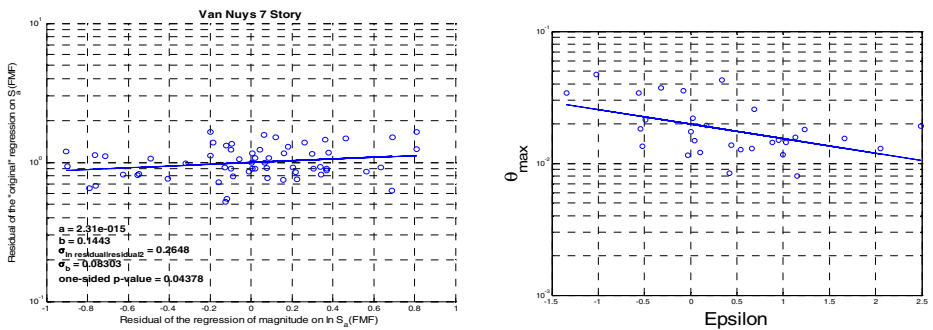
Figure 1. (a) Shows MIDR residuals (given S_a) versus magnitude; (b) shows residuals versus epsilon. Baker(2004b).

Therefore one can ignore M (as S_a is sufficient with respect to it for this structure), but epsilon needs further consideration, for example, as a member of *X* or by careful record selection as discussed above. Further epsilon deserves to be considered as a candidate for inclusion in an improved scalar or vector IM, one that would eliminate the insufficiency of S_a with respect to epsilon and, given its clear explanatory power, should decrease the dispersion in predicting the MIDR (Baker (2004b)). Figure 2

shows that the scalar IM proposed by Luco discussed above not only strongly reduces dispersion (vis-a-vis S_a), but also shows apparent sufficiency with respect to situations where near-source directivity effects may be important. Improved IM's, while reducing the requisite number of nonlinear structural analyses, may come with a price. Luco's predictor, for example, requires the development of a new attenuation law. Vector IM's require new attenuation information (e.g., correlations) and/or PSHA computer code modifications.
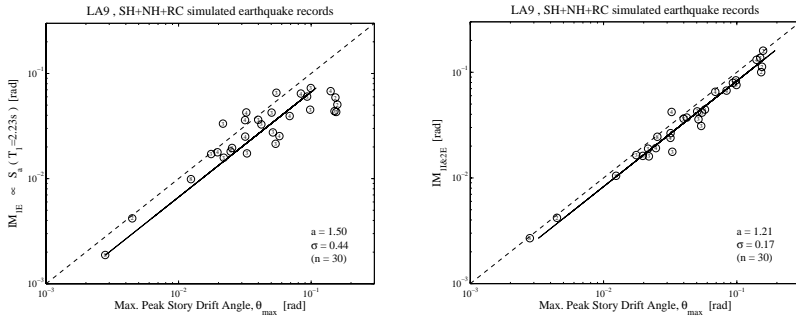
Figure 2. (a) Regression of MIDR versus (in effect) *Sa*; (b) regression versus the Luco IM. The records are geophysical synthetic accelerograms for a site near the Hayward Fault simulating 30 repetitions of an event rupturing all three segments of that fault. (Luco, 2002).

3. PROBABILISTIC ASSESSMENT

3.1 The Basics

Probabilistic assessment of structures for PBSD has been both researched and applied in various fields in various degrees. For example, the U.S. nuclear power industry has used Seismic PRA's (Probabilistic Risk Assessments) for two decades (Kennedy, 1980)) applying it to virtually all the plants in the country under the IPEEE program. Much more recently, the U.S. building industry has produced guidelines for probabilistic assessment of steel moment-resisting frames (FEMA-SAC (2000), Cornell(2002)). Both of these approaches are based on integration over the product of the hazard curve times some representation of the probability of a specified limit state given the IM level. Both procedures call for the explicit quantification of both the aleatory ("random") and epistemic ("knowledge") sources of uncertainty. The former method is based on fragility curves (*P[C|IM])* and provides a mean estimate of the limit state annual frequency. The latter document is based on a non-linear displacement-based "load and resistance factor" (LRFD-like) scheme derived from a distributions of displacement demand and displacement capacity; it sets criteria in terms such as a 90% confidence that the annual frequency of collapse is less than 1/2500 (i.e., explicitly separating epistemic and aleatory uncertainty).

PEER has put forward PBSA methodologies which can be represented by its "framing equation",

$$\lambda(\mathbf{DV}) = \iiint G(\mathbf{DV} \mid \mathbf{DM}) \mid dG(\mathbf{DM} \mid \mathbf{EDP}) \mid\mid dG(\mathbf{EDP} \mid \mathbf{IM}) \mid\mid d\lambda(\mathbf{IM}) \mid \qquad (1)$$

which is described in some detail[4] and applied in this workshop in Deierlein (2004), Krawinkler (2004), and Miranda (2004). Suffice it to say here that the integral is designed to isolate a pair-wise sequence of four (generally vector-valued) random variables representing ground motion intensity (*IM*), structural responses such as MIDR and peak floor accelerations (*EDP*), damage states (*DM*) and finally "decision variables" (*DV*) such as lives and dollars. The pair-wise sequences presume that the variables are only simply coupled, or that each variable is, to use the word from above, "sufficient" with respect to those before it in terms of its prediction of those after it. For example, it assumes that *P[DM =x|EDP = y and IM = z]* = *g(y)* and not of[5] *y* and *z*. In the context of PBSA it permits the specialist in each subject (e.g., cost estimation) to deal only with prediction of costs from given damage states without worrying about what ground motion or structural deformations caused the damage. Binary limit state analysis (such as assessment of collapse frequency) can be thought of as a special case when the DV is scalar and binary, DV = 1 being the collapse event. This formulation contains as special cases most of the common limit state and loss estimation schemes. One such is that using "fragility curves" which typically represent the probability of some binary limit state (collapse, severe economic loss, etc.) as a function of ground parameter (IM) such as PGA. Such a result is obtained if the second two integrals are collapsed leaving $\lambda(DV = 1) = \int G_{DV|IM}(0 \mid IM) \mid d\lambda(IM) \mid$ in which $G_{DV|IM}(0|IM)$ is the fragility curve resulting from using one or methods (e.g., Monte Carlo simulation) to find the probability of the limit state (collapse, for example) as a function of, say, PGA or S_a. We shall use this in an example below. (Note that the probability that the binary limit state variable is 1 is the probability that it is *strictly* greater than 0.)

Even with the simplifications inherent in the PEER framing equation the specification of the necessary probability distributions and the "propagation" of those uncertainties (i.e., the numerical computation of the integral) can be a daunting task. The specification of the aleatory and epistemic uncertainties requires inputting joint distributions such as the $G_{EDP|IM}$ and $G_{DM|EDP}$ when for, say, detailed PBSA economic loss estimation, the number of relevant *EDP*'s may be a vector of at least two to four per floor (e.g., peak IDRs and floor accelerations) and each potential loss-producing element in the PBSA model of the building (structural members, partitions, expensive laboratory equipment, etc.) may in principal deserve a random variable

---

[4] The G functions are complementary cumulative distribution functions, i.e., the probability that a random variable strictly exceeds the argument. The absolute values of their derivatives are probability density functions in the continuous case.

[5] To the probabilistic this is a kind of Markovian dependence.

(i.e., an element in the **DM** vector) to represent its continuous (e.g., maximum crack width in an RC joint, Pagni (2004)) or multi-level discrete (e.g., partition damage state, Miranda (2004)). In short, these vectors are very large, and even the proposed limitation to pair-wise joint distributions implies numerous modeling decisions, simplifications, and numerical input parameter estimates. Simplifications used in practice and research to date include (1) "lumping" many loss elements in a single representative one (e.g., all partitions on a given floor), which is equivalent to assuming perfect dependence among them; (2) limiting the dependence of each DM element to a single EDP element (e.g., the partition damage state on floor j depends only on the IDR in floor j), and (3) second-moment level modeling (e.g., regressions of DM on EDP or DV on DM, etc.), which is equivalent to limiting probabilistic dependence specification to simply a correlation coefficient. Further, specification of epistemic uncertainty implies that similar kinds of specification be provided for, at a minimum, the parameters in the aleatory probabilistic models, e.g., second-moment characterization of the (uncertain) mean values of all the EDP's for a given IM level (e.g., Baker (2003)). This might reflect epistemic uncertainty in the engineering models of nonlinear dynamic behavior adopted in the structural analyses (e.g., Ibarra (2003)). Limited experience and data will insure that there are research opportunities in all these directions for years to come.

The numerical assessment of the probabilistic PBSA model can be conducted in a variety of technical ways which need not be the primary focus of the modeler/analyst. These include analytical or numerical integration, Monte Carlo ("dumb" and/or "smart"), first-order, second-moment methods, FORM or SORM, etc., plus appropriate hybrids of two or more of these methods (e.g., Baker (2003), Porter (2004)). For example, the nature of the highly nonlinear and detailed dynamic analyses of MDOF frames suggests that the IM to EDP step will defy formal random vibration analysis and always require random sampling of accelerograms and numerical dynamic analysis (e.g., Monte Carlo perhaps coupled with regression or response surface analysis), as suggested in the three options outlined above. The uncertainty in the structural parameters may be included by Monte Carlo within these multiple runs, perhaps with special experimental designs, or again by response surface methods and/or FOSM methods. Like these uncertainties in structural parameters and models, limited data may always limit the effective specification of damage and economic loss data to little more than second moment specifications and associated methods.

3.2 Examples

In this section we present two simple examples of application of the PEER framing equation for the structural limit state case. The first is formal and the second includes numerical results; both employ analytical integration to "solve" the equation. While such solutions require the adoption of certain simplifying assumptions they can provide simplicity and transparency.

3.2.1 A DCF Displacement-Based Format

Under certain assumptions about the analytical forms of the distributions and relationships in the framework equation (e.g., Cornell (2002), Jalayer (2003)) it is possible to obtain an closed form solution to the PEER framework equation for the case when DV is a binary (i.e., limit state) variable, the IM is a scalar such as S_a, the EDP or demand is a scalar such as MIDR, and the (random) capacity is measured in the same terms (e.g., MIDR):

$$\lambda_{Limit\ State} = \lambda_{S_a}(\hat{C}) \exp[\frac{k^2}{2b^2}(\beta_{D|S_a}^2 + \beta_C^2)] \tag{2}$$

in which $\hat{C}$ is the median displacement capacity, the β's are dispersions of MIDR given S_a and of capacity as indicated, the b and k are parameters reflecting the dependence of drift on Sa and λ_{Sa} on S_a respectively, and λ_{Sa} is the S_a hazard curve.

For purposes of assessment of safety compliance (or "checking"), this limit state frequency result can be set equal to the allowable limit frequency (e.g., 1/2500 per year), and the result inverted to provide a LRFD-like code checking inequality. We call this a Demand and Capacity Factor (DCF) format as here demands and capacities are measured in dynamic displacement, not force terms, as is preferred for explicitly nonlinear problems. Several equivalent alternative formats are available. For example, the tolerable limit state frequency, λ_o, is satisfied if:

$$\gamma_{D|S_a} \cdot \hat{D}_{S_a^{\lambda_o}} \leq \phi_C \cdot \hat{C} \tag{3}$$

in which $\hat{D}_{S_a^{\lambda_o}}$ is the median drift displacement demand at ground motion level $S_a^{\lambda_o}$, which is in turn the Sa level associated with hazard level λ_o, and the capacity and demand factors have forms such as $\phi_C = \exp[-\frac{k}{2b}\beta_C^2]$. Note that $\hat{D}_{S_a^{\lambda_o}}$ can be found by Option C above by analyzing n' records at simply one S_a level, implying a total sample size of only 10 or less. A format such as this amplified to include epistemic uncertainty effects is the basis of the FEMA SMRF guidelines (FEMA (200X)).

3.2.2 Global Collapse Assessment via an IM-based Procedure

In this section we demonstrate an IM-based version of the limit state global dynamic instability collapse. Applying the same assumptions alluded to just above (Section 3.2.1) a formula for the collapse limit state frequency can be developed from the reduced IM or fragility form of the PEER framework equation stated above (Section 3.1), $\lambda(DV=1) = \int G_{DV|IM}(0|IM)|d\lambda(IM)|$:

$$\lambda_{Limit\ State} = \int_{S_a} F_C(s_a)|d\lambda_{Sa}(s_a)| = \lambda_{S_a}(\hat{C})\exp(\frac{1}{2}k^2\beta_{RC}^2) \tag{4}$$

(noting that the probability that the binary decision variable, *DV*, is strictly greater than zero (given the IM level) is simply the probability that the capacity (as measured in IM terms) is less than the IM demand, i.e., the cumulative distribution function, F_C, evaluated at the given IM demand level). Here the dispersion measure, β_{RC}, is that of the randomness or aleatory or record-to-record variability in the capacity. The plot of the F_C of a IM-based global instability capacity is shown in Fig. 1 (Krawinkler (2004)). It was developed from incremental dynamic analyses pushed to the "flat line" (Vamvatsikos, (2002)).
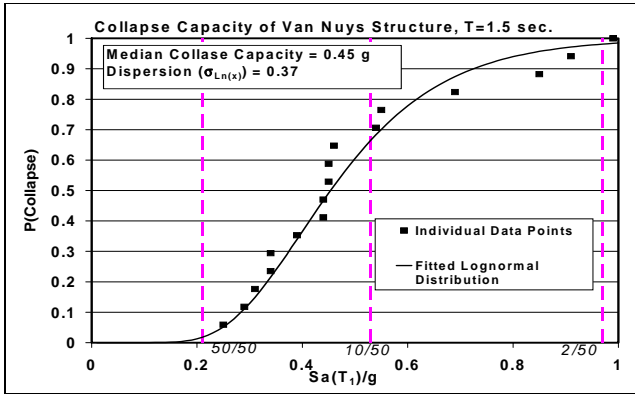
Figure 3. Cumulative distribution function, F, for global instability capacity in IM (S_a) terms. (Krawinkler 2004).

When supplemented with two unit median (lognormal) random variables with dispersions β_{UC} and β_{UH}, to reflect epistemic uncertainty in respectively the median capacity and the hazard curve frequencies, the limit state frequency above becomes an (epistemically uncertain) lognormal random variable, whose mean estimate is (Cornell (2002), Jalayer (2003)):

$$\overline{\lambda}_{Limit\ State} = \int_{S_a} \overline{F}_C(s_a)\,|\,d\overline{\lambda}_{S_a}(s_a)\,| = \overline{\lambda}(\hat{\hat{C}})\exp(\frac{1}{2}k^2\beta_{RC}^2)\exp(\tfrac{1}{2}k^2\beta_{UC}^2) \tag{5}$$

in which $\overline{F}_C$ is the mean estimate of the CDF of the capacity and the mean estimate of the hazard curve is $\overline{\lambda}_{S_a}(s) = \hat{\lambda}_{S_a}(s)\exp(\frac{1}{2}\beta_{UH}^2(s))$. $\hat{\hat{C}}$ is the median estimate of the median capacity. The dispersion (standard deviation of the natural log) of the limit state frequency is $\beta_{\lambda_{Limit\ State}} = \sqrt{\beta_{UH}^2 + k^2\beta_{UC}^2}$. Note that the mean estimate can be determined directly from a mean estimate of the hazard curve and that confidence bands on the limit state frequency can be obtained from these two β parameters and a standard Gaussian table. Finally note that the epistemic uncertainty depends on both that in the hazard (demand) and that in the capacity, the latter modified by the

parameter k (the slope of the hazard curve when plotted in a log-log form) which is in essence a Jacobian insuring that the two net dispersions are reflecting uncertainty in common (i.e., frequency) terms. As shown in Figure 3 the value of capacity random or aleatory dispersion, β_{RC}, in that example is about 0.37. Representative values for β_{UC} and β_{UH} might be 0.5 and 0.35 in coastal California, while k there (for S_a in the moderate period, here 1.5 seconds, and order 10^{-3} hazard range) might be 2.3. For a case in which the best (median) estimate of the median, $\hat{C}$, is 0.45g (as in Figure 3) and the mean estimate of the hazard at this level is 0.0025, the mean estimate of the collapse limit state frequency is 0.0068 or $(1.44)(1.9) = 2.7$ times the (mean estimate of the) likelihood that ground motion exceeds the estimated median capacity. The increase reflects the indicated product of the effects of aleatory and epistemic uncertainty (respectively) in the capacity (Eq. 5). In this case the mean estimate of the hazard curve at 0.45g is only 6% larger than the median estimate due to the low estimate of the β_{UH} value; this 6% ground motion hazard uncertainty effect on the mean limit state estimate will be larger in many locations and at lower hazard levels of usual safety interest. On the other hand at non-coastal California or analogous high seismicity areas the slope k will typically be lower reducing the impact of the capacity uncertainties. The total epistemic uncertainty in the limit state frequency, $\beta_{\lambda_{Limit\ State}} = \sqrt{\beta_{UH}^2 + k^2 \beta_{UC}^2}$, is about 1.45 and is dominated in this case by the second term, reflecting the factors just cited and the high epistemic uncertainty we now face as professionals trying to estimate the highly nonlinear, near-collapse regime, which is governed by factors such as P-delta and post-peak force decay in the hysteretic models of nonlinear elements.

ACKNOWLEDGEMENTS

REFERENCES

Deierlein, G. (2004). Overview of a comprehensive framework for earthquake performance assessment. *Proceedings Inter. Workshop on Performance Based Design*, Bled, Slovenia, June.

Krawinkler, H., F. Zareian, R. Medina, and L. Ibarra. (2004). Contrasting performance-based design with performance assessment. *Proceedings Inter. Workshop on Performance Based Design*, Bled, Slovenia, June.

Miranda, E., H. Aslani, and S. Taghavi. (2004). Assessment of seismic performance in terms of economic losses. *Proceedings Inter. Workshop on Performance Based Design*, Bled, Slovenia, June.

Jalayer, F. (2003). Direct Probabilistic Seismic Analysis: Implementing Non-Linear Dynamic Assessments. PhD Theses, Dept, of Civil and Environmental Engr., Stanford University.

Iervolino, I., and C. A. Cornell. (2004). "Record Selection for Nonlinear Seismic Analysis of Structures", Accepted for publication, *Earthquake Spectra*.

Baker, J., and C. A. Cornell. (2004b). A vector-valued ground motion intensity measure consisting of spectral acceleration and epsilon**.** Manuscript in preparation.

Carballo, J. E., C. A. Cornell. (2000). Probabilistic seismic demand analysis: spectrum matching and design, Report No. RMS-41, Reliability of Marine Structures Program, Department of Civil and Environmental Engineering, Stanford University.

Kennedy, R. P., C. A. Cornell, R. D. Campbell, S. Kaplan, and H. F. Perla. (1980). Probabilistic Seismic Safety Study of an Existing Nuclear Power Plant, *Nuclear Engineering and Design*, Vol. 59, No. 2, August, pp. 315-338.

FEMA-SAC. (2000). Recommended seismic design criteria for new steel moment-frame buildings. Report No. FEMA-350, SAC Joint Venture, Federal Emergency Management Agency, Washington, DC.

Baker, J., and C. A. Cornell. (2003). Uncertainty Specification and Propagation for Loss Estimation Using FOSM Methods, Report 2003/07, PEER, Berkeley, CA, Nov. 2003

Ibarra, L. (2003). Global collapse of frame structures for seismic excitations. Ph. D. Dissertation, Dept. Of Civil and Environmental Engineering, Stanford Univ., Stanford, CA, USA.

Porter, K. A., (2004). Propagation of Uncertainties from IM to DM, Chapter 6, PEER Performance-Based Earthquake Engineering Methodology: Structural and Architectural Aspects, Van Nuys Testbed Committee, Report in Progress. PEER, Berkeley, CA.

Cornell, C. A., F. Jalayer, R. Hamburger, and D. Foutch. (2002). The probabilistic basis for the 2000 SAC/FEMA steel moment frame guidelines, *Journal of Structural Engineering*, Vol. 128, No. 4, pp. 526-533, April 2002.

Jalayer, F., and C. A. Cornell. (2003). A technical framework for probability-based demand and capacity factor design (DCFD) seismic formats, Report 2003/6, PEER, Berkeley, CA, Nov., 2003

Vamvatsikos, D., and C. A. Cornell. (2002). Incremental dynamic analysis*, Earthquake Engineering and Structural Dynamics*, 31(3): 491-514, March

Luco, N. et al. (2002). Probabilistic seismic demand analysis at a near-fault site using ground motion simulations based on a kinematic source model," Proceedings 7th U.S. National Conference on Earthquake Engineering, Boston, MA, July.

Bazzurro, P., and C. A. Cornell. (2002). Vector-valued probabilistic seismic hazard analysis. Proceedings 7th U.S. National Conference on Earthquake Engineering. Boston, MA, July.

Baker, J., and C. A. Cornell. (2004a). Choice of a vector of ground motion intensity measures for seismic demand hazard analysis, 13th World Conference on Earthquake Engineering, Vancouver, Canada, August.

Pagni, C. A., and L. N. Lowes. (2004). Tools to enable prediction of the economic impact of earthquake damage in older RC beam-column joints, *Proceedings Inter. Workshop on Performance Based Design*, Bled, Slovenia, June.

POST-EARTHQUAKE FUNCTION OF HIGHWAY OVERPASS BRIDGES

Kevin MACKIE[1] and Božidar STOJADINOVIĆ[2]

ABSTRACT

Bridges are a crucial part of the transportation network in a region struck by an earthquake. Whether the bridge has collapsed or not determines if a road is passable. Ability of a bridge to carry traffic load after an earthquake determines the weight of trucks that can cross it and the speed at which such traffic may move. Extent of structural damage in bridges as structural systems and bridge components determines the cost and the time required to repair them. Today, post-earthquake bridge evaluation is qualitative and empirical rather than quantitative. The goal of our research is to provide an engineering basis for quick and reliable evaluation of the ability of a typical highway overpass bridge to function after an earthquake.

The PEER probabilistic performance-based evaluation approach provides the framework for bridge function evaluation. Three limit states, repair cost, traffic function, and collapse are addressed. An analytical study was performed that links engineering demand parameters for a family of typical U.S. highway overpass bridges to ground motion intensity measures. The PEER structural element performance database and reliability analysis tools were used to link engineering demand measures to damage measures. Finally, a number of decision variables were developed that describe the considered limit states in terms of measures of induced damage. This paper presents the analytical models involved in bridge post-earthquake function evaluation, the decision variables and their correlation to the considered limit states, and the fragility curves that represent the probability of exceeding a given limit state in a high seismic risk zone in the U.S.

Keywords: Performance-based earthquake engineering; Fragility; Decision variables; Damage limit state.

1. INTRODUCTION

Can we get there? How quickly? How heavy a load can be transported? How much will it take to repair any damage? How long will that take? These are the questions posed by emergency managers, recovery planners and structural engineers after an earthquake. The answers are in the state of highway infrastructure in a region struck

---

[1] *Doctoral Candidate, Dept. of Civil and Env. Engineering, University of California, Berkeley, Berkeley, CA 94720-1710, mackie@ce.berkeley.edu*
[2] *Associate Professor, Dept. of Civil and Env. Engineering, University of California, Berkeley, Berkeley, CA 94720-1710, boza@ce.berkeley.edu*

by an earthquake, of which bridges are an integral part. Today, answers to these questions are more qualitative than quantitative, mostly based on experience and engineering intuition rather than results of analyses and engineering evaluations. Furthermore, after an earthquake decisions must be made quickly: there is often no time to perform extensive engineering investigations. The goal of our research is to provide an engineering basis for evaluating the ability of a typical highway bridge to function after an earthquake. We address three limit states:

1. Repair limit state: to assess how much it may cost to repair a bridge;
2. Traffic function limit state: to assess the magnitude of traffic load that can be safely carried by a damaged bridge; and
3. Collapse limit state: to asses if the bridge is passable or not.

The highway overpass bridges under consideration in this study were chosen because they represent close to 90% of all bridges in typical regional highway networks in the U.S. (Basöz 1997). The particular bridges, typical for California, are detailed in (Mackie 2003). In summary, these reinforced concrete highway overpass bridges have two equal spans, a single bent with a single column, a pile shaft foundations, and roller abutment supports. Variations of a number of the bridge design parameters were studies, but are not the subject of this paper.

2. PROBABILISTIC FRAMEWORK

The Pacific Earthquake Engineering Research Center's (PEER) probabilistic performance-based design and evaluation approach provides the framework for bridge function evaluation. Data from seismology studies was used to assess the ground motion intensity measures (IM). Structural analysis using finite element models was performed to links engineering demand parameters (EDP), for a family of typical U.S. highway overpass bridges, to ground motion intensity measures using OpenSees software for non-linear dynamic seismic structural response simulation. The PEER structural element performance database was used to link engineering demand parameters to damage measures (DM) in typical bridge structural elements such as columns. A combination of finite element simulations and reliability analyses were employed to develop damage measures pertinent to bridge function. Finally, a number of decision variables were developed that describe the considered limit states in terms of measures of induced damage.

Previous research (Mackie 2003) has produced a sizeable collection of information regarding Probabilistic Seismic Demand Models (PSDM) that relate EDPs to IMs. PSDMs are generated using Probabilistic Seismic Demand Analysis (PSDA). Two approaches to PSDA include the cloud approach to vary the seismic demand (IM), and a scaling approach to reach prescribed intensity levels. The resulting PSDMs may assume any mathematical form; however, erudite choices simplify the evaluation using the PEER framework. Selections of PSDMs that are optimal in this regard are detailed elsewhere (Mackie 2003). One studious PSDM form is linear in log space.

$$\ln(EDP) = a + b\ln(IM) \tag{1}$$

Probabilistic capacity, or damage, models have also been the subjects of previous research (Berry 2003). Experimental observations of damage to structural components can be used to generate damage fragility curves conditioned on measures of response (EDPs). These curves are usually specified at discrete damage limit states (DM), therefore making a closed form mathematical model impossible. However, using reliability techniques for both structural component damage and for bridge-level loss of function, it is possible to describe a damage model in the same lognormal form as the demand model (Equation 2).

$$\ln(DM) = c + d\ln(EDP) \tag{2}$$

The PEER framework then provides a convenient methodology for generating both annual frequencies of exceeding discrete DM limit states and damage fragility curves:

$$P\left[DM > dm^{LS} \mid IM = im\right] = \int P[DM \mid EDP] \, dP[EDP \mid IM] \, dedp \tag{3}$$

Using Equations 1 and 2, the two terms in the kern of Equation 3 are simply lognormal CDFs and PDFs, respectively. In Equation 3, it is assumed that there is no dependence between successive terms in the integral. For example, DMs in the first term of the kern are conditioned on EDP values only, without considering the IMs.

Finally, to discuss decision limit states, loss models need to be developed that relates the damage states (DM) to decision variables (DVs). Once again, this relationship can be discrete, such as in current seismic performance criteria, or it can be continuous. For simplicity, the loss model is also assumed to have lognormal form

$$\ln(DV) = e + f\ln(DM) \tag{4}$$

The PEER framework then provides a simple extension to produce decision fragility curves.

$$P[DV \mid IM] = \iint P[DV \mid DM] \, dP[DM \mid EDP] \, dP[EDP \mid IM] \, dedp \cdot ddm \tag{5}$$

3. LIMIT STATES

Limit states for highway bridges are formulated at two levels: the component and the system. The component level addresses the affect of bridge structural component's damage on the post-earthquake response strategy. Specifically, components are

assessed for damage and corresponding repair costs or repair times are estimated. For example, damage could be considered in piles, pile caps, columns, expansion joints, abutment wing walls, approach slab and embankment, and numerous other locations. The system level addresses the overall performance of the bridge as a whole in a post-earthquake scenario. For a highway bridge, functionality is primarily measured in terms of the traffic load carrying capacity, lane closures, allowed axle loads and speed limits. The total cost in a post-earthquake scenario is the summation of the component, or direct losses, and the loss of functionality, or indirect losses.

3.1   Repair Cost

The repair cost limit state presented in this paper addresses only damage to the bridge column because of current limitations in available reconnaissance and research data for other bridge components. The data used in our study was collated into the PEER Structural Performance Database (http://nisee.berkeley.edu/spd/). Consequently, bridge longitudinal drift ratio was selected as the EDP describing the column demand, while discrete damage observations (DMs) selected from the database include concrete cover spalling, longitudinal rebar buckling, and column failure. Column failure was defined as the first observation of reinforcing bar fracture. Therefore, the DM can be thought of as component damage with specific values ranging from spalling to failure. Finally, reconnaissance data (Basöz 1997) was used to generate a loss model relating the damage to repair costs.

3.2   Traffic Function

The traffic function limit state presented in this paper addresses the bridge system as a whole in order to generate information about loss of its functionality. Functionality is defined in terms of the lateral and vertical load carrying capacity of the bridge. This capacity was assessed analytically using pushover and pushunder analyses pre- and post-earthquake because hardly any experimental data exists on the system performance of bridges. PSDMs for functionality use the residual load carrying capacity (units of force) as the EDP. Reliability analyses were performed to appraise capacity levels pre-earthquake. These are then compared to post-earthquake residual capacities to generate a bridge level DM that describes the percentage loss of load carrying capacity. It then remains up to engineers to determine the form of the loss model that relates the losses in capacity to changes in traffic loading and speed. A sample loss model is presented in this paper to facilitate application of the methodology and further discussion as to a more practical mathematical form.

3.3   Collapse

Collapse of a modern bridge is an unacceptable performance goal in California. Therefore, it was necessary to define the collapse or collapse prevention limit state in

terms of global and local bridge performance. An approach for defining collapse in terms of observed damage and decision limit states is presented here. While it would be possible to arbitrarily assign a traffic volume (decision) loss limit state to the collapse prevention state, it is more intuitive to use a combination of damage limit states. This combination involves both observable damage to bridge components and loss of overall bridge function.

4. COMPONENT-LEVEL DECISION: REPAIR COST

The probabilistic seismic demand model for this case was formulated previously (Mackie 2003). This PSDM relates $Sa(T_1)$, and IM, and drift ratio of the column in the longitudinal direction, an EDP. Simulation using cloud analysis was performed using OpenSees (http://opensees.berkeley.edu/) to obtain the PSDM. Assuming a lognormal distribution, determination of the two unknown parameters in Equation 1 yields a=-4.18 and b=0.885. The CDF curves, obtained by integrating over the full range of IM values, describe the demand fragility. Plots of these fragility curves and more detailed repair cost examples are presented elsewhere (Mackie 2004a).

Transition from demand to damage fragility is done using damage data observed in experiments. Given experimental data points in the PEER Structural Performance Database (Berry 2003), column damage states were regressed versus column design parameters using conventional linear regression. The resulting equation can be used to predict the mean (or median) EDP at which a specified level of damage was observed. CDFs can then be developed using an assumption about the statistical variation of the data to describe the probability of exceeding a damage state (DM), given a demand level (EDP). Alternatively, parameterized non-linear regressions may yield more suitable equations for describing the mean relationship between demand and damage. Such equations exist for bar buckling and cover spalling in bridge columns (Berry 2003).

The total probability theorem used to formulate the expression for damage fragility (Equation 3) can be used to convolve the damage model and the demand model. The result is a traditional damage fragility curve that shows the probability of exceeding a damage limit state as a function of ground motion IM. This damage fragility is shown in Figure 1 for the three DM limit states used in the damage model, namely spalling, bar buckling and column failure. Such a set of fragility curves can be immediately used to assess the change in the probability of exceedance of a limit state with the change of ground motion intensity. For example, a design scenario earthquake has an expected intensity of $Sa(T_1) = 1000$ cm/s^2. The probability of spalling is 1.0, but the probability of bar buckling is only 0.88. Similarly, the probability of column failure is slightly less at 0.75.

The component-level damage most directly implies repair cost, a direct cost economic decision variable. Alternatively, repair time could be considered as a decision variable, as it may be a more relevant decision variable for important arteries in a transportation network than repair cost.
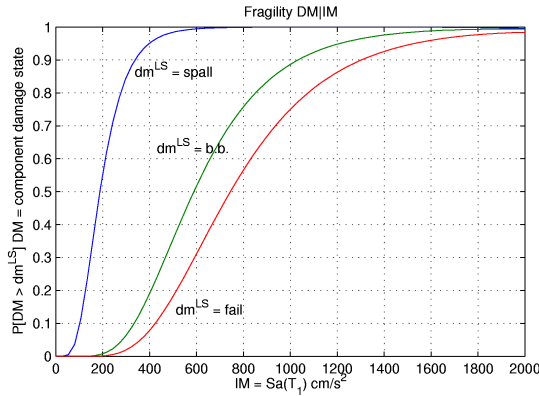
Figure 1. Bridge column damage fragility curves.

From data compiled for the Northridge earthquake for HAZUS, a modified repair cost ratio (RCR) as a function of damage for typical bridges was developed (Basöz 1999). HAZUS damage states of slight, extensive, and complete were assumed to correspond to the DM values of spalling, bar buckling, and column failure, respectively. A relationship between repair cost, normalized by replacement value, and damage is shown in Figure 2. The repair cost ratio is therefore a continuous decision variable (DV) variable, but with discrete input points. By assuming the value of the DM variable is, in fact, the median drift ratio for each damage limit state, it is possible to provide a smooth closed-form function with numerical values on the ordinate. Equation 5 is utilized to produce several decision limit state fragility curves for RCR values expressed as percent of the replacement cost. They are shown in Figure 3.
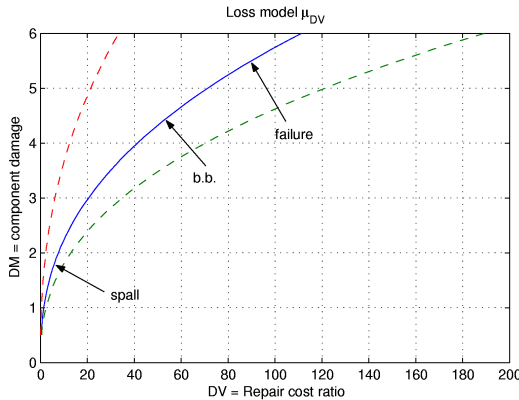
Figure 2. Bridge column repair cost loss model.
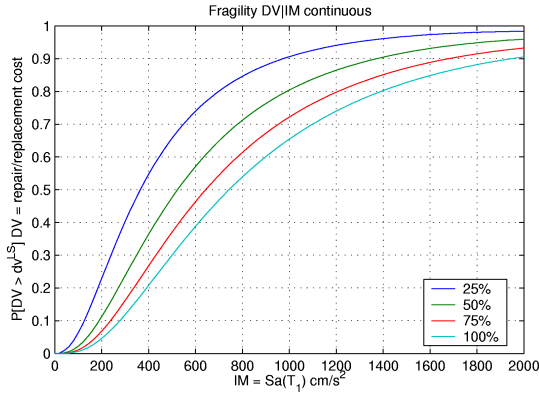
Figure 3. Bridge column component decision fragility curves.

For example, an earthquake with intensity of $Sa(T_1) = 1000$ cm/s^2, there is a 91% probability that the repair cost will exceed 25% of the replacement cost. This probability drops to 65% for exceeding the entire replacement cost. It should be noted that it may not be possible to obtain a complete distribution function if the given discrete damage states do not cover the full range required for the decision variable limit states. Due to the large amount of uncertainty in the loss model and the lack of other DV choices, cost data on other bridge components and assessment of system-level effects for reinforced concrete highway bridges cannot be done without additional research focused on damage assessment and repair cost modeling.

5. BRIDGE-LEVEL DECISION: TRAFFIC FUNCTION

Four methods for predicting post-earthquake damage fragilities from first-shock earthquakes, the corresponding interim models, and interim variables are detailed in Mackie (Mackie 2004b) for damage fragilities. Only a brief summary of each method and their comparison are provided here, followed by extensions from damage to decision fragilities. The loss model, which relates a damage variable to the loss of capacity decision variable, proposed herein, is shown Figure 4.

5.1 Method A: Direct Method

The direct method is an application of the PEER framework (Equation 5) directly to bridge-level interim models. Therefore, the approach is the same as the one use for component-level decisions: Equation 5 is evaluated numerically for a range of IM, EDP, DM and DV values to produce the DV fragility surface of Figure 5. The fragility surface is a convenient method of visualizing numerous decision limit states on the same plot. Each black line on the surface is a single DV fragility curve. The

major drawback of this method when applied to bridge-level decisions is a large model error. This results in low confidence (large dispersion) in predicting the median relationship between engineering response and earthquake intensity. This uncertainty is propagated through the subsequent models and results in a significant lack of confidence in the damage and decision fragilities.
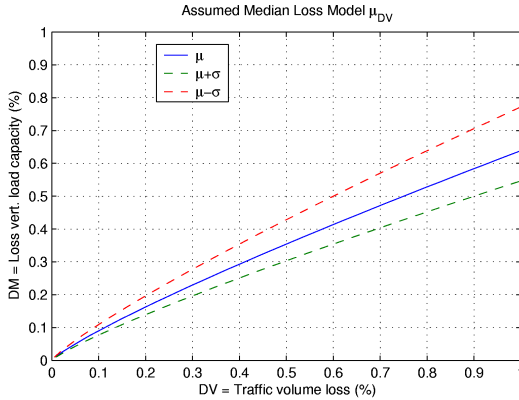
Figure 4. Bridge load-carrying capacity loss model.
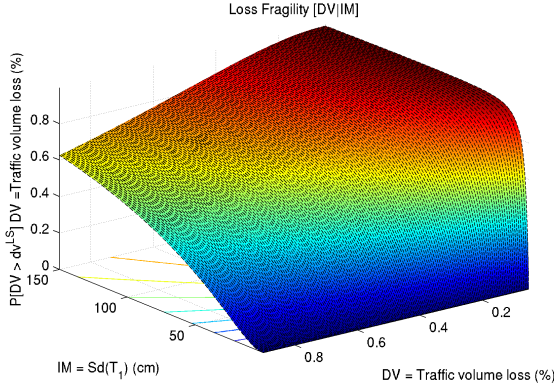
Figure 5. Decision fragility surface generated using the direct method.

Other shortcomings are also apparent: there is a large jump in probabilities of exceedance a DV for small IM values. This is not realistic, as it is expected that damage would start to accumulate only at higher earthquake intensities, not during the elastic response of the bridge. Nevertheless, as these bridge-level models are derived by direct application of the PEER framework, they are useful as benchmarks.

5.2   Method B: MDOF Residual Displacement Method

This method introduces residual displacement U_{res} as an intermediate response parameter to improve the PSDM relating bridge-level engineering response parameters and earthquake intensity (IM). Analytical simulations were then used to relate residual displacement of the bridge and its vertical and horizontal load carrying capacity degradation due to a combination of material and geometric nonlinearities. The resulting DV fragility formulation is shown in Equation 6.

$$P[DV|IM] = \iiint P[DV|DM] \, dP[DM|EDP] \, dP[EDP|U_{res}] \, dP[U_{res}|IM] \qquad (6)$$

Once again, it is assumed that the EDP can be conditioned solely on U_{res}, without any additional IM information. While there is lower uncertainty in the $EDP|U_{res}$ correlation, this method also suffers from large model error due to the large uncertainty in the residual displacement demand model. However, it does provide a more realistic prediction of the onset of bridge-level damage. Comparison between all four methods for a DV limit state of 25% traffic volume loss is shown in Figure 6.

5.3   Method C: SDOF Residual Displacement Method

This method is equivalent to Method B, except the residual displacements are obtained from residual displacement spectra (Kawashima et al., 1998) rather than analysis of actual bridge models. This method was affected to reduce the uncertainty in the residual displacement demand model. The single-degree-of-freedom (SDOF) oscillator properties were selected based on the initial elastic period of the bridge and an R-factor obtained from demand model simulations. While the method does result in slightly reduced uncertainty, the median prediction is largely dependent on the selection of SDOF oscillator properties.

5.4   Method D: EDP Conditioning Method

In an attempt to further reduce the interim uncertainty (model error), maximum displacement U_{max} is introduced and correlated with residual displacement U_{res}. This is achieved by integrating over maximum displacement and residual displacement in the third term of Equation 5. The expanded third term is shown in Equation 7. Application of Equation 7 requires the EDP to be conditioned on U_{res} only (no U_{max} information), and U_{res} to be conditioned on U_{max} only (no IM information). This was verified by showing that dependence of the residuals on U_{max} and IM, respectively, is small.

$$P[EDP|IM] = \iint P[EDP|U_{res}] \, dP[U_{res}|U_{max}] \, dP[U_{max}|IM] \qquad (7)$$

An efficient demand model relating maximum displacement U_{max} (or drift ratio) and $Sa(T_1)$ is used in the last term of the kern in Equation 7. The middle term in Equation 7 is derived using simulation (Mackie 2004b). The first kern term in Equation 7 was computed in Method B. Using a DV limit state of 25% of traffic volume reduction, the four methods are compared in Figure 6. The values of ζ, the lognormal parameter that describes the dispersion of the model, of the four methods are 0.96, 0.80, 0.73, and 0.46, respectively. Therefore, while even Method D has fairly high uncertainty, its prediction of the median value is better than the direct application of Equation 5.
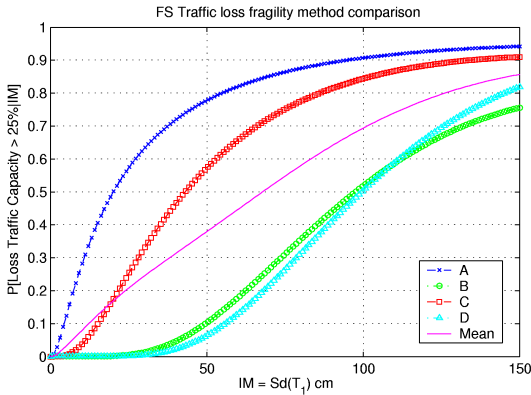
Figure 6. Comparison of Methods A through D for decision fragilities.

6. COLLAPSE-RELATED DECISION

The collapse-prevention limit state used in this paper is a combination of the loss of lateral and vertical load capacity limit states shown in Table 1 (Mackie 2004a). A bridge would be considered closed, i.e., in collapse-prevention limit state, if the lateral load carrying capacity had been reduced by 25% or the vertical load carrying capacity had been reduced by 50%. Thus, the remaining traffic volume crossing this bridge is zero. These values are used as an example and will be changed once more data becomes available. The damage fragility surfaces lateral (longitudinal) and vertical directions are presented in (Mackie 2004b). For the purposes of this example, the direct method (Method A) was used in order to maintain consistency between the lateral and vertical directions. Both of the limit states are plotted in Figure 7 along with the probability of closure, defined as the union of the two damage limit states.

The probability of the union was approximated as a series system with the correlation coefficient computed using the response load carrying data for the lateral and vertical directions. As would be expected, the correlation ($\rho = 0.85$) between vertical and lateral loss of load carrying capacity is high. The probability was

calculated using a 2 dimensional multi-normal CDF. Only 2 damage limit states were chosen to allow closed form integration of this CDF; however, it may be of further benefit to describe collapse in terms of both the loss of lateral and vertical load carrying capacity and the residual displacement of the bridge piers.

Table 1. Bridge performance level table: proposed values for limit states

Objective name	Traffic capacity remaining (volume)	Loss of lateral load carrying capacity	Loss of vertical load carrying capacity
Immediate access	100%	< 2%	< 5%
Weight restriction	75%	< 2%	< 10%
One lane open only	50%	< 5%	< 25%
Emergency access only	25%	< 20%	< 50%
Closed	0%	> 20%	> 50%
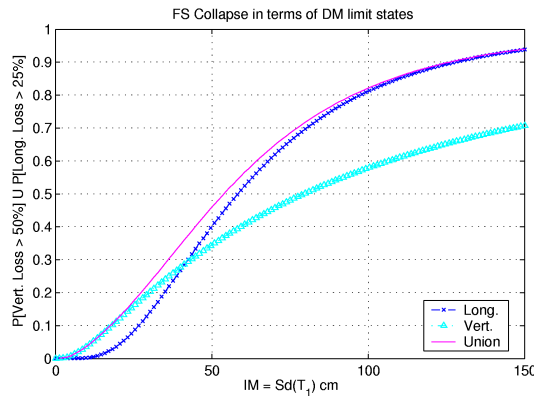
Figure 7. Collapse-prevention limit state fragility curves.

7. CONCLUSIONS

An engineering basis for quantitatively evaluating the ability of a typical highway bridge to function after an earthquake was presented in this paper for three limit states: repair cost, traffic function, and collapse-prevention. The PEER framework was utilized to cast these limit states in terms of damage and decision fragility curves. For the repair cost limit state, component-level (column) damage and loss data was used in a direct application of the PEER integral. However, for the bridge-level traffic function limit state, several methods of obtaining the decision fragilities were introduced, the best method using EDP conditioning. Finally, an example of combining damage limit states to define the collapse-prevention limit state was presented. The resulting fragility curves for all limit states can be used by engineers

and decision-makers to assess the performance of a typical highway bridge in a given earthquake scenario, and evaluate the changes in bridge performance under varying earthquake intensity scenarios. Ongoing research is focused on refining the values of decision variables using feedback from bridge engineers and additional analytical studies.

ACKNOWLEDGEMENTS

REFERENCES

Baker, J. W., and C. A. Cornell. (2003). Uncertainty specification and propagation for loss estimation using FOSM methods. *PEER Report 2003/07, University of California, Berkeley*.

Basöz N., and A. S. Kiremidjian. (1997). Evaluation of bridge damage data from the Loma Prieta and Northridge, CA earthquakes. *Report No. 127, John A. Blume Earthquake Engineering Center, Stanford, California.*

Basöz N., and J. Mander (1999). *Enhancement of the highway transportation lifeline module in HAZUS*. Washington: National Institute of Building Sciences.

Berry, M. P., and M. O. Eberhard (2003). Performance models for flexural damage in reinforced concrete columns. *PEER Report*. Submitted for publication.

Kawashima K., G. A. MacRae, J. Hoshikuma, K. K. Nagaya. (1998) Residual displacement response spectrum. *Journal of Structural Engineering*; 124(5): 523–530.

Mackie, K., and B. Stojadinović. (2003). Seismic demands for performance-based design of bridges. *PEER Report*. Submitted for publication.

Mackie, K., and B. Stojadinović. (2004a). Fragility curves for reinforced concrete highway overpass bridges. *Proceedings 13th World Conference on Earthquake Engineering* Paper no. 1553. Submitted for publication.

Mackie, K., and B. Stojadinović. (2004b). Residual displacement and post earthquake capacity of highway bridges. *Proceedings 13th World Conference on Earthquake Engineering* Paper no. 1550. Submitted for publication.

MODELING CONSIDERATIONS IN PROBABILISTIC PERFORMANCE BASED SEISMIC EVALUATION OF HIGHWAY BRIDGES

Sashi K. KUNNATH[1] and Leah I. LARSON[2]

ABSTRACT

Limitations associated with deterministic methods to quantify demands and develop rational acceptance criteria have led to the emergence of probabilistic procedures in performance-based seismic engineering (PBSE). The Pacific Earthquake Engineering Research (PEER) performance-based methodology is one such approach. In this paper, the impact of certain modeling decisions made at different stages of the evaluation process is examined. Modeling, in the context of this paper, covers hazard modeling, structural modeling, damage modeling and loss modeling. The specific application considered in this study is a section of an existing viaduct in California: the I-880 interstate highway. Several simulation models of the viaduct are developed, a series of nonlinear time history analyses are carried out to predict demands, measures of damage are evaluated and the closure probability of the viaduct is estimated for the specified hazard at the site. Results indicate that the assessment is particularly sensitive to the dispersion in the demand estimation, which in turn is influenced by the ground motion scaling procedure.

Keywords: Bridge; Fragility functions; Nonlinear time-history analysis; Performance-based seismic engineering; Seismic evaluation; Soil-foundation interaction.

1. INTRODUCTION

Early attempts in probabilistic seismic evaluation can be traced to the development and application of fragility curves. A formal implementation utilizing a probabilistic approach in seismic evaluation and design materialized with FEMA-350 (2000). The PEER performance-based framework may be regarded as an extension and an enhancement of the procedure developed for FEMA-350 (Cornell et al., 2002). A conceptual description of the methodology, based on the total probability theorem, is expressed as follows:

$$\nu(\,DV\,) = \iint G(\,DV\,/\,DM\,)\,dG(\,DM\,/\,EDP\,)\,dG(\,EDP\,/\,IM\,)\,d\lambda(\,IM\,) \qquad (1)$$

[1] *Professor, Civil & Environmental Engineering, University of California, Davis, CA 95616*

[2] *Graduate Student, Civil & Environmental Engineering, University of California, Davis, CA 95616*

where $\nu(DV)$ is the probabilistic description of the decision variable (for example, the annual rate of exceeding a certain repair cost), *DM* represents the damage measure, *EDP* represents the engineering demand parameter (drift, plastic rotation, etc.) and *IM* represents the intensity measure (characterizing the hazard). The expression of the form *P(A/B)* is essentially a cumulative distribution function or the conditional probability that *A* exceeds a specified limit for a given value of *B*. The terms that appear in the above equation can be deaggregated using the total probability theorem that assumes that each operation is mutually independent. One useful application of Equation (1) is to derive the mean annual probability of exceeding a DV given an IM.

While probabilistic methods offer distinct advantages over deterministic approaches, it is important to be cognizant of the assumptions that underlie the framework. A closer look at the PEER methodology indicates that the resulting evaluation is a function of four separate modeling tasks: hazard, demand, damage and decision-making. Suppositions and simplifications are often introduced at various modeling phases that can impact the final outcome of the assessment. This paper attempts to investigate the sensitivity of modeling assumptions introduced at different stages of a performance-based evaluation using the PEER framework.

2. APPLICATION OF THE PEER METHODOLOGY TO AN EXISTING VIADUCT IN CALIFORNIA

The expected seismic performance of a section of the I-880 viaduct constructed in the mid-1990s as part of the California Department of Transportations (CALTRANS) Cypress Replacement Project in Oakland, California, is evaluated using the PEER PBSE framework. The specific issues investigated include: modeling of the site hazard and issues related to scaling the ground motions; modeling of the system, the level of detail that is needed to establish reliable estimates of performance, and issues related to soil-foundation-structure interaction (SFSI) and P-delta effects; considerations in damage modeling; and finally, the significance of subjective decisions made by bridge inspectors in post-earthquake reconnaissance.

2.1   Description of the Viaduct

The rebuilt segment of the I-880 (Figure 1) is a seven-frame structure consisting of 26 spans and a total length of approximately 1140 m. The site is located within 7-8 km of the Hayward Fault. The soils on the site near the San Francisco Bay consist of dense fill, Bay mud and sand, covering deep clay deposits. The superstructure is composed of 7 cast-in place reinforced concrete box girders, approximately 21.8 m wide, 2.0 m tall and 0.3 m in depth. All columns of the viaduct have rectangular cross-sections with circular reinforcement. While a majority of the columns have continuous moment connections at the column-deck and column-pile-cap region, some bents have pinned connections at either the column-pile-cap or column-deck

location. Transverse reinforcement consists of #8 (25 mm diameter) hoops at 100 mm center-to-center spacing for all columns. Longitudinal reinforcement consists of varying numbers of #14 (45 mm) bars arranged in 5 different configurations.
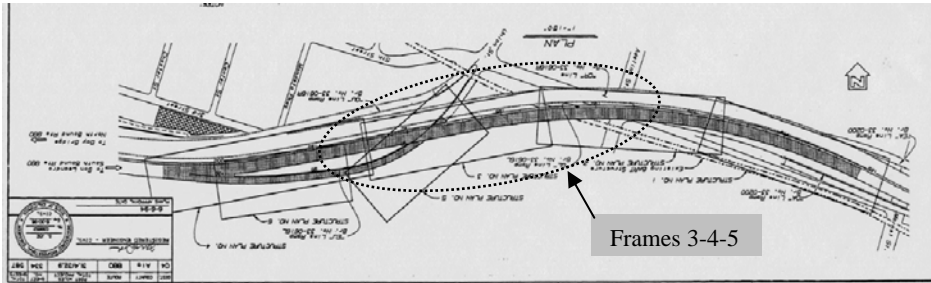
Frames 3-4-5

Figure 1. Plan view of the rebuilt I-880 viaduct.

2.2 Modeling the Viaduct

Two models were developed for the simulation studies: (i) a model comprising three inter-connected frames (denoted in Figure 1 as Frames 3-4-5) which incorporates connection elements at the hinge region between two adjacent frames; and (ii) a simple model of a single bent that was identified as the region of maximum demand in the three-frame model. The three-frame, 11-bent model, shown in Figure 2, was originally prepared by Bauer (2003).
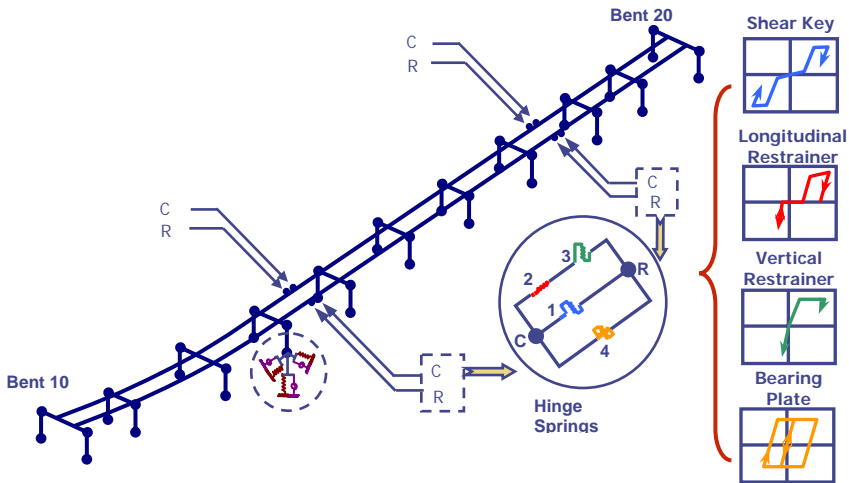
Figure 2. Simulation model of the I-880 viaduct.

Each bent, comprised of two columns joined by a single cap beam, is connected to the adjacent bents by a deck system that is assumed to remain elastic. Expansion joints between the frames, shown as C and R in the figure to denote a "Restrained" node and a "Constrained" node, are modeled using zero-length inelastic springs. Each hinge connection is composed of four springs representing the shear key, the longitudinal restrainer, the vertical restrainer, and the bearing plate. The properties of the longitudinal restrainer also model frame-to-frame impact in the compression direction of the spring following gap closure. The foundation system, consisting of 5x5 pile groups, was modeled by three translational and three rotational springs. The spring properties were derived from separate 3D finite element analyses of the soil-foundation system. Details of the model are reported in Bauer (2003).

3. PERFORMANCE-BASED EVALUATION PROCEDURE

The goal of the evaluation is to establish the closure probability of the viaduct for the expected hazard at the site. As is evident from Equation (1), the evaluation entails four independent modeling tasks beginning with the selection of earthquake records to characterize the site hazard and ending with the evaluation of the mean annual probability of closing the bridge.

3.1 Ground Motions, Hazard Curve and Intensity Measure (IM)

Uniform hazard spectra for S_D (soil) site conditions were developed by Somerville and Collins (2002) for the bridge site corresponding to three hazard levels: events with a 50%, 10% and 2% probability of being exceeded in 50 years (shown on the left in Figure 3). The spectra were generated for both strike-parallel (SP) and strike-normal (SN) directions. Several earthquake records with the required magnitude-distance combinations from strike-slip earthquakes were then selected. The components in the strike normal (SN) directions of each of these records were scaled so that the spectral acceleration at the natural period matches the corresponding value at the same period on the hazard spectra. The scale factor obtained for the SN direction is also used for the SP direction to preserve the relative scaling between all components of the recording. The intensity measure (IM) that was selected for the study is the 5% damped elastic spectral acceleration at the characteristic period of the structure. Selected ground motions are then scaled to this IM. The seismic hazard curve (also shown in Figure 3) was derived by plotting the return periods against the magnitude of the spectral accelerations at the characteristic structural period. The hazard curve can be approximated as a linear function on a log-log scale. To characterize the hazard curves, it is necessary to find the slope of the best-fit line through the logarithm of the three values characterized by coefficients k and k_0. The hazard curve is approximated by:

$$v(S_a) = k_0 (S_a)^{-k} \tag{2}$$
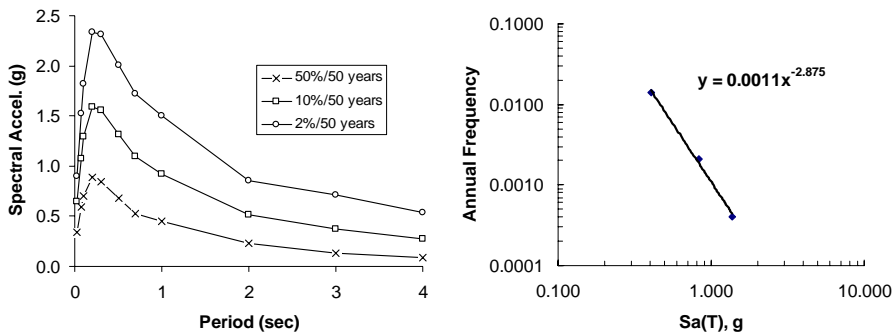
Figure 3. Uniform hazard spectra in fault-normal direction for the I-880 site and resulting hazard curve.

3.2   Seismic Demand (EDP Estimation)

All simulations were carried out using OpenSees (2004). Numerous demand measures can be monitored during the seismic response analysis, however, the eventual choice is influenced by the damage models that are available to correlate the EDPs to different damage states. In this study, the peak tangential drift of the individual columns was selected as the primary EDP measure.   This was dictated by the availability of damage measures and corresponding decision variables as indicated in the next two sections. Once the seismic demand parameters are computed, a best-fit curve through the median of the natural logarithm of the simulations is determined assuming a lognormal distribution, as follows:

$$EDP = a(S_a)^b \tag{3}$$

A typical set of simulations and the resulting curve-fit is displayed in Figure 4.
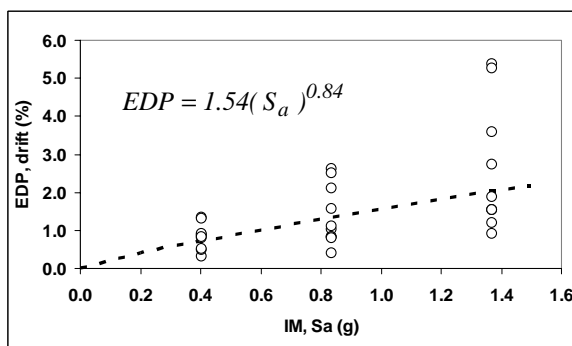
Figure 4. Typical set of simulations resulting in EDP-IM relationship.

69

3.3 Damage Modeling and Damage Measure (DM)

Based on work carried out at the University of Washington (Berry and Eberhard, 2003), the two damage measures considered in this study are the onset of concrete spalling and reinforcing bar buckling. Spalling of the concrete cover is an important damage measure because it represents the first flexural damage states wherein the repair costs may be significant. The onset of buckling of longitudinal reinforcing bars is another critical damage state because it significantly reduces the structure's functionality and has implications for structural safety. Based on extensive statistical analysis of experimental data, Berry and Eberhard proposed two fragility functions (shown on the left in Figure 5) that describe the probability of achieving these damage states given a seismic demand in terms of the tangential drift in the column.
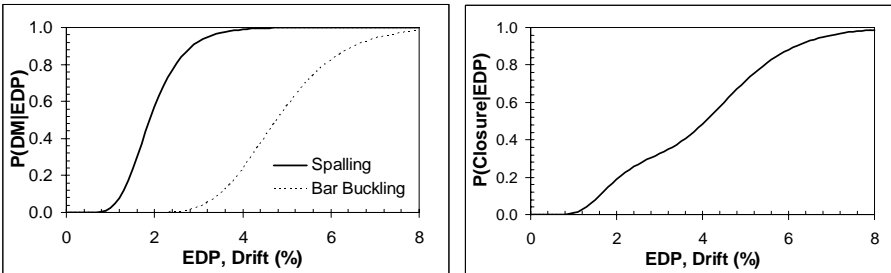
Figure 5. Likelihood of damage and closure probability as a function of EDP.

3.4 Decision Variable (DV)

Porter (2004) conducted a survey (Table 1) of a small group of bridge inspectors from departments of transportation across the country to determine how decisions on bridge closure are made. The respondents self-rated their expertise as 4 or 5 (on a 5 point scale) in responding to questions.

Table 1. Sample section of survey

Decision → Damage	No closure	Close 1-3 days	Close > 3days	Open with reduced speed
Horizontal offset at joint	< ½ in ½ - 1 in > 1 in	< ½ in ½ - 1 in > 1 in	< ½ in ½ - 1 in > 1 in	< ½ in ½ - 1 in > 1 in
Concrete Spalling	No Yes	No Yes	No Yes	No Yes
Bar Buckling	No Yes	No Yes	No Yes	No Yes

Results indicate that 33% of the respondents would likely close the bridge at least briefly (> 1 day) if they observed spalling. This figure increased to 100% for bar buckling. The data yield the following discrete probabilities:

$P(DV|Spalling = True) = 0.33$
$P(DV|Bar\ Buckling = True) = 1.00$

The fragility functions used to develop $P(DM/EDP)$ shown in Figure 5 can now be combined with the above discrete probabilities to determine the probability of closing the bridge given a demand estimate, as follows:

$$P(DV\mid EDP) = \int_{-\infty}^{\infty} P(DV\mid EDP)dP(EDP) = \sum_{i=1}^{2} P(DV\mid DM)P(DM\mid EDP) \quad (4)$$

The resulting probability distribution is also shown on the right in Figure 5. One final step remains. This involves integrating the seismic hazard curve into Equation (4). But before incorporating the hazard curve into the picture, it is necessary to find the probability of obtaining a dv given the EDPs resulting from a set of IMs (in a non-annual frequency format) (to distinguish between IM and dλIM):

$$P(DV > dv \mid IM) = \int_{0}^{\infty} P(DV\mid EDP)\left|\frac{dP(EDP\mid IM)}{dEDP}\right|dEDP \quad (5)$$

$P(EDP/IM)$ is evaluated assuming a lognormal distribution:

$$P(EDP > edp \mid IM = im) = 1 - \Phi\left(\frac{ln\left(\frac{edp}{a(im)^b}\right)}{\sigma_{ln\,edp\mid im}}\right) \quad (6)$$

Using the total probability theorem, the probability of closure given the seismic hazard curve implies:

$$P(DV > dv \mid \lambda IM) = \int_{0}^{\infty} P(DV > dv \mid IM)\left|\frac{dv(IM)}{dIM}\right|dIM \quad (7)$$

Equation (7) is evaluated numerically to obtain the annual probability of closure. The probability of closure in n ($n=50$) years is given by

$$P = 1 - (1 - P(DV > dv))^n \quad (8)$$

4. IMPACT OF MODELING DECISIONS

The probabilistic methodology outlined in the previous section is applied in the evaluation of the simulation model of the I-880 viaduct. EDPs were computed for ten ground motions for each hazard level. The EDP vs. IM relationship, as shown in Figure 4, was established for each variation of a model variable. The $P(DV/IM)$

distribution was then established for each set of simulations using the procedure discussed in Section 3. In general, the viaduct performed extremely well, with closure probabilities less than 1% in 50 years for all cases. The objective of the study, however, is to examine the consequences of model variations. The impact of assumptions made during the modeling phase of the evaluation is discussed in the remainder of this section.

4.1 Issues Related to Modeling

In this phase of the evaluation, the level of model detail is investigated. The median peak response of a critical bent (defined as the bent experiencing the maximum lateral drift) using the three-frame model is compared to the same response when a single frame model of the same bent is analyzed. Figure 6 indicates that the variation of demand with Intensity Measure (IM) is generally unaffected as is the probability of closure. When the hazard curve is integrated into the above distributions, the closure probability in 50 years for the multiple bent model is 0.95% and 0.46% for the single bent model. The difference appears to be significant but only because the maximum spectral acceleration for the 2%/50 year hazard is 1.4g which represents the initial tail of the distribution. The difference between the two closure probabilities is relatively insignificant for larger spectral magnitudes.
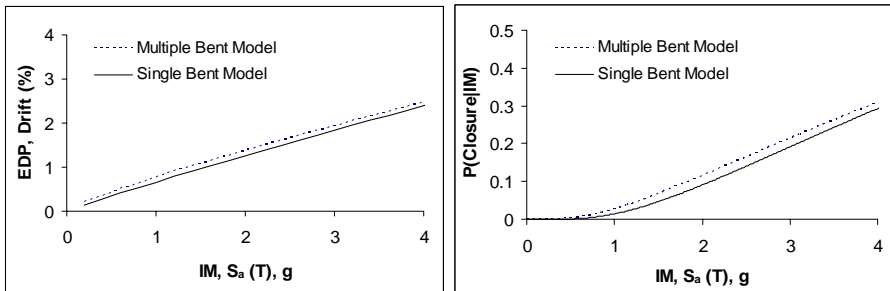
Figure 6. EDP-IM relationship and P(DV) for different system models.

4.1.1 P-Delta Effects

The single bent model was evaluated separately for P-delta effects. The difference in peak response for the model with and without P-delta effects was insignificant, as shown on the left in Figure 7. Axial forces on bridge columns tend to be quite low and most of the maximum drifts were 2% or less. Given this negligible variation, the closure probabilities of the two models were not further investigated.

4.1.2 Elastic vs. Inelastic Models

Figure 7 (right) also shows the difference between linear and nonlinear responses of the multiple frame model. In some cases, particularly for the 2%/50 year records, the variation is significant. However, for practical purposes, the differences are small enough to be ignored. The elastic model is based on effective stiffness properties (40% of initial stiffness for columns and 60% of initial stiffness for beams). The EDP-IM relationship and P(DV) distribution for the two cases are displayed in Figure 8. The results suggest that a simplified elastic model with effective stiffness properties is a reasonable approach to modeling such systems that are flexurally dominant and flexible (initial period greater than 0.5 seconds). When the hazard curve is integrated, the closure probability in 50 years for the nonlinear model is 0.95% and 0.85% for the linear model.
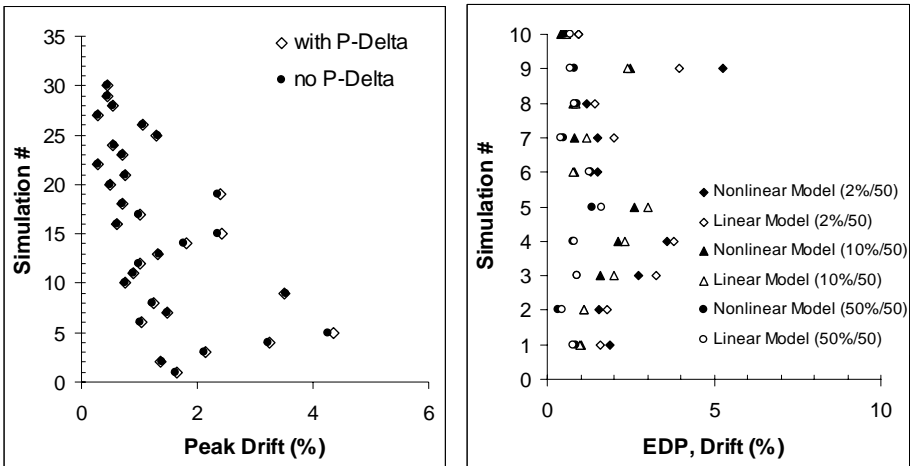
Figure 7. Effect of modeling details on peak system response.
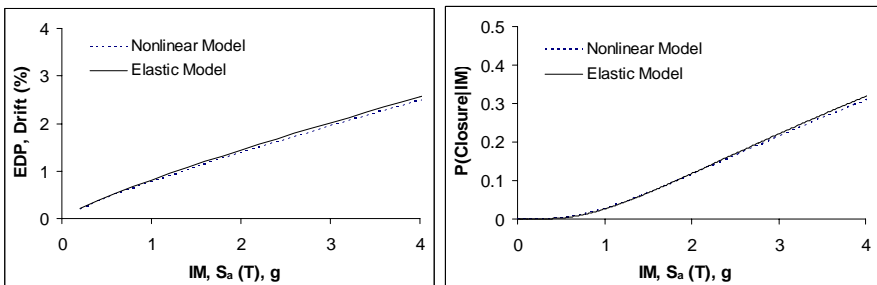
Figure 8. EDP-IM relationship and P(DV) for different member models.

4.1.3 Soil-Foundation-Structure Interaction (SFSI) Effects

The flexibility of the soil-foundation system was found to play a significant role in the response of the viaduct. Neglecting SFSI effects can result in a vastly different assessment of the bridge performance. As shown in Figure 9 the closure probability varies significantly depending on whether SFSI effects were incorporated or ignored. The likelihood of bridge closure in a 50-year period decreases by a factor of 5 (from 0.95% to 0.19%) if soil-foundation flexibility is disregarded.
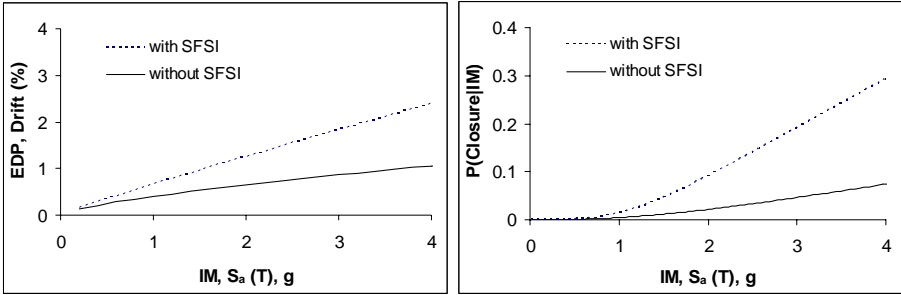
Figure 9. Effect of SFSI on EDP-IM relationship and P(DV).

4.2   Issues Related to Scaling and Transforming Ground Motions

Since the hazard curve is a function of the uniform hazard spectra, the process of scaling and transforming records can have a significant impact on the evaluation. Figure 9 shows the spectra of the original records, and the spectra after scaling and after transforming the fault normal records to the transverse direction of the bent. Since the transformation process alters the spectra and the magnitude at the characteristic period, the resulting peak responses exhibit larger dispersions.
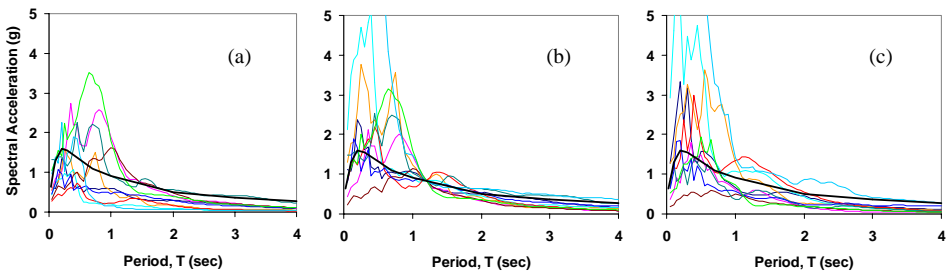
Figure 10. Effect of record transformation on spectral demand: (a) original records; (b) scaled to characteristic period; (c) transformed records.

The increased dispersion leads to higher closure probabilities. The effects of transforming ground motions and the effects of increased dispersion are confirmed in Figures 11–12. In Figure 12, the influence of scaling ground motions to a different characteristic period is demonstrated. Scaling the records at T=0.6s results in increased demands and dispersion leading to higher closure probabilities. For example, the probability of closure in 50 years based on the evaluation using records scaled at T=1.2 seconds was previously reported to be 0.46% for the single bent model. When the records are scaled at T = 0.6 seconds instead, the probability increases to 1.69%. Additionally, if the dispersion in the latter case is assumed to increase from 0.614 to 0.75, the probability of closure becomes 2.95%.
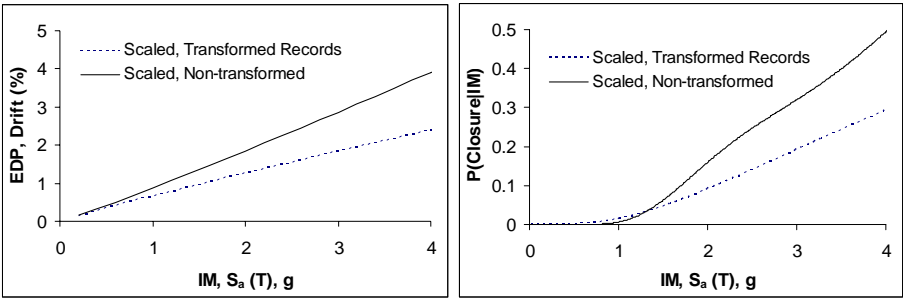
Figure 11. Effect of scaling and transformation on EDP-IM and P(DV).
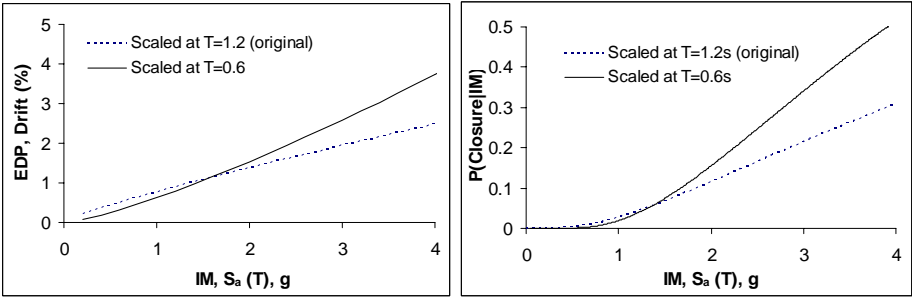
Figure 12. Effect of hazard curve and response dispersion on EDP-IM relationship and P(DV|IM).

The choice of the characteristic period at which the ground motion scaling is carried out presents certain challenges. For example, the initial period of the fixed-base model of the viaduct is in fact 0.6 seconds. The initial period of the model with soil-foundation springs increases to about 0.8 seconds for the single bent model. The value of T = 1.2 seconds corresponds to the system with effective stiffness properties.

The closure probability is significantly influenced by the dispersion and demands resulting from the choice of the period at which the ground motions are scaled.

5. FINDINGS AND CONCLUSIONS

The estimated closure probabilities for all cases investigated in this study were quite small. Hence, the effects of model variations were not immediately apparent though the order of difference in the closure probabilities was considerable in some cases. Closure probabilities are controlled by the following factors: (i) the selected characteristic period of the model, since ground motions need to be scaled to the spectral magnitude of the hazard spectra at this period — changes in the spectral ordinates change the coefficients that appear in Equations 2 and 3 and are carried throughout the evaluation process; (ii) the dispersion of the response estimates — larger dispersions lead to larger estimates of damage; and (iii) the decision variables relating damage to closure — if decisions are not made rationally and consistent with the degree of damage, then the integrity of the entire evaluation process can be compromised.

ACKNOWLEDGEMENTS

REFERENCES

Bauer. (2003). *Simulation Models for the Nonlinear Seismic Response of the I-880 Viaduct.* M.S. Thesis, Department of Civil and Environmental Engineering, University of California, Davis.

Berry, M., and M. Eberhard. (2003). "Column Deformation Demands at Bar Buckling," ASCE Structures Congress, Seattle.

Cornell, C. A., F. Jalayer, R. O. Hamburger, and D. A. Foutch. (2002). "Probabilistic Basis for 200 SAC Federal Emergency Management Agency Steel Moment Frame Guidelines." *ASCE Journal of Structural Engineering*, 128 (4), 526–533.

FEMA-350. (2000). *Recommended Seismic Design Criteria for New Steel Moment-Frame Buildings*. Developed by the SAC Joint Venture for the Federal Emergency Management Agency, Washington D.C.

OpenSees. (2004). "Open System for Earthquake Engineering Simulation." http://opensees.berkeley.edu.

Porter, K. (2004). "A Survey of Bridge Practitioners to Relate Damage to Closure." California Institute of Technology, unpublished report.

Somerville, P., and N. Collins. (2002). "Ground Motion Time Histories for the I880 Bridge, Oakland." URS Corporation, Pasadena, CA.

AN ANALYSIS ON THE SEISMIC PERFORMANCE LEVELS OF BRIDGES

Kazuhiko KAWASHIMA[1]

ABSTRACT

This paper presents an analysis on the seismic performance criteria and levels of bridges based on a questionnaire survey to 100 civil engineers. Analysis is presented for design criteria, period and cost of repair, expectation and problems, and analytical tools in the performance-based seismic design.

Keywords: Performance-based design; Seismic design; Bridges; Performance criteria; Analytical tools; Seismic damage.

INTRODUCTION

In seismic design of bridges, it is important to have clear seismic performance criteria. The basic concept of seismic design philosophy and performance criteria is more or less similar among the current codes worldwide. For small-to-moderate earthquakes bridges should be resisted within the elastic range of the structural components without significant damage, and bridges exposed to shaking from large earthquakes should not cause collapse. The performance requirements depend on the importance of bridges.

For example, Table 1 shows the performance criteria and performance matrix of bridges in Japan (JRA 2002). Function evaluation ground motions and safety evaluation ground motions are considered under the 2 level seismic design. Middle-field ground motions generated by earthquakes with magnitude of about 8 (Type-I ground motions) and near-field ground motions generated by earthquakes with magnitude of about 7 (Type-II ground motions) are used. The seismic performance is classified in terms of safety, function and reparability.

However the expression in the performance criteria and goals is general and vague. For example, what does "maintain safety for collapse" mean? Is it allowed that bridges cannot be repaired after an earthquake if only collapse can be avoided, or should damage be within a certain level so that bridges can be repaired? What "retain function in a short time after an earthquake" means? How shortly the damaged bridge should be repaired?

---

[1] *Professor, Department of Civil Engineering, Tokyo Inst. of Technology, Tokyo, Japan, Email: kawasima@cv.titech.ac.jp*

Table 1. Seismic performance goals

(a) Seismic performance goals

Design Ground Motions		Standard Bridges	Important Bridges
Function Evaluation		SP-1	
Safety Evaluation	Type-I (Middle field)	SP-3	SP-2
	Type-II (Near-field)		

(b) Seismic performance levels

Performance Levels	Safety	Function	Reparability	
			Short term (Emergency)	Long term
SP-1: Functional	Maintain safety for collapse	Keep function	No emergent repair is required	Only minor repair
SP-2: Limited damage	Maintain safety for collapse	Regain function in a short time after an earthquake	Emergent repair can regain function	Permanent repair without difficulty
SP-3: Prevent critical damage	Maintain safety for collapse	-	-	-

In reality there is a variety of demands on the seismic performance goals and levels by filed engineers. For example, they sometimes request to build bridges so that at least central few lanes can be functional under a certain velocity control for heavy emergent traffic to transport medical equipments and foods within 48 hours after an earthquake.

A survey was conducted in the Research Committee on Performance-based Seismic Design of Structures, Japan Association for Earthquake Engineering to evaluate the current understanding of civil engineers on the seismic performance criteria and goals. This paper introduces a part of the analysis on the seismic performance criteria and goals surveyed by a questionnaire survey.

QUESTIONNAIRE SURVEY

A questionnaire survey was conducted in September 2003 for 21 items on the performance-based seismic design, including the design philosophy and performance criteria, expected and actual periods for repair, initial construction and repair costs, expectation and problems of the performance-based seismic design, and analytical methods and tools. The survey was delivered by e-mails to civil engineers (20-60 years old) in governmental organizations, consultants, general contractors, bridge fabricators, and academic. Replies were obtained from 100 civil engineers. This survey aimed of collecting current practice and understanding on design philosophy and requirements, and did not intend to evaluate statistical-basis evaluation.

The survey stood on the condition that destructive damage occurred by a damaging earthquake in an urban area with over several thousands victims as well as seriously deteriorated functions in a wide range of area and facilities resulted by extensive damage of buildings, transportation facilities and utility facilities. The questions were directed to standard bridges, excluding special long bridges.

SEISMIC PERFORMANCE LEVELS

One of the most important decisions in design is the levels of seismic performance. Six goals and levels as shown in Table 2 were shown to engineers to select two per engineer. Since there were engineers who did not reply or replied only one level, those were classified "no answer" in Table 2. Number of replies as well as cross correlation with the experience of 1995 Kobe earthquake, which will be described later, are presented in Table 2.

Among six levels, Level 1 and Level 2 are a pair of questions. Level 2 intends that "it is allowed for engineers to design bridges so that collapse can be avoided no matter how extensive damage which results in long suspension of traffic occurs because it is not economically feasible to design bridges so that they do not suffer damage under a rare earthquake such as the Kobe earthquake." On the other hand, Level 1 intends that "since the roads and railways are essential infrastructures in urban areas, socio-economic damage (indirect damage) resulted by bridges damage must be extensively larger than the direct damage. Furthermore, it takes weeks even to arrange materials and human resources once an urban area is extensively deteriorated by an earthquake. Therefore it is required to design bridges so that they do not suffer extensive damage to an extent that they require emergency repair even under a rare earthquake such as the Kobe earthquake."

Excluding "no answer" (23.5%), Level 2 had the highest support of 23% from the engineers. This may be reasonable because Level 2 is now widely accepted in the engineering community worldwide. On the other hand, Level 1 had support of 14.5%. It is noted that the higher level of seismic performance in Level 1 had support of nearly 2/3 of the support of Level 2.

It is interesting to note that the support rate of Levels 1 and 2 depends on whether they experienced 1995 Kobe earthquake or not. If one classifies 100 engineers into two groups, i.e., the group who experienced Kobe earthquake (personally experienced the Kobe earthquake, involved in rescue and repair, or involved in design and analysis of damage bridges) and the group who did not experience Kobe earthquake, the support ratio for Level 1 was 17.9% in the group who experienced the Kobe earthquake, but it was only 10.6% in the group who did not experience the Kobe earthquake. This may be regarded that the engineers who have experienced Kobe earthquake intend to set higher seismic performance level than the group who did not experience Kobe earthquake.

The second highest support (15%) was directed to Level 6, i.e., "the seismic performance level depends on the amount of investment. However it is civil engineers

Table 2. Seismic performance goals

Choose two among the following six goals which are close to your professional opinion on the seismic performance levels	(1) Experienced the Kobe earthquake	(2) No experience to Kobe earthquake	(3) Total
(1) Since the roads and railways are essential infrastructures in urban areas, socio-economic damage (indirect damage) resulted by damage of bridges must be extensively larger than the direct damage. Furthermore, it takes several weeks even to arrange materials and human resources once an urban area is extensively deteriorated by an earthquake. Therefore it is required to design bridges so that they do not suffer extensive damage in an extend that they require emergency repair even under the Kobe earthquake.	19(17.9%)	10(10.6%)	29(14.5%)
(2) It is not economically feasible to design bridges so that they do not suffer damage under a rare earthquake such as the Kobe earthquake. It must be thus allowed for engineers to design bridges so that collapse can be avoided no matter how extensive damage which results in long term suspension of traffic occurs. Saving lives must be the goal.	25(23.6%)	19(20.2%)	46(23.0%)
(3) It is not meaningful for bridges to be functional when an urban area is extensively and widely deteriorated. Consequently, Sustaining extensive damage on bridges is acceptable.	2 (1.9%)	3 (3.2%)	5 (2.5%)
(4) Criticism was raised by public after the 1995 Kobe earthquake on the collapse of bridges. Public expects that bridges are so designed that they do not collapse. The philosophy that only collapse should be prevented with allowing extensive damage to occur is realized only among engineers.	10(9.4%)	10(10.6%)	20(10.0%)
(5) The seismic performance depends on the amount of investment. Engineer's mission is to do their best within given investment and boundary conditions. Because budget is limited, it is difficult to prevent extensive damage during destructive earthquakes such as the 1995 Kobe earthquake.	14(13.2%)	13(13.8%)	27(13.5%)
(6) The seismic performance level depends on the amount of investment. However it is civil engineers who decide the design force levels and the performance goals. We make design calculations according to design codes, but are we really trying to design bridges so that damage can be avoided? We should deliver our engineering knowledge for preventing damage.	19(17.9%)	11(11.7%)	30(15.0%)
(7) No answer	17(16.0%)	26(27.7%)	47(23.5%)
Subtotal	106(100%)	84(100%)	200(100%)

who decide the design force levels and the performance goals. We make design calculations according to design codes, but are we really trying to design bridges so that damage can be avoided? We should deliver our engineering knowledge for preventing damage." This Level 6 was in pair of Level 5, i.e., "the seismic performance depends on the amount of investment. Engineer's mission is to do best within a given investment and boundary conditions. Because budget is limited, it is difficult to prevent extensive damage during destructive earthquakes such as the 1995 Kobe earthquake." Level 6 had slightly higher support than Level 5.

It is interesting to note that the selection of Levels 5 and 6 also depends on the experience of Kobe earthquake. Similar to the comparison of Levels 1 and 2, if we classify into the group who experienced Kobe earthquake and the group who did not experience the Kobe earthquake, the support ratio was 13.8% and 11.7 % for Levels 5 and 6, respectively, in the group who did not experience Kobe earthquake, while it was 13.2% and 17.9%, respectively, in the group who experienced Kobe earthquake. The fact that the support ratio for Level 6 is higher by 6.2% in the group who experienced Kobe earthquake than the group who did not experience Kobe earthquake shows the importance of strong involvement in determination of the seismic performance levels including appropriate investment level, instead of only doing our best within a given boundary condition.

EXPECTED AND ACTUAL REPAIR PERIODS

Expected Period for Repair

How soon bridges which had suffered damage by an earthquake can be repaired and re-accessed is one of the important decisions in the determination of seismic performance levels. It was surveyed here from two points; one is the repair period in which bridges damaged are expected to repair after the earthquake (expected period for repair) and the other is the repair period which may be possible in the current practice after the earthquake (actual period for repair). The expected period for repair is shown below, and the actual period for repair will be discussed in the next section.

Table 3 summarizes the expected period for repair of bridges. The highest support was directed to "within a week" (24%) followed by "within 3 days" (23%), "within a month" (14%), and "within 3 months (10%)." Few supported "immediate, i.e., damage which requires repair should not be allowed" (2%) and "within a half day" (5%).

Actual repair period was long after Kobe earthquake. For example, when columns failed in shear and a plate girder deck suffered buckling at web plates and lower flange plates near the supports, it took 3 weeks to temporarily confine the columns by new reinforced concrete and to shore up the deck. It took weeks for survey and design, and it took months to fabricate structural members. Stock of structural members for replacement, such as bearings and expansion joints were not available. It should be noted if damage occurred at only a bridge, temporary shoring

of the bridge might be possible in a week. However, since extensive damage occurred in a wide area, it was unable to conduct temporary shoring for a number of bridges shortly after the Kobe earthquake.

Table 3. Expected period of repair of bridges after the earthquake

How soon should we repair bridges when buildings and infrastructure suffered extensive damage in a wide urban region?	(1) Experienced Kobe earthquake	(2) Did not experience Kobe earthquake	(3) Total
(1) immediate, i.e., damage which requires repair should not be allowed	2(3.8%)	0	2(2%)
(2) within a hour	0	1(2.1%)	1(1%)
(3) within 3 hours	0	0	0
(4) within a half day	3(5.7%)	2(4.3%)	5(5%)
(5) within a day	3(5.7%)	3(6.4%)	6(6%)
(6) within 3 days	9(17.7%)	14(29.8%)	23(23%)
(7) within a week	11(20.8%)	13(27.7%)	24(24%)
(8) within 3 weeks	4 (7.5%)	3 (6.4%)	7(7%)
(9) within a month	11 (20.8%)	3 (6.4%)	14(14%)
(10) within 3 months	5 (9.4%)	5 (10.6%)	10(10%)
(11) within a half year	3 (5.7%)	2 (4.3%)	5(5%)
(12) No answer	2 (3.8%)	1 (2.1%)	3(3%)
Subtotal	53 (100%)	47 (100%)	100(100%)

Table 4. Actual period of repair of bridges after the earthquake

How soon can we repair bridges when buildings and infrastructure suffered extensive damage in a wide urban region?	(1) Experienced Kobe earthquake	(2) Did not experience Kobe earthquake	(3) Total
(1) immediate, i.e., damage which requires repair may not occur	0	0	0
(2) within a hour	0	0	0
(3) within 3 hours	0	0	0
(4) within a half day	0	0	0
(5) within a day	1(1.9%)	0	1(1%)
(6) within 3 days	1(1.9%)	0	1(1%)
(7) within a week	6(11.3%)	10(21.2%)	16(16%)
(8) within 3 weeks	3(5.7%)	10 (21.2%)	13(13%)
(9) within a month	10(18.9%)	9 (19.1%)	19(19%)
(10) within 3 months	13(24.5%)	4 (8.5%)	17(17%)
(11) within a half year	14(26.4%)	12 (25.5%)	26(26%)
(12) No answer	5 (9.4%)	2 (4.2%)	7(7%)
Subtotal	53 (100%)	47 (100%)	100(100%)

It is interesting to clarify whether the experience of Kobe earthquake affected the estimate of expected repair period. In the group who experienced Kobe earthquake, the highest support was directed to "within a month" and "within a week" (both are 20.8%), followed by "within 3 days" (17.7%), while it was "within 3 days" (29.8%) followed by "within a week" (27.7%) in the group who did not experience the Kobe earthquake. It seems that there is not essential difference on the estimate between the two groups.

Actual Period for Repair

Table 4 shows how the engineers evaluate the actual repair period. The highest estimate was "within a half year" (26%) followed by "within a month" (19%) and "within 3 months" (17%). It is noted that those actual repair periods are much longer than the expected periods describe above.

There exists an apparent difference on the estimate of actual repair period depending on the experience for Kobe earthquake. The top 3 estimate was "within a half year" (26.4%), "within 3 months" (24.5%) and "within a month" (18.9%) in the group who experienced the Kobe earthquake, while it was "within a half year" (25.5%), "within 3 weeks" (21.2%) and "within a week" (21.2%) in the group who did not experienced Kobe earthquake. It is important to have not armchair theory but proper estimate on the repair period of structural members so that the seismic performance levels can be appropriately determined in design.

How Should We Account Realistic Demands on Repair Period in Design?

If we are asked to design a bridge which can be accessed "within a week" and a bridge which can be accessed "within 3 weeks" after the earthquake, how can we take such a difference of repair period into account in seismic design?

Table 5 shows the results on how we can take account of two different demands on repair period. Although 22% and 15% replied that they can take account of this difference in design by differentiating residual drift after the earthquake and ductility capacity, respectively, majority (54%) replied that it was unable to consider such a difference based on the current design technology. We need a breakthrough technology which enables to incorporate such realistic demands in design.

COST OF INITIAL CONSTRUCTION AND REPAIR

It is always the augments how much increase of initial cost can be validated for enhancing the seismic performance. Obviously, it is more costly to construct bridges with higher seismic performance. However if the cost increase is limited, engineers may want to construct bridges with enhanced seismic performance. Arakawa and Kawashima analyzed the dependence of construction cost on the intensity of lateral seismic force under various conditions (Arakawa and Kawashima 1986), and they

Table 5. How can we differentiate the demand of repair period between "within a week" and "within 3 weeks" in design ?

How can we take difference of the repair period of "within a week" and "within 3 weeks" into account in design ?	Number and percentage
(1) Design by differentiating ductility factor	15 (15%)
(2) Design by differentiating flexural strength	3 (3%)
(3) Design by differentiating residual drift after an earthquake	22 (22%)
(4) Design by differentiating the lateral force	3 (3%)
(5) It is unable to differentiate the two demands based on the current technology	54 (54%)
(6) Others	3 (3%)
(7) No answer	0
Total	100 (100%)

Table 6. How much more initial cost is required to construct "damage free bridges"?

How much times investment than the current level is required to construct "damage-free bridges"?	Number and percentage
(1) 10% more cost	4 (4%)
(2) 30% more cost	32 (32%)
(3) 50% more cost	25 (25%)
(4) 100% more cost	20 (20%)
(5) 200% more cost	5 (5%)
(6) Others	10 (10%)
(7) No answer	4 (4%)
Total	100 (100%)

Table 7. How repair cost should be in comparison with initial investment?

How should the repair const be in comparison with the initial investment?	Number and percentage
(1) Repair is not necessarily requested	12 (12%)
(2) Within 10%	11 (11%)
(3) Within 20%	23 (23%)
(4) Within 30%	30 (30%)
(5) Within 40%	19 (19%)
(6) Within 50% or over	1 (1%)
(7) No answer	4 (4%)
Total	100 (100%)

concluded that the dependence of initial cost on lateral seismic force was not sensitive, excluding special cases such as the bridges constructed on very weak soils.

Our final target is to develop technology which enables to construct bridges which are free from any closure to traffic (referred hereinafter as "damage-free bridge"). If this is technically feasible, it is interesting to know how much cost increase compared to the current level makes it possible to construct "damage-free" bridges. It is noted here that the cost means the direct cost of construction of superstructures, substructures and other related structural members. Table 6 shows the replies from the engineers. The highest support was directed to "30% more cost than the current level" (32%), which was followed by "50% more cost" (25%) and "100% more cost" (20%). There are large scatterings in the replies.

Construction cost of superstructures vs. substructures in an ordinary bridge is generally in the range of 60-70% vs. 40-30%. Because cost increase of superstructures for enhancing the seismic performance is generally limited, the cost increase of 30%, which had the highest support as above, means a 1.75-2 times the current cost for substructures. Very simply, construction cost of substructures is proportional to their volume. Therefore, if the height is the same, the construction cost is virtually proportional to the sectional areas of substructures. Since shear strength is approximately proportional to the sectional area and the flexural strength is approximately proportional to the square root of the area cubed, the 1.75-2 times the current cost brings approximately 1.75-2 times increase of shear strength and 2.3-2.8 times increase of flexural strength. This may be more than enough to construct "damage-free" bridges.

A question was raised here whether we should design bridges so that they can be repaired after the earthquake. If bridges should be repaired, how much cost can be validated to repair after the earthquake. Table 7 shows the replies by engineers. The highest support was delivered to "within 30% of the initial construction cost" (30%), followed by "within 20%" (23%) and "within 40%" (19%). There are opinions that "repair is not necessarily required" (12%).

It is important to have realistic evaluate on initial construction cost and repair cost to have consensus on the seismic performance levels of bridges.

EXPECTATIONS FOR PERFORMANCE-BASED DESIGN

Table 8 shows what engineers expect in the performance-based seismic design. The highest expectation was to "make design rational by appropriately choosing the performance criteria depending on bridge" (40.5%), followed by "determine the design force appropriately depending on the site condition" (16.5%) and "introduce probabilistic concept in the determination of design force, analysis and evaluation" (12.5%). On the other hand, little expectation was directed to "use of the most favorable analytical models and tools" (1%). It seems that extensive use of nonlinear static analysis (pushover analysis) and linear and nonlinear dynamic response analysis

Table 8. What do you expect in the performance-based seismic design?

What do you expect in the performance-based seismic design? Choose 2 maximum from below.	Number and percentage
(1) Make design rational by appropriately choosing the performance criteria depending on bridges	81 (40.5%)
(2) Determine the design force appropriately depending on the site condition	33 (16.5%)
(3) Use the most favorable analytical models and tools	2(1%)
(4) Want to propose new structural type not yet ever constructed	18 (9%)
(5) Eliminate unnecessary sections and members to have well balanced bridges	16 (8%)
(6) Introduce probabilistic concept in the determination of design force, analysis and evaluation	25 (12.5%)
(7) Want to declare the copy right of design and construction	4 (2%)
(8) Other	4 (2%)
(9) No answer	17 (8.5%)
Total	200 (100%)

Table 9. Use of dynamic response analysis in performance-based design

How do you want to use dynamic response analysis in the performance-based seismic design?	Number and percentage
(1) Want to use dynamic response analysis more extensively, because input data for pushover analysis are the same with the input data for dynamic response analysis. Furthermore, pushover analysis is inconvenient because it cannot be used for some types of bridges with predominant higher modes, while dynamic response analysis can be used to all bridges regardless of the types.	28 (28%)
(2) Want to use dynamic response analysis more extensively for bridges to which pushover analysis provides poor application. Want to use pushover analysis for bridges to which the equivalent static analysis provides good application.	46 (46%)
(3) Current level of balance between pushover analysis and dynamic response analysis is appropriate	9 (9%)
(4) Want to use pushover analysis more, because dynamic response analysis is inconvenient for determination of sections	9 (9%)
(5) Others	8 (8%)
(6) No answer	0
Total	100 (100%)

after the Kobe earthquake is one of the reasons why limited expectation was directed to this goal.

Table 9 shows how the engineers regard dynamic response analysis compared to pushover analysis. A majority opinion is that they intend to "use dynamic response analysis more extensively for bridges to which pushover analysis provides poor application. They intend to use pushover analysis for bridges for which the equivalent

Table 10. Problems of performance-based design

What do you think the barriers for performance-based seismic design? Choose from the followings based on the assumption that necessary cost-up of design by increasing steps and times is paid by clients.	Number and percentage
(1) It is trouble because many decisions have to be made	7 (7%)
(2) Time for design increases	2 (2%)
(3) Current technology is insufficient to meet realistic and practical demands and requirements	10 (10%)
(4) Require engineers with higher engineering background, knowledge and skill	30 (30%)
(5) Design is controlled by a designer or a design group with high technical background, and the design cannot be approved by others	21 (21%)
(6) Risk and responsibility increase	20 (20%)
(7) Others	10 (10%)
(8) No answers	0
Total	100 (100%)

static analysis provides good application" (46%). Subsequent opinion is that they intend to "use dynamic response analysis more extensively, because input data for pushover analysis are nearly the same to the input data for dynamic response analysis. Furthermore, pushover analysis is inconvenient because it takes more man-power and it cannot be used for some types of bridges with predominant higher modes, while dynamic response analysis can be used for all bridges regardless the types" (28%). On the other hand, few opinions were directed to "current level of balance between pushover analysis and dynamic response analysis is appropriate" (9%) and "use pushover analysis more, because dynamic response analysis is inconvenient for determination of sections" (9%).

Table 10 shows problems which the engineers are concerned about in the performance-based seismic design. The largest problem was that "engineers with higher engineering background, knowledge and skill are required" (30%). This is followed by "design is controlled by a designer or a design group with high technical background, and the design cannot be approved by others" (21%), "risk and responsibility increase" (20%), and "current technology is not matured to meet realistic and practical demands and requirements" (10%). On the other hand few pointed out "it is trouble for having several decisions" (7%) and "it increases time for design" (2%).

CONCLUSIONS

Seismic performance criteria and levels were clarified based on a questionnaire survey to 100 civil engineers. The following conclusions may be deduced based on the results presented herein:

(1) Experience of a damaging earthquake makes the engineers to set higher seismic performance levels. The group who experienced 1995 Kobe earthquake recognized the importance of strong involvement in determination of the seismic performance levels including appropriate investment level, instead of only doing their best within a given boundary conditions.

(2) The experience of Kobe earthquake affects the estimate of actual period of repair. The group who experienced Kobe earthquake estimated the actual repair period longer than the group who did not experience Kobe earthquake.

(3) Based on the current technology, it is not possible to take account of the difference of demands for accessible time between "within a week" and "within 3 weeks" in design. We need a breakthrough technology which enables to incorporate realistic demands in design.

(4) There exist large scatterings in the estimate of cost increase which is required to construct bridges which are free from any closure to traffic (damage-free bridges). How much cost can be validated for repair had large scattering in replies from the engineers. Realistic evaluation on the initial cost and repair cost is important to set clearer performance goals.

(5) In the performance-based seismic design, the engineers expect to make design rational by setting the performance criteria depending on bridges. Little expectation was directed to use the most favorable analytical models and tools.

(6) The engineers intend to use dynamic response analysis more extensively in the performance-based seismic design. About a half engineers want to use dynamic response analysis for bridges to which pushover analysis is poor, while approximately a quarter engineers intend to use dynamic response analysis instead of pushover analysis because the input data for dynamic response analysis are nearly the same with the input data for pushover analysis

(7) The engineers pointed out that higher engineering background, knowledge and skill required for engineers is the largest barrier for the seismic performance-based design. They also pointed out problems that design is controlled by only a designer or a design group with high technological background, and risk and responsibility increase in the performance-based seismic design.

REFERENCES

Arakawa, T., and K. Kawashima. (1986). Dependence of construction cost of bridges on the lateral force coefficient. *Civil Engineering Journal*. 28(2): 64-69.

Japan Association for Earthquake Engineering. (2004). Current state and future problems of the performance-based seismic design of structures, Research Committee on Performance-based Seismic Design.

DEVELOPMENT OF NEXT-GENERATION PERFORMANCE-BASED SEISMIC DESIGN GUIDELINES

Ronald O. HAMBURGER[1]

ABSTRACT

The Applied Technology Council has initiated the ATC-58 project to develop next-generation performance-based seismic design guidelines applicable to the design of new buildings and upgrade of existing buildings. The guidelines will enable: design of buildings capable of better or more reliable performance than code-based procedures; provide a rational basis for the design of structures using new technologies and structural systems; and provide a means of improving the reliability and effectiveness of current building code procedures. Performance will be expressed directly in terms of the probable financial, human, and occupancy interruption losses caused by earthquake damage. Performance may be expressed as expected losses, given specific design events, average annual values, considering all events that may occur and the probability of each, or probable maximum losses over a given time interval, as best suits the decision-making style of individual stakeholders. Performance assessment procedures employed by the guidelines are based on the framework developed by the Pacific Earthquake Engineering Research Center. Though primarily intended to guide the design of buildings to resist the effects of earthquakes, the guidelines are intended to be compatible with performance-based design procedures currently under development by others to address, fire, blast and other extreme hazards. The ATC-58 project is funded by the Federal Emergency Management Agency.

Keywords: Design criteria; Performance-based engineering.

1. INTRODUCTION

Since the initial development of building code provisions for earthquake resistance, the primary intent of code criteria has been to protect life safety by providing reasonable assurance that buildings would not collapse in anticipated levels of shaking. Following the 1989 Loma Prieta and 1994 Northridge earthquakes, structural engineers in the United States began development of structural design procedures that would reduce the financial and other losses associated with earthquake damage. The resulting criteria and methodologies came to be known as "performance-based design." Interest in these procedures has spread throughout the international earthquake engineering community.

---

[1] *Principal, Simpson Gumpertz & Heger, Inc. San Francisco, California, USA*

Present performance-based seismic design practice for buildings in the United States is embodied in appendices to the *Recommended Lateral Force Requirements and Commentary* (SEAOC, 1999) and the *FEMA-356* (ASCE, 2002) national rehabilitation guidelines. These documents define a series of discrete performance levels, ranging from states of little damage and earthquake impact (e.g., Immediate Occupancy) to states of near complete damage and total loss (e.g., Collapse Prevention), and provide methods of relating these damage states to response quantities predicted by structural analysis (e.g., interstory drift, individual member force demand).   These methodologies have had substantial impact on U.S. engineering practice and have experienced widespread application, particularly for the evaluation and upgrade of existing buildings.   Further, the basic performance framework for these performance-based procedures has been adopted by model building codes in the U.S. and extended to other design conditions including wind, snow, fire and blast. Despite this success, it is clear that substantial improvements can be made. Current procedures evaluate performance on the basis of local rather than global behavior, do not adequately characterize the performance of nonstructural components and systems, provide no guidance on how to proportion a structure, other than by iterative trial and error procedures, are of unknown reliability and are tied to performance levels that do not directly address the needs of the decision makers who must select the appropriate performance criteria for specific projects.

In September 2001, the Federal Emergency Management Agency contracted with the Applied Technology Council to develop next-generation performance-based seismic design guidelines intended to address these shortcomings. The resulting ATC-58 project, a broad program based on the *FEMA-349 Action Plan* (EERI, 2000), is intended to be implemented over a ten year period in partnership with the three national earthquake engineering research centers, the United States Geologic Survey, the National Earthquake Engineering Simulation program as well as industry associations and other interested parties. It will culminate with the publication of next-generation performance-based seismic design guidelines for buildings as well as companion publications intended to assist decision makers in using and taking advantage of performance-based approaches. Though primarily intended to address seismic design, substantial efforts are being made to ensure that the guidelines are developed compatibly with parallel efforts to develop performance-based design criteria for resistance to other extreme loads including fire and blast.

Guidelines development is occurring in two phases. The first phase comprises development of building performance assessment guidelines. In a major departure from prior performance-based approaches, rather than expressing performance in terms of arbitrary performance levels, the next-generation procedures characterize performance directly in terms of the probable life loss, repair costs and occupancy/functionality interruption times resulting from earthquake damage. The evaluation procedures closely follow the framework for performance-based earthquake engineering, developed by the Pacific Earthquake Engineering Research Center, in which probable earthquake losses are calculated by integrating over the

ground shaking hazard, probable structural response given intensity, probable damage given response and probable loss given damage (Deierlein, 2004). Calculated performance may be expressed in a variety of forms including average annual loss, expected loss at a specified hazard level, or probable maximum loss, as best suits individual stakeholders and decision makers. The effects of aleatory and epistemic uncertainty are directly accounted for in these performance calculations. In the second phase, performance-based design procedures will be developed to allow engineers to efficiently determine appropriate combinations of structural stiffness, strength, damping and ductility, as well as installation procedures for nonstructural components to achieve various levels of performance capability. Stakeholders' guides will be developed to assist decision makers in selecting appropriate performance objectives as the basis for building development projects.

2. BASIC METHODOLOGY

Figure 1 illustrates the performance-based design process. It includes selection of appropriate performance objectives, development of one or more preliminary designs the designer believes will be capable of achieving these objectives, assessment of each design's ability to perform as desired, and revision of the design until the desired performance capability is successfully demonstrated. The first phase of the ATC-58 project is focused on development of a robust methodology for assessing the performance capability of a design. Steps in this process are discussed below. Later phases of the project will include development of recommendations for standardized design performance objectives for different types of structures and the development of guidelines that will enable engineers to develop preliminary designs that have performance capabilities close to those desired, so that the overall performance-based design process can be efficiently prosecuted.
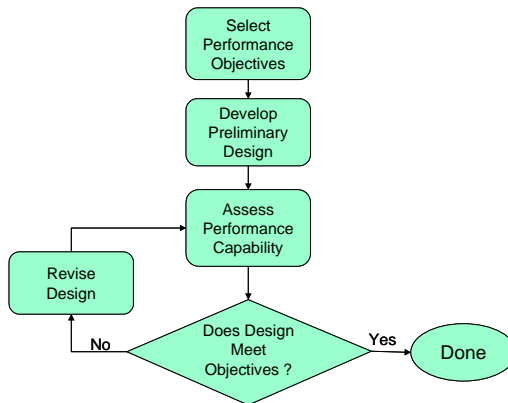
Figure 1. Performance-based design process.

2.1   Performance Objectives

An important goal of the ATC-58 project is to utilize performance objectives that are quantifiable and predictable, as well as meaningful and useful for the decision makers who must select or approve the objectives used as a basis for design. Decision makers are a disparate group that includes building developers, facility managers, risk managers, lenders, insurers, public agencies, regulators and individual members of the public. Each of these decision makers view seismic performance from a different perspective and select desired performance using different decision making processes. Regardless of the specific process used, selection of appropriate performance will involve development of an understanding of the risk associated with a given choice and the resources that must be invested to reduce this risk beyond certain thresholds. To facilitate this process, in the ATC-58 project performance objectives are expressed as the risk of incurring three specific kinds of earthquake induced loss. These include direct financial losses (dollars) associated with the cost of repairing or replacing damaged facilities, earthquake-induced life losses (deaths and serious injuries) and lost use of facilities (downtime) while they are being repaired, replaced or otherwise restored to service.

Different decision makers characterize these risks and determine acceptable levels of risk in different ways. Therefore the next-generation guidelines permit alternative methods of stating performance objectives including: expected losses, given the occurrence of a specific earthquake scenario, annualized losses, or the expected loss over a given period of years, each expressed together with a level of confidence associated with the estimate. Examples include Probable Maximum Losses (estimates of the 90% confidence level loss given a specific event), average annual loss (the mean loss per year averaged over many years) or the 500-year loss (that loss which has a 10% chance of being exceed in 50 years). Many other similar means of expression will be accommodated.

2.2   Perform Preliminary Design

The preliminary design for a building includes definition of all features that are significant to its probable future seismic performance. This includes the building's site characteristics, its basic configuration, materials of construction and structural systems, foundation type, stiffness and strength, and to the extent that response modification technologies such as seismic isolation or energy dissipation systems are incorporated in the design, the characteristics of these systems. Review of losses experienced by buildings in past earthquakes clearly indicates that except in those buildings where gross structural failure or collapse occurred, most economic and occupancy losses were the result of damage to nonstructural components and systems. Therefore, the preliminary design must also include consideration of the types of nonstructural components and systems that are to be installed in the building and the way in which they will be installed.

Vulnerability of buildings to losses related to nonstructural performance is highly dependent on the occupancy of the building. Laboratories and manufacturing facilities with clean room environments, for example, have systems with different vulnerabilities, and are more likely to experience occupancy interruption as a failure of these systems, than do office and residential occupancies. Thus, the preliminary design for a building must consider not only the typical building systems, such as electric power supply and distribution, heating ventilating and air conditioning systems, and fire protection but also critical tenant-installed systems and equipment.

Current performance-based design procedures provide little guidance to designers on how to select or proportion the structural and nonstructural systems in their buildings to achieve desired performance. Designers engaged in performance-based design must rely heavily on their personal intuition and judgment to develop designs they believe will be capable of the desired performance, and which they can then evaluate for performance acceptability. Although generally, increased structural stiffness, strength and energy dissipation capacity improve performance of structural systems, it is not clear that they have the same effect on the performance of nonstructural systems. Stronger and stiffer structures, though more resistant to structural damage then weaker, more flexible structures, transmit greater shaking to the nonstructural components and systems mounted in the building and may actually cause greater damage of these systems. Therefore, arriving at preliminary designs to satisfy a given set of performance objectives is not a trivial task. Later phases of the ATC-58 project will focus on developing tools to assist the designer to efficiently prepare preliminary designs that are suitable to buildings of different configurations, occupancies and performance objectives.

2.3 Performance Capability Assessment

Figure 2 illustrates the performance assessment process. It initiates with a characterization of the site hazard, that is, the probability that the building will experience various levels of ground shaking, characterized by an intensity measure (*IM*), such as peak ground acceleration, spectral response acceleration at the fundamental mode of the structure, inelastic spectral displacement at the fundamental mode of the structure, or other similar measure. It is possible that hazard functions for several different intensity measures will be required to assess the performance of a given building. As an example, spectral response acceleration or displacement at the fundamental mode of the structure may be the best *IM* to predict structural damage, while the damage experienced by nonstructural components and systems, particularly those mounted at grade, may be better predicted by peak ground acceleration.

Structural analysis is used for two basic purposes: prediction of structural response quantities (engineering demand parameters or *EDP*s) that can be used as predictors of the damage sustained by the structure, and, prediction of the intensity of demands placed on nonstructural elements and systems supported by the structure, at different intensities of ground motion.
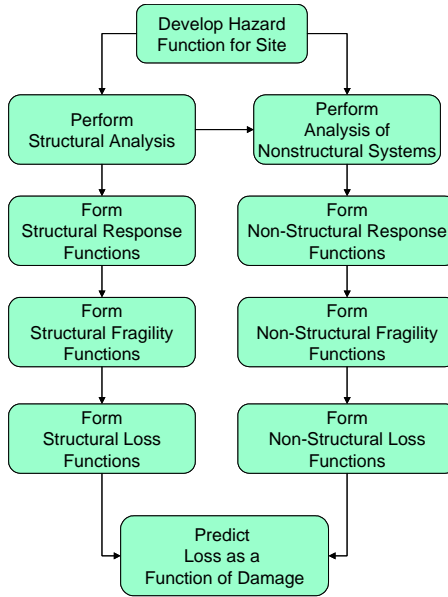
Figure 2. Performance assessment process.

To illustrate application of the process, we focus on the first of these two uses and for this discussion, use 1st mode elastic spectral response acceleration (S_{a1}) as our *IM* and peak interstory drift at each story level ($[\delta_i]$) as our *EDP*. For a given ground motion record, scaled to a specific value of S_{a1}, we can perform a nonlinear time history analysis of the structure and predict $[\delta_i]$. The values of $[\delta_i]$ predicted by this analysis will depend on several factors including our assumptions as to the structure's mass, stiffness, strength, damping, and hysteretic characteristics as well as the specifics of the ground motion record itself. If a different ground motion record were selected, but all of the modeling parameters left unchanged, we would predict somewhat different values for $[\delta_i]$, and, if we were to repeat this process using several different records, all scaled to the same S_{a1}, each, would in general, result in somewhat different $[\delta_i]$ predictions. If we believe each of these records is equally representative of the particular intensity of motion, the result is a random distribution of $[\delta_i]$ that can result from this particular ground motion intensity. This distribution can be characterized by a mean or median value and a measure of its random variation. If this process is repeated for a range of ground motion intensity values, it is possible to develop a structural response function that indicates the probable distribution of $[\delta_i]$ for different levels of ground motion intensity (S_{a1}). Figure 3 illustrates a structural response function of this type for a hypothetical single story structure, showing the median, 10% and 90% confidence bands for $[\delta_i]$ as a function of S_{ai}.
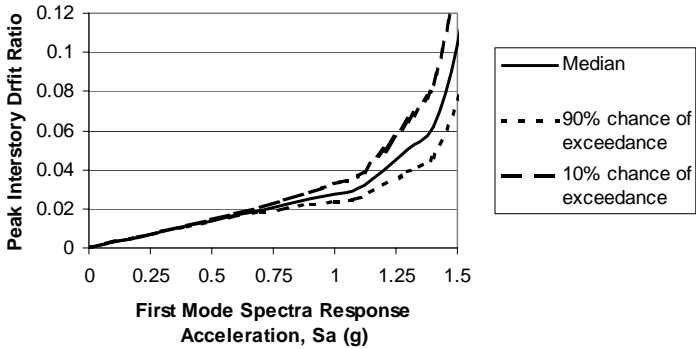
Figure 3. Representative structural response function.

In developing the structural response function illustrated in figure 3, the stiffness, mass, damping and hysteretic parameters for the structure were held invariant, as if the true value of these parameters was precisely known. While most likely values for these parameters can be estimated, in fact, the true values are seldom, if ever, known, and there is some uncertainty as to their precise values. To the extent the values for modeling parameters used in the analyses are inaccurate, the resulting structural response function for the building may either over- or under- predict response at a given ground motion intensity. While it is essentially impossible to predict the exact value of any of these parameters, it is possible to estimate most likely values for each, as well as measures of the potential variation. If a series of analyses are performed, varying these parameters consistent with the expected distributions, it is possible to predict the additional variation in response resulting from these uncertainties. The effect of these additional uncertainties is to broaden the scatter associated with the response function. This is illustrated in Figure 4.
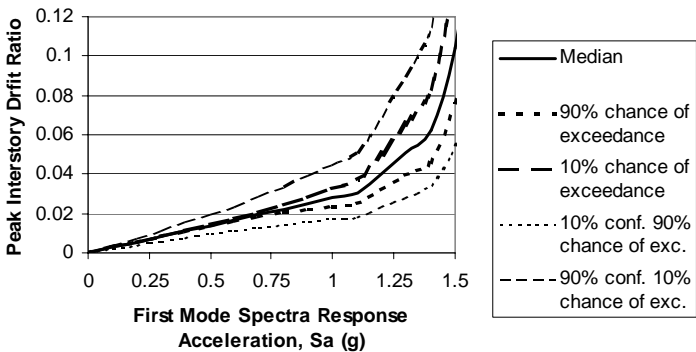
Figure 4. Structural response with aleatory and epistemic uncertainty.

For a real structure, the task of defining these uncertainty bounds considering the various random variables involved is a complex process requiring many analyses. As an alternative to this complex process, it is possible to estimate the confidence bounds by assuming that the variability can be represented by a standard distribution, typically lognormal, and by selecting a coefficient of variation based on either expert judgment or the variability observed in analysis of a limited number of standard structures. This will likely be the approach adopted by ATC-58 project, with engineers guided into performing analyses of the structure at several intensity levels and then applying standard variability measures to the computed response based on structure type and characteristics.

Damage is related to response through structural fragility functions, which indicate the probability that a structure will experience damage greater (or less) than a certain level, given that it experiences certain response, as measured by the *EDP*. Fragilities are expressed as probability distributions, rather than deterministic relationships in order to account for the uncertainty inherent in the process of predicting structural damage as a function of structural response. This uncertainty is associated with such factors as the random character of structural response to individual ground motion records and the inability of simple *EDP*s to distinguish between this response variation and the damage it causes. For example, two different ground motions may each produce 3% peak interstory drift demand in a structure, however, one ground motion may cycle the structure to this drift level one time then restore the structure to small oscillations about its neutral position while the second ground motion may cycle the structure to this drift level several times and leave the structure displaced nearly to this level. Clearly the latter motion will be more damaging of the structure than the first, though the value of the *EDP* is the same. Such effects are not predictable unless the precise ground motion and structural response is known. Other sources of uncertainty include lack of precise definition of material strength and construction quality.

In the ATC-58 project we propose to parameterize damage by tracking the condition of individual structural elements and components, as well as by tracking the global state of the building structure. For example, for moment-resisting steel frames, local damage measures include panel zone yielding, beam plastic hinging, beam flange buckling, and welded joint fracturing, while measures of global damage are various levels of residual interstory drift (e.g., 1%, 2%, 3%, etc. up to collapse) on a story by story basis. Each of these damage states (e.g., beam flange buckling, or residual drift of 2%) has different implications with regard to potential injury, repair effort and cost, and occupancy interruption. Figure 5 presents representative fragility curves for damage states for moment-resisting steel frame structures developed based on data generated under the FEMA/SAC program (Roeder, 2000) and Figure 6 presents a similar fragility curve for global damage states. The consequences of each of these individual damage measures must be aggregated on a system basis, over the entire structure.
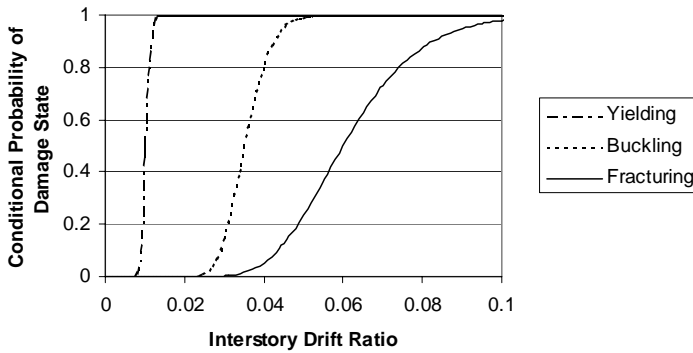
Figure 5. Representative structural fragility — local damage states.
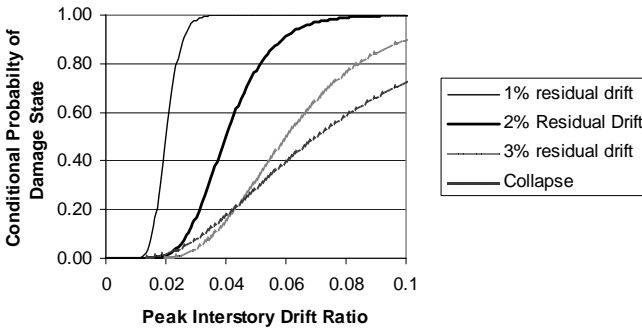
Figure 6. Representative structural fragility — global damage states.

Nonstructural fragilities serve the same purpose as structural fragilities. The *EDP* used to predict nonstructural component or system damage will, in general, be different than that used to predict structural damage. *EDP*s that are likely to be useful for predicting damage of nonstructural components mounted on or within a structure include peak floor response accelerations at the fundamental mode of the nonstructural component and peak inter-story drift at the levels of attachment of the component. Damage states that may be meaningful for nonstructural components and systems include loss of function, loss of structural integrity and toppling. Each class of nonstructural component or system, such as suspended ceilings, fire sprinkler systems, and interior partitions will have different fragility functions, tied to several different *EDP*s. These can be determined through collection of earthquake performance data on damage sustained by actual installations, through laboratory testing programs and in some cases, through structural analysis, just as would be done for the building structure itself. There are so many types of nonstructural components in a building that it is an impractically difficult task for the ATC-58 project to develop

all of the nonstructural fragility functions required to simulate a building's performance. The project will rely on independent researchers and the suppliers of nonstructural components for much of this data. An important task of the ATC-58 project is the development of standard procedures for establishment of nonstructural fragility parameters so that independent researchers and component suppliers can develop this data. Figure 9 is a hypothetical fragility curve for a single drift-sensitive nonstructural component (exterior curtain walls) showing the probability of various damage states: cracking of panels, breakage of glass, fallout of glass, and failure of panel connections, as a function of interstory drift. The fragilities shown in the figure are illustrative only and are not representative of real data.
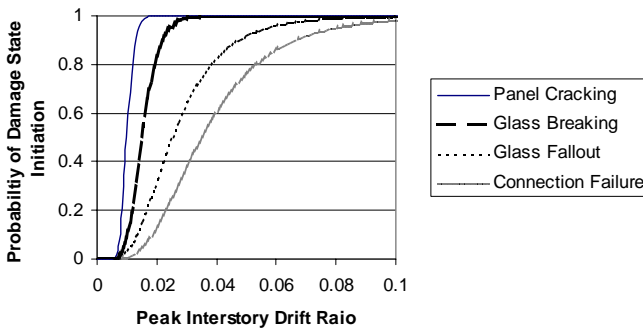
Figure 7. Representative nonstructural fragility curve.

Loss functions are used to estimate the probable value of the various losses, including repair costs, life loss and loss of use, given that the structure and nonstructural components and systems are damaged to different levels. Loss functions related to repair cost and restoration time can be developed by theorizing different levels of damage to representative buildings and asking general contractors and cost estimator to develop estimates of the cost and time to complete repair work. Estimation of losses and repair times associated with restoration of damaged facilities tend to be highly uncertain and are dependent on such random factors as the efficiency of the contractor, the availability and pricing of labor and materials in the post-earthquake environment, weather conditions, the occurrence of aftershocks, the time necessary to effect designs for the repair, the specific repair methods developed by individual engineers, and whether or not the building will remain partially occupied while repairs are implemented. Other uncertainties include the Owner's efficiency in retaining design teams and contractors to perform the necessary work, the availability of insurance or other sources of funding for the repair work, and the occupancy of the building and its tolerance to operations during repair work. Figure 8 is a hypothetical loss function for the repair costs associated with damaged steel moment connections. Similar loss functions will be developed for other types of structural and nonstructural damage and for restoration times.
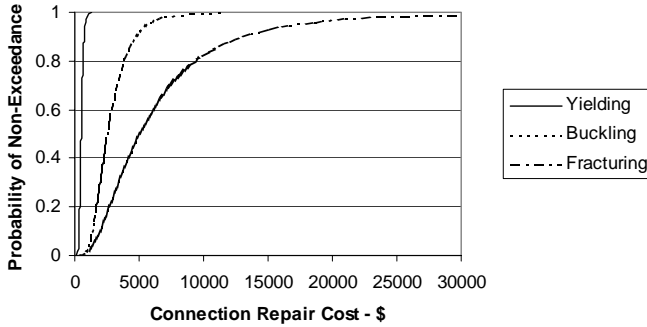
Figure 8. Example loss function for moment resisting steel frames.

Loss functions for life losses can be developed by evaluating historical data on the number of serious and fatal injuries in buildings of different construction characteristics that experienced different levels of damage. Comparisons of this type typically show that life losses are negligible unless partial or total collapse occurs. By convolving the likelihood that persons are in a portion of a building that is subject to collapse at the time an earthquake occurs, with the statistical rate that collapse has resulted in various levels of injury in the past, it is possible to develop loss functions that relate the probability of serious injury and life loss to the collapse damage state.

Once the hazard function, structural and nonstructural response functions, and damage and loss functions for a building have been formed it is possible to complete the performance assessment process by estimating the risk of the various losses in terms meaningful to the different decision makers who must select the desired building performance that will serve as the basis for .design. The simplest form of loss prediction consists of determining the expected value of a loss (deaths, dollars, or down time) given that the structure experiences a specific intensity of ground motion that may for example, represent an event with a 10% probability of exceedance in 50 years. The process starts by determining the conditional probability that structural response, in our previous example interstory drift (δ_i), will be to a given level, if the structure experiences this level of ground motion intensity. This is determined by evaluating the response function for the structure (e.g., Figure 4) at the given intensity level. The next step is to determine the total probability that the structure will be damaged to each of the possible damage states (DS_j). This is performed by integrating the conditional probability of experiencing each of the damage states $P(DS_j|\delta_i)$ as a function of interstory drift, δ_i, e.g., from Figures 5, 6 and 7, with the probability of experiencing different levels of δ_i obtained from the response function. Finally, the expected loss is computed by summing the probable value of the loss ($PV(\text{Loss}|DS_j)$, e.g., from loss functions such as Figure 8, given the occurrence of a damage state times the total probability of experiencing each of the damage states $P(DS)$ summed over all possible damage states, or in equation form:

$$\text{Expected Loss} = \iint PV\left(Loss\middle|DS_j\right)P\left(DS_j\middle|\delta_i\right)P(\delta)d(DS)d(\delta) \tag{1}$$

The average annual value of the loss can be obtained by realizing that the expected loss calculated in equation (1) is actually the probable loss given that a specific intensity of ground motion is experienced. Equation (1) can be used to evaluate the expected loss at each of a number of ground motion intensity levels, and the average annual loss can be calculated as the sum of the expected loss at each intensity level (EL_k) factored by the annual probability of experiencing each intensity level, and summing this over all possible intensity levels, or, in equation form:

$$\text{Average Annual Loss} = \iiint PV\left(Loss\middle|DS_j\right)P\left(DS_j\middle|\delta_i\right)P\left((\delta_i\middle|Sa_k\right)P\left(Sa_k\right)d(DS)d(\delta)d(Sa) \tag{2}$$

The average annual loss can be summed, statistically, to provide the expected loss over any desired interval of years. By calculating the combined uncertainty in the losses associated with the hazard, response, damage and loss functions, it is possible to estimate the expected losses at specified levels of confidence to produce other performance measures such as the popular Probable Maximum Loss (PML).

3. SUMMARY

When completed, the ATC-58 guidelines have the potential to revolutionize the practice of performance-based design. They will introduce the practicing structural engineer to the use of probabilistic structural reliability techniques and in the process, clarify the likelihood that performance-based designs will actually achieve intended performance. More important, they will enable the engineer to provide decision makers information that will be directly useful in selecting appropriate performance criteria for building design and upgrade projects.

REFERENCES

American Society of Civil Engineers (ASCE). 2002. *Prestandard and Commentary for Seismic Rehabilitation of Buildings*, *Report No. FEMA-356*, Federal Emergency Management Agency, Washington, D.C.

Deierlein, G. G. 2004. "Overview of a Comprehensive Framework for Earthquake Performance Assessment." In *Proceedings of the International Workshop on Performance-Based Seismic Design,* Bled, Slovenia, p.15.

Earthquake Engineering Research Institute (EERI). 2000. *Action Plan for Performance-Based Seismic Design*, *Report No. FEMA-349*, Federal Emergency Management Agency, Washington, D.C.

Roeder, C. 2000. *State of Art Report on Connection Performance, Report No. FEMA 355D*, Federal Emergency Management Agency, Washington, D.C.

Structural Engineers Association of California (SEAOC). 1999. R*ecommended Lateral Force Requirements and Commentary, Appendix G, Performance-based Design*, International Code Council, Whittier, CA, 1999.

APPLICATIONS OF PERFORMANCE-BASED ENGINEERING TO RISK MANAGEMENT DECISIONS

Craig D. COMARTIN SE[1]

ABSTRACT

Performance-based engineering procedures (PBE) promises significant related improvement in the capability to manage seismic risks effectively and efficiently from a business perspective. This paper first previews the document *FEMA 440: Performance and Risk Assessment for Buildings in Extreme Events* that proposes to use risk as the fundamental characterization of building performance. The three basic risk parameters are deaths and serious injuries, economic losses due to direct damages, indirect economic and societal losses attributable to loss of use of a facility due to damage. Once these basic parameters are quantified they can be reformulated to address the specific needs of various stakeholder decision makers. This is illustrative with several practical application examples.

Keywords: Performance-based engineering; Risk analysis; Risk management.

INTRODUCTION

This paper summarizes portions of a document currently being prepared as one product of the ATC 58 to develop next-generation performance-based seismic design guidelines (Hamburger, 2004). *FEMA 440: Performance and Risk Assessment for Buildings in Extreme Events* will present the results of project efforts to date to determine effective ways to characterize and communicate concepts of building performance to both design professionals and the numerous stakeholders and decision makers whose lives and financial interests are dependent on the performance of buildings that may be subject to earthquakes, fires, blasts and other extreme hazards. The primary objectives are to:

- establish a basic characterization of performance of buildings in extreme events that is technically sound and comprehensive from an engineering perspective.
- illustrate how this basic characterization can be adapted to the multiple specific needs of individual decision makers.

1 President, CDComartin, Inc.
427 13th Street
Oakland, California 94612
ccomartin@comartin.net

The following sections address each of these objectives. The basic concepts apply to many extreme hazards, but they are illustrated with seismic shaking. Examples of actual applications to buildings are also included.

THE USE OF RISK TO CHARACTERIZE PERFORMANCE

Building performance is defined effectively for a given building, at a given location, in terms of three basic risk parameters. Each of these is an aggregation, or integration, of potential losses over the life of the building from the hazard of interest. The basic risk parameters are these aggregations for:

- deaths and serious injuries.
- economic losses due to direct damage.
- economic and societal losses that indirectly occur as a result the loss of use of a damaged building or facility (downtime).

These can be expressed in a number of different forms (e.g., annualized loss, net present value of expected losses, annual probability of exceeding a certain loss). Note that conversion from one format to another is a relatively simple numerical transformation. Thus each basic risk parameter has a unique value regardless of the form of expression. The median values of the basic risk parameters also have an associated reliability as a measure of uncertainty.

This characterization of performance derives directly from the Pacific Earthquake Engineering Research Center Framing equation (Moehle, 2003) as illustrated in Figure 1.

$$v(DV) = \iiint G\langle DV|DM \rangle \, | \, dG\langle DM|EDP \rangle \, | \, dG\langle EDP|IM \rangle \, | \, d\lambda(IM)$$
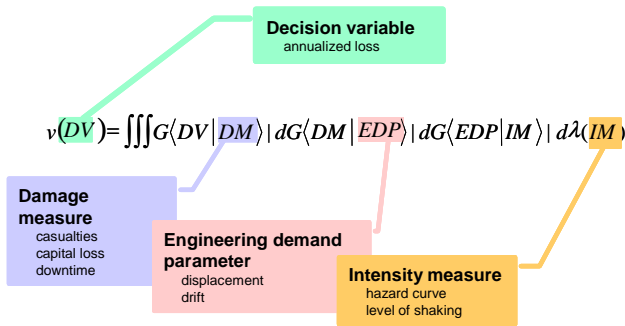
Figure 1. PEER framing equation and example parameters for seismic shaking.

The basic risk parameters are the decision variables for the three categories of losses (deaths, dollars, downtime). Figure 1 includes example parameters for engineering demand and intensity measure for seismic shaking; however, the basic concept can be applied to other extreme hazards using appropriate alternative parameters. (Deierlein, 2003 and Whittaker, 2003).

PRACTICAL ADAPTATION FOR STAKEHOLDER DECISIONS

The implementation the performance-based design using the basic risk parameters is illustrated in Figure 2. While the characterization of performance with the basic risk parameters is technically sound and practical from an engineering perspective, the results of the performance assessment are not useful directly to all stakeholders. As shown in Figure 2 the results are reformulated to address the specific decision making needs of various stakeholders. Some of these are summarized in the following.

Minimum Performance Standards (Code Compliance)

One of the important goals of the ATC 58 project is to develop performance based design procedures that can be used in codes and standards. Traditionally, codes have not stated the performance they are intending to achieve with their prescriptive provisions, except through broad, highly qualitative statements that their intent is to protect the public safety. The basic risk parameters that can be derived from the performance assessment can either be used to demonstrate that a design meets the performance criteria, or alternatively, can be used to improve the statements of performance criteria currently contained in the codes. For example, the primary purpose of seismic provisions in present prescriptive codes is to provide for a minimum level of public safety. The casualties risk parameter that is an output from the performance assessment methodology provides a quantifiable measure of safety for a building design. With this tool in place, codes could specify a maximum allowable life safety risk. This could be in the form, of not greater than a 10% chance of single life loss, given a 500-year event, or in the alternative but similar form, less than a 0.0002 chance per year of single life loss. Similarly, codes could require maximum levels of risk associated with capital losses or downtime depending on the importance or function of a facility (e.g., public buildings, hospitals). This format would be a much more useful and transparent code basis.

Conventional Performance Objectives

Similar to the code application described above, the performance levels of current performance-based design procedures such as *FEMA 356* (BSSC, 2000) and *ATC 40* (ATC, 1996) could be indexed easily using the basic risk parameters a performance assessment. The performance assessment could also be used to de-aggregate losses, if desired. This allows the estimation of losses associated with a specified seismic hazard level (e.g., casualties expected for a 500 year event). De-aggregation to deterministic events is also possible.

Specialized Decision Variables

Individual stakeholders will have interest in particular information on the risk implications of design decisions that will be most useful to their decision processes. Corporate risk managers, for example, may be most interested in project down time, as the loss of use of a facility for an extended period could affects not only short term profits but long term market share and viability. Lenders will typically be interested in downtime as well, because if a borrower is unable to use a building for an extended period of time, or obtain rents from tenants, they may be unable to service their loan. Insurers will typically be interested in likely repair costs, but may also be interested in downtime as they may underwrite lost income from operations due to damage. Building officials will typically be more interested in risk to life. The basic risk parameters can be easily re-formatted to provide such information. For example,

- What is the chance of a death or serious injury due to an earthquake in my building in the next 20 years?
- Can I be 90% sure that an earthquake will not put me out of business with a capital loss of over a million dollars in the next 50 years?
- Is there greater than a 10% chance that our hospital will be unable to accept new patients for more than a week after an earthquake in the next 50 years?
- Is there greater than a 10% chance that fire stations in a city will be unable to service the fire department following a major earthquake?
- What is the likely repair cost for my building in the event of a large earthquake?

The use of performance-based engineering to characterize losses in terms of risk enables the engineer, facility owner, building tenant, city planner, and others, to answer important questions such as these in economic terms. For example:

Should the owner retrofit a facility to reduce earthquake losses?
The engineer formulates the basic risk parameters in dollars for the existing facility then discounts them to a net present value. The engineer then conceptually develops a retrofit design to address the deficiencies of the facility and estimates the associated cost. Using the retrofit design the engineer can then repeat the calculation of losses for the retrofitted facility, again expressed in present value. These should be less than the losses for the un-retrofitted case. The difference represents the economic benefit of the retrofit. If the benefit exceeds the retrofit cost, the retrofit is a good investment. Many decision makers will divide the benefit (net present value of loss reduction) by the cost to obtain a cost benefit ratio or return on investment measure. Then an optimal level of retrofit could be determined by repeating this exercise until a maximum cost/benefit ratio is obtained.

For a new facility, is it preferable to use shear walls or unbonded braces as the lateral-force-resisting system?
The engineer performs a conceptual design and cost estimate for both options, then determines the net present value of the basic risk parameters for each option. If the

cost premium for the more expensive alternative is less than benefit in terms of reduced expected losses, the additional cost is economically justified.

For an industrial production facility, is it advisable to design for performance greater than required by the building code?

The engineer formulates a design and cost to meet the minimum requirements of the code as a baseline and estimates the basic risk parameters. One or more alternative designs can be prepared to improve expected performance beyond the baseline. The additional costs of these alternatives compared to the baseline costs is are an investment in seismic risk management. The reduction in the present value of basic risk parameters (from code design to upgraded criteria) represents the return on the investment.

Should an owner invest in a design for higher performance or transfer (or accept) the risk?

An economic analysis can identify the optimal investment in risk reduction through improved performance. Beyond some level the incremental return on investment drops. An owner may choose to supplement the design with risk transfer through insurance or simply accept it. By understanding the excess risk and the probabilistic distribution of that risk over a range of hazard levels, the owner is in a better position to develop a risk transfer and management plan that more precisely meets his tolerance and capacity needs.

Where does investing in seismic risk management fit into an owner's overall business plan?

Once the engineer determines the risks and rate of return on investments in risk reduction, risk transfer, or other seismic risk management strategies, the owner can make a comparison with other business investments (e.g., equipment, research, personnel). An owner typically has finite resources with which to invest; he must therefore make decisions that select the best investments from among competing demands on capital.

Should a community upgrade existing low-income housing with retrofit design or phase it out with newly designed replacement facilities?

Many towns and communities face great economic and social challenges in providing decent housing for the less privileged. Current code provisions, including those addressing seismic issues, are most often an impediment because of cost implications. The proposed characterization of performance and related analysis techniques might show that significant new or retrofit construction cost savings could be realized (compared to compliance with a prescriptive code) while still meeting sufficient levels of life safety.

How can home owners or builders using the non-engineered construction provisions of the code efficiently improve seismic performance?

It is not very likely that the analysis procedures envisioned for this project will be used directly to design many single family homes. Most homes are now built by contractors complying with prescriptive directions in a special section of the code for

non-engineered construction. Nonetheless, the proposed performance characterization and related analysis procedures enable the investigation and documentation of risks associated with these provisions in general. They can also be used to evaluate the effectiveness and efficiency of changes or alternatives. Eventually, the non-engineered provisions might include optional upgrades that can be prioritized and correlated to local seismicity. This would give home owners, buyers, and builders more options than they currently have.

There are significant uncertainties associated with seismic risks including estimating ground motion hazard, structural capacity, and losses. The preceding discussions represent these parameters simplistically as expected values. In reality, they are central (median or mean) values associated with individual probabilistic distributions. The risk-based approach to seismic performance characterization enables the tracking of uncertainty directly. For example, using the expected (central) values of the performance parameters the chance that the predicted losses from earthquakes are exceeded is 50%. They are equally likely to be less than the expected values. If an owner wishes to increase reliability to a higher level the probabilistic framework enables an upward adjustment of losses for a higher degree of confidence (e.g., 90%) that they will not be exceeded.

This is another important advantage of these procedures. Since codes are primarily concerned with life safety, they are naturally intended to be conservative. It would be publicly unacceptable, for example, to design a building based precisely on median values of hazard and capacity, if the result was that one-half of buildings would perform well, protecting their occupants, and one-half would not. When owners make decisions about enhancing performance however, to protect their capital and business operations, rather than conservative estimates of performance outcomes, they want to understand the median expected losses and the variance about that median. In this way, they can define a design based on their own risk tolerance and compare investments in risk management and reduction with other known business risks.

EXAMPLE APPLICATIONS

The proposed basic approach to seismic performance characterization and analysis has been used in a very rudimentary form in the past few years. The following are some examples of recent practical applications. In reviewing the examples, one should keep in mind that the procedures that were used, although conceptually similar to those envisioned for the future, are very simplistic. For example, damage is estimated strictly from a global perspective without investigating component behavior directly. The basic inelastic analysis procedure are nonlinear static as opposed to the more detailed response history analyses. Also, each application had to be developed and implemented from scratch without the benefit of guidelines or special purpose analysis tools. As a result, there are large uncertainties associated with the results.

The future techniques will improve the accuracy of the results significantly and provide practitioners with consensus-based guidance on reliable procedures.

Selection of an Appropriate Structural System for a Critical Facility

The University of California at Berkeley is building a new state-of-the art laboratory building to replace an existing building. The $200 million facility will serve the needs of important bioscience research for the next thirty to fifty years that are funded at a current annual rate of $40 million. The design engineer proposed the use of unbonded braces, a new structural system with enhanced performance characteristics, with the goal of protecting the University's investment and future research capabilities. However, as a public institution, receiving government funding, the University had to justify use of the new system, which was a more expensive alternative than a more conventional system would still meet the minimum requirements of the State of California Building Code, such as concentric braced steel frames. Figure 2 presents an architectural rendering of the building together with information on the development cost, projected value of building contents and of the economic loss to the University projected for each year that the building is out of service.

Item	Cost
Capital	$160 million
Contents	$50 million
Business Interruption	$40 million annually

Figure 2. Example building at the University of California at Berkeley.

The engineers developed designs for both the proposed unbonded brace frame system and a conventional braced frame system. The unbonded brace design was estimated to be approximately $1.2 million more expensive than the conventionally braced system. Using, presently available tools, that are rely heavily on the judgment of the analyst as to economic losses and structural damage, an economic analysis was performed for each system to quantify the potential loss of capital, contents and

research revenue using the basic procedures outlined in the previous sections. As illustrated in Figure 3, the evaluation suggested that the unbonded brace system would reduce annual losses due to earthquakes by $139K. Using a discount rate of 5%, the net present value of this reduction over the life of the building was calculated as $2.5M or more than twice the extra cost (see Figure 4). The equivalent return on investment using the unbonded braces in place of the conventionally braced frame was estimated at approximately 11%. As shown in Figure 5, the analysis suggested that the investment would theoretically pay for itself in approximately 15 years, far less than the 50 year projected lifetime.

UC Berkeley – Stanley Hall

$139K reduction in expected annual losses for unbonded braces compared to conventional system
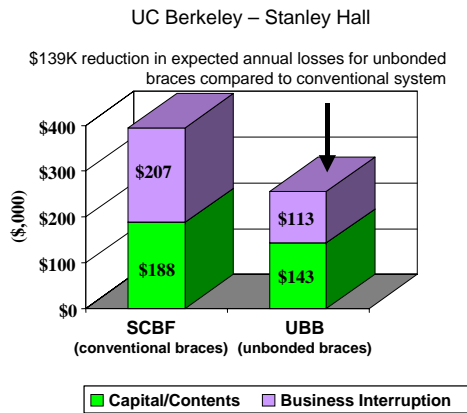
Figure 3. Reduction in expected annual earthquake losses attributable to the use of unbonded braces in place of conventional braces.

UC Berkeley – Stanley Hall

$2.5M reduction in the present value of expected losses for unbonded braces compared to conventional system (assuming 5% discount rate)
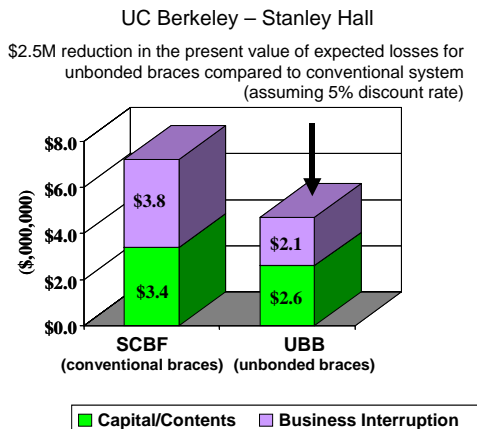
Figure 4. Reduction in the net present value of expected earthquake losses attributable to the use of unbonded braces in place of conventional braces.

UC Berkeley – Stanley Hall
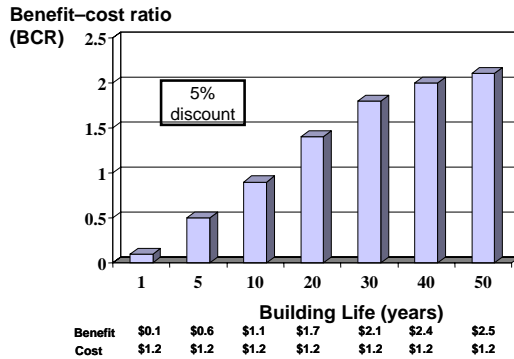
Figure 5. Ratio of benefits to costs for use of unbonded braces in place of conventional braces.

Recognizing the uncertainties involved, the basic parameters were varied to explore the sensitivity of the results to the basic assumptions. The analysis did not include direct consideration of some potential losses that are difficult to quantify. These include the loss of research faculty that might move to other institutions while repairs are made to the building, the losses associated with on-going experiments, and the sizable effect of the loss of the facility on the economy of the local community. The analysis, coupled with these qualitatively expressed considerations, provided sufficient evidence to support the investment in the enhanced system.

Enhanced Performance Objectives

San Leandro is a city on the San Francisco Bay, about eight kilometers from the Hayward Fault. Recently a national chain of automobile dealerships proposed to build a new sales and repair facility in the city. The projected cost of the building is $5 million with an inventory value of $2 million and projected gross annual revenue of nearly $4 million. The owner's lender required earthquake insurance in order to finance the project because of the proximity of the site to a major earthquake fault. The best quote on earthquake insurance the owner could find was $150,000 per year. The owner had both a long-term interest in reducing future potential losses, and a desire to reduce the amount of earthquake insurance the bank would require.

Using tools available today, an analysis was performed to estimate potential losses in a design level earthquake. The analysis suggested that for a large earthquake on the nearby fault, repair costs would approach about 40% of the replacement cost of the building. Most lenders require that this expected loss be less than 20% to remove insurance requirements. The design engineer developed an enhanced structural design that would reduce the expected losses. The design added structural elements and

increased the size of others. The total expected cost of the enhancements were estimated to be $200,000.

Reanalyzing the building with the proposed enhancements, the expected losses dropped to 16%. Furthermore, the expected reduction in capital, contents and business interruption losses on an annualized basis over the projected building life showed an overall return on investment of nearly 14%. This alone convinced the owner to implement the enhanced design. However, the greater value came when the owner presented the lender with the proposed enhancements and risk analysis. The lender agreed to waive the earthquake insurance if the enhancements were implemented. This made the effective return over 77%. Importantly, most of the return was in "hard dollars;" an insurance check that did not have to be written every year.

Insurance versus Seismic Upgrade for Enhanced Performance

The owner of a large precast concrete tilt-up warehouse south of San Francisco leases the building to several tenants. Recognizing the vulnerability of the older style of construction close to the Hayward fault, the owner purchased earthquake insurance on the property. The insurance covers 60% of the capital losses but has a 10% deductible that must be paid by the owner before any recovery from the insurance company. This policy ensures that, at most, the owner will recover only about 50% of the losses after an earthquake. The insurance company recently raised the cost of insurance to about 2.5% of the maximum recoverable amount. This means that the owner would have to suffer a complete loss every 40 years, on average, to justify the cost of insurance.

The owner was concerned about the volatility of the insurance market, especially considering that the rental market did not allow him to pass on insurance costs to the tenants. The owner wanted to develop a mitigation plan that would reduce the dependence on insurance. Performance-based engineering procedures were used to devise the mitigation solution and estimate capital losses in a design level event. The scope of the retrofit solution was adjusted to bring the median losses to approximately 15% of the projected replacement cost of the building. The reduction in expected loss made insurance far less attractive, or necessary, as a risk management tool. The cost of the strengthening solution was estimated at $130,000.

Based on financial analysis (Figure 6) the owner decided to cancel his insurance policy and invest the cost of the premium toward mitigation. This will finance the retrofit over a four-year period. The owner has made the decision to accept the risk over the next four years that a damaging earthquake could occur. After the mitigation is completed, however, the owner's investment will be generating a positive return on investment. They will achieve an equal measure of capital protection without having to buy insurance. Furthermore, the retrofit will reduce business interruption losses, for which they were not previously insured. The application of performance-based engineering and risk analysis procedures was able to offer the owner a quantitative

motivation to change the way they were spending money. The result was that the owner got more value without additional cost.

```
Current condition (with insurance)
  Year 1-
         Max. potential loss          $3,000,000
         Annual expected loss                      ($15,000)
         Annual expected insurance recovery         $7,500
         Annual insurance cost                     ($40,000)
            Total annual costs                                  ($47,500)

Mitigation condition (without insurance)
  Year 1-4
         Max. potential loss          $3,000,000
         Annual expected loss                      ($15,000)
         Annual expected insurance recovery            $0
         Annual insurance cost                         $0
         Annual mitigation cost                    ($40,000)
            Total annual costs                                  ($55,000)

  Year 5 and beyond
         Max. potential loss            $750,000
         Annual expected loss                       ($3,750)
         Annual expected insurance recovery            $0
         Annual insurance cost                         $0
         Annual mitigation cost                        $0
            Total annual costs                                   ($3,750)

Net rate of return on mitigation over 20 years                      62%
```

Figure 6. Example analysis of value of insurance versus mitigation.

REFERENCES

ATC. 1996. *The Seismic Evaluation and Retrofit of Concrete Buildings, Volumes 1 and 2*, ATC-40 Report, Applied Technology Council, Redwood City, California, www.atcouncil.org.

BSSC. 2000. *A Prestandard and Commentary for the Seismic Rehabilitation of Buildings*, prepared by the Building Seismic Safety Council; published by the Federal Emergency Management Agency, FEMA 356 Report, Washington, DC, www.fema.gov.

Deierlein, G., and S. Hamilton. 2003. Probabilistic framework of performance-based fire engineering and design, *Proceedings from the 2003 Designing Structures for Fire Conference — Baltimore, 2003*, Society of Fire Protection Engineers.

Hamburger, R. O. 2004. Development of next generation performance-based seismic design guidelines, *Proceedings of the International Workshop on Performance-based Seismic Design,* Bled, Slovenia, published by the Pacific Earthquake Engineering Research Center (PEER).

Moehle, J.P. 2003. "A Framework for Performance-Based Engineering", *Proceedings of the Tenth US-Japan Workshop on Improvement of Structural Design and Construction Practices*, Maui, Hawaii, 2003, Applied Technology Council, Redwood City, California, www.atcouncil.org or peer.berkeley.edu.

Whittaker, A. S., R. O. Hamburger, C. Comartin, R. Bachman and C. Rojahn. 2003. "Performance based engineering of building structures," *Proceedings*, 73rd Shock and Vibration Symposium, SAVIAC, San Diego, CA.

CHANGING THE PARADIGM FOR PERFORMANCE BASED DESIGN

Michael ASTRELLA[1] and Andrew WHITTAKER[2]

ABSTRACT

The principal investments in building construction are made in non-structural components and contents (NCCs). An efficient performance-based design paradigm should focus on these key investments and a new design paradigm is needed in order to do so. Structural framing systems should be selected on the basis of the required performance of NCCs. Protective systems appear to offer significant advantages over traditional framing systems in terms of both smaller median demands and smaller dispersion in demand for acceleration- and displacement-sensitive NCCs. The impact of structural framing system type on the NCCs demands is illustrated through response-history analysis of a 1960s-era hospital building located in Southern California.

Keywords: Performance; Investment; Protective systems; Design paradigm; Nonstructural.

1. INTRODUCTION

To date, tools for performance-based earthquake engineering have focused on performance *assessment* of structural framing. Only modest attention has been paid to *assessment* of nonstructural components and contents (NCCs) and to the development of tools for *design* of structural framing and NCCs.

HAZUS (NIBS 1997) provides important information on the financial importance of NCCs in a wide variety of building structures. Figure 1 displays the average percent investment in structural framing, nonstructural components and building contents for three types of building structures: office, hotel and hospital. In all cases, the investment in the structural framing is less than 20% of the total investment, and the percent investment in hospital construction is a mere 8% of the total. If a goal of performance-based earthquake engineering is to protect financial investments by minimizing total cost (including construction cost, annual maintenance cost and annualized earthquake-damage-related cost), close attention must be paid to those parts of a building in which the greatest investment is made.

[1,2]*Department of Civil, Structural and Environmental Engineering, University at Buffalo, State University of New York, Buffalo, NY 14260*

Traditionally, structural engineers have paid scant attention to NCCs because their design and detailing had not formed part of the structural-engineering scope of work. In those cases where structural engineers have designed and detailed NCCs, the components have been analyzed and designed (albeit indirectly) for the output of the structural framing. We contend that such an approach is inappropriate and that the performance-based design process should focus first and foremost on the most significant investments in the building, namely, the nonstructural components and contents.
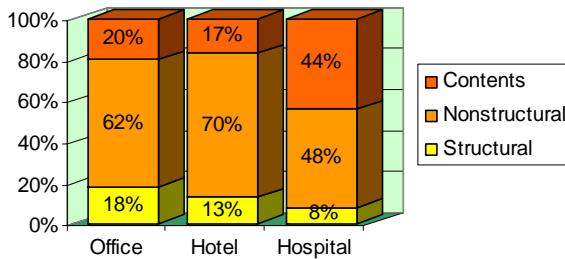
Figure 1. Investments in building construction (after E. Miranda).

2. UPDATING THE DESIGN PARADIGM

Figure 2 (from Hamburger) below illustrates the flow of a performance-based design procedure. Step 2 in the procedure involves selecting a preliminary design of the framing system (framing layout, system type, material, etc), which is then analyzed in step 3 for *performance capability*. In a robust performance assessment, this step would include design of both structural components and nonstructural components. If the computed performance is unacceptable, the design of the structural and nonstructural components is revised and then re-analyzed for performance capability.
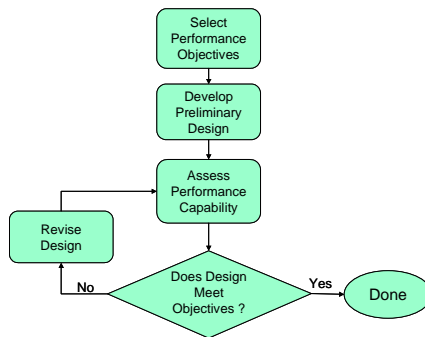
Figure 2. A performance-based design procedure (after R. Hamburger).

Ideally, the preliminary design of step 2 would satisfy, or come close to satisfying, the performance objective(s) selected for the building to avoid multiple design iterations. Assuming that fragility functions are developed in sufficient number and detail to characterize the vulnerability of NCCs for common building occupancies, guidance will be required to assist the structural engineer to select the structural system type (incl. material, seismic framing system, strength, ductility) that will deliver the intended building performance.

Studies are under way at the University at Buffalo to aid in the identification of optimal structural framing systems, noting that the optimal solution will vary as a function of the performance objectives. Weak and flexible, strong and stiff, and *protected* framing systems are being studied. A hospital structure was chosen for the baseline building because of the high value (measured as a percentage of the total investment) of the nonstructural components and building contents in such buildings (see Figure 1). Sample *preliminary* results from these studies are presented in the following sections with emphasis on demands on acceleration- and drift-sensitive NCCs. Results for velocity-sensitive components will be presented in Astrella (2004).

3. NORTHRIDGE HOSPITAL ASSESSMENT

The MCEER demonstration hospital is sited in Northridge, California, close to the epicenter of the 1994 Northridge earthquake. The building is a four story rectangular structure with a penthouse; the building was constructed in the early 1970s. The lateral-load resisting system is composed of perimeter steel moment-resisting frames and two interior moment-resisting frames in the transverse direction.

To facilitate analysis of the hospital building, a simplified mathematical model of the building was prepared: the penthouse was eliminated, the chamfered southwest corner of the building was eliminated and the framing was made both regular and symmetric about each horizontal axis. Two views of the building are presented in Figure 3: a building elevation and a plan view showing gridlines. The plan dimensions of the building are 83.8 m by 17.2 m and the story heights (1st to 4th) are 4.1 m, 3.8 m, 3.8 m and 3.8 m. In the transverse direction, the width of the exterior bays is 4.9 m and the width of the interior bay is 7.4 m. The moment-resisting frames are located on grids B, F, J, N, 2 and 5. All remaining frames were constructed with semi-rigid seat angle beam-to-column connections.

To illustrate the impact of structural-system choice on the response of acceleration- and drift-sensitive NCCs, the building was further simplified and analyzed in the north-south direction only. Specifically, the building was sliced along grid line H (the building centerline) and the moment frame of grid line F was relocated to grid lines H and B: producing a regular and symmetric building with no torsional response. Column bases on grid lines H and B were fixed, reflecting the in-situ conditions; all remaining column bases were pinned.

a. building elevation

b. plan view
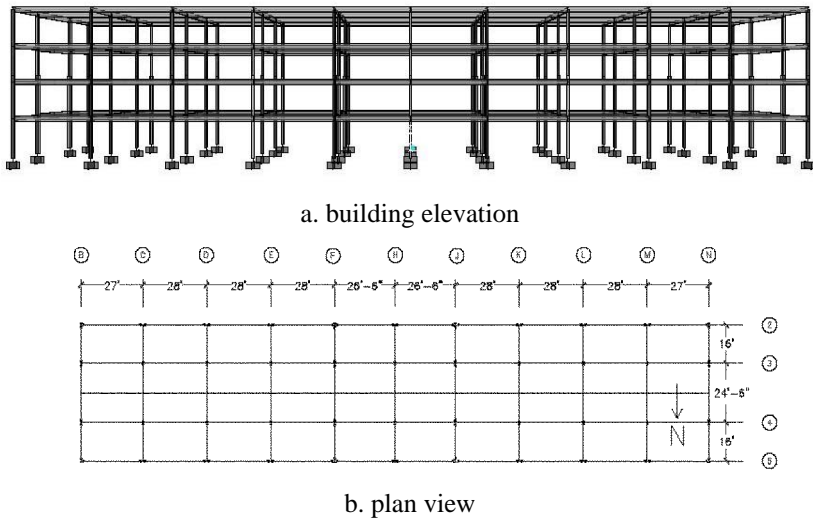
Figure 3. MCEER demonstration hospital.

Protection of structural framing systems against gross damage during severe earthquake shaking motivated the initial development (in the 1970s and 80s) and implementation (1980s) of seismic protective systems: seismic isolation bearings and supplemental passive damping devices. Hospital buildings were early candidates for the use of protective systems because of the need to maintain hospital function after a major earthquake: essentially eliminating damage to the structural framing. Nowadays, seismically isolated buildings are designed to restrict substantial (or all) inelastic action to the isolators in maximum capable earthquake shaking. Buildings incorporating supplemental dampers are designed typically to restrict substantial inelastic action (damage) to the damping devices in design and maximum earthquake shaking and thus to eliminate damage to components of the gravity-load-resisting system.

Fifteen mathematical models representing different traditional and *protected* lateral-force-resisting systems were developed in the OpenSees software environment (http://opensees.berkeley.edu/) for analysis and evaluation. The 15 models are summarized in Table 1; the baseline model was M3. The *traditional* framing systems are M3 and M6: moment-resisting frames. Buckling restrained braces (BRBs), displacement-dependent dampers, were implemented in M7. Fluid viscous dampers (FVDs), velocity-dependent dampers, were implemented in M8 and M9. Models M10 through M13 include linear viscoelastic seismic isolation bearings: one mathematical model used for low- and high-damping rubber bearings. Models M14 and M15 include bilinear seismic isolation bearings: the mathematical model used typically for lead-rubber and Friction Pendulum™ bearings. Much additional information will be available in Astrella (2004).

Table 1. Description of mathematical models

Model	Description	T_1 [1] (secs)
M1	Baseline model of 1970s in-situ building; designed for the strength and drift limits of the 1970 Uniform Building Code; best-estimate model for *non-moment*-resisting connections.	0.70
M2	Similar to M1 except rigid connections used for *non-moment*-resisting connections.	0.68
M3	Similar to M1 except pinned connections used for *non-moment*-resisting connections.	0.71
M4	1960s variant of M1: design drift limits of M1 not imposed.	1.74
M5	Similar to M4 except rigid connections used for *non-moment*-resisting connections.	1.58
M6	Similar to M4 except pinned connections used for *non-moment*-resisting connections.	1.81
M7	M6 augmented with buckling restrained braces (BRBs) to provide approximately a 300% increase in lateral stiffness. BRBs installed in paired diagonal braces in the exterior bays on grid lines B and H.	0.97
M8	M6 equipped with fluid viscous dampers (FVDs) to provide approximately 25% of critical damping in the first mode. FVDs installed in paired diagonal braces in the exterior bays on grid lines B and H.	1.81
M9	M6 equipped with fluid viscous dampers (FVDs) to provide approximately 40% of critical damping in the first mode. FVDs installed in paired diagonal braces in the exterior bays on grid lines B and H.	1.81
M10	M3 equipped with viscoelastic seismic isolation bearings; isolated period is 2.5 seconds; approximately 10% of critical damping in the first mode.	2.60
M11	M3 equipped with viscoelastic seismic isolation bearings; isolated period is 2.5 seconds; approximately 20% of critical damping in the first mode.	2.60

Table 1. — *Continued*

M12	M3 equipped with viscoelastic seismic isolation bearings; isolated period is 3.5 seconds; approximately 10% of critical damping in the first mode.	3.57
M13	M3 equipped with viscoelastic seismic isolation bearings; isolated period is 3.5 seconds; approximately 20% of critical damping in the first mode.	3.57
M14	M3 equipped with coupled bilinear seismic isolation bearings: $Q_d = 0.06W$; second-slope isolation period is 2.5 seconds; isolator yield displacement is 25 mm.	2.60[1]
M15	M3 equipped with coupled bilinear seismic isolation bearings: $Q_d = 0.06W$; second-slope isolation period is 3.5 seconds; isolator yield displacement is 25 mm.	3.57[1]

1. First mode period in transverse (short) direction.
2. Period calculation based on second slope (post-yield) isolator stiffness.

Preliminary results are presented in this paper for 11 of the 15 models: M3, M6, M7, M8, M9, M10, M11, M12, M13, M14 and M15. Seismic demands on NCCs in the 11 buildings was assessed by nonlinear response-history analysis in the transverse (north-south) direction only. The earthquake histories used for the response-history analysis were those generated for a NEHRP Soil Type S_D (firm soil) site in Los Angeles as part of the SAC Steel Project (Sommerville et al. 1997). Three bins of 20 histories were developed, each representing a different probability of exceedance (2% in 50 years, 10% in 50 years and 50% in 50 years). The response spectrum for each history in the 10% in 50 year (hereafter denoted 10/50) bin is shown in Figure 4a. The median, 16th and 84th percentile spectra are shown in Figure 4b together with the target spectral ordinates (shown circled) at periods of 0.3, 1, 2 and 4 seconds, to provide the reader with information on the variability in the earthquake histories used in the response-history analysis.
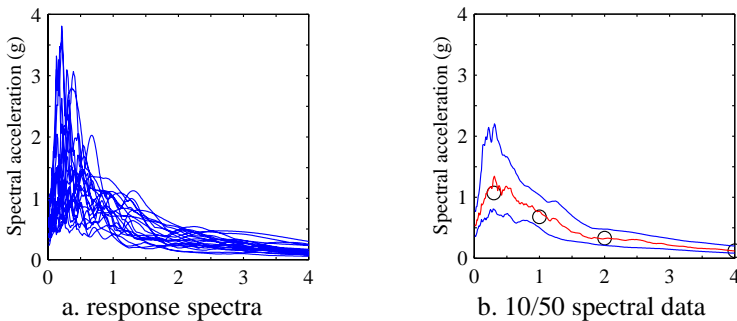

a. response spectra   b. 10/50 spectral data

Figure 4. Binned 10/50 ground motion data for response-history analysis.

Sample results from the response-history analysis are presented in Figures 5 through 9 for the 10/50 motions. Figure 5 presents a summary of the maximum drift responses for the 11 models noted above. Median, maximum, minimum, 16th percentile and 84th percentile results are presented assuming that the maximum responses are lognormally distributed. Drift data (relative displacement as a percentage of height) are presented for the 1st, 2nd and 4th stories and the roof.[3] The horizontal axis in each subplot denotes the model number (e.g., M3 per Table 1). The yield drift in each story for M3 and M6, based on nonlinear static analysis, are shown in the subplots of Figure 5 to identify the degree of inelastic action (damage) in the non-isolated building frames. The trends of Figure 5 are well established, namely, that adding lateral stiffness, viscous damping and seismic isolation reduce interstory drift. As expected, the drifts in the isolated frames (M10 through M15) are substantially smaller than those in the *traditional* frames (M3 and M6) and the frames equipped with supplemental damping devices (M7, M8 and M9). The addition of the displacement and velocity-dependent dampers led to significant reductions in the median maximum displacement response of the weak and flexible frame (M6). Based on median response data, a) the traditional moment frames (M3 and M6) each sustained structural damage; b) damage in the building equipped with BRBs (M7) was limited primarily to the BRBs (except in the 4th story, indicating that an increase in BRB size is needed); and c) the viscous damped frames (M8 and M9) sustained negligible damage. For the non-isolated buildings (M3, M6, M7, M8 and M9), the coefficient of variation in the peak roof drift is greatest (0.33) for M6 (mean peak roof drift = 2.3 %) and smallest (0.28) for M9 (mean peak roof drift = 0.95 %). The addition of viscous dampers (M8 and M9) to the weak and flexible building (M6) reduced substantially the median maximum roof drift (by 44% for M8 and 56% for M9) and the coefficient of variation in the maximum roof drift (from 0.33 for M6 to 0.29 for M8 and 0.28 for M9).

Figure 6 summarizes the maximum *peak* floor acceleration responses at the 2nd, 3rd, 4th and roof levels. Median, maximum, minimum, 16th percentile and 84th percentile results are presented assuming that the maximum responses are lognormally distributed. The trends seen in the four subplots of Figure 6 are also well established, namely, that adding lateral stiffness increases peak floor accelerations, and adding viscous damping or seismic isolation bearings reduce peak floor accelerations. For the non-isolated models, the coefficient of variation in the peak 2nd floor acceleration is greatest (0.37) for M7 (mean peak acceleration = 0.98 g) and smallest (0.30) for M8 and M9 (mean peak acceleration = 0.49 g). The addition of viscous dampers to the weak and flexible building (M6) reduced the median peak 2nd floor acceleration (by 29% for M8 and M9) and the coefficient of variation in the peak 2nd floor acceleration (from 0.32 for M6 to 0.30 for M9).

---

[3] The earthquake shaking is imposed at the first ground level (A1) in the non-isolated models M3, M6, M7, M8 and M9, and at the basement level (A0) for the isolated models M10, M12, M13, M14 and M15.

a. 1st story   b. 2nd story

c. 4th story   d. roof drift
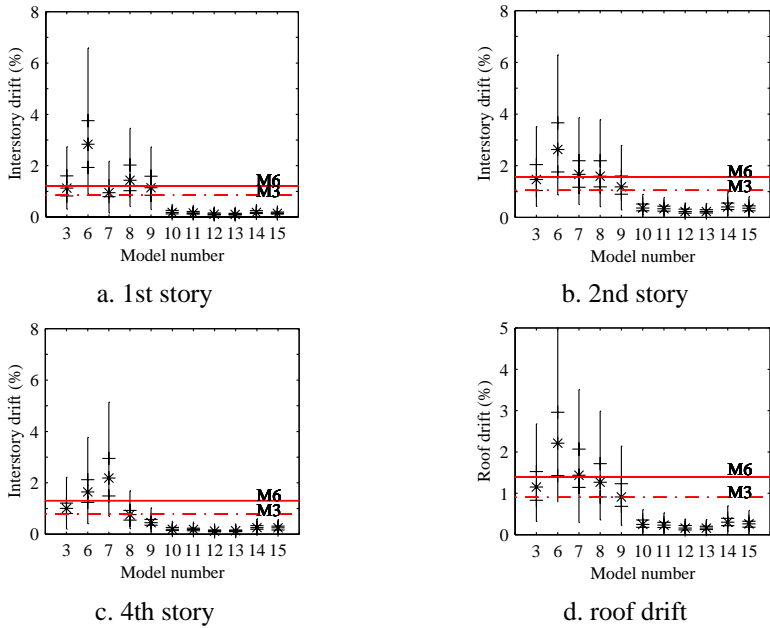
Figure 5. Maximum drift responses for 10/50 earthquake histories.

a. 2nd floor   b. 3rd floor

c. 4th floor   d. roof
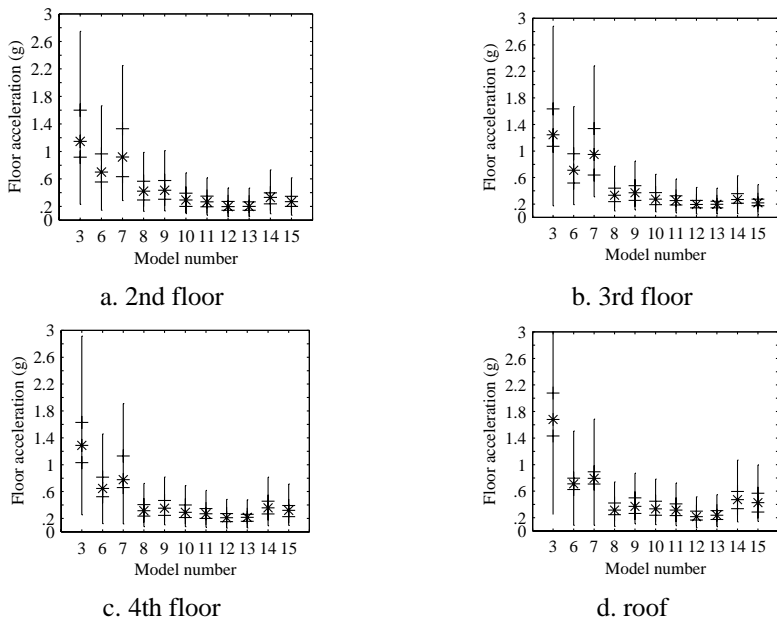
Figure 6. Maximum acceleration responses for 10/50 earthquake histories.

In FEMA 273/356, the intersection of the median capacity (pushover) and median demand (hazard) curves is termed a *performance point*. Such a point, although instructive, provides no information on the impact of uncertainty and randomness on the capacity and demand calculations and by extension on the building performance. Reinhorn extended the concept of the performance point to a *performance space*, to account for both uncertainty and randomness in a rigorous manner. Figure 7 presents performance points using median maximum drift (ID*) and median peak floor acceleration (A*) as the performance metrics; ID* and A* are defined in the figure. Alternate groupings of ID* and A* (e.g., A2/ID1) might be more appropriate for nonstructural components such as suspended ceiling systems. (In Figure 7a, the median peak 1st floor acceleration of each of the non-isolated models is equal to the median peak ground acceleration. In the isolated models, the 1st floor acceleration is measured above the isolation interface.) In terms of demands on NCCs, performance points adjacent to the origin are preferable to those points remote from the origin. On the basis of the chosen metrics, the performance of the buildings equipped with supplemental fluid viscous dampers or seismic isolation bearings is superior to that of the *traditional* moment-frame buildings or the building equipped with BRBs.

a. 1st floor (A1), 1st story (ID1)

b. 2nd floor (A2), 2nd story (ID2)

c. 4th floor (A4), 4th story (ID4)
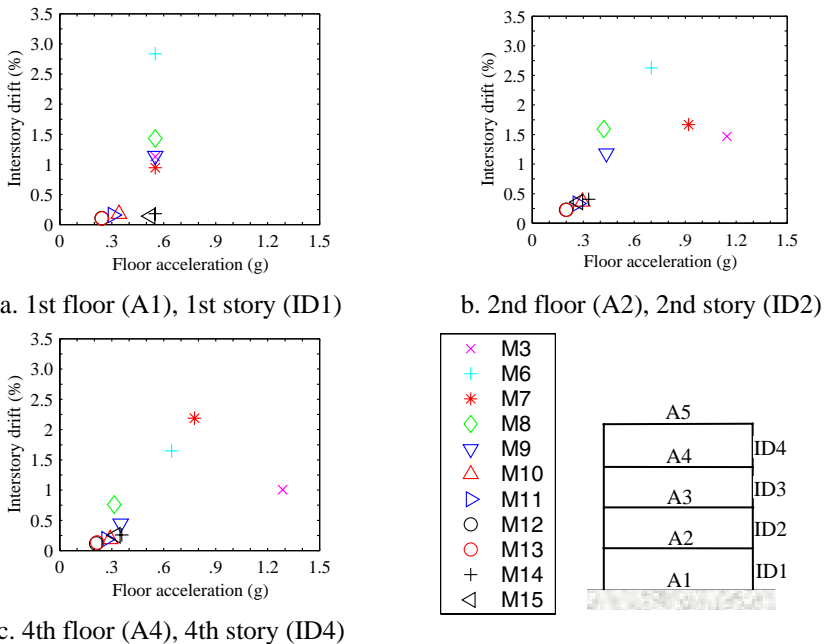
Figure 7. Performance points for 10/50 earthquake histories.

121

Figure 8 presents one possible form of the *performance space*, in which only ground motion variability has been considered. Herein, the performance space is a box defined by the 16th and 84th percentile maximum drift and zero-period floor acceleration responses. An optimal performance space should be small in size (indicating small variability in displacement and acceleration responses) and located close to the origin.

a. 1st floor (A1), 1st story (ID1)

b. 2nd floor (A2), 2nd story (ID2)

c. 4th floor (A4), 4th story (ID4)
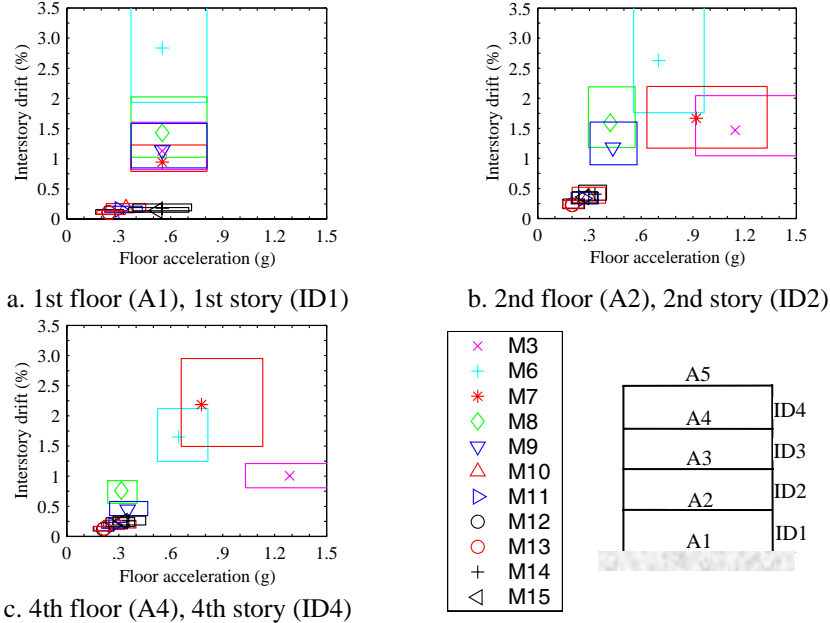
Figure 8. Performance spaces for 10/50 earthquake histories.

On the basis of the data presented in Figure 8, the performance of the isolated buildings is superior to that of the other buildings in terms of smaller displacement and acceleration demands on NCCs. Of the remaining *traditional* and *protected* lateral-force-resisting systems, the buildings equipped with fluid viscous dampers (M8 and M9) outperform the remaining 3 buildings (M3, M6 and M7).

For many acceleration-sensitive NCCs, peak floor acceleration alone is an inefficient predictor of damage: an observation made years ago by engineers tasked with designing mechanical systems in nuclear power plants. Better estimates of the vulnerability of acceleration-sensitive NCCs can be developed through the use of floor (in-structure) acceleration spectra. Median 5% damped median floor acceleration spectra for the 2nd floor (A2) and 4th floor (A4) of the 11 models for the 10/50 earthquake histories are presented in Figures 9a and 9b. The stiff and strong moment frame building (M3) and the building equipped with BRBs (M7) produce the highest spectral acceleration demands across a frequency range from 1 Hz to 100 Hz. The smallest acceleration demands are associated with the viscous damped frames

(M8 and M9) and the isolated frames (M10 through M15). Importantly, the spectral peaks of the moment-frame structures (M3 and M6) are suppressed through the addition of viscous damping: an observation reported first by Pavlou and Constantinou (2004).

a. 2nd floor (A2)

b. 4th floor (A4)

c. normalized 4th floor (A4)
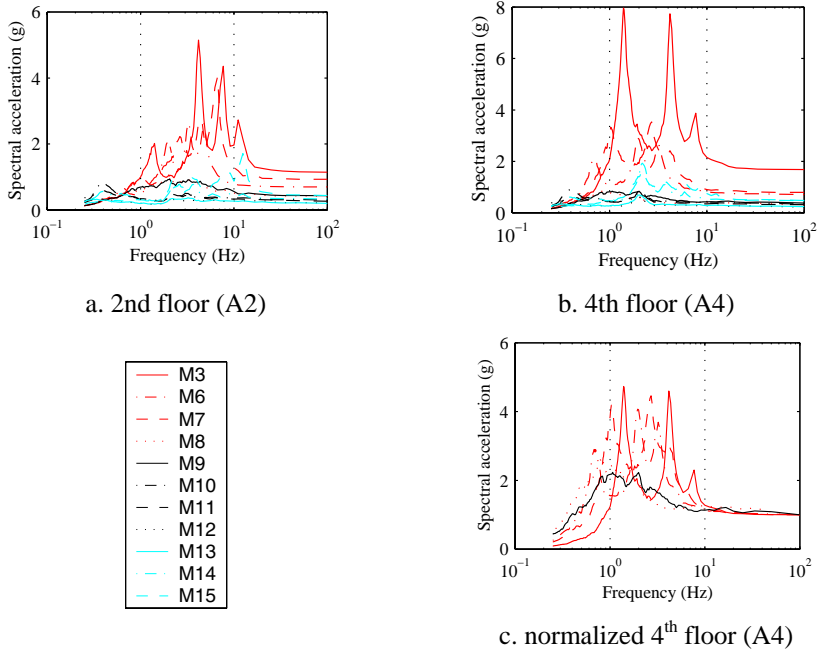
Figure 9. Floor acceleration spectra for 10/50 earthquake histories.

Normalized 5-percent damped 4th floor acceleration spectra are presented in Figure 9c for the 5 non-isolated buildings (M3, M6, M7, M8 and M9). The figure shows the amplification of the peak floor acceleration as a function of structural framing system. For the same peak floor acceleration, the performance of the viscous damped buildings, M8 and M9, is clearly superior to the *traditional* moment-frame buildings and the building equipped with BRBs.

4. CLOSING REMARKS

The next generation tools for PBEE will recognize the substantial financial investment in nonstructural components and contents (Figure 1). Significant research work is underway at the three NSF-funded earthquake research centers to develop performance assessment tools for NCCs (Whittaker and Soong, 2003).

To reduce losses in buildings in future earthquakes, the current performance-based design paradigm must be updated to shift the focus to NCCs. The geometry, type and materials that comprise a structural framing system should be selected by the

structural engineer so as to protect the primary investment: the NCCs. Guidance on the appropriate choice of structural framing system to meet NCCs-driven performance objectives is needed. The *preliminary* studies reported in this paper illustrate the benefits of seismic protective systems in reducing the median seismic demand and/or the variability in seismic demand on acceleration- and displacement-sensitive NCCs. On the basis of the limited studies reported herein, framing systems incorporating seismic isolation bearings and/or supplemental fluid viscous dampers appear to offer superior performance to traditional framing systems.

ACKNOWLEDGMENTS

REFERENCES

Astrella, M. (2004). "Changing the paradigm for performance-based earthquake design." *M.Sc. Thesis*, Department of Civil, Structural and Environmental Engineering, State University of New York, Buffalo, NY, August.

FEMA. (1997). "NEHRP Guidelines for the seismic rehabilitation of buildings." *Report FEMA 273*, Washington, D.C.: Federal Emergency Management Agency.

NIBS. (1997). "Earthquake loss estimation technology — HAZUS; user's manual." Washington, D.C.: National Institute of Building Sciences.

Pavlou, E., and M. C. Constantinou. (2004). "Response of nonstructural components in structures with damping systems." Paper submitted for review, *Journal of Structural Engineering*, Reston, VA: American Society of Civil Engineers.

Somerville, P., N. Smith, S. Punyamurthula, and J. Sun. (1997). "Development of ground motion time histories for Phase 2 of the FEMA/SAC Steel Project." *Technical Report SAC/BD-97/04*, Sacramento, CA: SAC Joint Venture.

Whittaker, A. S., and T. T. Soong. (2003). "An overview of nonstructural components research at three U.S. Earthquake Engineering Research Centers." *Proc., ATC Seminar on Seismic Design, Performance, and Retrofit of Nonstructural Components in Critical Facilities*, Report ATC-29-2, Redwood City, CA: Applied Technology Council.

THE ATC-58 PROJECT PLAN FOR NONSTRUCTURAL COMPONENTS

Robert E. BACHMAN[1]

ABSTRACT

The Applied Technology Council (ATC) with sponsorship from the Federal Emergency Management Agency has initiated a project to develop next-generation performance-based seismic design guidelines that will apply to both new and existing buildings (the ATC-58 project). The project includes a significant focus on non-structural components in recognition of the major economic losses associated with damage of non-structural components observed in recent earthquakes. In this paper, the plan for development of guidelines for the nonstructural components portion of the project is presented. The planned guidelines will cover the process of designing, testing, verifying and installing nonstructural components and will provide guidance on how one would go about assessing the probable life loss, repair costs and downtime associated with various design alternatives, as well as the associated indirect economic impacts. When implemented the plan will provide tools that will allow these losses to be reduced in the future in a practical and reliable way. The effort involved in compiling probabilistically based performance data and acceptance criteria for the many structural and nonstructural systems that comprise the building inventory is an immense task which is beyond the funding ability of any single private or public agency. Therefore, it is anticipated that much work associated with developing this performance data and acceptance criteria will be performed outside the project and will continue on for many years.

Keywords: Design criteria; Performance-based engineering; Nonstructural components.

1. INTRODUCTION

The Applied Technology Council with sponsorship of the Federal Emergency Management Agency (FEMA) has commenced on a project to develop next-generation performance-based seismic design guidelines (The ATC-58 Project). The guidelines are to be applicable to the design of new buildings as well as to the upgrade of existing buildings. The guidelines are to address both the design of building structural systems and the nonstructural components housed within the buildings. There is a significant project focus on nonstructural components in recognition of the major economic losses associated with damage of nonstructural components observed in recent earthquakes. The guidelines will be probabilistically

---

[1] *Principal, Robert E. Bachman, Consulting Structural Engineer, Sacramento, California, USA*

based to allow performance to be evaluated for specified levels of seismic hazard with defined reliability and levels of confidence.

Performance-based seismic design originally evolved as a concept whereby the desired performance level (e.g., immediate occupancy) for a given structure (including the nonstructural components housed within), along with a specified level of shaking, are defined at the initiation of the design process. The decision-maker is asked to select one or more of these performance levels, and a ground motion event or hazard level for which this performance is to be achieved and the designer is expected to develop a design capable of meeting these expectations. Under the ATC-58 project, this concept has evolved such that performance is defined in terms of the risk of life loss, direct economic loss (repair / replacement cost) and indirect economic loss (loss associated with facility downtime), considering either individual earthquake events or the entire range of events that may affect a facility. The designer will be provided with a procedure that is intended to allow determination as to whether the desired performance can be achieved. For critical facilities, the selected performance may be dominated by the need to have designated nonstructural components function following severe earthquakes.

Existing codes for the seismic design of new buildings are prescriptive in nature and are intended principally to provide for life-safety when the design level earthquake occurs. While current codes are intended to produce buildings that meet a life safety performance level for a specified level of ground shaking, they do not provide an explicit procedure that enables the designer to determine if other performance levels will be achieved, or exceeded. During a design level earthquake, a code-designed building should achieve the goal of preventing the loss of life or life-threatening injury to the occupants, but could sustain extensive structural and nonstructural damage and be out of service for an extended period of time. In some cases, the damage may be too costly to repair, with demolition being the only viable option.

With the publication of the NEHRP *Guidelines for the Seismic Rehabilitation of Existing Buildings* (FEMA 273 Report) in 1997, the technology available for the seismic rehabilitation of buildings greatly advanced beyond the technology available for the seismic design of new buildings. Designers were provided, for the first time, with a consistent set of procedures that enabled them to execute performance-based design. These procedures were further refined in the *Prestandard and Commentary for the Seismic Rehabilitation of Buildings* (FEMA 356), which was published in 2000. While these documents represent important and significant advances in seismic design practice, the FEMA 273/356 procedures have several significant shortcomings. First the procedures do not directly address control of economic loss, one of the most significant concerns of decision makers. Secondly, the procedures are focused on assessing the performance of individual building components, rather than the building as a whole. Most significantly, however, the reliability of the procedures in delivering the desired performance is not known and cannot easily be determined.

The development of next-generation guidelines for the ATC-58 project is currently planned to occur in two phases. The first phase comprises development of building performance assessment guidelines. In a major departure from prior performance based approaches, rather than expressing performance in terms of arbitrary performance levels, the next-generation procedures characterize performance directly in terms of the probable loss of life, repair costs and occupancy/functionality interruptions times resulting from earthquake damage. The evaluation procedures closely follow the framework for performance-based earthquake engineering developed by the Pacific Earthquake Engineering Research Center (PEER) in which probable earthquake losses are calculated by integrating over the ground shaking hazard, probable structural response given the ground motion intensity, probable damage levels given the structural response and probable loss given damage (Deierlein, 2004). In the second phase, performance-based design procedures will be developed to allow engineers to efficiently determine appropriate combinations of structural stiffness, strength and ductility, as well installation procedures for nonstructural components to achieve various levels of performance capability. Stakeholders' guides will be developed to assist in selecting appropriate performance objectives as the basis for building development projects.

Details regarding the background, budget and schedule of the ATC-58 project along with a description and example illustrations of the general methodology of the next-generation guidelines are provided in a companion paper in this conference (Hamburger, 2004). The remainder of this paper will focus primarily on the plan for developing the first phase performance assessment guidelines for nonstructural components for the project. The term nonstructural components covers a wide range of items that include all items in a building other than the building structural system and its foundation. Nonstructural components include all architectural elements such as cladding, glazing, ceiling systems and interior partitions that are permanently attached to the building. Nonstructural components also include all mechanical and electrical equipment such as fire sprinkler systems, water and sewer piping, HVAC (heating, ventilating and air conditioning) systems and electrical distribution and lighting systems that are permanently attached to the building. Nonstructural components may also include building contents such as furniture, movable partitions, computers, movable equipment and merchandise.

2. PERFORMANCE ASSESSMENT PROCESS

The performance assessment process, illustrated in Figure 1 below, begins with definition of one (or more) ground motion *Intensity Measures* (*IM*s) that should capture the important characteristic(s) of earthquake ground motion that affect the response of the structural framing and nonstructural components and building contents. The *IM*, which for the building structural system may be a ground motion parameter, such as peak ground acceleration, peak ground velocity, peak ground displacement, a spectral response quantity such as spectral displacement, velocity or

acceleration, or another parameter. *IM's* are expressed typically as a function of mean annual probability of exceedance, *p*[*IM*], which is specific to the location of the building and its mechanical characteristics (e.g., first and second mode periods). Most nonstructural components and systems, unlike structures, are not directly affected by the ground shaking, but rather are affected by motion or shaking of the structure to which they are attached or upon which they are supported. Therefore, for nonstructural components and systems, except those mounted at grade, the *IM* must characterize not the intensity of the ground shaking, but rather the intensity of the response motion of the building structure at the points of attachment of the nonstructural components.
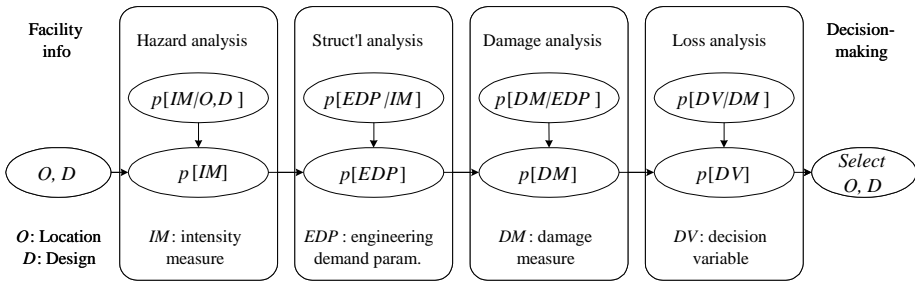
Figure 1. Steps in the performance assessment process (Moehle 2003).

For building structures, the second step of the assessment process is to determine *Engineering Demand Parameters* (*EDPs*) that describe the response of the structure as a whole and of its individual structural components. This is accomplished by structural response simulations using the ground shaking *IM*s and corresponding earthquake motions. Similarly, for nonstructural components, *Nonstructural Engineering Demand Parameters* (*EDP-Ns*) that describe the response of the nonstructural components and contents to earthquake shaking transmitted to them by the supporting structure, must be determined. Many nonstructural components act essentially as rigid bodies and have no response that is distinctly different than the motion of the structure that supports them. For these classes of nonstructural components, *EDP-Ns* that quantify the structural response, e.g., peak interstory drift demands, may be used directly to predict nonstructural performance. However, some nonstructural components have inherent flexibility and will either amplify or attenuate the motions transmitted to them by the structure and in the process, will experience motions that are different from those experienced by the supporting structure. For this class of nonstructural components, the second step in the performance assessment process is to select structural *EDPs* calculated from the predicted response of the structure, that predict the severity of shaking the nonstructural components are subjected to. An example of such a structural *EDP* is a floor response spectrum. In essence, these structural *EDPs* serve as *IMs* for the nonstructural components. Then

128

for these flexible nonstructural components, a third step is accomplished by performing structural response simulations of the nonstructural components using the structural *EDPs* as inputs to the nonstructural response calculations. The products of this step are conditional probabilities of experiencing nonstructural component response of different levels, *p[EDP-N/IM]*, which can then be integrated with the *p[IM]* to calculate mean annual probabilities of exceeding each nonstructural *EDP-N, p(EDP-N)*.

Next, the *EDP*s for the structural and nonstructural components and building contents are linked to *Damage Measures* (*DM*s) that describe the physical condition of those components and contents. *Damage Measures* include *effective* descriptions of damage to characterize the functionality, occupancy-readiness, life safety consequences and necessary repairs of or to the building including nonstructural components and systems. The product of this step are conditional probabilities, *p[DM/EDP]*, which are then integrated with *p[EDP]* to calculate the mean annual probability of exceedance for the *DM*, *p[DM]*.

The final step in the performance assessment process is the calculation of *Decision Variables* (*DV*s) that serve to translate damage estimates into quantities that are useful to those tasked with making risk-related decisions. The *DV*s under development at this time at PEER relate to one or more of the three decision metrics Figure 2.1, direct *dollar* losses, *downtime* (or restoration time), and *deaths or serious injuries* (casualties). The products of this step are conditional probabilities, *p[DV/DM]*, which are then integrated with *p[DM]* to calculate the mean annual probability of exceedance for the *DV*, *p[DV]*.

3. PLANS FOR NONSTRUCTURAL COMPONENTS

To support the development of the performance assessment guidelines for nonstructural components, the following tasks are currently planned during the first phase of the ATC-58 Project.

1. Identify *EDP-Ns* that are useful and efficient in predicting damage of nonstructural components. Establish the linkage between building *EDPs* and nonstructural *EDP-Ns*.

2. Identify the structural systems and components that are important to the performance of buildings and identify damage states that are meaningful to each of these components and systems. This task includes grouping these systems and components into broad categories that have similar damage states and similar *EDP-Ns* which best relate to the damage states.

3. Develop generalized preliminary fragility functions and associated loss functions for each of the broad categories identified in Task 2. These functions will be initially developed based on best available data and on expert opinion.

4. Develop standard procedures including testing protocols for quantifying the performance capabilities (fragility and loss functions) for the various types of components and systems.

5. Develop a framework for adjusting the generalized fragility and loss functions with available and more accurate and reliable fragility and loss functions for specific components and systems obtained by testing, analysis or empirical observations.

6. Development guidelines describing the Performance Assessment Procedure and provides examples which illustrate usage of the procedures.

In the remaining portions of this section, the above tasks are described in more detail.

3.1   Identify Nonstructural Engineering Demand Parameters

Traditional nonstructural engineering demand parameters (*EDP-Ns*) found in current codes and first generation performance based guidelines are limited to component forces and for some limited cases interstory relative displacement (drifts). Component force demands are determined by applying a lateral load to the center of mass of the component and then typically computing the forces in the component's bracing and attachments. Some nonstructural items such as cladding are specifically designed using interstory drift as the *EDP-N*. Typically, drift demand for cladding was determined based on the maximum drifts permitted for the structural system and not on the actual computed drift for the specific structure. Internal member forces caused by or imposed by interstory drifts were then added to the forces resulting from other loadings when drift was a consideration. In code-based designs and present performance based design guidelines, nonstructural component design forces are calculated using indirect and imprecise procedures based on empirical relationships. Therefore the result is traditional *EDP-Ns* do not necessarily correlate well with observed damage of nonstructural components in earthquakes.

For the next generation performance based engineering guidelines, an important criteria in the selection of *EDP-Ns* will be the correlation of *EDP-Ns* with damage. It is desirable for the *EDP-Ns* to be both useful and efficient. For an *EDP-N* to be useful, it must be compatible with the structural analysis or testing protocol which is used evaluate the nonstructural component response. An *EDP-N* is efficient if the variability associated with prediction of response and associated tend to be small. In this task, *EDP-Ns* of significance will be identified. The primary focus initially will be to identify *EDP-Ns* that are directly associated with building response motions such as interstory drift and peak floor acceleration. Other building response motions that are likely to be of significance include spectral acceleration of the floor at the fundamental period of the nonstructural component. A plot of a 5% damped roof response spectra and ground response spectra measured in a 19 story building during the Northridge earthquake is shown in Figure 2. It should be noted that the roof

spectra is several times larger than the ground spectra. For building contents subject to sliding and toppling, the *EDP-N* may be more associated with peak floor velocity. A second class of *EDP-Ns* which will be investigated are those associated with calculated analysis determination. For example, a significant *EDP-N* is likely to be the inelastic rotation of a pipe joint where the input to the pipe stress analysis is floor spectra and relative displacements of the floors.
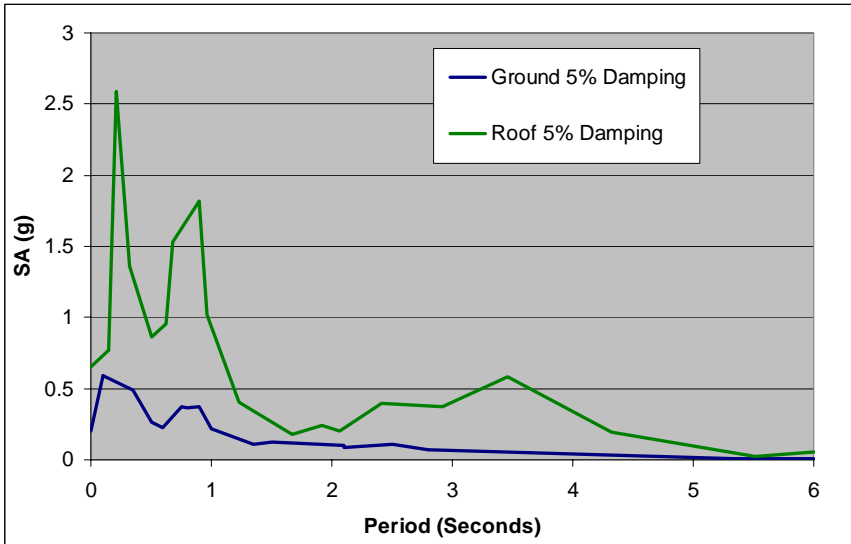
Figure 2. Measured 5 % damped elastic response spectra —19-story bldg.

3.2 Identify and Categorize Significant Nonstructural Systems and Components

As noted earlier, nonstructural components includes all items attached to or contained within a building other than the primary structural system. There are really countless types of nonstructural systems and components and it would be impractical to develop a performance prediction methodology that explicitly considered all the components that exist in any one building let alone the entire inventory of buildings that must be addressed. However, it should be possible to identify certain components and systems that that have particularly important and significant consequences with regard to life loss or serious injury, repair costs and downtime and categorize them into several broad group which have similar performance characteristics and engineering demand parameters. Similarly it should be possible to identify components which have a lesser impact and to similarly categorize them.

In this task, general broad categories will be identified such as systems/components that could, if damaged:
1. leak
2. result in fire ignition
3. prevent safe building occupancy
4. result in significant repair costs
5. result in a serious falling hazard
6. prevent critical functionality
7. result in serious business losses

These broad categories might be subdivided into *EDP-N* sensitivity. For example, the following 5 categories of *EDP-Ns* might be identified.
1. Relative Displacement between Floors (drift)
2. Peak Floor Acceleration
3. Peak Spectral Acceleration of Floor at Fundamental Period of Component
4. Peak Velocity of Floor
5. Peak Stress in an individual component (e.g., tank or pipe)

Individual significant components would next be identified and then categorized into one the categories and subcategories. For example, a drywall partition might be categorized as a component that may result in significant repair cost when damaged and subcategorized as having an *EDP-N* of drift. An uninterruptible power supply might have be categorized as having critical functionality and be subcategorized as having an *EDP-N* of peak spectral acceleration at the fundamental period of the component. A comprehensive and systematic categorization would be done of all components judged to be significant to either life loss or injury, repair cost or downtime. Remaining components would not be categorized but instead lumped in a few general categories. At this point we are using the term "bin" as an identifier for the broad categories.

3.3 Develop Generalized Fragility and Loss Functions

In this task, generalized fragility functions will be developed for each bin identified in the previous task. The fragility functions would utilize the *EDP-N(s)* identified for the bins. The fragility functions would initially be developed based on available resources and expert opinion.

Nonstructural fragilities are functions that relate the probability that a nonstructural component will experience damage greater (or less) than a certain level, given that it is driven to a certain level of response, as measured by the nonstructural engineering demand parameter. As is the case with building response functions, fragilities are expressed as probability distributions, rather than deterministic relationships in order to account for the variability and uncertainty inherent in the process of predicting nonstructural damage as a function of nonstructural response.

The variability is associated with such factors as the random character of the primary structural and associated nonstructural response to individual ground motion records and the inability of simple engineering demand parameters to distinguish between this response variation and the damage it causes. For example, two different ground motions may each produce peak interstory drift demands of 4 inches in a structure, however, one of these ground motions may cycle the structure to this drift level one time then restore the structure to small oscillations about its original position while the second ground motion may cycle the structure to this drift level several times and leave the structure displaced nearly to this level. Clearly the latter motion will be more damaging of the structure than the first motion, though the value of the engineering demand parameter is the same. Such effects are not predictable unless the precise ground motion and structural response is known. Uncertainty is introduced through such factors as lack of precise definition of material strength and construction quality.

In order to form fragility functions it is first necessary to establish measures of damage. A variety of such measures are possible. Damage states that may be meaningful for nonstructural components and systems could include "no damage," "leakage," "loss of function," "loss of structural integrity" and "toppling". In general, each category of nonstructural component or system will have different fragility functions perhaps tied to several different *EDP-Ns*.

While initially the fragility functions for the broad categories will be established by expert opinion, over time they can be determined more rigorously determined through collection of earthquake performance data on damage sustained by actual installations, through laboratory testing programs and in some cases, through structural analysis, just as would be done for the building structure itself. For critical equipment which must function, the fragility data may come from seismic qualification testing.

In some cases the fragility level may be associated with some mean design level. For example, under systems which have high repair cost, we may have a subcategory of components that are sensitive to peak floor accelerations. A component that is designed for twice the force might have a fragility that is twice as high.

Also as part of this task loss functions would be developed corresponding to each of the fragility functions. Loss functions indicate the probability of incurring various levels of loss, given that a structure or nonstructural component or system is damaged to a given level, expressed in such parameters as repair cost (dollars), lives lost (deaths) and hours of lost service or occupancy (downtime). These curves show the probability, that loss will be less than or equal to an indicated amount, given that the building is damaged to a given level. Loss functions can be constructed for a given building or class of buildings, by postulating damage to the structure (or nonstructural component/system) that is representative of a damage level for which there is an available fragility function, and estimating the losses associated with this damage. By varying the assumptions, or exploring the level of uncertainty associated with these

assumptions inherent in these estimates, it is possible to determine probability distributions of the possible losses, as a function of the damage state.

Loss functions tend to incorporate significant uncertainty as compared with hazard curves, response functions and fragility curves because they are highly dependent on human factors including the owner's ability to act rapidly in retaining the necessary design professionals and construction contractors to effect repairs, the efficiency with which the design professionals and contractors operate and the speed with which building departments approve proposed repair programs.

The loss functions would initially be normalized and would indicate what percentage of the replacement cost would be needed to repair all the components in category. Loss functions would also be developed for downtime and deaths and injuries for each of the broad categories and *EDPs-Ns*.

3.4   Development of Standardized Procedures for Establishing Fragilities

A key element in predicting the performance of nonstructural components is having reliable measurements of the extent of damage that occurs to components when they are subject to given levels of *EDP-Ns*. This extent of damage provides a measure of fragility of the components. One primary method for establishing fragility for nonstructural components is by component or system testing. Currently there are three primary methods of fragility testing; (1) shake table testing that measures the fragility of components which are primarily acceleration sensitive, (2) racking testing which measures the fragility of components which are primarily sensitive to horizontal relative displacements (drift sensitive) and (3) component cyclic testing which measures axial and/or rotational fragility (capacity) of subcomponents of nonstructural components such as pipe joints or braces. Some fragility tests are currently being conducted which two or all three of the above methods in the procedures and approaches.

One of the common needs in all fragility methods is accepted protocols for testing. Testing protocols provide the details of how the test is to be conducted and the test motions that are to be imparted onto the component by the test machines. With such accepted protocols in place, results can be duplicated and validated and standardized fragilities for individual components developed. Without such protocols, extrapolations with large variability are introduced into the fragility data. ATC is working in cooperation with the three NSF earthquake engineering centers (PEER, MCEER and MAE) to develop the protocols.

Standardized procedures for establishing fragility functions and loss functions based on fragility testing, experience data and detailed structural analysis will also be developed as part of this task. Also included in this task will be the development of procedures to how to convert existing and available fragility data in fragility functions and associated loss functions that are consistent with newly established data. It is a long term goal of the project to eventually develop a sanctioned database of fragility

functions for a wide variety of nonstructural components of significance that can be used with confidence to predict performance.

3.5 Development of Framework to Adjust Generalized Fragility/Loss Functions

Overtime it is expected that many more fragility and loss functions will become available for individual nonstructural components. This task will provide a framework and associated procedures for adjusting the generalized fragility and loss functions developed in Task 2 above to account for newly available functions. The procedure may take the form of explaining how to subtract on the component of interest from the generalized functions and perhaps having the individual component or system of interest separately identified in the aggregation. This would permit a better understanding of the key limiters of performance through deaggregation.

3.6 Document Performance Assessment Procedures and Provide Examples

The final task of the performance assessment phase of this project is to document and the performance assessment procedure. The documentation would cover the full scope of the project including defining the ground motion hazard, structural and nonstructural assessment, development of loss functions and loss aggregation and other decision information needed by decision makers to make informed decisions. It is expected that the documentation may include the step-by-step process that an engineer would need to follow in order to do a performance assessment. It would also include commentary and provide background material on the procedure development. Also examples would be provided that would illustrate the use of the procedures.

4. SUMMARY

The ATC-58 guidelines have the potential to revolutionize the practice of performance-based design for nonstructural components when the project is completed. Nonstructural components while well recognized as the dominating contributor to losses in recent earthquakes and a major contributor to downtime losses have not received serious attention in previous performance–based earthquake engineering guideline development. With the attention provided to nonstructural components in this project along with the use of probabilistic structural reliability techniques, the likely-hood that performance-based designs will actually achieve intended performance should greatly improve. More importantly, decision makers will be provided information that will be directly useful in selecting appropriate performance criteria for building design, nonstructural design and upgrade projects.

REFERENCES

American Society of Civil Engineers (ASCE), (2002). *Prestandard and Commentary for Seismic Rehabilitation of Buildings*, *Report No. FEMA-356*, Federal Emergency Management Agency, Washington, D.C.

Deierlein, G. G. (2004). "Overview of a Comprehensive Framework for Earthquake Performance Assessment." In Proceedings of the *International Workshop on Performance-Based Seismic Design,* Bled, Slovenia, pp. 15.

Earthquake Engineering Research Institute (EERI), (2000). *Action Plan for Performance-Based Seismic Design*, Report No. FEMA-349, Federal Emergency Management Agency, Washington, D.C.

Hamburger, R. O. (2004). "Development of Next-Generation Performance-Based Seismic Design Guidelines" *Proceedings of the International Workshop on Performance-Based Seismic Design,* Bled, Slovenia.

Moehle, J. P. (2003). "A framework of performance-based earthquake engineering," Proceedings, *Tenth U.S.-Japan workshop on Improvement of Building Seismic Design and Construction Practices,* 2003, Report ATC-15-9, Applied Technology Council, Redwood City, CA.

Structural Engineers Association of California (SEAOC), (1999), *Recommended Lateral Force Requirements and Commentary, Appendix G, Performance-based Design*, International Code Council, Whittier, CA, 1999.

SIMPLIFIED PBEE TO ESTIMATE ECONOMIC SEISMIC RISK FOR BUILDINGS

Keith A. PORTER[1] and James L. BECK[2]

ABSTRACT

A seismic risk assessment is often performed on behalf of a buyer of large commercial buildings in seismically active regions. One outcome of the assessment is that a probable maximum loss (*PML*) is computed. *PML* is of limited use to real-estate investors as it has no place in a standard financial analysis and reflects too long a planning period for what-if scenarios. We introduce an alternative to *PML* called probable frequent loss (*PFL*), defined as the mean loss resulting from an economic-basis earthquake such as shaking with 10% exceedance probability in 5 years. *PFL* is approximately related to expected annualized loss (*EAL*) through a site economic hazard coefficient (*H*) introduced here. *PFL* and *EAL* offer three advantages over *PML*: (1) meaningful planning period; (2) applicability in financial analysis (making seismic risk a potential market force); and (3) can be estimated by a rigorous but simplified PBEE method that relies on a single linear structural analysis. We illustrate using 15 example buildings, including a 7-story nonductile reinforced-concrete moment-frame building in Van Nuys, CA and 14 buildings from the CUREE-Caltech Woodframe Project.

Keywords: Simplified methods; Loss estimation; Seismic risk; Real-estate investment.

1. INTRODUCTION: SEISMIC RISK IN REAL-ESTATE INVESTMENTS

Seismic risk enters into several important real-estate decision-making processes: performance-based design of new buildings, purchase of investment property, seismic retrofit of existing buildings, and the purchase of earthquake insurance. We focus on one of the more common of these: the purchase by real-estate investors of existing commercial property in seismic regions.

Every time a purchase in excess of about $10 million in replacement value (roughly 50,000 to 100,000 sf) is to be financed by a commercial mortgage, the lender requires an assessment of the earthquake probable maximum loss (*PML*). The *PML* has no standard quantitative definition (Zadeh 2000), although working definitions involve the loss associated with a large, rare event. One definition is the 90th percentile of loss given shaking with mean recurrence time of 475 years. Lenders typically refuse to underwrite the mortgage if the *PML* exceeds 20% to 30% of the

---

replacement cost of the building, unless the buyer purchases earthquake insurance—a costly requirement that often causes the investor to decide against bidding.

If the *PML* hurdle is passed, bidders typically proceed to ignore seismic risk, for good reasons: (1) they plan on the order of 5-10 yr, so an upper-bound loss associated with 500-yr shaking is largely meaningless for investment sensitivity studies; (2) *PML* cannot be used in a financial analysis of return on equity or other standard financial performance metrics; and (3) *PML* cannot be used to compare seismic retrofit benefits with costs. Thus, the main seismic risk metric in one of the most common seismic risk decision situations provides owners little value for risk-management decision-making.

Two potentially useful performance metrics are expected annualized loss (*EAL*), which measures the average yearly loss when one accounts for the frequency and severity of various levels of loss, and mean loss given shaking in a reasonable upper-bound event during the investor's planning period. We introduce such a metric and refer to it as probable frequent loss (*PFL*), to evoke *PML* with a briefer planning period. The bidder who knows *EAL* can include it as an operating expense in the financial analysis. *PFL* can be used in the sensitivity studies commonly performed during bidding. We present three increasingly simple performance-based earthquake engineering (PBEE) methods to estimate *EAL* and *PFL*.

2. THREE METHODS TO CALCULATE INVESTOR'S SEISMIC RISK

2.1 *EAL* Method 1: Integrate Vulnerability and Hazard at Several IM Values

Assuming independence of intensity and of loss between earthquakes, *EAL* can be calculated as

$$EAL = V \int_{s=0}^{\infty} y(s)|G'(s)|ds \tag{1}$$

where V denotes the replacement cost of the building, s refers to the seismic intensity measure (*IM*), $y(s)$ is the mean seismic vulnerability function (defined here as the average repair cost as a fraction of V, given s), $G(s)$ is the mean annual frequency of exceeding shaking intensity s, and $G'(s)$ is its first derivative with respect to s.

In practice, $y(s)$ and $G(s)$ are evaluated at $n+1$ discrete intensity levels $s_0, s_1, \ldots s_n$. We denote these by $y_0, y_1, \ldots y_n$, and $G_0, G_1, \ldots G_n$, respectively. We assume $G(s)$ varies exponentially between the discrete values of s, and that $y(s)$ varies linearly, i.e.,

$$G(s) = G_{i-1} \exp\left(m_i\left(s - s_{i-1}\right)\right) \quad \text{for } s_{i-1} < s < s_i \tag{2}$$

$$y(s) = y_{i-1} + \Delta y_i / \Delta s_i \cdot \left(s - s_{i-1}\right) \quad \text{for } s_{i-1} < s < s_i \tag{3}$$

$$m_i = \ln\left(G_i / G_{i-1}\right)/\Delta s_i \quad i = 1, 2, \ldots n \tag{4}$$

$$\Delta s_i = s_i - s_{i-1} \quad i = 1, 2, \ldots n \tag{5}$$

$$\Delta y_i = y_i - y_{i-1} \quad i = 1, 2, \ldots n \tag{6}$$

One can show (Porter et al. 2004) that *EAL* is then given by

$$EAL = V \sum_{i=1}^{n} \left(y_{i-1} G_{i-1} \left(1 - e^{m_i \Delta s_i} \right) - \frac{\Delta y_i}{\Delta s_i} G_{i-1} \left(e^{m_i \Delta s_i} \left(\Delta s_i - \frac{1}{m_i} \right) + \frac{1}{m_i} \right) \right) + R \qquad (7)$$

where R is a remainder term for values of $s > s_n$, and has an upper bound of $VG(s_n)$ if $y(s) \leq 1$. We refer to the method of calculating *EAL* by Equation [7] as Method 1.

Information on $G(s)$ is increasingly available (e.g., Frankel and Leyendecker 2001). To determine $y(s)$ requires either (1) large quantities of empirical post-earthquake survey data (which for various reasons do not exist in reliable form); (2) the exercise of expert opinion; or (3) PBEE analysis along lines pursued by the Pacific Earthquake Engineering Research (PEER) Center.

To create $y(s)$, we employ a PBEE methodology called assembly-based vulnerability (ABV). ABV is described in detail elsewhere (e.g., Porter et al. 2001). It meets the two main criteria set out by Hamburger and Moehle (2000) for a second-generation PBEE methodology: system-level performance evaluation (e.g., economic loss, casualties, and repair duration, or "dollars, deaths, and downtime") and rigorous propagation of all important sources of uncertainty. In summary, ABV has six steps:

1. Facility definition. The facility is defined by its location and design, including site soil, structure and nonstructural assemblies. One creates an inventory of the damageable assemblies and identifies the structural-response parameter (interstory drift ratio, member force, etc.) that would cause damage to each assembly. By assembly, we mean a collection of components, assembled and in place, defined according to a standard taxonomic system, e.g., RS Means Co. Inc. (1997).

2. Ground-motion selection. One selects a ground-motion time history and scales all of its accelerations by a constant to achieve the desired value of s. We measure s by spectral acceleration at the facility's small-amplitude fundamental period of vibration, $S_a(T_1)$, and limit scaling of recorded time histories to a factor of 2. The scaled ground-motion time history is denoted here by $a(t)$.

3. Structural analysis. One creates a structural model and performs a nonlinear time-history structural analysis to determine structural responses, referred to as engineering demand parameters (*EDP*). The structural model is stochastic, meaning that component masses, damping, and force-deformation behavior (denoted here by M, ζ, and *FD*) are treated as uncertain, having prescribed probability distributions.

4. Damage analysis. Each damageable assembly has an uncertain capacity to resist damage. Damage is parameterized via an uncertain, discrete damage measure, denoted by $DM \in \{0, 1, \ldots N_{DM}\}$, where $DM = 0$ corresponds to no damage. Each level of DM is defined by prescribed repairs. For an assembly with $N_{DM} = 1$, one compares the *EDP* to which it is subjected with its uncertain capacity, denoted by R. If $R < EDP$, the assembly is damaged, otherwise not. For an assembly with $N_{DM} \geq 2$, the DM is the maximum value dm such that $R_{dm} < EDP$. If $N_{DM} \geq 2$, it is necessary to ensure that $R_{dm} \leq R_{dm+1}$ for $dm < N_{DM}$. A method to do so is shown in step 6. The

result of the damage analysis is the number of damaged assemblies of each type (indexed by j) and level of damage (indexed by dm), denoted here by $N_{j,dm}$.

5. Loss analysis. Each assembly type and damage state has an associated uncertain repair cost, which we denote by $C_{j,dm}$. The total direct repair cost is the sum of the number of damaged assemblies of each type (j) and damage state (dm) times the unit cost to repair each. One adds the quantity of repainting required (the total painted area of each room, hallway, or other line of sight that has at least one damaged assembly that must be repainted) times the unit cost to repaint. To this subtotal is added contractor overhead and profit (denoted here by C_{OP}), treated here as a factor of the total direct repair cost. The result is the total repair cost. This is divided by the building replacement cost to produce a sample of the damage factor, Y:

$$Y = \frac{1}{V}\left(1 + C_{OP}\right) \sum_{j=1}^{N_j} \sum_{dm=1}^{N_{dm}} N_{j,dm} C_{j,dm} \tag{8}$$

6. Propagate uncertainty. There are many uncertain parameters in the analysis. One way to propagate them is Monte Carlo simulation (MCS). In an MCS approach to ABV, each variable, denoted generically by X, has an associated cumulative distribution function (CDF), denoted by $F_x(x)$, which gives the probability that X will take on a value less than or equal to a particular value x. In a single loss simulation, one samples a value of each uncertain variable in steps 2 through 5 according to its CDF, and calculates a sample Y. One way to sample an X is to generate a sample u of a random number uniformly distributed between 0 and 1. The sample of X is given by

$$x = F_X^{-1}\left(u\right) \text{ where } u \sim U(0,1) \tag{9}$$

The vector of uncertain variables is denoted here by $\underline{X} = [a(t), M, \zeta, FD, R, C, C_{OP}]^{\mathrm{T}}$. Each component in the vector can itself have more than one component. Lacking a probabilistic model for $a(t)$, a suite of historical ground-motion time histories can be used and assigned equal probability. Each uncertain variable is simulated per Equation [9]. Steps 2–5 are performed, producing one sample of Y. The process is repeated many times at a given level of s to produce many samples of Y. The distribution of the samples is treated as the distribution of Y. One repeats this process at many levels of s to produce the uncertain seismic vulnerability function $Y(s)$.

Damage analysis for an assembly with $N_{DM} \geq 2$ requires more than simply simulating each capacity R_{dm} according to its distribution and comparing with EDP, owing to the necessity that $R_{dm} \leq R_{dm+1}$ for $dm < N_{DM}$. When $N_{DM} \geq 2$, one evaluates the CDF of DM for each assembly, conditioned on EDP, which we denote by $F_{DM|EDP=x}(dm)$. We denote the CDF of capacity R_{dm} by $F_{R,dm}(x)$ and calculate:

$$
\begin{aligned}
p\left[DM = dm \mid EDP = x\right] &= 1 - F_{R,(dm+1)}\left(x\right) & dm = 0 \\
&= F_{R,dm}\left(x\right) - F_{R,(dm+1)}\left(x\right) & 1 \leq dm < N_{DM} \\
&= F_{R,dm}\left(x\right) & dm = N_{DM}
\end{aligned}
\tag{10}
$$

$$F_{DM|EDP=x}\left(dm\right) = 1 - F_{R,dm+1}, \quad 0 \le dm < N_{DM}$$
$$= 1 \qquad dm = N_{DM} \tag{11}$$

$$dm = F_{DM|EDP=x}^{-1}\left(u\right); u \sim U(0,1) \tag{12}$$

where $p[A|B]$ denotes the probability of A given B. For many assembly types and damage states, it is reasonable to take $F_{R,dm}(x)$ as a cumulative lognormal distribution,

$$F_{R,dm}\left(x\right) = \Phi\left(\ln\left(x/\hat{x}\right)/\beta\right) \tag{13}$$

where Φ is the cumulative standard normal distribution and $\hat{x}$ and β are the median and logarithmic standard deviation of capacity, which vary by assembly type and damage state. See Porter et al. (2001) and Beck et al. (2002) for examples.

Latin hypercube simulation (LHS). To enhance step 6, replace Equation [9] by

$$x = F_X^{-1}\left(u_1/N + u_2/N\right) \tag{14}$$

where N is the number of samples desired, u_1 is sampled from {0, 1, … N-1} with equal probability and without replacement, and $u_2 \sim U(0,1)$. Replace Equation [12] by

$$dm = F_{DM|EDP=x}^{-1}\left(u_3/N + u_4/N\right) \tag{15}$$

where u_3 is sampled from {0, 1, … N-1} with equal probability and without replacement and $u_4 \sim U(0,1)$. LHS ensures that the simulations produce samples from the tails of each distribution as well as the body.

2.2   *EAL* Method 2: Use Probable Frequent Loss

One can simplify method 1 by evaluating $G(s)$ and $y(s)$ at only two points, taking

$$G\left(s\right) = G\left(s_{NZ}\right)\exp\left(m\left(s - s_{NZ}\right)\right) \tag{16}$$

$$y\left(s\right) = 0 \qquad\qquad s < s_{NZ}$$
$$= a\left(s - s_{NZ}\right) \qquad s_{NZ} \le s \le s_U \tag{17}$$
$$= y_U \qquad\qquad s_U < s$$

where s_{NZ} is defined such that $y(s_{NZ}) = 0+$, i.e., the value of s where loss first becomes nonzero, and s_U denotes the value of s where y reaches an upper-bound y_U such as 1.0.

   Given a value of s_{NZ} such as $S_a(T_1) = 0.05$g, one can determine a by calculating the mean seismic vulnerability function at some value $s_{NZ} \le s_{EBE} \le s_U$, where s_{EBE} denotes the site shaking intensity in an event referred to here as the *economic-basis earthquake* (EBE), named to evoke the design-basis earthquake (DBE) of older codes, with a hazard level more relevant to repair costs than to life safety. We refer to mean loss given the EBE as the *probable frequent loss* (PFL), in imitation of and contrast with the *PML*. One can define the EBE as the event causing a level of shaking with 10% exceedance probability in 5 yr, although other moderate shaking levels also produce reasonable results. The shaking level s_{EBE} can be calculated, e.g., using Frankel and Leyendecker (2001), adjusting for site classification by using F_a or F_v, as appropriate, from the International Building Code (International Code Council 2000).

There is good reason to define EBE this way. To test the life-safety of a structural design, engineers have historically considered upper-bound shaking (10% exceedance probability) during the building's design life (e.g., 50 years), referring to this level of shaking as the DBE. To examine an upper-bound economic loss during the owner's planning period, it is consistent to use the same exceedance probability (10%) during that planning period (5 yr). We could define EBE as the event causing the site shaking intensity with 50% exceedance probability in 50 years, an event treated by FEMA 356 (ASCE 2000) that would be only slightly stronger than the 10%/5-yr event, but favor the suggested definition for its value to risk communication. EBE is defined for meaning to the investor, for whom 50 years is too long a planning period and 50% exceedance probability does not suggest an upper-bound intensity. Our 10%/5-yr definition of EBE more directly addresses the concerns of the investor.

Returning to EAL, we denote the mean annual frequencies of a site exceeding s_{NZ}, s_{EBE}, and s_U by G_{NZ}, G_{EBE}, and G_U, respectively. Then

$$a = PFL\big/\big[V \cdot \big(s_{EBE} - s_{NZ}\big)\big] \tag{18}$$

$$m = \ln\big(G_{EBE}/G_{NZ}\big)\big/\big(s_{EBE} - s_{NZ}\big) \tag{19}$$

$$s_U = s_{NZ} + y_U\big/a$$
$$= s_{NZ} + y_U V\big(s_{EBE} - s_{NZ}\big)\big/PFL \tag{20}$$

One can show (Porter et al. 2004a) that substituting [16] through [20] into [1] leads to

$$EAL = PFL \cdot \big[\big(G_{NZ} - G_U\big)\big/\ln\big(G_{NZ}/G_{EBE}\big)\big] \tag{21}$$

If $s_U \gg s_{NZ}$, as expected, then $G_U \ll G_{NZ}$, leading to:

$$EAL \approx PFL \cdot H \tag{22}$$

where

$$H \equiv G_{NZ}\big/\ln\big(G_{NZ}/G_{EBE}\big) \tag{23}$$

We refer to H as the *site economic hazard coefficient*. It can be mapped as a scalar for a given fundamental period, site classification, and s_{NZ}. Its units are yr^{-1}. Equation [22] still requires that one estimate PFL somehow. One can use Method 1 with one the intensity level s_{EBE}, which requires multiple PBEE simulations. This is Method 2.

2.3   *EAL* Method 3: PFL and Linear ABV

We further simplify the analysis by noting that at moderate s, around s_{EBE}, the structural response may be adequately modeled using linear spectral analysis. Further, since only mean loss at s_{EBE} is required, we can avoid some aspects of ABV that are intended to quantify damage and uncertainty. Method 3 employs a simplified PBEE approach called linear assembly-based vulnerability (LABV). It has four steps:

1. Facility definition. Same as in Methods 1 and 2.

2. Hazard analysis. Determine s_{EBE} as in Method 2.

3. Structural analysis. Calculate *EDPs* using the first-mode spectral response. We denote by ϕ_1, L_1 and M_1, the building's fundamental mode shape, modal excitation, and modal mass, respectively. For example, considering one frame direction, the *EDP* for a segment of wallboard partition on the mth story would be the interstory drift along that column line, estimated as

$$EDP \approx \frac{s_{EBE}}{\omega_1^2}\left(\frac{\phi_{1(m+1)} - \phi_{1m}}{h_m}\right)\frac{L_1}{M_1} \tag{24}$$

where $\omega_1 = 2\pi/T_1$, ϕ_{1m} is the component of the fundamental mode shape at floor m, and h_m refers to the height of story m.

4. Damage and loss analysis. Let c_{dm} denote the mean cost to restore an assembly from damage state dm; it can be calculated by standard cost-estimation principles. We denote by $c(x)$ the mean cost to repair one assembly given that it has been exposed to $EDP = x$. We refer to $c(x)$ as the mean assembly vulnerability function, calculated by

$$c(x) = \sum_{dm=1}^{N_{DM}} c_{dm} p[DM = dm \mid EDP = x] \tag{25}$$

where $p[DM=dm|EDP=x]$ is given by Equation [10]. Mean assembly vulnerability functions can be created and archived for later use. See Porter et al. (2004) for examples. This is not a new idea. Czarnecki (1973) proposed several, as did Kustu et al. (1982), who normalized by the assembly replacement cost. Because construction contractors estimate repairs in terms of labor hours and dollar amounts, we find it simpler to deal with c_{dm} directly (i.e., not normalized). Introducing subscript k to index particular assemblies and c_{OP} to denote the mean value of C_{OP}, *PFL* is given by

$$PFL = (1 + c_{OP}) \sum_{k=1}^{N} c_k(x_k) \tag{26}$$

where N is the number of building assemblies. *EAL* is then given by Equation [22].

3. CASE STUDIES

Van Nuys Hotel Building. To compare the three methods, we begin with an actual highrise hotel building located in Van Nuys, CA. It is a seven-story, eight-by-three-bay, nonductile reinforced-concrete moment-frame building built in 1966. It suffered earthquake damage in 1971 and 1994, after which it was seismically upgraded. We analyzed the building in its pre-1994 condition. See Beck et al. (2002) and Porter et al. (2002a) for details of the hazard model, structural model, component capacity distributions and unit repair costs. We performed 20 simulations at each of 20 levels of *IM*: $S_a(1.5 \text{ sec}, 5\%) = 0.1, 0.2, \ldots 2.0g$, producing 400 simulated values of *Y*.

We took masses as perfectly correlated, normally distributed, with coefficient of variation (COV) equal to 0.10, per Ellingwood et al. (1980). We took damping as

normally distributed with mean value of 5% and coefficient of variation of 0.40, as derived in Beck et al. (2002). Structural members were taken as having deterministic stiffnesses (including post-yield, unloading, etc.) but with yield and ultimate force and deformations that are perfectly correlated, normally distributed, with COV of 0.08, per Ellingwood et al. (1980). We took component capacities and unit repair costs as lognormally distributed; see Beck et al. (2002) for damage states, repair efforts, and parameters of the lognormal capacity distributions. We took C_{OP} as uniformly distributed between 15% and 20%. A professional cost estimator provided all costs.

Figure 1(a) shows the resulting vulnerability function; Figure 1(b) shows the site seismic hazard function. Each circle in Figure 1(a) represents one simulation. The jagged line shows mean loss at each S_a level. The smooth curve is a polynomial fit to the data. Each simulation includes one nonlinear time-history structural analysis using one simulation of the building's uncertain mass, damping, and force-deformation characteristics, one simulation of the capacity of each of 1,233 structural and nonstructural components, and one simulation of the unit-repair cost for each of 9 combinations of component type and damage state. The structural analyses took approximately 12 hours of computer time; the loss analysis took an hour. The most time-consuming portion of the analysis was creating the structural model. Figure 1 shows that, for S_a up to about 0.5g, a linear approximation for $y(s)$ is reasonable; and that beyond 0.5g, $G'(s)$ is so small that the integrand of Equation [1] makes little contribution, supporting the approximation for $y(s)$ in Equation [17].

We applied Methods 1, 2, and 3 to this case-study building, producing the results shown in Table 1. Note that *PFL* for Method 2 was taken from the Method-1 analysis at $s = s_{EBE}$. Agreement between the methods is reasonable: Methods 2 and 3 produce *EAL* estimates within about 30% of that of Method 1. That Method 3 produces a reasonable estimate is particularly promising: at least in this case, one need not create a nonlinear structural model to get a reasonable estimate of *PFL* and *EAL*.
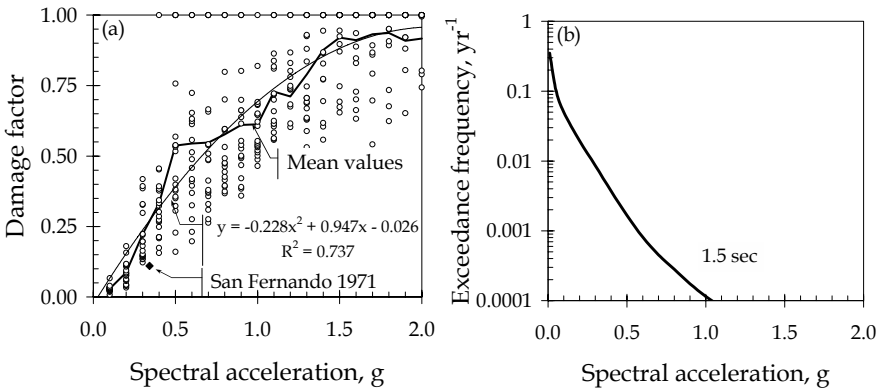

Figure 1. (a) Seismic vulnerability and (b) site hazard for Van Nuys building.

Table 1. Approximation of seismic risk for Van Nuys case study

	Method 1	Method 2	Method 3
s_{NZ}	N/A	0.05g	0.05g
s_{EBE}	N/A	0.20g	0.20g
$G(s_{NZ})$, yr^{-1}	N/A	0.1026	0.1026
$G(s_{EBE})$, yr^{-1}	N/A	0.0195	0.0195
H, yr^{-1}	N/A	0.0617	0.0617
PFL	N/A	$613,000	$930,000
EAL	$53,600	$37,800	$57,400

We performed three additional tests. First, we evaluated Equation [7] at each of n = 1, 2, … 20, for Δs = 0.1g. Figure 2 shows the result: the EAL considering only $S_a \leq$ 0.1g, then $S_a \leq$ 0.2g, etc. Figure 2(a) plots the results against S_a; Figure 2(b), against mean recurrence time. They show that only about 15% of cumulative economic loss comes from events with PML-level shaking or greater ($S_a > 0.5g$). As important as the 500-year earthquake is for life safety, it is largely irrelevant for cost. About half the EAL for this building results from events with $S_a \leq 0.25g$, whose mean recurrence time is 85 years or less. About 35% of loss is due to $S_a \leq s_{EBE}$. Ideally, loss from $S_a \leq s_{EBE}$ would be near 50% of EAL, making s_{EBE} is a good representative scenario shaking level, but the fraction will likely vary between buildings, so a cumulative EAL fraction of 35% at the s_{EBE} defined this way seems acceptable.

CUREE-Caltech Woodframe Project Buildings. As a second test, we compared Methods 1 and 2 using 14 hypothetical but completely designed buildings from the CUREE-Caltech Woodframe Project (Porter et al. 2002b). The buildings are variants of four basic designs referred to as index buildings (Reitherman and Cobeen 2003). They include a small house (single story, 1,200 sf, stucco walls, no structural sheathing), a large house (two stories, 2,400 sf, some walls with structural sheathing, stucco exterior finish), a three-unit townhouse (two stories, 6,000 sf total, some walls with structural sheathing, stucco exterior finish), and an apartment building (three stories, 13,700 sf, 10 dwelling units, and tuck-under parking). Each index building included four or more variants: poor-, typical-, and superior-quality versions, and one or more retrofits or above-code or alternative designs. We considered these woodframe buildings located at an arbitrary site in Los Angeles, CA, at 33.9°N, 118.2°W. Using Frankel and Leyendecker (2001) to determine site hazard and adjusting for NEHRP site classification D, we find s_{EBE} = 0.4g. Of the 19 buildings examined in Porter et al. (2002b), 14 have nonzero mean loss at s_{EBE}.
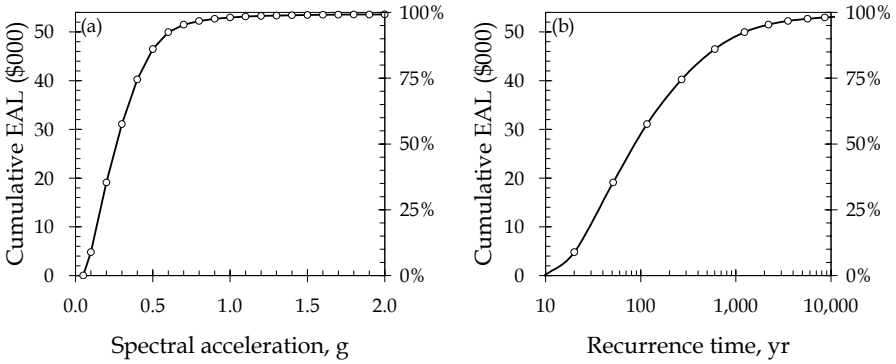
Figure 2. Dominance of frequent events in EAL for Van Nuys building.

Figure 3 shows *EAL* for the Van Nuys and 14 woodframe buildings calculated by Method 1 (referred to in the figure as "exact") and by Method 2 (referred to as "approximate"). We denote Method-1 *EAL* by EAL_1, define estimation error as

$$\varepsilon \equiv \left(EAL_2 - EAL_1\right)/EAL_1 \tag{27}$$

and take the error for each case-study building as a sample of ε. We find the sample mean and sample standard deviation of this error are $\overline{\varepsilon}$ = 0.12 and s_ε = 0.52, respectively. Thus, for these 15 buildings, the use of s_{EBE} defined as the shaking with 10% exceedance probability in 5 yr produces a fairly modest (12%) error in the estimate of *EAL*, relative to the exact method, which requires analysis of the complete seismic vulnerability function.

As a final test, we calculated the error if one defines s_{EBE} as shaking with 50% exceedance probability in 50 yr, and found $\overline{\varepsilon}$ = 0.06 and s_ε = 0.47. Defining EBE this way produces slightly more accurate results for the case-study buildings than using shaking intensity with 10% exceedance probability in 5 yr (as we have done), although at a the cost of meaningful risk communication.
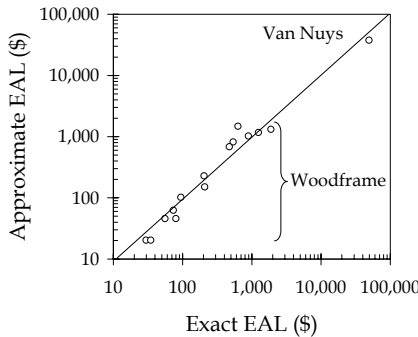

Figure 3. Comparing *EAL* by methods 1 and 2 for 15 sample buildings.

146

The *EAL* values shown in Figure 3 might be quite meaningful to the real-estate investor. In the case of the Van Nuys building, whose replacement cost is approximately $7.0M and whose annual net operating income is on the order of $1M, an *EAL* of $54,000 represents a significant expense. The *EAL*s for the poorer-performing woodframe buildings can exceed $1,000. This would be a significant expected annual expense for a small investor, of the same order as homeowner insurance (Insurance Information Institute 2003).

4. CONCLUSIONS

Through a case study of a nonductile reinforced-concrete moment-frame building, we show that repair costs can be dominated by small, frequent events, rather than rare, *PML*-level losses. Using this example and that of 14 woodframe buildings, we show that expected annualized loss (*EAL*) is approximately proportional to a scenario loss referred to as the probable frequent loss (*PFL*). The constant of proportionality, referred to as the site economic hazard coefficient (*H*), can be mapped or tabulated for use by engineers or investors. *PFL* can be defined as the mean loss conditioned on the occurrence of shaking with 10% exceedance probability in 5 years. This is the economic-basis earthquake, EBE, named in imitation of the design-basis earthquake (DBE) of older codes. An approach called linear assembly-based vulnerability (LABV) can reasonably estimate *PFL* and *EAL* with one simplified PBEE analysis.

This methodology can inform a common opportunity for seismic risk-management: the purchase of commercial buildings in seismically active regions. Current practice produces little information to help investors consider seismic risk. Consequently, the opportunity for risk-management is usually missed. The problem might be alleviated by using *PFL* rather than (or in addition to) *PML*. *PFL* offers several advantages as a performance metric: (1) it better reflects upper-bound loss during an investor's planning period than does *PML*; (2) it can be multiplied by *H* to estimate *EAL*, which can be used as an operating expense, thereby making seismic risk more of a market force; (3) it can be readily calculated by a single, simplified PBEE simulation using linear structural analysis; and (4) by this method, PBEE can bring rigor to the most-common seismic risk-management opportunity for commercial buildings.

REFERENCES

American Society of Civil Engineers. 2000. *FEMA 356 Prestandard & Commentary for the Seismic Rehabilitation of Buildings*, FEMA, Washington, D.C.
Beck, J. L., K. A. Porter, R. V. Shaikhutdinov, S. K. Au, T. Moroi, Y. Tsukada, and M. Masuda. 2002. *Impact of Seismic Risk on Lifetime Property Values,* CUREE, Richmond, CA, http://resolver.caltech.edu/caltechEERL:2002.EERL-2002-04

Czarnecki, R.M., 1973. *Earthquake Damage to Tall Buildings, Structures Publication 359,* Massachusetts Institute of Technology, Cambridge, MA.

Ellingwood, B., T. V. Galambos, J. G. MacGregor, and C. A. Cornell. 1980. *Development of a Probability-Based Load Criterion for American National Standard A58,* National Bureau of Standards, Washington, D.C.

Frankel, A., and E. V. Leyendecker. 2001. *Uniform Hazard Response Spectra & Seismic Hazard Curves for the United States,* US Geological Survey, Denver, CO.

Hamburger, R. O., and J. P. Moehle. 2000. "State of performance-based engineering in the United States," *2nd U.S.-Japan Workshop on Performance-Based Earthquake Engineering Methodology for Reinforced Concrete Building Structures*, Sapporo, Japan, September 2000.

Insurance Information Institute, 2003. *Facts and Statistics: Homeowners Insurance*, www.iii.org/media/facts/statsbyissue/homeowners/ .

International Code Council. 2000. *International Building Code,* ICBO, Whittier, CA.

Kustu, O., D. D. Miller, and S. T. Brokken. 1982. *Development of Damage Functions for Highrise Building Components*, URS/Blume, San Francisco, CA.

Porter, K. A., J. L. Beck, and R. V. Shaikhutdinov. 2002a. "Sensitivity of building loss estimates to major uncertain variables," *Earthquake Spectra*, 18 (4), 719-743

Porter, K. A., J. L. Beck, and R. V. Shaikhutdinov. 2004a (expected). "Simplified estimation of economic seismic risk for buildings," *Earthquake Spectra.*

Porter, K. A., J. L. Beck, H. A. Seligson, C. R. Scawthorn, L.T. Tobin, and T. Boyd. 2002b. *Improving Loss Estimation for Woodframe Buildings*, CUREE, Richmond, CA.

Porter, K. A., A. S. Kiremidjian and J. S. LeGrue. 2001. "Assembly-based vulnerability of buildings and its use in performance evaluation," *Earthquake Spectra,* 17 (2), 291-312.

Reitherman, R., and K. Cobeen. 2003. *Design Documentation of the Woodframe Project Index Buildings*, CUREE, Richmond, CA.

R.S. Means Co., Inc.. 1997. *Means Assemblies Cost Data*, Kingston, MA.

Zadeh, M. M.. 2000. "Understanding risk management," *Financial Management of Earthquake Risk,* Earthquake Engineering Research Institute, Oakland CA, 1-14.

ASSESSMENT OF SEISMIC PERFORMANCE IN TERMS OF ECONOMIC LOSSES

Eduardo MIRANDA[1], Hesameddin ASLANI[2] and Shahram TAGHAVI[2]

ABSTRACT

An approach for describing the seismic performance of buildings as a continuum and in terms of economic losses is presented. Two alternative measures of economic losses are described and discussed. In the proposed approach the total loss in a building due to physical damage is treated as a random variable and it is computed as the sum of the losses in individual structural and nonstructural components. Economic losses are computed using a fully probabilistic approach that permits the explicit incorporation of uncertainties in the seismic hazard at the site, in the response of the structure, on the fragility of individual structural and nonstructural components, and on the costs associated with the repairs or replacement of individual building components. Physical damage is estimated by combining structural response parameters such as interstory drift ratio or peak floor acceleration with component fragility functions. Results from an existing non-ductile seven story reinforced concrete building are presented to illustrate the proposed loss estimation methodology.

Keywords: Performance-based seismic design; Probabilistic loss estimation; Fragility function; Correlation; Loss deaggregation.

1. INTRODUCTION

The goal of performance-based seismic design (PBSD) is to design facilities that satisfy the performance expectations of their owners. Implicit in PBSD when applied to buildings is the need to predict the performance of the structure, its non-structural components and contents for a wide range of possible earthquake ground motion intensities.

Recent research conducted at the Pacific Earthquake Engineering Research (PEER) Center aims at describing the seismic performance of structures quantitatively by continuous variables rather than discrete performance levels such as those used in FEMA 356 document. The three continuous variables studied by PEER include: economic (e.g., dollar) losses, downtime and fatalities. The present work is focused on economic loss estimation.

---

[1] *Assistant Professor, Dept. Civil and Envir. Engrg., Stanford University, Stanford, CA, 94305-4020*

[2] *Ph.D. Student, Dept. Civil and Envir. Engrg., Stanford University, Stanford, CA, 94305-4020*

There are many studies on seismic loss estimation. However, most previous studies have been aimed at estimating losses on a regional basis for a large number of facilities (e.g., ATC-13, Hazus, etc.) as opposed to a more accurate estimation of economic losses in individual facilities. For a comprehensive literature review on different loss estimation approaches, the reader is referred to FEMA 249 (1994).

The objective of this work is to summarize research conducted by the authors aimed at quantifying the seismic performance in specific buildings in terms of economic losses. In the proposed approach the total loss in a building due to physical damage is treated as a random variable and it is computed as the sum of the losses in individual structural and nonstructural components. Economic losses are computed using a fully probabilistic approach that permits the explicit incorporation of uncertainties in the seismic hazard at the site, in the structural response, on the fragility of individual structural and nonstructural components, and on the costs associated with the repairs or replacement of individual building components. Physical damage is estimated by combining structural response parameters such as interstory drift ratio or peak floor acceleration with component fragility functions. The proposed approach is illustrated by applying it to a non-ductile seven-story reinforced concrete building.

2. MEASURES OF ECONOMIC LOSS

There are many possible measures of economic losses that can be used to describe seismic performance. Only two measures of economic loss are discussed here. For a more complete discussion of alternative economic losses the reader is referred to Miranda and Aslani (2003) and Krawinkler and Miranda (2004). The first economic loss measure is the expected annual loss, which corresponds to the economic loss that, on average, occurs every year in the building. The expected annual loss provides quantitative information to assist stakeholders in making risk management decisions. In particular, owners, lending institutions, insurers, and other stakeholders can use expected annual losses to compare, for example, annual revenues versus expected annual losses. Similarly, they can compare annual earthquake insurance premiums to annual expected losses, etc.

The second measure of economic loss discussed here is the probability of having an economic loss equal or greater than a certain amount, which provides information of the probability of experiencing an economic loss larger than a certain amount (e.g., the probability of loosing more than one million dollars due to earthquake damage in the building). This second measure of economic loss also provides economic losses associated with particular probabilities of being exceeded (e.g., the total dollar loss that has 1% probability of being exceeded in 50 years).

The expected annual loss in a building $E[L_T]$ over a time period t can be computed as (Rosenblueth 1976, Wen et al. 2001)

$$E[L_T] = \int_0^t \int_0^\infty e^{-\lambda \tau} E[L_T | IM] |dv(IM)| d\tau \tag{1}$$

where $e^{-\lambda\tau}$ is the discounted factor of the loss over time t, λ is the discount rate per year, $E\,[\,L_T\,|\,IM\,]$ is the expected loss in the building corresponding to a ground motion intensity, IM, $\nu(IM)$ is the mean annual rate of exceeding a ground motion intensity IM. In (1) the time period t can correspond to the design life of the structure, the remaining life of an existing structure or another reference time period. For purposes of setting design actions in building codes or for setting insurance premiums long t are usually assumed (Rosenblueth, 1976) and the effect of the finite life span of the facility becomes negligible.

Since collapse (C) and non-collapse (NC) are mutually exclusive damage states, the expected loss in a building conditioned on ground motion intensity IM, can be computed using the total probability theorem as follows

$$E[L_T\,|\,IM] = E[L_T\,|\,NC,IM]\cdot[1 - P(C\,|\,IM)] + E[L_T\,|\,C]\cdot P(C\,|\,IM) \qquad (2)$$

where $E[L_T\,|\,NC,IM]$ is the expected loss in the building provided that collapse does not occur for ground motions with an intensity level $IM=im$, $E[L_T\,|\,C]$ is expected loss in the building when collapse occurs in the building and $P(C/IM)$ is the probability that the structure will collapse conditioned on ground motion intensity.

The expected total loss in the building provided that collapse does not occur at a ground motion intensity $IM=im$, $E[L_T\,|\,NC,IM]$, is computed as the sum of the losses in individual components of the building as

$$E[L_T\,|\,NC,IM] = E\left[\sum_{i=1}^{N}(a_i\cdot L_i\,|\,NC,IM)\right] = \sum_{i=1}^{N}a_i\cdot E[L_i/NC,IM] \qquad (3)$$

where $E[L_i/NC,IM]$ is the expected normalized loss in the ith component given that global collapse has not occurred at the intensity level im, a_i is the replacement cost of component i and L_i is the normalized loss in the ith component defined as the cost of repair or replacement in the component normalized by a_i. Details on the computation of $E[L_T\,|\,NC,IM]$ and $E[L_T\,|\,IM]$ are given in Aslani and Miranda (2004b).

The mean annual frequency of exceedance of a certain level of economic loss l_T is computed as

$$\nu[L_T > l_T] = \int_0^\infty P[L_T > l_T\,|\,IM]\cdot\left|\frac{d\nu(IM)}{dIM}\right|dIM \qquad (4)$$

where $P[L_T>l_T\,|\,IM]$, is the probability of exceeding a certain level of loss for a given IM. For values smaller than 0.01 the mean annual frequency of exceedance of a loss l_T is approximately equal to the mean annual probability of exceedance.

In Eq. (4), $P(L_T > l_T\,|\,IM)$ can be assumed lognormally distributed (Aslani and Miranda 2004b). On the basis of this assumption only the first two moments of the probability distribution are required to evaluate this conditional probability. The first moment, the expected value, is given by equation (2) while the variance of the loss, is computed as follows

$$\sigma^2_{(L_T>l_T|IM)} = \sigma^2_{(L_T|NC,IM)}\cdot[1 - P(C\,|\,IM)] + \sigma^2_{(L_T|C)}\cdot P(C\,|\,IM)$$

$$+\{E[L_T\,|\,NC,IM] - E[L_T\,|\,IM]\}^2\cdot[1 - P(C\,|\,IM)] + \{E[L_T\,|\,C] - E[L_T\,|\,IM]\}^2\cdot P(C\,|\,IM) \qquad (5)$$

where $\sigma^2_{(L_T|C)}$ is the variance of the total loss in the building given that collapse has occurred and $\sigma^2_{(L_T|NC,IM)}$ is the variance of the total loss in the building given that collapse has not occurred at intensity level *im* which can be computed as a function of the dispersion in the losses of individual components as follows

$$\sigma^2_{[L_T|NC,IM]} = \sum_{i=1}^{N} \sum_{j=1}^{N} a_i \cdot a_j \cdot \rho_{L_i,L_j|NC,IM} \cdot \sigma_{L_i|NC,IM} \sigma_{L_j|NC,IM} \tag{6}$$

where $\sigma_{L_i|NC,IM}$ is the dispersion of the loss in the *i*th component when collapse has not occurred at intensity level *im*, and $\rho_{L_i,L_j|NC,IM}$ is the correlation coefficient between the losses in the *i*th and *j*th components conditioned on *IM* when collapse has not occurred.

The correlation between the losses in two individual components conditioned on the ground motion intensity level, $\rho_{L_i,L_j|NC,IM}$, can be computed as

$$\rho_{L_i,L_j|NC,IM} = \frac{\sigma_{L_iL_j|NC,IM}}{\sigma_{L_i|NC,IM}\sigma_{L_j|NC,IM}} \tag{7}$$

where $\sigma_{L_iL_j|NC,IM}$ is the covariance of the loss between the *i*th and *j*th components conditioned on *IM*, when collapse has not occurred. As will be explained later, this correlation is a function of three correlations: (1) the correlation of the engineering demand parameters *EDP* (i.e., response parameters) that have an influence on the components; (2) the correlation of the damages in the components conditioned on the *EDP*; and (3) the correlation between the repair/replacement costs of the components associated with a given damage state. The proposed approach not only takes into account the correlation between losses in individual components but also the variation of this correlation with changes in the ground motion intensity level.

3. BUILDING-SPECIFIC LOSS

3.1 Structural Response Estimation

In the proposed approach the mean annual frequency of exceedance of the *intensity measure*, *IM*, (i.e., the seismic hazard curve) is from a conventional probabilistic seismic hazard analysis. For the United States this information is readily available at closely spaced grid points, that permit to obtain seismic hazard curves for any zip code or any geographical coordinates in the country.

The selection of the parameter to be used to characterize the ground motion intensity for the structure (i.e., the intensity measure IM) depends on a number of aspects such as the fundamental period of vibration of the structure, the response parameters of interest, location of interest within the structure, level of nonlinearity, etc.
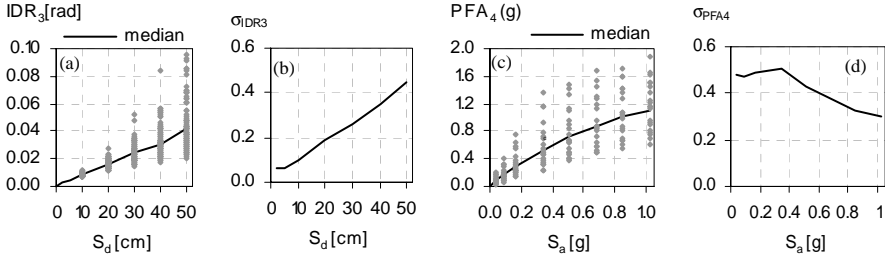
Figure 1. Variations of the probability parameters of *EDP*s with changes in the elastic displacement spectral ordinate, *S*$_d$: (a) median of IDR1 (b) dispersion of IDR1 (c) median *PFA*$_{roof}$ (d) dispersion of *PFA*$_{roof}$.

In this study the use three different parameters as *IM*'s was investigated. The first one is the elastic displacement spectral ordinate of a single-degree-of-freedom, *SDOF*, system evaluated at the fundamental period of vibration of the building, $S_d(T_1)$. The second *IM*, is the maximum displacement $\Delta_i(T_1)$ of a bilinear *SDOF* system with the same period and strength as that of the building. The third parameter that was studied as *IM* is the peak ground acceleration (*PGA*).

The probability that a structural response parameter, referred in PEER as *engineering demand parameter*s (*EDP*), exceeds a certain value conditioned on a given ground motion intensity P(*EDP*|*IM*) is obtained by using the results of non-linear response history analyses (Miranda and Aslani 2003). Ground motions are scaled, such that all have the same intensity measure and the analysis is repeated for increasing levels of intensity. Figure 1 shows the variations of the median and dispersion of the interstory drift ratio at the first story, *IDR*$_1$, and of the peak floor acceleration at roof level, *PFA*$_{roof}$ of a non-ductile seven-story reinforced concrete building. The figure shows changes in central tendency and dispersion of these two response parameters for five increasing levels of elastic displacement intensity S_d. For each intensity level 80 nonlinear response history analyses were performed. Gray dots in the figure represent results for individual ground motions. It can be seen that considerable variability exists in the response of the structure from one record to another. In general, the response will increase as the ground motion intensity increases; however, the trend is not necessarily linear. Several simplified approaches assume the dispersion to remain constant with changes in ground motion intensity. As shown in the figure for the case of drift in the first floor, the level of dispersion exhibits a sharp increase with the increasing *IM*. However, dispersion will not always increase. For example, dispersion in upper stories was observed to decrease with increasing *IM*. Figures 1c and 1d presents similar results but for the peak floor acceleration at the roof, *PFA*$_{roof}$. In this case, the acceleration demand increases with increasing S_d, but the demand tends to saturate with increasing level of nonlinearity. It can be seen that dispersion sharply decreases with increasing level of ground motion intensity. It is noteworthy that the variations of the dispersion of the *EDP* with changes in *IM* shown here are very large both for *IDR*$_1$ and *PFA*$_{roof}$.
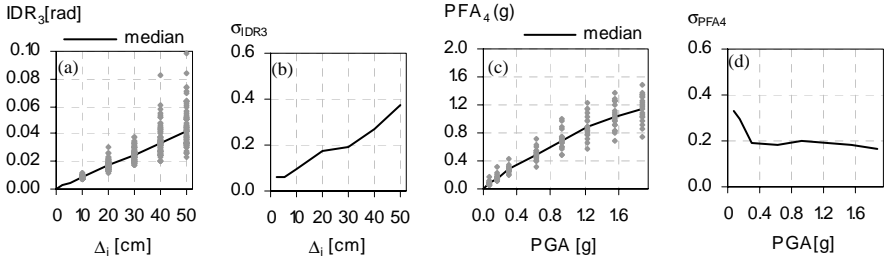
Figure 2. (a) Variations of median and dispersion of IDR_1 with changes in the inelastic spectral ordinate, Δ_i; (b) variations of median and dispersion of PFA_{roof} with changes in PGA.

Figure 2a presents the variations of the median and dispersion of IDR_1 with changes in IM, when using inelastic spectral ordinates $\Delta_i(T_1)$ as the intensity measure. Comparison of figures 1 and 2 shows that using $\Delta_i(T_1)$, as the intensity measure leads to lower levels of dispersion for IDR_1, particularly at higher level of intensity. Figure 2b shows the variations of peak floor acceleration demands at the roof when PGA is used to characterize the ground motion intensity. Comparing figure 1 and 2 shows that using PGA as the intensity measure leads to lower levels of dispersion than those computed when $S_d(T_1)$ is used as IM. This agrees well with previous observations, which indicate that when a significant portion of the exposed value is sensitive to floor accelerations (e.g., in museums, clean rooms, laboratories, etc.) acceleration-based intensity measures lead to smaller dispersions in response and hence a smaller number of ground motions may be used (Taghavi and Miranda 2003b).

3.2 Damage Estimation

Once the response of the structure has been computed, an estimation of the damage in individual components can be obtained through the use of fragility functions. Fragility functions are curves that permit the estimation of the probability that a structural or non-structural component will be in a certain damage state when it is subjected to a certain level of EDP.

For each component, damage states, referred in PEER as *damage measures DM*, associated with different repair actions were identified. Fragility functions for each damage state were then developed using the results of experimental results available in the literature. Many studies have concluded that the structural response parameter that is best correlated with structural damage is the interstory drift ratio, *IDR*. Therefore, this parameter was used to develop fragility functions of structural components. Analysis of the results of various damage states indicates that fragility functions can be assumed to have a lognormal distribution. Therefore, only two parameters, namely the median and logarithmic standard deviation of the EDP, are required to define the fragility function corresponding to a certain damage state.

Figure 3a, shows an example of fragility function for the first damage state of a reinforced concrete column in the building. It is observed that the *EDP,* which in this case corresponds to the interstory drift ratio, associated to certain damage states of structural components exhibits a very large scatter. In order to reduce the uncertainty in damage estimation for these damage states *fragility surfaces* were developed (Aslani and Miranda 2004a). In a fragility surface the mean and standard deviation of *EDP* corresponding to a damage state are evaluated as a function of a new parameter, α, which allows the incorporation of additional information. The parameter α can incorporate information on the element (e.g., geometry, detailing, etc.), its loading and or a combination of the two. The probability of exceeding the damage state is then estimated as a function of the level of *EDP* in the component but also as a function of the parameter α. Figures 3b and 3c present examples of the fragility surfaces developed to estimate the probability of experiencing a shear failure and or the loss of vertical load carrying capacity in non-ductile reinforced concrete columns For more details on the fragility curves and fragility surfaces of structural components the reader is referred to Aslani and Miranda 2004a.

Consistent with parameters used in FEMA 356, fragility functions for non-structural components were developed as a function of either *IDR* and *PFA*. Non-structural components were assumed to be sensitive to only one of these parameters. Figure 4a presents an example of fragility functions developed for gypsum board partitions as a function of the level of the *IDR* imposed to the partition. Figure 4b presents an example of fragility functions developed for suspended ceilings as a function of the level of the *PFA* in the component. More details on the fragility of nonstructural components are presented in Taghavi and Miranda (2003a).

3.3 Estimation of the Probability of Collapse

As shown in Eqs (2) and (5) both the expected value of the losses and the dispersion of the losses for a given ground motion intensity require an estimate of the probability of collapse. Two different approaches were used to estimate the probability of collapse. In one approach collapse was produced by the occurrence of lateral dis-
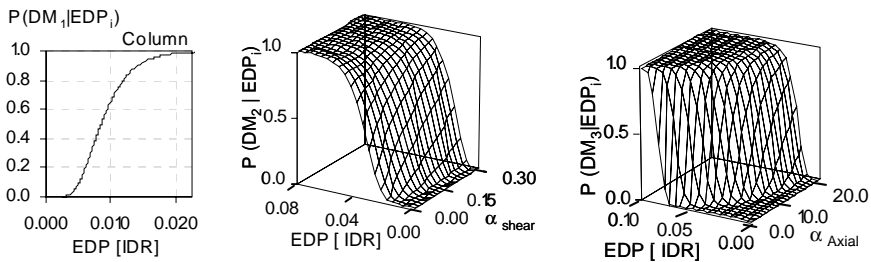

Figure 3. Fragility assessment of non-ductile reinforced concrete columns.
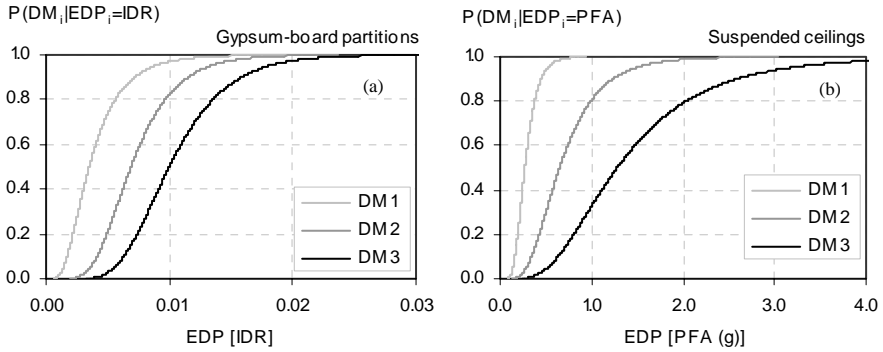
Figure 4. Fragility functions of drift-sensitive and acceleration-sensitive non-structural components at different damage measures; (a) gypsum-board partitions, (b) suspended ceilings.

placements that lead to a dynamic instability in the structure. In the second approach it was assumed that the structure could collapse even if the lateral displacements were not very large but enough to cause damage states that could trigger the loss of vertical carrying capacity in structural members. The second type of collapse triggering mechanism is particularly important in the case of non-ductile structures. In order to get an estimate of the probability of collapse due to the loss of vertical carrying capacity of structural components it was assumed that if a loss of vertical carrying capacity occurred in either a column of a slab column connection, such failure would trigger a progressive collapse of the structure. As shown in Aslani and Miranda (2004b), with this assumption the probability of collapse due loss of vertical carrying capacity (LVCC), $P(C_{LVCC}|IM)$, is equal to the largest probability of any individual structural element that can loose its vertical carrying capacity

$$P\left(C_{LVCC} \mid IM\right) = \max_{\forall i} \left[P\left(LVCC_i \mid IM\right)\right] \tag{8}$$

where $P\left(LVCC_i \mid IM\right)$ is the probability of losing the vertical carrying capacity in the ith component conditioned on IM and is computed as

$$P\left(LVCC_i \mid IM\right) = \int_0^\infty P\left(LVCC_i \mid EDP_i\right) \cdot \left| dP\left(EDP_i \mid IM\right)\right| \tag{9}$$

where $P\left(LVCC_i \mid EDP_i\right)$ is the probability of the ith component losing its vertical carrying capacity given that it is subjected to a deformation level equal to edp. $P\left(LVCC_i \mid EDP_i\right)$ is computed from fragility surfaces, developed for $LVCC$ damage states on the basis of experimental studies on structural components. $dP\left(EDP_i \mid IM\right)$ is the probability density function of EDP_i conditioned on IM, which can be estimated from a probabilistic response analysis. Figure 5, presents a graphical presentation of the steps to estimate $P(C_{LVCC}|IM)$, using Eqs. (8) and (9).
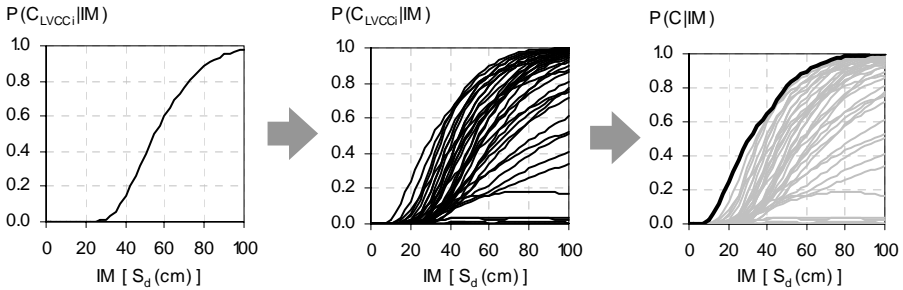
Figure 5. Different steps of estimation of the probability of collapse of the system conditioned on _IM_.

3.4 Repair or Replacement Costs Estimation

For each component loss functions are developed to estimate the cost of repair or cost to replace each component. Loss functions are functions that provide information on the probability of exceeding a certain level of repair or replacement cost given that the component is in the damage measure, *DM*. Examples of these functions are given in Aslani and Miranda (2004a).

3.5 Modeling Correlation between Losses in Individual Components

Estimation of the correlation between losses in individual components requires information on the correlation at three different levels; *EDP | IM* level, *DM | EDP* level and *DV | DM* level. The correlation at the response level, *EDP | IM* is estimated based on the results from nonlinear response history analyses. The correlation at the damage level, *DM | EDP*, is mathematically modeled by categorizing components into certain groups in terms of their damageability and estimating the joint probability of two components being at different damage states conditioned on the level of deformation each of them is subjected to. The correlation at the repair cost level, *DV | DM*, is estimated from the information on the correlation between different tasks required to repair the component.
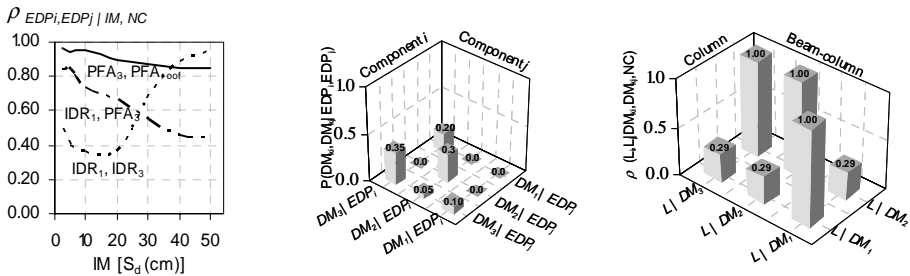

Figure 6. Variations of the required parameters to estimate the correlation of losses in individual components.
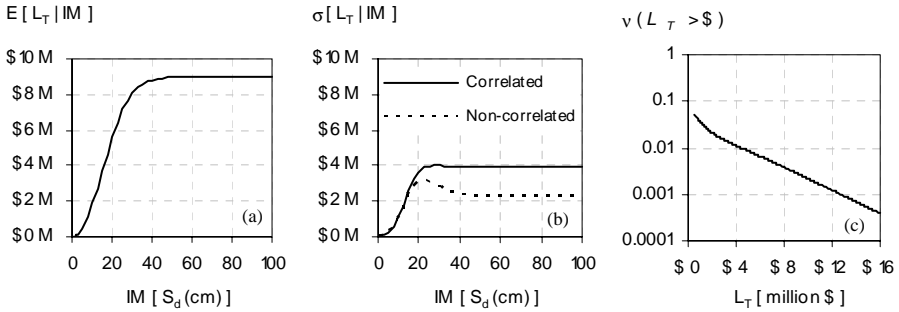
157

Figure 7. (a) Expected loss at different levels of intensity, (b) dispersion of loss at different levels of intensity, (c) building loss curve.

Figure 6 presents examples of each of the correlation at each of the above three level. Figure 6a shows how the correlation between different types of *EDP* varies as the ground motion intensity increase. Shown in Figure 6b is an example of the joint probability distribution of two components being at different damage states. Figure 6c shows the correlation between repair costs for a column and a beam-column connection.

3.6   Building Loss Estimation

Figure 7a presents the variations of the expected loss at different levels of intensity, $E[L_T|IM]$, estimated for the case study building. It can be seen that for this building losses rapidly increase at small levels of ground motion intensity. Figure 7b presents the variations of the dispersion of the loss of the building with increasing level of ground motion intensity for two cases: when losses in individual components are assumed to be correlated and when they are assumed non-correlated. It can be seen that correlation has significant effects on the uncertainty of the loss. For example, at S_d=20 cm assuming that the losses are uncorrelated leads to an underestimation of 25% of the dispersion of the loss.

The loss curve for the case study building is shown in Figure 7c where it can be seen that losses smaller than $1,000,000 have relatively high mean annual frequencies of exceedance.

4. LOSS DEAGGREGATION

Similarly to seismic hazard deaggregation (McGuire, 1995) building losses can also be disaggregated. In particular, it is interesting to investigate the ground motion intensities that most contribute to expected annual losses in a building. Figure 8 provides three examples of loss deaggregation. Figure 8a presents the contribution of collapse and non-collapse expected loss to the total loss at different levels of intensity. It can be seen in the figure that at small levels of intensity, (S_d<25cm), the contribution of non-collapse losses dominates the expected losses. Figure 8b provides similar information for the contribution of structural and non-structural losses to the
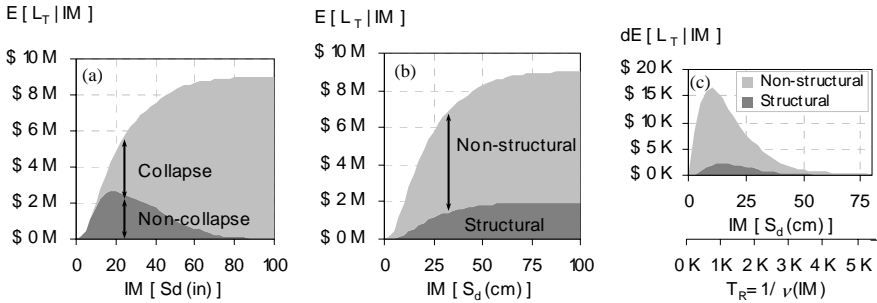
Figure 8. Loss deaggregation results: (a) contribution of collapse and non-collapse losses to the total loss at different levels of intensity, (b) contribution of structural and non-structural losses to the total loss at different levels of intensity, (c) deaggregation of the expected annual loss.

total loss. It can be send that losses are primarily produced by damage to non-structural components.

Figure 8c presents loss deaggregation results for the expected annual loss. It can be seen that for the case study building the earthquakes with S_d smaller than 50 cm, (return periods, T_R of less than 3500 years), contribute 96% to the expected annual loss, 81% of which comes from non-structural components and only 15% corresponds to structural components.

5. CONCLUSIONS

A methodology is proposed to estimate the seismic performance of buildings in terms of economic losses. The methodology explicitly incorporates the uncertainties corresponding to the seismic hazard, to the response of the structure, to the damage incurred in different components and to the repair or replacement cost of damaged components. Generic procedures are proposed to improve the estimation of various sources of uncertainty that contribute to the loss estimation methodology. Specifically, the concept of fragility surfaces is introduced which leads to smaller dispersions while estimating damage and provides a powerful tool to estimate the conditional probability of system collapse. Furthermore, the effects of correlation between losses in individual components are explicitly considered. It is concluded that the correlation between losses at the component-level can significantly increase the dispersion in the losses in the building.

As part of the study, the use different of different parameters as ground motion intensity measures was investigated. It is concluded that for drift-sensitive components, using inelastic spectral displacement ordinates leads to lower dispersion of building response than those computed using elastic spectral ordinates. For acceleration-sensitive components, it was observed that peak ground acceleration, *PGA*, provides smaller levels of dispersion of peak floor accelerations compared to those computed using elastic spectral ordinates as intensity measure.

Finally, the results from the loss estimation methodology were disaggregated in order to determine the contribution of different ground motion levels and different components on losses in the building. Examples on deaggregation were presented to identify the contribution of structural and nonstructural components to expected losses and contributions of collapse and non-collapse to expected annual losses.

REFERENCES

Aslani, H., and E. Miranda. (2003). Probabilistic assessment of building response during earthquakes. *Procs. Applications of Statistics and Probability in Civil Engineering ICASP9*, Der Kiureghian, Madanat & Pestana (eds.), Millpress, Rotterdam.

Aslani, H., and E. Miranda. (2004a). Probabilistic damage assessment for building-specific loss estimation. *PEER report*. Pacific Earthquake Engineering Research Center, University of California at Berkeley, Berkeley, California.

Aslani, H., and E. Miranda. (2004b). Investigation of the effects of correlation for building-specific loss estimation. *PEER report in preparation*, Pacific Earthquake Engineering Research Center, University of California at Berkeley, Berkeley, California.

Building Seismic Safety Council (BSSC). FEMA 356. (2000). Prestandard and commentary for the seismic rehabilitation of buildings. Federal Emergency Management Agency, Washington, D.C.

FEMA 249. (1994). Assessment of the state-of-the-art earthquake loss estimation methodologies. Federal Emergency Management Agency, Washington, D.C.

Krawinkler, H., and E. Miranda. (2004). Performance-based earthquake engineering. Chapter 9 of *Earthquake Engineering: from engineering seismology to performance-based engineering*, CRC Press, 2004.

McGuire, R. K. (1995). Probabilistic Seismic Hazard Analysis and Design Earthquakes: Closing the Loop, *Bull. Seismological Soc. America*, 85, 1275–1284.

Miranda, E., and H. Aslani. (2003). Building-specific loss estimation methodology. *Report PEER 2003-03*, Pacific Earthquake Engineering Research Center, University of California at Berkeley, Berkeley, California.

Rosenblueth, E. (1976). Towards optimum design through building codes. *Journal of the structural division-ASCE*; 1976; 102, (3), 591–607

Taghavi, S., and E. Miranda. (2003a). Response assessment of nonstructural elements. *Report PEER 2003-04*, Pacific Earthquake Engineering Research Center, Richmond, California.

Taghavi, S., and E. Miranda. (2003b). Probabilistic study of peak floor acceleration demands in linear structures. *Procs. Applications of Statistics and Probability in Civil Engineering ICASP9*, Der Kiureghian, Madanat & Pestana (eds.), Millpress, Rotterdam.

Wen, Y. K., and Y. J. Kang. (2001). Minimum building life-cycle cost design criteria, I: Methodology. *J. Struct. Engineering*, ASCE, 127 (3), 330–337.

SEISMIC RESILIENCE OF COMMUNITIES — CONCEPTUALIZATION AND OPERATIONALIZATION

Michel BRUNEAU[1] and Andrei REINHORN[2]

ABSTRACT

A conceptual framework which defines the seismic resilience of communities and quantitative measures of resilience in a manner that can be useful for a coordinated research effort focusing on enhancing this resilience is one of the main themes at the Multidisciplinary Center for Earthquake Engineering Research (MCEER). This framework relies on the complementary measures of resilience: "Reduced failure probabilities", "Reduced consequences from failures", and "Reduced time to recovery". The framework also includes quantitative measures of the "ends" of robustness and rapidity, and the "means" of resourcefulness and redundancy. The ultimate objective of this work is to make the concepts that are presented here adaptable for the analysis of various critical infrastructure elements (both as individual systems and as interrelated sets of systems) exposed to both natural and man made disasters.

Keywords: Performance; Resilience; Recovery; Redundancy; Socio-economic.

1. INTRODUCTION

As part of the conceptualization of a framework to enhance the seismic resilience of communities (Bruneau et al. 2003), seismic resilience has been defined as the ability of a system to reduce the chances of a shock, to absorb a shock if it occurs (abrupt reduction of performance) and to recover quickly after a shock (re-establish normal performance), as described in Bruneau et al. (2003). More specifically, a resilient system is one that shows:

1. Reduced failure probabilities,
2. Reduced consequences from failures, in terms of lives lost, damage, and negative economic and social consequences,
3. Reduced time to recovery (restoration of a specific system or set of systems to their "normal" level of performance)

A broad measure of resilience that captures these key features can be expressed, in general terms, by the concepts illustrated in Figure 1, based on the notion that a

---

[1] *Director Multidisciplinary Center for Earthquake Engineering Research and Professor Department of Civil, Structural, and Environmental Engineering (CSEE) , University at Buffalo, State University of New York, Buffalo, NY, 14260*

[2] *Clifford Furnas Professor CSEE, University at Buffalo, State University of New York, Buffalo, NY, 14260*

measure, Q(t), which varies with time, can be defined to represent the quality of the infrastructure of a community. Specifically, performance can range from 0% to 100%, where 100% means no degradation in quality and 0% means total loss. If an earthquake occurs at time t_0, it could cause sufficient damage to the infrastructure such that the quality is immediately reduced (from 100% to 50%, as an example, in Figure 1). Restoration of the infrastructure is expected to occur over time, as indicated in that figure, until time t_1 when it is completely repaired (indicated by a quality of 100%). Hence, community earthquake loss of resilience, R, with respect to that specific earthquake, can be measured by the size of the expected degradation in quality (probability of failure), over time (that is, time to recovery). Mathematically, it is defined by:
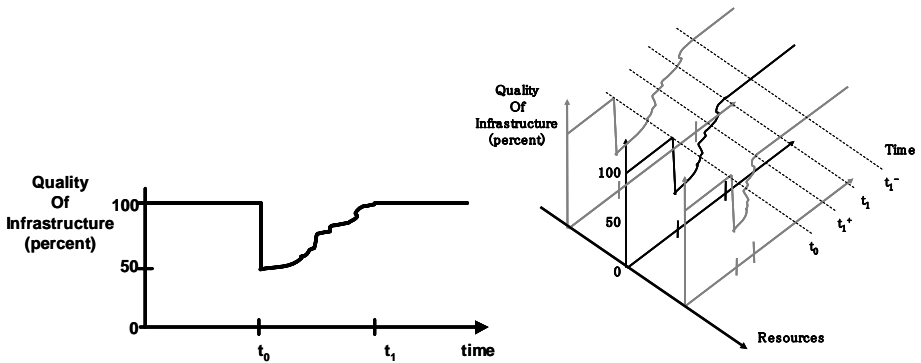
$$R = \int_{t_0}^{t_1} [100 - Q(t)]dt$$

Figure 1. Resilience functions: basic (left), multi-dimensional (right).

For a geographically distributed system designed to provide a standardized service, such as a power grid, or a water distribution network, the problem is simpler, as the vertical axis in Figure 1 could be a quantifiable value, such as kilowatts, gallons, or households provided with service. However, for critical systems for which the deliverable is not a simple engineering unit, such as for the case of acute care facilities, the vertical axis is harder to define, not to mention quantify.

This paper presents concepts developed in attempts to quantify the seismic resilience of acute care facilities. The problem is framed in a broader societal context, from which is formulated a sub-problem that can be addressed and quantified through a coordinated large-scale multidisciplinary earthquake engineering research effort. The engineering tools that could result from an implementation of the concepts presented here could contribute and be integrated into decision support tools, which in turn could be use for the formulation of strategies and policies at a higher level.

2. RESILIENCE CONCEPTS

Resilience for both physical and social systems can be further defined as consisting of the following properties:

- Robustness: strength, or the ability of elements, systems, and other units of analysis to withstand a given level of stress or demand without suffering degradation or loss of function;
- Redundancy: the extent to which elements, systems, or other units of analysis exist that are substitutable, i.e., capable of satisfying functional requirements in the event of disruption, degradation, or loss of functionality;
- Resourcefulness: the capacity to identify problems, establish priorities, and mobilize resources when conditions exist that threaten to disrupt some element, system, or other unit of analysis.
- Rapidity: the capacity to meet priorities and achieve goals in a timely manner.

As such the vertical and horizontal axes in Figure 1 (left) address the ends of resilience, namely robustness and rapidity. However, Figure 1 can be expanded in 3-D and 4-D to capture the means of resilience as is illustrated in Figures 1 (right) by a third axis, that added resources can be used to reduce time to recovery. In theory, if infinite resources were available, time to recovery would asymptotically approach zero. Practically, even in the presence of enormous financial and labor capabilities, human limitations will dictate a practical minimum time to recovery.

3. RESILIENCE OF ACUTE CARE FACILITIES

Residents in seismic areas have expressed their strong expectation that acute care facilities should be available and operational following an earthquake (Nigg 1998). As such, fulfillment of this expectation would significantly contribute to enhancing the seismic resilience of communities. California has already taken steps in that direction by enacting ordinance SB1953 which requires that acute care facilities be retrofitted by 2030 to a level that would allow them to be fully operational following an earthquake.

To quantify the seismic resilience, the quantity to be measured by the vertical axis of the resilience chart must first be defined.

A first option is to quantify quality of life as the percentage of healthy population (Figure 2). Using
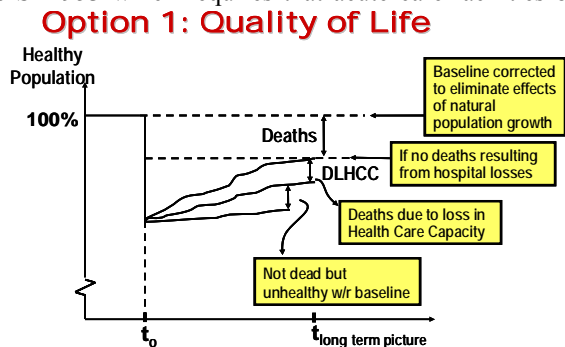

Figure 2. Quality of life — measure of performance.

the total healthy population in absence of an earthquake as a reference basis, and normalizing it to eliminate the effect of population growth over time, the horizontal line drawn at 100% on the vertical axis represents the healthy population that resides in an area that could be affected by a scenario earthquake. A first drop in population health would occur when individuals are killed by seismically deficient structures. Injuries suffered during the earthquake would account for the remaining reduction in the healthy population at time t_0. In the best of scenario, in absence of hospital losses, all these injuries would heal, and no more deaths would be added to the toll. Conversely, deaths due to loss in health care capacity (DLHCC) would occur, i.e., deaths that could have been prevented if the health care system capability had not been reduced by the earthquake. This approach has the advantage that it seeks to quantify the impact of an earthquake on the health of a population, a significant measure for the purpose of policy making.

A second, alternative, option focuses on relating the seismic resilience of facilities to the number of patients/day that can be provided as a measure of the treatment capacity of the health care facilities (Figure 3). For example, prior to an earthquake, the impact of SB1953 is shown (Figure 3) as resulting in the loss of some patients/day capacity, as some hospitals are expected to close. Following the major loss of patients/day capacity directly attributed to the earthquake, is the short burst of recovered patients /day capacity as a con-sequence of the "parking-lot" medicine provided outside of hospital facilities. In Figure 3, for convenience, two distinct and concurrent recovery activities are illustrated as sequential, namely: repair of capacity and rebuilding of capacity.
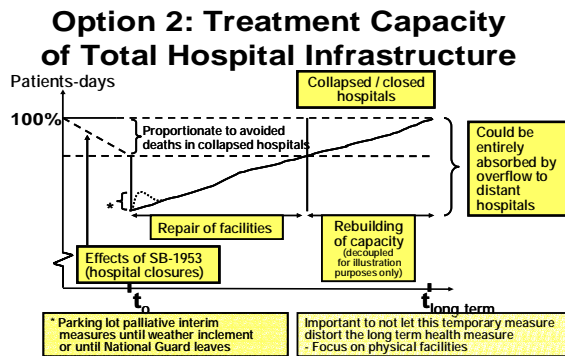
Figure 3. Hospital capacity — measure of performance.

The advantage of this second approach is that it focuses on the physical infrastructures and their ability to provide their intended function, which facilitates engineering quantification. This framework makes it possible for a coordinated earthquake engineering research effort to contribute in a focused and effective manner to the broader problem. While the engineering effort and resources needed to completely address all issues likely still requires the concerted efforts of multiple government agencies and considerable funding, it is possible for smaller scale engineering efforts to develop some of the tools and methodologies that could be integrated into decision support systems. In this respect, these engineering

quantification tools could be used to assess whether the seismic resilience is enhanced or not, i.e., whether a set of interventions reduce the loss in patient-day capacity, or if a local overflow can be absorbed globally, and how long will take to restore capacity.

4. RESILIENCE OF STRUCTURAL AND NON-STRUCTURAL COMPONENTS

A first step toward the above objectives is the definition and quantification of engineering resilience. This is illustrated here by focusing on the resilience of structural and non-structural components.

In light of the considerable uncertainties inherent to the field of earthquake engineering (both in the demands estimated through engineering seismology, and

Figure 4. Probabilistic aspect of seismic resilience, (structural integrity example).

in the capacities that ensue from the non-linear inelastic seismic performance of the structure), the quantification of seismic resilience proceeds through a probabilistic frame-work, as illustrated in Figure 4. A serviceability level is defined as a small loss in structural integrity. A collapse level is defined as the maximum loss of integrity prior to collapse; other resilience curves are shown to represent various structural integrity conditions between the serviceability and collapse levels, and the fact that a proportional coupling often (but not always) exists between the time to recovery and the initial loss of structural integrity. It is also illustrated that over time, structural integrity could return to the initial pre-earthquake condition, to less than this condition (e.g., cracking in some structural element may never be repaired), or above this condition if the structure is repaired to a superior seismic performance level. The bell-curves show that these integrity levels are random variable.

One way to achieve quantification of engineering seismic resilience is through the concept of Multidimensional Bell-curve of Response. Therefore, for the purpose of this discussion, the probability distribution surface schematically shown in Figure 5 is used. Viewed from above, the surface can be expressed by isoprobability contours. Spherical contours are used here for expediency. Floor pseudo-accelerations (PSA floor) and interstory drifts (S_d floor) express the Limit Space (LS), with specific structural and non-structural limit states shown by dotted lines; for the former, a serviceability limit state (cracking of concrete structural elements) and a collapse limit state are indicated. Deterministic limit states are used here, but need not be.

Floor acceleration and inter-story drift are therefore the structural response probabilistic parameters considered here by the bell distribution. The probability that response exceeds a specific limit state can be directly calculated from the volume under the surface distribution exceeding the specified limit. For a given structural response, retrofit measures that would allow the non-structural components to resist greater floor accelerations (i.e., move up the acceleration limit state dotted line in Figure 5) would directly translate into a smaller volume under the probability distribution surface, and thus a smaller probability of

Figure 5. Probability that response exceeds limit space: (a) non-structural limit states vs. structural limit states; (b) different sequence of limit states.

exceedence of the limit state. However, modifications to the structural system change the probable structural response, which is equivalent to sliding the multidimensional bell-curve within the limit space (i.e., moving along the dotted arrows in Figure 5). For example, stiffening the structural system in a manner that reduce interstory drifts would move the response surface to the left of the limit space of Figure 5, and could also move it upward or downward, depending on the initial structural period (although the former is more likely). Structural damage during an earthquake would weaken the structure, moving the response surface toward the right and possibly downward (solid arrow in Figure 5), resulting in greater intersect with the drift-controlled limit states.

Quantification of the seismic resilience curve is first presented for the case of linear-elastic structural response. For this and all subsequent cases considered, the vertical axis of the resilience curves is in terms of "investment value" in the structural system, or the non-structural system. The left part of Figure 6 illustrates that there is no structural loss (i.e., no drop in the value of structural investment) when the

structure remains elastic. This is equivalent to having no significant intersect between the probabilistic response surface and the structural limit states in Figure 5a. However, such intersect exists in the limit space for the non-structural components, and the magnitude of this intersect (i.e., probability of exceeding the limit space) can be calculated, and is expected to increase as a function of the earthquake return period. Figure 6c expresses the resulting probability of exceeding the limit space as a function of the earthquake hazard (itself expressed in probability of exceedence over 50 years, in a manner compatible with code documents — 50%, 10% (500 years return period), and 2% probability of exceedence.. The probable non-structural loss, P_{NSL}, can be expressed by the product of the probability of exceeding the limit state, P_{LS}, and of the value of the non-structural investment, NS_{INV}. For the probable exceedence of the limit space shown in Figure 6c for a design level corresponding to a 500-year return period, Figure 6b shows the resulting non-structural resilience curve, with the probable non-structural losses at time t_o. The time at full recovery to pre-earthquake conditions, t_1, is entirely related to repair of non-structural damage.

Quantification of the seismic resilience curve for the case of non-linear inelastic structural response differ from the previous case by the presence of a structural loss (i.e., a drop in the value of structural investment due to damage) measurable from the fragility concept since there is now a quantifiable intersect between the probabilistic response surface and the structural limit states in Figure 5b. Figure 7b expresses the resulting probability of exceeding the limit space, P_{LS}, as a function of the earthquake hazard, and Figure 7a the corresponding probable loss in the structural investment, P_{LS}. If another earthquake was to occur at time t_o^+, the probability of exceeding the limit state would be significantly greater (as shown in Figure 7b), and a further loss in the structural investment (possibly to collapse) would occur.
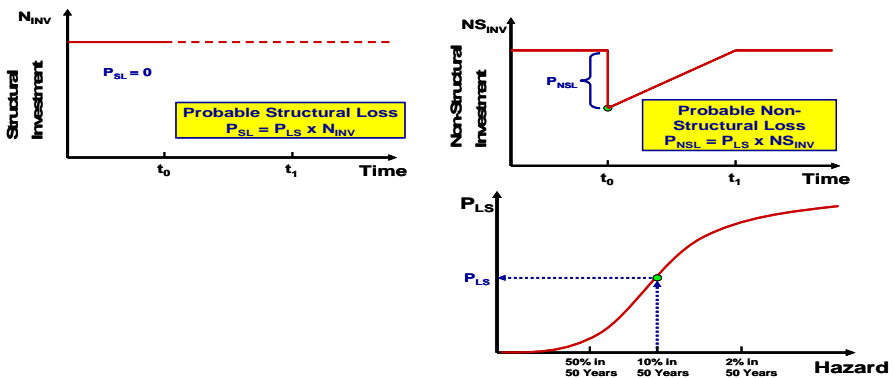

Figure 6. Probable non-structural loss in case of linear-elastic structural response.

The probable non-structural loss would be calculated as before, with the only difference that if the same earthquake was to re-occur at time t_o^+, the probability of exceeding the non-structural limit space could increase or decrease, depending on the type of non-structural components, and the extent of structural damage (e.g., a "softer" damaged structure might undergo lower floor accelerations but greater floor interstory drifts). For the purpose of Figures 7c and 7d, the assumption of greater probability of non-structural damage is made.
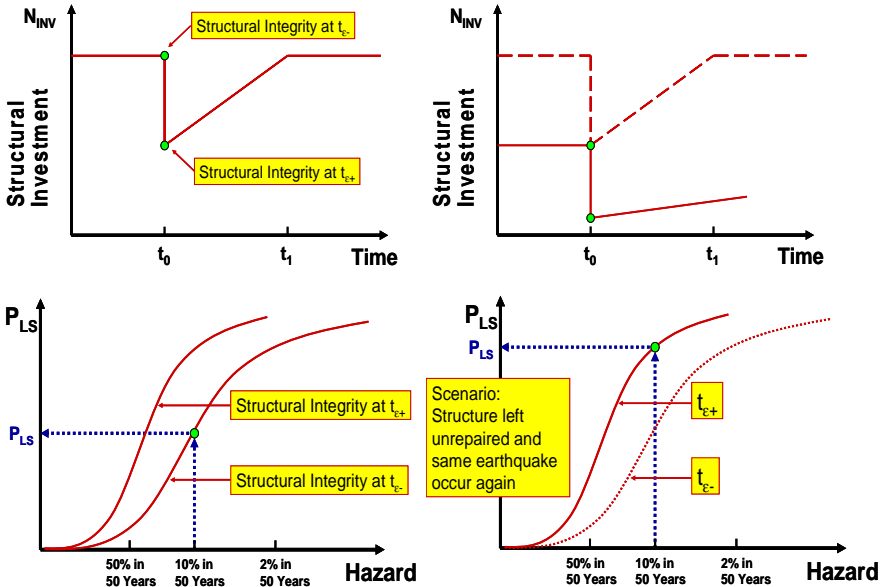
Figure 7. Case of structural seismic response: (a) Structural resilience curve and corresponding loss in structural integrity as obtained from; (b) Probability of structural loss before earthquake; (c) New structural resilience curve if structure left unrepaired, based on; (d) probability of failure upon repeat of earthquake.

Structural repairs progressively shift the curve of probable losses back to the original condition that existed at the instant before t_o (thus equal to the condition at t_1). This requires a financial investment and one could quantify the cost required to shift from one probabilistic curve to another (unlikely to be a linear relationship). The rate of repair also provides a measure of the rapidity dimension of the resilience curve. Note, that repairs to non-structural components may also be required, and that it is possible to increase the value of the investments (on the basis of the same non-structural components and equipments here, not by adding more of them) to above the pre-earthquake condition, enhancing seismic resilience by reducing the probability of losses in a future repeat of the same earthquake. The benefit of retrofitting prior to an earthquake can also be assessed and quantified using the resiliency concept presented in Figures 8. To illustrate how this is achieved, the fragility curves at times t_o^- and t_o^+

of Figure 7a will be used. It is assumed that the relativity of this pair of fragility curves for a given structure remains the same, and that seismic retrofit prior to an earthquake is equivalent to sliding of the fragility curves along the horizontal axis such that a greater earthquake is required after retrofit to produce the same probable loss of the structural investment. Failing the availability of a theory to quantitatively substantiate this assumption of constant relationship between pairs of fragility curves for a given structural condition, this will be referred here as the "Reinhorn-Bruneau Sliding Pair of Fragility Curves" assumption. As shown in Figure 8, once the structure has been retrofitted, the investment in the structural system has been increased, which translates into the elevated resilience curve of Figure 8b. Furthermore, should the same expected earthquake occurs (with a return period corresponding to 10% change of exceedence in 50 years for the example in Figure 8a), the probable loss in structural investment due to damage is also reduced, as shown by the corresponding drop between time t_0^- and t_0^+ in Figure 8b.
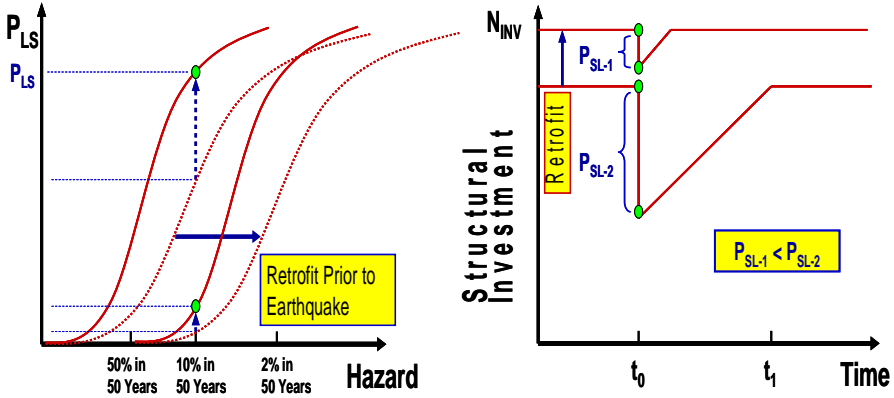
Figure 8. Non-linear structural seismic response: (a) Bruneau/Reinhorn assumption of sliding proportional fragility curve sets; (b) Enhancement of resilience curve to reduced probability of losses due to seismic retrofit prior to earthquake.

The corresponding impact of either structural damage or seismic retrofit on the fragility and resilience curves of non-structural component for the case of non-linear structural seismic response and non-retrofitted non-structural components is somewhat unknown. For example, structural damage could result in a more flexible structure, which would have greater displacements but smaller floor accelerations upon a recurrence of the same earthquake at time t_0^+. The total probability of losses in non-structural component would depend on the response distribution (the Demand) and the limit space (the Capacity).

169

To establish the relationships between various engineering measures and loss of patients/day capability requires integrating (quantitatively) component fragilities (including non-structural, structural, geotechnical, etc.) into a system resilience (using the same units as presented in this paper).

5. CLOSING REMARKS

A possible final quantification of seismic resiliency assessment could be stated in a format suitable for some stakeholders: "There is a 95% chance that 80% of hospitals can operate at 90% of their capacity within 5 days following an earthquake". This is a statement that addresses a measure of loss of capacity (90% of capacity), an assessment of time to recovery (within 5 days), integration over a geographically distributed system as an option (80% of hospitals).

At this time, communities cannot articulate such resiliency objectives, as they cannot operate at this level of sophistication. This is partly because the tools to support such statements do not yet exist. Research is most needed to develop such tools, which decision makers will then be able to use to formulate the numbers themselves. However, in formulating policies anchored in quantitative resiliency targets, one must recognize that resiliency targets, while important objectives, are not to be taken as absolutes. This points to the need for a quantitative probabilistic framework and tools anchored in engineering procedures to guide decision makers in consideration of policies, rather than to focus on numerical values in a "one-size fits all" approach.

In the end, willingness to invest in pre-earthquake mitigation measures aimed at reducing seismic resilience is intrinsically tied to the earthquake risk as perceived by the stakeholders. Quantitative resiliency measures, integrated into decision support tools, will help respective stakeholders better understand their exposure and options by providing well "anchored" data from which they can re-assess their perceptions.

ACKNOWLEDGMENTS

REFERENCES

Bruneau, M., S. Chang, R. Eguchi, G. Lee, T. O'Rourke, A. Reinhorn, M. Shinozuka, K. Tierney, W. Wallace, D. von Winterfelt. (2003). "A Framework to Quantitatively Assess and Enhance the Seismic Resilience of Communities", EERI Spectra Journal, Vol.19, No.4, pp.733-752.

Nigg, J. M. (1998). Empirical findings based on research conducted under NSF Grant No. CMS-9812556. "Perceptions of Earthquake Impacts and Loss-Reduction Policy Preferences among Community Residents and Opinion Leaders," J. M. Nigg, Principal Investigator.

PERFORMANCE AND DISPLACEMENT-BASED EARTHQUAKE LOSS ESTIMATION OF URBAN AREAS

Rui PINHO[*]

ABSTRACT

Code implementation of performance-based seismic design requires the definition of multiple design levels, each of which is coupled with different performance limit states that structures must then comply to. The definition of such pairs of design and performance levels should ideally be based on cost-benefit considerations derived from reliable and computationally efficient loss models, which, at their core, feature sound deformation-based principles and procedures that lead to an explicit and accurate account of structural performance. This work describes preliminary efforts in developing such a loss model, where distribution of damage states at a specific location, and for any given earthquake ground motion, can be readily estimated through a set of analytically-derived relationships that correlate building displacement capacity and height, which in turn can be related to displacement demand. Uncertainty in geometrical, material and limit state properties of a building class is also explicitly accounted for, without compromising the elegance of the procedure. In this way, studies on regional or national levels may still be effectively carried out, even when the triggering of multiple earthquake scenarios, as opposed to the use of probabilistic hazard maps and uniform hazard spectra, is employed to realistically assess seismic demand and its consequences on the built environment.

Keywords: Displacement-based assessment; Earthquake loss estimation; RC structures.

1. INTRODUCTION

1.1 Preamble

The main objective of performance-based seismic design, for both new and existing structures, is to control all earthquake losses, including direct and indirect economic losses in addition to the fundamental life-safety objective. As widely acknowledged, this requires the definition of multiple design levels, each coupled with different performance limit states to which structures must then comply to. As noted by Bommer (2004), however, arbitrary choices, as opposed to sound technical principles, seem to have played the decisive role in the choice of the design levels that are nowadays employed in the majority of seismic design codes (e.g., spectral

---

[*] *European School for Advanced Studies in Reduction of Seismic Risk (ROSE School), Pavia, Italy*

acceleration with a 475-year return period for the life-safety limit state of non-critical buildings). The rationale underlying the current endeavour is that the definition of such pairs of design and performance levels should instead be based on cost-benefit considerations derived from reliable and computationally efficient loss models, which, at their core, feature sound deformation-based principles and procedures that lead to an explicit and accurate account of structural performance.

This paper describes the first efforts in developing such a loss model, where the distribution of damage states across a particular class of buildings at a specific location and for any given earthquake ground motion can be readily estimated through a set of analytically derived relationships that correlate building displacement capacity and height, which in turn can be related to displacement demand.

1.2 Proposed Methodology

A new approach to displacement-based assessment of structural vulnerability of reinforced concrete moment resisting frames has been proposed by Pinho *et al.* (2002) and subsequently developed in a deterministic framework by Glaister and Pinho (2003). Crowley *et al.* (2004) refined the approach and extended it into a fully probabilistic framework that incorporates the variability in the parameters that define both the demand and the capacity.

The procedure uses mechanically-derived formulae to describe the displacement capacity of classes of buildings at three different limit states. These equations are given in terms of material and geometrical properties, including the average height of buildings in the class. By substitution of this height through a formula relating height to the limit state period, displacement capacity functions in terms of period are attained; the advantage being that a direct comparison can now be made at any period between the displacement capacity of a building class and the displacement demand predicted from a response spectrum.
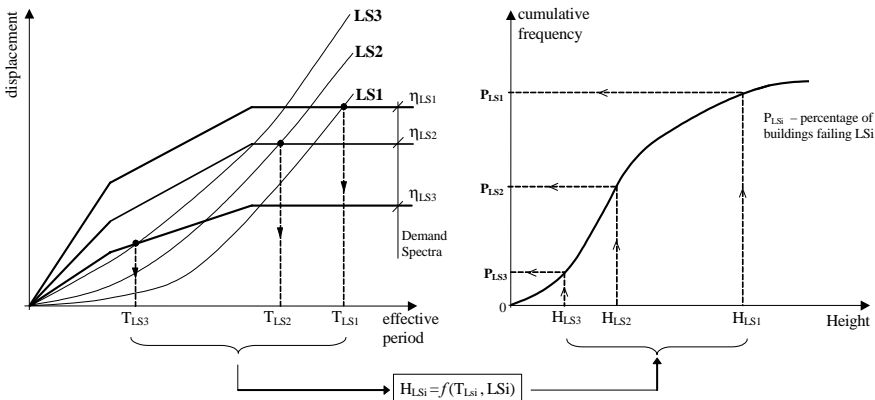

Figure 1. A deformation-based seismic vulnerability assessment procedure.

The original concept is illustrated in Figure 1, above, whereby the range of periods with displacement capacity below the displacement demand is obtained and transformed into a range of heights using the aforementioned relationship between limit state period and height. This range of heights is then superimposed on to the cumulative distribution function of building stock to find the proportion of buildings failing the given limit state. The inclusion of a probabilistic framework into the method, however, has meant that the simple graphical procedure outlined in Figure 1 that treated the beam- or column-sway RC building stock as single building classes can no longer be directly implemented, but instead, separate building classes based on the number of storeys need to be defined, as noted in subsequent sections.

2. DETERMINISTIC IMPLEMENTATION

2.1 Classification of Buildings

The initial step required in this method is the division of the building population into separate building classes. A building class is to be considered as a group of buildings that share the same construction material, failure mechanism and number of storeys; e.g., reinforced concrete moment resisting frames of 3 to 5 storeys, exhibiting a beam-sway failure mode. A decision regarding whether a moment resisting frame will exhibit a beam-sway or a column-sway mechanism may be made considering the construction type, construction year and presence of a weak ground floor storey.

2.2 Structural and Non-Structural Limit States

Damage to the structural (load-bearing) system of the building class is estimated using three limit states of the displacement capacity. The building class may thus fall within one of four discrete bands of structural damage: none to slight, moderate, extensive or complete. A qualitative description of each damage band for reinforced concrete frames is given in the work by Crowley *et al.* (2004) along with quantitative suggestions for the definition of the mechanical material properties for each limit state, taken from the work of Priestley (1997) and Calvi (1999).

Damage to non-structural components within a building can be considered to be either drift- or acceleration-sensitive (Freeman *et al.*, 1985; Kircher *et al.*, 1997). Drift-sensitive non-structural components such as partition walls can become hazardous through tiles and plaster spalling off the walls, doors becoming jammed and windows breaking. Acceleration-sensitive non-structural components include suspended ceilings and building contents. At present, only drift-sensitive non-structural damage is considered within this methodology, using three limit states of drift capacity. Interstorey drift can be used to predict drift-sensitive non-structural damage. Freeman *et al.* (1985) report that studies on dry wall partitions indicate an initial damage threshold at a drift ratio of 0.25%, and a threshold for significant damage at drift ratios between 0.5 to 1.0%. However, to ensure three non-structural

limit states, the suggestions given by Calvi (1999) have been followed (see Crowley *et al*., 2004). The non-structural components will again fall within one of four bands of damage: undamaged, moderate, extensive or complete.

2.3 Displacement Capacity as a Function of Height

The demand in this methodology is represented by a displacement spectrum which can be described as providing the expected displacement induced by an earthquake on a single degree of freedom (SDOF) oscillator of given period and damping. Therefore, the displacement capacity equations that are derived must describe the capacity of a SDOF substitute structure and hence must give the displacement capacity, both structural and non-structural, at the centre of seismic force of the original structure. In the following sub-sections, structural displacement capacity formulae for moment-resistant reinforced concrete frames exhibiting a beam- or column-sway failure mechanisms are presented.

2.3.1 Structural Displacement Capacity

By considering the yield strain of the reinforcing steel and the geometry of the beam and column sections used in a building class, yield section curvatures can be defined using the relationships suggested by Priestley (2003). These beam and column yield curvatures are then multiplied by empirical coefficients to account for shear and joint deformation to obtain a formula for the yield chord rotation. This chord rotation is equated to base rotation and multiplied by an effective height to produce the displacement at the centre of seismic force of the building.

The effective height is calculated by multiplying the total height of the structure by an effective height coefficient (ef_h), defined as the ratio of the height to the centre of mass of a SDOF substitute structure (H_{SDOF}), that has the same displacement capacity as the original structure at its centre of seismic force (H_{CSF}), and the total height of the original structure (H_T), as explicitly described in the work by Glaister and Pinho (2003).

The yield displacement capacity formulae for beam- and column-sway frames are presented in Equations (1) and (2) respectively; these are used to define the first structural limit state.

$$\Delta_{Sy} = 0.5 ef_h H_T \varepsilon_y \frac{l_b}{h_b} \tag{1}$$

$$\Delta_{Sy} = 0.43 ef_h H_T \varepsilon_y \frac{h_s}{h_c} \tag{2}$$

Post-yield displacement capacity formulae are obtained by adding a post-yield displacement component to the yield displacement, calculated by multiplying together the limit state plastic section curvature, the plastic hinge length, and the height/length of the yielding member. The post-yield displacement capacity formulae for RC beam-

and column-sway frames are presented here in Equations (3) and (4), respectively. In this formulation, the soft-storey of the column-sway mechanism is assumed to form at the ground floor. Straightforward adaptation of the equations could easily be introduced in the cases where the soft-storey is expected to form at storeys other than the ground floor, but this is not dealt with herein.

$$\Delta_{SLsi} = 0.5 ef_h H_T \varepsilon_y \frac{l_b}{h_b} + 0.5 \left(\varepsilon_{C(Lsi)} + \varepsilon_{S(Lsi)} - 1.7 \varepsilon_y \right) ef_h H_T \tag{3}$$

$$\Delta_{SLsi} = 0.43 ef_h H_T \varepsilon_y \frac{h_s}{h_c} + 0.5 (\varepsilon_{C(Lsi)} + \varepsilon_{S(Lsi)} - 2.14 \varepsilon_y) h_s \tag{4}$$

A detailed account of the derivation of Equations (1) through to (4) can be obtained from the work of Glaister and Pinho (2003). These equations employ the following parameters:

Δ_{Sy}	structural yield (limit state 1) displacement capacity
Δ_{SLsi}	structural limit state i (2 or 3) displacement capacity
ef_h	effective height coefficient
H_T	total height of the original structure
ε_y	yield strain of the reinforcement
l_b	length of beam
h_b	depth of beam section
h_s	height of storey
h_c	depth of column section
$\varepsilon_{C(Lsi)}$	maximum allowable concrete strain for limit state i
$\varepsilon_{S(Lsi)}$	maximum allowable steel strain for limit state i

2.3.2 Non-Structural Displacement Capacity

In the derivation of the non-structural displacement capacity equations for beam-sway frames, the effective height coefficient cannot be used directly because, rather than mechanically deriving a base rotation capacity, as in the structural displacement capacity formulation, it is the roof deformation capacity that is directly obtained (see Crowley *et al.*, 2004). Hence a relationship between the deformation at the roof and the deformation at the centre of seismic force is required. The factor relating these two displacements is named a shape factor (S) and it can be found from the displacement profiles suggested by Priestley (2003) for beam-sway frames of various heights. The non-structural displacement capacity of the SDOF substitute structure (Δ_{NSLsi}) for a given limit state i can thus be found by multiplying the roof displacement by the shape factor to give the displacement at the centre of seismic force of the structure, as presented in Equation (5), where ϑ_i stands for the drift ratio capacity at limit state i (Crowley *et al.*, 2004).

$$\Delta_{NSLsi} = S\vartheta_i H_T \tag{5}$$

For column-sway frames, the potential for concentration of non-structural damage at the ground floor should be considered. Thus it is assumed that once the first floor reaches the limit state interstorey drift capacity, then the non-structural damage limit state has been attained. Therefore it should be ascertained whether the displacement at the first floor (Δ_{NS1st}), obtained by multiplying the interstorey drift with the storey height, is greater than the first floor structural yield displacement (Δ_{Sy1st}), found by multiplying the yield base rotation by the height of the first storey. As shown by Crowley *et al.* (2004), the above effectively means that the non-structural displacement capacity of column-sway frames for limit states before structural yielding, ascertained at the first floor, may be found using Equation (6) whilst for limit states occurring after structural yielding at the first floor, Equation (7) applies.

$$\Delta_{NSLsi} = 0.67\vartheta_i H_T \tag{6}$$

$$\Delta_{NSLsi} = \vartheta_i h_s + 0.43(ef_h H_T - h_s)\varepsilon_y \frac{h_s}{h_c} \tag{7}$$

2.4 Period of Vibration of Buildings as a Function of Height

Simple empirical relationships are available in many design codes to relate the fundamental period of vibration of a building to its height. However, these relationships have been realised for force-based design and so produce lower bound estimates of period such that the base shear force becomes conservatively predicted. The use of a reliable relationship between period and height is a fundamental requirement in this methodology, so that the displacement capacity formulae can be accurately defined in terms of period and directly compared with the displacement demand; however with a conservative period-height relationship the displacement demand would generally be under-predicted. Therefore, Crowley and Pinho (2004) carried out an extensive parametric study to derive a suitable relationship between yield period and height, which is given in Equation (8). For post-yield limit states, on the other hand, the limit state period of the substitute structure can be obtained by the secant stiffness to the point of maximum deflection on an idealised bi-linear force-displacement curve, which, as demonstrated by Glaister and Pinho (2003), leads to an expression (Equation (9)) that depends on elastic period (T_y) and ductility (μ_{Lsi}) alone.

$$T_y = 0.1H_T \tag{8}$$

$$T_{Lsi} = T_y \sqrt{\mu_{Lsi}} \tag{9}$$

2.5 Displacement Capacity as a Function of Period

Inspection of the displacement capacity equations given above renders clear that, in order for the capacity curves to be graphically superimposed onto a period-dependent demand curve (response spectra), as suggested in Figure 1, it is necessary to replace all H_t terms present in these capacity equations with period-dependent functions. Such step has been carried out by Glaister and Pinho (2003), leading to a set of capacity equations that are conceptually identical to Equations (1) to (7), but conveniently defined in terms of effective period, rather than height. For the sake of succinctness, however, such formulae are not reproduced here, being nonetheless found in Crowley *et al.* (2004).

2.6 Displacement Demand

Displacement response spectra are used in this method to represent the input from the earthquake to the building class under consideration. The relationship between equivalent viscous damping (ξ) and ductility (μ), used to account for the energy dissipated through hysteretic action at a given level of ductility, is presented in the following equation:

$$\xi = a\left(1 - \mu_i^{-b}\right) + \xi_E \tag{10}$$

where a and b are calibrating parameters which vary according to the characteristics of the energy dissipation mechanisms, whilst ξ_E represents the equivalent viscous damping when the structure is within the elastic, or pre-yield, response range. Values of a=25, b=0.5 and ξ_E=5%, suggested by Calvi (1999), are currently adopted.

The equivalent viscous damping values obtained through Equation (10), for different ductility levels, can then be combined with Equation (11), proposed by Bommer *et al.* (2000) and currently implemented in EC8 (CEN, 2003), to compute a reduction factor η to be applied to the 5% damped spectra at periods from the beginning of the acceleration plateau to the end of the displacement plateau;

$$\eta = \left[10/(5 + \zeta)\right]^{1/2} \tag{11}$$

3. PROBABILISTIC FRAMEWORK

The first-order reliability method (FORM) can be used to calculate the approximate cumulative distribution function of a non-linear function of correlated random variables, such as the limit state displacement capacity function and limit state period function. Once the cumulative distribution functions of the demand and the capacity have been found, the calculation of the probability of exceedance of a specified limit state can be obtained using the standard time-invariant reliability formulation (e.g.,

Pinto *et al*., 2004). The probability of being in a particular damage band may then be obtained from the difference between the bordering limit state exceedance probabilities.

3.1 Probabilistic Treatment of the Demand

The cumulative distribution function of the displacement demand can be found using the median displacement demand values and their associated logarithmic standard deviation at each period. The cumulative distribution function can be used to obtain the probability that the displacement demand exceeds a certain value (x), given a response period (T_{Lsi}) for a given magnitude-distance scenario.

The displacement demand spectrum that might be used in a loss estimation study could take the form of a code spectrum or else a uniform hazard spectrum derived from PSHA for one or more annual frequencies of exceedance. Both of these options have drawbacks in being obtained from PSHA wherein the contributions from all relevant sources of seismicity are combined into a single rate of occurrence for each level of a particular ground-motion parameter. The consequence is that if the hazard is calculated in terms of a range of parameters, such as spectral ordinates at several periods, the resulting spectrum will sometimes not be compatible with any physically feasible earthquake scenario. Furthermore, if additional ground-motion parameters, such as duration of shaking, are to be incorporated – as they are in HAZUS (FEMA, 1999), in the definition of the inelastic demand spectrum – then it is more rational not to combine all sources of seismicity into a single response spectrum but rather to treat individual earthquakes separately, notwithstanding the computational penalty that this entails. Another advantage of using multiple earthquake scenarios as opposed to PSHA is the facility of being able to disaggregate the losses and identify the earthquake events contributing most significantly to the damage.

The approach recommended therefore is to use multiple earthquake scenarios, each with an annual frequency of occurrence determined from recurrence relationships. For each triggered scenario, the resulting spectra are found from a ground-motion prediction equation. In this way, the aleatory uncertainty, as represented by the standard deviation of the lognormal residuals, can be directly accounted for in each spectrum. The cumulative distribution function of the displacement demand can then be compared with the joint probability density functions of displacement capacity and period (Section 3.2), and the annual probability of failure for a class of buildings can be found by integrating the failure probabilities for all the earthquake scenarios (see Crowley *et al.*, 2004).

3.2 Probabilistic Treatment of the Capacity

As has been presented previously, the limit state displacement capacity (Δ_{Lsi}) of each building class can be defined as a function of the fundamental period (T_{Lsi}), the geometrical properties of the building, and the mechanical properties of the

180

construction materials. Similarly, the limit state period (T_{Lsi}) of each building class can be defined as a function of the height (or number of storeys), the geometrical properties of the building, and the mechanical properties of the construction materials. The uncertainty in Δ_{Lsi} and in T_{Lsi} is accounted for by constructing a vector of parameters that collects their mean values and standard deviations. By assigning probability distributions to each parameter, FORM can be used to find both the cumulative distribution function (CDF) of the limit state displacement capacity, conditioned to a period, and the CDF of the limit state period, which are then combined to create the joint probability density function of capacity.

3.2.1 Probabilistic Modelling of Geometrical Properties

A given building class within a selected urban area may comprise a large number of structures that present the same number of storeys and failure mode, but that feature varying geometrical properties (e.g., beam height, beam length, column depth, column/storey height), due to the diverse architectural and loading constraints that drove their original design and construction. Since such variability does affect in a significant manner the results of loss assessment studies (see Glaister and Pinho, 2003), it is duly accounted for in the current method by means of the probabilistic modelling described below.

Clearly, one could argue that by carrying out a detailed inspection of the building stock, such variability could be significantly reduced (in the limit, if all buildings were to be examined, it could be wholly eliminated), however at a prohibitive cost in terms of necessary field surveys and modelling requirements (vulnerability would then be effectively assessed on a case-by-case basis). This epistemic component of the geometrical variability of reinforced concrete members has been modelled in the present work by means of normal or log-normal probability distribution functions, derived from European building stock data, as described in Crowley *et al.* (2004).

3.2.2 Probabilistic Modelling of Reinforcing Bar Yield Strain

Mirza and MacGregor (1979) have suggested that once a probabilistic distribution for yield strength has been found, it can be divided by a deterministic value of the modulus of elasticity, which features a very low coefficient of variation, to produce the distribution of the yield strains. These two researchers have also concluded, through a series of experimental parametric studies, that a normal distribution would accurately represent the variability of reinforcement bars' yield strength, in the vicinity of the mean, whilst a beta distribution correlated well over the whole range of data. The coefficient of variation in the yield strength was found to be between 8% - 12% when data were taken from different bar sizes from many sources. More recently, the Probabilistic Model Code (JCSS, 2001) has also suggested that a normal distribution can be adopted to model the yield strength of steel. Therefore, a normal distribution for the steel yield strength (and subsequently yield strain) has been adopted in the current work.

The main difficulty in assigning a probability distribution to the yield strength of the steel used in a group of buildings, however, is the possibility that different grades have been used, which would lead to a distribution with multiple peaks and troughs (see Crowley *et al.*, 2004). One approach to solve this problem could be to calculate the probability of failure for the building class given each possible steel grade, using the normal distribution to model the dispersion for each grade, and then to compute a weighted average of failure, knowing or judging the use of each steel grade within the building class. The validity of such an approach would become questionable, however, if different steel grades were often used within individual buildings.

3.2.3 Probabilistic Modelling of Limit States Threshold Parameters

Dymiotis *et al*. (1999) have studied the seismic reliability of RC frames using interstorey drift to define the serviceability and ultimate structural limit states. They have found that a lognormal distribution may be used to describe the variability in interstorey drift for both limit states. Therefore, the variability in non-structural limit states, defined in this work as a function of interstorey drift limiting values, will be represented by means of lognormal distributions, using the mean drift ratios that have been suggested by Crowley et al. (2004).

Kappos *et al*. (1999), on the other hand, report the ultimate concrete strain reached in 48 tests of very well-confined RC members. A simple statistical analysis of this data shows that it would appear that in the case of limit state sectional strains a lognormal distribution is also able to describe the variability of these parameters. Hence, and since for the structural limit states it is the sectional steel and concrete strains that define respective boundaries, it would appear that a lognormal distribution may also be applied to describe the variability in these limit state parameters. Again, the mean values suggested by Crowley et al. (2004) are employed, in tandem with assumed coefficients of variation.

3.2.4 Probabilistic Modelling of Scatter in Empirical Relationships

A number of empirical relationships have been used to derive the functions of displacement capacity and period that have been presented in Section 2. These include empirical expressions for the plastic hinge length members and the yield curvature of RC members, all of which are discussed in Glaister and Pinho (2003), and an additional empirical parameter employed in the formula derived by Crowley and Pinho (2004) to relate the height of a building to its yield period. All of the aforementioned relationships rely on empirical coefficients to relate one set of structural properties to another, as for example the coefficient of 0.1 in the yield period vs. height equation, $T_y = 0.1H_T$. The mean value and standard deviation of these coefficients have been taken from the studies carried out to derive those formulae, with a normal distribution being used to model the respective dispersion.

4. CONCLUSIONS

Owing to its transparency, theoretical accuracy and computational efficiency, the procedure presented herein is particularly suitable for loss estimation studies. The definition of the displacement capacity is transparent as one may use any chosen number of storeys, geometrical, material or limit state threshold properties in the equations and adapt these easily for use in any part of the world. The conceptual soundness of the methodology has been preliminarily examined by Crowley *et al.* (2004) through a comparison of vulnerability curves derived using this procedure and those provided in HAZUS; the curves derived using the proposed method led to more realistic vulnerability models which appear to be consistent with field observations following destructive earthquakes. Finally, the large decrease in computational effort required for earthquake loss estimations for scenario events due to the direct consideration of the ground motion uncertainty is also a significant advantage of the proposed methodology.

The above effectively means that the method does cater for rigorous, scenario-based approaches that can be applied to large areas within a reasonable timescale. In this manner, it will be possible for iterative loss assessment studies to be carried out for a given urban area under events with varying return periods and assuming different levels of building stock vulnerability, considering the effects, along with respective costs, of different design code requirements and/or structural upgrading policies. The above could provide politicians, planners and code drafters with quantitative information to inform and guide their decisions, thus allowing the calibration of local regulations for optimum balance between societal investment and public risk, rather than being based on pre-selected return periods whose basis is somewhat arbitrary.

REFERENCES

Bommer, J. J. (2004). Earthquake actions in seismic codes: can current approaches meet the needs of PBSD? *This volume.*

Bommer, J. J., A. S. Elnashai, and A. G. Weir. (2000). Compatible acceleration and displacement spectra for seismic design codes. *Proceedings 12th World Conference on Earthquake Engineering*, Auckland, New Zealand, Paper no. 207.

Calvi, G. M. (1999). A displacement-based approach for vulnerability evaluation of classes of buildings. *Jrnl Earthqu. Eng.* 3(3), 411-438.

Comité Européen de Normalisation (2003) Eurocode 8, Design of Structures for Earthquake Resistance – Part 1: General rules, seismic actions and rules for buildings, Pr-EN 1998-1. Final Draft. December 2003.

Crowley, H., and R. Pinho. (2004). Period-height relationship for existing European reinforced concrete buildings. *Jrnl Earthqu. Eng.* 8(SP1).

Crowley, H., R. Pinho, and J. J. Bommer. (2004). A probabilistic displacement-based vulnerability assessment procedure for earthquake loss estimation. *Bull. Earthqu. Eng.*: 2 (2).

Dymiotis, C., A. J. Kappos, and M. K. Chryssanthopoulos. (1999). Seismic reliability of RC frames with uncertain drift and member capacity. *ASCE Jrnl Struct. Eng.* 125(9): 1038-1047.

FEMA. (1999) *HAZUS99 — Earthquake Loss Estimation Methodology: User's Manual*, Federal Emergency Management Agency , Washington D.C.

Freeman, S. A., D. L. Messinger, W. L. Casper, L. W. Mattis, F. R. Preece, and R. E. Tobin. (1985). Structural Moments No. 4. Drift Limits: Are they realistic? *Earthqu. Spectra* 1(2): 203-390.

Glaister, S., and R. Pinho (2003). Development of a simplified deformation-based method for seismic vulnerability assessment. *Jrnl Earthqu. Eng.* 7(SP1): 107-140.

Joint Committee for Structural Safety (JCSS). (2001). *Probabilistic Model Code - Working document, last update 13/03/2001*. (online). Available from URL: www.jcss.ethz.ch.

Kappos, A. J., M. K. Chryssanthopoulos, and C. Dymiotis. (1999). Uncertainty analysis of strength and ductility of confined reinforced concrete members, *Eng. Struct.* 21: 195-208.

Kircher, C. A., A. A. Nassar, O. Kustu and W. T. Holmes. (1997). Development of building damage functions for earthquake loss estimation. *Earthqu. Spectra* 13(4): 663-682.

Mirza, S. A., and J. G. MacGregor. (1979). Variability of mechanical properties of reinforcing bars. *ASCE Jrnl Struct. Div.* 105(ST5): 921-937.

Pinho, R., J. J. Bommer and S. Glaister (2002). A Simplified Approach to Displacement-Based Earthquake Loss Estimation Analysis. *Proceedings 12th European Conference on Earthquake Engineering*, London, England, Paper no. 738.

Pinto, P. E., R. Giannini, and P. Franchin. (2004). *Methods for seismic reliability analysis of structures*. Pavia, Italy: IUSS Press.

Priestley, M. J. N. (1997). Displacement-based seismic assessment of reinforced concrete buildings. *Jrnl Earthqu. Eng.* 1(1): 157-192.

Priestley, M. J. N. (2003). *Myths and fallacies in earthquake engineering – Revisited, The Mallet-Milne Lecture*. Pavia, Italy: IUSS Press.

Restrepo-Velez, L. F., and J. J. Bommer. (2003). An exploration of the nature of the scatter in ground-motion prediction equations and the implications for seismic hazard assessment. *Jrnl of Earthqu. Eng.* 7(SP 1): 171-199.

Restrepo-Velez, L. F. (2004). A simplified mechanical-based procedure for the seismic risk assessment of unreinforced masonry buildings. *Individual Study*, ROSE School, Pavia, Italy.

Sasani, M., and A. Der Kiureghian. (2001). Seismic fragility of RC structural walls: displacement approach. *ASCE Jrnl Struct. Eng.* 127(2): 219-228.

PARAMETERIZED VULNERABILITY FUNCTIONS FOR AS-BUILT AND RETROFITTED STRUCTURES

Seong-Hoon JEONG[1] and Amr S. ELNASHAI[2]

ABSTRACT

In this study, preliminary results from an approach whereby a set of vulnerability functions are derived based on the three basic response quantities of stiffness, strength and ductility. Once the basic three characteristics of a structural system are defined and the response database is constructed, the vulnerability functions for various limit states can be constructed without recourse to further simulation.

Keywords: Parameterized vulnerability function; Fast demand estimation; Response parameters; Response database.

1. INTRODUCTION

The use of vulnerability functions, defined as a relationships between ground shaking intensity and the probability of reaching or exceeding a certain response level, for assessment of seismic losses is in increasing demand, both for pre-earthquake disaster planning and post-earthquake recovery and retrofitting programs. This is due to the difficulties associated with analyzing individual structures and the importance of obtaining a global view of anticipated damage or effects of intervention, before or after an earthquake, respectively. Apart from the regional loss assessment application of vulnerability functions, they are useful in probabilistic assessment of damage to individual structures taking into account material and input motion randomness.
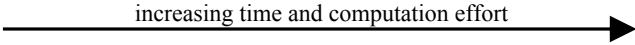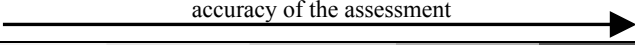
Various methods of vulnerability assessment differ in the required resources and precision of the assessment results. Therefore, the choice of a method should be made considering the tradeoff between effort and precision, as conceptually shown in Table 1. Observed vulnerability methods resort to statistics of real damages from past earthquakes and its details are given in (Rossetto and Elnashai 2003). Seismic risk assessment methods in ATC-13 and ATC-14 are examples of vulnerability functions based on expert opinions and score assignment respectively, and details of these methods are discussed in (Lang 2002). Vulnerability functions derived from simple

---

[1] *Research Assistant, Civil Engineering Department, University of Illinois at Urbana-Champaign*
[2] *Willette Professor, Civil Engineering Department; Director, Mid-America Earthquake Center, University of Illinois at Urbana-Champaign, Urbana, Illinois, USA*

analytical models generally have significant limitations due to simplicity of the models, use of response spectra or other simple representations of ground shaking (Calvi 1999).

Table 1. Comparison of vulnerability assessment methods (Lang 2002)

Methods	1 observed vulnerability	2 expert opinions	3 simple analytical models	4 score assignment	5 detailed analysis procedure
Effort	increasing time and computation effort →				
Precision	accuracy of the assessment →				
Application	building stock				individual building

The aim of the method proposed in this paper is to obtain precise assessment results closing up to those of the vulnerability assessment using detailed analysis procedure with a very quick and simple procedure.

2. OVERVIEW OF THE PROPOSED METHODOLOGY

Vulnerability functions may be derived analytically by simulation. Even for a limited number of random variables and for modest ranges of variation, the simulation effort is very considerable, reaching several hundreds of thousands of analyses. Every time the structure is replaced or even modified, the repetition of the simulation is required. It is hereafter proposed to parameterize the problem in such a manner that a generic set of vulnerability functions will be derived. The parameters influencing the shape of the functions are related to (i) stiffness, closely related to serviceability limit state, (ii) strength, closely related to damage control limit states and (iii) ductility, closely related to collapse prevention. By using the latter parameters with a response database which is a collection of pre-run inelastic response analyses of structures with a wide range of response parameters, the vulnerability functions are directly obtained without the need for simulation. This feature, allows consideration of various structural configurations in the decision making of earthquake mitigation strategies, by reducing the time and effort in the derivation of vulnerability functions.

Fig. 1 represents the procedure to derive parameterized vulnerability functions. In the latter figure, the effect of a specific repair method on the vulnerability curve is calculated through three main steps: (i) determination of response parameters after repair, (ii) response estimation using Response Database (RD) of which the detail is presented in the following section and (iii) construction of vulnerability functions with various limit states (L.S.).
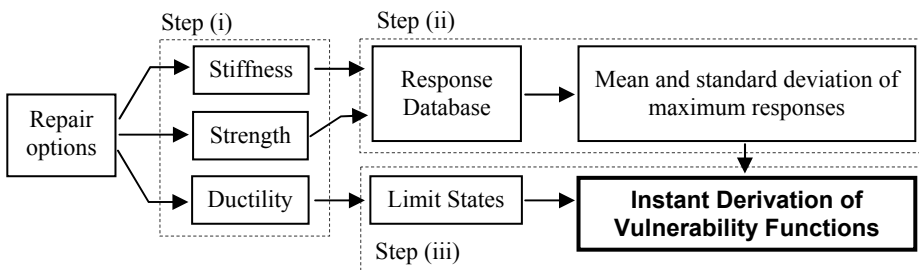
Figure 1. Overall procedure of the parameterized vulnerability function.

It is noteworthy that response estimation (Step (ii)) can be performed without considering the effect of ductility supply. This is due to the fact that once the yield point is determined by stiffness and strength ultimate displacement capacity does not affect the shape of the capacity curve which, in this study, determines the response of a structure. The effect of ductility is implemented in determining the limit states (L.S.) to derive vulnerability functions. If the limit states are determined by displacement or displacement based damage index, it is very easy to determine limit states according to the ductility variation. Otherwise, the relationship between ductility and limit states needs to be defined before deriving vulnerability functions.

3. DEMAND ESTIMATION METHODOLOGY EMPLOYING RESPONSE DATABASES

The objective of this study is to provide a tool for the construction of vulnerability functions for a wide range of structures with known response parameters. In the proposed method, the vulnerability function is constructed using parameterized structural response characteristics (stiffness, strength and ductility) and the Response Database. Simulation is therefore no longer needed. The structural response parameters are defined for the single-degree of freedom (SDOF) system that is equivalent to the complex structure. The response database is a collection of pre-run dynamic analysis results for a range of structural response parameters. The proposed methodology has conceptual analogy with earthquake response spectra, because it (i) utilizes simplified structural models (SDOF system), (ii) obtains maximum value of response history and (iii) constructs curves which replace dynamic response history analyses.

3.1 Structure of the Response Database

The database is designed to store information of structural responses as statistical parameters and its structure is represented in Fig. 2. The basic element of structuring the database is the process of obtaining a set of mean and standard deviation of maximum responses and this is the first step of constructing the response database.
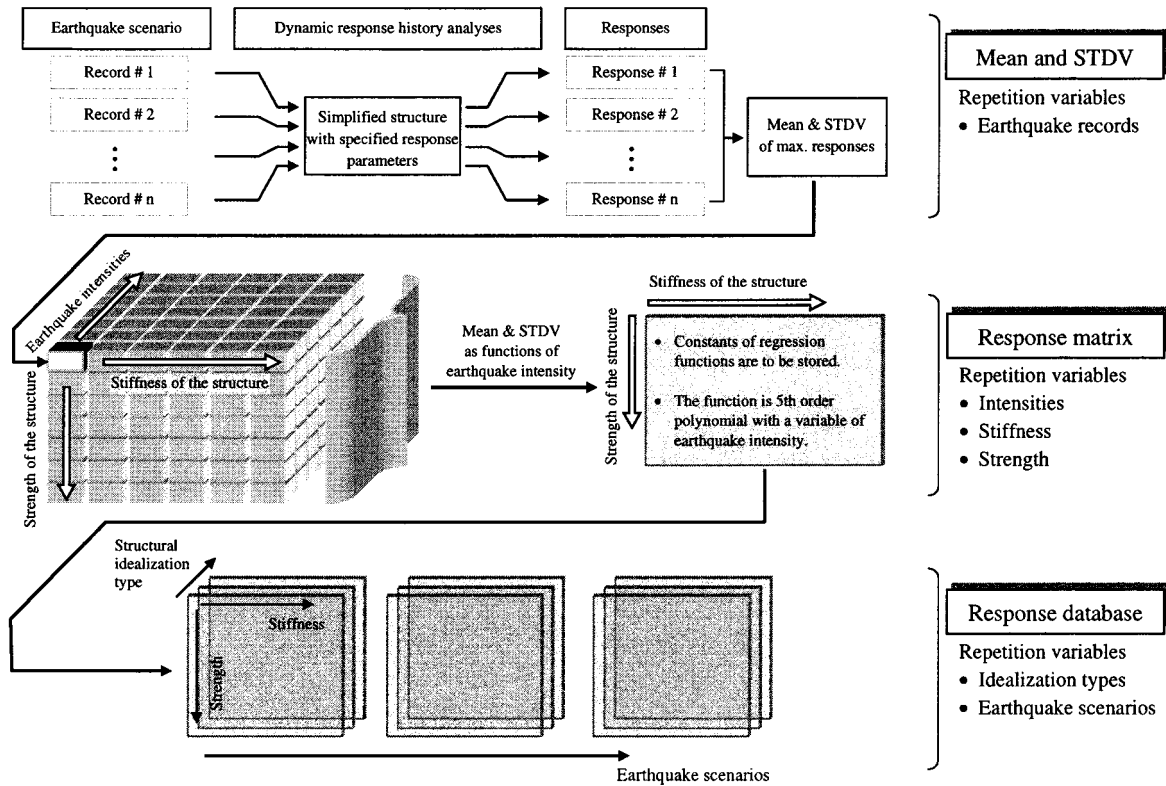
187

Figure 2. Structure of the response database

A group of response time histories obtained from dynamic response history analyses with a series of ground motions are summarized in two statistical parameters; mean and standard deviation of maximum responses. Then, the latter process is repeated for a range of earthquake intensities and structural response parameters to construct the response matrix. The dimension of the response matrix can be reduced by representing the mean and standard deviation as functions of earthquake intensities. After this step, the response matrix contains constants of regression functions that represent mean (μ) and standard deviation (σ) of maximum displacement demand. Finally, the response database is constructed by summing the response matrices for various earthquake scenarios and structural idealization types.

3.2 Probability Distribution

The effect of variability in member capacity on the global response is very small compared to that of variability in the ground motion. Therefore, in this paper, earthquake ground motion is considered as the only random variable. As an illustrative example in this paper, a set of artificial ground motions is used. The latter ground motions are synthesized to simulate an earthquake event for lowland soil profile in Memphis, TN, USA and entitled 'Scenario #3' among three scenarios generated as a part of Mid-America Earthquake (MAE) Center research project HD-1 (Hazard Definition). Scenario #3 consists of ten records simulating an earthquake event of magnitude (M_w) 5.5 and a focal depth of 20 km with 84 percentile level (one standard deviation above the mean value) from the prediction model. Details are discussed in (Romero et al. 2001).

A vulnerability curve is a cumulative conditional probability of structural response exceeding a prescribed limit states for a range of earthquake intensities. In this paper, maximum displacement is utilized to represent response of structures and it is assumed to be a log-normally distributed random variable. This means that the logarithm of the maximum displacement has a normal probability distribution, as shown in Fig. 3 (a). In order to examine the validity of the assumed probability distribution, log-normal probability paper is constructed as shown in Fig. 3 (b). The three sets of sample data plotted on the latter probability paper are obtained from dynamic response history analyses of three different structures that have the same strength ratio (0.2) but different periods (0.3, 0.6 and 0.9 sec.). Ten records of the earthquake scenario for lowland profile in Memphis with PGA of 0.2g were utilized for the analyses. The plotting position of a sample data is determined by calculating its cumulative probability then its inverse, standard normal variate. The cumulative standard normal probability of the mth value among the N data (x_1, x_2, . . . , x_N, arranged in increasing order) of the logarithm of maximum displacement is determined by $m/(N+1)$ and its basis is discussed in (Gumbel 1954).

Since the horizontal axis of the probability paper is the standard normal variate, s, which is the inverse of the standard normal cumulative probability, a linear relationship between the vertical and horizontal axes guarantees that the vertical axis

can be used as a random variable of normal distribution. In Fig. 3 (b), the vertical axis is logarithm of the maximum displacement, and thus the linearity of a set of sample data shows that the probability distribution of logarithm of maximum displacement is normal. This verifies that the choice of probability distribution (log-normal distribution) in the context of the derivation presented hereafter is appropriate.
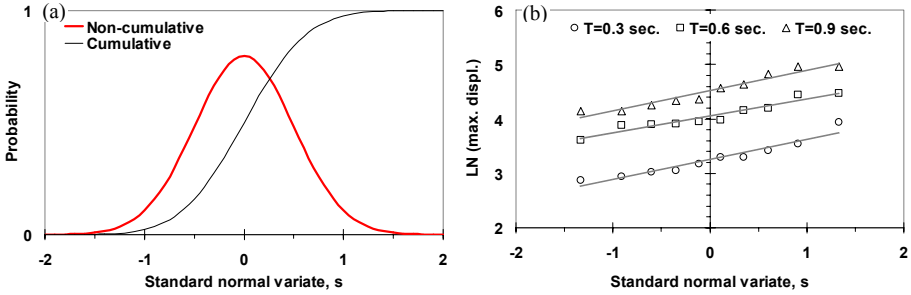

Figure 3. Probability distribution and probability paper; (a) standard normal probability distribution, (b) log-normal probability paper (S.R.=0.2).

3.3   Fast Demand Estimation

The response database is a collection of pre-analyzed responses for a wide range of structures in the format of statistical correlation parameters. Therefore, the response estimation of a structure can be instantly carried out because it entails only reading the corresponding value from the latter database according to the given response parameters such as stiffness and strength of the structure. Additionally the latter database enables the analyst to construct vulnerability functions by dealing with only two statistical parameters (mean and standard deviation) instead of massive data from a group of dynamic response history analyses. This feature renders the construction of vulnerability functions much easier than the conventional methods. Concurrently, the fidelity of information is maintained because the cumulative normal or log-normal distribution that is used to represent the probability distribution of maximum response depends on only the mean and standard deviation of the used random variables.

3.3.1 Response Parameters

In order to obtain mean (μ) and standard deviation (σ) of maximum responses using the database, the analyst needs to determine the structural idealization type and response parameters. In this paper, a bi-linear structural model was utilized, as shown in Fig. 4. The period and the non-dimensional strength ratio (S.R.) are utilized as the most convenient parameters. Strength ratio (S.R.) is defined as the ratio of lateral yield strength (P) to the total weight (W) of the structure. This is a convenient parameter that is used extensively in seismic design practice. It is noteworthy that the approach presented in this paper is independent of the assumption of bilinear

190

response, and the Response Database may be derived for a tri-linear or other shape of pushover curve.
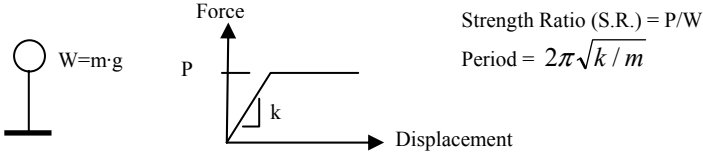

Figure 4. Bi-linear model and response parameters.

3.3.2 Statistical Estimation of Maximum Response

As indicated in Fig. 2, the mean (μ) and standard deviation (σ) of maximum displacement response from a series of inelastic dynamic response history analyses are collected and organized in tabular form. An example of the latter table, the response matrix of the mean value in Fig. 2, is represented in Appendix I. Each cell of the table contains six constants of a fifth order polynomial regression function and represents mean or standard deviation of the maximum displacements as a function of earthquake intensity, as shown in Eq. (1).

$$y = a_1 \cdot x^5 + a_2 \cdot x^4 + a_3 \cdot x^3 + a_4 \cdot x^2 + a_5 \cdot x^1 + a_6 \tag{1}$$

Where x is earthquake intensity and y is mean or standard deviation of the response quantity.

The analyst can instantly obtain mean values (μ) and standard deviation (σ) of maximum displacement as functions of earthquake intensity, provided that the response parameters (period and strength ratio) are prescribed and the response database is ready to be utilized. As an example of response estimation by the above-described method, a set of plots of mean value (μ) and standard deviation (σ) for elastic-perfectly-plastic (EPP) structures with elastic period of 0.8 sec. and strength ratios (S.R.) of 0.1, 0.2 and 0.3 is shown in Fig. 5.
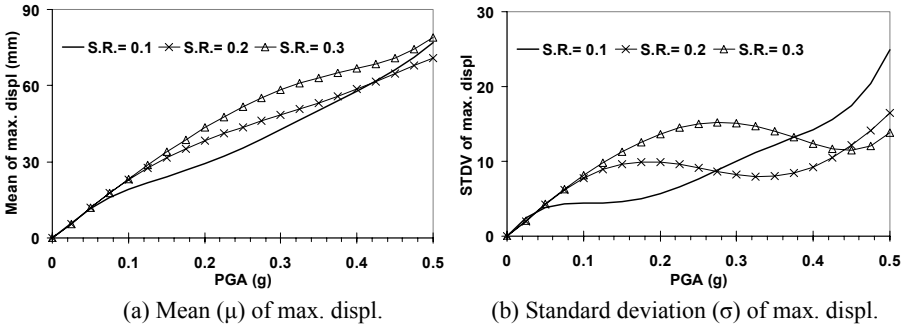

(a) Mean (μ) of max. displ.   (b) Standard deviation (σ) of max. displ.

Figure 5. Mean and standard deviation as functions of earthquake intensity.

4. DERIVATION OF THE VULNERABILITY FUNCTION

The procedure of calculating the probability of the maximum response exceeding a given limit state (L.S.) is described as follows:

1. Define the coefficient of variation (C.O.V.) and median of the maximum response as

$$\text{C.O.V.: } \delta = \sigma/\mu \qquad \text{Median: } x_m = \frac{\mu}{\sqrt{1+\delta^2}} \tag{2}$$

where, σ is the standard deviation and μ is the mean value.

2. Determine the displacement limit state (L.S.) associated with a specific damage level.

3. Calculate the conditional cumulative probability for the log-normal distribution as

$$\Phi\left(\frac{\ln(L.S.)-\lambda}{\xi}\right), \quad \lambda = \ln x_m, \quad \xi = \sqrt{\ln(1+\delta^2)} \tag{3}$$

4. Calculate the probability of maximum displacement exceeding a given limit state as

$$\text{Prob (max. displ.} > L.S.) = 1 - \Phi\left(\frac{\ln(L.S.)-\lambda}{\xi}\right) \tag{4}$$

Whilst the effect of stiffness and strength change on the vulnerability curves are considered by response using the Response Database, the effect of ductility change (Δu_i) can be implemented into the calculation procedure of conditional probability by changing the limit states (L.S.), as shown in Fig. 6.
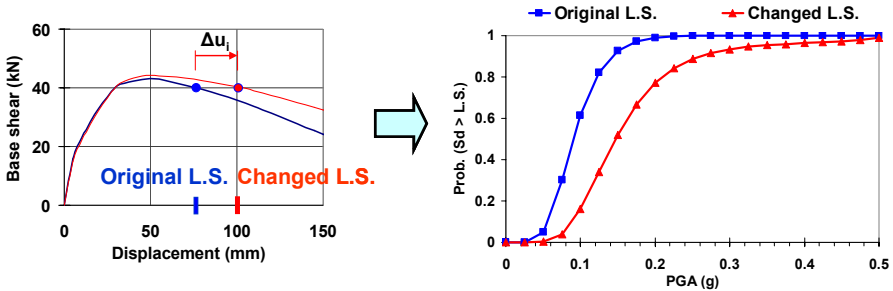

Figure 6. Effect of ductility change on vulnerability functions.

Sample derivation of vulnerability functions corresponding to various displacement limit states, for the same structures shown in Fig. 5 (elastic-perfectly-plastic, T=0.8 sec. and S.R.=0.1; 0.2;0.3), are presented in Fig. 7.

(a) L.S. = 20 mm

(b) L.S. = 40 mm

(c) L.S. = 60 mm

(d) L.S. = 80 mm
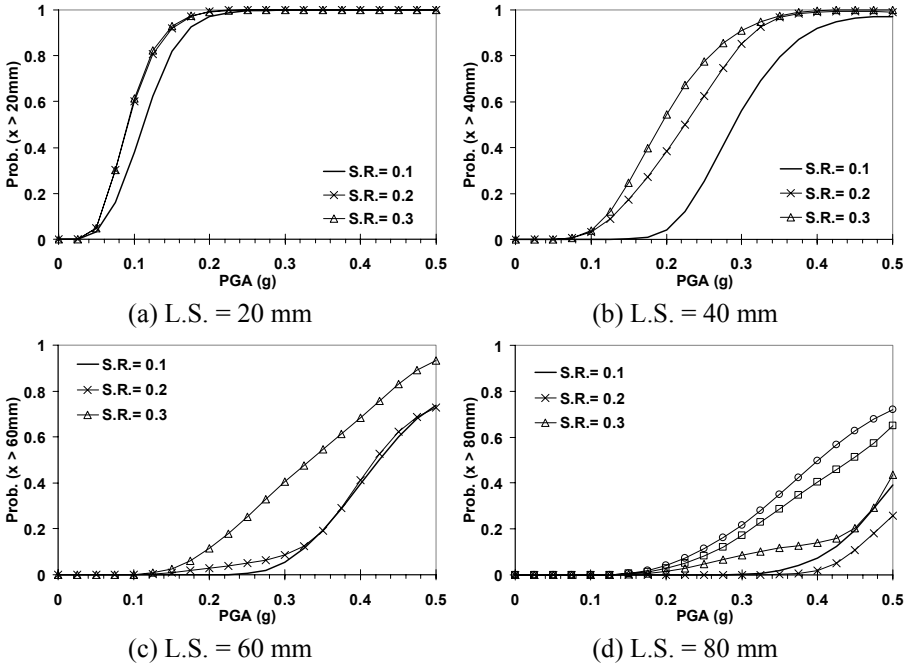
Figure 7. Vulnerability functions for various limit states (L.S.).

Sources of uncertainty can be categorized as (i) errors of ignorance and simplification, (ii) measurement errors and (iii) statistical errors (Geysken et al., 1993). In each category, various uncertainties exist and their quantification is complex (Singhal and Kiremidjian 1998). The uncertainties can be implemented in the derivation of vulnerability function as below:

$$\text{Prob (max. displ.} > \text{L.S.)} = 1 - \Phi(\frac{\ln(L.S._m) - \lambda}{\sqrt{\beta_1^2 + \beta_2^2 + \cdots + \beta_n^2}}) \tag{5}$$

where $L.S._m$ is the median value of a displacement limit state and β_i (i=1, 2, $\cdots$, n) represent various uncertainties. These can be demand uncertainty, capacity uncertainty and modeling uncertainty as in (Wen et al. 2004) or simply response and capacity uncertainty (Dimova and Hirata 2000). Modeling of uncertainty is not presented in this paper, though its importance in seismic loss assessment cannot be over-emphasized.

5. CONCLUSIONS

Derivation of vulnerability functions for a class of structures requires many analyses (tens or even hundreds of thousands), especially when a large number of random variables is considered. These will then have to be re-derived for different structural configurations as well as for different repair and/or strengthening methods. In this paper, a new analytical vulnerability assessment framework based on deriving a Response Database was proposed. The Response Database is an accumulation of pre-analyzed inelastic response of structures with a wide range of stiffness and strength. Therefore, with pre-determined stiffness, strength and a set of records, the database provides mean value and standard deviation of inelastic response quantities of the corresponding structure without the need for further analysis. The effect of ductility variation is included by changing the limit states in the calculation of cumulative conditional probability.

The implications of the success of the developed approach are wide-ranging. For cases of selection between different retrofitting options, the parameterized vulnerability functions approach gives rapid estimates of probabilities of various damage levels being inflicted onto the structures under consideration, given only the stiffness, strength and ductility for each alternative retrofitting scheme. Additionally, the presented vulnerability assessment methodology enables the analyst to practically investigate the vulnerability of large number of structural configurations. Therefore, this method blends very well with Consequence-Based Engineering (Abrams et al. 2002) where the vulnerability assessment for generic structural systems in a large region is sought. This approach is being implemented into the Mid-America Earthquake Center seismic loss assessment system MAEViz.

ACKNOWLEDGMENT

APPENDIX I. RESPONSE MATRIX FOR MEAN VALUE (μ) OF MAXIMUM DISPLACEMENT

EPP (Elastic-Perfectly Plastic) structure under records for Memphis, Lowlands soil profile, Scenario #3 (M=5.5 at Memphis, TN with focal depth 20 km)

S.R.		Period (sec.)												....
		0.2	0.4	0.6	0.8	1	1.2	1.4	1.6	1.8	2	2.2	2.4	
0.025	a_1	-2053.20	-1799.50	3993.60	-12511.00	-14142.00	6481.00	12945.00	1994.10	-6332.50	-10515.00	-7383.70	1818.90	
	a_2	3849.10	2678.80	-2723.20	16516.00	18417.00	-8232.20	-17754.00	-5258.80	7126.70	13956.00	11854.00	690.11	
	a_3	-2681.80	-1323.70	-328.19	-7799.40	-8318.00	3965.30	9077.60	4609.40	-2049.60	-6022.10	-6134.90	-1682.80	
	a_4	865.28	259.81	486.79	1580.10	1544.90	-855.88	-2074.70	-1608.70	-120.96	833.08	1082.30	440.90	
	a_5	27.94	123.45	65.74	25.28	54.60	242.03	363.57	366.71	254.32	178.84	143.22	162.69	
	a_6	-0.09	-1.38	2.07	3.09	3.13	1.22	-0.84	-0.98	0.51	1.38	1.43	0.73	
0.050	a_1	-1443.80	-5822.70	7218.20	21152.00	34835.00	2993.30	-6074.80	6579.10	-4843.90	-20906.00	2686.00	8019.50	
	a_2	600.35	9847.80	-12664.00	-27038.00	-44184.00	-4142.80	8421.90	-7684.20	4877.80	27075.00	-2542.50	-10461.00	
	a_3	33.72	-6161.00	7627.40	11716.00	19480.00	2527.80	-3307.90	3651.20	-1176.00	-12345.00	558.10	4654.80	
	a_4	149.35	1711.90	-1815.40	-1919.10	-3510.90	-843.48	139.15	-1111.30	-269.82	2230.50	-9.74	-853.39	
	a_5	59.46	-55.39	285.44	238.10	399.87	299.49	271.32	370.92	310.55	82.80	210.83	258.94	
	a_6	-0.96	3.31	-2.46	0.97	-2.10	-0.13	0.37	-1.33	-1.46	3.05	0.23	-1.25	
0.075	a_1	-8191.30	5907.00	-10807.00	-215.82	-15211.00	8049.60	1616.80	5203.30	5376.50	11576.00	-8245.90	-493.92	
	a_2	11311.00	-7795.30	14472.00	-2222.80	13140.00	-10168.00	-2796.80	-8021.90	-3546.80	-14034.00	9798.20	769.34	
	a_3	-5692.10	3105.60	-6360.80	2612.70	-2213.70	4912.50	1933.50	4654.50	15.83	5693.60	-4150.40	-370.15	
	a_4	1380.90	-240.56	1041.50	-828.59	-469.25	-1241.50	-820.84	-1429.00	133.32	-976.59	741.99	71.42	
	a_5	-58.89	78.27	75.04	214.72	275.10	347.49	367.69	433.08	246.32	305.23	164.03	192.35	
	a_6	1.75	1.13	1.99	1.37	-0.75	-1.21	-2.23	-3.42	0.30	-1.35	1.06	0.11	
0.100	a_1	-2038.70	3544.80	-17130.00	15596.00	4264.90	10393.00	-18126.00	-19994.00	-4348.90	-5253.10	4137.60	327.31	
	a_2	4296.30	-5296.30	24925.00	-22208.00	-4094.80	-15177.00	23978.00	26240.00	5394.00	6485.90	-4928.90	-369.23	
	a_3	-3092.80	2618.80	-12817.00	11893.00	2122.40	8192.00	-11143.00	-11977.00	-2725.50	-2964.00	2040.70	149.44	
	a_4	1035.50	-350.11	2724.80	-2833.10	-777.55	-2095.30	1959.30	2040.70	548.22	584.40	-356.53	-26.09	
	a_5	-60.26	93.06	-88.11	404.17	287.64	446.97	147.20	163.17	218.71	191.81	241.43	199.54	
	a_6	2.33	1.04	6.51	-2.79	-0.80	-3.91	2.50	2.25	0.83	1.01	-0.50	-0.04	
0.125	a_1	10177.00	9971.80	15657.00	3214.00	12098.00	-13304.00	11872.00	-10045.00	7735.50	3347.30	-3560.50	0.00	
	a_2	-11910.00	-14160.00	-16887.00	-6870.60	-16522.00	14840.00	-11390.00	16895.00	-8652.00	-4468.90	4154.40	0.00	
	a_3	4520.00	7192.20	5777.90	5307.90	8536.00	-5253.40	3233.80	-9765.50	3130.30	2059.40	-1736.30	0.00	
	a_4	-470.49	-1423.30	-691.29	-1753.40	-2149.90	445.25	-383.50	2144.60	-454.22	-398.02	312.42	0.00	
	a_5	46.01	188.16	155.42	357.62	417.20	270.37	296.04	116.82	284.80	268.14	193.89	197.69	
	a_6	0.36	-0.96	1.84	-2.27	-4.05	-0.53	-0.22	3.84	-0.40	-0.66	0.47	0.00	
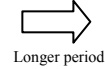
Longer period
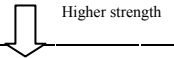
Higher strength

REFERENCES

Abrams, D. P., A. S. Elnashai, and J. E. Beavers. (2002). "The Mid-America Earthquake Center for research program towards development of consequence-based-seismic risk mitigation." *International Conference on Advances and New Challenges in Earthquake Engineering Research*, Harbin, China, August 15-18.

ATC-13. (1985). "Earthquake damage evaluation data for California." Applied Technology Council, Redwood City, California.

ATC-14. (1987). "Evaluating the seismic resistance of existing buildings." Applied Technology Council, Redwood City, California.

Calvi, G. M. (1999). "A displacement-based approach for vulnerability evaluation of classes of buildings." *Journal of Earthquake Engineering,* 3(3), pp. 441-438.

Dimova, S. L., and K. Hirata. (2000). "Simplified seismic fragility analysis of structures with two types of friction devices." *Earthquake Engineering and Structural Dynamics,* 29, pp. 1153-1175.

Geysken, P., A. Der Kiureghian, and P. Monteiro. (1993). "BUMP: Bayesian updating of model parameters." UBS/SEM-93/06, University of California at Berkeley.

Gumbel, D. J. (1954). "Statistical theory of extreme values and some practical applications." Applied Mathematics Series 33, National Bureau of Standards, Washington, D.C.

Lang, K. (2002). "Seismic vulnerability of existing buildings." IBK Bericht, Bd. 273, Institute of Structural Engineering, Swiss Federal Institute of Technology, Zurich, Switzerland.

Rossetto, T., and Elnashai, A. S. (2003). "Derivation of vulnerability functions for European-type RC structures based on observational data." Engineering Structures, 25(10), pp. 1241-1263.

Singhal, A., A. S. Kiremidjian (1998). "Bayesian updating of fragilities with application to RC frames." *Journal of Structural Engineering,* ASCE, 124(8), pp. 922-929.

Wen, Y. K., B. R. Ellingwood, and J. Bracci. (2004). *Vulnerability function framework for consequence-based engineering.* MAE Report 04-04, Mid-America Earthquake Center, University of Illinois at Urbana-Champaign.

SEISMIC FRAGILITY OF SMALL EQUIPMENT AND CONTENTS

Tara HUTCHINSON[1] and Samit RAY CHAUDHURI[2]

ABSTRACT

This paper presents analytically developed seismic fragility curves for unattached bench-mounted equipment and contents. The emphasis of the study is on rigid scientific equipment, which is often placed on the surface of ceramic laboratory benches in science laboratories or other buildings. Although theoretical solutions are available to determine the seismic response of rigid sliding blocks and research has been conducted to develop the analytical fragility curves, previous studies have not considered the uncertainty of important input parameters and how they affect the shape and distribution of the curves. Moreover, for scientific equipment mounted on benches, limited experimental data are available regarding the dynamic characteristics of the typical support systems and the equipment frictional behavior.

For this study, only uniaxial seismic excitation is considered to provide insight into the contributions and sensitivity of the fragility to different uncertain parameters. Uncertain parameters considered in this study include: (i) static and kinetic coefficients of friction and (ii) supporting (bench and building) characteristics. In this paper, generalized fragility curves for sliding-dominated equipment are provided for use in seismic performance assessment.

Keywords: Nonstructural response; Seismic fragility; Equipment response; and Friction.

1. INTRODUCTION

Scientific equipment such as analyzers, microscopes, centrifuges, monitors, and computer workstations, are often placed on the surface of ceramic laboratory benches in science laboratories. Damage to these items has gained significant attention following recent earthquakes, largely due to the potential for significant economic losses and/or research downtime. Many of these types of scientific equipment are fairly costly and loss of functionality would result in total economic loss of the equipment itself. In addition, in hospital or other critical buildings, failure of such equipment may hinder emergency response efforts immediately after an earthquake. However, in comparison with structural systems, there is little research on the performance of these equipment and contents, particularly with respect to understanding the characteristics of the varied support (bench and building) conditions and their frictional behavior.

---

[1] *Asst. Professor, Dept. of Civil and Environmental Engineering, University of California, Irvine*
[2] *Graduate Student, Dept. of Civil and Environmental Engineering, University of California, Irvine*

In general, these types of bench-mounted scientific equipment are short and rigid, thus, imposed seismic excitation results in a sliding-dominated response, rather than a rocking-dominated response. An example of a typical science laboratory bench-shelf system, with equipment mounted onto the surface of the bench, is shown in Figure 1. Upon sliding, there is concern that the equipment may be damaged either by falling from the bench-top surface or through impact with neighboring equipment or surrounding sidewalls. The probability that either potential limit states will be exceeded is often expressed in the form of a seismic fragility curve. A seismic fragility curve associates the probability of exceedance of a defined limit state (a damage measure, DM) with an engineering demand parameter (EDP). An EDP may be considered an input parameter to the fragility curve, for example, maximum floor acceleration or maximum inter-story drift.

Figure 1. Typical bench-mounted equipment within a Science Laboratory (Photo courtesy of Mary Comerio).

Since the sliding of unrestrained rigid equipment is initiated when the acceleration at the top of the supporting element overcomes the resistance due to friction between the two surfaces of contact, considering the acceleration amplification due to a support element (such as a furnishing element) in the fragility curve development is very important. Science laboratory benches often have uni-strut railing systems providing a pinned support at the floor and ceiling to anchor the bench, creating a system with some flexibility. The result may be that the natural frequency of the laboratory bench system lies within the acceleration sensitive zone of the input floor response spectrum, and may therefore experience acceleration amplification. However, since the sliding response is nonlinear, it is not possible to determine the response of the equipment by simply scaling the input acceleration to account for the bench amplification. This has also been observed by other researchers [e.g., Shao and Tung (1999) and Garcia and Soong (2003)].

1.1 Background and Previous Work

Research has been conducted to understand the toppling and sliding behavior of unrestrained rigid equipment under seismic excitation. Perhaps the first analytical formulation describing the fundamental equations of motion for rigid unattached bodies was presented by Shenton and Jones (1991). In later work, Shenton (1996) investigates the criteria for sliding and rocking and sliding-rocking of rigid body modes. Shao and Tung (1999) cast the problem into a statistical formulation, studying

the mean and standard deviation of sliding relative to a rigid base considering an ensemble of 75 real earthquake motions. This work also considered the probability of over turning and rocking for rigid bodies. Similarly, Choi and Tung (2002) studied the sliding behavior of a freestanding rigid body under the action of base excitation. The objective of this study was to estimate the amount of sliding when a rigid body is subjected to real earthquake motion. In this context, Choi and Tung (2002) apply an extension of Newmark's (1965) work, using absolute base spectral displacement rather than maximum velocity, as was done by Newmark (1965).

Studies have reported the effect of sliding response due to both vertical acceleration and base frictional coefficient [e.g., Taniguchi (2002), Garcia and Soong (2003)]. Taniguchi (2002), for example, investigated the nonlinear seismic response of free-standing rectangular rigid bodies on horizontally and vertically accelerating rigid foundations. The equations of motion and associated boundary conditions corresponding to commencement and termination of liftoff, slip and liftoff-slip interaction motions are provided. Applying a large number of time histories Taniguchi (2002) found that the response of the body is sensitive to small changes in the friction coefficient and slenderness of the body, and to the wave properties and intensity of ground motions. It was also observed that vertical excitation adds irregularities to the behavior, as it excites or dampens the response depending upon the direction. Recent work by Garcia and Soong (2003) provide analytically developed seismic sliding fragility curves using design spectrum compatible time histories. Two different damage measures (DMs) are considered for development of sliding fragility in the study of Garcia and Soong (2003): (i) excessive relative displacement and (ii) excessive absolute acceleration. This study concluded that the sliding response is very sensitive to the coefficient of friction. It was also observed that neglecting vertical acceleration might lead to unconservative estimates of sliding.

Although previous studies have contributed to determining sliding response estimation, both in a deterministic and probabilistic sense, consideration of uncertain parameters in this estimation has not been provided. For sliding bodies in a realistic building setting, even small environmental changes (e.g., moisture, dust, etc.), can change the interface resistance characteristics. Furthermore, from the aforementioned discussion, it is clearly that considering the supporting structure (bench and building) is important. These two uncertain issues are the focus of this paper.

2. ANALYTICAL FORMULATION

2.1 Pure Sliding under Horizontal Excitation

Considering the free body diagram of the rigid equipment shown resting on the top of a bench in Figure 2, the condition describing the onset of the movement of the body may be expressed as:

$$|m\ddot{x}(t)| \geq \mu_s mg \tag{1}$$

where $\ddot{x}(t)$ = acceleration at the top of the bench, m = mass of the equipment and g = acceleration due to gravity. In Figure 2, $\dot{x}(t)$ and $x(t)$ = absolute velocity and displacement of the top of the bench, $\ddot{u}(t)$, $\dot{u}(t)$, and $u(t)$ = acceleration, velocity and displacement of the equipment with respect to bench top. The static and kinetic coefficients of friction, μ_s and μ_k, respectively, are used to represent the frictional resistance between the bench-top surface and the equipment. The kinetic coefficient of friction may be represented as a fraction ϕ of the static coefficient of friction (i.e., $\mu_k = \phi \mu_s$). Equation (1) assumes the bench has negligible motions in the vertical direction. Once the equipment begins sliding on the bench, the equation of motion of the equipment may be expressed as (Shenton and Jones, 1991):

$$m(\ddot{x}(t) + \ddot{u}(t)) = -S(\dot{u}(t))\mu_k mg \tag{2}$$

where, $S(\dot{u}(t))$ = signmum function,

$$S(\dot{u}(t)) = 1; \ (\dot{u}(t) > 0) \tag{3}$$
$$S(\dot{u}(t)) = -1; \ (\dot{u}(t) < 0) \tag{4}$$

Therefore, the sliding continues until the relative velocity of the mass equals to zero (i.e., $\dot{u}(t) = 0$) and commences again if Equation (1) is satisfied.
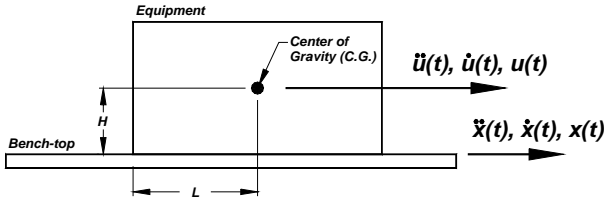

Figure 2. Schematic diagram of bench top supporting a rigid piece of equipment.

2.2   Bench Dynamic Characteristics

The bench system may be idealized as a single-degree-of-freedom (SDOF) system in the horizontal direction, with the mass of the equipment resting on the bench-top. It is also reasonable to assume negligible slippage between the base of the bench and the floor surface, since the bench is anchored at the base to the floor. The equation of motion of the bench-top may then be expressed as:

$$\ddot{x}(t) + 2\zeta_n \omega_n \dot{x}(t) + \omega_n^2 x(t) = -\ddot{x}_g(t) \tag{5}$$

where $\ddot{x}_g(t)$ = the floor motion (or the motion at base of the bench), ω_n = the natural circular frequency and ζ_n = damping ratio, of the system. Applying equation (5), the bench-top time history may easily be obtained when the floor time history is known and thus this bench-top motion may be considered as input to the base of the equipment for the sliding analysis. This cascade approach neglects the dynamic

200

interaction between the bench and the equipment in the same way as it neglects the interaction between the bench and floor. Such an assumption is reasonable for most installed bench systems, since the frequency of the bench system is much higher than that of the building structure and the mass of the bench is negligible compared with the buildings' mass. Dynamic characteristics regarding representative bench systems required to solve equation (5) were determined using shake table and low amplitude modal (hammer) experiments applied to full-scale specimens (Hutchinson and Ray Chaudhuri, 2003). Through the dynamic testing, the natural frequency and associated damping were determined to range from f_n = 10 to 15 Hz and ζ_n = 3 to 12% for systems arranged in the transverse and longitudinal directions.

3. SYSTEM AND PARAMETERS CONSIDERED FOR FRAGILITY CURVE DEVELOPMENT

Fragility curves are developed for bench-mounted rigid equipment considering different: (i) types and magnitudes of damage measures (displacement and velocity), (ii) coefficients of static and kinetic friction, and (iii) support characteristics (bench and building). In addition, the overall uncertainty due to the range of excitations (provided by the different structures and at the ground level) is considered. The following sections describe the system parameters selected as well as the probabilistic formulation adopted for constructing these curves.

3.1 Ground Motions

In this study, 22 measured ground motions are scaled to different hazard levels of 50, 10, and 2% in 50 years, resulting in a total of 32 input motions (Sommerville 2002). Hazard level scale factors are determined by matching site-specific spectral ordinates at the fundamental period of a numerical building model (discussed in the following section). The ground motions are derived from actual ground motion records considering their magnitude and distance of fault from site at which records are collected. The list of the ground motions used along with their different peak parameters is provided in Sommerville (2002). The resulting range of peak ground accelerations (PGA) encompasses the coefficient of friction for the equipment of interest, with PGA = 0.26 – 2.5g. The range of peak ground velocity (PGV) for these motions is PGV = 14 – 352.4 cm/sec, and the range of peak ground displacements (PGD) for these motions is PGD = 1.2 – 141.2 cm.

3.2 Numerical Model of a Representative Science Building

For this study, a numerical model of a representative science building where such equipment would be found is constructed. The influence of other building types is also considered and described in subsequent sections. However, the first building of consideration, herein termed the *RC* building, is a seven-story reinforced concrete

science building. The lateral load-resisting system of this building consists of coupled shear walls in the transverse direction and perforated shear walls in the longitudinal direction. A numerical model was developed in OpenSees (2003) for this structure, using a representative 2D section of the building along the transverse direction [Figure 4(a), (Lee and Mosalam, 2002)]. The building has a reasonable amount of nonlinearity contributed through coupling beams connected to elastic, rigid shear walls. The first and second modal periods of the numerical model were determined as 0.28 and 0.64 seconds, respectively. Nonlinear time history analyses were performed using a modified Newton-Raphson solution strategy.

3.3   Probabilistic Formulation

The approach adopted uses the 32 ground motions propagated through the *RC* building, to generate 224 ground and floor level motions for construction of the fragility curves. The bench-top acceleration is determined using experimental values of bench dynamic behavior. Bench-top acceleration time histories are then considered as input and for the different coefficients of friction of the equipment considered, with their uncertainty in mean and standard deviation, the absolute maximum displacement and velocity relative to the bench are determined. Engineering judgment must then be applied in the selection of limit states for the DMs considered. Upon analyses of the results, if the limit state is exceeded, then the probability of exceeding that limit state is unity and if the limit state is not exceeded then the probability is zero. This process is continued for each of the EDP values. To develop the fragility curves, the framework of probability theory is applied, with the underlying assumption that the probability of exceeding a particular limit state is a lognormal distribution. Shake table results conducted on these types of equipment, indicate that with increasing input accelerations, the dispersion in terms of response displacement of the equipment increases (Hutchinson and Ray Chaudhuri, 2003; Konstantinidis and Makris 2003). These results, combined with χ^2 goodness-of-fit tests, which indicate low significance levels, substantiate the selection of a lognormal distribution. The probability of exceeding a particular limit state is therefore given by:

$$F(a_i) = \Phi\left(\frac{\ln(a_i / m)}{\sigma}\right) \tag{6}$$

where if peak horizontal floor acceleration (PHFA) is selected as the EDP, $F(a_i) =$ probability of exceeding a particular limit state for a given PHFA a_i, m and σ = the median and log-standard deviation of the lognormal distribution, respectively, and $\Phi(x) =$ the value of the standard normal for the variable x. Provided the median and log-standard deviation of the lognormal distribution are evaluated, for each a_i one may determine the probability that a particular limit state has been exceeded.

To determine m and σ, the maximum likelihood theory is used (Shinozuka et al. 2000). Considering, for any case with the PHFA a_i, the probability of exceeding a limit state is provided by $F(a_i)$, and for any case in which the limit state is not exceeded, the probability of exceeding that limit state is then provided by $(1 - F(a_i))$. The likelihood function $L(m,\sigma)$ may then be expressed as:

$$L(m,\sigma) = \left(\prod_{i=1}^{p} F(a_i) \right) \left(\prod_{j=1}^{n-p} (1 - F(a_j)) \right) \tag{7}$$

where n = the total number of data points, p = number of cases in which the limit state is exceeded, therefore, $(n$-$p)$ = number of cases in which the limit state is not exceeded. To obtain the maximum values of $L(m,\sigma)$, the following two conditions must be satisfied:

$$\frac{\partial \ln L(m,\sigma)}{\partial m} = 0 \tag{8}$$

$$\frac{\partial \ln L(m,\sigma)}{\partial \sigma} = 0 \tag{9}$$

Solving the above two-dimensional optimization problem numerically m and σ may be determined. After obtaining m and σ, the probability of exceeding a limit state for any PHFA a_i may be determined using Equation (6).

4. RESULTS AND DISCUSSION

4.1 Sample Fragility Curves

Figure 3 provides a sample of the generated fragility curves, where a high and low bound of μ_s (= 0.3 and 0.7) and ϕ (= 0.5 and 0.9) are selected and damage measures of (a) DM = 5cm, (b) DM = 10cm, (c) DM = 30 cm/sec and (d) DM = 50 cm/sec are shown. Note that the selection of μ_s and ϕ were based on repeated static pull and inclined base tests performed on a subset of typical bench-mounted laboratory equipment (Ray Chaudhuri and Hutchinson, 2004a). Selected DM values were based on review of the general layout of typical laboratories, engineering judgment and observations during shake table testing of these types of systems. Comparing (a) to (b), as the DM increases, the fragility curve becomes flatter, i.e., both the median and log-standard deviation increase. It may also be noted that for higher μ_s values, the spread between high and low ϕ (= 0.5 and 0.9) is larger. In Figure 3(b), large changes in PHFA are required to increase the probability of exceedance only moderately, at the largest resistance parameters (μ_s = 0.7 and ϕ = 0.9), i.e., the curve is very flat in comparison with other curves shown. Figure 3 implies that when other parameters

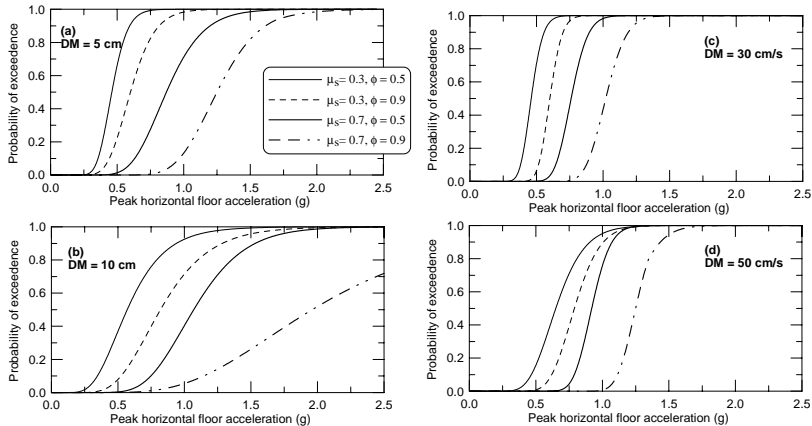remain the same, the magnitude of sliding displacement is less for equipment with higher μ_s and ϕ values.

Figure 3. Effect of μ_s and ϕ on seismic fragility curves, considering different DMs.

4.2   Effect of Building Characteristics on the Fragility Curves

To study the effect of the dynamic behavior of different building structures on the fragility curves, two additional 8-story building models are constructed. These buildings, with a steel moment resisting frame (SMRF) construction; have been previously considered by Santa-Ana and Miranda (2000). Both structures have the same floor plan consisting of three bays in each direction. However, column and beam details vary between the two buildings, such that one is relatively flexible, while the other is relatively stiff. The buildings have a uniform mass distribution and a non-uniform lateral stiffness distribution over their height. They were designed using the lateral load distribution specified in the 1994 Uniform Building Code (ICBO, 1994), with member stiffness tuned to obtain fundamental periods of vibration for each structure representative of those obtained from earthquake records of instrumented existing SMRFs. The fundamental periods of vibration for these two structures are T_1 = 1.92 and 1.19 seconds, for the flexible and stiff structures, respectively. In the following discussion, the nomenclature *Steel-1* and *Steel-2* is used to refer to the flexible and stiff structure, respectively.

   Numerical models of these structures were developed in OpenSees (2003) for these structures, considering a representative 2D frame of the building in the transverse direction [Figures 4(b) and (c)]. Both geometric nonlinearity and material nonlinearity are accounted for the model. A lumped mass model is used, with the buildings assumed fixed at the ground surface. Two percent Rayleigh mass proportional damping is used and kinematic material hardening is assumed.

Nonlinear time history analyses are performed using the same 32 ground motions and fragility curves are generated with the resulting 256 (8 floors x 32) motions. Bench amplification is accounted for, considering representative values of $f_n = 10Hz$ and $\zeta_n = 10\%$. Figure 5(a) and (b) show a comparison of the fragility curves for a mean sliding displacement of 5 cm, considering the three different buildings. It may be observed from these curves that for a damage measure of 5 cm mean sliding, the median values and the log-standard deviations of the lognormally distributed fragility curves are smaller for the steel buildings, than that of the *RC* building. This implies that given a particular value of the PHFA, sliding distances are more for longer period structures. This can be attributed to the motion amplification at the floor levels for the comparatively flexible steel buildings. From these analyses, the mean absolute acceleration amplification was 1.52, 2.19 and 1.00 for *Steel-1*, *Steel-2*, and *RC*, with associated *cov* values of 0.35, 0.39, and 0.21, respectively.
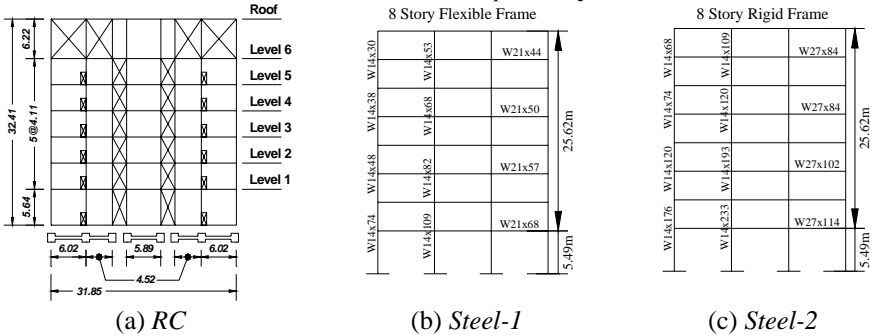

(a) *RC* (b) *Steel-1* (c) *Steel-2*

Figure 4. Building models used in this study: (a) transverse bay of a seven-story reinforced concrete building, modeled by Lee and Mosalam (2002) (*RC*), (b) and (c) two eight-story steel moment frame buildings (*Steel-1* and *Steel-2*). (units in meters).
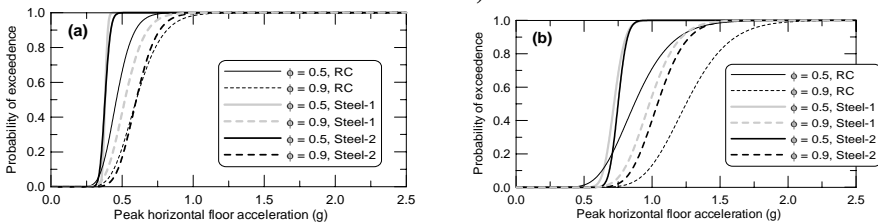

Figure 5. Effect of different building types on fragility curves for DM = 5cm and: (a) $\mu_s = 0.3$ and (b) $\mu_s = 0.7$. ($f_n = 10Hz$ and $\zeta_n = 10\%$).

4.3   Development of Generalized Fragility Curves

Although fragility curves may be developed on a per-equipment basis, generalized curves, with broader applicability to categories of equipment, and considering a range

of sliding thresholds, are desirable. Table 1 shows the classification selected for the bench-mounted science equipment of interest in this study. Fragility curves are now given in terms of their median m and coefficient of variation cov (log-standard deviation/median) for incrementally calculated DMs and the equipment categories noted in Table 1. Figure 6 shows a sample of these generalized curves for the low base resistance equipment (Category 1). It should noted, that for development of these fragility curves, an incremental DM of 0.2 cm is selected.

Table 1. Equipment categorized by their base resistance

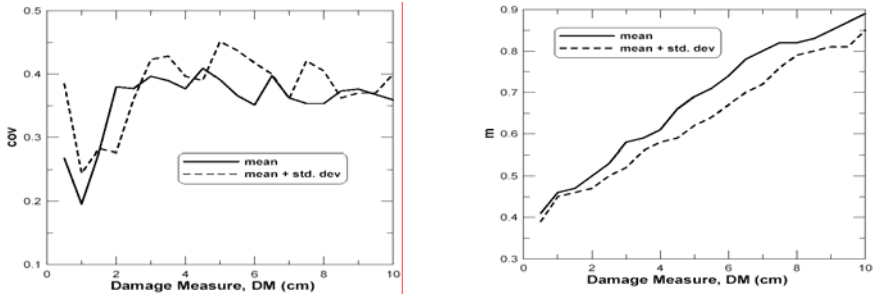| Category	Description	Science Equipment[3]	Average μ_s	Average ϕ
1	Low base resistance	Large Microscope Indy	0.35	0.90
2	Low-medium base resistance	38 cm CRT 43 cm CRT	0.45	0.90
3	Medium base resistance	Technicon Analyzer Indigo, Octane	0.65	0.95
4	Medium-high base resistance	Eppendorf Centrifuge	0.70	0.90
5	High base resistance	48 cm CRT	0.85	0.95

Figure 6. Lognormal parameters (m and cov) for DM = maximum relative displacement, bench-mounted equipment category 1 ($\mu_s = 0.35$, $\phi = 0.90$).

Figure 6 illustrates that for a damage measure of 3cm or more the lognormal parameters follow a straight-line trend. Therefore, both m and cov, may be simplified by a least square regression. The median m may be simplified as a straight line of the form, $m = b_1DM + c_1$ and the cov can be assumed as a straight line parallel to abscissa (i.e., $cov = c_2$). Using these simplified expressions for m and cov, re-arranging the terms of Equation 6 and neglecting smaller order terms, one can express the PHFA in terms of the DM for a given probability of exceedence as a simple quadratic of the form:

$$PHFA = \bar{c}_1 + \bar{c}_2 DM + \bar{c}_3 DM^2 \tag{10}$$

---

[3] Testing results of these equipment items presented in Ray Chaudhuri and Hutchinson (2004a)

where the PFHA is in g's, DM is the damage measure in cm, and $\bar{c}_1$, $\bar{c}_2$, $\bar{c}_3$ are constants depending upon the equipment category and the probability of exceedence. For example, for equipment with Category 1, the coefficients become, $\bar{c}_1 = 0.35$, $\bar{c}_2 = 0.0374$ and $\bar{c}_3 = -0.0017$ for a 5% probability of exceedence. A family of curves similar to Figure 6, and summary statistics for use in Equation 10, for the categories listed in Table 1, and considering other damage measures are provided in Ray Chaudhuri and Hutchinson (2004b).

5. CONCLUSIONS

In this paper, seismic fragility curves, associating the probability of exceedance of a defined limit state (a damage measure, DM) with an engineering demand parameter (EDP), are developed for a range of rigid, sliding-dominated science equipment mounted on bench surfaces. For this study, only uniaxial seismic excitation is considered to provide insight into the contributions and sensitivity of the fragility to different uncertain parameters. Uncertain parameters considered in this study include: (i) static and kinetic coefficients of friction (μ_s and μ_k) and (ii) supporting (bench and building) characteristics. Fragility curves are developed for a stiff reinforced concrete (*RC*) building, and two flexible steel buildings (*Steel-1* and *Steel-2*). A simple approach for generalizing these curves is presented, which will be useful where an unknown magnitude of DM is desired in seismic performance assessment.

ACKNOWLEDGEMENTS

REFERENCES

Choi, D., and C. C. D. Tung. (2002). "Estimating sliding displacement of an unanchored body subjected to earthquake excitation." *Earthquake Spectra*. 18(4): 601–613.

Garcia, L. D., and T. T. Soong. (2003). "Sliding fragility of block-type non-structural components. Part 1: Unrestrained components." *Earthquake Engineering and Structural Dynamics*. 32: 111–129.

Hutchinson, T. C., and S. Ray Chaudhuri. (2003). "Bench and shelf-mounted equipment and contents: shake table experiments." *In the Proceedings of the Applied Technology Council Seminar on Seismic Design, Performance, and*

Retrofit of Nonstructural Components in Critical Facilities. ATC-29-2. Newport Beach, CA. pp. 485-499.

Konstantinidis, D., and N. Makris. (2003). "Experimental and analytical studies on the seismic response of slender laboratory equipment." *In the Proceedings of the Applied Technology Council Seminar on Seismic Design, Performance, and Retrofit of Nonstructural Components in Critical Facilities. ATC-29-2.* Newport Beach, CA. pp. 399-411.

Lee, T. H., and K. Mosalam. (2002). "OpenSees seismic analysis of the LSA Building." Draft Report submitted to Pacific Earthquake Engineering Research (PEER) Center. 45 pp.

Newmark, N. M. (1965). "Effects of earthquakes on dams and embankments." *Geotechnique* XV(2): 139-159.

OpenSees. (2003). *Open System for Earthquake Engineering Simulation.* Pacific Earthquake Engineering Research (PEER) Center. University of California, Berkeley. On-line documentation at: http://opensees.berkeley.edu/.

Ray Chaudhuri, S., and T. C. Hutchinson. (2004a). "Characterizing Frictional Behavior for Use in Predicting the Seismic Response of Unattached Equipment." *In the Proceedings of the 11th International Conference on Soil Dynamics & Earthquake Engineering. (SDEE 2004).* Berkeley, California. January. pp. 368-375.

Ray Chaudhuri, S., and T. C. Hutchinson. (2004b). "Performance characterization of bench- and shelf-mounted equipment and contents." Final report to Pacific Earthquake Engineering Research (PEER) Center Report 2004/xx. (In Preparation).

Santa-Ana, P. R., and E. Miranda. (2000). "Strength reduction factors for multi-degree-of-freedom systems". *In the Proceedings of the 12th World Conference on Earthquake Engineering (WCEE).* New Zealand. Paper number 1446. 8 pp.

Shenton, H. W. III and N. P. Jones. (1991). "Base excitation of rigid bodies. I: formulation." *Journal of Engineering Mechanics, ASCE.* 117: 2286–2306.

Shenton, H. W. III. (1996). "Criteria for initiation of slide, rock, and slide-rock rigid-body modes." *Journal of Engineering Mechanics, ASCE.* 122(7): 690–693.

Shao, Y., and C. C. Tung. (1999). "Seismic response of unanchored bodies." *Earthquake Spectra.* 15(3): 523–536.

Shinozuka, M., M. Q. Feng, H. K. Kim, and H. S. Kim. (2000). "Nonlinear static procedure for fragility curve development." *Journal of Engineering Mechanics, ASCE.* 126(12): 1287-1295.

Sommerville, P. (2002). "Ground motion time histories for the UC lab building." Unpublished Pacific Earthquake Engineering Research (PEER) Center Report.

Taniguchi, T. (2002). "Non-linear response analyses of rectangular rigid bodies subjected to horizontal and vertical ground motion." *Earthquake Engineering and Structural Dynamics.* 31: 1481–1500.

TOOLS TO ENABLE PREDICTION OF THE ECONOMIC IMPACT OF EARTHQUAKE DAMAGE IN OLDER RC BEAM-COLUMN JOINTS

Catherine A. PAGNI[1] and Laura N. LOWES[2]

ABSTRACT

A critical step in performance-based seismic design is the prediction and definition of earthquake performance using terms that are meaningful to building owners. Recently, economic impact, defined as the cost of repairing earthquake damage and the building downtime required to complete the repair work, has been adopted as a meaningful measure of building performance. To enable earthquake engineers to predict the economic impact of earthquake loading, models are required linking the engineering measures used traditionally to define building performance with damage, repair methods, economic loss and repair time.

The work presented here develops these models for older reinforced concrete beam-column joints. The results of previous research are used to develop empirical relationships between damage states and traditional engineering response measures, such as inter-story drift, joint deformation and number of loading cycles. The proposed damage states are characterized by parameters such as concrete crack width, extent of concrete spalling and yielding and buckling of reinforcement. The results of previous research and practical experience by engineers and contractors are used to define a series of repair methods that can be used to restore a damaged joint to its original condition. Each damage state is associated with a specific repair technique, and probabilistic models are developed to enable prediction required repair.

Keywords: Beam-column joint; Damage; Repair; Fragility function.

1.   INTRODUCTION

Research at the Pacific Earthquake Engineering Research Center (PEER) and elsewhere to advance performance-based earthquake engineering has resulted in an awareness by the earthquake engineering community of the needs to (1) define performance using terms that are understood by and of valuable to building owners and (2) employ a probabilistic framework that supports the propagation of uncertainty through the process. The PEER framework equation (http://peer.berkeley.edu):

$$\nu(DV) = \int \int \int G\langle DV|DM \rangle dG\langle DM|EDP \rangle dG\langle EDP|iM \rangle d\lambda(IM) \tag{1}$$

[1] *PACE Civil, Inc., Redding, CA USA*

[2] *Dept. of Civil Engineering, University of Washington, Seattle, WA USA*

was developed to accommodate these needs. In this equation, probabilistic functions link earthquake intensity measures (IMs) with engineering demand parameters (EDPs). This relationship brings the engineer to what was traditionally the end of the analysis. However, the PEER framework equations also provides a basis for going beyond EDPs by employing probabilistic relationships that link EDPs with damage measures (DMs) and subsequently DMs with decision variables (DVs). Specifically, in Eq. 1, $\nu(DV)$ is the mean annual probability that the decision variable DV exceeds a specific value, $G\langle DV|DM\rangle$ is the conditional probability that DV exceeds a specific value given a particular value of DM, $dG\langle DM|EDP\rangle$ is the derivative (with respect to DM) of the conditional probability that DM exceeds a limit value given a specific value of EDP, $dG\langle EDP|IM\rangle$ is the derivative (with respect to EDP) of the conditional probability that EDP exceeds a limit value given a specific value of IM, and $d\lambda(IM)$ is the derivative of the seismic hazard curve, $\lambda(IM)$.

Multiple approaches are appropriate for incorporating information about building response into Eq. 1. For example, a building-specific EDP, such as maximum roof drift, could be used to predict *the* damage state of the building, or component-specific EDPs could be used to predict the damage state of individual component, with the damage state of the building defined by the cumulative damage states of all of the components. It is generally accepted that the latter approach provides an opportunity to introduce more information into the process and thereby reduce uncertainty. The models developed here support the latter approach. Specifically, the results of previous research and practical experience are used to develop probabilistic relationships linking EDPs with DMs for one type of structural component, older beam-column building joints.

2. EXPERIMENTAL DATA

A critical phase of this research effort was the identification of experimental data characterizing the progression of earthquake damage in older beam-column joints. The criteria used to choose laboratory test specimens, the characteristics of the experimental test specimens, and variation in test specimens that could be expected to affect damage progression are discussed in the following sections.

2.1 Criteria Used To Identify Appropriate Laboratory Test Specimens

Three criteria were used to identify experimental data sets for use in this study. First, only laboratory specimens representative of pre-1967 construction were used. A review of construction drawings for buildings designed prior to 1979 for construction on the West Coast (Mosier 2000) were used as a basis for defining design details for older joints. Table 1 lists Mosier's statistics for critical joint design parameters. The

joint test specimens used in the current study fell within the ranges observed by Mosier for joints designed prior to 1967, with two exceptions:

- 5 of the 21 specimens included in this study have joint transverse reinforcement. For these specimens, transverse steel ratios ranged from 0.2% to 0.4%. These volumes were considered to be sufficiently low, in comparison with the post-1967 average, to be representative of pre-1967 construction.
- 3 of 21 specimens included in this study had beam bottom reinforcement that was discontinuous through the joint. For these specimens, the bond index was higher than the maximum observed by Mosier (2000).

Table 1. Design details for pre–1979 beam-column joints

Design year	Volumetric Transverse Steel Ratio (%)			Shear Stress Demand $/f_c$			Beam Bar Bond Index $\mu = d_b f_y / 2 l_d \sqrt{f_c}$		
	ave.	min.	max.	ave.	min.	max.	Ave.	min.	max.
Pre-1967	0.0	0.0	0.2	0.21	0.09	0.30	21	12	38
1967-1979	0.9	0.0	2.1	0.15	0.06	0.29	23	14	43

Note: In defining the bond index, μ, d_b, is the diameter of the reinforcing bar, f_y is the yield strength of the bar, l_d is the anchorage length within the joint assumed to be equal to the column depth, and f_c is the concrete compressive strength and units are inches and pounds.

Second, only laboratory test specimens with the same basic configuration and load history were used. All of the specimens represented sub-assemblages from two-dimensional building frames and comprised the joint, the beams framing into the joint and extending to mid-span, and the columns framing into the joint and extending to mid-height. Lateral loading was applied as a shear force the top of the column and reacted by shear forces at the base of the column and beam ends. Lateral load was applied pseudo-statically using displacement control. In some cases, a constant axial load was applied at the top of the column to represent gravity load.

Third, only test specimens for which sufficient data characterizing the progression of damage in the beam-column joint were used. While all experimental researchers provide data characterizing the load-displacement response of laboratory test specimens, the detail and consistency with which damage data are reported in the literature varies substantially. In many cases, the lack of sufficient damage data eliminated joint specimens for use in this study.

2.2 Experimental Data Used in the Study

A review of the literature resulted in four test programs and twenty-one test specimens that met the above criteria:

- *Meinheit and Jirsa (1977)* investigated the impact of joint transverse reinforcement on response. Data from one (MII) of the eleven specimens

tested by Meinheit and Jirsa are used; sufficient data are provided for this specimen.

- *Pessiki et al. (1990)* investigated the earthquake response of older building components. Data from seven (P2-P5, P7-P9) of the test specimens are used.
- *Joh et al. (1991a, 1991b)* investigated the impact on earthquake response of 1) joint transverse reinforcement, 2) beam transverse reinforcement and 3) torsion due to beam eccentricity. Three specimens from these studies (JXO-B8, JXO-B1, and JXO-B2) are used.
- *Walker (2001)* and *Alire (2002)*: evaluated the impact of joint shear stress and load history. These studies conclude that joints maintain strength and adequate stiffness when drift demand less than 1.5% and shear stress demand is less than $10\sqrt{f'_c}$. Data from all of the specimens (PEER*, CD*, PADH*) are used.

Design details and loading data for these specimens are listed in Table 2.

Table 2. Design details and load data for experimental test specimens

Specimen	f'c (psi)	Shear Stress Demand / f'c	Shear Stress Demand / sqrt(f'c) (psi)	Transverse Steel Volume Ratio (%)	Maximum Bond Index, μ	Column Axial Load / f'cAg	Drift History*	Column Splice Above Joint	Ratio of Beam to Column Width
PEER14	4606	0.16	10.9	0.00	18.7	0.11	Standard	no	1.00
PEER22	5570	0.20	14.6	0.00	24.9	0.09	Standard	no	1.00
CD1514	4322	0.18	11.6	0.00	19.3	0.12	High-cyc.	no	1.00
CD3014	6171	0.14	11.3	0.00	16.1	0.08	High-cyc.	no	1.00
CD3022	5533	0.21	15.5	0.00	25.0	0.09	High-cyc.	no	1.00
PADH14	6218	0.15	11.7	0.00	16.1	0.08	Unsym.	no	1.00
PADH22	5259	0.22	15.7	0.00	25.6	0.10	Unsym.	no	1.00
PEER09	9500	0.13	12.6	0.00	16.7	0.10	Standard	no	1.00
PEER15	9500	0.19	18.7	0.00	26.7	0.10	Standard	no	1.00
PEER41	5000	0.17	12.2	0.00	29.6	0.10	Standard	no	1.00
P2	5000	0.19	13.2	0.00	34.8	0.27	Standard	yes	0.88
P3	4000	0.21	13.2	0.00	34.6	0.34	Standard	yes	0.88
P4	4000	0.20	12.7	0.00	34.6	0.34	Standard	yes	0.88
P5	4000	0.22	13.6	0.23	38.0	0.34	Standard	yes	0.88
P7	3000	0.19	10.5	0.00	52.5	0.46	Standard	yes	0.88
P8	3000	0.19	10.3	0.00	39.4	0.46	Standard	yes	0.88
P9	4000	0.15	9.60	0.00	39.5	0.10	Standard	yes	0.88
MII	6060	0.25	19.7	0.44	25.1	0.25	Standard	no	0.85
JXO-B1	3901	0.12	7.51	0.27	19.9	0.17	Standard	no	0.67
JXO-B2	3269	0.24	13.8	0.27	19.9	0.17	Standard	no	0.50
JXO-B8	3429	0.19	11.1	0.27	19.5	0.15	Standard	no	0.93
Min.	3000	0.12	7.5	0.00	16.1	0.08			0.50
Max.	9500	0.25	19.7	0.44	52.5	0.46			1.00
C.O.V.	0.36	0.19	0.22	1.90	0.36	0.67			0.14

Note: A *standard* drift history comprises 1–3 cycles to increasing maximum drift demands, a *high-cycle* history comprises 10 or more cycles to increasing maximum drift demands, and an *unsymmetrical* history comprises multiple cycles to varying maximum and minimum drift demands.

The specimens listed in Table 2 have design details typical of pre-1967 construction and were subjected to similar simulated earthquake load histories in the laboratory. However, as suggested by the data in Table 2 there are variations in both the design details and gravity loading. These variations contribute to variability in the observed damage patterns and progression.

3. IDENTIFYING DAMAGE STATES, ENGINEERING DEMAND PARAMETERS AND METHODS OF REPAIR

3.1 Engineering Demand Parameters

Within the context of this study, an engineering demand parameter (EDP) is a scalar or functional quantity that defines the earthquake demand on a joint at any point in the load history. Since the objective of the current study is to develop models for use in predicting joint damage given an EDP value, we are seeking to find the EDP that most accurately and precisely predicts joint damage. Since data characterizing the response of the laboratory test specimens discussed previously are used to develop models linking EDPs with damage states and methods of repair, the domain of potential EDPs is limited to the data published by the experimental researchers.

A review of the literature and the experimental data provides a basis for identifying a series of five potential EDPs:

- *Maximum inter-story drift:* Drift is a simply demand measure provided by all researchers, and there is consensus within the earthquake engineering community that drift is a measure of earthquake demand. However, inter-story drift comprises flexural deformation of beams and columns as well as joint deformation. Thus, it is an imperfect measure of joint deformation demand.
- *Number of load cycles:* Like drift, the number of load cycles is a simply demand measure provided by all researchers and there is consensus within the earthquake engineering community that the number of load cycles has an impact on the observed response of components.
- *Maximum joint shear strain*: Joint shear strain represents a substantial improvement over inter-story drift, since it is a measure only of joint deformation demand. However, joint shear strain data are provided by few researchers; the sparsity of these data may increase model uncertainty.
- *Drift in combination with the number of load cycles:* The results of previous research suggest that earthquake demand on a component is best characterized by a function that includes a measure of displacement demand and a measure of the number of load cycles. Given the availability of drift as a measure of joint deformation demand, a functional EDP that includes inter-story drift and number of load cycles is proposed:

$$F = aD^b + cN^d \qquad (2)$$

where D is the maximum drift and N is the number of load cycles (computed using the drift history). Empirical parameters in Eq. 2 are calibrated to minimize the dispersion of the data and are defined as follows: a=0.252, b=0.645, c=0.0178, d=0.819.

- *Joint shear strain in combination with the number of load cycles:* A functional EDP that includes both maximum joint shear strain and number of load cycles is considered the most desirable EDP:

$$F = a\gamma^b + cN^d \qquad\qquad (3)$$

where γ defines the maximum joint shear strain, N defines the number of load cycles (computed using the drift history) and empirical parameters are defined as follows: a = 1.46, b = 0.481, c=0.200, d = 0.309.

3.2 Damage States

Damage measures (DMs) describe the damage sustained by a component during an earthquake. In this study, damage is quantized into discrete damage states. Data characterizing the development of damage in the previously discussed laboratory test specimens as well as research results, documentation providing guidelines for post-earthquake repair and interviews with professional were used to identify a series of damage states that (1) best characterize the progression of damage in reinforced concrete beam-column joints and (2) best determine the appropriate method of repair for the component. These damage states are

1. Initial cracking at the beam-column interface
2. Initial cracking within the joint area
3. Maximum crack width is less than 0.02 in. (5 mm)
4. Maximum crack width is greater than 0.02 in. (5 mm)
5. Beam longitudinal reinforcement yields
6. Maximum crack width is greater than 0.05 in. (1.3 mm)
7. Spalling of at least 10% joint surface concrete
8. Joint shear strength begins to deteriorate
9. Spalling of more than 30% joint surface concrete
10. Cracks extend into the beam and/or column
11. Spalling of more than 80% joint surface concrete
12. Crushing of concrete extends into joint core
13. Failure due to (a) buckling of longitudinal steel reinforcement, (b) loss of beam longitudinal steel anchorage within the joint core, or (c) pull-out of discontinuous beam longitudinal steel reinforcement

3.3   Methods of Repair

The method of repair required to restore a component to its original, pre-earthquake condition, provides a basis for estimating the economic impact of earthquake loading. Information was collected from multiple sources to identify appropriate techniques for repairing earthquake damage to RC components and to link these repair methods with the range of previously identified damage states. The primary references consulted were *FEMA 308 Repair of Earthquake Damaged Concrete and Masonry Wall Buildings* (ATC 1998) and *ACI 546R-96 Concrete Repair Guide* (ACI Com. 546 1996). In addition, the results of previous research by others were used to verify the adequacy of repair methods and to identify which repair methods would be employed for which damage states (Karayannis 1998, Filiatrault and Lebrun 1996, Tasai 1992, Jara et al. 1989). Additionally, practicing engineers and contractors were consulted to verify linkages between repair methods and damage states (Coffman and Kapur 2003, Runacres 2003, Savage 2003).

Review of the relevant sources results in identification of five methods of repair that would be appropriate for restoring joints to original condition (Table 3). These methods of repair include five basic repair techniques: repair cosmetic finishes, epoxy inject concrete cracks, patch spalled concrete, remove and replace crushed concrete, replace reinforcing steel. Review of the relevant sources also provided a basis for linking these methods of repair with specific damage states (Table 3). While the probabilistic framework employed for prediction of economic impact (Eq. 1) would suggest that there should be a probabilistic relationship linking each repair method with a set of damage states, there are insufficient data available to calibrate such models.

Table 3. Methods of repair for joints

Method of Repair	Activities	Damage States
0. Cosmetic Repair	Replace and repair finishes.	0-2
1. Epoxy Injection	Inject cracks with epoxy and replace finishes.	3-5
2. Patching	Patch spalled concrete, epoxy inject cracks and replace finishes.	6-8
3. Replace Concrete	Remove and replace damaged concrete, replaces finishes	9-11
4. Replace Joint	Replace damaged reinforcing steel, remove and replace concrete, and replace finishes.	12

4. PREDICTION OF REQUIRED REPAIR METHOD

Using the experimental data collected as well as the damage states and methods of repair identified from the literature, a series of fragility curves were developed for use

in predicting damage as well as repair method given an EDP. The steps in the development process are discussed in the following sections.

4.1   Damage versus EDP

Experimental data characterizing the progression of damage for the test specimens were used to generate data sets linking the thirteen damage states with the three primary EDPs: drift, number of load cycles and joint shear strain. The functional EDPs, defined by Eq. 2 and Eq. 3, were calibrated to minimize the dispersion of the data for all damage states about a line spanning the range of damage states and functional values from 0 to 1. Figure 1 shows damage-EDP data for the five EDPs.

(a) drift   (b) number of cycles   (c) joint shear strain

(d) F(D,N) per Eq. 2   (e) F(γ,N) per Eq. 3
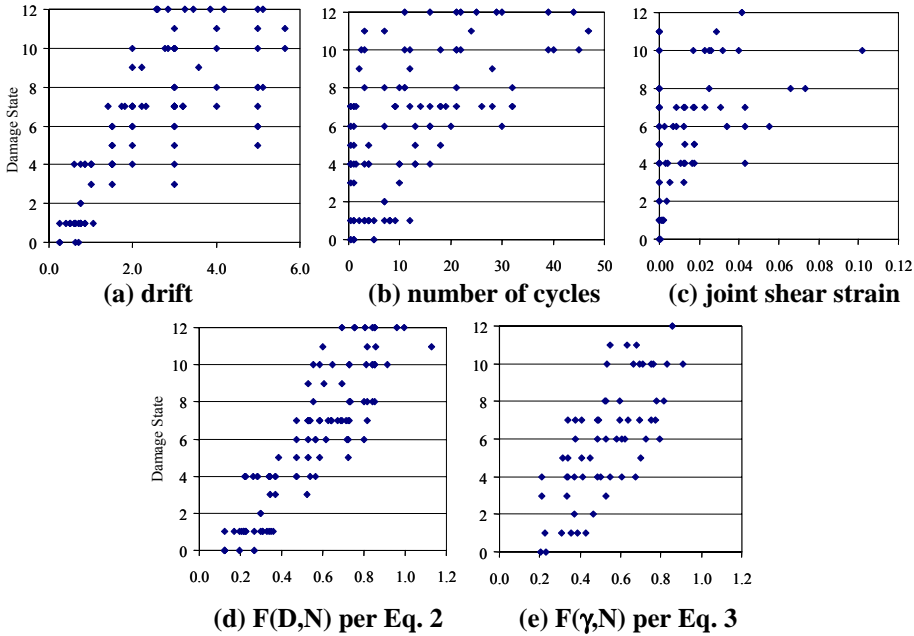
Figure 1. Damage versus EDP.

The scatter of the data in Figure 1 reinforces the need for probabilistic models linking EDPs with damage and repair. The variability in these data is due in part to variability in test specimen design and loading; however, it is due also to the data collection procedures used in the laboratory. The typical procedure used in earthquake testing in the laboratory is as follows:
1. A half-cycle of loading to a new maximum displacement demand, at which point loading is paused to allow for identification of new cracks and regions of spalling, measurement of new and existing cracks and picture taking.

2. Loading in the reversed direction to a new minimum displacement demand, at which point loading is paused to allow for data collecting as above.
3. Multiple additional full load cycles, typically two additional cycles, to the new maximum and minimum displacement demand levels.

Thus, in monitoring the progression of damage, it is not possible to know exactly the displacement demand level at which damage occurred, only that it occurred prior to reaching a particular maximum displacement demand level. Further it is not possible to differentiate between damage that occurs during the second cycle to a maximum displacement demand level from that which occurs during the third cycle or from that which occurs during the first cycle to an increased maximum displacement demand.

4.2 Predicting the Required Method of Repair

4.2.1 Grouping Damage Data for Using in Prediction Method of Repair

The data presented in Figure 1 were used to develop models defining the probability of earthquake damage requiring, at least, the use of a specific method of repair. These data could have been used to generate fragility curves defining the probability that joint damage would meet or exceed a specific damage state. However, since the ultimate objective of this effort was the prediction of economic impact, the development of damage-state prediction models was not considered to be necessary.

To generate repair-method prediction models, the data in Figure 1 were combined so that individual data points define a specific EDP value and the required method of repair associated with that EDP value. This combination was accomplished using the relationships in Table 3. Because several damage states are linked with each methods of repair, there are several plausible approaches to *combining* the data:

- Method One: All of the EDP-damage state pairs are used for each method of repair. This results in the most data. This also results in the data being biased towards higher EDP levels.
- Method Two: For each individual specimen, the lowest EDP-damage state data point associated with each method of repair is used. This results in no more than 21 data points for each method of repair. This also results in the data being slightly biased towards higher EDP levels, but the bias is less than for combination Method One.
- Method Three: Only data for the lowest damage state are used for each method of repair. This method results in the fewest data for each method of repair.

All three approaches were employed for all five EDPs. For each combination method, the sample mean and coefficient of variation were computed for the EDP-method of repair data sets. Combination Method Two was identified as the preferred method for use in the study. This method resulted in the smallest coefficient of variation for the EDP-method of repair data as well as well-spaced means.

4.2.2 Modeling the Data Using Standard Probability Distributions

The data in Figure 1, combined into method of repair groups using combination Method Two as discussed in Section 4.2.1, were used to generate fragility functions defining the probability that a joint would require at least a particular method of repair given a specific value of an EDP. Standard cumulative probability distribution functions (CDFs) may be used to define fragility functions. In the current study, three standard CDFs were calibrated to fit the data using the Method of Maximum Likelihood. The standard distributions considered included

- Lognormal distribution: Commonly employed distribution. Requires positively valued data.
- Weibull distribution: Less commonly used distribution. The distribution allows for a stronger influence of extreme-valued data. This is desirable for the current application where small-demand values are important.
- Beta distribution: Less commonly used distribution. Allows for an upper and lower bound to be defined for the distribution, which may be desirable for the current application.

The three CDFs were tested using three standard goodness-of-fit tests to identify a preferred distribution for use in modeling the data:

- The Chi-Square test: For accurate results, this test requires that the total number of data points exceed 50. This was not the case here, so the accuracy of these results is questionable.
- The Kolmogorov-Smirnov (K-S) test: This test is exact for all sample sizes, but requires that the distribution parameters not be estimated from the data. This was not the case here, so the accuracy of this test also is questionable.
- The Lillefors test: This test is exact for all sample sizes and is designed for situations in which distribution parameters are estimated from the data set. This test is appropriate only for the normal distribution; however, by considering the log of the data, this test can be used to evaluate the lognormal distribution. This was done for the current study.

Application of these tests indicated that the Beta distribution was not appropriate for use in modeling the data and that the Weibull and lognormal distributions were equally good. The lognormal distribution was chosen as the preferred distribution for this study because of its widespread use in comparison to the Weibull distribution.

4.2.3 Proposed Fragility Functions

Figure 2 shows the proposed fragility functions linking method of repair with EDP for three of the five EDPs. Given a specific EDP value and a specific method of repair, these models define the probability that joint damage will be such that, at a minimum, the specific method of repair will be required to restore the joint to its original condition. Fragility functions are shown only for three of the five proposed EDPs because only for these EDPs do the fragility functions have well spaced means and low coefficients of variation. These factors result in the progression from a relatively

low probability of requiring a specific method of repair to a relatively high probability occurring over a very small EDP range, and thus make the fragility function better suited for use in predicting economic impact. Note that for the functional EDP defined by maximum joint shear strain and number of load cycles, a fragility function is not provided for method of repair 4, as insufficient data were available for calibration of this function.
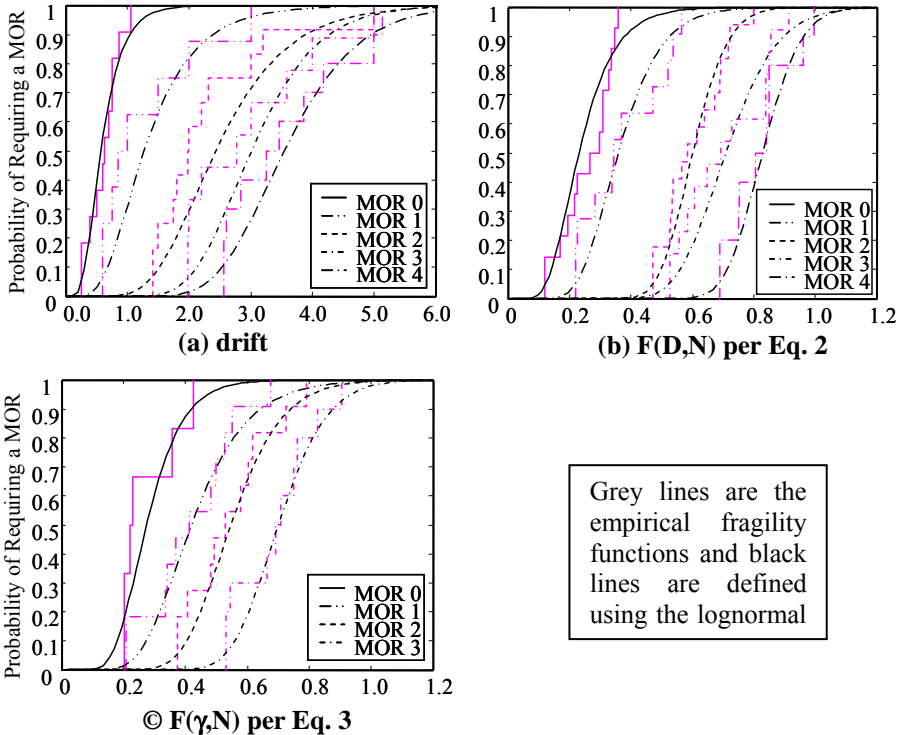

Figure 2. Probability of meeting or exceeding a method of repair (MOR).

5. CONCLUSIONS

The results of previous research as well as the practical experience of structural engineers and contractors were used as a basis for developing probabilistic defining the method of repair required to restore a pre-1967 joint to original condition as a function of traditional engineering demand parameters. These models provide a basis for evaluating the economic impact of earthquake loading of a building. Multiple approaches were considered in developing the probabilistic models. It was found that defining engineering demand using inter-story drift or a nonlinear function of inter-story drift and number of load cycles resulted in the best models. It was found also

that the defining demand using a nonlinear function of maximum joint shear strain and number of load cycles offers the potential for reduced model uncertainty; however, insufficient data are available to define this model for all methods of repair. Additional data are required defining the progression of damage in older joints as a function of the three primary EDPs: drift, number of load cycles and joint shear strain.

REFERENCES

Alire, D. (2002). "Seismic Evaluation of Existing Unconfined RC Joints." *M.S. Thesis*. Seattle: University of Washington.

ACI Com. 546. (1996). *ACI 546R-96: Concrete Repair Guide*. Farmington Hills: ACI.

Applied Technology Council. (1998). *FEMA 308: Repair of Earthquake Damaged Concrete and Masonry Wall Buildings."* Washington D.C.: FEMA.

Coffman, H., and J. Kapur. (2003). WA Dept. of Transportation. In-person interview.

Filiatrault, A., and I. Lebrun. (1996). "Seismic Rehabilitation of Reinforced Concrete Joints by Epoxy Pressure Injection Technique". *ACI SP-160: Seismic Rehabilitation of Concrete Structures*: Farmington Hills: ACI. 73-92.

Jara, M., Hernandez, Garcia, and Robles. (1989). "The Mexico Earthquake of September 19, 1985-Typical Cases of Repair and Strengthening of Concrete Buildings." *Earthquake Spectra* 5(1): 175-181.

Joh, O., Goto, and Shibata. (1991a). "Influence of Transverse Joint and Beam Reinforcement and Relocation of Plastic Hinge Region on Beam-Column Joint Stiffness Deterioration." *ACI SP-123: Design of Beam-Column Joints for Seismic Resistance*. Ed., J. Jirsa. Farmington Hills: ACI.

Joh, O., Goto, and Shibata. (1991b). "Behavior of Reinforced Concrete Beam-Column Joints with Eccentricity." *ACI SP-123: Design of Beam-Column Joints for Seismic Resistance*. Ed., J. Jirsa. Farmington Hills: ACI.

Karayannis, C. G., C. E. Chalioris, and K. K. Sideris (1998). "Effectiveness of RC Beam-Column Connection Repair using Epoxy Resin Injections." *Journal of Earthquake Engineering* 2(2): 217-240.

Meinheit, D., and J. Jirsa. (1977). *The Shear Strength of Reinforced Concrete Beam-Column Joints.* Austin: University of Texas, Dept. of Civil Engineering. 217 pp.

Mosier, W. G. (2000). "Seismic Assessment of Reinforced Concrete Beam-Column Joints." *M.S. Thesis*. Seattle: University of Washington. 218 pp.

Pessiki, S. P., Conley, Gergely and White. (1990). *Seismic Behavior of Lightly-Reinforced Concrete Column and Beam-Column Joint Details.* NCEER-90-0014. Buffalo: National Center for Earthquake Engineering.

Runacres, R. (2003). Contech, Inc. Telephone interview.

Savage, S. (2003). Coughlin, Porter, and Lundeen. In-person interview.

Tasai, A. (1992). "Effective Repair with Resin for Bond Failure of RC Members." *Proceedings of the 10WCEE*. 5211-5216.

Walker, S. (2001). "Seismic Performance of Existing RC Beam-Column Joints." *MS Thesis.* Seattle: University of Washington.

SEISMIC FRAGILITY ANALYSIS OF STRUCTURAL SYSTEMS

Paolo E. PINTO[1], Paolo FRANCHIN[1], Alessio LUPOI[1], Giorgio LUPOI[2]

ABSTRACT

A method is presented for the evaluation of the seismic fragility function of realistic structural systems. The method is based on a preliminary, limited, simulation involving non linear dynamic analyses performed to establish the probabilistic characterisation of the demands on the structure, followed by the solution of a system reliability problem with correlated demands and capacities. The results compare favourably well with the fragility obtained by plain Monte Carlo simulation, while the associated computational effort is orders of magnitude lower. The method is demonstrated with an application to a 3D RC building structure subjected to bi-directional excitation.

Keyword: Fragility functions.

1. INTRODUCTION

Fragility functions can be obtained through a variety of methods that range from expert judgment (ATC13,1985), to data analysis on observed damages (Singhal 1998, Shinozuka 2000), to fully analytical approaches, as for example in Cornell 2002, Gardoni 2003, Franchin 2004, Au 2003.

A feature common to most of the approaches of the latter category is the use of a reduced number of simulations to compare probabilistically the maximum structural responses with the corresponding capacities. The difference among them lie essentially in their balance between cost and accuracy, i.e., in their ability to account economically for all the aspects entering the reliability problem. These latter include:

- The possibility of the structure reaching collapse in more than one failure mode (system reliability problem)
- The degree of dependence among the possible failure modes
- The uncertainty in the capacity of the structure (due to the approximate nature of the models)

---

[1] *Dept. Struct. & Geotech. Eng., University of Rome "La Sapienza", Rome, Italy*
[2] *European School for Advanced Studies in Reduction of Seismic Risk, Pavia, Italy*

- The influence on the dynamic response of the variability of the system parameters

In the paper a method is presented which is simple and, at the same time, able to account for all of the above mentioned aspects. The method takes profit of ideas and proposals that have appeared in different forms in the recent literature, though not formulated in a similarly coherent framework. It is presented here together with an application of realistic character that offers the possibility of exploring its features, among which effectiveness and practicality are believed to be the most attractive ones.

2. RELIABILITY METHOD

In the basic formulation of this method the variability of the response/demand is assumed to be due only to that of the ground motion, i.e., the structural response, given the input, is deterministic.

In case the performance of the structure can be characterised by a single failure mode, or when one mode is dominant over the others, denoting by D_k the maximum demand in this failure mode due to the k-th accelerogram and by C the corresponding capacity, completely defined by its cumulative distribution function $F_C(\ )$, the probability of failure conditional on the sample ground motion k is given by:

$$P_{f,k} = \Pr\{C \le D_k\} = F_C(D_k)$$
(1)

By repeating the analysis with a number of accelerograms, the probability of failure unconditional with respect to sample variability can be simply obtained as:

$$P_f = \frac{1}{n}\sum_{k=1}^{n} P_{f,k}$$
(2)

where the number of samples must be large enough to ensure stable estimates of .

In general, failure may occur according to different modes of comparable importance (e.g., flexural failure, shear failure, joint failure, etc.) in different members of the structure. If the failure events can be considered as independent and arranged in series, the probability of failure of the system is easily evaluated as:

$$P_{f,k} = \Pr\left\{\bigcup_{i=1}^{m} C_i \le D_{ik}\right\} = 1 - \prod_{i=1}^{m}\left(1 - P_{f,ik}\right) = 1 - \prod_{i=1}^{m}\left[1 - F_{C_i}(D_{ik})\right]$$
(3)

which is the generalisation of Eq.(1) for the case of m independent modes.

In Eq.(2) the dependence of P_f on the intensity of the seismic action is omitted: the fragility function is obtained by calculating P_f for a convenient number of intensity values. The simplest version of the procedure is comprised in Eq.(2) and (3). Consideration of the correlation between failure modes, of the influence of the variability of the mechanical parameters on the demand and of possible non serial arrangements of the failure events are all areas where the basic procedure can be improved, as indicated in the following.

In a general formulation of the problem, both the demands and the capacities should be considered as functions of the basic variables $\mathbf{x}$, i.e., $C_i = C_i(\mathbf{x})$ and $D_i = D_i(\mathbf{x})$. In the basic procedure this dependence is ignored for what concerns the demand and only partially accounted for at the capacities level through their marginal distributions $F_{C_i}(\cdot)$. Actually, a significant degree of correlation normally exists among the capacities C_i's. This correlation can be evaluated based on that existing among the basic random variables $\mathbf{x}$ they have in common.

In practice, most formulae for the capacity of failure modes of reinforced concrete members are built upon a relatively weak mechanical basis, to which elements of empirical origin are added. These formulae are presumed to be unbiased (i.e., to provide a correct prediction of the mean value), but they are accompanied by a significant scatter due to modelling error. Since the capacity is generally a positive quantity, the general format of these formulae is additive when expressed in terms of some transformation of the capacity:

$$C_i = \mu_{C_i}(\mathbf{x}) + \varepsilon_{C_i}$$

(4)

or multiplicative as in:

$$C_i = \mu_{C_i}(\mathbf{x}) \cdot \varepsilon_{C_i}$$

(5)

In the former case ε_{C_i} is usually assumed to be a zero mean Gaussian random variable, while in the latter it can be assumed to be a unit mean Lognormal variable. It has to be observed that for distinct failure modes the corresponding random variables ε_{C_i} and ε_{C_j} are usually considered as independent and this reduces the correlation between the capacities C_i and C_j.

Coming now to the demands, rather than calculating the failure probability conditional on the k-th sample of ground motion, as in the basic procedure, the results D_{ik} from the entire set of non linear structural analyses can be used to compute the statistics of the D_i's, which include mean values μ_{D_i}, standard

deviations σ_{D_i} and correlation coefficients $\rho_{D_i D_j}$. The i-th demand can then be expressed, similarly to the corresponding capacity, as:

$$D_i = \mu_{D_i}(\boldsymbol{\mu}_{\mathbf{x}}) \cdot \varepsilon_{D_i}$$

(6)

where the mean value μ_{D_i} of the demand is evaluated at the mean value of the basic variables $\boldsymbol{\mu}_{\mathbf{x}}$, ε_{D_i} can be assumed to be Lognormal with unit mean, standard deviation equal to the i-th demand coefficient of variation $\delta_{D_i} = \sigma_{D_i} / \mu_{D_i}$ and correlation coefficient with ε_{D_j} equal to $\rho_{ij} = \rho_{D_i D_j}$.

Apart from the dependence of the demands on the basic variables $\mathbf{x}$, all the elements are in place to evaluate the probability of failure of a completely general system (not necessarily serial):

$$P_f = \Pr\left\{ \bigcup_{j=1}^{n_C} \bigcap_{i \in I_{C_j}} C_i(\mathbf{x}, \boldsymbol{\varepsilon}_C) \le D_i(\boldsymbol{\varepsilon}_D) \right\}$$

(7)

with n_c cut-sets $\mathbf{C}_j$ (I_{C_j} denoting the set of indices of the failure modes belonging to the j-th cut set).

The system reliability problem in Eq.(7) can be evaluated either by FORM, first solving each component/failure mode and then using the multi-normal approximation for general systems, or by Monte Carlo simulation, which is simpler and in this case is comparatively inexpensive since it does not require any structural analysis.

As a final step, it remains to account for the dependence of the demands on $\mathbf{x}$. One possible approximate way of doing it is to consider this dependence as linear around the mean value of $\mathbf{x}$. This involves the first order partial derivatives of the demands with respect to $\mathbf{x}$ evaluated in the mean $\boldsymbol{\mu}_{\mathbf{x}}$ of the basic variables. The latter, often called *sensitivities* with respect to the system parameters, can be computed either numerically by a finite difference scheme, i.e., repeating the analysis for perturbed values of the parameters, or, more efficiently, by the Direct Differentiation Method (Franchin 2004, Kleiber 1997). In practice, the sensitivities $\partial D_i / \partial x_j$ are computed as the mean values of the derivatives conditional on sample accelerogram:

$$\frac{\partial D_i}{\partial x_j} = \frac{\partial}{\partial x_j}\left(\frac{1}{n} \sum_{k=1}^{n} D_{ik} \right) = \frac{1}{n} \sum_{k=1}^{n} \frac{\partial D_{ik}}{\partial x_j}$$

(8)

where the derivatives $\partial D_{ik}/\partial x_j$ are calculated at the time instants where the corresponding maxima occur.

The demand in failure mode i can thus be rewritten accounting for its (linearised) dependence on $\mathbf{x}$ as:

$$D_i(\mathbf{x}) = \mu_{Di}(\mathbf{\mu_x})\varepsilon_{D_i} + \sum_j \frac{\partial D_i}{\partial x_j}\left(x_j - \mu_{x_j}\right) \tag{9}$$

and the reliability problem can be written, similarly to Eq.(7), as:

$$P_f = \Pr\left\{\bigcup_{j=1}^{n_C}\bigcap_{i\in I_{Cj}} C_i(\mathbf{x}) \le D_i(\mathbf{x})\right\} \tag{10}$$

where now it is understood that the vector $\mathbf{x}$ includes, besides the basic variables, also the capacity error terms ε_C's and the demands variability terms ε_D's.

3. APPLICATION

The method described in the previous section is applied in the fragility analysis of a three-storey 3D RC structure (Figure 1), designed solely for gravity loads according to the design and construction practice of the early 70's in southern Europe, i.e., including plan irregularity, strongly eccentric beam-column connections, overall poor detailing. The building has been designed, constructed and pseudo-dynamically tested under bi-directional loading within the framework of the EU funded project SPEAR (Negro 2004).
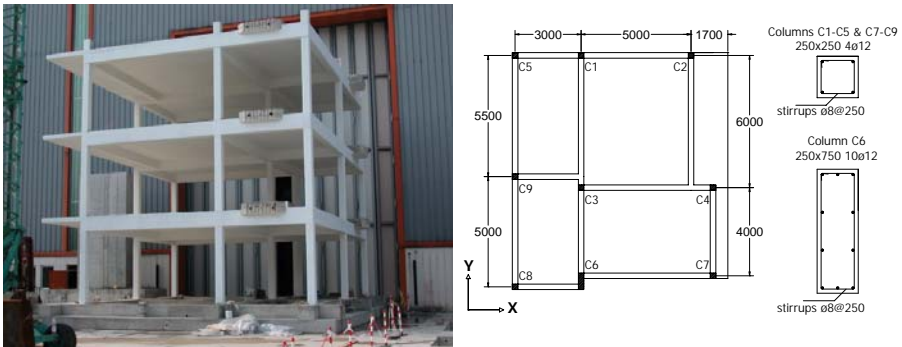
Figure 1. Photo of the test structure outside the lab (left) and plan of the framing (right).

The first three modes of vibration of the structure, evaluated considering cracked stiffness properties, are shown in Figure 2, Left to Right. The first mode is predominantly flexural parallel to axis X ($T = 0.8s$), the second mode is predominantly flexural parallel to axis Y ($T = 0.72s$), while the third is predominantly torsional ($T = 0.64s$).
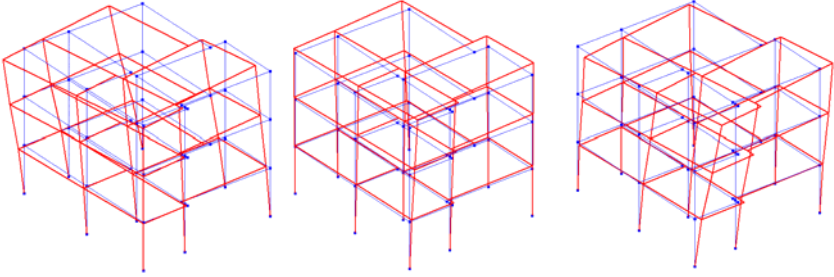

Figure 2. First three modal shapes.

3.1 Modes of Failure and Definition of Collapse

Failure of the structure is defined in terms of the columns failures only. The latter can be either in flexure or in shear. Failure in flexure is defined as the attainment of the ultimate compression strain at the core concrete $\varepsilon_{cc,u}$.

The shear failure mode capacity is given by the shear strength model suggested in Kowalsky 2000, which is chosen since it allows evaluation of capacity under bi-axial loading. The model considers the shear capacity as the sum of three distinct components:

$$V = \left(V_c + V_s + V_p\right) \cdot \varepsilon_V \tag{11}$$

where V_c represents the concrete contribution, V_s the transverse steel contribution, and V_p the axial load contribution to shear resistance, respectively. The expressions for the three contributions are given in fib Bull.24, 2003, where the model, originally calibrated to circular columns, is extensively evaluated finding a mean value of the ratio of experimental to calculated results equal to 0.86 for rectangular sections and a corresponding CoV of 26.1%. A model correction term, ε_V is therefore included in Eq. (11).

Failure of the structure is defined as the series system of the flexural and shear failure modes of all columns.

3.2 Random Variables

Four random variables are considered in this application. These are three material parameters, the concrete strength and ultimate compressive strain, and the steel yield stress, and the model error term in Eq. (11). Mean values and coefficients of variation are reported in Table 1. All random variables are assumed to be log-normally distributed.

Table 1. Characterisation of random variables used in the application

		Mean	CoV
	f_c	25 [MPa]	0.20
Material properties	f_y	450 [MPa]	0.20
	$\varepsilon_{\varepsilon_{cc,u}}$	0.006	0.35
Model uncertainty	ε_V	0.86	0.26

3.3 Seismic Action

Ten rock/stiff soil records are selected from the PEER data base in the magnitude range from 6 to 7 and the distance range from 25 to 60km. The acceleration response spectra of the two orthogonal components of the un-scaled records are shown in Figure 3. The "stronger" component is defined as that having highest spectral acceleration at the effective fundamental period of the structure $T = 0.8s$. In the analysis the stronger component has been applied along direction Y of the building (see Figure 1, Right). For the determination of the fragility the stronger components are all scaled at the same (increasing) intensity, while the weaker ones are kept in the same ratio to the corresponding stronger ones as for the un-scaled records.
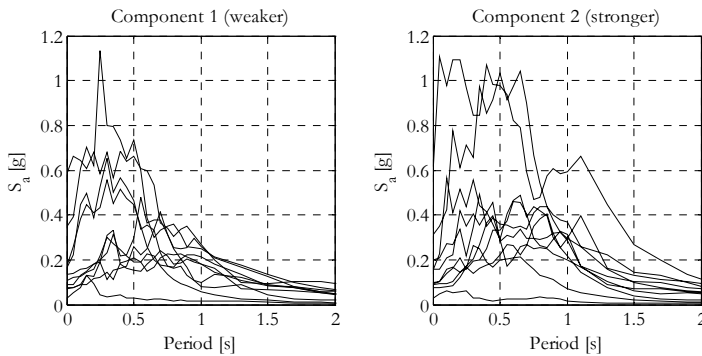
Figure 3. Acceleration response spectra of the 10 selected accelerograms (PEER database: URL: http://peer.berkeley.edu/smtcat).

Details about the ten records selected are reported in Table 2.

Table 2. Recorded accelerograms used in the application

	Name	Date	Station name	M	R	S_a (T=0.8s) [g]	
					[km]	Strong	Weak
1	Friuli	06/05/76	Tolmezzo	6.5	37.7	0.542	0.357
2	Loma Prieta	18/10/89	Apeel 7 Pulgas	7.1	47.7	0.290	0.181
3	Victoria Mexico	09/06/80	Cerro Prieto	6.4	34.8	0.477	0.305
4	Spitak Armenia	07/12/88	Gukasian	7.0	30.0	0.436	0.166
5	Imperial Valley	15/10/79	Cerro Prieto	6.9	26.5	0.415	0.162
6	Coalinga	02/05/83	Parkfield-Vineyard Canyon	6.5	32.3	0.262	0.256
7	Northridge	17/01/94	Sandberg - Bald Mtn.	6.7	43.4	0.255	0.123
8	Friuli, Italia	06/05/76	Barcis	6.5	49.7	0.018	0.032
9	Palm Spring	08/07/86	Santa Rosa Mountain	6.0	55.4	0.113	0.132
10	Kobe	16/01/95	TOT	6.9	57.9	0.378	0.252

3.4   Results

The 3D finite element model of the frame structure is analysed with the PEER structural analysis package OpenSees. Non-linear flexibility-based elements with fibre section discretisation are used for all members. Bi-linear hysteretic steel and Kent-Scott-Park concrete models are employed. P-delta effect is included.

The number of records (10 records) has been established based on past experience. The adequacy of this number for this 3D building subjected to bi-directional excitation in order to provide stable estimates of the statistics of the response needs to be checked. This has been done for a number of response quantities. Figure 4 shows the evolution of mean value and CoV of one of them with the number of records used, for a random ordering of the latter. It is noted that, starting from 6-8 records, both the mean and the CoV estimates become sufficiently stable. The same figure also shows the evolution of one of the several correlation coefficients of the considered response with the other quantities. Stabilisation is achieved in this case with 4-5 records only, but in general 6-8 records are needed.
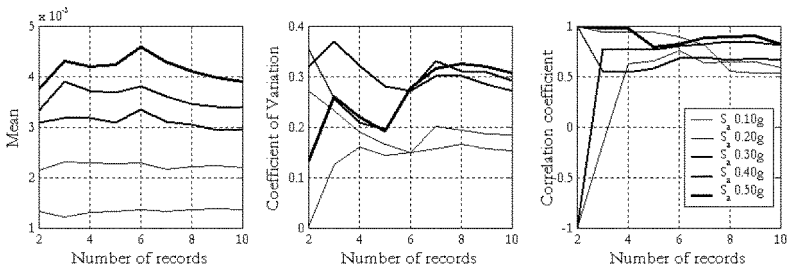

Figure 4. Stability of mean and CoV of one selected demand (concrete compressive strain on a critical column C6, first floor); stability of correlation coefficient of the compressive strain demand in C6 and C4.

228

The variability of the response increases with the seismic intensity and stabilises at around 30% for the higher values. This relatively low variability indicates that the chosen intensity measure, $S_a(T = 0.8s)$, is effective in reducing the ground-motion-induced variability and, hence, the number of records (non-linear analyses) required for a target confidence in the estimates.

The statistics of the demands for all elements, including their mean, standard deviations and correlation coefficients, as well as their derivatives with respect to f_c and f_y, are evaluated from the results of the non-linear analyses, carried out for parametrically increasing values of the seismic intensity.

Figure 5 shows sample results for the flexural and shear demands at the first floor on column C6, which is among those critical in determining the total fragility.
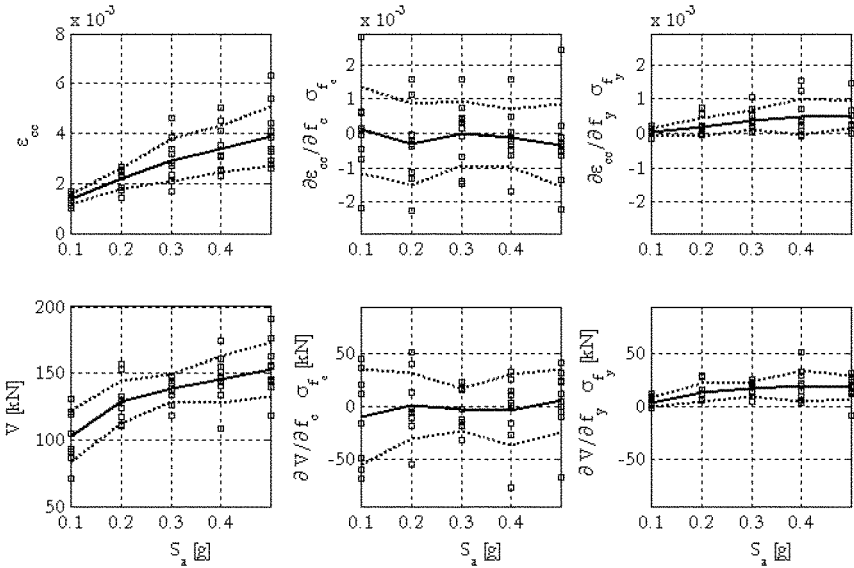
Figure 5. Column C6: maximum concrete strain (above) and shear force (below) versus seismic intensity: demand and sensitivities with respect to f_c and f_y.

The dependence of the flexural demand ε_{cc} is almost linear on the seismic intensity, which confirms, even for this rather complex system, the approximate validity of the equal-displacement rule: for the higher intensity values, in fact, the column is well within the inelastic range. The adjacent plots show the sensitivities of ε_{cc} with respect to f_c and f_y (multiplied by the corresponding standard deviations, in order

229

to allow a quantitative assessment of their relative importance). It can be noted that in fact their influence is almost insignificant in this case, which is another way of confirming that displacement-related response quantities such as ε_{cc} are only weakly dependent on strength-related mechanical parameters.

For what concerns the shear demand, after yielding of the column extremities, as expected the curve tends to flatten. Again, the adjacent plots show the sensitivities of the shear demand with respect to f_c and f_y. While the first one is on the average zero, the second one shows that for a positive variation of the yield stress the increase in shear demand is independent of the PGA value. This is expected, since the variation in shear force due an increase in the yield stress remains constant along the hardening branch.

Finally, it is worth commenting that the sensitivities of the response with respect to the capacity variables $\varepsilon_{cc,u}$ and ε_V have not been computed. This fact comes unavoidably from a limitation of the available analytical tools, which do not allow to account in the course of the analysis for the modification of the response due to the attainment of the capacity in some of the members. Hence, any perturbation in the capacity parameters would go undetected during the analysis, yielding identically zero derivatives.

3.4.1 Fragility Curves

Once the demand variables are statistically determined, reliability analysis can proceed as indicated in Section 2. The most straightforward and accurate way to evaluate the system probability of failure in Eq. (10) is to resort to Monte Carlo simulation. It is recalled that at this stage no more structural analyses are needed and that a trial of the MC simulation simply consists of sampling from the joint distribution of $\mathbf{x}$ (in this case $f_c, f_y, \varepsilon_{cc,u}, \varepsilon_V$) and checking the state of the system. It is worth observing that the evaluation of the entire fragility by MC simulation at this last stage of the procedure usually involves less effort than a single non-linear dynamic analysis.

Figure 6 (Left) contains the fragility curves for the structure, evaluated by Eq. (10), as well as by simpler alternative procedures. In particular, the simplest one is that based on the assumption of independence among the failure modes (Eq. (3)), while in the second alternative the sensitivities are ignored, as suggested by their modest influence on the response (see Figure 5).

One can note that the independence assumption leads to quite different results from the other curves, that are considerably more severe in the upper part of the fragility.

The closeness between curves (a) and (c), i.e., between considering or ignoring the dependence of the demands on $\mathbf{x}$ through the sensitivities, is a further indication that in many cases, such as the present one, the dominant effect is the ground-motion-induced variability, which tends to overshadow that related to structural randomness.
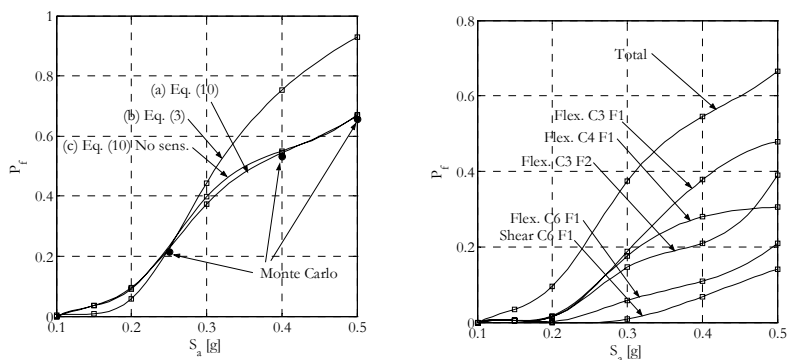
Figure 6. Fragility curves: LEFT (a) full system (b) independent components (c) full system without sensitivities; RIGHT contribution of the main failure modes to the total fragility.

Figure 6 (Left, full circles) also shows a limited validation by "regular" Monte Carlo simulation. It is recalled that this simulation differs from that used to evaluate Eq.(10) in that it requires non linear analyses to be performed for different samples of **x** and associated random selection of a record (from those used for collecting the demand values). The target coefficient of variation of the probability estimate is decreasing with increasing probability, ranging from 0.10 to 0.01, the total number of simulations for all points in the curve being above 5000. The match between simulation results and those from the proposed procedure is quite good.

Finally, Figure 6 (Right) shows the total fragility (Eq.(10)) together with those relative to the most important individual failure modes. This plot gives an important indication of the modes that dominate global failure (flexural in column C3 at the first and second floor, flexural in columns C4 and C6 at the first floor and shear along Y in column C6, first floor).

ACKNOWLEDGEMENTS

REFERENCES

Applied Technology Council (ATC). 1985. Report 13: *Earthquake damage evaluation data for California.* Redwood City, CA.

Au S. K., J. L. Beck. 2003. Subset simulation and its application to seismic risk based on dynamic analysis, *ASCE J. Eng. Mech.* Vol.129(**8**):901-917.

Cornell A. C., F. Jalayer, R. Hamburger, D. Foutch. 2002. The probabilistic basis for the 2000 SAC/FEMA steel moment frame guidelines. *ASCE J. Eng. Mech.* 128(**4**):526-533.

Federation international du Bêton (*fib*). 2003. Bulletin 24: "Seismic assessment and retrofit of reinforced concrete buildings" prepared by Task Group 7.1. Lausanne, Switzerland.

Franchin P., A. Lupoi, P. E. Pinto, M. I. J. Schotanus. 2004. Seismic fragility analysis of RC structures: use of response surface for a realistic application, in *Proceedings of 13th World Conf. Earthq. Eng.* Vancouver, B.C., Canada, Aug.1-6.

Franchin P. 2004. Reliability of uncertain inelastic structures under earthquake excitation. *ASCE J. Eng. Mech.* Vol.130(**2**):180-191.

Gardena P., K. M. Mosalam, A. Der Kiureghian. 2003. Probabilistic seismic demand models and fragility estimates for RC bridges. *J. Earthq. Eng.* Vol.7 (special Issue 1):79-106.

Kleiber M., H. Antùnez, T. Hien, P. Kowalczyk. 1997. Parameter sensitivity in nonlinear mechanics: theory and finite element computations. John Wiley & Sons, NY.

Kowalsky M .J., M. J. N. Priestley. 2000. Improved analytical model for shear strength of circular reinforced concrete columns in seismic regions. *ACI Struct. J.*, Vol.97(**3**):388-396.

Negro P., E. Mola, J. F. Molina, G. E. Magonette. 2004. Full-scale bi-directional Pad testing of a torsion ally unbalanced three-storey non-seismic RC frame. *In Proc. of the 13th World Conference on Earthquake Engineering,* Paper N. 968. Vancouver, Canada, August.

Shinozuka M., M. Q. Fang, J. Lee, T. Magnum. 2000. Statistical analysis of fragility curves. *ASCE J. Eng. Mech.* Vol.126(**12**):1224-1231.

Singhal A., A. Kiremidjian. 1998. Bayesian updating of fragilities with application to RC frames. *ASCE J. Struct. Eng.* Vol. 124(**8**):922-929.

SOME DEVELOPMENTS ON PERFORMANCE-BASED SEISMIC DESIGN OF MASONRY STRUCTURES

Sergio M. ALCOCER[1], Juan G. ARIAS[2] and Leonardo E. FLORES[3]

ABSTRACT

Performance-based earthquake engineering aims at improving the seismic-risk decision-making process through assessment and design methods such that a building attains specific levels of performance under given specified earthquake demands. Masonry design and construction have been traditionally developed on an empirical basis; until recently, improvements had been attained through a trial-and-error process, more than through rigorous mechanics principles and models. Current prescriptive assessment and design methods fail to describe most common limit states accepted for structures made of other materials. In this paper, current design practices and new approaches under development, based on experimental data from static and dynamic tests, are presented. To assess the seismic performance of typical Mexican confined masonry houses, results of a series of shaking table underway are included. A performance criteria and a simple analytical model, aimed at predicting the nonlinear response of masonry structures, are introduced. Measured and calculated responses are compared to evaluate the adequacy of modeling assumptions. Differences indicate the need of improvement of nonlinear modeling of complex confined masonry walls.

Keywords: Confined masonry; Walls; Design; Limit states; Testing; and Evaluation.

1. INTRODUCTION

1.1 Housing in Mexico

As many other countries, Mexico experiences a very large housing deficit that has accumulated over decades. Limited economic growth and scarce financial incentives in the country have been two of the primary reasons for the estimated 4.3 million houses that need to be either built or refurbished. Although the deficit is concentrated in urban areas, rural villages experience much of the same problems, but with more

---

[1] *Director, Institute of Engineering, UNAM, Apartado Postal 70-472, Mexico DF, 04510, salcocem@iingen.unam.mx*

[2] *Research assistant, Institute of Engineering, UNAM, Apartado Postal, 70-472, Mexico DF, 04510, jara@iigen.unam.mx*

[3] *Researcher, National Center for Disaster Prevention, CENAPRED, Av. Delfin Madrigal 665, Mexico DF, 04360, lfc@cenapred.unam.mx*

limited possibilities of overcoming the situation due to a more constrained economical position.

The structural system most widely used consists of load-bearing masonry walls with cast-in-place (or prefabricated) reinforced concrete (RC) slabs. Confined masonry is the preferred masonry system in Mexico, used to build houses ranging from low-cost to expensive and architecturally sophisticated residences. Confined masonry walls are confined vertically and horizontally with tie-columns, TCs, and bond beams, BBs, respectively. In Mexican buildings, such elements have very small cross-sectional dimensions, typically equal to the wall thickness. Confining elements are intended to tie structural walls and floor/roof systems together, and to improve wall energy dissipation and deformation capacities. When properly designed and detailed, an increase in lateral strength can be quantified. Walls are built with handmade or industrialized brick units, which may be made either of cement or clay, and which may be solid or hollow; handmade solid clay units prevail.

1.2 Earthquake Performance of Confined Masonry Houses

Seismic behavior of masonry buildings in Mexico City has been generally satisfactory due to the low drift and acceleration demands in the soft-soil area, where most of construction is located, because of the distinctly different fundamental period of vibration of the buildings as compared to the fundamental frequency of the ground motion. In near-epicentral regions, however, large damages have been observed during strong ground shaking in inadequately confined masonry structures. In contrast, well-confined masonry structures, with a reasonable symmetric wall layout, have shown excellent performance, with no damage even in brittle finishes. Loss estimations after recent earthquakes (Alcocer et al., 2001; Lopez et al., 2001) indicated that approximately one-third of the total losses, including direct and indirect losses, have occurred in the housing sector. Loss estimations after disasters are quite recent in Mexico, and information is not detailed enough to differentiate between structural and non-structural damages.

1.3 Research Significance

Any effort to improve performance, through the development of design and assessment methodologies, and by tailoring capacities (structural and nonstructural) to seismic hazard regions in the country (demands), is well justified, from the social and economical stand point, because: (1) important differences are observed in the structural design criteria used in housing projects (e.g., ratios of ultimate strengths to design loads); (2) in some cases, architectural considerations are of primary importance whereas structural and nonstructural performances are unimportant; (3) 70% of the housing construction does not comply with construction codes and is developed without the participation of trained engineering professionals (Meli and Alcocer, 2004); and (4) a house is the most important and cherished family asset. In

this paper, initial results of a research underway aimed at evaluating the seismic performance of masonry structures is presented.

2. SEISMIC DESIGN OF CONFINED MASONRY CONSTRUCTION

2.1   Seismic Behavior

Seismic behavior of confined masonry walls has been studied through quasi-static cyclic loading and via shaking table tests. Recently, cyclic loading experiments have been conducted on full-scale isolated walls and on 2D and 3D wall subassemblages. Typically, in such tests a drift-controlled cyclic program, with monotonically-increasing drift amplitudes, has been applied. Variables studied have included walls aspect ratio, wall flexural coupling (i.e., flexural-to-shear capacity ratio), wall vertical stresses applied to simulate gravity loads, type of unit (e.g., handmade solid clay, industrialized multiperforated clay, semi-industrialized cement), type of mortar, TC detailing (e.g., percentage of transverse reinforcement), percentage of horizontal reinforcement along the mortar joints, and the size of a welded wire fabric connected to the walls. Details of recent experimental programs and test results can be found elsewhere (Aguilar, 1996; Alcocer and Meli, 1995; Alcocer, 1996; Alcocer et al., 1996; Alcocer and Zepeda, 1999). Shaking table tests have been carried out on small scale specimens (Alcocer and Muria, 2000; Alcocer et al., 2004). Recently, half scale one-, two- and three-story structures, which represented a prototype structure, were tested under recorded and artificial ground motions that represented credible earthquakes probable to occur on the Mexican Pacific coast.

Typical hysteresis curves of confined masonry walls with and without horizontal reinforcement along the mortar joints are shown in Fig. 1. Initial behavior is linear elastic until first inclined masonry cracking occurs. With further cycling at higher drift levels, cracking concentrates near the diagonals (mainly in a wide, single crack) thus dividing the wall into triangular blocks limited by the main cracks. At this stage, wall stiffness has considerably decayed and strength (maximum load) is provided by friction and brick/block interlock, and through shear resistance of TC's ends. After this stage, shear degradation of wall strength takes place because of brick crushing and spalling, and of shearing off of the TC ends. Confined masonry walls horizontally reinforced with high-strength deformed wires generally exhibits a superior behavior in terms of strength, energy dissipation and deformation capacity. At wall strength, an array of widely distributed, fine cracking, suggests the formation of a diagonal compression field, which is balanced, in the horizontal direction, by forces resisted by the wires.

2.2   General Requirements for Analysis and Design

Mexican masonry standards allow the use of a simplified method of analysis to distribute the earthquake-induced lateral loads among the walls in symmetric and

buildings, up to five stories high (Gobierno, 2004). For all cases, an equivalent static lateral force analysis and/or a modal analysis are specified. Details on analysis requirements can be found elsewhere (Alcocer et al., 2003; Gobierno, 2004).
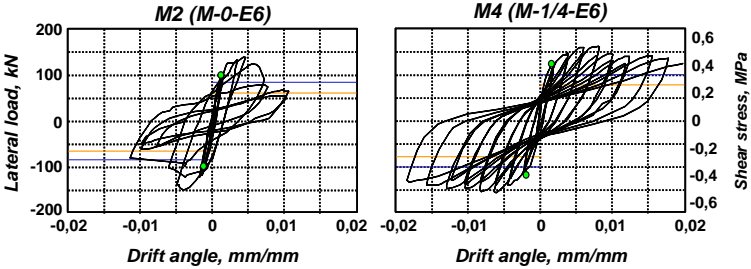

**Figure 1. Typical hysteresis curves of confined masonry walls without and with horizontal reinforcement.**

In structures analyzed with methods other than the simplified method, inelastic interstory drifts shall be checked. These values are calculated through multiplying the elastic drift angles, obtained in the analysis from a reduced set of lateral forces, by the seismic behavior factor, Q. The seismic behavior factor Q is equal to 2 for confined masonry walls built with solid units or with multiperforated bricks with horizontal reinforcement and exterior tie-columns; 1 for unreinforced masonry; and 1.5 for other cases. Calculated inelastic drift angles shall not exceed allowable values, which were derived from experimental results, and are intended to be consistent with a moderate level of damage, generally accepted in Mexico as a desirable performance of housing under the design earthquake. For example, for confined masonry walls built with solid units, allowable inelastic lateral drift angle is 0,0025.

Masonry standards prescribe the spacing of TCs and BBs, as well as their reinforcement detailing (Fig. 2). The masonry contribution to shear strength is calculated from Eq. 1, in which FR is the strength reduction factor, AT is the wall transverse area, and P is the vertical load acting on the wall. This equation is intended to predict the shear force at first diagonal cracking, and was calibrated from experimental results.

$$V_{mR} = F_R (0.5 v_m^* A_T + 0.3 P) \leq 1.5 F_R v_m^* A_T \tag{1}$$

The contribution of the horizontal reinforcement to shear strength is determined from Eq. 2, in which η is an efficiency factor (see Fig. 3), p_h is the percentage of horizontal reinforcement, and f_{yh} the specified yield stress of the horizontal reinforcement. In this regard, "horizontal reinforcement" refers to steel wires embedded along the joint mortar and also refers to the horizontal wires of a steel welded wire mesh properly anchored to the masonry and covered with a cement-based mortar.

$$V_{sR} = F_R \, \eta \, p_h \, f_{yh} \, A_T \tag{2}$$

Figure 2. Confined masonry requirements.
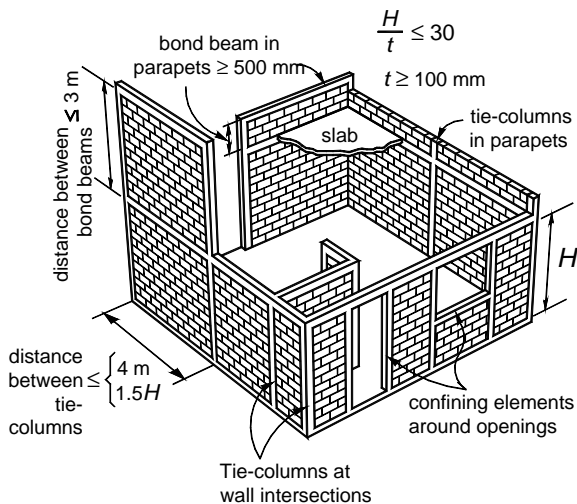
The efficiency factor η was derived from experimental data (Aguilar 1996, Alcocer 1996b, 1999). This factor corresponds to that recorded at the allowable inelastic lateral drift discussed before. The upper limit on ph is related to the masonry crushing strength. The lower limit corresponds to the percentage of horizontal steel needed to maintain the strength at first diagonal cracking.

3. ANALYTICAL MODEL FOR CONFINED MASONRY

A hysteretic model intended to perform nonlinear dynamic analyses was developed and calibrated from tests carried out on full scale wall structures (Flores and Alcocer, 1996). The model is applicable to confined masonry walls built with handmade clay bricks and cement mortar, with or without horizontal reinforcement. The envelope curve follows a tri-linear backbone curve where first inclined cracking, strength and ultimate strength (and their corresponding drift angles) are key engineering parameters in its definition. The hysteresis model follows stiffness decay rules for the loading and unloading branches. To obtain the best-fit curve, measured stiffness of the loading and unloading branches in the experimental hysteresis loops were normalized by the measured initial stiffness.

Measured stiffnesses were obtained as the slope of the secant drawn from the point with zero load of the previous half-cycle to the peak in the next half-cycle. Initial stiffness was the slope of the secant line drawn at a point where the slope of the envelope curve changes significantly.
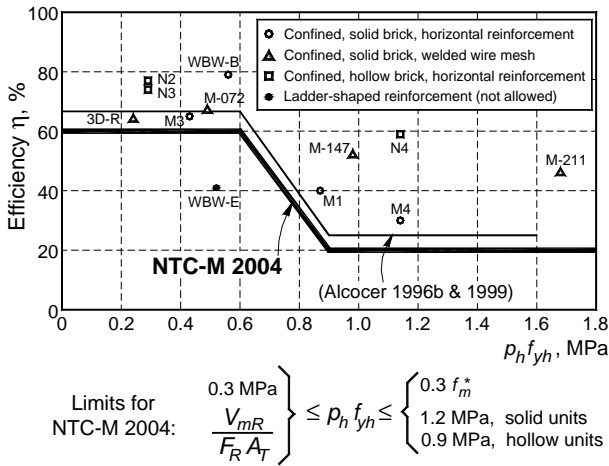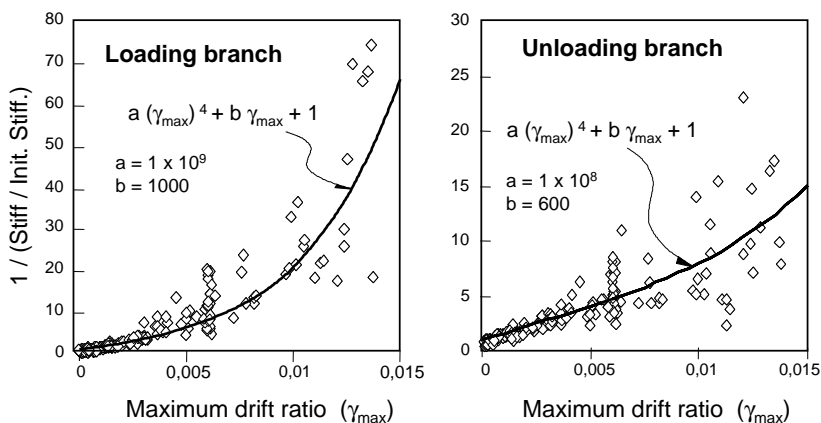
Figure 3. Efficiency factor of horizontal reinforcement for contributing to wall shear strength.

The normalized stiffness degradation curves for the loading and unloading branches, for confined masonry walls without horizontal reinforcement, and the best-fit curve of the data are shown in Fig. 4. According to the model proposed, loading stiffness is constant until reaching the envelope. If higher drifts are imposed, the loading branch will follow the envelope. To compute the stiffnesses for the loading and unloading branches for the next half-cycle, the maximum drift angle reached must be recorded. This implies that stiffness decay in the loops will not be calculated if the drift ratios were smaller than a value reached before. Calibration criteria and results can be found elsewhere (Flores and Alcocer, 1996).

4. SEISMIC PERFORMANCE EVALUATION OF CONFINED MASONRY STRUCTURES

4.1   Performance Criteria for Masonry Structures

Based on experimental results and damage observations in the laboratory and in the field, performance criteria for confined masonry structures made of solid clay units are suggested (Table 1). Three limit states were identified, namely, serviceability, reparability and safety.

Figure 4. Normalized stiffness degradation curves for the loading and unloading branches.

The serviceability limit state is associated to the onset of masonry inclined cracking, which typically occurs at drift angle of the order of 0,15%. Such value is quite variable, depending upon the type of masonry unit, wall flexural-to-shear capacity ratio, among other factors. Evidently, at this state, damage is minor. For the reparability limit state, it was decided to associate it to the formation of the full inclined cracking, and the penetration of such cracking into TC ends. It has been observed in the lab that the residual crack width at such limit state is of the order of 2 mm, and that a drift angle is approximately 0,25%. The safety limit state corresponds to wall shear strength, typically characterized by large masonry cracks (with a residual width of 5 mm) and considerable damage at TC ends. Damage in TC occurs in the form of yielding of TC longitudinal reinforcement due to shearing and onset of cracking crushing and spalling.

Performance criteria presented in Table 1 were developed keeping in mind the need for repair of a masonry structure after a moderate-to-severe event (reparability limit state). In this regard, three basic repair methods were considered: injection of an adhesive component (epoxy or Portland cement-based materials); jacketing (mortar overlays reinforced with welded wire meshes, or composite overlays); and placement of additional horizontal reinforcing bars within mortar joints. Rehabilitation techniques where made consistent with the damage and structural response (Fig. 5).

Table 1. Performance criteria for confined masonry structures with solid clay units

Limit state	Criterion	Residual crack width, mm	Drift angle, %
Serviceability	Onset of masonry inclined cracking (cracking strength)	0,1	0,15
Reparability	Inclined cracking fully formed over masonry wall; hairline cracking into tie-columns; onset of masonry crushing	2	0,25
Safety	Shear strength of wall; wall cracking penetrates into tie-column ends; yielding of tie-column reinforcement due to shearing; onset of tie-column crushing	5	0,40
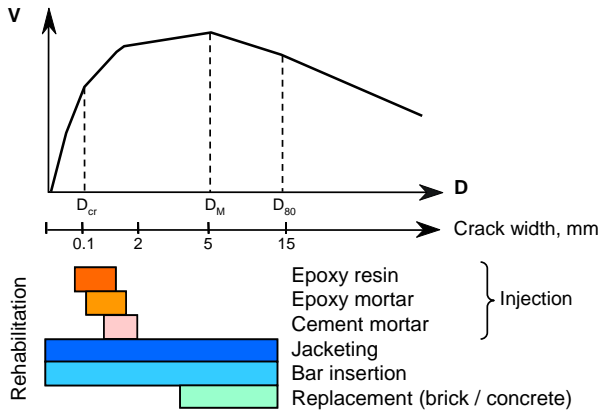
Figure 5. Typical rehabilitation schemes considered for confined masonry structures.

4.2 Seismic Evaluation through Shaking Table Tests

In order to assess the seismic performance of typical confined masonry houses, as well as to evaluate the performance criteria and the analysis model developed, a series of shaking table tests have been carried out. Details of the testing program and main results can be found elsewhere (Alcocer et al., 2004). Specimens were half-scale models of one- (M1) and three-story (M3) houses constructed in Mexico. Walls were made of hand-made solid clay bricks. Dimensions and wall layout of M3 are shown in Fig. 6. Two earthquake motions recorded in epicentral regions in Mexico were used as basis for the testing program. One was the motion recorded in Acapulco, Guerrero,

in April 25, 1989, during a M=6,8 earthquake with PGA=0,34g. The other was that recorded in Manzanillo, Colima, in October 10, 1995, during a M=8,0 quake with PGA=0,40g. Both records were considered as Green functions to simulate larger magnitude events (i.e., with larger instrumental intensity and duration). For the Acapulco record, earthquakes with magnitudes 7.6, 7.8, 8.0 and 8.3 were simulated, whereas for the Manzanillo record, earthquakes with magnitudes 8.1, 8.2 and 8.3 were simulated. Final pattern of cracking is also shown in Fig 6.
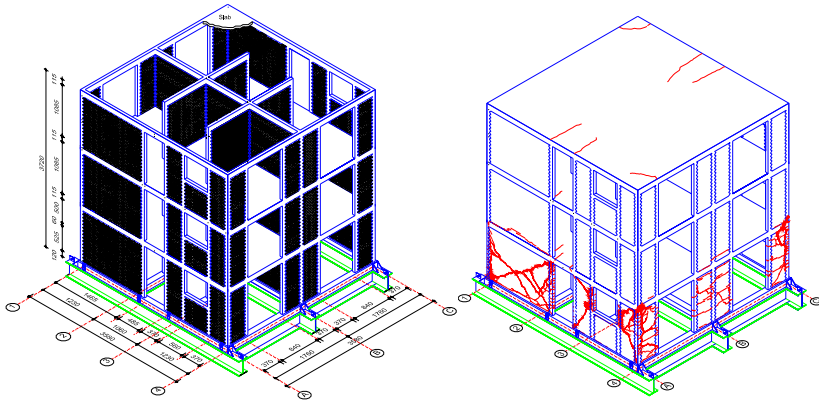
Figure 6. Geometry and final crack pattern of the 3-story specimen.

The envelope curve for M3 is shown in Fig. 7. Different markers were used depending on the specimen wall layout. Square markers correspond to the specimen with the original wall layout. For this structure, the wall density index was 4,1 percent. The wall density index was calculated as the ratio of the wall area in the direction of loading and the floor plan area. Round markers relate to the specimen response after walls indicated in the figure were removed, thus leading to a lower wall density index (2,9 percent). Wall removal in the middle axis evidently modified the trend of the envelope curve. In an effort to visualize a possible envelope should the original wall index had been kept constant, envelope values for the modified specimen were affected by the ratio of the wall density indexes, namely, 4,1 / 2,9=1,4. The envelope of this virtual specimen is shown with triangles. After comparing the envelope curves of the one- and three-story specimens, as well as the force and drift ratio values for the three limit states identified, it is apparent the similitude in the response. The latter supports the idea that the performance of the three-story structure, M3, was controlled by the first story which, in turn, was governed, as in M1, by shear deformations.

Because the analytical model strongly relies on the stiffness degradation curve, the stiffness decay was assessed through calculating the cycle stiffnesses, K_p at representative cycles. Normalized peak-to-peak stiffness - first story drift ratio curves for M1 and M3 models are shown in Fig 7. The peak-to-peak stiffnesses were normalized with respect to the initial stiffness of M1 and M3. Stiffness decay was observed at low drift ratios, even before first inclined cracking became apparent. This phenomenon is attributed to incipient wall flexural cracking, and perhaps, to some micro-cracking (invisible to the naked eye) in masonry materials, local loss of mortar bond and adjustment of brick position. After first inclined cracking, but before reaching strength, the decay increased with drift ratio. At larger drift ratios, K_p remained nearly constant. At this stage, stiffness decay is associated to cracking and crushing in masonry walls and RC confinement members. Also shown in the graph is the stiffness decay trend measured in static cyclic testing (shown with markers only). It is apparent the difference in the rate of stiffness decay among specimens tested dynamically and statically. This difference must be taken into account when revising the hysteresis model in the future.
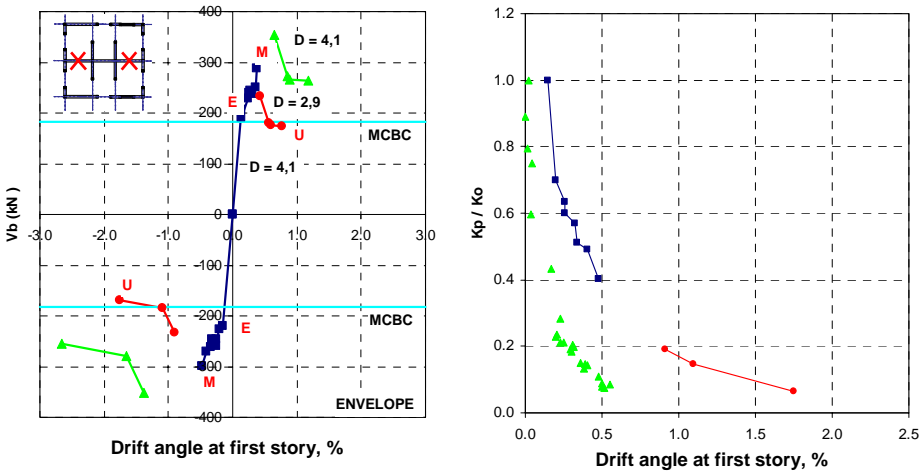
Figure 7. Envelope curve of M3, and stiffness degradation curves of M1, M3 and static tests (shown with markers).

4.3 Comparison between Measured and Calculated Response

Measured response from the shaking table tests were compared to calculated responses using the abovementioned hysteretic model (still using the stiffness decay rule derived from static tests). For modeling purposes, it was assumed that inelastic behavior in the structure was concentrated at the ground story and that shear deformations (shear plastic hinge) would control the response. These features have been observed in the field, and were corroborated during the shaking table tests.

Calculated and measured responses, in terms of base shear and first story drift angles, for M3 model and for the M8.3 artificial ground motion are presented in Fig. 8. It is apparent that a good agreement was reached in the base shear response, but some differences were noted in the drift response. Evidently, such difference indicates the need to improve the nonlinear modeling of complex confined masonry, with emphasis on better capturing the effect of confinement, especially at large drift angles, and of perpendicular walls.
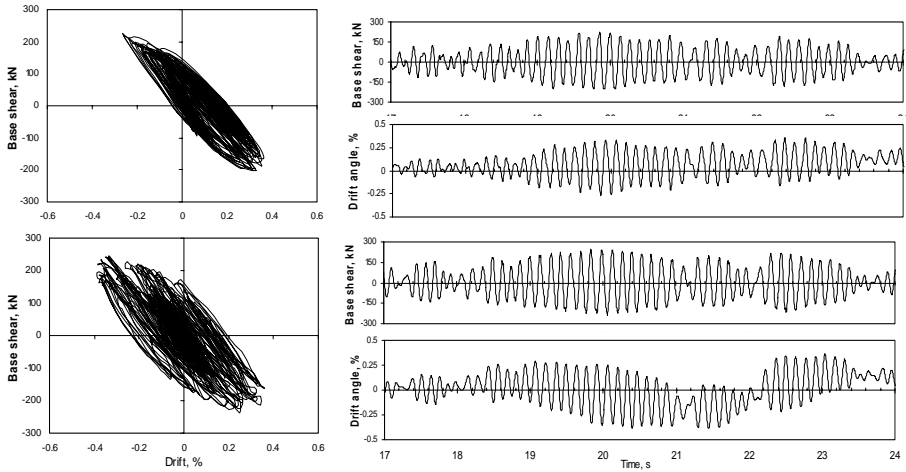
Figure 8. Calculated (top) and measured responses of M3.

5. CONCLUDING REMARKS

To assess the seismic performance of typical Mexican confined masonry houses, a series of shaking table tests are underway. A series of recorded and artificial ground motions, consistent with the seismic hazard of the Mexican Pacific coast, were used as input. Engineering design parameters have been developed and have been compared to experimental results. Aimed at predicting the nonlinear response of masonry structures, a simple analytical model has been developed from static cyclic tests. With this model, the response of the models tested at the shaking table was calculated. Comparisons of the measured and calculated responses indicated good agreements in base shear, but some differences in drift. This difference indicates the need to improve the nonlinear modeling of complex confined masonry, with emphasis on capturing the rate effect on stiffness decay, as well as the effect of confinement and of perpendicular walls.

ACKNOWLEDGEMENTS

REFERENCES

Aguilar, G., R. Meli, R. Diaz, R. Vazquez-del-Mercado (1996). Influence of horizontal reinforcement on the behavior of confined masonry walls. *Proceedings 11WCEE*, paper no. 1380.

Alcocer, S . M., and R. Meli (1995). Test program on the seismic behavior of confined masonry structures. *The Masonry Society Journal*, 13 (2): 68-76.

Alcocer S. M. (1996). Implications derived from recent research in Mexico on confined masonry structures. *Proceedings CCMS Symposium*, 82-92.

Alcocer S. M., J. A. Pineda, J. Ruiz, and J. A. Zepeda (1996). Retrofitting of confined masonry walls with welded wire mesh. *Proceedings 11WCEE,* paper no. 1471.

Alcocer S. M., and J. A. Zepeda (1999). Behavior of multi-perforated clay brick walls under earthquake-type loading. *Proceedings 8NAMC*.

Alcocer, S. M., and D. Muria-Vila (2000). Ensayos en mesa vibradora de sistemas de muros de mampostería confinada a escala 1:3. *Información Tecnológica*, 11-5, 113-122.

Alcocer S. M., G. Aguilar, L. Flores, D. Bitran, R. Duran, O. A. López, M. A. Pacheco, C. Reyes, C. M. Uribe, and M. J. Mendoza (2001). *The June 15, 1999 Tehuacán earthquake* (in Spanish). Mexico City: Centro Nacional de Prevención de Desastres, ISBN 970-628-601-2.

Alcocer S. M., J. Cesin, L. E. Flores, O. Hernandez, R. Meli, A. Tena, and D. Vasconcelos (2003). The new Mexico City building code requirements for design and construction of masonry structures. *Proceedings 9NAMC*.

Alcocer, S. M., J. G. Arias and A. Vazquez (2004). Response assessment of Mexican confined masonry structures through shaking table tests. *Proceedings 14WCEE,* paper no. 2130.

Flores, L. E., and S. M. Alcocer (1996). Calculated response of confined masonry structures. *Proceedings 11WCEE,* paper no. 1830.

Gobierno del Distrito Federal (2004). *Normas Técnicas Complementarias para Diseño y Construcción de Estructuras de Mampostería* (in Spanish), Mexico City: Gobierno del Distrito Federal.

Lopez O. A., C. Reyes, R. Duran, D. Bitran, and J. Lermo (2001). *The September 30, 1999 Oaxaca earthquake* (in Spanish). Mexico City: Centro Nacional de Prevención de Desastres, ISBN 970-628-609-8.

Meli, R., and S. M. Alcocer (2004). Implementation of Structural Earthquake-Disaster Mitigation Programs in Developing Countries. *Natural Hazards Review*, 5-1, ISSN 1527-6988, 29-39.

DISPLACEMENT BASED SEISMIC DESIGN AND PERFORMANCE EVALUATION TESTS OF A FULL-SCALE BRB COMPOSITE FRAME

K.C. Tsai[1], Y.T. Weng[2], M.L. Lin[3], C.H. Chen[3] and P.C. Hsiao[4]

ABSTRACT

This paper introduces a full-scale 3-story 3-bay CFT buckling restrained braced (CFT/BRB) frame specimen tested recently in the Taiwan National Center for Research on Earthquake Engineering using pseudo dynamic test procedures and internet testing techniques. The test frame was loaded to simulate the responses under ground motions corresponding to earthquake hazards for a highly seismic location with 50%, 10%, and 2% chance of exceedance in 50 years. The frame specimen was designed by displacement-based seismic design (DSD) procedures considering a target inter-story drift limit of 0.025 radian for the 2% in 50 years hazard level. This paper summarizes the analytical studies made before and after the tests and evaluates the frame performance. CFT/BRBF performed extremely well after the application of six earthquake load effects. Very minor changes on stiffness and damping were observed as evidenced from the free vibration tests conducted after each earthquake pseudo dynamic test. The peak story drift reached 0.023 radian at the first story after applying the 2/50 design earthquake on the specimen. Tests confirmed that the DSD procedure adopted in the design of the specimen is effective in limiting the ultimate story drift. Tests also confirmed that the response of the CFT/BRB frame can be satisfactorily predicted by using either OpenSees or PISA3D.

Keywords: Concrete filled tube (CFT); Buckling restrained brace (BRB); Passive control; Displacement-based seismic design; Networked pseudo dynamic test; Nonlinear analysis.

1. INTRODUCTION

In October 2003, a full-scale 3-story 3-bay CFT column with the buckling restrained braced composite frame (CFT/BRBF) specimen (Fig. 1) was tested in a Taiwan-US-Japan Cooperative Research Program (Tsai et al. 2004, Chen et al. 2004, Lin et al. 2004). The 3-story prototype structure is designed for a highly seismic location either in Taiwan or United States. The typical bay width is 7m and typical story height is 4m. The total height of the frame, including the footing, is about 13m. The 2.15 meters wide concrete slab is adopted to develop the composite action of the beams. Measuring 12 meters tall and 21 meters long, the specimen is among the largest frame

tests of its type ever conducted. The frame was tested using the pseudo-dynamic test procedures applying input ground motions obtained from the 1999 Chi-Chi and 1989 Loma Prieta earthquakes, scaled to represent 50%, 10%, and 2% in 50 years seismic hazard levels. Following the pseudo-dynamic tests, since none of the brace was fractured, quasi static loads were applied to cyclically push the frame to large inter-story drifts up to the failure of the braces. Being the largest and most realistic composite CFT/BRB frame ever tested in a laboratory, the tests have provided a unique data set to verify both computer simulation models and seismic performance of CFT/BRB frames. This experiment also provides great opportunities to explore international collaboration and data archiving envisioned for the Networked Earthquake Engineering Simulation (NEES) program and the Internet-based Simulations for Earthquake Engineering (ISEE) (Wang et al. 2004) launched recently in USA and Taiwan, respectively. This paper describes the analytical predictions and the experimental results, and evaluates the seismic performance of the frame specimen. Inelastic static and dynamic time history analyses were conducted using PISA3D (Lin and Tsai 2003) and OpenSees (Open System for Earthquake Engineering Simulation), developed at National Taiwan University and Pacific Earthquake Engineering Research Center (PEER), respectively.

2. A FULL SCALE CFT/BRB COMPOSITE FRAME

The 3-story CFT/BRB frame shown in Fig. 1 is employed in this experimental research. The prototype three-story building consists of 6-bay by 4-bay in plane. In the two identical prototype CFT/BRB frames, only the two exterior beam-to-column joints (Fig. 1) in each floor are moment connections, all other beam-to-column connections are assumed not to transfer any bending moment. The BRBs are installed in the center bay. Square CFT columns are chosen for the two exterior columns while the center two columns are circular CFTs. Story seismic mass is 31.83 ton for the 1st and 2nd floors, 25.03 ton for the 3rd floor for each CFT/BRB frame (half of the building). The material is A572 Gr.50 for all the steel beams and columns, while the compression strength *fc'* of the infill concrete in CFT columns is 35MPa. In all the analyses, the material's strength for steel and concrete is based on the actual strength obtained from the material tests. The supporting beams above the BRBs satisfy the capacity design principle considering the strained hardened BRBs and an unbalanced vertical load resulted from the difference of the peak BRB compressive and tensile strengths. The fundamental vibration period is about 0.68 second. Three different types of moment connections, namely through beam, external diaphragm and bolted end plate types, varying from the first floor to the third floor were fabricated for the exterior beam-to-column connections. Three types of BRBs, including the single-core, double-cored and the all-metal BRBs, were adopted in the three different floors. In particular, two single-cored unbonded braces (UBs), each consisting of a steel flat plate in the core, were donated by Nippon Steel Company and installed in the second floor. Each UB end to gusset connection uses 8 splice plates and 16-24mmϕ F10T

bolts. The two BRBs installed in the third story are double-cored constructed using cement mortar infilled in two rectangular tubes (Tsai et al. 2002) while the BRBs in the first story are also double-cored but fabricated with all-metal detachable features (Tsai and Lin 2003). Each end of the double-cored BRB is connected to a gusset plate using 6- and 10-24mmφ F10T bolts at the third and first floor, respectively. No stiffener was installed at the free edges of any gusset before the testing.
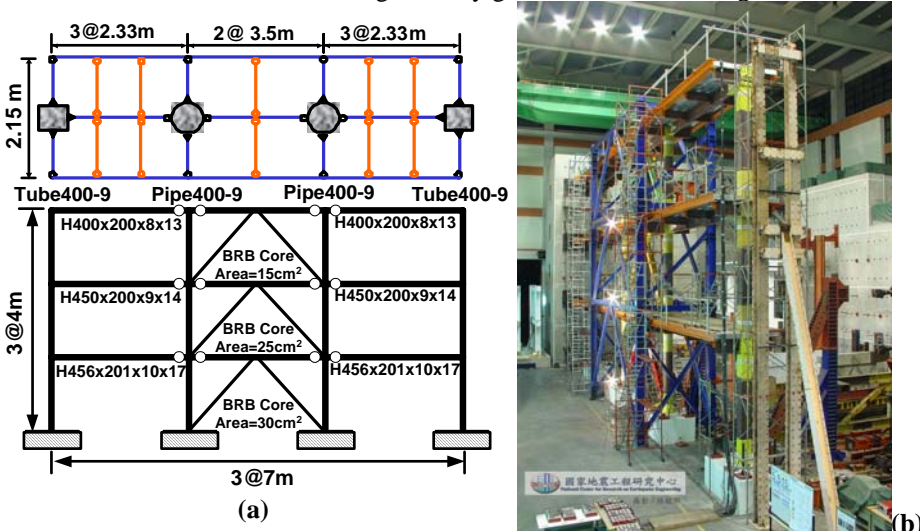

Figure 1. (a) Plan and elevation of the full-scale CFT/BRB composite frame (b) Photo of the CFT/BRB test frame.

3. DESIGN PROCEDURE FOR A CFT/BRB FRAME

The design procedures (Tsai et al. 2004) adopted for the CFT/BRBF consist of the following steps: (1) Select an initial desired displaced shape for the structure, (2) Determine the effective displacement by translating the actual MDOF structure to the substituted SDOF structure, (3) Estimate system ductility from the properties of BRB members, (4) Determine the effective period of the substituted SDOF structure from an inelastic design displacement spectrum, (5) Compute the effective mass, effective stiffness, and design base shear, (6) Distribute the design base shear over the frame height, (7) Design the members for the CFT/BRB frame. There are some key points in these steps described above. First, the story drift θ_{yi} corresponds to the brace yielding can be estimated as:

$$\theta_{yi} = 2 \cdot \varepsilon_{cy} / \gamma \cdot \sin 2\phi \qquad (1)$$

where ε_{cy} is the yielding strain of the brace center cross section, γ is the ratio between a specific elastic axial strain of the brace center segment and the corresponding elastic averaged strain of the entire brace (computed from the brace

end work-point to work-point). And ϕ is the angle between the horizontal beam and the brace. Thus, if θ_{mi} is the target drift of the ith story calculated from the target displacement profile, then the story ductility can be computed from:

$$\mu_i = \theta_{mi} / \theta_{yi} \tag{2}$$

After calculating all the story ductilities from Eq. 2, the average of all story ductilities is taken as the system ductility. Second, the beam framing into the braces are designed by capacity design principle. This requires the consideration of the horizontal brace force components as beam axial loads and the flexural demand resulted from a vertical unbalanced concentrated force of $0.1\,\Omega_h P_y sin\,\phi$ acting upward at the center of the beam span as depicted in the free body diagram Fig. 2. Noted that P_y is the nominal tensile yield strength of brace, the factor of 0.1 considers the 10% difference between the peak compressive and tensile strengths, and Ω_h represents the effects of strain hardening. Applying LRFD specifications:

$$P_u /(\phi_c P_n) \geq 0.2 : P_u /(\phi_c P_n) + \frac{8}{9} M_u / \left[\left(1 - \frac{P}{P_e}\right) \phi_b M_n \right] \leq 1.0 \tag{3}$$

where $P_n = F_{cr} A_g$, $P_e = \dfrac{\pi^2 EI}{(kl)^2}$, $\phi_c = 0.75$ (*tension*) or 0.85 (*compression*), $\phi_b = 0.9$

Note that the bottom beam flange is not laterally braced except by transverse beams at the center point of span. Accordingly, P_n and M_n in Eq. 3 are conservatively computed (without considering the effects of the concrete slab) from an unbraced length of 3.5 m for the capacity design of left beam segment shown in Fig. 2.
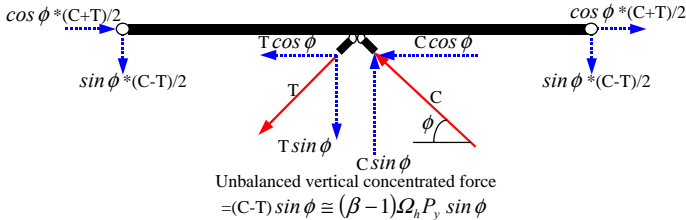

Figure 2. Free body diagram of a beam supporting the BRBs.

The final selections of structural members are given in Table 1.

Table 1. Selection of member sizes and grades

Member	Beam Sizes and Core Cross Sectional Area of Braces (A572 GR50)		
Location	1FL	2FL	3FL
Beam (mm)	H456×201×10×17	H450×200×9×14	H400×200×8×13
Brace (cm^2)	30	25	15
Dimension of Columns (A572 Gr.50) unit : mm	CFTs: C1: Tube: 350×9, C2: Pipe: 400×400×9		

4. EXPERIMENTAL PROGRAM

Figures 3a and 3b consider Taiwan seismic code draft updated in 2002. It stipulates, for a hard rock site, the $S_a(T=1 \text{ sec})$ values for earthquake hazard of 10% chance of exceedance in 50 years (10/50 Design Earthquake, DE) and 2/50 (Maximum Considered Earthquake, MCE) earthquakes as 0.68g and 0.91g, respectively. The 5% damped S_a values for TCU082EW records are also shown on Figs. 3a and 3b. The corresponding PGA values for the 10/50 and 2/50 levels of excitations are 0.46g and 0.62g, respectively, for the TCU082EW record. Similarly, for the LP89g04NS record, the corresponding PGA values for the 10/50 and 2/50 levels of excitations are 0.40g and 0.54g, respectively.
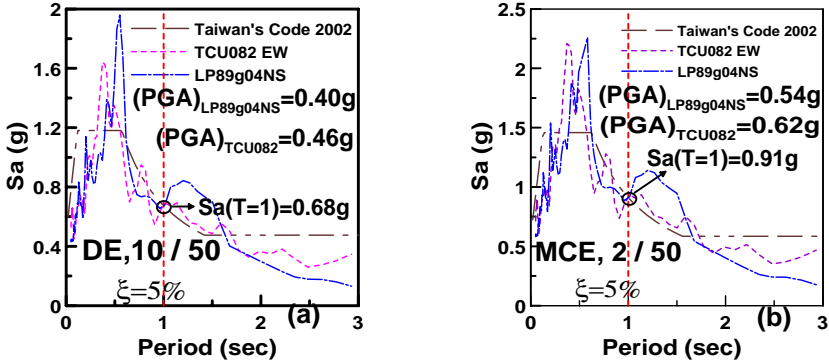
Figure 3. Design acceleration spectra (a)10/50 (b)2/50 hazard level.

As shown in Fig. 4, the two earthquake records are TCU082EW (from the 1999 ChiChi earthquake) and LP89g04NS (from the 1989 Loma Prieta earthquake), both of which are considered to represent general motions without near-field directivity effects. The original test plan was to scale these two records in acceleration amplitude to represent four separate pseudo-dynamic loading events, which were sequenced as follow: (1) TCU082 scaled to represent a 50/50 hazard intensity, i.e., with a 50% chance of exceeding in 50 years, (2) LP89g04 scaled to a 10/50 hazard intensity, which represents the design basis earthquake, (3) TCU082 scaled to a 2/50 hazard, and (4) LP89g04 scaled to a 10/50 hazard — identical to loading (2). The records scaling is based on matching the spectral acceleration at one second period to the specified earthquake hazard levels.
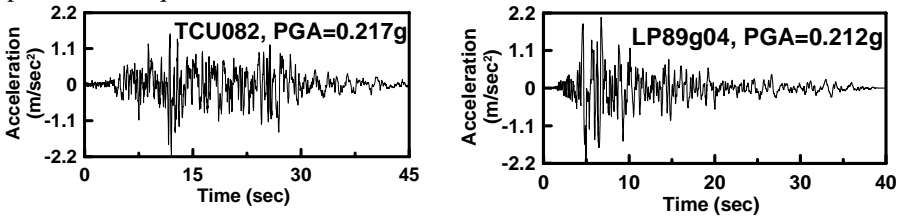

Figure 4. Original ground accelerations used in test (before scaling).

Fig. 5 shows the actual applications of the ground motions in the PDTs for the CFT/BRB frame specimen. As noted above, four earthquake ground accelerations scaled to three different PGAs were planned for the PDT of the CFT/BRB frame specimen. However, some unexpected events encountered during the testing. In the Test No. 1, due to the buckling of the gusset plate occurred at the brace to beam connection in the first story, the test stopped at the time step of 12.3 second. Then stiffeners were added at the free edges of all the gusset plates underneath the three floor beams. Then test resumed using the same ground accelerations as Test No.1 but in reversed direction. Until Test No.4, the PDT test was stopped at the time step of 12.54 second as the crack on the top of concrete foundation near the gusset plate for the south BRB-to-column joint were observed. After one pair of angles was installed bracing the stiffener to the two anchoring steel blocks, the test resumed again by applying the same earthquake acceleration as that proceeded in Test No. 4. After all, a total of six PDTs were conducted, and all the BRBs were not damaged. Therefore, cyclic increasing uniform story drifts were imposed until the failure of the BRBs. Since the scheduled PDT and cyclic tests were completed with failures only in bracing components including the BRBs, UBs and the gusset plates, it was decided that Phase-2 tests be conducted after repairing the damaged components. It adopted the same two earthquake records but scaled to match the spectral acceleration at the first mode period to the specified earthquake hazard levels. The ground motion accelerations applied in Phase 2 PDTs are also shown in Fig. 5 (Chen et al. 2004). All the key analytical predictions and the experimental responses were broadcasted from a website (http://cft-brbf.ncree.gov.tw).
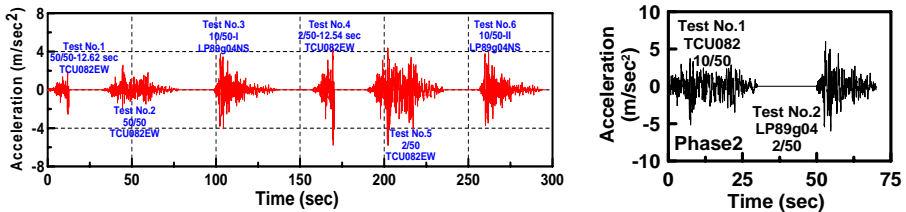

Figure 5. Ground acceleration time history in PDTs.

5. ANALYTICAL MODELS

5.1 PISA3D Model

In the application of PISA3D, all BRBs were modeled using the two-surface plastic (isotropic and kinematic) strain hardening truss element (Fig. 6). All the beam members were modeled using the bi-linear beam-column elements (Fig. 7). Considering the strength degrading behavior of the concrete, all the CFT columns were modeled using the three-parameter degrading beam-column elements as shown

in Fig. 8. A leaning column is introduced in the PISA3D frame model in order to simulate the 2nd order effects developed in the gravity columns.
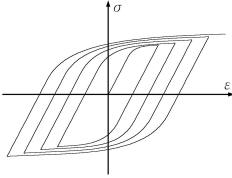

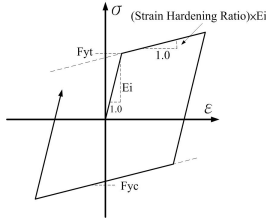**Figure 6. Two-surface plasticity hardening truss element.**
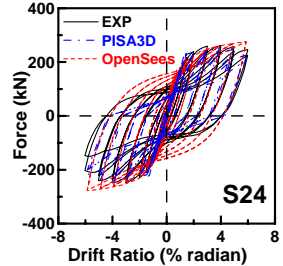

Figure 7. Bilinear element model.

Figure 8. Drift ratio and force hysteresis of CFT column.

5.2 OpenSees Model

All the CFT columns and steel beams of the frame are modeled by the flexibility-based nonlinear beam-column fiber elements with discretized fiber section model. The uniaxial bilinear steel material model (Steel01) is the basic model that incorporates isotropic strain hardening adopted in the analyses. The uniaxial Kent-Scott-Park concrete material model (Concrete01) is adopted and no tensile concrete strength is considered. All BRBs were modeled using the truss element. The Menegotto-Pinto steel material (Steel02) with isotropic and kinematic strain hardening was used for the truss element. A leaning column arrangement has also been adopted in OpenSees model. The frame model presented in this paper utilizes the measured material properties of steel beams, CFT tubes, and the infill concrete for the CFT columns.

6. ANALYTICAL AND EXPERIMENTAL RESULTS

Figs. 9 and 10 present the roof experimental displacement time history, and the 1st inter-story drift versus story shear relationships obtained in Test No. 5. The peak value of roof displacement is about 208-mm and the peak story drift is at 1st story of about 0.025 radian. It is evident that the roof displacements and the brace hysteretic behavior simulated either by PISA3D or OpenSees shown in Figs. 9 and 10 are satisfactory. Fig. 11 shows the peak story shear distributions under the applications of 50/50, 10/50 and 2/50 three earthquake load effects. It is confirmed that the analyses have predicted the experimental peak shears extremely well. Fig. 12 shows that except the roof floor, experimental peak lateral floor displacements well agree with the target design responses for both the 10/50 and 2/50 two events. Tests (Fig. 13) also confirmed that experimental peak inter-story drifts of 0.019 and 0.023 radians well agree with the target design limits 0.02 and 0.025 radians prescribed for the 10/50 and 2/50 events, respectively.
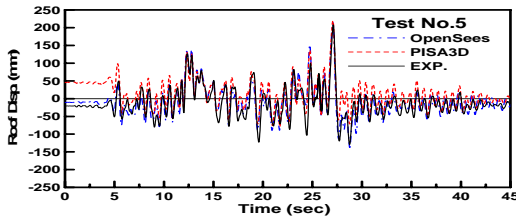
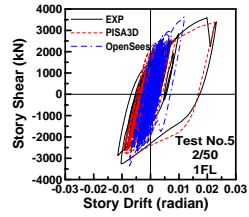**Figure 9. Roof displacement time history in Test No. 5.**

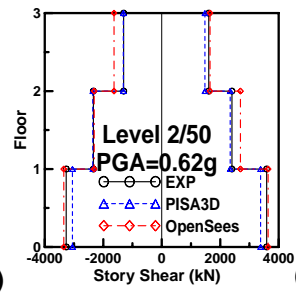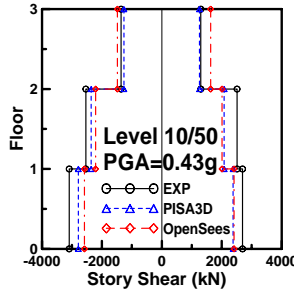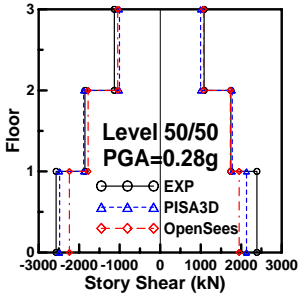**Figure 10. Hysteresis of 1st Story in Test No. 5.**

Figure 11. Peak story shear distribution of CFT/BRB frame specimen (a)50/50 (b)10/50 (c)2/50.
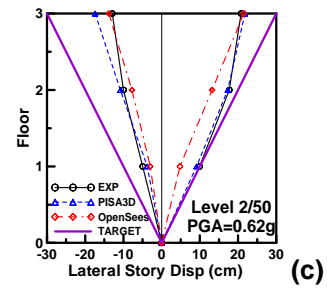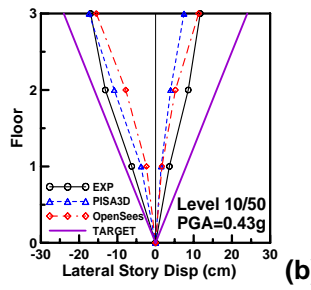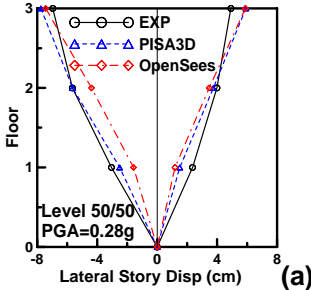

Figure 12. Peak story displacement distribution of CFT/BRB frame specimen (a)50/50 (b)10/50 (c)2/50.
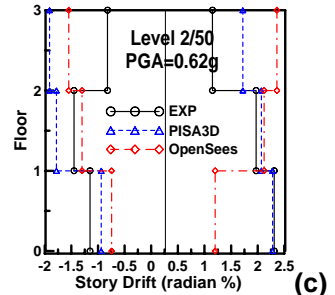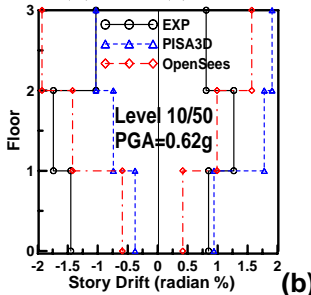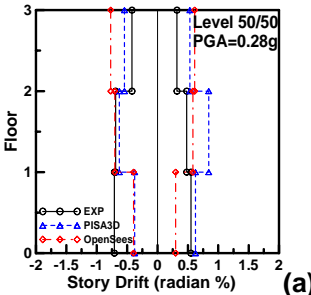

Figure 13. Peak inter-story drift distribution of CFT/BRB frame specimen (a)50/50 (b)10/50 (c)2/50.

252

Figure 14 gives the analytical and experimental roof displacement time history of CFT/BRB frame specimen obtained in the Test No. 3 and Test No. 5. respectively. It is evident that the lateral displacements of CFT/BRB frame predicted either by OpenSees or Pisa3D are satisfactory. Table 2 shows the maximum and minimum lateral displacements of the predicted and measured response for the Test No. 2, Test No. 3, Test No. 5 and Test No. 6, respectively. The differences between the analytical and experimental responses are also shown in Table 2.

Table 2. Roof displacement comparisons and differences

Events	Lateral Displacement (cm)						Error (%)			
	TEST		OpenSees		PISA3D		OpenSees		PISA3D	
	max	min	max	min	max	min	max	min	max	min
Test No.2 (50/50)	4.9	-7.0	5.9	-7.4	5.9	-7.7	17	5	17	9
Test No.3 (10/50-I)	11.7	-17	11.3	-15.5	7.5	-17.4	4	10	56	2
Test No.5 (2/50)	20.8	-12.9	21.5	-13.8	21.8	-10.8	3	7	5	19
Test No.6 (10/50-II)	18	-13.2	15.3	-10	16.8	-7.1	18	32	7	86
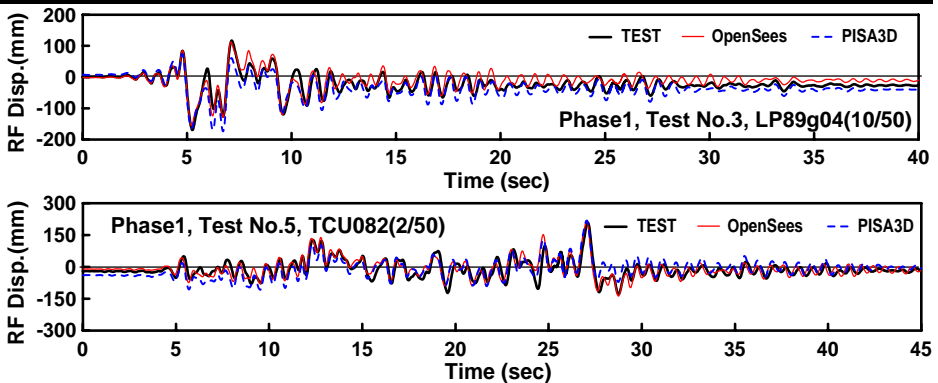
Figure 14. Roof displacement time history in Tests No. 3 and No. 5.

Fig. 11 and Fig.15 show that the predictions agree extremely well with the experimental story shear time history response and the peak story shears. As shown in Table 3, it's found that the maximum story shear differences between the prediction and the test result are only 19% and 13% for OpenSees and PISA3D, respectively.

Table 3. Base shear comparison

Events	Story Shear (10^3 kN)						Error (%)			
	TEST		OpenSees		PISA3D		OpenSees		PISA3D	
	max	Min	max	min	max	min	max	min	max	min
Test No.3 (10/50-I)	2.7	-3.1	2.4	-2.6	-2.8	2.4	13	19	13	11
Test No.5 (2/50)	3.6	-3.3	3.3	-3.4	3.4	-3	9	3	6	10

Figure 15. Base shear history in Tests No. 3 and No. 5.

In the Test No. 2, braces started to experience plastic deformation at the first and the second floors. As shown in Table 4, by computing the linear responses between the axial force versus core displacement of braces before yiel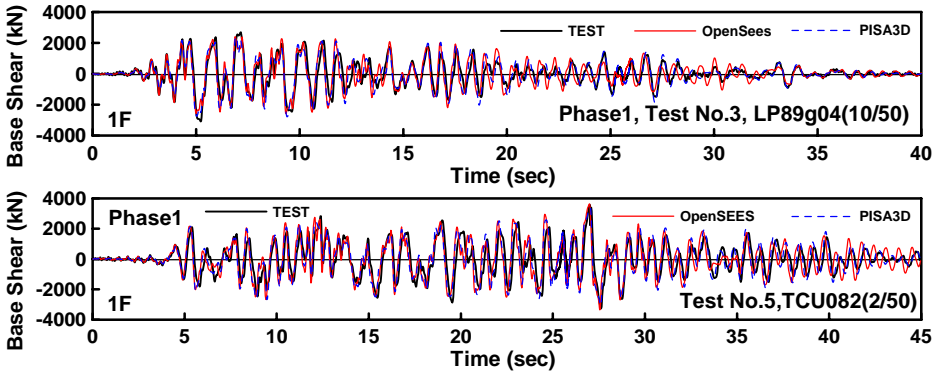ding, it is confirmed that the initial stiffness of the BRBs of the specimen is rather close to the design value. This suggests that the unbonding mechanism of the BRBs is effective in these BRBs. After the application of six earthquake effects in Phase 1 tests, it is found that the UBs and BRBs performed rather satisfactorily without evident failure. Furthermore, the BRBs dissipated most of hysteretic energy absorbed by the structure in different levels of earthquake intensities (Fig. 16). In each case, the energy dissipated by the north BRB is almost the same as that by the south BRBs in each floor suggesting the accurate transformation of the strain gauge readings into the brace axial forces. In the meantime, the ultimate story drift of the BRB composite frame was controlled rather effectively under the effects of the design earthquakes.

Table 4. Effective stiffness of BRBs or UBs

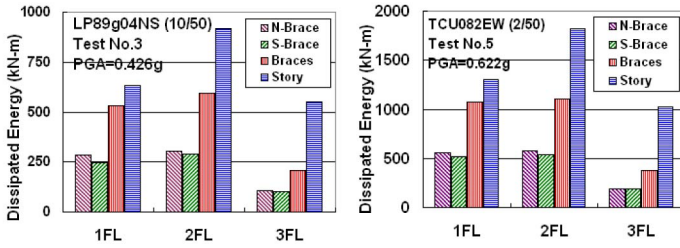|	Experiment		Analysis		error (%)	
	N (kN/mm)	S (kN/mm)	N (kN/mm)	S (kN/mm)	N	S
3BRB	91.5	88.0	87.35	87.4	4.7	0.7
2UBB	183.0	181.4	191.1	191.1	4.2	5.1
1BRB	193.0	184.3	185.9	185.9	3.8	0.8

Figure 16. Comparison of dissipated energy in tests.

7. KEY EXPERIMENTAL OBSERVATIONS

As noted previously, since the scheduled PDT and cyclic tests in Phase-1 study were completed with failures only in bracing components including the BRBs, UBs and the gusset plates, it was decided that Phase-2 tests be conducted after repairing the damaged components. Phase-2 tests not only allowed to make the best use of the 3-story, 3-bay frame but also aimed to investigate the performance of the stiffened gussets plates and the new BRBs. Before the Phase-2 tests, the laterally buckled gusset under the 3rd floor beam had been removed before installing a new one. In addition, stiffeners were welded at the free edges of the heat straightened gusset at all the brace to column joints (Fig. 17). Six new BRBs, two all metal double cored construction for the 1st story and four concrete filled double cored for the 2nd and 3rd stories (Fig.18) have been installed. Analytical predictions and actual experimental results were also broadcasted during the all the Phase-2 tests.

Figure 17. Buckling of the gusset at the brace to column joint after Phase-1 tests.

Figure 18. Added stiffeners at the free edges of the gusset at the brace to column joint before Phase-2 tests.

8. CONCLUSIONS

Based on the test and analytical results, summary and conclusions are made as follows:

- Test results confirm that the earthquake responses of the 3-story 3-bay CFT-BRB frame and members can be satisfactorily predicted using both PISA3D and OpenSees.
- The peak story drift reached 0.025 radian in Phase 1 tests after applying the 2/50 design earthquake on the specimen. It appears that the DSD procedure adopted in the design of the specimen is effective in limiting the ultimate story drift under the effects of the design earthquake.
- CFT/BRBF performed extremely well after the application of six earthquake load effects. In addition, according to the free vibration tests conducted after each earthquake pseudo dynamic test, the stiffness and damping of the specimen only changed slightly.
- Stiffeners added along the free edges of the gusset plate are effective in preventing out-of-plane instability of the brace-to-column connections. However, it also introduces flexural demands on the BRBs. Further researches are required to study the BRB end connections.
- All the moment connections survived all the Phase-1 and Phase-2 tests without failure. The BRBs effectively control the story drift and reduce the nonlinear demand imposed on these moment connections.
- Tests confirmed that the networked testing architecture implemented for the ISEE is very effective in disseminating real time test results through the internet.

REFERENCES

Tsai, K. C., Y. T. Weng, S. L. Lin, and S. Goel. (2004). "Pseudo-dynamic Test of A Full-scale CFT/BRB Frame: Part 1 - Performance Based Specimen Design", Proceedings, Paper No. 750, 13th World Conference on Earthquake Engineering, Vancouver, Canada.

Chen, C. H., P. C. Hsiao, J. W. Lai, M. L. Lin, Y. T. Weng, and K .C. Tsai. (2004). "Pseudo-Dynamic Test of a Full-Scale CFT/BRB Frame: Part 2 - Construction and Testing", Proceedings, Paper No. 2175, 13th World Conference on Earthquake Engineering, Vancouver, Canada.

Lin, M. L., Y. T. Weng, K. C. Tsai, P. C. Hsiao, C. H. Chen, and J. W. Lai. (2004). "Pseudo-dynamic Test of A Full-scale CFT/BRB Frame: Part 3 - Analysis and Performance Evaluation", Proceedings, Paper No. 2173, 13th World Conference on Earthquake Engineering, Vancouver, Canada.

Tsai, K. C., Y. C. Hwang, C. S. Weng, T. Shirai, and H. Nakamura. (2002). "Experimental Tests of Large Scale Buckling Restrained Braces and Frames." Proceedings, Passive Control Symposium 2002, Tokyo Institute of Technology, Tokyo.

Lin, B. C., and K. C. Tsai. (2003). "User Manual for the Platform and Visualization of Inelastic Structural Analysis of 3D Systems PISA3D and VISA3D." Center for Earthquake Engineering Research, National Taiwan University, Report No. CEER/R92-04.

Tsai, K. C., and S. L. Lin. (2003). "A Study of All Metal and Detachable Buckling Restrained Braces." Center for Earthquake Engineering Research, National Taiwan University, Report No. CEER/R92-03.

Wang, S. J., K. J. Wang, Y. S. Yang, W. C. Cheng, C. C. Yeh, and K. C. Tsai. (2004). "ISEE: Internet-Based Simulations for Earthquake Engineering Part II: The Application Protocol Approach", *Proceedings*, Paper No. 1548, 13th World Conference on Earthquake Engineering, Vancouver, Canada.

REAL-TIME DYNAMIC HYBRID TESTING OF STRUCTURAL SYSTEMS

Andrei REINHORN[1], Mettupalayam V. SIVASELVAN[2], Zach LIANG[2] and Xiaoyun SHAO[3]

ABSTRACT

The development and implementation of a novel structural testing method involving the combined use of shake tables, actuators, and computational engines for the seismic simulation of structures is presented herein. The hybrid simulation is intended to discover through physical testing the behavior of parts or whole substructure assemblies for which knowledge is limited, while the known parts of the structural system can be simulated analytically. The result of the hybrid simulation provides information of the entire system without need for whole system testing. The structure to be simulated is divided into one, or more, experimental and computational substructures. The interface forces between the experimental and computational substructures are imposed by actuators and resulting displacements and velocities are fed back to the computational engine. The earthquake ground motion is applied to the experimental substructures by shake tables. The unique aspect of the above hybrid system is force-based substructuring. The hybrid simulation can be implemented as pseudo-dynamic or real time dynamic methods. While the former has a long history of applications, while the latter was developed recently owing to the availability of newest technologies and investments done by the George E Brown Network for Earthquake Engineering Simulations.

Keywords: Hybrid testing; Dynamics; Experimentation; Analysis, Control.

1. INTRODUCTION

Simulation of structures under seismic loads is usually performed either experimentally or computationally. Experimental results are used to develop and calibrate computational models of structural components and assemblies. These computational models are used to predict the response of structures. Further experiments are then performed to validate and refine the computational models. Structural simulation is thus an iterative process involving alternate stages of experimentation and computation.

---

[1] *Clifford C. Furnas Professor*

[2] *Project Engineer, G. E. Brown Network for Earthq. Eng. Simulation (NEES),*

[3] *Ph.D. Candidate,*

Dept. of Civil, Structural and Environmental Eng. University at Buffalo

This paper describes a new method of *real-time dynamic* seismic simulation of structures which involves combined use of experimentation and computation and some of the above iteration can potentially be performed online. The new development was facilitated by the new George E. Brown Network for Earthquake Engineering Simulation (NEES) deployment which provides unique opportunities for integrated experimentation and computing.

This novel structural simulation method involves the combined use of shake tables, actuators, and computational engines. The structure to be simulated is divided into one or more experimental and computational substructures. The interface *forces* between the experimental and computational substructures are imposed by actuators and resulting displacements and velocities are fed back to the computational engine (See Figure 1). The earthquake ground motion can be applied to the experimental substructures by actuators as interpreted displacements (Pseudo-Dynamic Technique) or by one or more shakes tables

Figure 1. Substructure testing.

(Real-Time Dynamic Hybrid Technique). The unique aspect of the latter, the real-time dynamic hybrid system is the force-based sub-structuring. Since the shake tables induce inertia forces in the experimental substructures, the actuators have to be operated in dynamic force control as well. The resulting experimental-computational infrastructure is more versatile than previously deployed techniques.
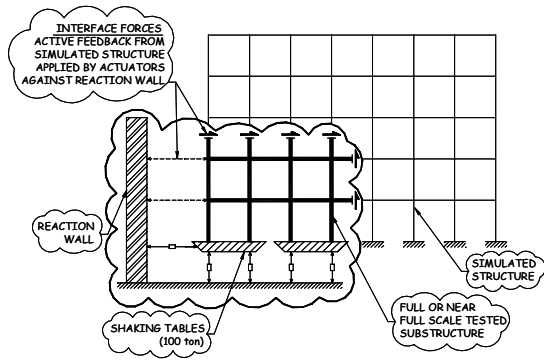
2. COMPUTATIONAL ISSUES

The simulation of structural dynamic response became a routine in the design of modern construction. Most simulations are done using computational tools which were verified by alternative analysis techniques or by experiments. The response of inelastic structures or other non linear systems is very difficult to assess. The time domain numerical simulation of structures under dynamic excitation is usually carried out by using either the modal superposition method (for elastic structures), or by direct integration methods. Appropriate assumptions have to be made in order to predict and calculate the response of the simulated structure. In particular, the direct integration methods utilized in dynamic testing are actually performed step-by-step. Not only the analytical errors are accumulated gradually, but the selection of sampling periods also affects the accuracy and stability of this integration process. More modern techniques based on State Space Approach (Sivaselvan and Reinhorn,

2004) can be formulated using system transition matrices derived from exact solutions. Such solutions are exact for elastic structures and present minimal errors for inelastic structures (Chu et al., 2002). Most recently analytical techniques based on Hamiltonian-Lagrangian formulations (Sivaselvan and Reinhorn, 2004) proved that inelastic problems with severe degradation, sudden breaks and repetitive impacts, as well as progressively collapsing structural assemblies can be solved with stable solutions using energy minimization techniques. These techniques and others developed in recent years still need experimental verification and identification of unknown phenomena neglected in modeling.

3. SUBSTRUCTURE TESTING OF LARGE SPECIMENS

Several experimental procedures are used to simulate and test the behavior of structural systems and components under earthquake loads. These include (1) Quasi-static testing (2) Shake-table testing (3) Effective force testing (4) Pseudo-dynamic testing and (5) Real Time Dynamic Hybrid testing (this paper). The Real-Time Dynamic Hybrid simulation, a form of substructure testing technique, allows only parts of the structure for which the analytical understanding is incomplete to be tested experimentally.
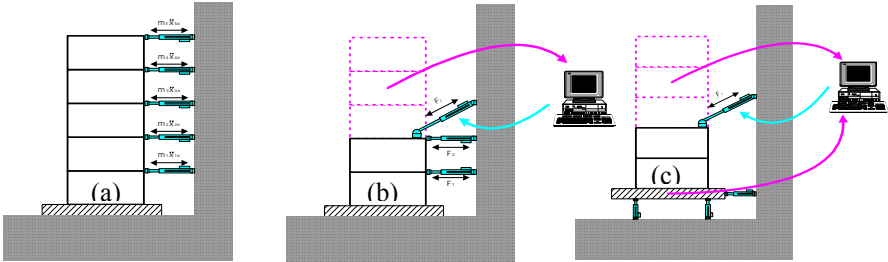

Figure 2. Modern methods for "dynamic" testing (a) effective force (b) pseudo-dynamic (c) real-time dynamic.

But in contrast to other existing testing methods, the last testing method allows substructures to be tested in the context of structural assemblies under dynamic conditions so that they can be subject to realistic load histories. The real-time testing allows the rate-dependent effects to be captured accurately. Moreover when the real time evaluation of the structure is combined with real time identification of properties the resulting computational system becomes a reliable tool for analytical studies.

The substructure testing was developed in the '80s and formulated by numerous researchers (Nakashima 1985, Mahin et al. 1985, Shing et al., 1985). As a traditional form of substructure testing technique, the pseudo dynamic test is an experimental technique for simulating the earthquake response of structures and structural components in the time domain. The test was developed in the early 1970s, having a

history of nearly thirty years. In this test, the structural system is represented as a discrete spring-mass system, and its dynamic response to earthquakes is solved numerically using direct integration. Unlike conventional direct integration algorithms, in the pseudo dynamic test the restoring forces of the system are not modeled but are directly measured from a test conducted in parallel.

Because of various advantages of this test over the shaking table test, which is known to be the most direct method to simulate the earthquake responses of structures, the test has been introduced in many research institutions throughout the world. As an extension of this testing technique, the pseudo dynamic test with a real-time control was developed in the 1990s. A few of the notable developments are presented in Nakashima et al. (2003).

Real-time dynamic hybrid testing, the main subject of this paper, extends the above testing techniques by allowing for testing substructures under realistic dynamic loads and for representing rate-dependent and distributed inertia effects accurately. While the fast pseudo-dynamic (mentioned above) and the real-time dynamic hybrid testing use substructures for physical testing and online computations to simulate the global system in real-time, the latter technique includes the inertia effects are part of the physical system testing.

The newly developed George E Brown Network for Earthquake Engineering Simulation, developed experimental and computational infrastructure for implementation of Pseudo-Dynamic Testing (University of Illinois, Lehigh University), Fast Pseudo-Dynamic Testing (University of Colorado, University of California at Berkeley, Univeristy at Buffalo) and the most advanced Real-Time Dynamic Hybrid Testing (University at Buffalo). Description of those installations can be found at http://www.nees.org/.

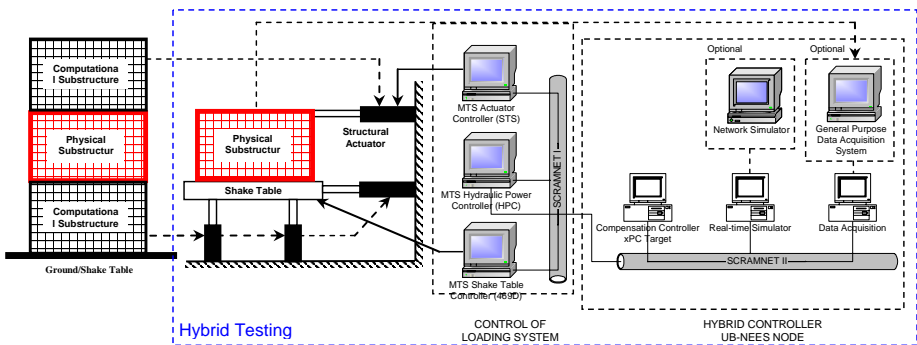## 4. FORMULATION OF NEW HYBRID TESTING TECHNIQUE

Figure 3. Schematic of real-time dynamic hybrid test system.

Real-time Dynamic Hybrid Testing (RTDHT) shown in Figure 2(c) is a novel structural testing method involving the combined use of shake tables, actuators, and computational engines for the seismic simulation of structures.

The structure to be simulated is divided into a physical substructure and one or more computational substructures. The interface forces between the physical and computational substructures are imposed by actuators and resulting displacements and velocities are fed back to the computational engine. The earthquake ground motion, or motion of other computational substructures, is applied to the experimental substructure by shake tables. A schematic of the RTDHT system is shown in Figure 3. A detailed description of the implementation follows:

5. SUBSTRUCTURING METHODS

The RTDHT implies first determining the model of the physical substructure being tested within the whole structural model identifying the interface parameters. A three-story model is shown in Figure 4 with its parameters. If u_g is the motion of the ground with respect to the inertial reference frame. u_i and x_i are the motions of the ith story with respect to the fixed reference frame and with respect to the ground respectively, then $u_i = u_g + x_i$. Defining the first and third floor in Figure 4 as *computational substructures* and the second floor as the *experimental substructure* as shown also in Figure 4, the equations of motion in the inertial reference frame are then given by:
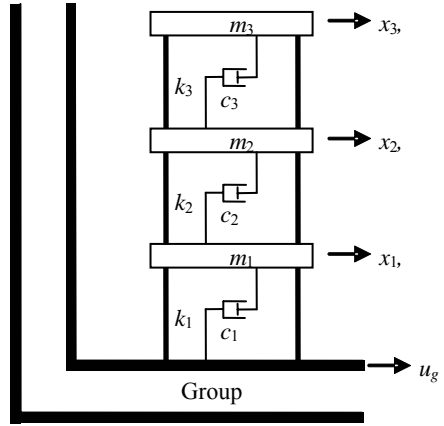

Figure 4. Three-story model.

$$
\begin{aligned}
&m_1\ddot{u}_1 + (c_1 + c_2)\dot{x}_1 &&- c_2\dot{x}_2 &&+ (k_1 + k_2)x_1 &&- k_2 x_2 &&= 0 \rightarrow \text{Computational Substructure 2}\\
&m_2\ddot{u}_2 - c_2\dot{x}_1 + (c_2 + c_3)\dot{x}_2 - c_3\dot{x}_3 &&&&- k_2 x_1 + (k_2 + k_3)x_2 - k_3 x_3 = 0 \rightarrow \text{Experimental Substructure}\\
&m_2\ddot{u}_2 &&- c_3\dot{x}_2 + c_3\dot{x}_3 &&&&- k_3 x_2 + k_3 x_3 = 0 \rightarrow \text{Computational Substructure 1}
\end{aligned}
\tag{1}
$$

By considering the influence of the *experimental substructure* as external disturbance, the equations of the *computational substructures* may be written as:

$$
m_1\ddot{x}_1 + c_1\dot{x}_1 + k_1 x_1 = -m_1\ddot{u}_g + \underbrace{k_2(x_2 - x_1) + c_2(\dot{x}_2 - \dot{x}_1)}_{\substack{\text{Force measured at the base}\\\text{of experimental substructure}}}
$$

$$
m_3\ddot{x}_3 + c_3\dot{x}_3 + k_3 x_3 = -m_3\ddot{u}_g + \underbrace{k_3 x_2 + c_3\dot{x}_2}_{\substack{(k_3 * \text{displacement} + c_3 * \text{velocity}) \text{ of}\\\text{experimental substructure}}}
\tag{2}
$$

The equation governing the *experimental substructure* rearranged using the relative displacement $x_{21} = x_2 - x_1$. Then equation (2) becomes:

$$
m_2(\ddot{u}_1 + \ddot{x}_{21}) + c_2\dot{x}_{21} + k_2 x_{21} = k_3(x_3 - x_2)
\tag{3}
$$

Being able to use both a shake table and an actuator to excite the experimental substructure introduces several possibilities for the application of the first floor acceleration $\ddot{u}_1$ and the thirds story force $k_3(x_3 - x_2)$: (a) Apply the acceleration using the shake table and the force using the actuator.; alternatively (b) Apply the ground acceleration using the actuator as well (as in the Effective Force method); (c) Yet another alternative is obtained by rearranging equation (3) as follows:

$$m_2 \left[\underbrace{\ddot{u}_1 - \frac{k_3}{m_2}(x_3 - x_2) + \ddot{x}_{21}}_{\text{Equivalent acceleration}} \right] + c_2 \dot{x}_{21} + k_2 x_{21} = 0 \tag{4}$$

The equivalent acceleration can be applied using the shake table only. However, the first story acceleration and the third story force can each be divided into two components, one to be applied by the shake table, and the other by the actuator. The actuator is assumed fixed in the inertial reference frame, while the structure is in a non-inertial frame attached to the shake table. The actions are shown below:

$$\text{Shake table acceleration, } \ddot{u}_t = \underbrace{\alpha_1(s)\ddot{u}_1}_{\substack{\text{First story contribution} \\ \text{to shake table acceleration}}} \underbrace{-\alpha_3(s)\frac{k_3}{m_2}(x_3 - x_2)}_{\substack{\text{Third story contribution} \\ \text{to shake table acceleration}}}$$

$$\text{Actuator Force, } F_a = \underbrace{-\left[1 - \alpha_1(s)\right]m_2\ddot{u}_1}_{\substack{\text{First story contribution} \\ \text{to actuator force}}} + \underbrace{\left[1 - \alpha_3(s)\right]k_3(x_3 - x_2)}_{\substack{\text{Third story contribution} \\ \text{to actuator force}}} \tag{5}$$

where $\alpha_1(s)$ and $\alpha_3(s)$ are frequency dependent splitting function such as for example band-pass filters. Such a splitting has several advantages discussed by Kausel (1998), Reinhorn and Sivaselvan (2004). The above substructuring and force splitting strategies are:

- If $\alpha_1(s) \neq 0$ and $\alpha_3(s) \neq 0$, then the control requires a shake table and an actuator to implement the substructure testing.
- If $\alpha_1(s) = 0$ and $\alpha_3(s) = 0$, however, two possibilities exist:
  - In dynamic testing, the inertia is part of the experimental system, whereas in pseudo-dynamic testing, inertia effects are computed.
  - Thus for hybrid testing ($\alpha_1(s) \neq 0$ or $\alpha_3(s) \neq 0$) or dynamic hybrid testing, the actuator should operate in force control.

Such a unified view of hybrid simultaneous computation and experimentation testing systems provides a better perspective to develop algorithms and software.

6. DYNAMIC FORCE CONTROL

The implementation of the RTDHT requires therefore implementation of force control in the hydraulic actuators. This control is sensitive to the acceleration and force

measurements, to the modeling of the compressibility of fluid, to the nonlinearities of the servo control system (servo valves) and other stiffness. The authors developed two approaches for dynamic force control:

The first approach is using the convolution method with a compensation technique that is based on identification of the frequency response function (FRF) of the system and modifying the force input by the inverse of the FRF. The operation is done in the time domain by evaluating the convolution integral. The forces are calculated based on Equation 6 with $\alpha_1(s) = 1$ and $\alpha_3(s) = 0$. Without the compensation the implementation is not feasible. The system was tested for free vibrations, and base motion–white noise and earthquakes. The performance for the

Figure 5. Pilot test for white noise.

white noise of the 2-dof and the 1-dof hybrid set-up is shown in Figure 5. The hybrid system simulates the 2-dof over the entire frequency range except for the very low frequencies with errors of up to 5%.
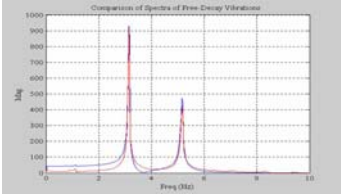
The second approach is based on control characteristics of hydraulic actuators. A hydraulic actuator is a rate-type device or velocity source; however, hydraulic actuators are typically designed for good position control. In contrast for force control, a force source is required. Thus force control using hydraulic actuators is an inherently difficult problem. Actuators designed for position control have stiff oil columns, making force control very sensitive to control parameters and often leading to instabilities. Moreover friction, stick-slip, breakaway forces on seals, backlash etc. cause force noise, making force a difficult variable to control.

Motivated by these observations and by the fact that causality requires a flexible component in order to apply a force in the force control scheme described here, a spring is introduced between the actuator and the structure as shown in Figure 6. Notice that the scheme (1) intentionally introduced series spring, K_{LC}, which assumes the role of the oil spring and (2) there is no force feedback loop.
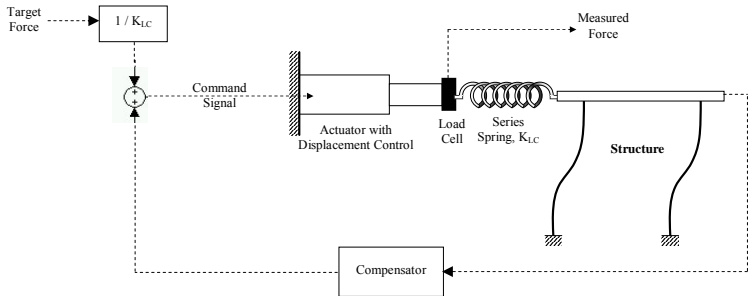
Figure 6. Proposed force control scheme.

The actuator behaves as a displacement device. Hence the actuator in the control scheme of Figure 6 is operated in closed-loop displacement control with a PIDF

controller. Although the system as a whole controls force function, *internally the actuator operates in closed-loop displacement control*. Hence, there is no need for an additional force feedback loop to ensure stability. More details on these developments are presented elsewhere by Reinhorn et al., 2004.

7. DISTRIBUTED REAL-TIME ARCHITECTURE

The real-time hybrid system is implemented using a distributed architecture that uses Shared Random Access Memory Network (SCRAMNET[TM]), a very low-latency replicated shared memory fiber optic network. The architecture of hardware-software controller (see right side of Figure 3) allows for flexibility in the design of the real-time operating system and in the implementation of the components used. There are three units which form the controller:

1. **The Compensation Controller** which contains the cascade control loop for force control presented above. This controller also compensates for time-delays that are inherent in the physical system.

2. **The Real-time Simulator** which simulates the computational sub-structures. The architecture has been designed so that this simulator could be seamlessly replaced by one at a remote location or a Supercomputer, if necessary.

Figure 7. Computational infrastructure.

3. **The Data Acquisition System** (DAQ) that is used for feedback from the experimental substructure as well as for archiving information during the test. .

The controller operates in a synchronous-asynchronous manner. The controller was developed to allow parallel operations of each of the three units while sharing only essential information through a "pool" memory provided by the 1μsec update rate SCRANNET. Each individual component / unit operates at each own time rate, accessing the shared memory when needed, without delaying other units. The compensation controller is designed to compensate also for all other latencies in communications, computing and hydraulic operations. The current implementation at University at Buffalo uses the architecture shown above which allows substituting the Simulation Component with any computational device — such as a supercomputer operating in a Grid.
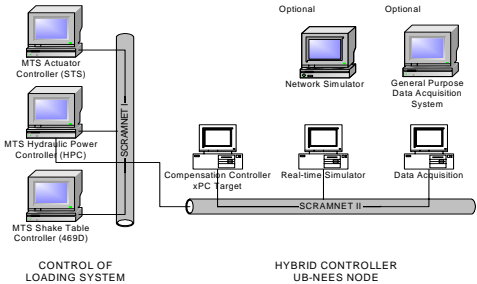
8. REAL-TIME HYBRID TESTING IMPLEMENTATION

A series of hybrid tests were performed on a two-story structure with the first story built on the shake table and the second story simulated (see Figure 8).
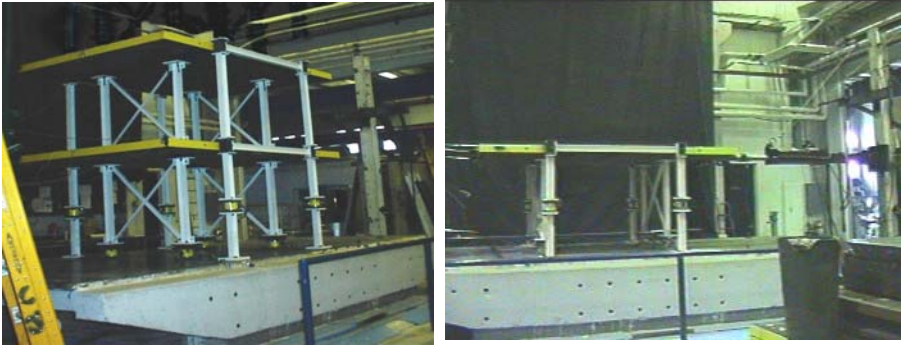
Figure 8. Two stories (left) and hybrid test on shake table (right).

A sample result from a sine-sweep test is .shown in the frequency domain in Figure 9. The result is compared with a computational simulation of the two story model. The result shows a small discrepancy in the damping representation. This is the subject of current work.

The results from real-time hybrid tests are presented for two cases:

- Two stories structure — tested and analyzed using h shake table motion.
- Hybrid system: one story with an actuator on physically tested on shake table
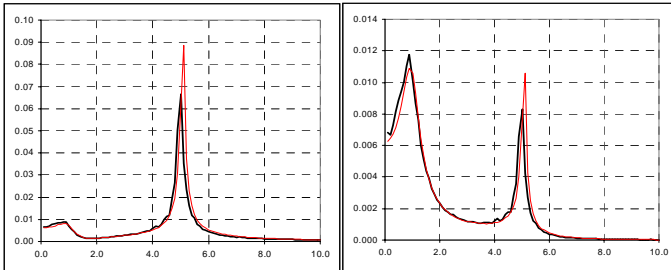
Figure 9. Results of simulation experiments.

The results in Figure 9 (on left) show the transfer function of the system measured during the experiment and the reference computation at first floor. Figure 9 (on right) shows the computed reponse of the virtual second story from measured data versus the analytical simulation. The hybrid test is capable to achieve both amplitude and frequency content with minor differences — attributed to the resolution of the data acquisition system The rest of discrepancies are believed to stem from unmodelled damping in the system and from some latency.

9. CONCLUDING REMARKS

The Real Time Dynamic Hybrid Testing System is implementing combined physical testing and computational simulations to enable dynamic testing of sub-structures

including the rate and inertial effects while considering the whole system. The paper presents a new force control scheme with a predictive compensation procedure which enabled the real-time implementation. The new system was tested through bench tests and medium scale pilot testing successfully. The procedures are implemented in the full / large scale University at Buffalo NEES node which includes 2 six-degree-of-freedom shake tables and three high-speed dynamic actuators and a structural testing system controller (STS) capable to implement the control algorithms presented above.

ACKNOWLEDGEMENTS

REFERENCES

Chu, S. C., T. T. Soong, and A. M. Reinhorn. (2002). "Real-Time Active Control Verification via Structural Simulator", *Journal of Engineering Structures*, 24 (3) 343–353.

Horiuchi, T., et al. (1999). Real-time hybrid experimental system with actuator delay compensation and its application to a piping system with energy absorber, Journal of Earthquake Engineering and Structural Dynamics, 28(11), 1121–1141.

Kausel, E. (1998), New seismic testing method I: Fundamental concepts, Journal of Engineering Mechanics-ASCE, 124(5): 565–570.

Mahin, S. A., P. B. Shing, C. R. Thewalt. (1985). Pseudo dynamic method for seismic testing, *J. Struc. Engrg.*, ASCE, 115(8), 2113–2128.

Nagarajaiah, S., A. M. Reinhorn, and M. C. Constantinou. (1992). Experimental-Study of Sliding Isolated Structures with Uplift Restraint, Journal of Structural Engineering-ASCE, 1992 118(6): 1666–1682.

Nakashima, M., H. Kato, and E. Takaoka.(1992). Development of real-time pseudo dynamic testing, Journal of Earthquake Engineering and Structural Dynamics, 21(1), 79–92.

Reinhorn, A. M., M. V. Sivaselvan, Z. Liang, and X. Shao. (2004). Real-time Dynamic Hybrid Testing of Structural Systems, 13th World Conference on Earthquake Engineering, Vancouver, B.C., August 1–6, Paper No. 1644.

Shing, P. B., and S. A. Mahin. (1985). Computational aspects of a seismic performance test method using on-line computer control, *Earthquake Engineering and Structural Dynamics*, 13, 507–526.

Sivaselvan, M., and A. M. Reinhorn. (2004). Nonlinear Structural Analysis towards Collapse Simulation: A Dynamical Systems Approach, Technical Report MCEER-04-0005, MCEER, University at Buffalo.

ROLES OF LARGE-SCALE TEST FOR ASSESSMENT OF SEISMIC PERFORMANCE

Masayoshi NAKASHIMA, Tomohiro MATSUMIYA, Dawei LIU, and Keichiro SUITA[1]

ABSTRACT

A full-scale test on a three-story steel moment frame was conducted, with the objectives of acquiring "real" information about the damage and collapse of a steel moment frame under cyclic loading, interaction between the structural frame and nonstructural elements and examining the capacity of numerical analyses commonly used in seismic design and analysis to trace the real cyclic behaviour. The outline of the test structure and test program is presented; results on the interaction between the frame and exterior finishes are introduced; and correlation between the experimental results and the results of pre-test and post-test numerical analyses is discussed.

Keywords: Steel moment frame; Full-scale test; Collapse; Nonstructural elements.

1. INTRODUCTION

"Performance-based engineering" has become a standard norm for research, development, and practice of earthquake engineering particularly after the 1994 U.S. Northridge and 1995 Hyogoken-Nanbu (Kobe) earthquakes (Performance, 1995; Recommended, 2000; NEHRP, 2000; Notification, 2000; Midorikawa et al., 2003). Relevant themes of challenges range from the characterization of strong motions and their effects on the structural response, quantification of multiple levels of performance associated with the functionality, damage, and safety limit states, examinations into the interaction of various nonstructural components and building contents with building performance, among many others. To verify individual research findings and assure the expected performance of innovative developments and practices, *real data* obtained from "observations" and "experiments" are essential. They are rather difficult to acquire, however. A large earthquake event occurs very scarcely, which makes it difficult to monitor or measure the real behavior of structures at such an event. Interaction between member and system behavior is known to be complex; hence tests on a structural system that has much redundancy are indispensable. Building structures, however, are massive, and it is difficult to

[1] *Disaster Prevention Research Institute, Kyoto University, Gokasho, Uji, Kyoto, 611-0011 JAPAN*

fabricate and load them in the laboratory, whereas miniature models are known to fail to duplicate the prototype behavior because of lack of similitude. Considering these circumstances, the writers conducted an experimental project in which a full-scale, three-story steel building frame was loaded quasi-statically to failure. The primary objectives of the project were: (1) to acquire realistic data about performance, progress of damage, and final failure of the concerned frame in deformation ranges that are far beyond those considered in contemporary seismic design; (2) to examine the interaction between the local damage induced into individual members and elements and the global damage sustained by the structural frame; (3) to observe effects of RC floor slabs on the behavior of steel moment frames; (4) to examine the interaction between the structural system and exterior finishes; and (5) to calibrate the capacity of numerical analyses to trace the behavior to collapse. This paper reports on the outline of the test and the results about the overall behavior, interaction between the structural frame and exterior finishes, and ability of a plastic-hinge based nonlinear analysis to trace the experimental cyclic behavior. Other issues of interest, i.e., interaction between the local damage and global behavior, effects of composite action, and behavior to final collapse are being explored, and preliminary findings are presented elsewhere (Matsumiya et al. 2004a; Matsumiya et al 2004b).

2. TEST STRUCTURE

The test structure was a three-story, two-bay by one-bay steel moment frame as shown in Fig.1, having a plan dimension of 12 m (in the longitudinal direction) by 8.25 m (in the transverse direction). The structure was designed following the most common design considerations exercised in Japan for post-Kobe steel moment frames. That is, the columns were made of cold-formed square-tubes, beams were made of hot-rolled wide-flanges, the through-diaphragm connection details were adopted, in which short brackets were shop-welded to the columns [Fig.2(a)]. The columns with short brackets were transported to the test site, and they were connected horizontally to beams by high-strength bolts. Metal deck sheets were placed on top of beams, with studs welded to the beam top flanges through the metal deck sheets. Wire-meshes were placed above the metal deck sheets, and concrete was placed on site. Fabrication and construction procedures adopted for the test structure faithfully followed those exercised in real practice (Nakashima et al., 1998). Exception was the column bases. Instead of embedding anchor bolts in the foundation RC beams, anchor bolts were fastened in short, deep steel beams, which in turn were securely tied down to the strong floor [Fig.2(b)].

The two-planes placed in parallel in the longitudinal direction were nearly identical, but one plane, called the "South" plane, had a floor slab extended on the exterior side by 1.5 m, while the other plane, called the "North" plane, had a floor slab that terminated at the beam end (Fig.1). This overhang was designed to make it possible to directly measure the effects of RC floor slabs from the difference in resistance between the two planes. The columns were extended to the approximate

mid-height in the third story, at which level steel braces were connected horizontally to the columns by high strength bolts through gusset plates. The braces served to achieve a rigid-diaphragm action in this plane, while the column rotations at the top were permitted by the out-of-plane flexibility of the gusset plates. Two quasi-static jacks, one in each longitudinal plane, were placed in this level, as shown in Fig.1.
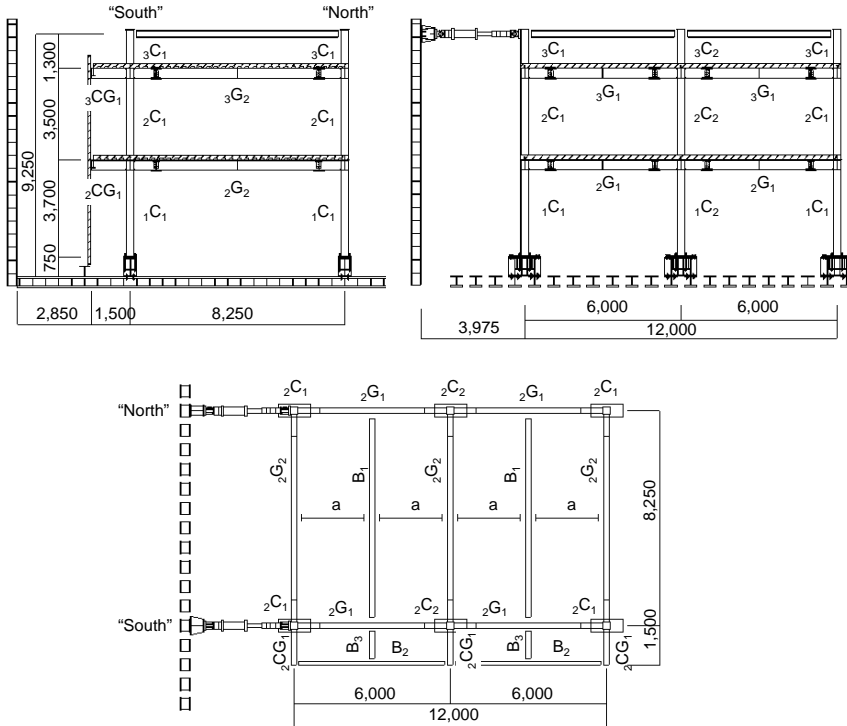
Member		Section	Member		Section (Stud bolt)
Column	$_1C_1$	□-300x9	Beam	$_2G_1$	H-400x200x9x16 (19φ h=110 Single@200)
	$_1C_2$	□-300x12		$_2G_2$	H-400x200x9x16 (19φ h=110 Single@200)
	$_2C_1$	□-300x9		$_3G_1$	H-400x200x9x16 (19φ h=110 Single@200)
	$_2C_2$	□-300x9		$_3G_2$	H-400x200x9x16 (19φ h=110 Single@200)
	$_3C_1$	□-300x12		$_2CG_1$	H-400x200x8x13 (19φ h=110 Single@200)
	$_3C_2$	□-300x16		$_3CG_1$	H-400x200x8x13 (19φ h=110 Single@200)
Anchor bolt	M33	length=740 (110)		B_1	H-400x200x8x13 (16φ h=110 Single@300)
	M36			B_2	H-300x150x6.5x9 (No)
Base plate		50x475x475		B_3	H-200x100x5.5x8 (16φ h=110 Single@300)
Mesh		6φ 150x150		a	H-200x100x5.5x8 (No)

Unit: mm

Figure 1. Plan and elevation of test structure (unit: mm).

Another feature of the test structure was the exterior finishes (cladding) installed during the test. ALC (autoclaved lightweight concrete) panels were placed on one edge of the floor to examine the effects of nonstructural elements on the hysteretic behavior of the test structure. The ALC panels were installed along the floor edge of the "South" plane (the one with the overhang).
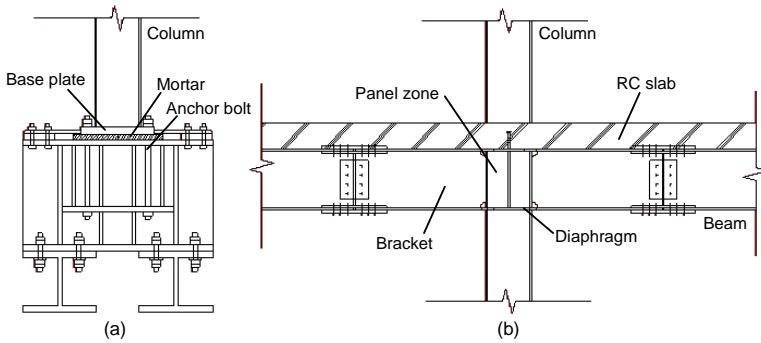
Figure 2. Connection details: (a) column base connection; (b) beam-to-column connection.
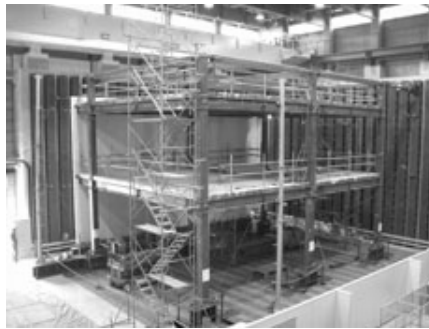
Figure 3. Overview of test structure (with ALC panel).

3. LOADING PROGRAM

As shown in Fig.1, two quasi-static jacks were arranged for horizontal loading. Each jack was placed at one end of the test structure and at the mid-height of the third story. An identical displacement was applied to both jacks. The two planes acted nearly independently; that is, no transfer of the force between the two planes was observed. Figure 4 shows the loading program used in the test. Quasi-static cyclic loading with increasing displacement amplitudes was adopted, and either two or three

cycles were repeated for each amplitude. The displacement was expressed in terms of the overall drift angle, defined as the horizontal displacement at the loading point relative to the loading height (i.e., 8.5 m). Overall drift angles of 1/200 rad, 1/100 rad, 1/75 rad, 1/50 rad, 1/25 rad, and 1/20 rad were adopted. An on-line pseudodynamic test was also conducted in the medium range of loading (after the 1/75 rad amplitude loading and before the 1/50 rad amplitude loading). After loading to the 1/20 rad amplitude, the jacks were dismounted once, and installed again with a 0.6 m long shim, and reloaded again to the maximum overall drift angle of 1/15 rad to examine the failure behavior. A computer controlled on-line test system was used for the test. The system was able to ensure flexible control in either the displacement or force mode as well as to conduct fully automatic loading and measurement. The full detail of the control system is described in Nakashima et al., 1995 and Nakashima and Liu, 2003.
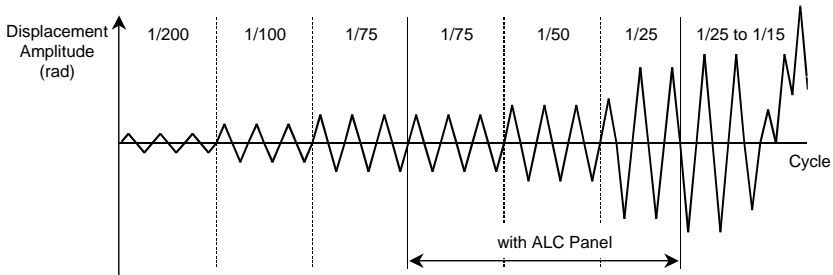
Figure 4. Loading program.

4. MEASUREMENT

A load cell attached to the head of each jack measured the horizontal load applied by the jack. A digital displacement transducer that had a resolution of 0.01 mm was used to measure the displacement of the jack. Four strain gauges were glued on the column surface at two cross-sections, each located at a distance of 1 m inward either from the column top or bottom. The cross-sections remained elastic; thus the bending moments applied at the cross-sections were estimated from the corresponding curvatures. The shear force applied to the column was estimated as the sum of the two bending moments divided by the distance between the measured cross-sections. The column axial force was estimated from the average of the strains measured by the column strain gauges. The beam shear force was estimated from the difference between the axial forces exerted into the two columns, one located on the top of and the other located underneath the concerned beam. Shear deformations of the panel zones, deformations of the floors in the direction orthogonal to the loading direction, rotations and lateral displacements of the column bases, and out-of-plane rotations and displacements of the beams were also measured by displacement transducers

273

having a variety of gauge lengths. Furthermore, many strain gauges were glued on the beam flanges and webs in the vicinity of beam-to-column connections as well as on the anchor bolts at the column bases. A total of 283 data channels were connected to the measuring system.

5. TEST RESULTS

5.1 Overall Behavior
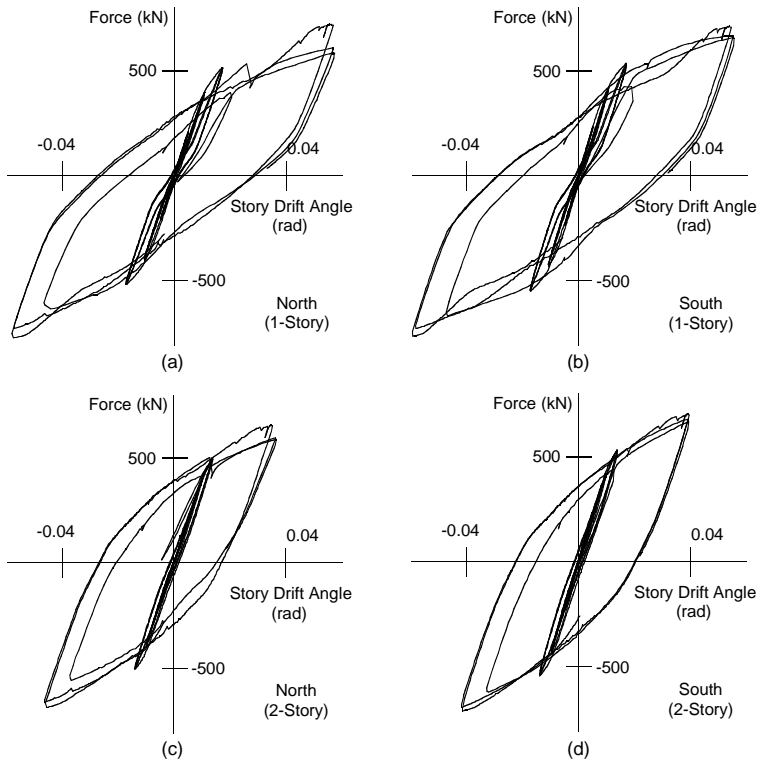
Figure 5. Story shear versus story drift angle relationships: (a) first story in north plane; (b) first story in south plane; (c) second story in north plane; (d) second story in south plane.

Figure 5 shows the story shear versus story displacement relationships. The relationships are presented with respect to the story (the first and second stories) and plane (the "North" and "South" planes). The story shear force was the load applied by the jack placed in the concerned plane. In the relationships, those obtained from

the tests with ALC panels were excluded. For loading not smaller than the 1/75 amplitude, beams, panel-zones, and column bases sustained plastic deformations, which indicates balanced participation of individual components to the overall deformations. Pinching behavior in the second and third cycles relative to the first cycle was notable for the 1/75 amplitude and greater. This was primarily due to yielding and progress of plastic deformations of the anchor bolts. Such yielding was accepted in designing the test structure.

5.2   Interaction with Exterior Finishes
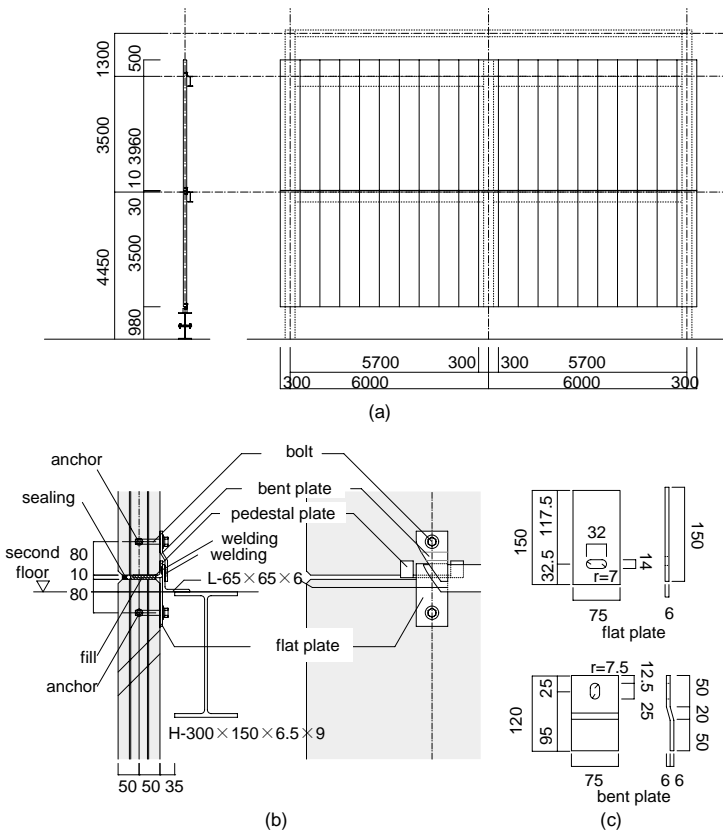
Figure 6. Installation of ALC panels: (a) elevation; (b) attachment to edge beam; (c) plates with slotted hole.

The effects of exterior finishes on the stiffness and strength of the tested frame were observed by the direct comparison between the tests with the 1/75 and 1/25 amplitudes, because for those two amplitudes, tests were conducted one time without

the ALC panels and the other time with them. The panels were attached to the edge beam of the "South" plane. Configuration of the ALC panels and the attachment details are shown in Fig.6. The ALC panels had a width of 600 mm, a height of either 3,500 mm (the first story) or 3,960 mm (the second story) mm, and a thickness of 100 mm [Fig.6(a)]. Each panel had a stud bolt embedded in the mid-width location near the top and bottom edge. The bolt was inserted to the slotted hole of a small steel plate [Fig.6(c)]. The plate was welded to a small angle, and the angle was welded to the edge beam [Fig.6(b)], both prior to the installation of the ALC panels. The slotted holes were used to ensure rigid movement of the ALC panels during the horizontal response of the frame. This detail has been adopted widely in Japan particularly after the 1995 Kobe earthquake, in which quite a few damage instances were observed for ALC panels (Reconnaissance 1995). Figure 7 shows the "South" plane's story shear versus story drift relationships obtained for the two amplitudes, with the solid lines without the ALC panels and the broken lines with. As evidenced from the figures, the ALC panels did not affect either the stiffness or strength for both amplitudes. Product specifications of ALC panels commonly specify an allowable story drift of 1/75 to 1/50 for use in practice. The test results showed excellent performance of the ALC panels and adequacy of the attachment details. No visible cracks were observed in the ALC panels except for minor cracks and spalling of concrete at the bottom of the panels in the first story.

(a)   (b)
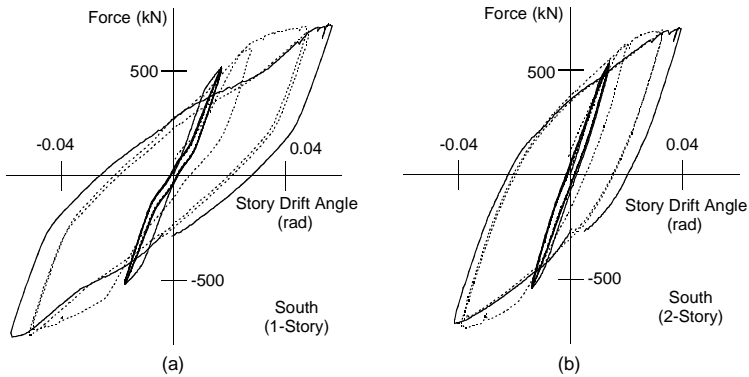
Figure 7. Effect of ALC panels on hysteretic behavior: (a) first story; (b) second story (solid lines = without panels; dotted lines = with panels).

5.3   Accuracy of Numerical Analysis

Figure 8(a) shows the results of pushover analyses conducted in the course of the design of the test structure, together with the experimental results. The program employed was based on the direct stiffness method with member-by-member representation. Plastic hinges inserted at member ends represent plastification, with

the relationship between the moment and plastic rotation taken to be bilinear. In Japan, such analyses are commonly adopted in seismic design practices. Since the analyses were carried out prior to the test, nominal strength values were adopted for the material strengths. The four cases shown in Table 1 were analyzed. In some cases of analyses, composite action with RC floor slabs was taken into account, and both the stiffness and strength of composite beams were adjusted using the concept of "effective width." Using the effective width stipulated in the Japan's composite slab guideline, the elastic stiffness of the beams was enlarged by 1.8 times, and the positive moment strength was enlarged by 1.5 times, respectively. In some cases of analyses, panel-zone behavior, i.e., the size, flexibility, and yielding of panel-zones were also considered. The panel-zone strength was enlarged by 1.3 times the values calculated using the design equations. This is also a common practice in Japan to allow for rather significant hardening sustained by panel-zones. In all cases, no strain hardening after reaching the respective strength was considered. This is again a common seismic design practice in Japan. According to comparison between the test and analysis [Fig. 8(a)], the elastic stiffness and yield strength are very close to each other; in particular the difference (for both the elastic stiffness and yield strength) is not greater than 1% for Case 4. This observation indicates that numerical analyses commonly used in seismic design is very reasonable in terms of the prediction of the two most important structural properties, i.e., the elastic stiffness an yield strength.

Table 1. Analysis cases in pushover analysis

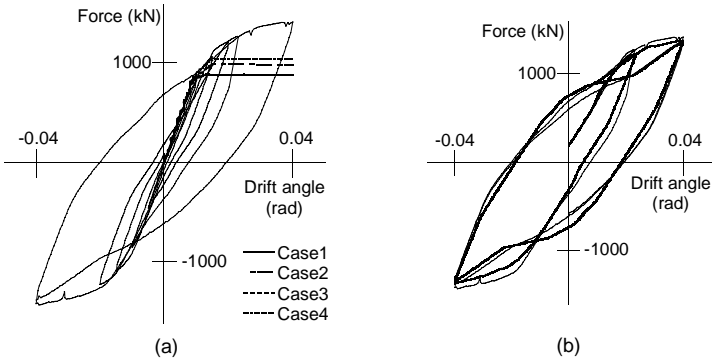| Analysis case	Composite action	Panel-zone effect
Case 1	Not considered	Not considered
Case 2	Considered	Not considered
Case 3	Not considered	Considered
Case 4	Considered	Considered

Figure 8. Comparison between test and numerical analysis: (a) before test; (b) after test.

To examine how accurately numerical simulation is able to trace the experimental cyclic behavior, the analysis program adopted for the pushover analyses was used again. This analysis this time was different from the previous analysis in the following aspects. Yield strength values obtained from the associated coupon tests were used instead of the nominal strength values, resulting in a 31% increase for beams, a 32-35% increase for columns, and a 5-8% increase for column bases. Strain hardening after yielding was included, with the modulus of strain hardening (relative to the elastic stiffness) determined by trial and errors. Increase of moment capacity by composite action was adjusted based on the experimental results. A slip model was incorporated to represent the hysteretic behavior of the column bases that involve significant pinching.

Figure 8(b) shows comparison between the experimental and numerical results for the cycles of 1/25 amplitude. In the development of the analytical curves, 5, 5, and 13% of strain hardening were adopted for the columns, column bases, and beams and panel-zones, respectively. The positive moment capacity was increased by 20% to allow for composite action. The thin and bold lines are the experimental and analytical curves. Correlation between the experimental curves and analytical curves obtained for the frame model is excellent, with the difference in the maximum strength not greater than 2.6% (positive) and 4.7% (negative), and the difference in the dissipated energy (areas of enclosed loops) not greater than 4.0%. Pinching behavior notable particularly in the first story is also reproduced very reasonably.

Analysis parameters (degree of strain hardening and increase in the positive bending moment) were chosen in reference to the experimental results; hence the analyses are typical post-analyses and are not fair in terms of "prediction." The writers' contention is that the analyses commonly used in daily design and analysis practices are reasonable enough to duplicate the inelastic behavior up to the drift angle of 1/25, which is significantly larger than the range of deformations considered in contemporary seismic design, if strain hardening and composite action are estimate properly. How to estimate reasonable strain hardening and composite action is a subject of further exploration.

6. CONCLUSIONS

This paper introduced the outline and some results of the cyclic loading tests applied to a full-scale, three-story, two-bay by one-bay steel moment frame. Notable observations obtained in this paper are summarized below.

(1) Balanced deformations between the beams, panel-zones, and column bases (primarily due to yielding of the anchor bolts) were observed. Pinching behavior was notable for cyclic loading with larger amplitudes (up to 1/25 in the overall drift angle) primarily because of cyclic yielding and resulting slip-type hysteresis experienced at the column bases.

(2) The effect of ALC panels (used for exterior finishes) on the structural behavior was nearly null up to the story drift angle of 1/25 rad, indicating that the

attachment details adopted for installation of ALC panels were very satisfactory in terms of the detachment of the panels from the frame response.

(3) Pushover analyses conducted prior to the tests predicted the elastic stiffness very reasonably and the strength with a good amount of conservatism. This indicates that present numerical analyses commonly adopted in daily design practices are adequate as design tools.

(4) Including strain hardening after yielding and composite action, numerical analyses were able to duplicate the cyclic behavior of the test structure with great accuracy, although a reasonable procedure to determine the degrees of hardening and composite action is yet to be explored.

REFERENCES

Matsumiya, T., D. Liu, M. Nakashima, and K. Suita. (2004). Test on Collapse Behavior of 3D Full-Scale Steel Moment Frames Subjected to Cyclic Loading. *Proceedings of the Seventh Pacific Conference of Steel Structures*, March 24-27.

Matsumiya, M., K. Suita, P. Chusilp, and M. Nakashima. (2004). Full-Scale Test of Three-Story Steel Moment Frames for Examination of Extremely large Deformation and Collapse Behavior. *Proceedings of the 13th World Conference on Earthquake Engineering*, Vancouver (to be presented).

Midorikawa, M., I. Okawa, M. Iiba, and M. Teshigawara. (2003). Performance-Based Seismic Design Code in Japan. *Earthquake Engineering and Engineering Seismology*, Taiwan, Vol.4, No. 1:12−25.

Nakashima, M., T. Akazawa, and H. Igarashi. (1995). Pseudo Dynamic Testing Using Conventional Testing Devices. *Journal of Earthquake Engineering and Structural Dynamics*, Vol.24, No.10:1409-1422.

Nakashima, M., K. Inoue, and M. Tada. (1998). Classification of Damage to Steel Buildings Observed in the 1995 Hyogoken-Nanbu Earthquake. *Engineering Structures*, Vol.20, No.4-6:271-281.

Nakashima, M., and D. Liu. (2003). Instability and Complete Failure of Steel Columns Subjected to Cyclic Loading. *Journal of Engineering Mechanics, ASCE*, (accepted for publication).

Nakashima, M., T. Minami, and I. Mitani. (2000). Moment Redistribution Caused by Beam Fracture in Steel Moment Frames. *Journal of Structural Engineering*, ASCE, Vol.126, No.1:137-144.

FEMA 368. (2000). *NEHRP Recommended Provisions for Seismic Regulations for New Buildings and Structures.* Federal Emergency Management Agency, Building Seismic Safety Council, Washington, D.C.

Ministry of Land, Infrastructure and Transport. (2000). *Notification No.1457-2000, Technical Standard for Structural Calculation of Response and Limit Strength of Buildings.* (in Japanese).

SEAOC Vision 2000 Committee. *Performance-Based Seismic Engineering of Buildings.* (1995). Structural Engineers Association of California, Sacramento CA.

FEMA 350. (2000). *Recommended Seismic Design Criteria for New Steel Moment-Frame Buildings.* Federal Emergency Management Agency, Building Seismic Safety Council, Washington, D.C.

Steel Committee of the Kinki Branch of the Architectural Institute of Japan. (1995). *Reconnaissance Report on Damage to Steel Building Structures Observed from the 1995 Hyogokken-Nanbu Earthquake.* Osaka.

FULL-SCALE LABORATORY TESTING: STRATEGIES AND PROCEDURES TO MEET THE NEEDS OF PBEE

Artur PINTO[*], Paolo NEGRO[*], Fabio TAUCER[*]

ABSTRACT

Performance-Based Seismic Design (PBSD) and Risk Assessment are recalled in view of the definition of structural testing procedures and protocols. A few tests performed at ELSA in support of the European Design Code (Eurocode 8) and on assessment and retrofit of existing structures are summarized. As examples of more advanced testing techniques, a brief review of 3D tests performed on an in-plan irregular building and of Pseudo-dynamic (PSD) tests with nonlinear substructuring carried out on bridges is made. The contribution and role of testing to the challenging development and implementation of PBSD are addressed.

   Keywords: Performance and risk assessment; Earthquake-testing protocols; Eurocode 8; Calibration tests; PSD tests; 3D pseudo-dynamic tests; Hybrid (physical/numerical) online simulation.

1. INTRODUCTION

Earthquake testing has always played a central role in the development of earthquake engineering (EE) research and practice. There are primary aspects related to validation of modeling and analysis procedures, together with aspects related to structural innovation (new materials, assemblages, etc.), which often require the adoption of laboratory experimentation.

   In Europe there is a specific case of intensive use of experimental facilities and associated numerical exploitation of experimental results for the calibration of the European Norms for design (Eurocode 8 for seismic design), whose enforcement is foreseen for 2007. Contrarily to most of the existing codes worldwide, Eurocodes are new codes, not built on any specific existing code, and embody many innovations, including a clear statement on performance requirements and compliance criteria (see details in (Fardis, 2004)). There was therefore a need to check performance of structures designed to Eurocodes and to check capacities and limit-state requirements. In fact, since the beginning of the 90's a large experimental research work has been carried out in Europe, at the European Laboratory for Structural Assessment (ELSA)

---

[*] *ELSA Laboratory, Joint Research Center, European Commission, 21020 Ispra (VA), Italy*

reaction-wall laboratory of the Joint Research Centre (JRC) and at many other laboratories and universities equipped with shaking-tables and other testing facilities.

The near future challenge of the experimental facilities is how to respond to the needs of Performance-Based Earthquake Engineering (PBEE), more specifically Performance-Based Seismic Design, and ultimately, how to contribute to the development and implementation of a future generation of design codes based on performance concepts. The primary issue for experimentalists and associated researchers is to fully understand the concepts of PBEE, concerning capacity assessment, demand and multi-level performance verification. There are several aspects to take into account, as component, assemblage and structure testing should be thoroughly considered. Regarding 'structure testing', there is a need to define appropriate testing protocols, which include loading type, intensity and test sequence, together with any variables representative and relevant to the control of performance, on the basis of realistic loading conditions for different test levels. Intensity, sequence and number of tests represent a compromise between an ideally refined response/capacity evaluation and the need to limit the number of sequential tests on the same model causing unrealistic cumulative damage. This requires a close interaction between various actors, namely experimentalists and analysts.

In order to meet the requirements of PBSD there is also a need for experimental facilities capable to handle complex structures and systems, including 3D earthquake response, to understand real effects of phenomena like soil-structure interaction (SSI) and to combine physical and numerical testing online and offline in a sort of 'real-virtual testing environment' where local and global, point and field digital measuring and visualization systems and corresponding processing can provide detailed information on demands and on the corresponding consequences, namely type and evolution of physical damage.

2. PERFORMANCE BASED SEISMIC DESIGN

Seismic design has experienced a substantial evolution in the last 50 years achieving the fundamental objective of life safety and accepting/incorporating solutions and technologies that enable critical facilities to remain operational after major seismic events. The present seismic design codes state clear objectives in terms of life safety (strength and ductility requirements), which can be mostly achieved, and state also objectives in terms of damage control that are typically checked indirectly, meaning that damage control checks are derived from demands based on the values calculated from ultimate limit states.

As economical aspects are also becoming overriding objectives in our societies, measurable consequences of earthquakes, such as structural and non-structural damage (e.g., repair costs) in earthquake events, as well as other economical consequences (e.g., loss of operation/revenue) and 'non-measurable' consequences, such as social impacts (quality of life), should be considered in the planning and design of our infrastructures, living and production facilities. As a matter of fact, the

economic losses resulting from the last major events in the U.S. and Japan can be considered as the motivation for PBEE, which is deemed to provide an appropriate platform to achieve safer and more economic constructions.

The conceptual frameworks proposed in the USA for PBEE (Krawinkler, 1999), such as Vision 2000, can be considered as a step forward on a more rational seismic design and assessment/redesign of engineered facilities. In fact, explicit consideration of multi-level performance objectives together with specific seismic intensities leads to a more controllable/predictable seismic performance. This represents a significant improvement relatively to the single-level explicit approach of current design codes because it requires explicit consideration and check of key performance objectives and it conveys it clearly to the designer that a structure is likely to be subjected to different seismic intensities during its life, including severe ones with low probability of occurrence.

However, this multi-performance approach still embeds a prescriptive concept, in the sense that the association of a series of performance objectives with specific input levels does not leave space to differentiated choices and might not satisfy the requirements and expectations of different stakeholders (the general public, owners, lenders, insurers, businesses and government). It is believed that decisions regarding acceptable earthquake risk should be left to the stakeholders and the scientific/technical communities should focus on the issues related to calculation of these risks and associated costs.

It is however advocated that a risk-based approach should be followed for seismic design. It should include prescriptive performance objectives related to safety as well as to other relevant macroeconomic minimum requirements (stakeholders: state and authorities) and leave the economic aspects on the other stakeholders, who are deemed to focus on the mitigation of the adverse economic consequences (Hadjian 2002). This mixed approach (minimum requirement performance – optimum-risk based) imposes minimum safety levels as well as minimum social adverse consequences and brings seismic design to a new level, where safety, design optimization (allowed trade-off between different performance levels) and innovation can coexist.

3. PERFORMANCE AND EXPECTED LOSSES FOR STRUCTURES DESIGNED ACCORDING TO CURRENT DESIGN CODES — ILLUSTRATIVE EXAMPLE

Reliability analysis and risk assessment of structures can be carried out following well-established methodologies. Difficulties may be encountered in system reliability approaches, for which correlation between different failure mechanisms exists as well as in the quantification of demand and capacity variabilities and loss (cost) functions. An application of reliability and risk assessment tools and methodologies to structures designed according to the Eurocodes was made by (Pinto, 1998). A case studied in this work is herein revisited to underline a few important aspects relevant to risk assessment and also to the definition of appropriate earthquake testing protocols.

The four-storey reinforced concrete frame building presented in Section 4.1 is the subject of this example. The structure was modeled numerically and was assumed to be in a High-seismicity zone in Europe with a hazard compatible with its design seismic action. Response simulations (non-linear models under earthquake input motions) were obtained for several input intensities (each using 5 artificially generated accelerograms). The response curve was approximated by an analytical function (average values of the simulation results) and a constant c.o.v. of 25% was assumed for the sectional lognormal distribution of the response. Performance curves were obtained for a few different cases (using the same number of 'experimental' points but distributed differently along the intensity ranges to approximate the response curves) and subsequently Annualized Earthquake Losses (AEL) were derived. It was concluded that the approximation of the structural response curves represents a key component of the risk assessment process, with very significant implications on the values of the expected earthquake losses. Approximation should be based on well-distributed 'experimental points' covering low, medium and high input intensities.
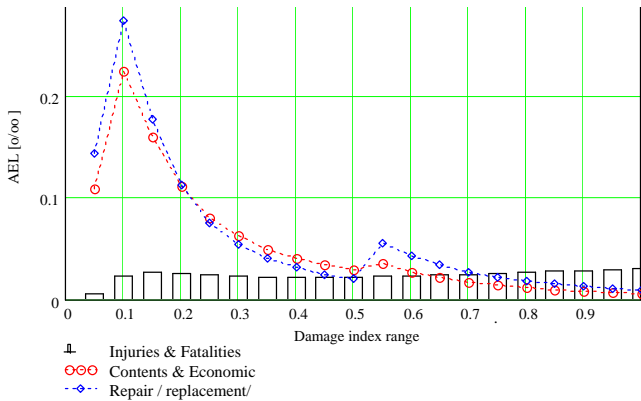
Figure 1. Contribution of damage ranges to total expected AEL.

There is another important aspect to take into consideration in the risk assessment process, which is concerned with the contribution of the damage ranges to the total expected losses. Fig. 1 shows the partial contribution of the damage ranges (0–0.05, 0.05–0.1, 0.1–0.15, …) to the total expected losses. It is noted that damage states in the vicinity of 0.1 are predominantly contributing to the repair and economic losses whereas 'human losses' are practically constant for all damage ranges other than for the damage values lower than 0.1, for which they are very limited.

The key concluding note is that reduction of economic losses is effective in the zones corresponding to low – low/medium damage indices, which can be addressed by the reduction of damage-inducing demands (e.g., drifts) corresponding to low-medium input intensities with high probability of occurrence.

4. OBJECTIVES AND OUTCOME OF STRUCTURAL TESTING

Experimental verification of the performance of structures subjected to earthquake input motions can be made through either shaking table (dynamic) tests or reaction-wall (pseudo-dynamic) tests; however, if strain rate effects are important and condensation to a reduced number of test DOFs is not realistic, dynamic testing should be sought. On the other side, if large-full scale models should be considered, pseudo-dynamic testing (PSD) becomes the appropriate solution because complex nonlinear phenomena are often accurately simulated only at full or large model scales. Furthermore, expansion of the time scale makes up for much more handy tests, in that the tests can be stopped at any critical event and be re-started if necessary. Furthermore, PSD testing allows hybrid (physical and numerical) online simulation of large structures and systems to be carried out by substructuring techniques already familiar to analysts.

The basic objectives of earthquake testing of structures can be summarized as: (i) to check the accuracy of numerical models and to adjust/calibrate model parameters. (modeling of single components may not capture the behavior of a complete structural system); (ii) to check structural performance for different input motion intensities (compare: demand, control variables and damage descriptions with capacity, limit state characterization and, ultimately, to reach collapse of the structure, which is normally associated with: (1) severe degradation of the structural properties often not accurately simulated by the analytical models, and/or (2) brittle failure modes not captured by the models); (iii) to build confidence and trust on the performance of new structural solutions, new design methods (e.g., new design codes) and innovative materials, as well as to provide evidence on good or bad performance (demonstration).

A test campaign normally involves a series of phases as described in Table 1. However, there is no standard procedure to conduct a test campaign. It should be tailored to the research/demonstration/qualification scope and objectives.

Table 1. Full-scale seismic tests: stages and corresponding description

Stage	Description
A0	Define scope and objectives of the experimental campaign
A	Define a test specimen representative of a class of structures
B	Subject test specimen to EQ ground motions with specific intensities, I1, I2, I3, …, corresponding to characteristic lifetime exceedance probabilities (e.g., 50, 10 and 2%) and achieve collapse stage (Ultimate capacity)
C	Record demands, in terms of deformation (e.g., drifts) and corresponding damage description
D	Carry out engineering quantification of damage (damage model, damage indices), taking into account the problem of cumulative damage resulting from sequential tests
E	Carry out calibration of damage cost functions relating drifts and/or damage indices with repair costs
F	Compare performances with corresponding performance objectives
G	Identify implications on modeling, design methods and procedures, redefinition of performance objectives

The minimal scope of structural seismic tests would be to check the performance of a model when subjected to the loading considered in its design and to check also its ultimate capacity in order to evaluate safety margins. In fact, the present limit-state based design codes explicitly consider one or two limit-states (safety and serviceability) and implicitly assume that the structure should be able to withstand (without collapse but with important/severe damage) earthquake intensities much higher than the design ones, which is achieved through capacity design (preferential-stable dissipation mechanisms) and requirements on ductility capacity. Explicit quantification of the seismic intensities associated to limit states other than safety is not given, nor performance is required to be checked. Therefore, one relies on prescriptive design procedures and on intended performances, which require verification and/or calibration. This has been the main scope of most of the tests performed at ELSA on structures designed according to the Eurocodes. Building and bridge models were tested and the results were used by the European research community and code-makers, to calibrate models, to refine some parts of the code (e.g., ductility classes, behavior factors), to introduce new design rules (e.g., structures with infill panels) and analysis methods, to introduce new materials (e.g., composite structures) and to introduce new technologies (base-isolation and distributed passive dissipation systems).

Two examples of the tests performed at ELSA in support of Eurocode 8 are given below. One is concerned with new structures and the corresponding tests were carried out for earthquake intensities corresponding to serviceability life-safety and ultimate capacity. The other is concerned with the assessment of existing structures, for which a test protocol tailored for life-safety and for ultimate capacity was adopted.

4.1 Testing of a Full-Scale 4-Storey RC Frame Building Designed According to the Eurocodes

The first experiments performed at ELSA in support of the European Codes consisted on a series of tests on a full-scale 4-storey RC frame building designed according to Eurocodes 2 and 8 (see Fig. 2). This was the first 'Eurocode structure', built and seismically tested for two different earthquake input motion intensities corresponding to serviceability and life-safety limit states. The structure was subsequently subjected to a displacement controlled cyclic test up to collapse in order to check its ultimate capacity. Earthquake intensities corresponding to 40% and 150% of the 'design-earthquake' (DE) were used in the PSD tests. Illustrative results are given in Fig. 2. Detailed description of the research programme, test results and analysis can be found elsewhere (Negro, 1996). It is however important to note that the low-level test caused only minor cracking in the structure and apparent low damage was sustained in the high-level test, with cracks remaining open only in the critical parts of the beams. Yielding of rebars took place in the beams plastic hinge zones and at the base of the ground floor columns, but neither spalling of concrete (only slight indication of spalling at the base of the 1st storey columns) nor buckling of rebars were observed.
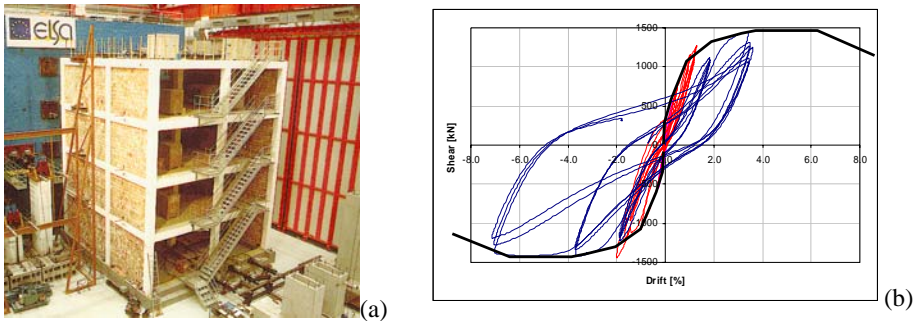
(a)   (b)

**Figure 2. R/C structure tested at ELSA: (a) Infilled frame configuration;
(b) Bare frame 1st storey shear-drift diagrams.**

Before the final cyclic collapse test, two additional pseudo-dynamic tests were
carried out: one with infill panels uniformly distributed along the height (see Fig. 2a)
and another one with infills at the all but the ground storey. The final cyclic test on
the bare frame was performed with imposed top displacement and inverted triangular
force distribution. Fig. 2b shows the first storey shear-drift diagrams for the tests on
the bare frame structure.

4.2   Assessment and Re-Design/Retrofit of Existing RC Frame Structures

A series of pseudo-dynamic tests on two full-scale models of a 4-storey R/C frame
(Fig. 3a) representative of existing structures designed without specific seismic
resisting characteristics (common practice of 40~50 years ago in South European
countries) were carried out at ELSA. Four testing campaigns were performed aiming
at: (1) vulnerability assessment of a bare frame; (2) assessment of a selective retrofit
solution; (3) earthquake assessment of an identical frame with infill masonry walls;
(4) assessment of shotcrete retrofitting of the infill panels.

Contrarily to the strategy adopted in the tests described in Section 4.1, which
aimed at the verification of serviceability and life-safety limit-states and check of the
ultimate capacity, the tests on the model representing existing structures were focused
on the behavior and performance for input motions corresponding to the design
actions of new structures as well as on the assessment of their ultimate capacity.
Therefore, an input motion corresponding to a 475 yrp was adopted for the first test
on the bare frame. The second test aimed at reaching ultimate capacity of the frames
and was carried out with an input motion intensity corresponding to 975 yrp. The tests
on the retrofitted structure and on the infilled frame structure adopted the same input
intensities in order to allow for direct comparison with the original configuration. A
subsequent PSD test with an intensity corresponding to 2000 yrp was carried out.
Illustrative results are given in Fig. 3b, whereas a detailed analysis of the test results
can be found elsewhere (Pinto, 2002).
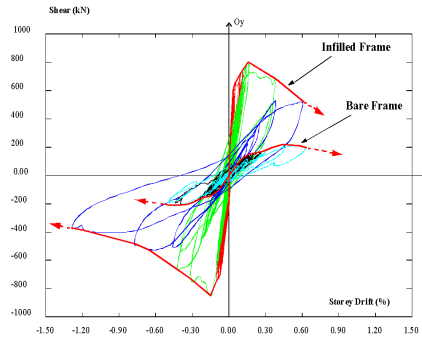
(a)   (b)

Figure 3. Tests on a full-scale models of an existing RC frame structure: (a) test set-up at ELSA; (b) first storey shear-drift diagrams and envelope curves for the bare and infilled frames.

5. NEW AND INNOVATIVE EXPERIMENTAL TECHNIQUES AND FACILITIES

In order to meet the requirements of PBSD there is also a need for experimental facilities capable of handling complex structures and systems, including 3D earthquake response, to understand the real effects of phenomena like SSI and to combine physical and numerical simulation online and offline in a sort of 'real-virtual testing environment'.

NEES represents a pioneering initiative on the creation of a network of experimental facilities and their users aiming at a collaborative research approach for the US earthquake engineering community. New experimental facilities were constructed, existing ones were upgraded and the communication infrastructure and tools for geographically distributed and hybrid (numerical and experimental) testing seems to be ready. The NEES facilities and associated vision are deemed to provide a valuable contribution to the development and implementation of PBSD as well as to investigate a series of phenomena in need of increased knowledge (e.g., SSI, asynchronous input motions). Moreover, the database of experimental results can constitute, in the medium/long term, a source for model development/calibration as well as for limit-state characterization and quantification.

Unfortunately, in Europe there is no similar specific programme financing new or upgrading existing earthquake engineering facilities, but there is a past experience of collaboration between EE facilities. In addition, ELSA has recently made substantial progress on the development and implementation of the PSD testing method with substructuring and on the development of advanced test setups, including for example 3D testing of buildings (2 horizontal translations and 1 rotation per storey). Examples of these types of tests and illustrative results are given below.

5.1 3D Tests on a Torsionally Unbalanced Structure

A substantial improvement of the testing capabilities has been obtained by the commissioning of a bi-directional PSD implementation.

In the framework of the research activity of ELSA, PSD testing of a real-size plan-wise irregular 3-storey frame structure is being carried out as the core of the research project SPEAR (Seismic PErformance Assessment and Rehabilitation of existing buildings). The project is specifically aimed at throwing light onto the behaviour of existing old RC frame buildings lacking seismic provisions. A balanced combination of numerical and experimental activities was considered, including a series of full-scale PSD tests on a torsionally unbalanced 3-storey RC frame structure, representing a common configuration of housing units in most earthquake-prone areas of Europe. The experimental phase focused on a real-size specimen (see Fig. 4). The first tests were carried out on the structure in its original, "as built" configuration. Following these tests, a light (i.e., member-level) retrofitting intervention (FRP wrapping of columns to improve ductility) was carried out. A new round of tests will be performed on the retrofitted configuration, so that the effectiveness of currently available guidelines for the design of retrofitting interventions will be judged. Finally, the damage inflicted by the second round of tests will be repaired and the structure more heavily retrofitted, by means of interventions aimed at improving the global structural configuration.
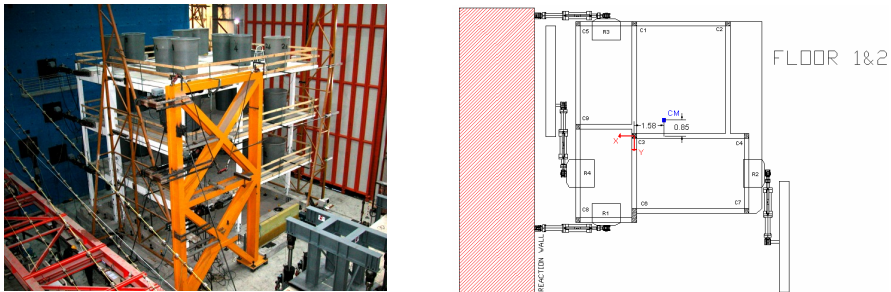
Figure 4. 3D tests on an full-scale model of a torsionally unbalanced RC structure: view of the model at the testing site (left); actuators layout and location of floor centre of mass (CM) (right).

The bi-directionality of the PSD test, consisting in the simultaneous application of the longitudinal and the transverse component of the earthquake to the structure (see Fig. 4), introduces a higher degree of complexity, from both the analytical and technical points of view, with respect to usual unidirectional PSD testing. In fact, three DOFs per storey need to be taken into account: two translations and one rotation along the vertical axis, as opposed to the single degree of freedom per storey that is usually taken into account in unidirectional PSD testing. Four actuators per storey were connected to the structure, three of which were strictly necessary. A redundant

number of actuators requires a more complex control strategy. The structure was subjected to two tests (with PGA of 0.15g and 0.20g) each test with one accelerogram in each direction. Illustrative results from the second test (0.20g) are given in Fig. 5, which shows rather different column drift histories resulting from the induced torsion of the building. Detailed analysis of the test results and test set-up can be found elsewhere (Negro, 2004).
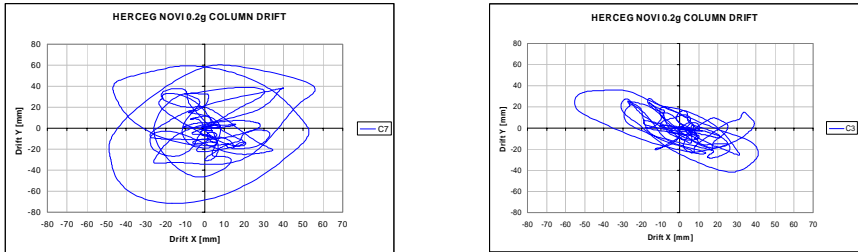
Figure 5. Second storey X and Y direction drifts for two external corner columns.

5.2   Integration of Numerical and Experimental Simulations

Another major advancement in testing techniques was obtained by the development of non-linear substructuring techniques in PSD testing.

ELSA already had a long experience on PSD testing with substructuring in application to bridges. PSD testing with linear substructuring was successfully applied to bridges at ELSA in the mid '90s (Pegon, 2000). A series of PSD tests were performed on regular and irregular bridges designed according to the Eurocodes, with the three piers of the model-bridge built and physically tested and the deck simulated numerically with linear FEM. The test campaign comprised also isolation solutions to tackle the irregularity problem and addressed the issue of asynchronous input motion (Pinto, 1996). An extension of this technique is the use of non-linear models for the numerical parts of the structure — "non-linear substructuring".
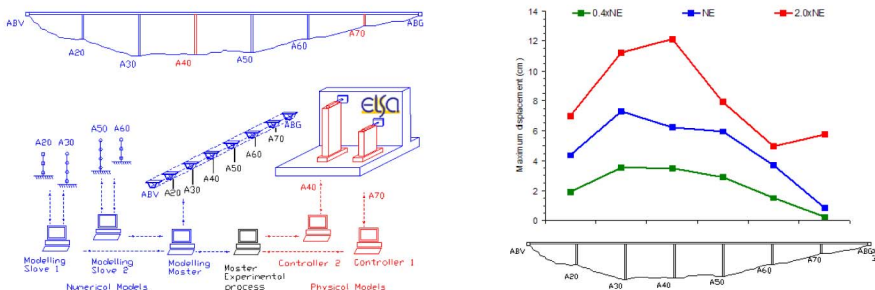
Figure 6. PSD testing with substructuring: application to bridges: test setup and EQ demands.

Non-linear substructuring was recently applied at ELSA allowing the assessment of the performance of a six-pier bridge to be made with physical testing of two piers and on-line simulation of the remaining piers (non-linear numerical models) and deck (linear numerical model). A schematic representation of the test set-up is shown in Fig. 6a). The bridge was tested for three input motion intensities corresponding to probabilities of exceedance of 50, 10 and 2%, in 75 years (tests: 0.4xNE, 1.0xNE and 2.0xNE). Recorded values of the maximum top displacement of the piers are shown in Fig. 6b). Detailed description and analysis of the results can be found elsewhere (Pinto, 2004).

5.3   Other Potential Applications of PSD Testing with Substructuring

Substructuring in pseudo-dynamic testing offers a series of possibilities, which can reduce costs of the experimental set-up and give way to the simulation of earthquake response of large-structures (long or tall) that would be impossible to accommodate in a laboratory (for example the case of bridges). Testing of isolation and dissipation devices with the structure simulated numerically and testing of a base isolated system (structure and dissipation or isolation devices) with online testing of the structure and with the devices tested apart from the structure have already been done at ELSA for buildings and bridges. Another interesting field where substructuring can be considered is SSI. On-line numerical simulation of the soil or structure behaviours can be achieved. There are also challenging objectives for geographically distributed PSD testing, continuous PSD testing and fast PSD testing (to cope with strain-rate requirements) and coupling of PSD and shaking table facilities.

Need and relevance to performance based seismic design of some of the above-mentioned possibilities and features might seem debatable. However, it is important to note that the tendency is to perform more reliable and accurate experiments and to move from element/sub-assemblage to systems testing (physical and hybrid), which encompasses the objectives of PBSD.

6. CONCLUSIONS

A series of tests performed at ELSA in support to the development and calibration of the Eurocodes and in support to the assessment and re-design of existing vulnerable structures have been presented. Focus has been placed on the issue of the definition of test protocols aiming at the assessment of the structure performance for different levels of the input motion. A performance-oriented test protocol would require several tests for different levels of the input motion. However, this may be unrealistic because sequential tests on the same structure would lead to unrealistic damage accumulation. A test protocol considering input motions corresponding to serviceability and life-safety limit-states with a subsequent test to derive ultimate capacity appears to be the most appropriate. It is underlined that a 'serviceability test' is indispensable to calibrate loss functions required in performance and risk-based design and assessment approaches. Non-structural elements must be also included in the test models.

New experimental facilities and test methods able to perform complex tests and to combine numerical and physical simulation should play an important role in the clarification of open issues in the design and assessment of structures, such as structural irregularity, SSI, variability and type of input motions and in the study of complex systems such as structures with dissipation devices, which may address the problem of excessive expected economic losses. Performance and risk-based design shall benefit from the creation of a comprehensive database of experimental results.

New measuring/recording systems, such as digital video systems to record response and damage during the tests will also provide better information and evidence on local and global damage evolution and allow better damage descriptions.

Assuming that performance based design is achieved, accepted and implemented, practice will move from prescriptive to performance-based codes widening the possibilities for creativity and innovation but also transferring more responsibility to the designer, to the owner and to other players in the process. Anticipating that recourse to testing and testing/simulation will be necessary, in particular for innovative solutions, it will be required to agree on a 'qualification procedure', focused on standard testing protocols, which provide realistic/reliable performance evaluation.

REFERENCES

Fardis, M. N. (2004). A European perspective to performance-based seismic design, assessment and retrofitting. (These proceedings).

Hadjian, A. S. (2002). A general framework for risk-consistent seismic design. *Engng Struct. Dyn.* 2002; 31:601-626.

Krawinkler, H. (1999). Challenges and progress in performance-based earthquake engineering. *International Seminar on Seismic Engineering for Tomorrow – In Honor of Professor Hiroshi Akiyama.* Tokyo, Japan, November 26, 1999.

Negro, P., A. V. Pinto, G. Verzeletti, G. E. Magonette. (1996). PsD tests on a four-story R/C building designed according to Eurocodes. *Journal of Struct. Engineering - ASCE*, Vol. 122, No. 11, 1409-1417.

Negro, P., E. Mola, F. Molina, G. Magonette. (2004). Full-scale PSD testing of a torsionally unbalanced three-storey non-seismic RC frame. *Proceedings of the 13th WCEE*, Vancouver, Canada.

Pegon, P., A. V. Pinto. (2000). Pseudodynamic testing with substructuring at the ELSA Laboratory. *Engng Struct. Dyn.* 2000; 29:905-925.

Pinto, A. V. (ed.). (1996). Pseudodynamic and shaking table tests on RC bridges, *ECOEST – PREC8 Report No.5*, LNEC, Lisbon.

Pinto, A. V. (1998). Earthquake performance of structures – behavioural, safety and economical aspects. *Special Publication N. I.98.111* (PhD Thesis), European Commission, Joint Research Centre, Ispra, Italy.

Pinto, A. V., H. Varum, J. Molina. (2002). Experimental assessment and retrofit of full-scale models of existing RC frames. *Proceedings of the 12th European Conference on Earthquake Engineering, EAEE*. London. Elsevier Science Ltd.

Pinto, A. V., P. Pegon, G. Magonette, G. Tsionis. (2004). Pseudo-dynamic testing of bridges using non-linear substructuring. *Earthquake Engng Struct. Dyn.* 2004; 33:1125-1146.

PERFORMANCE BASED ASSESSMENT — FROM GENERAL METHODOLOGIES TO SPECIFIC IMPLEMENTATIONS

Matej FISCHINGER[1], Darko BEG[1], Tatjana ISAKOVIĆ[1], Miha TOMAŽEVIČ[2], Roko ŽARNIĆ[1]

ABSTRACT

Two main objectives has been followed — to identify some potential pitfalls related to specific applications of general PBA procedures as well as to make an overview of the related experimental and analytical research in Slovenia. RC viaducts, lightly reinforced limited ductile RC walls, partial-strength steel connections, timber-frame buildings and masonry buildings are addressed. Efficient inelastic models are presented and validated with experiments and blind predictions. It is demonstrated that extrapolation of the standard push-over procedures from buildings to bridges should be done with care. Irregularity index is introduced to identify those viaducts to be preferably analyzed by inelastic time-history procedures. Multimode pushover procedures and torsionally flexible viaducts are analyzed in some depth. Global engineering demand parameters may fail to predict damage level in RC structures. Analyzed walls were heavily damaged at drifts below 1%, while local deformations at the base were close to ultimate values. It was demonstrated that asymmetric endplate bolted connections behave better than it would be expected considering low strength and ductility of the weaker side. Two-step mathematical model using universal longitudinal spring is proposed for dynamic analysis of timber-frame structures. Behavior factors and damage indices for masonry buildings are experimentally assessed.

Keywords: Performance based assessment; Bridges; RC walls; Partial-strength steel connections; Timber-frame buildings; Masonry structures.

1. INTRODUCTION

Performance based seismic engineering (PBSE) methodologies have been typically tested against limited number of structures belonging to well investigated structural types (predominantly building frames). Extrapolating these procedures to other, specific and/or less investigated systems, should be done with care. Bridges, especially viaducts with continuous deck, typically used in Europe, may belong to such category of structures as demonstrated in Chapter 2.

[1] *Faculty of Civil and Geodetic Engineering, University of Ljubljana, Jamova 2, Ljubljana, Slovenia*

[2] *Slovenian National Building and Civil Engineering Institute, Dimičeva 12, Ljubljana, Slovenia*

To evaluate some performance and damage criteria one may need advanced, experimentally verified analytical models and computational tools, in particular if the investigated system implies special, less-investigated and/or limited ductile structural details. The paper addresses a number of such specific systems recently investigated by Slovenian researchers, both experimentally and analytically — lightly reinforced structural walls (Chapter 3), steel frames with partial strength connections (Chapter 4), timber-frame buildings (Chapter 5) and masonry structures (Chapter 6).

There has been general impression that much more research effort in PBSE has been employed on the demand side than on the capacity side. Consequently relatively crude and loosely defined damage criteria (like 2% drift) are frequently used in conjunction with sophisticated and detailed demand evaluations. Some research results related to the capacity evaluation of the addressed structural systems is included in the paper.

In short, there are two main objectives of the presented paper — to identify some potential pitfalls related to specific applications of general PBA procedures as well as to make an overview of the related experimental and analytical research in Slovenia.

2. RC VIADUCTS WITH CONTINUOUS DECK

Extrapolation of the standard push-over procedures from buildings to bridges should be done with care, as it will be demonstrated in the case of the analysis of single-column bent RC viaduct in the transverse direction. There are several differences in structural system of such bridges compared to buildings: (a) The superstructure of the viaduct is often quite flexible in its own plane. Consequently, many modes can be excited during the response, depending on the instantaneous stiffness of the piers. (b) In bridges the structural elements resisting lateral load are usually situated in one plane only. Therefore, quite complex torsional (in the case of the roller supports at the abutments) and distorsional (in the case of the pinned supports at the abutments) response modes can be excited. (c) It is not straightforward to define characteristic force and deformation as well as deformation shape of viaduct structure for push-over analysis. All these may preclude the use of the inelastic static analysis. Thus, the objective of the reported research has been to identify the cases where the pushover analysis (either single mode or multi mode) is acceptable and the cases where more rigorous inelastic time-history analysis is required for typical European viaduct structures. Only one, irregular, torsionally sensitive viaduct (Fig. 1), which was experimentally tested in ELSA (Pinto 1996) and addressed by many researchers, is presented here as the main example. More complete results are available in (Isaković et al. 2003).

Many codes (i.e., EC8/2) would classify this viaduct as regular since (due to the very stiff central column) the eccentricity is 0.6%, which is less than 5%. Consequently simple single mode push-over procedure would be allowed and even encouraged by the code for this viaduct.
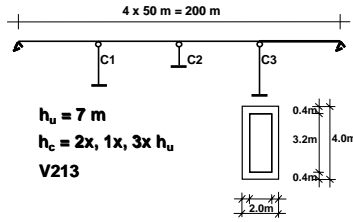
Figure 1. Irregular, torsionally sensitive viaduct V213.

2.1 Single Mode Procedures

Elastic single mode method (SM) grossly underestimates the displacement at the stiff side of the analyzed viaduct when compared with the results of the elastic multi mode (MM) method (Fig. 2). This is why the SM excites only first — torsional (asymmetric) mode, while the second — translational mode predominantly influences the displacement on the stiff side.
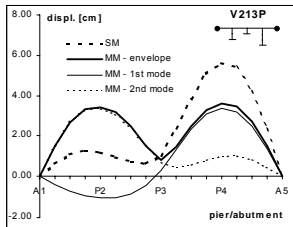
Figure 2. Influence of higher modes in viaduct V213.
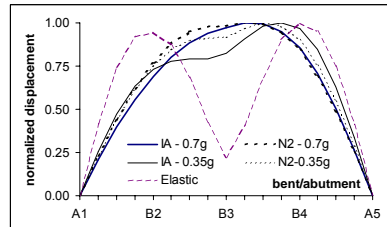
Figure 3. Displacements of viaduct V213.

Similar trend is observed in the case of inelastic analysis, but the importance of higher modes has diminished by increased level of yielding in piers. Results of standard, single mode push-over based procedure N2 (Fajfar and Fischinger, 1988) and inelastic time-history analysis (IA) are compared in Fig. 3 for two different load intensities ($a_{g,max}$ = 0.35g and 0.7g). Results are further compared with elastic MM method (see also Fig. 2). It is obvious that with the increased pier plastification the single mode associated with the (elastic) deck deformation prevails in the response. The conclusion, that in general single mode static methods can not be used for torsionally flexible structures has been frequently mentioned in the case of buildings (i.e., Rutenberg and Tso, 2004).

The research (Isaković et al. 2003) has indicated other important parameters that enhance the influence of higher modes and consequently increase the irregularity of bridge response as well as preclude the use of single mode methods. First of all this is the ratio of the stiffness of the deck and that of the piers (affected also by the level of plastification in piers). Others include eccentricity and type of constraints at the abutments.
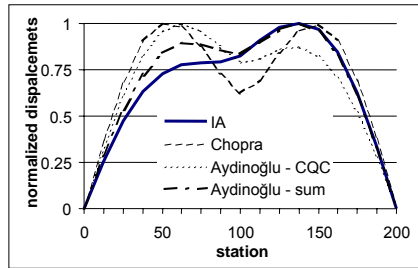
Figure 4. Normalized displacements of V213 (multi-mode and IA methods).

2.2 Multimode Procedures

Realizing the limited applicability of the single mode methods, several researchers have developed methods taking into account the influence of higher modes. However they were predominantly tested for building structures. For example, Chopra's method (Chopra 2002) is a push-over based procedure, where the structure is pushed using displacements shapes of all important modes, determined by the elastic multi-modal analysis. The results are then combined using SRSS rule. However, such an approach may not be applicable for irregular (i.e., torsionally flexible) viaducts (see Fig. 4), since the method does not take into account that the shape of the modes as well as their contribution to the total response are changing during the response.

Aydinoğlu (2004) takes into account variations of modes and variation of their importance during the response. Properties of a structure are changing according to the formation of the plastic hinges. The CQC rule is used to combine important modes. However, in the case of the viaduct V213 such an approach still overestimates the displacements on the stiff side of the viaduct (Fig. 4). It seems that this is due to the CQC combination rule, where the sign of the quantities is lost (neglected). If, in this particular case, contributions of different modes are simply summed, the results are much closer to the results of the inelastic time-history analysis. By definition any multi-mode spectral method depends on combination rules. Furthermore, no combination rule can be fully theoretically justified. Therefore, the research related to inelastic spectral multimode procedures is still a long way to go. The importance and influence of different combination rules was recognized and studied by Reinhorn and his associates (DeRue 1998) who analyzed the viaduct very similar to the V213.

2.3 Irregularity Index

Kawashima (2004) reports that in the questionnaire survey 46% of the 100 Japanese civil engineers answered that "they want to use dynamic response analysis for bridges to which push-over analysis provides poor application". But which are those bridges? V213 viaduct is one such example. Single mode methods do not work for this viaduct. Some multi mode methods may improve results, but the outcome is uncertain and

some procedures are (contrary to the opinion of their authors) quite complicated for the use in design.

An attempt was made (Isaković et al. 2003) to provide designers with a simple tool (a single number called irregularity index) to identify those bridges to be preferably analyzed by inelastic time history analysis rather than by the standard single mode N2 procedure. The concept of the proposed irregularity index is presented in Figure 5. It is based on the comparison of the displacement shapes obtained in the two iterations of the push-over in the N2 method (it could be used in the elastic range to determine the applicability of the Rayleigh's method, too). If the areas bounded by these displacements lines are very different, the displacements are changing during the response, and the inelastic time-history analysis is recommended. If not, the designer may proceed with further steps of the N2 procedure.

What is "very different" is still quite arbitrarily defined, but in general the index below 5 % defines conservatively the viaduct, which can be analyzed by push-over procedure (defined as regular viaduct). Some examples of regular and irregular bridges and corresponding irregularity indices are presented in Table 1.
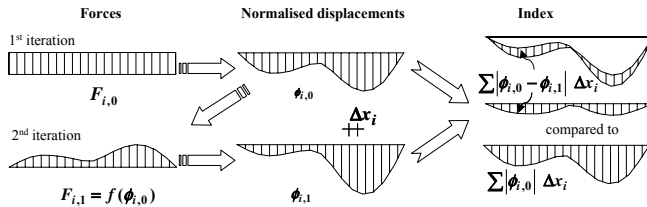
Figure 5. Definition of the irregularity index.

Table 1. Irregularity index for several types of viaducts (PGA = 0.35g)

Example of viaduct	Difference between SDOF and MDOF - D[%]	Irregularity index IRI [%]
V123 P	7.4	6.9
V213 P	7.9 ("weak" reinforc.) 14.4 ("strong" reinforc.) 4.4 (PGA = 0.7 g)	7.3 ("weak" reinforcement) 19.6 ("strong" reinforcement) 1.7 (PGA = 0.7g)
V121 P	7.2	9.3
V232 P	0.4	0.4
V213 R	45.5	17.4

P — viaducts with pinned supports at the abutments; **R — viaducts** with roller supports at the abutments; **weak reinforcement** — based on seismic forces in transverse direction; **strong reinforcement** — based on seismic forces in both directions

3. LIGHTLY REINFORCED LIMITED - DUCTILE RC STRUCTURAL WALLS

The research of the seismic response of RC walls has been rather limited in comparison to frames. In particular there are few research results related to thin, lightly reinforced and limited ductile walls in low- to medium-rise buildings with high wall-to-floor ratio. Such buildings are typical for central Europe. Recently, shaking table test of a 5-story cantilever wall designed according to EC8 (Fig. 6) was performed in the frame of the CAMUS 3 benchmark project. Large, 1:3 model was subjected to a sequence of 4 accelerograms. The wall was heavily damaged and close to collapse after the fourth run (Fig. 7). Blind prediction was made (Fischinger et al., 2004) using multiple-vertical-line-element model (MVLEM). In the frame of this paper only a few observations related to PBA issues will be addressed.

Figure 6. CAMUS 3 test.

Figure 7. Damage to the edge of the wall at the end of the test sequence (CAMUS 3).

3.1 Initial Damage

While MVLEM had demonstrated excellent performance in previous studies, bad correlation of predicted and experimental results (Fig. 8a) in the first (low level) run came as a negative surprise. Later it was explained by the benchmark organizers that the wall was subjected to additional loading during initial testing of the setup, prior to the main test. But, since there was no visible damage and the natural frequencies had not changed, they considered this preceding loading unimportant. However, if this preceding loading was considered in the analysis, the match would be very good (Fig. 8b). This example demonstrates that in RC structures damage is not easy to observe and define. Such initial damage, influencing subsequent response, might exist in many actual situations.
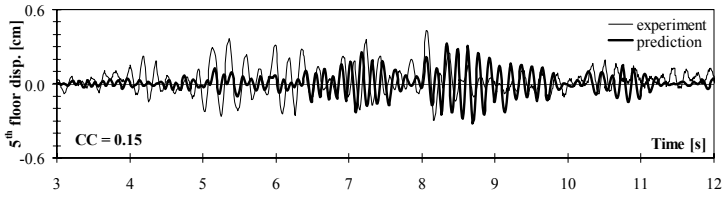
Figure 8a. Low level response — preceding load is not considered.
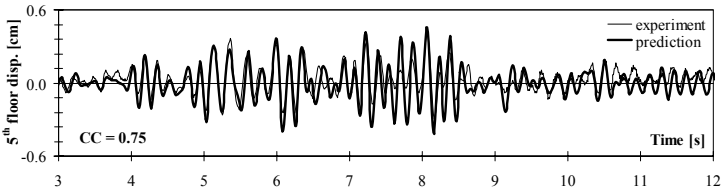
Figure 8b. Low level response — preceding load is considered.

3.2 Near Collapse Performance, Local Failure

The prediction for the last — fourth run was completely wrong (Fig. 9a). It was realized during post-experimental analysis that in the second run the boundary reinforcement at the base of the wall experienced large ductility demand. Since some (low-diameter) bars in that area were quite brittle, they most probably failed. Since the first author of this paper was interested only in global EDPs (like top displacement) he overlooked the possibility of this failure, which was not automatically detected either by DRAIN or by OpenSees. When the potentially fractured reinforcement was omitted in the analysis after the second run, the correlation between experiment and analysis was good (Fig. 9b). This example demonstrates that global damage measures may fail to predict damage level in RC structures. It should be emphasized that the top drift of the wall was less than 1% even in the fourth run, which should not indicate major damage by any accepted criterion. However, the wall, designed according to modern code, was very close to collapse (Fig. 7). It has been also demonstrated that standard models may have problems simulating near collapse behavior.
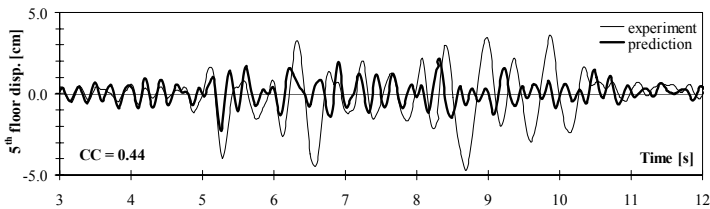
Figure 9a. Near collapse level — brittle reinf. is included into model.
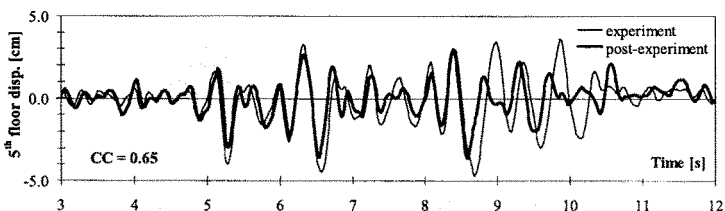
Figure 9b. Near collapse level — brittle reinf. is excluded from model.

3.3 Parametric Study

Using models and procedures calibrated within the CAMUS study and simplified non-linear assessment method N2, an extensive deterministic parametric study of idealized buildings with structural walls (Fig. 10) designed according to EC8 was done. The influence of the flanges and wall openings has not been considered.

The area of the wall was kept constant (A_{wall} = 1.0 m^2). The varied parameters included maximum ground acceleration ($a_{g,max}$ = 0.1g, 0.2g, 0.3g), seismic force reduction factor (behavior factor q = 1.5, 2, 3, 4, 5 in 6), number of stories (n = 5, 10, 15) and wall-to-floor ratio (ρ_1 = 1%, 1.5%, 2% in 3%). Axial force was calculated based on one half of the tributary area (considering walls in the perpendicular direction).
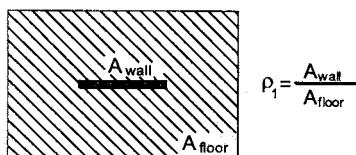
Figure 10. Idealized floor plan.
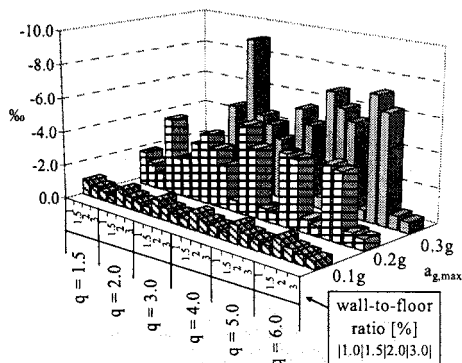
Figure 11. Maximum def. on the compression edges of the walls (10-story buildings).

The results will be presented at the 13th WCEE (Fischinger et al., 2004). Only one result is demonstrated here for illustration. The deformation of the compression edge was chosen as one of the EDPs indicating local damage related to required confinement. In Fig. 11 the deformation of the compression edge for 10-story buildings (the highest of the buildings typically built in Slovenia) is plotted as the function of the behavior factor (q) and wall-to-floor ratio (ρ_1) on one axis and $a_{g,max}$ on the other axes.

While the global drift of the buildings (not presented here; see Fischinger et al. 2004) never exceeded 1%, large compression deformations (more than 0.5%) were observed in higher buildings subjected to moderate earthquakes. In these cases, wall to floor ratio becomes very important. If this ratio is more than 2%, compression should be within acceptable range. However, confinement in needed in walls with lower wall-to-floor ratio.

This example might demonstrate that even simple deterministic studies using simplified push-over procedures may provide meaningful information about seismic vulnerability of structures.

4. PARTIAL-STRENGTH CONNECTIONS IN STEEL STRUCTURES

In steel construction in Slovenia partial-strength connections were very often used without assuring the rotation capacity of these connections. Especially asymmetrical end-plate bolted connections with extended end-plate at the upper and flush end-plate at the lower side of the connection were popular (see Fig. 12). They are suitable to resist gravity loading in non-sway frames and can be used also in sway frames when horizontal loading is not very important as in the case of moderate wind loading in non-seismic regions. In seismic conditions the tension can arise also at the weaker side of the connection, which then acts as a partial-strength connection with predominant non-ductile failure at bolts. Under the German influence this type of connections was introduced into Slovenia and sometimes used without sufficient precaution disregarding the fact that Slovenia is unlike Germany a seismic region.

To get an insight into the behavior of asymmetric endplate connections experimental and numerical investigations were performed. The main purpose of this work was to assess the sensitivity to weaker side collapse of the connections in earthquake conditions as well as further behavior of partly damaged frames.

4.1 Experimental Analysis

Tee shaped beam-column assembly was chosen to represent a part of a real frame around the connection. The beam part of the assembly was made of IBE 300 hot rolled profile and the column part of HEB 200 hot rolled profile. The tests were run under displacement control following the sinusoidal pattern with constant amplitude of approximately two times the yield displacement. The constant frequency of 0.5 Hz was applied.

The first specimen was able to withstand 93 cycles (Fig. 13) and the second one 118 cycles before collapsed. Relatively large number of cycles was obtained because the imposed displacement amplitude of two times the yield displacement is relatively small and can be expected in moderate earthquakes.
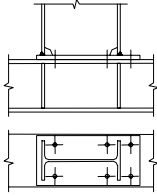
Figure 12. Asymmetric endplate bolted connection.
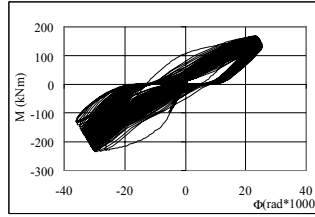
Figure 13. Moment-rotation diagram.
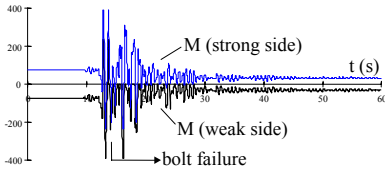
Figure 15. Moment-time diag.
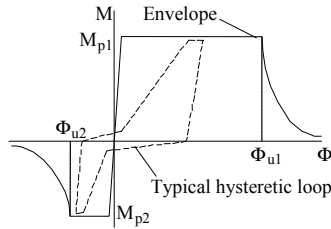
Figure 14. Modeling of the connection spring.

4.2 Numerical Modeling of the Connection

On the basis of the test results and calculations the connection behavior was modeled numerically. A rotational spring element was implemented into the computer program for nonlinear dynamic analysis DRAIN 2DX.

The numerical model (Fig. 14) of the connection includes asymmetric hysteretic behavior, pinching effect, low ductility for tension on the weak side of the connection due to the possibility of rupture of bolts. It can also represent the connection behavior after the possible rupture of the weak side bolts.

Time-history analysis was performed using computer program DRAIN 2DX. Simple one bay single story frames were run first to study the response of asymmetric connections and than an existing three story industrial building was analyzed. Two different real properly scaled accelerograms (Kobe-1995, Ulcinj-1979) were used. A typical response of simple frame connections is shown in the moment-time diagrams in Fig 15. Bolt failure at the weak side of the connection happened after the second strong shock.

4.3 Results

On the basis of the test results on connections and numerical simulations of frames it is possible to conclude that asymmetric endplate bolted connections behave in earthquake conditions better than it would be expected considering low strength and ductility of the weaker side of the connections. It is certainly not our aim to encourage

302

the use of such connections in earthquake resistant steel frames, but it is important to recognize that there is a potential resistance to seismic actions. Even after rupture of bolts on the weaker side, connections (and frames) can sustain further earthquake shocks acting as rigid in one and as pinned in the other direction. Stiffness of frames is decreased in this case but a collapse does not occur as long as the resistance is not reached also on the stronger side of a connection. An existing three story industrial building suffered rupture of bolts at the weaker side of two connections but the overall behavior of the frame was not affected importantly.

5. TIMBER-FRAME BUILDINGS

In light-frame buildings, shear walls are typically composed of wood framing and panel sheathing attached with dowel-type fasteners, usually nails. The dowel-type mechanical connections are performing in an inelastic manner. Consequently, the behavior of timber-frame wall panels to varying loads is inelastic. Deformability of shear wall reflects in elastic deformation of sheathing material and framing members and inelastic deformation of fasteners. For modeling the displacement response of shear wall it is very important to develop an accurate model for the orthotropic inelastic behavior of fasteners in wood materials.

5.1   Numerical Model

A two-step macro model for the calculation of the entire wood structure response has been developed (Fig. 16). Within the first step (cyclic analysis) each single woodframe wall is numerically analyzed on the basis of the known inelastic behavior of fasteners. The result of analysis is a hysteretic response of the wall. Based on this result, mechanical characteristics of inelastic spring that simulates the behavior of a physical body – woodframe wall are derived. In the second step of the analysis (dynamic analysis) the entire building structure is simulated with inelastic springs simulating load-bearing walls. The model is supported by two different software packages, i.e., DRAIN-2DX and CANNY-E. The results of two-dimensional analyses performed by DRAIN-2DX are used for the composition of three-dimensional structural model suitable for the prediction of response of analyzed wood framed building. Three-dimensional analysis is performed by CANNY-E program.

To model both, structural connectors and equivalent structural struts, an element, called ULS (Universal Longitudinal Spring) has been developed. The physical model is a longitudinal spring with appropriate length down to infinitely short dimension. The model had been originally developed for the modeling of masonry infill of reinforced concrete frames (Žarnić 1994) and later modified for the simulation of inelastic response of nailed sheathing to framing connections (Dujič & Žarnić 2003). It applies significantly modified hysteretic rules proposed by the authors of the IDARC program (Park et al. 1987) and original skeleton curve with ductility and

descending sections (Žarnić and Gostič 1997). These, universal hysteretic rules are presented in Figure 17.
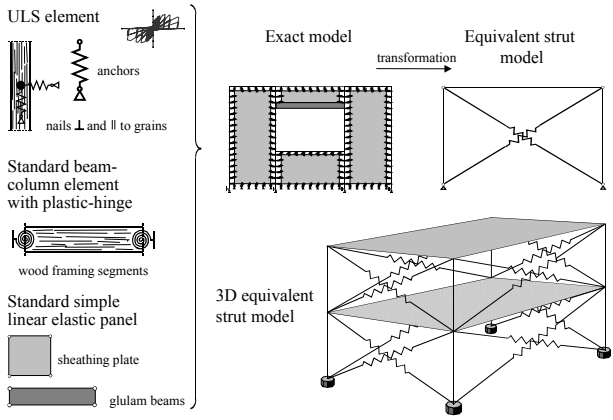
Figure 16. Two-step mathematical model for the dynamic analysis of timber-frame structures.
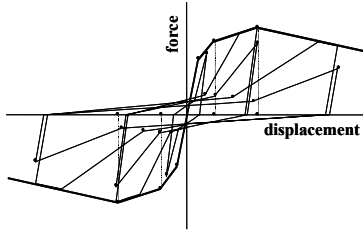
Figure. 17 ULS hysteretic model.

The mathematical model of load-bearing walls consists of the assemblage made of sheathing plates connected to wooden frame. In the mathematical model each nail is represented by two longitudinal inelastic spring elements. The first spring element simulates the behavior of the nail parallel to the grain of wood connection, while the second one represents the behavior of the nail perpendicular to the grain of wood connection. The framing members of the shear walls were modeled with linear elastic beam elements with plastic-hinges at both edges. Sheathing panels were modeled by linear elastic panel elements. The studs at the edges of sheathing segments were anchored with tie-downs or anchors, depending on the position of the stud, and modeled with inelastic spring elements.

The second step is the dynamic analysis of the 3D model performed with the CANNY-E program. The wood framed structure can be modeled as multi story

frame-floor system with equivalent strut bracing and stiff diaphragms representing slab and roof construction.

5.2   Implication of the Model

Efficiency of the model was demonstrated within the CUREE-Caltech Woodframe Project. The shake table tests on a full scale two-story wood framed residential building were carried out in Charles Lee Powell Laboratory in La Jolla, California. Blind prediction of the response of the tested structure was made (Dujič and Žarnić 2001). Good correlation between the numerical prediction and the test results demonstrated high efficiency of the mathematical model, although only very basic data were available (Dujič and Žarnić 2003).

6. MASONRY STRUCTURES

In the last years, part of the masonry research at Slovenian National Building and Civil Engineering Institute has been oriented towards obtaining information about the values of design parameters which would ensure adequate performance of newly designed masonry structures in seismic conditions. In one of the studies, the propagation of physical damage to masonry walls and structures under lateral load has been analyzed and an attempt has been made to find a correlation between the amount of damage and limit states, used in the seismic resistance verification. On the basis of the analysis of experimental results, it has been shown that, although the type of damage to masonry walls and buildings varies in dependence on construction system, such as plain, confined and reinforced masonry, the damage to structural walls can be classified and damage indexes I_d introduced in an uniform way. Typical values of I_d are presented in Fig. 18.
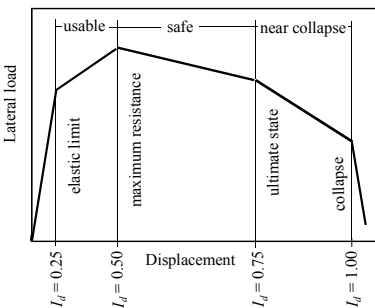
Figure 18. Seismic resistance envelope with characteristic limit states, states of usability of building, and attrib. damage indexes.
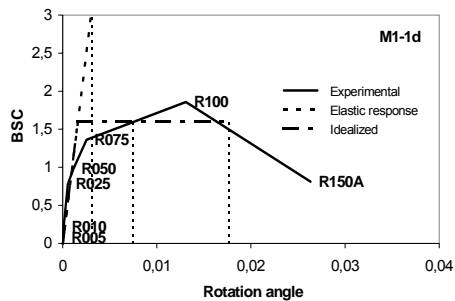
Figure 19. Experimental and idealized — base shear coefficient (BSC) - story rotation angle relationships obtained for a confined terraced house model

Recently, six models representing buildings of two different structural configurations and two different types of masonry materials have been tested on a unidirectional shaking table at ZAG: a two-story terraced house with main structural walls orthogonal to seismic motion and a three-story apartment house with uniformly distributed structural walls in both directions. Four models of the first and two models of the second type, built at 1:5 scale, have been tested. In the case of the terraced house, two models have been built as either partly or completely confined masonry structures (Table 2).

Table 2. Shaking-table tests — description of tested models

Design	Type	Material	Bed joint	Remarks
M1-1	Terraced house	Calcium silicate	Thin	no confinement
M1-2	Terraced house	Hollow clay unit	Normal	no confinement
M1-1c	Terraced house	Calcium silicate	Thin	confined staircase walls
M1-1d	Terraced house	Calcium silicate	Thin	fully confined walls
M2-1	Apartm. house	Calcium silicate	Thin	no confinement
M2-2	Apartm. house	Hollow clay unit	Normal	no confinement

The seismic behavior of the tested models has been analyzed in order to verify the Eurocode 8 proposed values of structural behavior q. The results of tests are summarized in Table 3, where the values of the maximum attained base shear coefficient BSC_{max}, evaluated on the basis of the known masses of the models concentrated at floor levels, and measured floor acceleration responses, as well as the measured values of the story rotation angle at the damage limit Φ_{dam} (corresponding to damage index $I_d = 0.25$), maximum attained resistance Φ_{Hmax} ($I_d = 0.50$) and ultimate limit (before collapse) Φ_u ($I_d = 0.75$) are given.

Table 3. Parameters of seismic resistance of the tested models at characteristic limit states

Model	BSC_{max}	Φ_{dam}	Φ_{Hmax}	Φ_u
M1-1	0.52	0.19%	0.82%	0.91%
M1-2	0.49	0.25%	0.56%	3.98%
M1-1c	0.99	0.26%	0.26%	3.96%
M1-1d	1.86	0.25%	1.31%	2.63%
M2-1	0.69	0.33%	0.33%	0.43%
M2-2	0.55	0.30%	0.66%	1.66%

As regards the influence of different quality of masonry materials on the seismic behavior of the tested building types, it can be seen that the models of both, terraced house and apartment house structural type, made of model materials simulating calcium silicate masonry units (models M1-1 and M2-1) exhibited substantially more brittle behavior than the models of the same type, but made of model materials simulating hollow clay units. However, there has been not much difference observed as regards the resistance. The confinement of structural walls with vertical R.C. confining elements in the case of the terraced house models M1-1c and M1-1d proved to be a successful measure of improving the seismic behavior of the terraced house type of structure as regards both lateral resistance and displacement capacity.

In the idealization of the experimentally obtained resistance envelopes, the story rotation angle (relative story displacement) at the point where 20% of strength degradation has occurred, has been defined as the ultimate story rotation angle (displacement) which the structure can resist without risking collapse. This assumption has been considered in the cases where no sudden collapse of the models (such as was the case of models M1-1 and M2-1) has been observed during the shaking tests. The rotation angle (displacement) at 20 % of strength degradation has been considered as ultimate in the evaluation of the idealized ultimate global ductility factor of the structure μ_u. However, substantial damage to structural walls of the models has occurred at that stage. Therefore and in order to fulfill also the "damage limitation" requirement, only part of the available displacement capacity has been taken into account in the evaluation of behavior factor q on the basis of the global ductility of the structure, limited by the displacement value where severe damage to structural walls occurs. This value has been arbitrarily chosen to be 3-times the value of story rotation at the damage limit $\Phi_u = 3\ \Phi_{dam}$. Typical evaluation is presented in Figure 19.

As has been found by this study, the ranges of values of structural behavior factor q, proposed in Eurocode 8 for different masonry construction systems, are adequate, though conservative. Since the experimental response has been evaluated, an increase in q factor values is expected as a result of overstrength of masonry structures, designed by usual design calculation methods.

The study also indicated that the values of q factor depend not only on the system of construction, but also on the properties of masonry materials and structural configuration, especially structural regularity, of the building under consideration. Therefore, experimental research is needed for the assessment of a particular value for a particular structural type specified on a national basis within the recommended range of values in the basic document. Although such tests are helpful, the values of behavior factor q cannot be assessed by means of only ductility tests of structural walls.

REFERENCES

Aydinoğlu, M. N. (2004). An improved pushover procedure for engineering practice: incremental response spectrum analysis IRSA. *Proc. of Int. Workshop on PBSD*, Bled.

Beg, D. et al. (1999). Behaviour of Unsymmetric Bolted Connections Subjected to Dynamic Loading. *Stability and Ductility of Steel Structures; Proc. 6th intern. colloq.*, Timisoara, Amsterdam: Elsevier.

Chopra, A. K. (2002). A modal pushover analysis procedure for estimating seismic demands for buildings *Earthquake Engineering and Structural Dynamics* 31:561-582.

DeRue, G. M. (1998). *Nonlinear static procedure analysis of 3D structures for design Applications*, Master of Science Thesis, University of New York at Buffalo.

Dujič, B., R. Žarnić. (2001). Numerical Model & Predictions — Team Slovenia. CUREE-Caltech Woodframe Project, *Proc. of the Int. Benchmark Workshop*, p. 15, University of California, San Diego, La Jolla, California, 2001.

Dujič B., R. Žarnić. (2003). Blind prediction of seismic response of timber-frame house. *Skopje earthquake: 40 years of European Earthquake Eng.: SE 40EEE*. Skopje, Macedonia.

Fajfar, P., M. Fischinger. (1988). N2 — a method for non-linear seismic analysis of regular buildings, *Proc. 9WCEE*, Tokyo-Kyoto, Vol. 5, pp. 111-116.

Fischinger M., T. Isaković, P. Kante. (2004). Seismic vulnerability evaluation of lightly reinforced walls. *Proc. of 13th WCEE*, Vancouver.

Isaković, T., M. Fischinger, and P. Kante. (2003). Bridges: when is single mode seismic analysis adequate?, *Structures and Buildings*, 156: SB2: 163 – 173.

Kawashima K. (2004). An analysis of the seismic performance levels of bridges. *Proc. of Int. Workshop on PBSD*, Bled.

Park, Y. J., A. M. Reinhorn, S. K. Kunnath. (1987). IDARC: Inelastic Damage Analysis of Reinforced Concrete Frame - Shear-Wall Structures. *Technical Report NCEER-87-0008*.

Pinto, A. V. (1996). *Pseudodynamic and Shaking Table Tests on R.C. Bridges*, ECOEST and PREC8 Report No. 5.

Rutenberg, V., W. K. Tso. (2004). Horizontally irregular structures: some recent developments. *Proc. of Int. Workshop on PBSD*, Bled.

Žarnić, R. (1994). Inelastic model of reinforced concrete frame with masonry infill – analytical approach. *Int. Journal of Engineering Modelling*, 7, 1-2, pp 47-54.

Žarnić, R., S. Gostič. (1997). Masonry Infilled Frames as an Effective Structural Sub-Assemblage. *Proc. of the Int. Workshop on Seismic Design Methodologies for the Next Generation of Codes*, Fajfar and Krawinkler (editors), Bled, Slovenia.

ON GROUND MOTION DURATION AND ENGINEERING DEMAND PARAMETERS

Edoardo COSENZA[1], Iunio IERVOLINO[1] and Gaetano MANFREDI[1]

ABSTRACT

Impact of records features in nonlinear demand assessment is a controversial issue in earthquake engineering. What Engineering Demand Parameter (EDP) is best correlated with ground motion duration related measures has not been thoroughly addressed yet. The study presented in this paper approaches the problem investigating whether duration matters by statistical analyses of significant study cases. Twenty four SDOF structures have been designed for the purpose, considering several oscillation periods, backbones and ductility levels. Six different EDP's, ranging from kinematics ductility to equivalent number of cycles, have been considered.

Nonlinear analyses deal with ordinary records, therefore soil site and specific near fault effects, such as directivity-induces pulses, are avoided during selection. One class of accelerograms is chosen to represent three specific duration scenarios, and another class is randomly selected from a large catalogue. Responses to different records sets are evaluated in each of the study cases.

Time-history median results are formally compared by statistical hypothesis test to asses the difference, if any, between non linear demands of the sets of records. Incremental Dynamic Analysis (IDA) curves are used to qualitatively assess duration effects as function ground motion Intensity Measure (IM), while quantitative impact of duration on EDP's is assessed by means of fragility curves.

Keywords: Duration; Energy; Engineering demand parameter; Incremental dynamic analysis; Hypothesis test; Fragility curves.

1. INTRODUCTION

1.1   Motivation and Framework

Duration issues in earthquake engineering deal both with capacity and demand. Definition of duration related capacity measures is a non-trivial issue, while it is not clear what EDP is affected by duration (CSMIP, 1993). The latter is approached in this study; aim is showing from a general prospective whether duration matters in nonlinear seismic demand analysis.

---

[1] *Department of Structural Analysis and Design, University of Naples Federico II, Italy*

The goal is pursued by investigating significant cases; SDOF periods are chosen to be representative of each of the four elastic design spectrum branches. Yielding strength is set to get two different ductility levels, comparatively "high" and "low". Evolutionary and non-evolutionary backbones are considered to simulate very different structural behaviors.

Real records sets have been chosen to be representative of three selected duration scenarios; other randomly selected accelerograms have been made available to perform statistical comparisons. Running nonlinear analyses of the SDOF structures, under the designed sets, allows monitoring six different demand measures expected to be differently sensitive to the duration content of ground motion. To establish if duration is an issue among different EDP's of the same structure, hypothesis test response are used; to investigate more deeply how it plays a role in demand analysis trend, and how quantitatively it affects differently structural response among different SDOF, IDA analyses and fragility curves are developed.

This complex experiments space may be helpful in clarifying that "it depends" whether duration matters in nonlinear seismic analysis. Importance of duration changes strongly as function of the chosen EDP while the general conclusion holds with the same EDP across all structural configurations.

1.2   Duration Measures Used in This Study

Total duration of ground motion is a not unique definition quantity, while empirical observations show how it is an important ground motion feature affecting the structural response.

In this study, structural damage evaluation is related to number and amplitude of plastic cycles induced by seismic excitation. I_D factor, introduced by Cosenza and Manfredi (1997) is a good predictor for computation of plastic cycles demand (Cosenza and Manfredi, 2000; Manfredi, 2001) and then it's used in the present study as the duration related index for records. It's defined as in (1) being related to the energy content of ground motion but also with energy dissipated by structural response.

$$I_D = \frac{\int_0^{t_E} a^2(t)dt}{PGA\,PGV} \tag{1}$$

In Eq. 1 $a(t)$ is the acceleration time-history of the ground motion, PGA and PGV are the peak ground acceleration and velocity respectively and t_E is the effective duration of the seismic event. Other definitions of duration indexes are available in literature, as said, hence, the problem is the definition of the earthquake duration in relation with the main energy contents (Cosenza and Manfredi 2000). With regard to this aspect, Trifunac and Brady have defined the effective duration t_D as the time elapsed between the 5% and the 95 % of the root mean square acceleration RMSA; Kawashima and Aizawa (1989) have introduced the bracketed duration t_B as elapsed

time between the first and last acceleration excursion greater than a percentage of PGA. Trifunac and Novikova have proposed a more refined determination of t_D as the sum of the record intervals with a total amount of RMSA greater than the 90 per cent. In the following comparison of I_D with other duration measures is reported for the records herein used.

2. METHODOLOGY

2.1   Study Cases

Study cases are made of four SDOF periods with three different backbones, each of those designed to have two target ductility levels. Demand on the twenty four SDOF structures defined in such way is investigated in terms of six EDP's. Influence of I_D is assessed by hypothesis test (Iervolino and Cornell, 2004); by statistical comparison of demand coming from different sets characterized by different I_D.

Trend of demand as function of intensity measure (IM) (e.g. spectral acceleration, Sa) (Fig. 1) is assessed by Incremental Dynamic Analysis (Vamvakistos and Cornell, 2002) since I_D insensitive to amplitude scaling of records. All records in the sets are individually scaled to get the desired spectral acceleration level for all the EDP's then the median of results is plotted versus spectral acceleration. If results for sets with different I_D are kept separated the three resulting curves provide a qualitative picture of differences in EDP's of I_D.
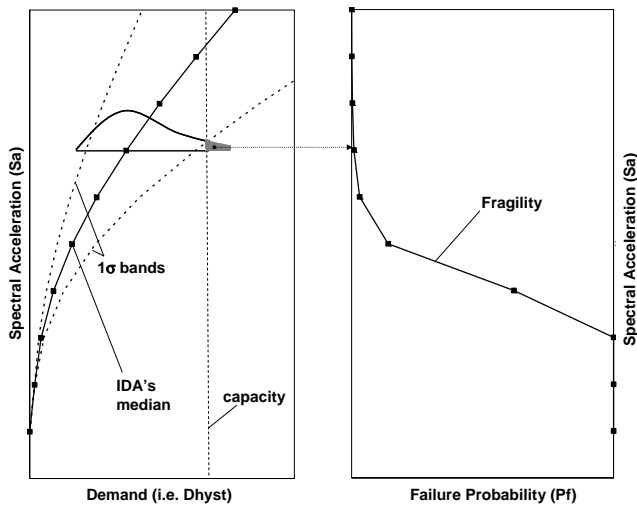
Figure 1.   IDA's based fragility example (T = 0.6 s - Elastic Perf. Plastic SDOF).

Assuming lognormal distribution of the results of different records around median of IDA curve (Fig. 1) and fixing a threshold representative of the structural

capacity, is possible to build up fragility curves for each set, those are representative of the I_D value specific for the set they refer to.

2.1.1 SDOF Periods and Backbones

Four different periods SDOF systems have been considered, *short* (0.1 sec), *moderate* (0.6 s), *long* (1.5 sec) and *very long* (4 sec) in order to investigate if conclusions come to at moderate periods seem to hold at extremes. Chosen periods are representative of different branches of the Eurocode design elastic spectrum. For each of the periods two yield strengths are selected dividing the elastic strength by a factor of 3 (DL3) and 6 (DL6) according to the design spectrum; damping is 5% of critical. Backbones investigated are: elastic perfectly plastic (EP) first as example case and elastic-plastic with hardening (EPH) which avoid possible instability of the first one (Fig. 2). Plus, a stiffness degrading model is considered such as modified Clough (MC) (Mahin and Bertero, 1981).
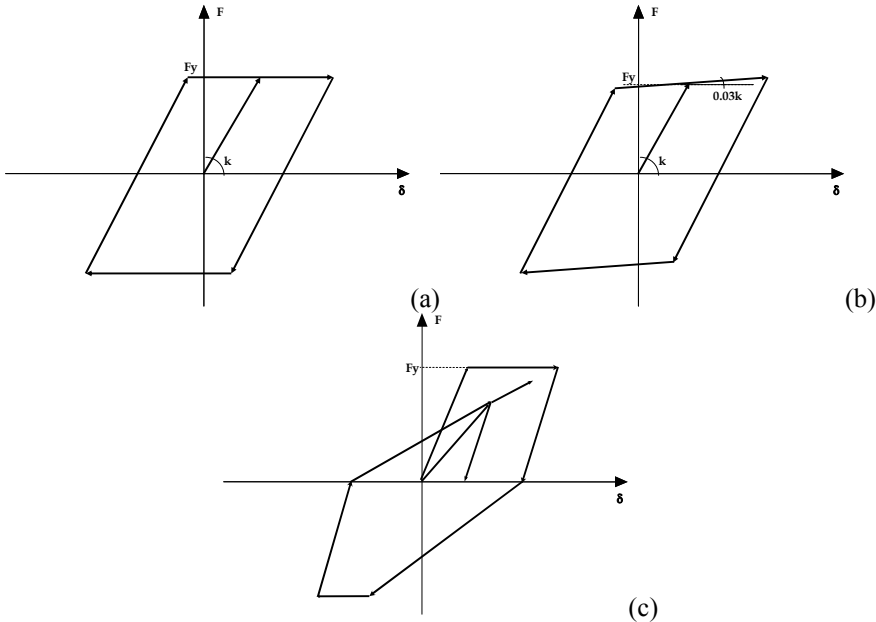
Figure 2. Backbones investigated: EPP (a), EPH (b), MC (c).

EPP model is a non evolutionary model as EPH; they're representative of peculiar structural situation such as welded connections steel frames without instability problems. EPP model is not evolutionary or degrading. Modified Clough model is evolutionary in terms of elastic stiffness; it has been added to the analyses to

cover a larger range of structural cases keeping it simple: still clearly separating elastic phase to inelastic phase.

2.1.2   Engineering Demand Parameters

Different demand measures are differently sensitive to earthquake duration, assess whether duration matters for EDP's is the main goal of the study. Has been shown poor correlation of duration indexes with displacement demand, while is of certain interest to see what happens changing the collapse criterion. Demand measures considered are: kinematics ductility (Dkin); cyclic ductility (Dcyc); plastic fatigue (Fp, b = 1.8); plastic fatigue (Fp, b = 1.5); hysteretic ductility (Dhist). Equivalent number of cycles (Ne) has also been considered since it's well correlated with the energy measure adopted in this study. Details about EDP definitions herein used may be found in Krawinkler and Nassar (1992), Cosenza et al. (1993), Fajfar and Vidic (1994) and Cosenza and Manfredi (2000). Fig. 3 summarize study cases, each dot is a particular designed SDOF structure. All SDOF's in Fig. 3 are investigated in terms of all six EDP's listed above.
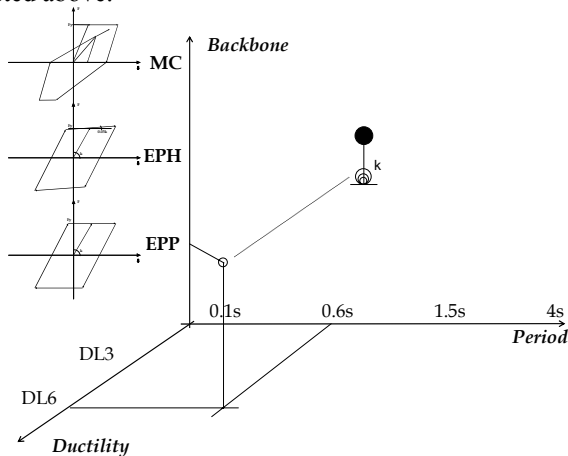
Figure 3. SDOF's analysis space.

2.2   Accelerograms

All the records herein considered came from the Pacific Earthquake Engineering Research Center (PEER) database, so that we may assume they all are processed the same. However all the accelerograms in both of the groups of sets have been selected with some boundary conditions in order to better reduce the influence of those factor that are not in the objective of the study. In particular only records from C-D NEHRP soil classes and coming from free field or one story building instrument housing have been considered. These features make the records definable as ordinary, avoiding site and housing response effects. Moreover, for addressing the selection issue the records

belong to the far field so that come from stations at over 25 km in distance in order to better avoid directivity pulse-type effects.

2.2.1 Class of Target Sets

Similarly to what presented in Iervolino and Cornell (2004) the target sets for the record selection study are designed to be representative of specific scenarios; i.e. duration. Three sets of 20 records each have been set up to be I_D specific in the median ($I_D = 5$, $I_D = 13$, $I_D = 20$). Scatter around the median values are due to unavailability of enough records with required features in the database, this scatter will affect results especially in $I_D = 20$ sets where it is stronger.

(a)

(b)
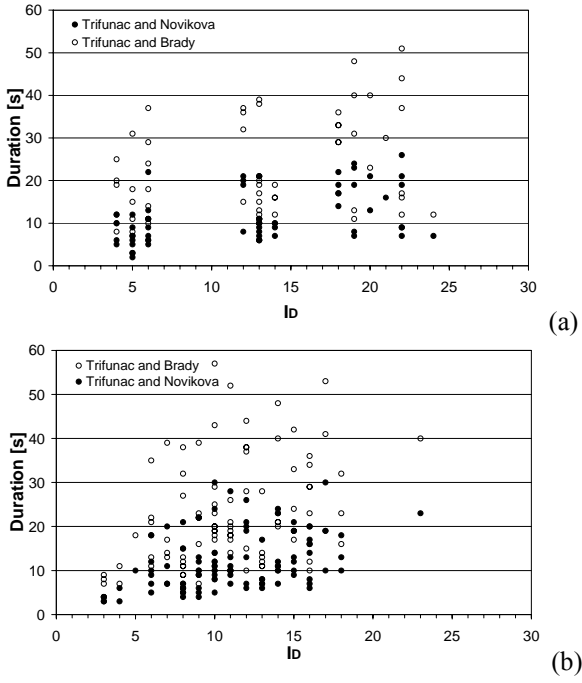
Figure 4. I_D vs. duration in the T (target sets) (a) and A (arbitrary sets) (b).

Duration characteristics of target sets are shown in Figure 4(a) where I_D is represented versus other duration definitions (Trifunac and Brady, 1975; Trifunac and Novikova, 1994). In order to best represent what might occur in the future and to reduce correlation due to event commonality, it is desirable to have the records in each set coming from different events. This requirement conflicts with the desire to have a large sample. Target sets have been split in two of size ten which is the order of magnitude used in recommended earthquake engineering practice, but also to formally compare different sets with the same I_D. The size ten sets are named: T5a,

T5b, T13a, T13b, T20a and T20b can be easily retrieved in the PEER on-line database.

2.2.2   *Class of Arbitrary Sets*

While part of the analysis is comparing sets with different specific I_D, has been considered useful to compare target set to sets randomly selected records which are not subjected to catalog limits and may give another proof if duration is an issue or not. These sets were chosen effectively randomly (in terms of I_D) from the catalog. The *arbitrary sets* are ten sets of ten records each. The records in each set are chosen randomly (without replacement) first from the list of events and then from the available distances within a certain event to the degree possible. Features of arbitrary sets are shown in Figure 4(b).The record samples used in this study have been found having correlation of about 40-45% between I_D and other duration measures.

3. RESULTS AND DISCUSSION

Selected result are presented in the following; for sake of brevity only analyses regarding one SDOF can be shown and only target-sets results can be reported; discussion of other study cases may be found elsewhere (Iervolino et al., 2004). The SDOF T = 0.6 s with the elastic-perfectly-plastic backbone has been chosen to be discussed since this period may be of special interest for earthquake engineering applications, while the EPP backbone is one of the most commonly used in this kind of study. However, is remarkable that conclusions hold similarly for all others SDOF and backbones study cases and for arbitrary class of sets, which can't be published here since they would require considerably longer discussion.

3.1   Hypothesis Tests

Testing the hypothesis that duration "doesn't matter" for EDP means that responses from different sets, characterized by different I_D, should give virtually the same results.   This statistical equivalence for each structural case can be assessed by statistically testing the ratio of the estimated medians (i.e. geometric mean) of the results of nonlinear analyses. In the following relations the ratio of the estimated median responses of two generic set (x, y) is defined as z in (1) while the estimation of the standard error can be evaluated β.

$$z = \frac{\overline{\theta}_x}{\theta_y}; \beta_z = \sqrt{\frac{\sigma^2_x}{n_1} + \frac{\sigma^2_y}{n_2}}$$ (2)

In (2) n_1 and n_2 are the sample sizes of the compared sets; σ_x and σ_y are the standard deviations of the natural logarithms of the two compared sets. Under the assumption that the responses are lognormal: the natural log of the responses ratio (z)

divided by β is distributed as a student-T with 18 degrees of freedom. The Null Hypothesis of the test is

H$_o$: responses of different sets are virtually the same

To the proof of this hypothesis we can associate a statistical significance level, which corresponds to the risk of rejecting H$_o$ when it is, in fact, correct.

Following tables show absolute values of ln(z)/β for T = 0.6 s SDOF with EPP backbone. The greater is this number the larges is the discrepancy between the responses in terms of standard error. In bold-italic are highlighted those results leading to rejection of the null hypothesis at 1.5 sigma confidence level. The matrices sub-diagonal show the comparison of different target-sets with the same median I$_D$; by definitions this results should be clean of rejections of null hypothesis since two sets with the same I$_D$ are built to be statistically equivalent.

Tables 1. Hypothesis test results T = 0.6 s — EPP SDOF.

Dkin	5a	5b	13a	13b	20a	20b
5a	0.00	-	-	-	-	-
5b	0.19	0.00	-	-	-	-
13a	*2.37*	*2.07*	0.00	-	-	-
13b	0.42	0.58	*2.72*	0.00	-	-
20a	0.70	0.50	1.44	1.05	0.00	-
20b	0.49	0.28	*1.80*	0.88	0.24	0.00

Dcyc	5a	5b	13a	13b	20a	20b
5a	0.00	-	-	-	-	-
5b	0.12	0.00	-	-	-	-
13a	0.12	0.21	0.00	-	-	-
13b	*1.61*	*1.52*	1.14	0.00	-	-
20a	0.93	0.94	0.63	0.56	0.00	-
20b	0.74	0.76	0.45	0.90	0.27	0.00

Fp b=1.8	5a	5b	13a	13b	20a	20b
5a	0.00	-	-	-	-	-
5b	0.07	0.00	-	-	-	-
13a	1.25	1.07	0.00	-	-	-
13b	0.05	0.03	1.16	0.00	-	-
20a	0.94	0.80	0.25	0.87	0.00	-
20b	1.35	1.17	0.11	1.26	0.36	0.00

Fp b=1.5	5a	5b	13a	13b	20a	20b
5a	0.00	-	-	-	-	-
5b	0.02	0.00	-	-	-	-
13a	*1.54*	1.39	0.00	-	-	-
13b	0.32	0.31	1.16	0.00	-	-
20a	1.30	1.19	0.16	0.95	0.00	-
20b	*1.74*	*1.58*	0.23	1.36	0.37	0.00

Dhist	5a	5b	13a	13b	20a	20b
5a	0.00	-	-	-	-	-
5b	0.16	0.00	-	-	-	-
13a	*2.46*	*2.25*	0.00	-	-	-
13b	1.15	1.14	1.25	0.00	-	-
20a	*2.34*	*2.17*	0.01	1.20	0.00	-
20b	*2.83*	*2.59*	0.45	*1.65*	0.42	0.00

Ne	5a	5b	13a	13b	20a	20b
5a	0.00	-	-	-	-	-
5b	0.44	0.00	-	-	-	-
13a	0.28	0.73	0.00	-	-	-
13b	*2.40*	*2.66*	*2.44*	0.00	-	-
20a	*2.50*	*2.75*	*2.51*	0.38	0.00	-
20b	*3.61*	*3.76*	*3.76*	*1.63*	1.11	0.00

Tabled results show that in the case of kinematics ductility there's no evidence to reject the null hypothesis and all the values are generally close to zero meaning similar responses under different I_D sets. Hysteretic ductility and equivalent number of cycles results strongly suggest that I_D matters in nonlinear demand analysis since H_o is rejected in almost all comparisons while it cannot be rejected if two sets with the same I_D are compared. Under this prospective Dkin rejection cases results may be explained. Under the assumption that duration doesn't matter in Dkin, results should be almost clean of values above 1.5 times the standard error but, 13a is not equivalent to 13b as proven by hypothesis test of direct comparison. However, pooling 13a-13b in one set (13) and comparing it with a pooled set (5) the comparison provides $|\ln(\bar{\theta}_5 / \bar{\theta}_{13})/\beta_{5,13}| = 1.2$ which leads to no rejection.

Plastic fatigue is expected to be sensitive to I_D, but the latter is not showing in the tables. To explain that it is worth to remember that hypothesis test are built to reject the null hypothesis; if they don't, it means that there's no reason to reject which may mean that there are not enough information to do it (too large dispersions or small sample sizes). This is why IDA's and fragility analyses have been performed. Those results will show sensitivity of Fp to I_D which cannot be assessed by hypothesis test due to large standard errors.

3.2   IDA Curves

Hypothesis test have been intended as preliminary results for testing target-sets behavior and made good cases for general proof of expected results. However, to assess the trend of EDP as function of spectral acceleration in the target-sets IDA's analyses have been performed; it has been possible since I_D index is insensitive to scaling by definition. Again, in the following figures IDA's trend are reported for T = 0.6 s SDOF with EPP backbone in the range of 0 to 1 [g] spectral acceleration. For the purpose of IDA, sets with the same I_D merged in one set (i.e. $\text{T5a} \cup \text{T5b} \equiv \text{T5}$) to increase the sample size (20 records each).

Results are reported in the median, dispersion results show broad residuals distribution particularly for T20 set where, as shown in Fig. 1a, I_D are much more disperse than other sets. Results show how I_D influence is undetectable in kinematics ductility while it becomes more and more influent moving towards hysteretic ductility where demand curves are ranked in the crescent sense of I_D. In fact, all plots refer to the same range (abscissa), then is possible to conclude, from the right shift of the curves, how the median of the demand increases progressively from Dkin to Fp and from Fp to Dhyst. This same trend has been shown, without exceptions, in all other study cases that are not reported here.

3.3   Fragility Curves

While IDA curves help in assessing qualitatively the trend of IDA in different EDP's while for quantitatively evaluate effects of duration related indexes may be useful to

get fragility curves from demand analyses (Fig. 1). In fact, they incorporate not only trend information but also results dispersion effects. Fragility curves regarding kinematics ductility don't show any significant effect of I_D on the failure probability (Fig. 6); all curves provide similar probabilities of failure and are not ranked on the plot by I_D. As expected form IDA results moving to plastic fatigue and hysteretic ductility or equivalent numbers of cycles, fragilities rank by I_D level; moreover median of fragility reduces indicating an easier collapse and slope increases showing greater differences in failure probability of different I_D sets.
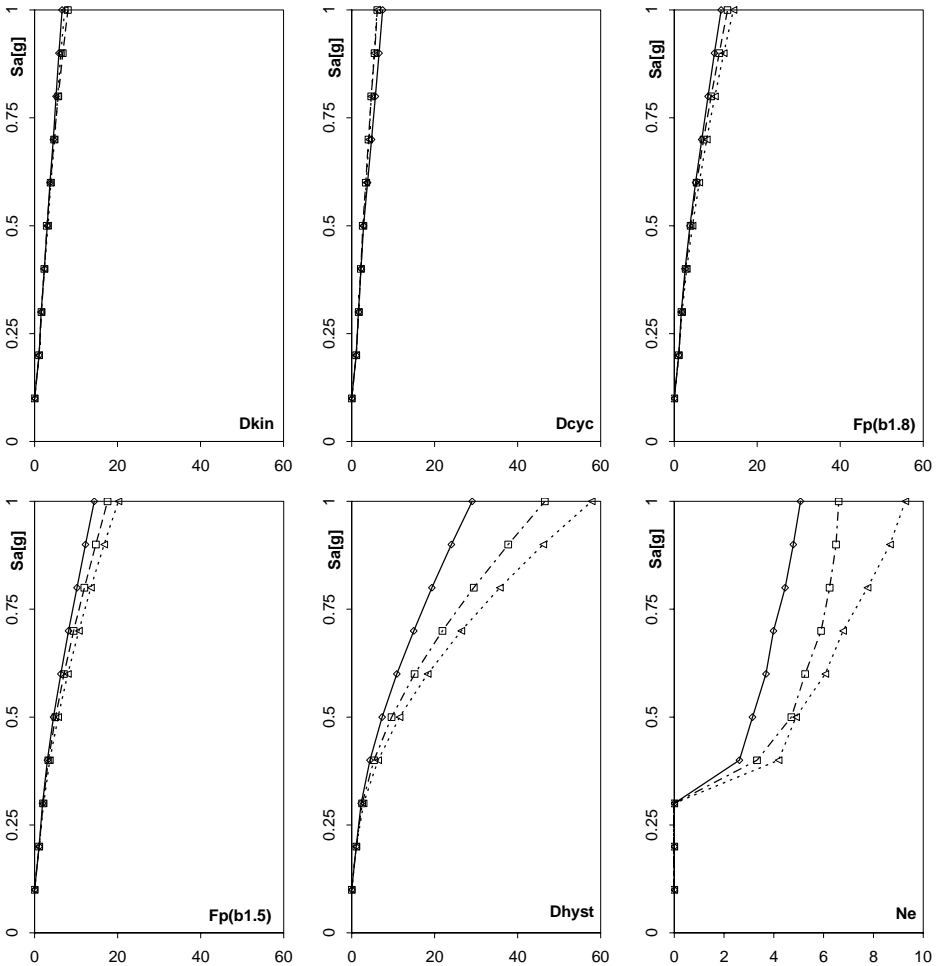
Figure 5. IDA curves for T = 0.6 s – EPP SDOF (◇ T5; ⊡ T13; △ T20).
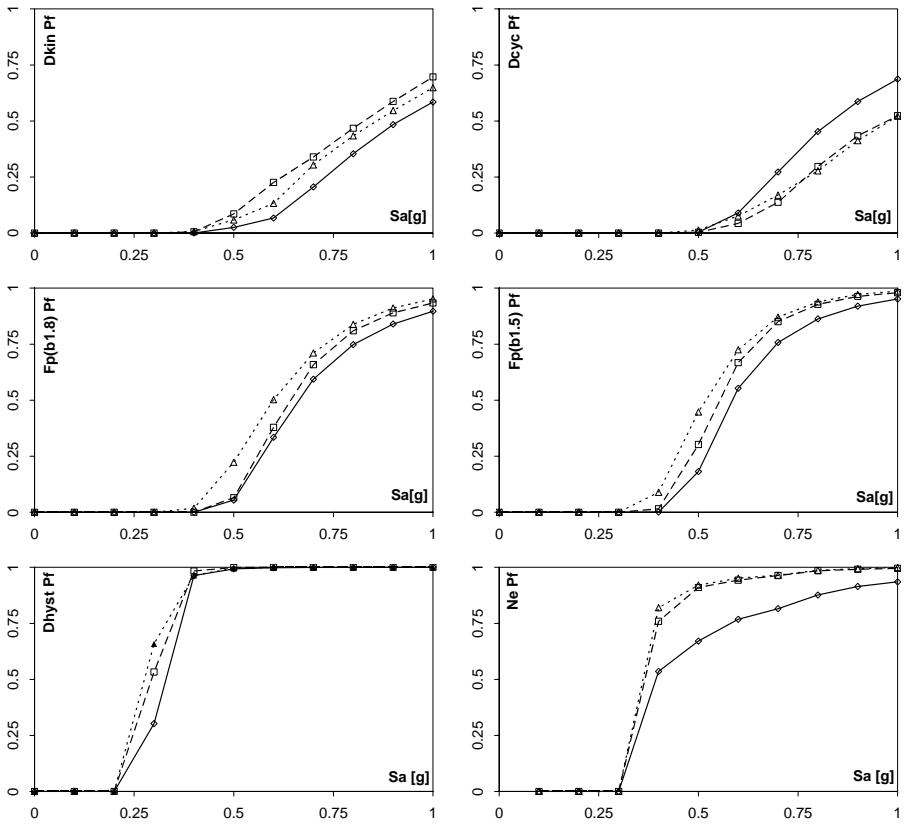
Figure 6. Fragility for T = 0.6 s – EPP SDOF (◇ T5; ⊡ T13; △ T20).

4. CONCLUSIONS

Effects of duration on seismic demand analysis have been proven in general sense. Results of this study show with different information levels on a statistical basis how ground motion duration related indices affect engineering demand assessment. Influence of I_D is proven generally on a test hypothesis prospective while the demand trends and fragility assessment add quantitative features to the statements. Kinematics and cyclic ductility seem to be not affected at all by I_D where no bias in the results can be proven while plastic fatigue (low b) and hysteretic ductility demand show a systematic dependence on duration. Even if selected results have been shown, investigators found the same general conclusion for all cases in broad ranges of period from 0.1 sec to 4 sec and for very different evolutionary and nonevolutionary-nondegrading backbones. Ultimately is shown how duration affects differently

different EDP's regardless of the kind of structure (SDOF) considered even though backbones are not equally sensitive to duration.

REFERENCES

Cosenza E., and G. Manfredi. (1997). *The improvement of the seismic-resistant design for existing and new structures using damage criteria*. In Fajfar P. and Krawinkler H. (eds). Seismic Design Methodologies for the Next Generation of Codes: Balkema 119-130.

Cosenza E., and G. Manfredi. (2000). Damage Indices and Damage Measures. *Prog. Struct. Engng. Mater.* 2: 50–59.

Cosenza E., G. Manfredi, R. Ramasco. (1993). The use of damage functionals in earthquake engineering: A comparison between different methods, *Earthquake Engineering and Structural Dynamics*, Vol. 22, pp.855-868.

CSMIP. (1993). *Impacts of Earthquake Strong-Motion Duration on Inelastic Structural Response Factors and on Ground-Motion Damage Potential* 1090-525.

Fajfar P., and T. Vidic. (1994). Consistent inelastic design spectra: hysteretic and input energy. *Earthquake Engineering and Structural Dynamics* 23: 523–532.

Iervolino I., and C. A. Cornell. *Record Selection for Nonlinear Seismic Analysis of Structures.* Submitted for publication to Earthquake Spectra.

Iervolino I., G. Manfredi, and E. Cosenza. (2004). Ground Motion Duration Effects in Nonlinear Seismic Structural Analysis. Submitted to *Earthquake Engineering and Structural Dynamics.*

Kawashima K., and K. Aizawa. (1989). Bracketed and normalized durations of earthquake ground acceleration. *Earthquake Engineering and Structural Dynamics.* 18: 1041-1051.

Krawinkler H., and A. A. Nassar. (1992). Seismic design based on ductility and cumulative damage demands and capacities. In: Fajfar P. and Krawinkler H. (eds) *Nonlinear seismic analysis and design of reinforced concrete buildings*. Oxford: Elsevier Applied Science 23–40.

Mahin S. A., and V. V. Bertero. (1981). An Evaluation of Inelastic Seismic Design Spectra. *Journal of Structural* D*ivision ASCE* 107, 1777-1795.

Manfredi G. (2001). Evaluation of seismic energy demand. *Earthquake Engineering and Structural Dynamic*s 30:485-499.

Trifunac M. D., and A. G. Brady. (1975). A study on the duration of strong earthquake ground motion. *Bulletin of the Seismological Society of America* 65(3): 581-626.

Trifunac M. D. and E. I. Novikova. (1994). Duration of strong ground motion in terms of earthquake magnitude epicentral distance, site conditions and site geometry. *Earthquake Engineering and Structural Dynamics* 23: 1023-1043.

Vamvatsikos D., and C. A. Cornell. (2002). Incremental Dynamic Analysis. *Earthquake Engineering and Structural Dynamics* 31(3):491-514.

ON DRIFT LIMITS ASSOCIATED WITH DIFFERENT DAMAGE LEVELS

Ahmed GHOBARAH[1]

ABSTRACT

Performance objectives in performance-based design procedures have been described in several ways according to the operational status of the structure or the level of damage sustained up to collapse. The selection of the appropriate drift associated with different levels of damage for the design is significant in terms economy and safety. The identification of drift levels associated with different states of damage remains one of the unresolved issues in the development of performance objectives in performance-based design and assessment procedures. The objective of this study is to develop the approach to establish the drift of different structural systems that is associated with different definable levels of damage to use as performance objectives in the design of new structures and the evaluation of the seismic resistance of existing structures.

Analytical and experimental data were used to examine the correlation between drift and damage of various structural elements and systems. The analytical procedures included time-history analysis, dynamic and static pushover analyses of various designs of reinforced concrete walls and moment resisting frames. Recently conducted tests as well as available experimental research results in the literature are reviewed for the appropriateness and consistency of the data. The experimental work included static and dynamic testing of walls and frame components.

It was found that the drift associated with various damage levels of different reinforced concrete elements and structural systems vary significantly. Two main sets of drift limits were defined for ductile and nonductile structural systems.

Keywords: Performance-based design; Performance objectives; Drift; Damage; Moment resisting frames; Walls.

1. INTRODUCTION

Earthquakes continue to cause substantial damage and loss of life in many parts of the world. Although many buildings designed to current codes did not collapse during recent earthquakes, the level of damage to structures was unexpectedly high. In addition to the high cost of repairs, economic loss due to loss of use was significant. Conventional methods of seismic design have the objectives to provide for life safety (strength and ductility) and damage control (serviceability drift limits).

[1] *Department of Civil Engineering, McMaster University, Hamilton, Canada*

Current code design procedures succeeded in reducing loss of life during major seismic events. However, much remains to be done in the area of damage reduction.

Performance-based design is a general design philosophy in which the design criteria are expressed in terms of achieving stated performance objectives when the structure is subjected to stated levels of seismic hazard. The performance targets may be a level of stress not to be exceeded, a load, a displacement, a limit state or a target damage state (Ghobarah 2001). Specifying structural performance objectives in terms of drift limits has not been extensively studied. A set of performance objectives defined in terms of drift was given by several publications such as SEAOC (1995) and FEMA (1997). The definition of comprehensive and realistic drift limits that are associated with known damage states remains one of the important unresolved issues in performance-based design procedures.

The relationship between performance objectives and damage is best illustrated by the typical performance curve shown in Figure 1. Vision 2000 defined performance objectives are marked on the capacity curve. In addition, the states of damage of the structure are identified on the capacity curve. The structure is considered to suffer no damage or sustain very minor damage up to concrete cracking. Between concrete cracking and the first yield of steel, the crack sizes are normally < 2 mm and damage is considered to be repairable. Past steel yield, the cracks are wider than 2 mm and repair becomes difficult, impractical or costly, thus the irreparable damage classification. The described performance applies to ductile systems. However, nonductile systems may suffer brittle failure at any drift level that is associated with repairable or irreparable damage states.

The structural response in terms of displacement can be related to strain-based limit state, which in turn is assumed related to damage. The defined performance of a structure in terms of a state of damage, strain or deformation gives better indicator of damage than stresses. However, relating displacement limits and drift of the structure to damage is an oversimplification since the level of damage is influenced by several other factors such as the structural system, the accumulation and distribution of structural damage, failure mode of the elements and components, the number of cycles and the duration of the earthquake and the acceleration levels in case of secondary systems.

The objective of this investigation is to develop the approach to quantify the drift limits associated with different damage levels for some reinforced concrete structural systems such as moment resisting frames (MRF) and walls.
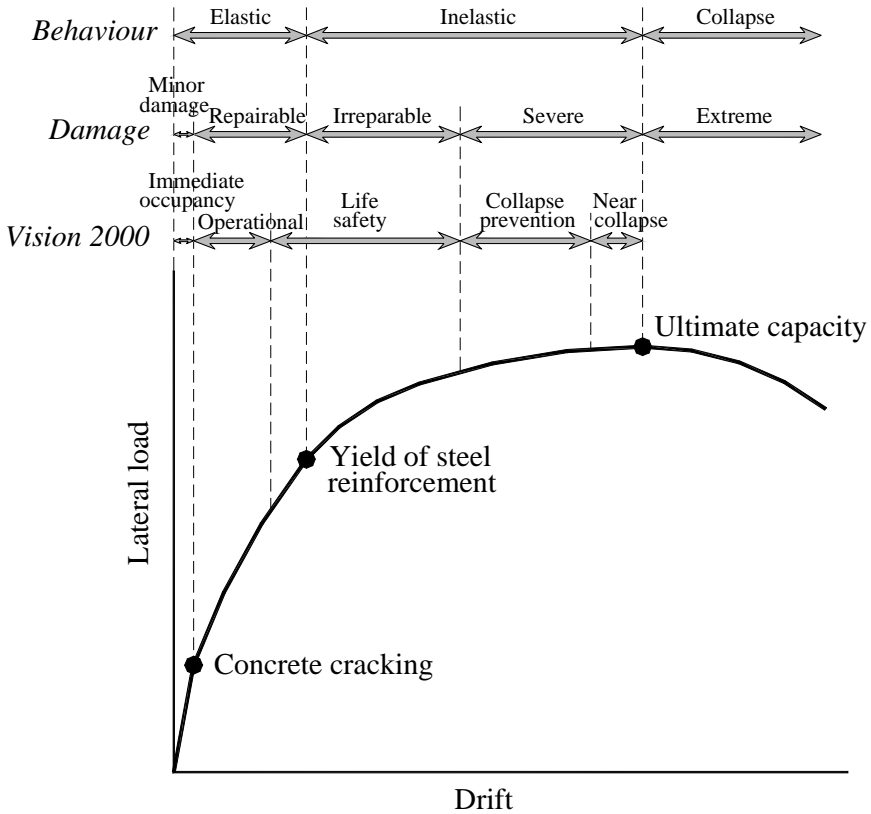
Figure 1. Typical structural performance and associated damage states.

2. DAMAGE

An attempt to develop a procedure to correlate damage of various structural systems to drift taking into account various ground motion characteristics, was made through the use of a damage index (Ghobarah et al. 1997). For effective design criteria, the correlation between damage and drift should be calibrated against experimental work as well as observed performance of structures during earthquakes when possible. Drift limits were found to vary and different sets should be developed for different structural systems such as nonductile and ductile moment resisting frame, moment resisting frame with infills, flexural structural walls and reinforced concrete squat shear walls.

There have been several attempts to describe damage levels of various structural systems (Rossetto and Elnashai 2003). The damage in terms of limits defined in this

study (No damage, Repairable, Irreparable and Severe damage states) associated with various performance levels of some structural systems such as nonductile and ductile moment resisting frames and frames with infills and walls, is described as follows:

(a) No damage: No structural damage is observed. Some fine cracks in plaster may exist.

(b) Repairable damage:
  - Light damage. Initiation of hairline cracking in beams and columns near joints and in walls. Cracking at the interface between frame and infills and near corners of openings. Start of spalling in walls.
  - Moderate damage. Flexural and shear cracking in beams, columns and walls. Some elements may reach yielding of steel.

(c) Irreparable damage: Yielding of steel reinforcement occurs in several elements. Cracks are larger than 2 mm. Residual deflection may occur. Ultimate capacity is reached in some structural elements and walls. Failure of short columns may occur. Partial failure of infills and heavy damage to frame members may take place. Severe cracking and bucking of steel in boundary elements of walls occurs.

(d) Extreme: Partial collapse of lateral and gravity load carrying elements of the structures is observed. Shear failure of columns. Shear failure of beams and columns causing complete failure of infills. Some reinforced concrete walls may fail.

(e) Collapse: The structure may be on the verge of collapse or may experience total collapse.

3. DRIFT

For the case of three performance levels (serviceability, damage control and life safety or collapse prevention), three corresponding structural characteristics (stiffness, strength and deformation capacity) dominate the performance. If more intermediate performance levels are selected, then it becomes difficult to define which structural characteristic dominate the performance. Different performance objectives may impose conflicting demands on strength and stiffness. The displacements or drift limits are also function of the structural system and its ability to deform (ductility). Design criteria may be established on the basis of observation and experimental data of deformation capacity. For example, near collapse the drift limits of ductile structural system are different from that of nonductile systems, which suggest that different drift limits will correspond to different damage levels for different structural systems.

3.1 Factors That Affect Drift

The displacements or drift of a structure are functions of several factors such as the stiffness or strength and the ability of the structural system to deform (ductility).

Other factors such as the applied load whether shear or flexure, confinement and shear span influence the structural deformations. An important factor in the behaviour of columns and walls is the effect of the axial load. The increase in the axial load increases the shear resistance of the member. In addition, it was found experimentally that the increase in axial load reduces the lateral drift.

Although the performance objectives and the description of the associated damage may remain unchanged, it is clear that several sets of drift definitions are required to establish the limits for various structural systems and elements such as:

- Reinforced concrete moment resisting frame (MRF)
  (a) Ductile well designed frames according to current codes. The established drift limits can be included in the code provisions.
  (b) Existing frame with nonductile detailing designed to earlier codes. The established drift limits can be used in the evaluation of the lateral load carrying capacity of existing structures.
  (c) Moment resisting frame with masonry infills.
- Structural walls
  (a) Flexural structural walls of aspect ratio (height/length) > 1.5.
  (b) Squat walls with predominantly shear behaviour of aspect ratio < 1.5.

3.2   Interstorey Drift Distribution and Damage

The roof drift is a useful simple measure of the overall structural deformation that is routinely calculated. It can be determined from nonlinear dynamic analysis, pushover analysis or the response of an equivalent single degree of freedom representation. Roof drift calculated using the gross section inertia is almost half the drift calculated using the cracked section inertia. Roof drift can be related to damage. However, the roof drift does not reflect the distribution of damage along the height of the structure and does not identify weak elements or soft storeys. The interstorey drift can be directly used in the design and serviceability check for beams and columns of the frame and can be correlated to damage at the floor level. A well-designed MRF structure would have an almost uniform interstorey drift distribution along its height. In this case, the relationship between the roof drift and the maximum interstorey drift is linear with approximately 38° slope as shown in Figure 2. For existing nonductile structures and poorly designed frames such as those with a soft storey, the maximum interstorey drift of the soft storey may indicate collapse while the roof drift will correspond to lower damage level. Therefore, the damage to the MRF can be considered influenced by two drift parameters: (a) the interstorey drift; and (b) its distribution along the height of the structure.
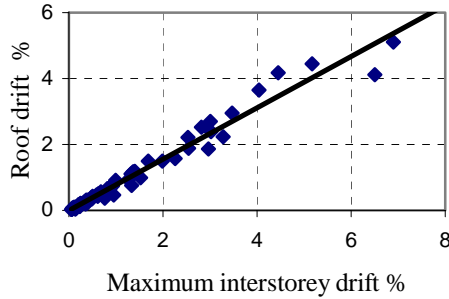
Figure 2. Relationship between maximum interstorey drift and roof drift of well-designed 3, 6, 9, and 12 storey MRFs subjected to several ground motion records.

To take into account a measure of the storey drift distribution along the height of the structure, a representative factor is proposed. The factor is called the *Storey Drift Factor* (SDF) and can be calculated by the formula:

$$SDF = \frac{\sqrt{\frac{1}{(n-1)^2} \sum_{i=1}^{n}(S_i - \overline{S})^2 \sum_{i=1}^{n}(S_i)^2}}{\overline{S}} \tag{1}$$

where n is the number of storeys, S_i is the maximum interstorey drift of floor i, and $\overline{S}$ is the mean value of the maximum interstorey drift ratios. A value of the SDF = 0 indicates equal interstorey drift along the height. A value close to 1 represents the case where the overall drift is caused by few storeys (e.g., soft storey).

Global damage can be related to damage at the element and storey levels using any damage index such as final softening. The results of the analysis of 10 ductile moment resisting frames are summarized in Table 1.

Table 1. Final softening damage index associated with various damage levels

State of damage	Element	Storey	Global
No damage	<0.2	<0.15	<0.10
Repairable damage			
(a) Light	<0.3	<0.2	<0.15
(b) Moderate	<0.4	<0.3	<0.2
Irreparable damage (>yield)	>0.4	>0.3	>0.2
Severe damage - Life safe - Partial collapse	0.6-0.8	0.5-0.7	0.4-0.6
Collapse	>0.8	>0.7	>0.6

4. MOMENT RESISTING FRAMES

4.1   Ductile MRF

The *storey drift factor* calculated using equation (1) for a number of ductile, well-designed MRFs can be correlated with damage as shown in Figure 3. The damage index used is the final softening representing the effect of stiffness degradation following the application of the load. This damage index was arbitrarily selected because of its simplicity. Other damage indices could have been also used. In Figure 3, zero damage index indicates no damage while 1 represents collapse. However in practical terms, the actual failure of the structure occurs at damage index values of 0.7 to 0.8. For ductile MRF, damage index values up to 0.2 represent repairable damage.

The plot in Figure 3 using SDF on the horizontal axis can be compared with a similar damage plot using the maximum interstorey drift shown in Figure 4. The figures are similar but not identical. Comparison between the two horizontal axes of Figures 3 and 4 gives a rough relationship between the maximum interstorey drift and the SDF values.

The SDF for the ductile reinforced concrete moment resisting frames is plotted with the ductility factor as shown in Figure 5. For SDF values from 0 to 0.2 the damage as measured by the final softening damage index is light. Moderate repairable damage is estimated for SDF values from 0.2 to 0.4. The start of yield as indicated by ductility >1 from figure 5 corresponds to SDF of 0.4, damage index of 0.15 and interstorey drift of 1.3. In the figure, the point marking the departure from ductility factor 1 is well defined. Past the yield point, damage increases and is considered irreparable. When using a large sample of frames, the mean damage index at frame yield is closer to 0.2. The maximum interstorey drift limits corresponding to various damage states for a ductile MRF are listed in Table 2.

Table 2. Drift ratio (%) limits associated with various damage levels

State of damage	Ductile MRF	Nonductile MRF	MRF with infills	Ductile walls	Squat walls
No damage	<0.2	<0.1	<0.1	<0.2	<0.1
Repairable damage (a) Light damage (b) Moderate damage	0.4 <1.0	0.2 <0.5	0.2 <0.4	0.4 <0.8	0.2 <0.4
Irreparable damage (>yield point)	>1.0	>0.5	>0.4	>0.8	>0.4
Severe damage - Life safe - Partial collapse	1.8	0.8	0.7	1.5	0.7
Collapse	>3.0	>1.0	>0.8	>2.5	>0.8
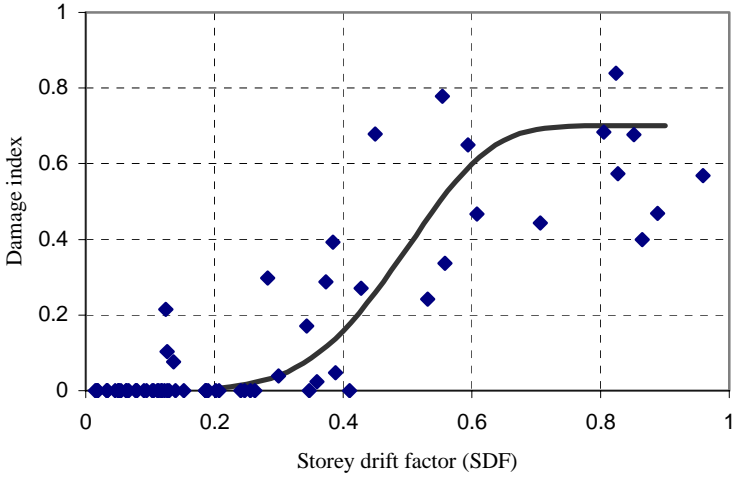
Figure 3. Correlation between the interstory drift factor and damage for a 3, 6, 9, and 12 storey MRFs.
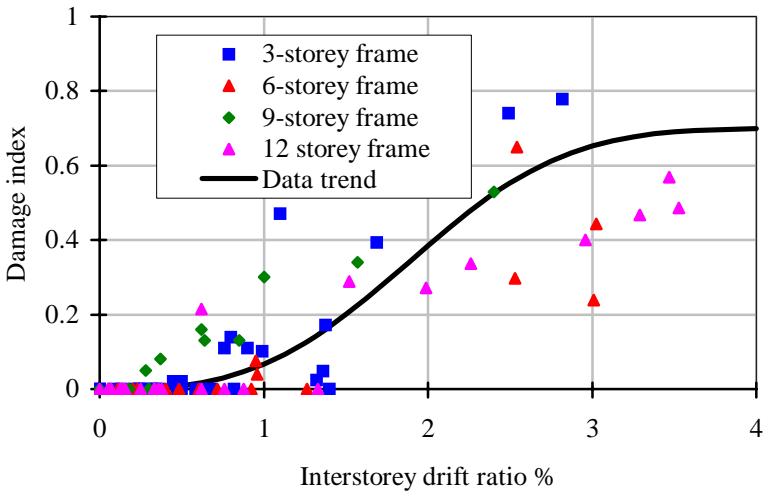
Figure 4. Damage at various drift levels of code designed 3, 6, 9, and 12 storey ductile MRFs.
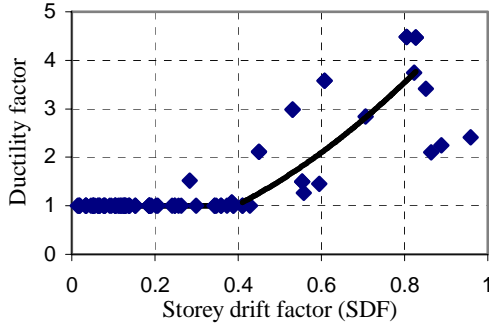
Figure 5. Correlation between ductility and the storey drift factor.

4.2 Nonductile MRF

MRF designed to earlier codes or without seismic detailing often suffer from poor confinement of lap splices, lack of shear reinforcement in the beam-column joints and inadequate embedment length of the beam bottom reinforcement at the column. These frames behave in a nonductile manner and may fail in brittle failure modes. As an example of the data used, the maximum interstorey drift is plotted against the damage index in Figure 6. The behaviour of several frames when subjected to a number of ground motions contributed the data shown in the figure. For nonductile MRF, the damage index corresponding to repairable damage limit is 0.4. This damage level corresponds to maximum interstory drift limit of 0.5%, which is considered to be the limit of irreparable damage as suggested by experimental observation. The maximum interstorey drift limits corresponding to various damage states of a nonductile MRF are listed in Table 2.
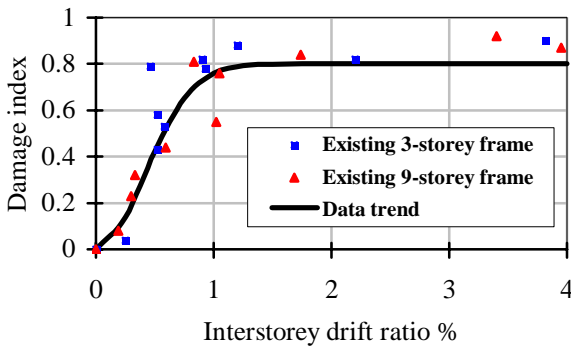
Figure 6. Relationship between maximum interstorey drift and damage for existing nonductile frames.

4.3 MRF with Infills

Several researchers have recently studied the behaviour of MRFs with infills (Lu 2002). Quality experimental data is becoming available. An example illustrating the effect of infills on the relationship between damage and maximum interstorey drift is shown in Figure 7. The load carrying capacity of infilled frame is higher than that of a bare frame. A moment resisting frame with infills gives roughly half the interstorey drift of a bare frame (Chiou et al. 1999) with twice the damage index. For example, 0.35 damage index corresponds to interstorey drift of bare MRF of 0.8%. Interstorey drift ratio of 0.8% corresponds to a damage index of a MRF with infills of 0.7, which is near collapse. The behaviour of infilled frame may not return to the behaviour of a ductile MRF after the failure of the masonry infills. The apparent lack of ductility for MRF with infills is because the pattern of masonry failure may cause brittle failure of the frame elements. This may be the case even for a well-designed frame that is ductile when tested without the infills. The maximum interstorey drift limits corresponding to various damage states of MRF with infills are listed in Table 2.
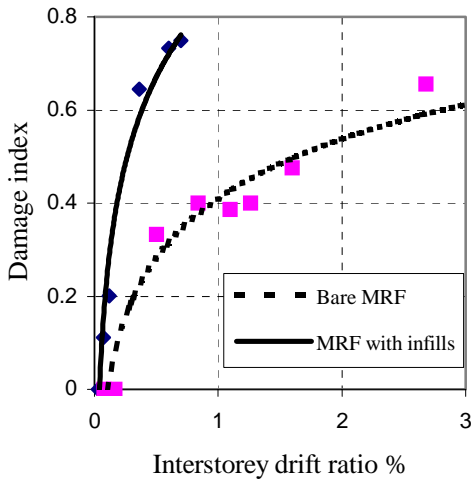
Figure 7. Behaviour of bare portal MRF and MRF with infills.

5. WALLS

Structural walls may act predominantly in shear or flexure depending on their aspect ratio and the applied loads. Squat walls may fail abruptly by one of several brittle modes of failure. There is a comprehensive volume of experimental research and post earthquake observation on the behaviour of walls (Duffey et al. 1994; Khalil and Ghobarah 2003; Kowalsky 2001; Wood 1991).

5.1   Flexural Structural Walls

An example of the behaviour of flexural walls is shown in Figure 8. Initially the wall stiffness is high. Yielding of the steel reinforcement in ductile flexural walls occurs at drift values of approximately 0.8%. The drift limits corresponding to various damage states of ductile flexural walls are listed in Table 2.

5.2   Squat Shear Walls

The relationship between damage and drift ratio for squat walls is shown in Figure 8. Initially under low levels of load, the behaviour of the squat wall is the same as ductile flexural walls. However, when shear cracks occur and are not arrested, the wall stiffness degrades rapidly reflecting a substantial increase in damage leading to abrupt failure. In the case of squat walls, it was experimentally observed that damage index of 0.3 represents the limit of repairable damage. This limit corresponds to relatively low drift ratio value of 0.4%. The steel yield point is normally not reached before shear failure occurs. The drift limit corresponding to various states of damage of squat shear walls are listed in Table 2.
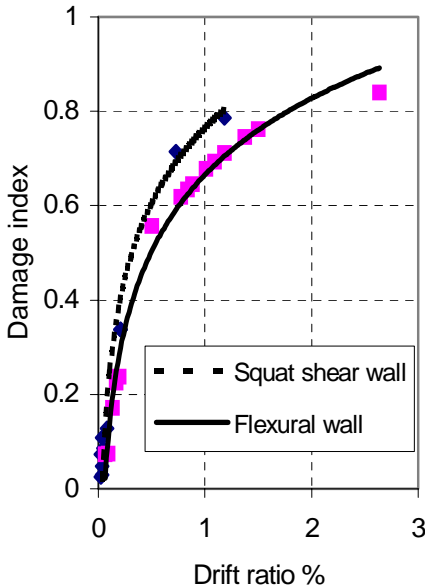
Figure 8. Shear and flexural behaviour of walls (Khalil and Ghobarah 2003).

6. CONCLUSIONS

Different sets of drift limits associated with various damage levels were defined for moment resisting frames (ductile, nonductile, with infills), flexural structural walls and squat shear walls. The defined performance levels were based on experimental data, field observations and measurements and theoretical analyses. At least two main sets of drift limits can be identified to represent various damage levels for the design of ductile systems and the assessment of the seismic resistance of nonductile ones.

Currently available drift limits were found to be conservative for ductile structures and nonconservative for nonductile structures.

Realistic drift calculations should be made using reduced gross inertia due to the cracked section properties.

The proposed drift limits representing various performance objectives of the structure can be further refined as additional test and analysis data are included.

REFERENCES

Chiou, Y-J., J-C. Tzeng, and Y-W Liou. (1999). Experimental and analytical study of masonry infilled frames. *Journal of Structural Engineering*, 125(10):1109-1117.

Duffey, T. A., C. R. Farrar, and A. Goldman. (1994). Low-rise shear wall ultimate drift limits. *Earthquake Spectra* 10(4):655-674.

FEMA. (1997). Guidelines for seismic rehabilitation of buildings. National Earthquake Hazard Reduction Program (NEHRP), Report FEMA 273, Federal Emergency Management Agency, Washington, D.C.

Ghobarah, A. (2001). Performance-based design in earthquake engineering: state of development. *Engineering Structures*, 23:878-884.

Ghobarah, A., N. M. Aly, and M. El Attar. (1997). Performance level criteria and evaluation. In: Fajfar P., Krawinkler, H., editors. *Seismic Design Methodologies for the Next Generation of Codes.* AA Balkema, Rotterdam: 207-215.

Khalil, A., and A. Ghobarah. (2003). Scale model testing of structural walls. *Response of Structures to Extreme Loading*, Toronto, Canada, Paper# 246, Elsevier, UK.

Kowalsky, M. J. (2001). RC structural walls designed according to UBC and displacement-based methods. *Journal of Structural Engineering*, 127(5):506-516.

Lu, Y. (2002). Comparative Study of Seismic Behavior of Multistory Reinforced concrete Framed Structures. *Journal of Structural Engineering*, 128(2):169 – 178.

Rossetto, T., and A. Elnashai. (2003). Derivation of vulnerability functions for European type RC structures based on observed data. *Engineering Structures* 25:1241-1263.

SEAOC. (1995). Vision 2000, Performance based seismic engineering of buildings. Structural Engineers Association of California, Sacramento, CA.

Wood, S. L. (1991). Performance of reinforced concrete buildings during the 1985 Chile earthquake: implications for the design of structural walls. *Earthquake Spectra*, 7(4):607-638.

MODAL PUSHOVER ANALYSIS: SYMMETRIC- AND UNSYMMETRIC-PLAN BUILDINGS

Anil K. CHOPRA [1] and Rakesh K. GOEL [2]

ABSTRACT

After a brief evaluation of methods currently standard in engineering practice to estimate seismic demands, this paper emphasizes modal pushover analysis, which is shown to provide considerably improved estimated of demands, while retaining the conceptual simplicity and computational attractiveness of current nonlinear static pushover procedures. Rooted in structural dynamics theory, this procedure is ready for practical application to symmetric-plan buildings and is promising for unsymmetric-plan buildings.

Keywords: Buildings; Nonlinear static procedure; Pushover analysis; Seismic demands.

1. INTRODUCTION

Currently, the structural engineering profession uses the nonlinear static procedure (NSP) or pushover analysis described in FEMA-356 (ASCE, 2000) and ATC-40 (ATC, 1996) documents to estimate seismic demands, which are computed by nonlinear static analysis of the structure subjected to monotonically increasing lateral forces with an invariant height-wise distribution until a predetermined target displacement is reached. Pushover analysis procedures have been improved in several ways. Adaptive force distributions that attempt to follow more closely the time-variant distributions of inertia forces have been proposed (Bracci et al., 1997, Elnashai, 2001, Gupta and Kunnath, 2000). An incremental response spectrum analysis procedure (IRSA) has been developed (Aydinoglu, 2003). Attempts have been made to consider more than the first mode in pushover analysis (Sasaki et al., 1998; Kunnath and Gupta, 2000; Matsumori et al., 1999). Based on structural dynamics theory, a modal pushover analysis procedure (MPA) has been developed that includes higher mode contributions to determine the total seismic demand (Chopra and Goel, 2002; Chopra and Goel, 2004).

The objectives of this paper are to (1) briefly evaluate procedures used in current structural engineering practice to estimate seismic demands for buildings; and (2)

[1] University of California, Berkeley, chopra@ce.berkeley.edu
[2] CalPoly State University, rgoel@calpoly.edu

outline and evaluate an improved procedure that retains the conceptual simplicity and computational attractiveness of current methods.

2. NONLINEAR STATIC PROCEDURE: CURRENT PRACTICE

The nonlinear static procedure (NSP) in FEMA-356 requires development of a pushover curve, a plot of base shear versus roof displacement, by nonlinear static analysis of the structure subjected first to gravity loads, followed by monotonically increasing lateral forces with a specified, invariant height-wise distribution. The limitations of force distributions in the FEMA-356 nonlinear static procedure are demonstrated in Figs. 1 and 2 where the resulting estimates of the median story drift and plastic hinge rotation demands imposed on the SAC buildings by the ensemble of 20 SAC ground motions are compared with the "exact" median value determined by nonlinear RHA of the buildings. The first-mode force distribution grossly underestimates the story drifts, especially in the upper stories, showing that higher-mode contributions are especially significant in the seismic demands for upper stories. Although the ELF and SRSS force distributions are intended to account for higher mode responses, they do not provide satisfactory estimates of seismic demands. The "uniform" force distribution seems unnecessary because it grossly underestimates drifts in upper stories and grossly overestimates them in lower stories of four buildings. The FEMA-356 lateral force distributions either fail to identify, or significantly underestimate, plastic hinge rotations in beams at uppers floors.
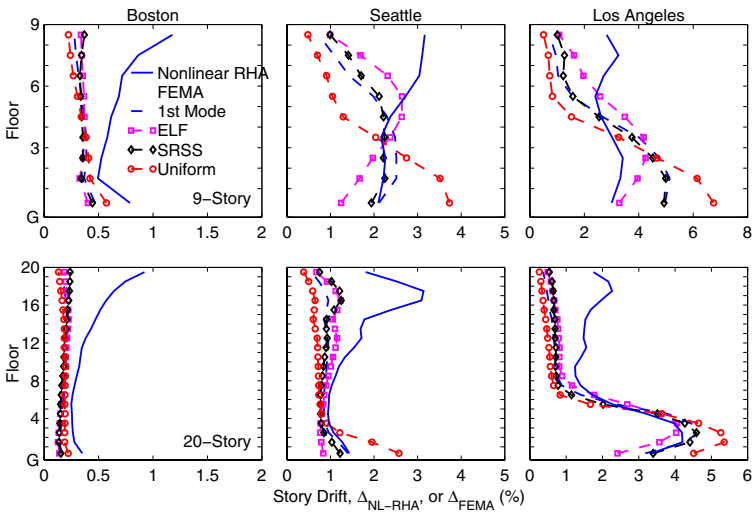
Figure 1. Median story drifts determined by nonlinear RHA and four FEMA-356 force distributions: 1st Mode, ELF, SRSS, and "Uniform."
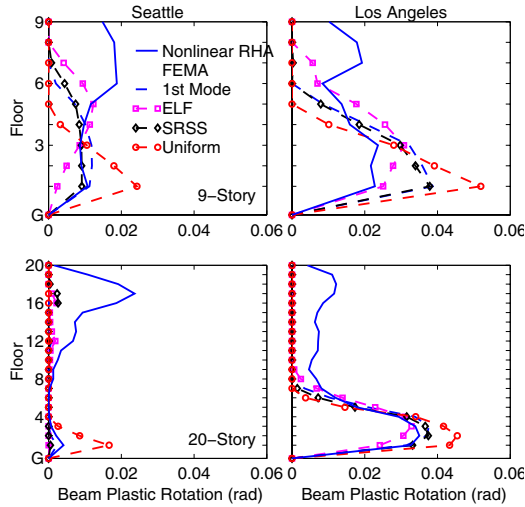
Figure 2. Median plastic rotations determined by nonlinear RHA and four FEMA-356 force distributions: 1st Mode, ELF, SRSS, and "Uniform."

3. IMPROVED NSP: MODAL PUSHOVER ANALYSIS

It is clear from the preceding discussion that the seismic demand estimated by NSP using the first-mode force distribution (or others in FEMA-356) should be improved. One approach is to include the contributions of higher modes of vibration to seismic demands.

3.1 Basic Concept

The equations of motion for a multistory building subjected to horizontal ground accelerations $\ddot{u}_g(t)$ or $\ddot{u}_{gy}(t)$ along the *x* and *y* axes, respectively, are the same as if the ground were stationary and the excitation was replaced by external forces, known as the effective earthquake forces:

$$\mathbf{p}_{\text{eff}}(t) = -\mathbf{M}\boldsymbol{\iota}_x\ddot{u}_{gx}(t) \quad or \quad -\mathbf{M}\boldsymbol{\iota}_y\ddot{u}_{gy}(t) \tag{1}$$

where the mass matrix $\mathbf{M}$ consists of three diagonal submatrices $\mathbf{m}$, $\mathbf{m}$, $\mathbf{I}_o$; $\mathbf{m}$ is associated with lateral degrees of freedom (DOF) and $\mathbf{I}_o$ with torsional DOF. The influence vectors $\boldsymbol{\iota}_x$ and $\boldsymbol{\iota}_y$ associated with *x* and *y* ground motions are as follows:

$$\boldsymbol{\iota}_x = \begin{Bmatrix} \mathbf{1} \\ \mathbf{0} \\ \mathbf{0} \end{Bmatrix} \qquad \boldsymbol{\iota}_y = \begin{Bmatrix} \mathbf{0} \\ \mathbf{1} \\ \mathbf{0} \end{Bmatrix} \tag{2}$$

respectively, where each element of **1** is equal to unity and of **0** is equal to zero. Thus, the effective earthquake forces are

$$\mathbf{p}_{\text{eff}}\left(t\right) = -\mathbf{s}\ddot{u}_g\left(t\right) = -\begin{Bmatrix} \mathbf{m1} \\ \mathbf{0} \\ \mathbf{0} \end{Bmatrix} \ddot{u}_{gx}\left(t\right) \quad or \quad \begin{Bmatrix} \mathbf{0} \\ \mathbf{m1} \\ \mathbf{0} \end{Bmatrix} \ddot{u}_{gy}\left(t\right) \tag{3}$$

The spatial distribution of the effective forces (Eq. (3)) over the building is defined by the vector **s** and the time variation by $\ddot{u}_g\left(t\right) = \ddot{u}_{gx}\left(t\right)$ or $\ddot{u}_{gy}\left(t\right)$. This force distribution can be expanded as a summation of modal inertia force distributions $\mathbf{s}_n$ (Chopra 2001, Section 13.3):

$$\mathbf{s} = \sum_{n=1}^{3N} \mathbf{s}_n = \sum_{n=1}^{3N} \Gamma_n \mathbf{M} \boldsymbol{\phi}_n \tag{4}$$

where $\boldsymbol{\phi}_n$ is the nth natural vibration mode of the structure consisting of three subvectors, $\boldsymbol{\phi}_{xn}, \boldsymbol{\phi}_{yn}$, and $\boldsymbol{\phi}_{\theta n}$, and

$$\Gamma_n = \frac{L_n}{M_n} \qquad M_n = \boldsymbol{\phi}_n^T \mathbf{M} \boldsymbol{\phi}_n \qquad L_n = \begin{cases} \boldsymbol{\phi}_{xn}^T \mathbf{m1} & \text{for} \quad \ddot{u}_{gx}\left(t\right) \\ \boldsymbol{\phi}_{yn}^T \mathbf{m1} & \text{for} \quad \ddot{u}_{gy}\left(t\right) \end{cases} \tag{5}$$

Thus

$$\mathbf{p}_{\text{eff},n}\left(t\right) = -\mathbf{s}_n \ddot{u}_g\left(t\right) \tag{6}$$

is the nth-mode component of effective earthquake forces.

In the MPA procedure, the peak response r_n of the building to $\mathbf{p}_{\text{eff},n}\left(t\right)$ — or the peak "modal" demand—is determined by a nonlinear static or pushover analysis using the modal force distribution

$$\mathbf{s}_n^* = \begin{Bmatrix} \mathbf{m} \boldsymbol{\phi}_{xn} \\ \mathbf{m} \boldsymbol{\phi}_{yn} \\ \mathbf{I}_o \boldsymbol{\phi}_{\theta n} \end{Bmatrix} \tag{7}$$

The peak modal demands r_n are then combined by an appropriate modal combination rule—SRSS for symmetric-plan buildings and CQC for unsymmetric-plan systems—to estimate the total demand. This procedure is directly applicable to the estimation of deformation demands (e.g., floor displacements and story drifts) but computation of plastic hinge rotations and member forces requires additional consideration.

Although modal analysis theory is strictly not valid for inelastic systems, the fact that elastic modes are coupled only weakly in the response of inelastic systems to modal inertia forces (Chopra and Goel, 2002, 2004) permitted development of MPA, an approximate procedure.

3.2   Summary of Procedure

The MPA procedure has been summarized as a sequence of computational steps to estimate floor displacements and story drifts for symmetric-plan buildings (Goel and Chopra, 2004a) and unsymmetric-plan buildings (Chopra and Goel, 2004).

3.3   Plastic Hinge Rotations and Member Forces

Although the total floor displacements and story drifts are computed by combining the values obtained from gravity load and "modal" pushover analyses for all modes contributing significantly to the demand, the plastic hinge rotations and member forces are not computed by this procedure. The rotations of plastic hinges can be estimated from the story drifts by a procedure presented earlier by Gupta and Krawinkler (1999). The member forces are computed from the total member deformations using the member force-deformation (or moment rotation) relationship, recognizing *P-M* interaction in columns. These procedures to compute member forces are described in Goel and Chopra (2004b).

4. EVALUATION OF MPA: SYMMETRIC-PLAN BUILDINGS

4.1   Higher Mode Contributions in Seismic Demands

Figures 3 and 4 show the median values of story drift and beam plastic rotation demands, respectively, including a variable number of "modes" in MPA superimposed with the "exact" result from nonlinear RHA. The first "mode" alone is inadequate in estimating story drifts, but with a few "modes" included, story drifts estimated by MPA are generally similar to the nonlinear RHA results.

The first "mode" alone fails to identify the plastic hinging in the upper floors of all buildings and also in the lower floors of the Seattle 20-story building. Including higher-"mode" contributions also improves significantly the estimate of plastic hinge rotations. In particular, plastic hinging in upper stories is now identified, and the MPA estimate of plastic rotation is much closer—compared to the first-"mode" result—to the "exact" results of nonlinear RHA.
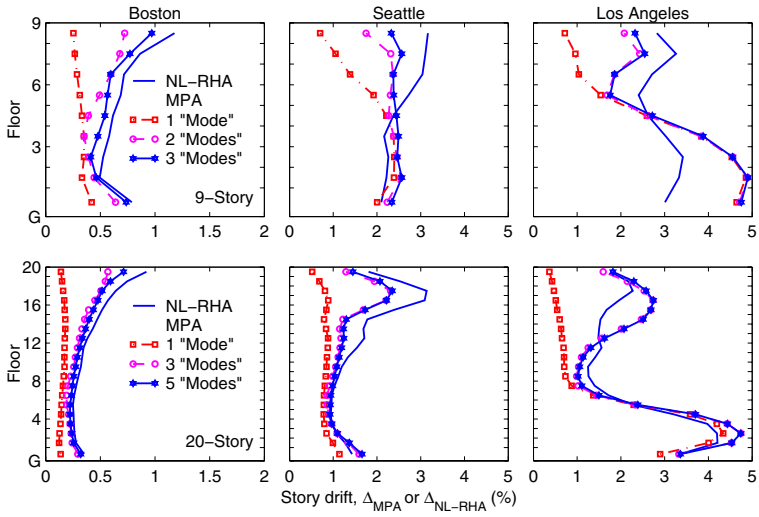
Figure 3. Median story drifts determined by nonlinear RHA and MPA with variable number of "modes"; P-Δ effects due to gravity loads are included.
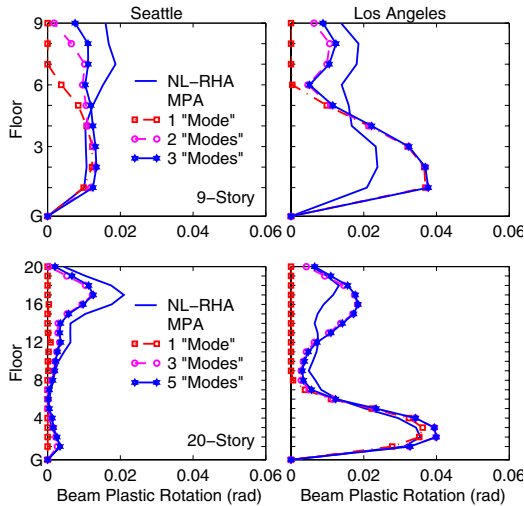
Figure 4. Median plastic rotations in interior beams determined by nonlinear RHA and MPA with variable number of "modes"; P-Δ effects due to gravity loads are included.
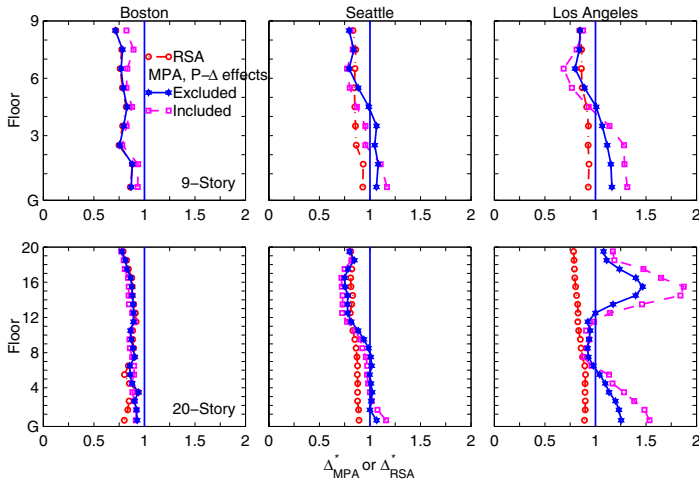
Figure 5. Median story drift ratios Δ^*_{MPA} for two cases: P-Δ effects due to gravity loads excluded or included and Δ^*_{RSA} for SAC buildings.

4.2 Accuracy of MPA

For each of the six SAC buildings, Fig. 5 shows the median of r^*_{MPA}, the ratio of response r computed by MPA and nonlinear RHA, for story drifts for two cases: gravity loads (and P-Δ effects) excluded or included; median values of r^*_{RSA} from elastic analyses are also shown. The median value of r^*_{RSA} being less than one implies that the standard RSA procedure underestimates the median response of elastic systems. Because the approximation in the RSA procedure for elastic systems is entirely due to modal combination rules, the resulting bias serves as a baseline for evaluating additional approximations in MPA for inelastic systems. The additional bias introduced by neglecting "modal" coupling in the MPA procedure depends on how far the building is deformed in the inelastic range. The increase in bias is negligible for both Boston buildings because they remain essentially elastic, slight for Seattle buildings because they are deformed moderately into the inelastic range, and significant for Los Angeles buildings, especially for the Los Angeles 20-story building because it is deformed into the region of rapid deterioration of lateral capacity, leading to collapse of its first-"mode" SDF system during six excitations. Because beam plastic rotations are directly related to story drifts, the MPA procedure is similarly accurate in estimating both demand quantities (Goel and Chopra, 2004a).

The MPA procedure estimates member forces to similar or better accuracy compared to story drifts. Such comparative results are presented for bending moments

and axial forces in columns in Figs. 6 and 7; similar results for bending moments and shear forces in beams and shear forces in columns are available elsewhere (Goel and Chopra, 2004b).
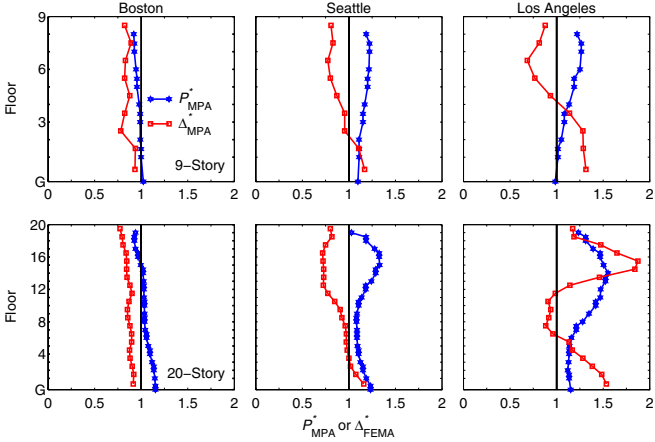
Figure 6. Median response ratios r^*_{MPA} **for column axial forces,** P^*_{MPA} **, and story drifts,** Δ^*_{MPA} **.**
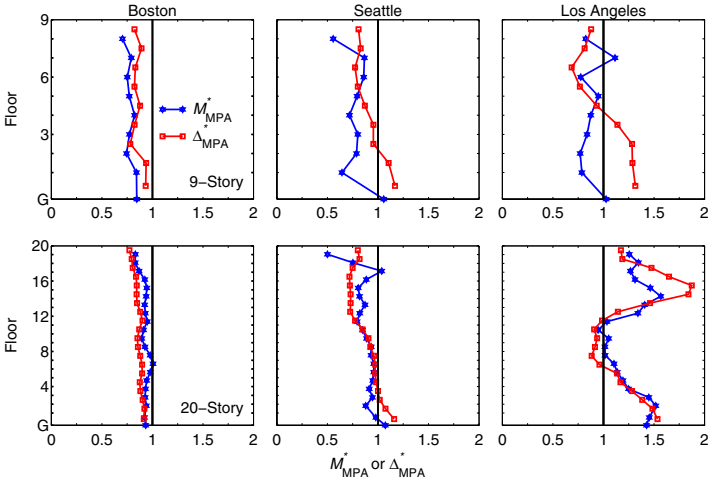
Figure 7. Median response ratios r^*_{MPA} **for column bending moments,** M^*_{MPA} **, and story drifts,** Δ^*_{MPA} **.**

5. EVALUATION OF MPA: UNSYMMETRIC-PLAN BUILDINGS

Computed were the seismic demands resulting from one of the SAC ground motions for the SAC-Los Angeles 9-story building, a symmetric-plan system, and three mass-eccentric systems, U1, U2, and U3, with different degrees of coupling between lateral and torsional motions as characterized by different values of the ratio of uncoupled lateral and torsional vibration periods. Figure 8 shows the story drifts at the right edge of the building plan including a variable number of "modal" pairs (or "modes" for symmetric building) in MPA superimposed with the "exact" result from nonlinear RHA. The first "modal" pair ("mode" for symmetric systems) alone is inadequate in estimating the story drifts, especially in the upper stories of the building, but with two "modal" pairs included, story drifts estimated by MPA are quite accurate.

For the excitation considered, the MPA results are accurate for two unsymmetric systems, U1 and U3, to a similar degree as they were for the symmetric building, which is apparent by comparing Figs. 8b and d with Fig. 8a; however, the results are less accurate for system U2 (Fig. 8c). Chopra and Goel (2004) demonstrated that this loss of accuracy is not because the system has very close natural periods and strong coupling of the lateral and torsional motions in each mode of vibration but because the roof displacement of system U2 due to the selected ground motion is considerably underestimated in the MPA procedure. This discrepancy occurs because the individual "modal" responses attain their peaks almost simultaneously, a situation for
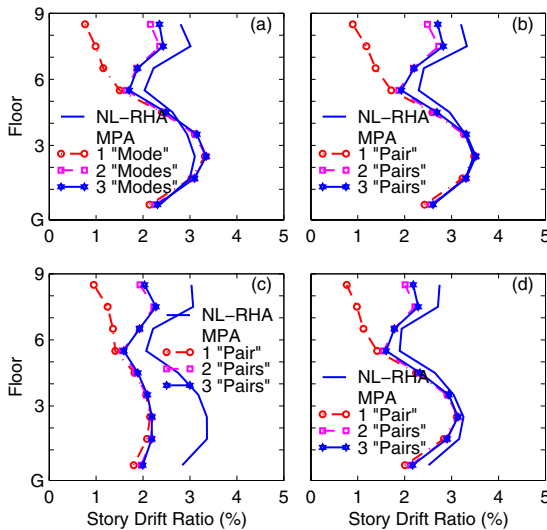
Figure 8. Story drifts determined by MPA with variable number of "modal" pairs (or modes) and nonlinear RHA: (a) symmetric building; (b), (c), and (d) unsymmetric-plan systems U1, U2, and U3.

341
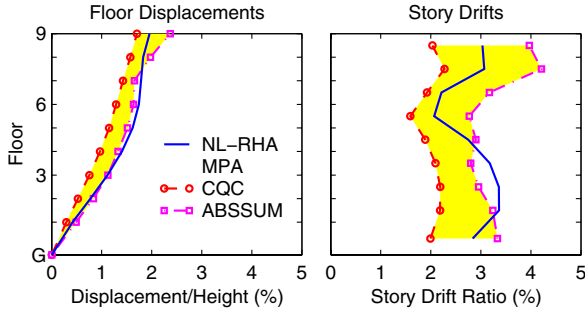
Figure 9. Responses at the right frame of unsymmetric-plan system U2 determined by MPA using CQC and ABSSUM rules and nonlinear RHA.

which the CQC modal combination rule is not valid. For such a case, the absolute sum (ABSSUM) rule may be more appropriate. Figure 9 shows that the "exact" demand is generally bounded by the two estimates determined by the MPA procedure using two different modal combination rules, CQC and ABSSUM.

The preceding scenario points to the need for evaluating the MPA procedure considering an ensemble of ground motions and documenting the bias and dispersion in this procedure applied to unsymmetric buildings, as has been accomplished for symmetric buildings (Chopra and Goel, 2004a). Such a statistical investigation is necessary for two reasons: First, the SRSS and CQC modal combination rules are based on random vibration theory and are intended for use when the excitation is characterized by a smooth response (or design) spectrum. Second, accurate estimation of roof displacement is necessary for the success of any pushover procedure and this usually is not assured for individual ground motions, as has been observed for the six SAC buildings (Chopra et al., 2003). For the Los Angeles 9-story building, the ratio of roof displacement values determined by MPA and nonlinear RHA varied from 0.66 to 1.70, with a median value of 1.21, over the 20 SAC ground motions.

6. CONCLUDING COMMENTS

Based on structural dynamics theory, the MPA procedure retains the conceptual simplicity and computational attractiveness of the standard pushover procedures with invariant lateral force distribution. Because higher-mode pushover analyses are similar to the first-mode analysis, MPA is conceptually no more difficult than procedures now standard in structural engineering practice. Because pushover analyses for the first two or three modal force distributions are typically sufficient in MPA, it requires computational effort that is comparable to the FEMA-356 procedure, which requires pushover analysis for at least two force distributions.

Without additional conceptual complexity or computational effort, MPA estimates seismic demands much more accurately than FEMA-356 procedures, as demonstrated by a comparison of Figs. 1 and 3 and Figs. 2 and 4. However, MPA is an approximate method that cannot be expected to always provide seismic demand estimates close to the "exact" results from nonlinear RHA. The total bias in the MPA estimate of seismic demands (including P-Δ effects) for Boston and Seattle buildings is about the same as the largest errors observed in the RSA procedure—which are tacitly accepted by the profession by using commercial software based on RSA. While MPA is sufficiently accurate to be useful in seismic evaluation of many buildings for many ground motions—and much more accurate than FEMA-356 procedures—its errors may be unacceptably large for buildings that are deformed far into the region of negative post-yield stiffness, with significant deterioration in lateral capacity, e.g., Los Angeles 20-story building subjected to the SAC 2/50 ensemble of ground motions. For such cases, MPA and most other pushover procedures cannot be expected to provide accurate estimates of seismic demands and they should be abandoned in favor of nonlinear RHA.

The computational effort in MPA can be further reduced by simplifying computation of the demands associated with higher vibration modes by assuming the building to be linearly elastic (Chopra et al., 2004). Such a modified MPA leads to a larger estimate of seismic demand, thus reducing the unconservatism of MPA results (relative to nonlinear RHA) in some cases and increasing their conservatism in others. While this increase in demand is modest and acceptable for systems with moderate damping, at least 5%, it is unacceptably large for lightly damped systems.

In practical application of MPA, the roof displacement for each modal pushover analyses can be estimated from the elastic spectrum defining the seismic hazard multiplied by the inelastic deformation ratio (Chopra and Chintanapakdee, 2004).

ACKNOWLEDGMENTS

REFERENCES

American Society of Civil Engineers (ASCE). (2000). Pre-standard and commentary for the seismic rehabilitation of buildings, *FEMA-356*, Federal Emergency Management Agency, Washington, D.C.

Applied Technology Council (ATC). (1996). Seismic evaluation and retrofit of concrete buildings. *Report No. ATC-40*, Redwood City, Calif.

Aydinoglu, M. N. (2003). An incremental response spectrum analysis procedure based on inelastic spectral deformation for multi-mode seismic performance evaluation. *Bull. Earthq. Engrg.*, 1:3-36.

Bracci, J. M, S. K. Kunnath, and A. M. Reinhorn. (1997). Seismic performance and retrofit evaluation for reinforced concrete structures. ASCE, *J. Struc. Engrg.*, 123:3-10.

Elnashai A. S. (2001). Advanced inelastic static (pushover) analysis for earthquake applications. *Struc. Engrg. Mech.*, 12(1):51-69.

Chopra, A. K. (2001). *Dynamics of Structures: Theory and Applications to Earthquake Engineering*, 2nd Ed., Prentice Hall, Englewood Cliffs, New Jersey.

Chopra, A. K., and R. K. Goel. (2002). A modal pushover analysis procedure for estimating seismic demands for buildings. *Earthq. Engrg Struc. Dyn.*, 31:561-582.

Chopra, A. K., R. K. Goel, and C. Chintanapakdee. (2003). Statistics of single-degree-of-freedom estimate of displacement for pushover analysis of buildings. ASCE, *J. Struc. Engrg.*, 119:459-469.

Chopra A. K., and C. Chintanapakdee. (2004). Inelastic deformation ratios for design and evaluation of structures: single-degree-of-freedom bilinear systems. ASCE, *J. Struc. Engrg.*, to appear.

Chopra, A. K., and R. K. Goel. (2004). A modal pushover analysis procedure to estimate seismic demands for unsymmetric-plan buildings. *Earthq. Engrg Struc. Dyn.*, to appear.

Chopra, A. K., R. K. Goel, and C. Chinatanapakdee. (2004). Evaluation of a modified MPA procedure assuming higher modes as elastic to estimate seismic demands. *Earthq. Spectra*, to appear.

Goel, R. K., and A. K. Chopra. (2004a). Evaluation of modal and FEMA pushover analyses: SAC buildings. *Earthq. Spectra*, 20(1):225-254.

Goel, R. K., and A. K. Chopra. (2004b). Extension of modal pushover analysis to compute member forces. *Earthq. Spectra*, submitted for publication.

Gupta, A., and H. Krawinkler. (1999). Seismic demands for performance evaluation of steel moment resisting frame structures (SAC Task 5.4.3). *Report No. 132*, John A. Blume Earthq. Engrg. Cen., Stanford Univ., Stanford, Calif.

Gupta, B., and S. K. Kunnath. (2000). Adaptive spectra-based pushover procedure for seismic evaluation of structures. *Earthq. Spectra*, 16:367-392.

Kunnath, S. K., and B. Gupta. (2000). Validity of deformation demand estimates using nonlinear static procedures. *Proc. U.S.-Japan Workshop on Performance-Based Earthq. Engrg. Methodology for R/C Bldg. Struc.*, Sapporo, Hokkaido, Japan.

Matsumori, T., S. Otani, H. Shiohara, and T. Kabeyasawa. (1999). Earthquake member deformation demands in reinforced concrete frame structures. *Proc. U.S.-Japan Workshop on Performance-Based Earthq. Engrg. Methodology for R/C Bldg. Struc.*, pgs. 79-94, Maui, Hawaii.

Sasaki, K. K, S. A. Freeman, and T. F. Paret (1998). Multimode pushover procedure (MMP)—A method to identify the effects of higher modes in a pushover analysis. *Proc. 6th U.S. Nat. Conf. Earthq. Engrg.*, Seattle, Wash.

AN IMPROVED PUSHOVER PROCEDURE FOR ENGINEERING PRACTICE: INCREMENTAL RESPONSE SPECTRUM ANALYSIS (IRSA)

M. Nuray AYDINOĞLU[1]

ABSTRACT

The practical version of improved pushover procedure *Incremental Response Spectrum Analysis (IRSA)* works directly with smoothed elastic response spectrum and makes use of the well-known *equal displacement rule* to scale modal displacement increments at each piecewise linear step of an incremental application of linear *Response Spectrum Analysis (RSA)*. IRSA can be readily applied to plan-symmetric as well as asymmetric multi-story buildings and irregular bridges involving multi-mode response at each piecewise linear step. Practical implementation of the procedure including P-delta effects is very simple and transparent.

Keywords: Equal displacement rule; Incremental response spectrum analysis; Modal capacity diagrams; Pushover analysis.

1. INTRODUCTION

The *Nonlinear Static Procedure (NSP)* based on *pushover analysis* has been recognized as a standard tool for the *deformation-based seismic evaluation* of existing and/or new structures (ASCE 2000, CEN 2003). In spite of the fact that the procedure has become very popular in recent years in structural earthquake engineering community, its development and implementation has been mostly intuitive, without being supported by a rational theory.

The procedure is assumed to rest on a modal coordinate transformation applied to a nonlinear multi-degree-of-freedom (MDOF) structural system by considering its fundamental mode only. However, since such a linear transformation is not possible for a nonlinear response, a linear elastic fundamental mode shape is generally adopted and it is assumed *invariant* for the purpose of defining the static-equivalent seismic load pattern to be applied to the structure. It is further assumed that various other invariant seismic load patterns can be used including the one, for example, based on a constant mode shape, which is expected, by intuition, to *bound* the possible solutions (ASCE 2000). In any case, nonlinear analysis of a MDOF system under an invariant load pattern is approximately reduced to the analysis of a simple, single-degree-of-

---

[1] *Department of Earthquake Engineering, Boğaziçi University, Kandilli Observatory and Earthquake Research Institute, 34680 Çengelköy — Istanbul, Turkey*

freedom (SDOF) system. In this regard pushover analysis serves for the approximate construction of the *backbone curve of the SDOF hysteresis* (Aydinoglu 2003), which is called the *capacity diagram* (Chopra and Goel 1999) or *capacity spectrum* (ATC, 1996). Thus seismic demand can be estimated in a simple manner using *inelastic response spectrum* concept (Fajfar 1999). Note that the capacity diagram is not explicitly used in the so-called *Displacement Coefficient Method* of FEMA 356 document (ASCE 2000), but its coordinates are implicitly considered in defining the *coefficients*.

It has to be admitted that the above-described *intuition-driven* approach has some serious problems and limitations. Firstly, the backbone curve of the SDOF hysteresis, i.e., the capacity diagram cannot be developed directly. Instead an auxiliary capacity curve, i.e., the so-called *pushover curve* is needed, but its coordinates are defined somewhat arbitrarily. The base shear and the roof displacement are traditionally selected for buildings, but it is problematic as to which displacement component to choose, for example, in bridges. On the other hand, it is not clear which *mode shape* is to be considered in the conversion process from the pushover curve to the capacity diagram. In some applications invariant linear elastic mode shape is adopted while in the others *instantaneous deformed shapes* due to invariant load patterns are used as if they were similar to *instantaneous mode shapes*.

Selecting the pushover curve coordinates arbitrarily and assuming an *artificial* mode shape for capacity diagram conversion may lead to inconsistent, even erroneous results. In this regard a typical but lesser known example is the misrepresentation of P-delta effects in buildings through conventional pushover curve (Aydinoglu 2004). The problem deals with the contribution of *equivalent P-delta forces* to the base shear. Note that generally linear shape functions are adopted for an approximate development of the *geometric stiffness matrix*, which represents P-delta effects (Clough and Penzien 1993). In a two-dimensional response of a building structure with rigid floor diaphragms, for example, this approximation leads to a *story P-delta moment* at each story (total story axial force times the story drift), which is then divided to the story height and thus converted to an equivalent force couple. Resultants of those forces help define a tri-diagonal geometric stiffness matrix, which is commonly used in most analysis software. It is clear that in calculating the contribution of P-delta forces to the base shear, the sum of those equivalent force couples vanishes at every story except in the first story (since the force at the bottom is not counted). This leads to an awkward situation, meaning that the ordinate of the conventional pushover curve actually represents the P-delta effect of *only the first story*! It may be argued that had the base overturning moment been selected as the ordinate of the pushover curve instead of the base shear, P-delta effects could have been represented more correctly.

It becomes evident that the main source of the above-mentioned problems is the invariant seismic load patterns *intuitively* used in the conventional pushover analysis, which in turn requires the development of a conventional pushover curve and the selection of an artificial mode shape for conversion to the capacity diagram. Actually,

for a response governed by the fundamental mode only, those problems can be easily overcome by using an *adaptive* procedure, in which instantaneous seismic loads and the corresponding deformed shape amplitudes are always compatible at each incremental step of a *piecewise linear analysis*, because both are expressed in terms of *instantaneous* mode shapes. In such an analysis procedure, plotting the conventional pushover curve is completely avoided and the capacity diagram of the *modal SDOF system*, which may include P-delta effects, can be developed directly for the seismic demand estimation (Aydinoglu 2003, 2004).

It should be stressed that even if the above-described adaptive procedure can be considered to provide the right answer to the single-mode pushover analysis, the main problem remains unresolved: Such an analysis can be reliably applied to only two-dimensional response of low-rise building structures regular in plan, where the seismic response can be assumed essentially governed by the fundamental mode. Hence it follows that improved procedures are required for high-rise and/or plan-irregular buildings and irregular bridges to account for higher-mode effects in a practical, but at the same time a rational manner. As a matter of fact significant efforts have been devoted in recent years to achieve this objective (Gupta and Kunnath 2000, Antoniou et al 2002, Chopra and Goel 2002). In this respect, *Incremental Response Spectrum Analysis (IRSA)* procedure has been introduced recently (Aydinoglu 2003). It is further extended to include P-delta effects (Aydinoglu 2004) and elaborated in this paper as an improved pushover procedure intended for use in routine engineering practice.

2. PRACTICAL IMPLEMENTATION OF INCREMENTAL RESPONSE SPECTRUM ANALYSIS (IRSA) PROCEDURE

Incremental Response Spectrum Analysis (IRSA) procedure is essentially based on a piecewise linear *Response Spectrum Analysis (RSA)* procedure applied at each incremental step of a pushover analysis (Aydinoglu 2003).

Adopting *lumped plasticity* approach, i.e., using plastic hinges to characterize the nonlinear behavior of structural members, any incremental *pushover step* (i) is defined in IRSA as representing a *piecewise linear* response increment in between the formation of two consecutive plastic hinges at discrete response points (i–1) and (i) during the so-called *pushover-history* process.

Applying modal expansion at the (i)'th piecewise linear pushover step, the increment of the displacement vector in the n'th mode, $\Delta \mathbf{u}_n^{(i)}$, can be expressed as

$$\Delta \mathbf{u}_n^{(i)} = \mathbf{\Phi}_n^{(i)} \Gamma_{xn}^{(i)} \Delta d_n^{(i)} \tag{1}$$

where $\Delta d_n^{(i)}$ represents modal displacement increment, $\mathbf{\Phi}_n^{(i)}$ denotes instantaneous mode shape vector and $\Gamma_{xn}^{(i)}$ refers to instantaneous participation factor for a ground motion in a given x direction. The eigenvalue analysis is governed by

$$(\mathbf{K}^{(i)} - \mathbf{K}_G^{(i)}) \, \mathbf{\Phi}_n^{(i)} = (\omega_n^{(i)})^2 \, \mathbf{M} \, \mathbf{\Phi}_n^{(i)} \tag{2}$$

in which $\mathbf{M}$ denotes mass matrix, $\mathbf{K}^{(i)}$ and $\mathbf{K}_G^{(i)}$ represent instantaneous (tangent) first-order stiffness and geometric stiffness matrices, respectively, the combination of which defines the instantaneous second-order stiffness matrix. Geometric stiffness matrix (Clough and Penzien 1993) accounts for P-delta effects with compressive axial forces taken positive. $\omega_n^{(i)}$ is the instantaneous natural frequency.

On the other hand, static-equivalent seismic load vector increment corresponding to the displacement vector increment given by Eq.1 can be written as

$$\Delta \mathbf{f}_{Sn}^{(i)} = (\mathbf{K}^{(i)} - \mathbf{K}_G^{(i)})\Delta \mathbf{u}_n^{(i)} = \mathbf{M}\boldsymbol{\Phi}_n^{(i)}\Gamma_{xn}^{(i)}\Delta a_n^{(i)} \qquad (3)$$

where $\Delta a_n^{(i)}$ refers to the modal pseudo-acceleration increment:

$$\Delta a_n^{(i)} = (\omega_n^{(i)})^2 \Delta d_n^{(i)} \qquad (4)$$

Modal displacement and modal pseudo-acceleration developed at the end of the (i)'th pushover step are calculated by adding their increments to those obtained at the end of the previous pushover step:

$$d_n^{(i)} = d_n^{(i-1)} + \Delta d_n^{(i)} \qquad ; \qquad a_n^{(i)} = a_n^{(i-1)} + \Delta a_n^{(i)} \qquad (5)$$

2.1 Modal Capacity Diagrams

A hypothetical nonlinear time-history analysis based on a piecewise linear mode-superposition method has led to a conclusion that modal pseudo-acceleration versus modal displacement diagrams, i.e., $a_n - d_n$ diagrams can be defined for each mode, which may be interpreted as *modal hysteresis loops* (Aydinoglu, 2003). The backbone curves of those loops, i.e. the envelopes of peak response points in the first quadrant, as shown in Fig. 1, are called *modal capacity diagrams*. According to Eq.4, the instantaneous slope of a given diagram is equal to the eigenvalue of the corresponding mode at the piecewise linear step concerned. By definition, first-mode capacity diagram is essentially identical to the *capacity spectrum* defined in the Capacity Spectrum Method (ATC 1996) of the conventional single-mode pushover analysis. Note that instantaneous slope of the first-mode capacity diagram or those of the few lower-mode diagrams could turn out to be negative due to P-delta effects when accumulated plastic deformations result in a negative-definite second-order stiffness matrix. A negative slope means a negative eigenvalue and thus an imaginary natural frequency, which leads to a modal response that resembles the non-vibratory response of an over-damped system (Aydinoglu and Fahjan 2003). The corresponding mode shape has a remarkable physical significance, representing the post-buckling deformation state of the structure under gravity loads and instantaneous static-equivalent seismic loads. Although structural engineers are not familiar with the negative (or zero) eigenvalues due to negative-definite (or singular) stiffness matrices, those quantities are routinely calculated by matrix transformation methods of eigenvalue analysis, such as the well-known Jacobi method (Bathe 1996).

2.2   Modal Scaling

The principal aim of IRSA is to estimate the above-defined modal displacement increments and accordingly the other modal response quantities of interest during an incremental application of a piecewise linear RSA. Hence a reasonable estimation of *relative* values of modal response increments, which may be called *modal scaling*, constitutes the most critical part of the development of IRSA.

An appropriate modal scaling procedure is proposed for IRSA in its inception stage (Aydinoglu 2003) where *inelastic spectral displacements* associated with the *instantaneous* configuration of the structure are used to scale the modal displacement increments. Interestingly, such a scaling procedure paves the way for adopting the *equal displacement rule* in practical applications where seismic input is defined via *smoothed elastic response spectrum*. According to this simple and well-known rule, spectral displacement of an inelastic SDOF system and that of the corresponding elastic system are assumed practically equal to each other provided that the effective initial period is longer than the *characteristic period* of the elastic response spectrum.

The characteristic period is approximately defined as the transition period from the constant acceleration segment to the constant velocity segment of the spectrum. For periods shorter than the characteristic period, elastic spectral displacement is amplified using a displacement modification factor, i.e., C_1 coefficient given in FEMA 356 (ASCE 2000). However such a situation is seldom encountered in mid- to high-rise buildings and long bridges with tall piers involving multi-mode response. In such structures, effective initial periods of the first few modes are likely to be longer than the characteristic period and therefore those modes automatically qualify for the equal displacement rule. On the other hand, effective post-yield slopes of the modal capacity diagrams get steeper and steeper in higher modes with gradually diminishing inelastic behavior (Fig. 1). Thus it can be comfortably assumed that inelastic modal displacement response in higher modes would not be different from the corresponding modal elastic response. Hence, smoothed elastic response spectrum may be used in its entirety for scaling modal displacements without any modification. As a reasonable further simplification for practice, elastic periods calculated in the first pushover step may be considered in lieu of the initial periods, the latter of which are estimated approximately from the bi-linearization of the modal capacity diagrams (Fig. 1b).
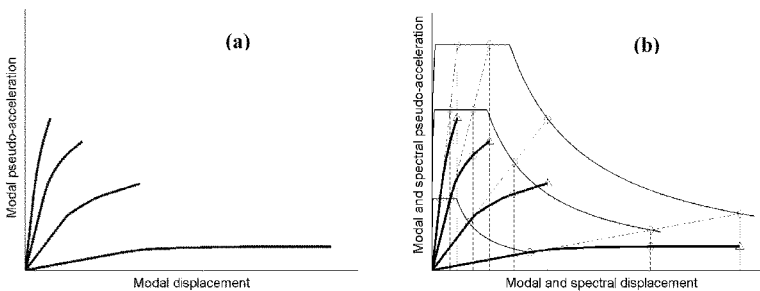
Figure 1. (a) Modal capacity diagrams, (b) scaling with equal displacement rule.

When equal displacement rule is employed, the scaling procedure applicable to modal displacement increments is simply expressed as (Aydinoglu 2003)

$$\Delta d_n^{(i)} = \Delta \tilde{F}^{(i)} S_{den}^{(1)} \tag{6}$$

where $\Delta \tilde{F}^{(i)}$ is an *incremental scale factor*, which is applicable to all modes at the (i)'th pushover step. $S_{den}^{(1)}$ represents the *initial elastic spectral displacement* defined at the first step (Fig. 1b), which is taken equal to the *inelastic spectral displacement* associated with the *instantaneous* configuration of the structure at any pushover step. Modal displacement at the end of the same pushover step can then be written as

$$d_n^{(i)} = \tilde{F}^{(i)} S_{den}^{(1)} \tag{7}$$

in which $\tilde{F}^{(i)}$ represents the *cumulative scale factor* with a maximum value of unity:

$$\tilde{F}^{(i)} = \tilde{F}^{(i-1)} + \Delta \tilde{F}^{(i)} \le 1 \tag{8}$$

Note that Eqs.6,7 actually represent a monotonic scaling of the elastic response spectrum progressively at each pushover step, which may be regarded analogous to the scaling of an individual earthquake record as applied in the *Incremental Dynamic Analysis (IDA)* procedure (Vamvatsikos and Cornell 2002). The spectrum scaling corresponding to the first yield and an intermediate step are indicated in Fig. 1b.

It is worth warning that equal displacement rule may not be valid at near-fault situations with forward directivity effect. On the other hand, legitimacy of the rule with P-delta effects is another important issue addressed elsewhere (Aydinoglu 2004).

It needs to be stressed that IRSA is a *displacement-controlled* procedure and therefore the above-mentioned monotonic spectrum scaling applies to spectral displacements only, not to the spectral pseudo-accelerations. If required however, a *compatible* modal pseudo-acceleration increment, $\Delta a_n^{(i)}$, corresponding to the increment of *scaled* modal displacement can be defined from Eqs.4,6 as

$$\Delta a_n^{(i)} = \Delta \tilde{F}^{(i)} S_{ain}^{(i)} \quad ; \quad S_{ain}^{(i)} = \frac{(\omega_n^{(i)})^2}{(\omega_n^{(1)})^2} S_{aen}^{(1)} \tag{9}$$

where $S_{ain}^{(i)}$ represents *compatible inelastic spectral pseudo-acceleration* and $S_{aen}^{(1)}$ refers to *initial elastic spectral pseudo-acceleration* corresponding to the elastic spectral displacement, $S_{den}^{(1)}$, defined at the first pushover step.

At this point, it may be worthwhile to point out the main difference of IRSA from an essentially similar incremental response spectrum analysis procedure developed by Gupta and Kunnath (2000). Note that the latter is a *load-controlled* procedure where modal pseudo-acceleration increments have been scaled at each step to define static-equivalent seismic load vector increments using *instantaneous elastic spectral pseudo-accelerations*, $S_{aen}^{(i)}$. The key point is the incompatibility of distribution of the so-defined instantaneous static-equivalent seismic loads with the resulting nonlinear instantaneous displacement response (see Eq.11 below for compatible seismic loads).

2.3 Pushover-History Analysis

Substituting Eq.6 into Eq.1 leads to the following expression for the displacement vector increment in the n'th mode at the (i)'th pushover step:

$$\Delta \mathbf{u}_n^{(i)} = \tilde{\mathbf{u}}_n^{(i)} \Delta \tilde{F}^{(i)} \quad ; \quad \tilde{\mathbf{u}}_n^{(i)} = \mathbf{\Phi}_n^{(i)} \Gamma_{xn}^{(i)} S_{den}^{(1)} \tag{10}$$

Although IRSA is a displacement-controlled procedure, utilizing Eqs.3,9 static-equivalent seismic load vector increment corresponding to the displacement vector increment given in Eq.10 may be written for an alternative load-controlled process:

$$\Delta \mathbf{f}_{Sn}^{(i)} = \tilde{\mathbf{f}}_{Sn}^{(i)} \Delta \tilde{F}^{(i)} \quad ; \quad \tilde{\mathbf{f}}_{Sn}^{(i)} = \mathbf{M} \mathbf{\Phi}_n^{(i)} \Gamma_{xn}^{(i)} S_{ain}^{(i)} \tag{11}$$

in which $S_{ain}^{(i)}$ is the compatible inelastic spectral pseudo-acceleration defined by Eq.9.

Note that in previous papers on the development of IRSA (Aydinoglu 2003, 2004), a different form of scale factor, namely the *inter-modal scale factor* had been used in pushover-history analysis. In the present paper, the above-given *incremental* and *cumulative scale factors* are directly used in the subsequent development.

Now, the increment of a *generic response quantity* of interest, such as the increment of an internal force, a displacement component, a story drift or the plastic rotation of a previously developed plastic hinge etc, may be written as

$$\Delta r^{(i)} = \tilde{r}^{(i)} \Delta \tilde{F}^{(i)} \tag{12}$$

in which $\tilde{r}^{(i)}$ is defined through a modal combination rule, such as Complete Quadratic Combination (CQC) rule as

$$\tilde{r}^{(i)} = \sqrt{\sum_{m=1}^{N_s} \sum_{n=1}^{N_s} (\tilde{r}_m^{(i)} \rho_{mn}^{(i)} \tilde{r}_n^{(i)})} \tag{13}$$

where N_s denotes the total number of considered in the analysis and $\tilde{r}_n^{(i)}$ refers to the response quantity obtained from $\tilde{\mathbf{u}}_n^{(i)}$ defined in Eq.10 or alternatively from $\tilde{\mathbf{f}}_{Sn}^{(i)}$ defined in Eq.11. $\rho_{mn}^{(i)}$ is the cross-correlation coefficient of the CQC rule. Thus, generic response quantity at the end of the (i)'th pushover step can be estimated as

$$r^{(i)} = r^{(i-1)} + \Delta r^{(i)} = r^{(i-1)} + \tilde{r}^{(i)} \Delta \tilde{F}^{(i)} \tag{14}$$

Note that each pushover step involves the formation of a new hinge, for which an incremental scale factor is calculated. In order to identify the next hinge and to estimate the response quantities at the end of the (i)'th pushover step, the generic expression given in Eq.14 is specialized for the response quantities that define the coordinates of the *yield surfaces* of all potential plastic hinges, i.e., biaxial bending moments and axial forces in a general, three-dimensional response of a framed structure. In the first pushover step, response quantities due to gravity loading are considered as $r^{(0)}$. Considering the yield conditions, the section that yields with the minimum positive incremental scale factor, $\Delta \tilde{F}^{(i)}$, helps identify the new hinge. In order to avoid iterative operations in hinge identification process, yield surfaces are

preferably linearized in a piecewise fashion, i.e., they are represented by finite number of lines or planes in two- and three-dimensional models, respectively.

Once the incremental scale factor is determined, the new value of the cumulative scale factor is calculated from Eq.8 and any response quantity of interest developed at the end of the (i)'th pushover step is obtained from the generic expression of Eq.14. If required, increments of modal displacements and modal pseudo-accelerations can be calculated from Eq.6 and Eq.4, respectively. Adding to those calculated at the end of the previous step, the new coordinates of all modal capacity diagrams may be obtained simultaneously from Eqs.5.

2.4 Estimating Seismic Demand: Peak Response Quantities

The above-described *pushover-history* procedure is repeated until cumulative spectrum scale factor defined by Eq.8 exceeds unity at the end of a given pushover step. When such a step is detected, which is indicated by superscript (p), incremental scale factor corresponding to this final pushover step is re-calculated from Eq.8 as

$$\Delta \tilde{F}^{(p)} = 1 - \tilde{F}^{(p-1)} \tag{15}$$

Peak value of the generic response quantity is again obtained from Eq.14 for i = p.

2.5 Summary of Practical Implementation of IRSA

A detailed derivation of IRSA is presented above for the sake of completeness. Note that the actual practical implementation of the procedure based on lumped plasticity model combined with smoothed response spectrum and equal displacement rule is very simple and transparent. The analysis stages to be applied at each pushover step of IRSA are summarized in the following:

(1) Run a linear response spectrum analysis (RSA) with a sufficient number of modes by considering the instantaneous second-order stiffness matrix corresponding to the current plastic hinge configuration. Preferably use a matrix transformation method (e.g., Jacobi method) in free-vibration analysis to accommodate singular or negative-definite matrices. Use the same spectral displacements, $S_{\text{den}}^{(1)}$, at all pushover steps as seismic input, which are defined only once at the first pushover step as elastic spectral displacements. Alternatively, compatible spectral pseudo-accelerations defined at each step by Eq.9 may be used. Obtain all response quantities of interest, $\tilde{r}^{(i)}$, by applying an appropriate modal combination rule (e.g., CQC rule — Eq.13).

(2) Specialize the generic expression of Eq.14 for the response quantities that define the coordinates of the yield surfaces of all potential plastic hinges, i.e., biaxial bending moments and axial forces in a general, three-dimensional response of a framed structure. Response quantities due to gravity loading are considered as $r^{(0)}$ in the first pushover step. Calculate the incremental scale factor, $\Delta \tilde{F}^{(i)}$, according to the yield conditions of all potential plastic hinges and identify the new yielded hinge.

(3) Calculate cumulative scale factor from Eq.8 and check if it exceeded unity. If exceeded, calculate the incremental scale factor, $\Delta \tilde{F}^{(p)}$, from Eq.15 for the final pushover step. If not, continue with the next stage.

(4) Calculate all response quantities of interest developed at the end of the pushover step from the generic expression of Eq.14. If the final pushover step has been reached, terminate the analysis. If not, continue with the next stage.

(5) Modify the current second-order stiffness matrix by considering the last yielded hinge identified at Stage (2) and return to Stage (1) for the next pushover step.

3. ILLUSTRATIVE EXAMPLES

3.1   3-D Pushover Analysis of a 9-Story Building with Mass Eccentricity

The first example is the 9-story benchmark steel building with basement designed for the Los Angeles area as part of the SAC project (Gupta and Krawinkler 1999). It has four identical moment resisting perimeter frames on each side as shown in Fig. 2a. Other details of modeling are given elsewhere (Aydinoglu, 2004). In order to create a 3-D mono-symmetrical response, mass centers of all floors are shifted eastward by a non-dimensional eccentricity of e=0.15. Earthquake ground motion is applied in N-S direction and defined through a standard response spectrum (ASCE 2000) with short-period and one-second spectral accelerations being 1.375 g and 0.80 g, respectively. Taking P-delta effects into account, 8 vibration modes are considered to adequately represent the coupled lateral-torsional response using CQC modal combination rule. Fig. 2b shows modal capacity diagrams with implementation of equal displacement rule. Fig. 2c, 2d, 2e show variations of peak floor displacements, story drift ratios and right-end beam plastic hinge rotations at central spans, respectively. Peak floor accelerations are shown in Fig. 2f. Response quantities are given for each perimeter frame and centre of mass (CM) where applicable. Intensity/demand curves are plotted in Fig. 2g in terms of maximum story drift ratios where the vertical axis indicates the seismic intensity measure (IM) defined as first-mode elastic spectral acceleration.
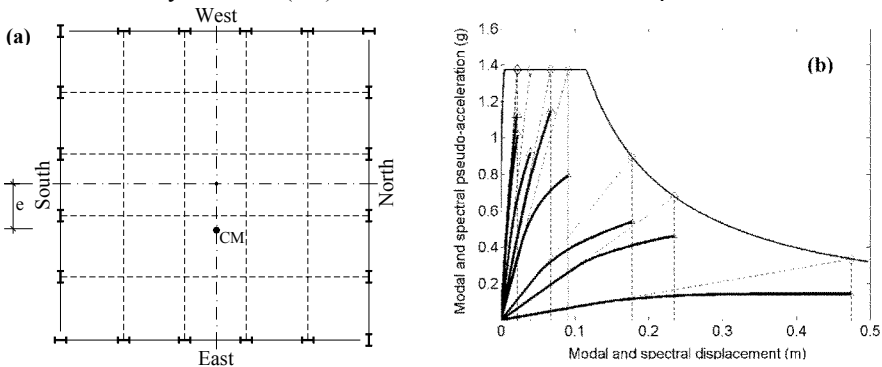
Figure 2. (a) Plan of 9-story steel building, (b) modal capacity diagrams,
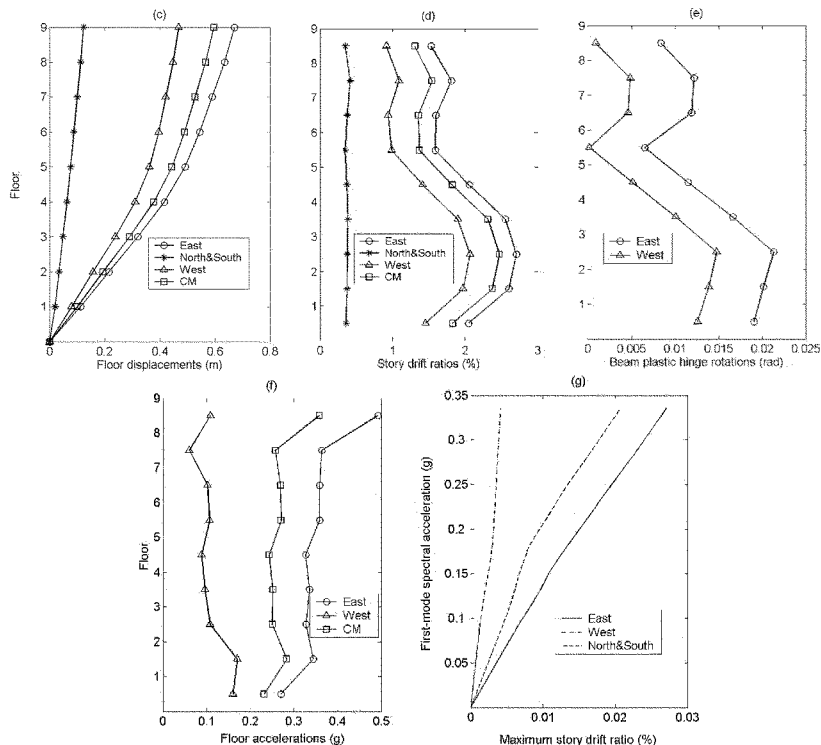
Figure 2—*continued.* (c) floor displacements, (d) story drift ratios, (e) plastic hinge rotations, (f) floor accelerations, (g) intensity/demand curves.

3.2   Pushover Analysis of a Long Viaduct in Transverse Direction

The second example is a 14 span, 789 m long *Sadabad – No.1 Viaduct* in Istanbul, constructed in late 1980's using *incremental launching method* with regular spans and side spans of 58 m and 46.4 m, respectively (Fig. 3a). Piers are of reinforced concrete box sections with plan dimensions of 3m x 4.7 m and a wall thickness of 0.45 m. Pier heights measured from top of the foundation to the soffit of the deck vary between 9 m and 48 m. Prestressed concrete deck is a 5 m deep box girder with a 12.3 m wide roadway slab (Fig. 3b). Plastic behavior is represented by plastic hinges located at pier bottoms. 8 vibration modes are considered in IRSA for transverse pushover analysis using the same smoothed response spectrum as above. Fig. 3c shows modal capacity diagrams and implementation of equal displacement rule at the onset of first yield and at the peak response. Given in Fig. 3d, 3e,3f are the transverse deck displacements, pier drift ratios and plastic hinge rotations, respectively, where the same response quantities obtained from a single-mode IRSA are superimposed for comparison.

Figure 3. (a) Viaduct side view, (b) cross-section, (c) modal capacity diagrams, (d) deck transverse displacements, (e) pier drift ratios, (f) plastic hinge rotations.

4. CONCLUSIONS

Incremental Response Spectrum Analysis (IRSA) is a recently introduced procedure attempting to replace the intuitive approach governing the current applications of single-mode and multi-mode pushover analyses with a rigorous one. The essential requirement of practicality in engineering applications dictates that pushover analysis including multi-mode effects should be simple enough without involving any time-history analysis. It means that seismic input is to be defined through a *smoothed response spectrum* and the analysis procedure should incorporate a modal combination technique based on peak modal response quantities. In fact IRSA is designed to satisfy all such requirements through an incremental application of the conventional *Response Spectrum Analysis (RSA)* procedure combined with an efficient use of the well-known *equal displacement rule*. As demonstrated through typical examples presented in this paper, IRSA can be readily applied to any 3-D structure including plan-asymmetric multi-story buildings and irregular bridges involving multi-mode response at each piecewise linear pushover step.

Based on the summary of IRSA provided in 2.5 above, the only major difference of IRSA from the conventional single-mode pushover may be identified as follows: The *static analysis* required at each step of the latter is effectively replaced in IRSA with a *response spectrum analysis* based on initial elastic spectral displacements, which makes the computer implementation extremely simple and straightforward.

REFERENCES

Antoniou, S., A. Rovithakis, and R. Pinho (2002). Development and verification of a fully adaptive pushover procedure. *Proc. of the 12th European Conf. on Earthquake Engineering, London.* Paper No.882.

ASCE-American Society of Civil Engineers (2000). Prestandard and commentary for the seismic rehabilitation of buildings (FEMA 356), Washington D.C.

ATC-Applied Technology Council (1996). Seismic evaluation and retrofit of concrete buildings (ATC-40). Redwood City, California.

Aydinoglu, M. N. (2003). An incremental response spectrum analysis based on inelastic spectral displacements for multi-mode seismic performance evaluation. *Bulletin of Earthquake Engineering*; 1(1): 3-36.

Aydinoglu, M. N., and Y. M. Fahjan (2003). A unified formulation of the piecewise exact method for inelastic seismic demand analysis including the P-delta effect. *Earthquake Engineering and Structural Dynamics*; 32(6): 871-890.

Aydinoglu, M. N. (2004). Incremental Response Spectrum Analysis (IRSA) procedure for multi-mode pushover including P-delta effects. *Proc. of the 13th World Conf. on Earthquake Engineering, Vancouver, Canada*. Paper No.1440.

Bathe, K. J. (1996). *Finite Element Procedures*. New Jersey, Prentice Hall.

CEN (2003). *Eurocode 8 — Design of structures for earthquake resistance*, Part 1, European Standard prEN 1998-1, Stage 49 Draft, October 2003, Brussels.

Chopra, A. K., and R. K. Goel (1999). Capacity-demand-diagram methods based on inelastic design spectrum. *Earthquake Spectra*; 15(4): 637-656.

Chopra, A. K., and R. K. Goel (2002). A modal pushover analysis for estimating seismic demands for buildings. *Earthquake Engineering and Structural Dynamics*; 31(3): 561-582.

Clough, R. W., and J. Penzien (1993). *Dynamics of structures*. 2nd Ed., New York, McGraw-Hill.

Fajfar, P. (1999). Capacity Spectrum Method based on inelastic demand spectra. *Earthquake Engineering and Structural Dynamics*; 28(9): 979-993.

Gupta, A., and H. Krawinkler (1999). Seismic demands for performance evaluation of steel moment resisting frame structures. The John A. Blume Earthquake Engineering Center, Stanford University, California, Report No.132.

Gupta, B., and S. K. Kunnath (2000). Adaptive spectra-based pushover procedure for seismic evaluation of structures. *Earthquake Spectra*; 16(2): 367-391.

Vamvatsikos, D., and C. A. Cornell (2002). Incremental dynamic analysis. *Earthquake Engineering and Structural Dynamics*; 31(3): 491-514.

EXTENSIONS OF THE N2 METHOD — ASYMMETRIC BUILDINGS, INFILLED FRAMES AND INCREMENTAL N2

Peter FAJFAR, Matjaž DOLŠEK, Damjan MARUŠIĆ and Iztok PERUŠ[1]

ABSTRACT

The N2 method is a relatively simple seismic analysis technique based on pushover analysis and inelastic response spectrum approach. Its basic variant is based on a number of assumptions, which impose restrictions to its applicability to general structural systems. Recent research has been aimed to extending the applicability of the method to plan-asymmetric buildings and to infilled reinforced concrete frames. Moreover, the incremental N2 (IN2) method has been developed as a simple alternative to incremental dynamic analysis (IDA). In the paper, the basic N2 method and the three extensions are summarised.

Keywords: Simplified non-linear analysis; Inelastic spectra; Reduction factors; Torsion; Infilled frames.

1. INTRODUCTION

In recent years, a breakthrough of simplified inelastic analysis and performance evaluation methods has occurred. Such methods combine the non-linear static (pushover) analysis of a multi degree-of-freedom (MDOF) model and the response spectrum analysis of an equivalent single-degree-of-freedom (SDOF) model. They can be used for a variety of purposes such as design verification for new buildings and bridges, damage assessment for existing structures, determination of basic structural characteristics in direct displacement based design, and rapid evaluation of global structural response to seismic ground motion of different intensities. An example is the capacity spectrum method (CSM), developed by Freeman (1998) and implemented in different variants in different regulatory documents in the USA and in Japan. Another example is the N2 method, which has been implemented into the final version of the Eurocode 8 standard (CEN 2003).

The simple basic variant of the N2 method cannot be applied to some structural systems with specific structural behaviour, e.g., to infilled reinforced concrete (RC) frames. Moreover, the basic variant of the N2 method is, like other simplified non-

linear methods, restricted to symmetric structures, which can be modelled by a planar structural model. In this paper, the extensions of the N2 method are summarized.

A pushover based non-linear analysis of plan-asymmetric buildings, which experience torsional rotations, proved to be a difficult problem. As a preliminary solution, it is proposed to determine the global displacement demand in each horizontal direction by a uni-directional pushover analysis of a 3D structural model, and to estimate the torsional influence from the results of elastic modal analysis of the same model. This proposal is based on results of limited parametric studies, which suggest that the torsional effects decrease with increasing intensity of ground motion and with related increase of plastic deformations. Consequently, torsional amplification determined by elastic analysis may represent a conservative estimate.

The N2 method employs inelastic spectra for the determination of seismic demand. Inelastic spectra are determined from the elastic demand spectra by using strength reduction factors. In the basic variant of the N2 method, simple R-μ-T relationships are used, based on equal displacement rule in medium- and long-period range of the spectrum. This assumption, although valid for many structural systems, is not appropriate for RC frames infilled with masonry, which are characterised by a strong stiffness and strength degradation after infill fails. Specific R-μ-T relationships have been developed for this type of structural systems. The example demonstrates how any R-μ-T relationship can be employed in the N2 method.

The result of an Incremental dynamic analysis (IDA) is an IDA curve, which represents the relation between a structural response parameter versus the intensity level of ground motion, and the corresponding variability. IDA requires a large number of inelastic time-history analyses of MDOF structural systems and is thus time consuming. An estimate of the IDA curve can be obtained by a series of N2 analyses, called IN2 (Incremental N2) analysis. An IN2 curve, which is the result of IN2 analysis, can be combined with generic variability for different structural systems, determined by parametric studies.

2. SUMMARY OF THE N2 METHOD — BASIC VARIANT

The N2 method (N comes from Nonlinear analysis and 2 comes from 2 mathematical models) was developed at the University of Ljubljana in mid-eighties. The formulation of the method in the AD format enables the visual interpretation of the procedure and of the relations between the basic quantities controlling the seismic response. For details about the basic version of the N2 method, limited to planar structural models, see e.g., (Fajfar and Gašperšič 1996 and Fajfar 2000).

In the N2 method, first the pushover analysis of the MDOF model is performed. Pushover curve is then transformed to the capacity diagram. The seismic demand for the equivalent SDOF system with a period T can be determined as follows: Elastic demand in terms of acceleration S_{ae} and displacement S_{de} is determined from the elastic spectrum. The inelastic acceleration demand S_a is equal to the yield acceleration S_{ay}, which represents the acceleration capacity of the inelastic system.

The strength reduction factor due to ductility R_μ, which will be denoted in this paper as R ($R \equiv R_\mu$), can be determined as the ratio between the accelerations corresponding to the elastic and inelastic system. The ductility demand μ is then calculated from inelastic spectra, which are defined by the period dependent relation between reduction factor and ductility (R-μ-T relation), and the inelastic displacement demand S_d is computed as $S_d = (\mu/R)S_{de}$. The target displacement, which represents the seismic demand of the MDOF model, is obtained as $D_t = \Gamma S_d$, where Γ is the transformation factor from the MDOF to the SDOF system.

In principle any R-μ-T relation can be used. A very simple and fairly accurate R-μ-T relation is based on the equal displacement rule in the medium- and long-period range. This relation is used in the basic variant of the N2 method. It has been implemented in Eurocode 8 and is discussed below. The application of the N2 method can be extended also to complex structural systems, for example to infilled frames (Chapter 4), provided that an appropriate specific R-μ-T relation is known.

For many years, the ductility factor method has been used in seismic codes. The basic assumption of this method is that the deformations of a structure produced by a given ground motion are essentially the same, whether the structure responds elastically or yields significantly. This assumption represents the "equal displacement rule". Using this rule, the ductility dependant reduction factor R is equal to ductility factor μ. The simple chart in Fig.1 is essential for understanding of the concept of reduction factors and of the ductility factor method. The educational value of the figure can be greatly increased by using the AD format, introduced by Freeman. In AD format, Fig.1 (force has to be divided by mass) can be combined with demand spectra (Fig.2). Fig.2, which enables a visualisation of the basic variant of the N2 method, resembles to the basic chart in capacity spectrum method. The main difference is in inelastic demand, which is defined by an inelastic spectrum rather than by an equivalent highly damped elastic spectrum. Inelastic spectrum in medium- and long-period range in Fig.2 is based on the equal displacement rule.
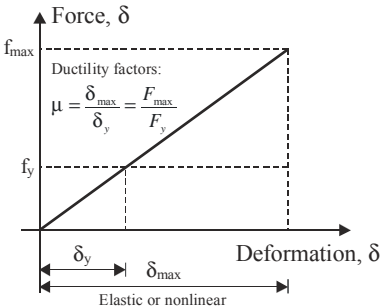

Figure 1. Basic diagram explaining the ductility factor method (re-plotted from Clough and Penzien 1975, p.603).
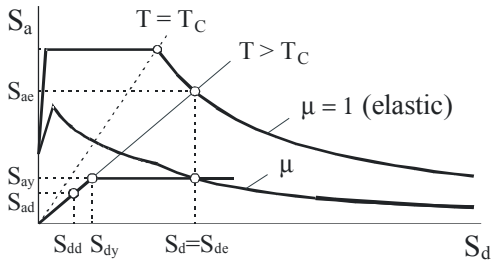
Figure 2. Elastic and inelastic demand spectra versus capacity diagram.

In Fig.2 the quantities relevant for the seismic response of an ideal elasto-plastic SDOF system can be visualised. Seismic demand is expressed in terms of accelerations and displacements, which are the basic quantities controlling the seismic response. Demand is compared with the capacity of the structure expressed by the same quantities. Fig.2 helps to understand the relations between the basic quantities and to appreciate the effects of changes of parameters. The intersection of the radial line corresponding to the elastic period of the idealised bilinear system T with the elastic demand spectrum S_{ae} defines the acceleration demand (strength) required for elastic behaviour, and the corresponding elastic displacement demand S_{de}. The yield acceleration S_{ay} represents both the acceleration demand and capacity of the inelastic system. The reduction factor R is equal to the ratio between the accelerations corresponding to elastic (S_{ae}) and inelastic systems (S_{ay}). If the elastic period T is larger than or equal to T_C, which is the characteristic period of ground motion, the equal displacement rule applies and the inelastic displacement demand S_d is equal to the elastic displacement demand S_{de}. From triangles in Figs.1 and 2 it follows that the ductility demand μ is equal to R. Fig.2 also demonstrates that the displacements S_{dd} obtained from elastic analysis with reduced seismic forces, corresponding to design acceleration S_{ad}, have to be multiplied by the total reduction factor, which is the product of the ductility dependent factor R and the overstrength factor, defined as S_{ay}/S_{ad}. The intersection of the capacity diagram and the demand spectrum, called also performance point, provides an estimate of the inelastic acceleration and displacement demand, as in the capacity spectrum method. This feature allows the extension of the visualisation to more complex cases, in which different relations between elastic and inelastic quantities and different idealisations of capacity diagrams are used, e.g., for infilled frames (see Fig.7a). Unfortunately, in such cases the simplicity of relations, which is of paramount importance for practical design, is reduced. Note that Fig.2 does not apply to short-period structures.

Fig.2 can be used for both traditional force-based design as well as for the increasingly popular deformation-controlled (or displacement-based) design. In these two approaches, different quantities are chosen at the beginning. Let us assume that the approximate mass is known. The usual force-based design typically starts by assuming the stiffness (which defines the period) and the approximate global ductility capacity. The seismic forces (defining the strength) are then determined, and finally displacement demand is calculated. In direct displacement-based design, the starting points are typically displacement and/or ductility demands. The quantities to be determined are stiffness and strength. The third possibility is a performance evaluation procedure, in which the strength and the stiffness (period) of the structure being analysed are known, whereas the displacement and ductility demands are calculated. Note that, in all cases, the strength corresponds to the actual strength and not to the design base shear according to seismic codes, which is in all practical cases less than the actual strength. Note also that stiffness and strength are usually related quantities. All approaches can be easily visualised with the help of Fig.2.

The relations apply to SDOF systems. However, they can be used also for a large class of MDOF systems, which can be adequately represented by equivalent SDOF systems. The combination with the nonlinear pushover analysis substantially increases the accuracy of the procedure compared to the traditional ductility factor method.

3. EXTENSION TO PLAN—ASYMMETRIC BUILDINGS

The original N2 method is, like other simplified non-linear methods, restricted to 2D analysis. In order to extend the applicability of the method to plan-asymmetric buildings, which require a 3D structural model, a procedure based on pushover analysis of a 3D building model was proposed in (Fajfar 2002) and implemented in (Fajfar et al. 2002). The test results have indicated that some improvements of the N2 method for asymmetric structures are still needed, therefore the research on inelastic structural response of asymmetric structures has been continued. Based on several extensive parametric studies reported in (Fajfar et al. 2004) we concluded that (a) the amplification of displacements determined by the elastic analysis can be used as a rough estimate also in the inelastic range and (b) any favourable torsional effect on the stiff side of torsionally stiff buildings, which may arise from elastic analysis, may disappear in the inelastic range. Based on these results, the following procedure is proposed, which represents a combination of non-linear static and linear dynamic analysis. It can be applied both for torsionally stiff and torsionally flexible buildings.

Two independent analyses in two horizontal directions are performed. For each direction, first a pushover analysis of a 3D structural model is made. The transverse elements should be included in the model. Lateral loads are applied in mass centres. Based on the obtained base shear – top displacement relationship, an equivalent SDOF system is determined. Top displacement corresponds to the mass centre. The transformation from the MDOF to the SDOF system and vice versa is the same as in the case of a 2D model. The procedure for determining the target displacement of the equivalent SDOF system is also the same as in the case of 2D analysis. Seismic demands (deformation quantities: displacements, storey drifts, rotations and ductilities, and quantities related to accelerations, which may be relevant for brittle elements and contents of the building) are determined by pushing the structure to the target displacement for each of two horizontal directions separately.

In the next step of analysis, a usual elastic modal analysis employing the same mathematical model as in pushover analysis and the same demand spectra as for determination of target displacement is performed for both directions of loading. Demand quantities obtained for two directions of loading are combined by the SRSS rule. The resulting seismic demand in terms of displacements at different locations at the top of the building is used for the determination of correction factors to be applied to the results of pushover analyses. A single correction factor is determined for each vertical plane of load-bearing elements (e.g., a structural wall or a plane frame) and it depends on the position of the plane in the plan. The correction factors are aimed to

introduce the elastic torsional influences (displacement shapes in the plan) at the top of the building, while preserving the absolute values of top displacements in mass centre and the vertical distributions (ratios) of seismic demand determined by two pushover analyses. Only amplification due to torsion is taken into account. Beneficial torsional effects, i.e., de-amplification of displacements compared to the displacements in the mass centre, is neglected.
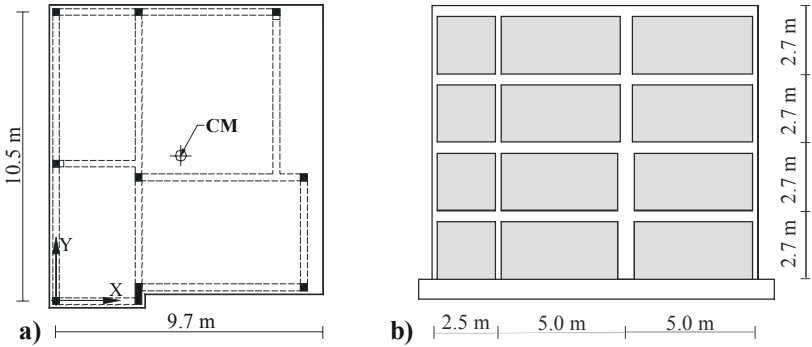
Figure 3. Test structures: (a) SPEAR building; (b) infilled frame.

In order to illustrate the proposed procedure, a three-storey RC frame structure (Fig.3a), tested pseudo-dynamically in full-scale in ELSA laboratory in Ispra within the SPEAR project, has been analysed. The mathematical model corresponds to pre-test analyses. Non-linear time-history analyses were performed with 7 two-component semi-artificial accelerograms, fitted to Eurocode 8 elastic spectrum. In Fig.4 envelopes of normalized displacements at the top of the building, obtained by time-history analyses for different intensities of ground motions, are compared with the results of elastic spectral analysis. Fig.4 indicates that, on the flexible sides (i.e., the upper and right hand side in Fig.3a), the torsional amplification generally decreases with increasing intensity of ground motion. On the stiff sides, the de-amplification is smaller than suggested by elastic spectral analysis. It may completely disappear or even an amplification may occur. The coefficient of variation of normalized displacements amounts to about 0.13 in X-direction and about 0.1 in Y-direction (at PGA = 0.3 g). According to the proposed extension of the N2 method, the displacement demand in both directions follows the elastic spectral line on the flexible sides and the horizontal line 1.0 on the stiff sides. The correction factors in different locations are determined as the ratios between the lines defined above and the lines obtained by the pushover (static) analysis. The target displacement, which is by definition the displacement demand at the top at mass centre, is determined by the usual procedure, applied in the N2 method. Comparison of the capacity diagram and demand spectra normalized to PGA = 0.3g is presented in Fig.5. There is a noticeable difference in pushover curves due to different sense of loading in Y-direction, while

in X-direction pushover curves practically overlap. Target displacements of the MDOF model, obtained by the N2 method, amount to about 12 cm in the X-direction and to 11.4 cm in the Y-direction. The values obtained by non-linear time-history analysis amount to 10.6 and 10.4 cm in X- and Y- direction, respectively. The corresponding coefficients of variation are about 0.10 and 0.25. The comparison of results suggests that the N2 method is conservative in both steps, i.e. when determining target displacement in CM and when determining the torsional amplifications.
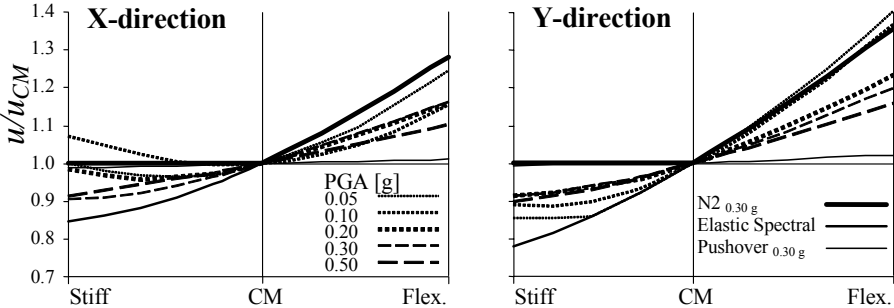
Figure 4. Envelopes of the normalised displacements at the top of the SPEAR building in the horizontal plane.
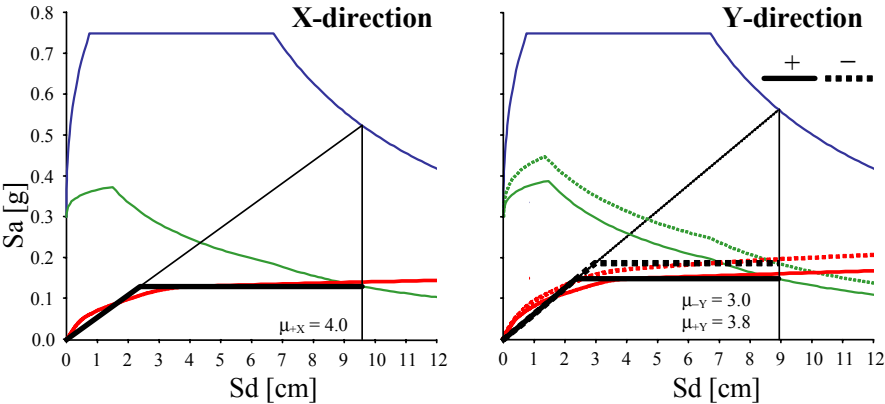
Figure 5. Capacity diagrams and demand spectra (PGA = 0.3 g).

4. EXTENSION TO INFILLED FRAMES

In order to employ the N2 method to infilled RC frames, a specific R-μ-T relation is needed. The basic characteristic of the pushover curve of infilled RC frames is a substantial decrease in strength and stiffness after the infill has begun to degrade. The

frame is usually able to resist the seismic loads after the infill fails. The pushover curve can be modeled with a four-linear force-displacement relationship as shown in Fig.6a. Based on an extensive statistical study of a SDOF mathematical model with a four-linear backbone curve and hysteretic behaviour typical for infill frames, a specific R-μ-T relation was determined (Dolšek and Fajfar 2004a). The relation depends on the basic parameters of the pushover curve (yield displacement D_y and yield force F_y, ductility at the beginning of softening of infills μ_s, and the ratio between the force at which infills completely collapse and yielding force r_u) and the corner periods of the acceleration spectrum T_C and T_D. T_C represents the corner period between the constant acceleration and constant velocity part of the spectrum of the Newmark-Hall type, and T_D represents the corner period between the constant velocity and constant displacement part of the spectrum.

$$\mu = \frac{1}{c}(R - R_0) + \mu_0 \tag{1}$$

where

$$
c =
\begin{cases}
0.7\left(\dfrac{T}{T_C}\right) & \cdots \quad R \le R(\mu_s), \quad T \le T_C \\[2ex]
0.7 + 0.3\Delta T & \cdots \quad R \le R(\mu_s), \quad T_C < T \le T_D^* \\[2ex]
0.7\sqrt{r_u}\left(\dfrac{T}{T_C}\right)^{\frac{1}{\sqrt{r_u}}} & \cdots \quad R > R(\mu_s), \quad T \le T_C \\[2ex]
0.7\sqrt{r_u}\,(1-\Delta T) + \Delta T & \cdots \quad R > R(\mu_s), \quad T_C < T \le T_D^* \\[2ex]
1 & \cdots \qquad\qquad\qquad\quad T > T_D^*
\end{cases}
\tag{2}
$$

with

$$T_D^* = T_D\sqrt{2 - r_u}\,, \quad \Delta T = \frac{T - T_C}{T_D\sqrt{2 - r_u} - T_C}\,, \tag{3}$$

$$
\mu_0 =
\begin{cases}
1 & \cdots \quad R \le R(\mu_s) \\
\mu_s & \cdots \quad R > R(\mu_s)
\end{cases}
\tag{4}
$$

and

$$
R_0 =
\begin{cases}
1 & \cdots \quad R \le R(\mu_s) \\
R(\mu_s) & \cdots \quad R > R(\mu_s)
\end{cases}
\tag{5}
$$

where

$$
R(\mu_s) =
\begin{cases}
0.7\left(\dfrac{T}{T_C}\right)(\mu_s - 1) + 1 & \cdots \qquad T \le T_C \\[2ex]
(0.7 + 0.3\Delta T)(\mu_s - 1) + 1 & \cdots \quad T_C < T \le T_D^* \\[2ex]
\mu_s & \cdots \qquad T > T_D^*
\end{cases}
\tag{6}
$$

As an example, an idealized force-displacement relation (pushover curve) and the *R-μ-T* relation for the given pushover curve are shown in Fig.6.

The coefficient of variation for ductility is strongly influenced by the dispersion of elastic displacement. It is higher for lower periods. As a rough estimate, a value of about 0.7 can be assumed for infilled frames with the fundamental period in the short period range (Dolšek and Fajfar 2004a).

Note that the idealized *R-μ-T* relation defined above is based on mean ductility obtained by statistical analysis, in which the reduction factor *R* was fixed. It is shown in (Dolšek and Fajfar 2004a) that such an approach is conservative both for design and assessment. In the same paper it is shown that a more realistic *R-μ-T* relation can be obtained if median is used as the central value instead of mean.

Knowing the *R-μ-T* relation, the usual N2 procedure, as described in Chapter 2, can be employed. Note, however, that the performance point, defining the seismic demand, is presented in the capacity-demand plot as the point where the horizontal line, at the acceleration S_{ay}, intersects the appropriate inelastic spectrum, and **not** the point, where the capacity diagram intersects the demand spectrum.

A similar extension of the N2 method can be made to any structural system, provided that an appropriate specific *R-μ-T* relation is available.
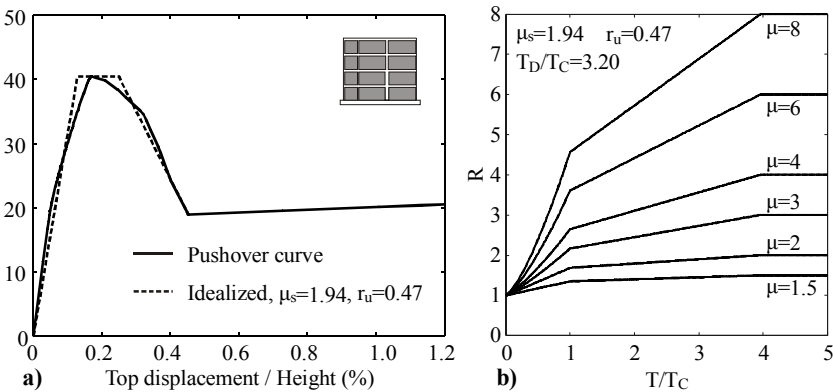
Figure 6. Infilled frame: (a) force-displacement relation, (b) R-μ-T relation.

5. INCREMENTAL N2 METHOD

The incremental N2 (IN2) method (Dolšek and Fajfar 2004b, 2004c) is a relatively simple non-linear method for determination of approximate IDA curves. An IDA curve is determined with non-linear dynamic analyses (Vamvastsikos and Cornell 2002), while each point of an IN2 curve (approximate IDA curve), which corresponds to a given seismic intensity, is determined with the N2 method.

In order to determine an IN2 curve, first the ground motion intensity measure and the demand measure have to be selected. The most appropriate pair of quantities is the

spectral acceleration and the top (roof) displacement, which allow also the visualization of the procedure (Fig.7a). Other relevant quantities, like maximum story drift, rotation at the column and beam end, shear force in a structural element and in a joint, and story acceleration, can be employed as secondary demand measures. They are related to roof displacement and can be uniquely determined if roof displacement is known. The secondary demand measures can be used, together with the main demand measure, for performance assessment at different performance levels.

Roof displacement and other relevant demand measures for a chosen series of spectral accelerations are determined by the N2 method. The shape of the IN2 curve depends on the inelastic spectra applied in the N2 method, which are based on the relation between strength reduction factor, ductility and period (the R-μ-T relation). If a simple R-μ-T relation, based on equal displacement rule in the medium- and long-period range, is used, the IN2 curve is linear for structures with period higher than T_C. A more complex R-μ-T relation is used for infilled RC frames (Eqs. 1 to 6). In this case IN2 curve is four-linear (Fig.7). Note that a bilinear relation is used already before yielding. Considering the piecewise linearity of the IN2 curve, only a few points have to determined in order to obtain the complete IN2 curve.

Usually the inelastic spectra, used in the N2 method, represent mean spectra and consequently the IN2 curve represents a mean curve. More specifically, the R-μ-T relation for infilled frames (Eqs. 1 to 6), represents an idealization of the R-μ-T relation, calculated for mean ductility given the reduction factor.

The determination of a point on the IN2 curve is visualised in Fig.7a. The point is defined with the pair: elastic spectral acceleration (1.07g), corresponding to the equivalent elastic period T, on the Y-axis, and the corresponding inelastic displacement demand (6.59cm) on the X-axis. By repeating the procedure for many levels of elastic spectral acceleration, the complete IN2 curve can be obtained as presented in Fig.7b.
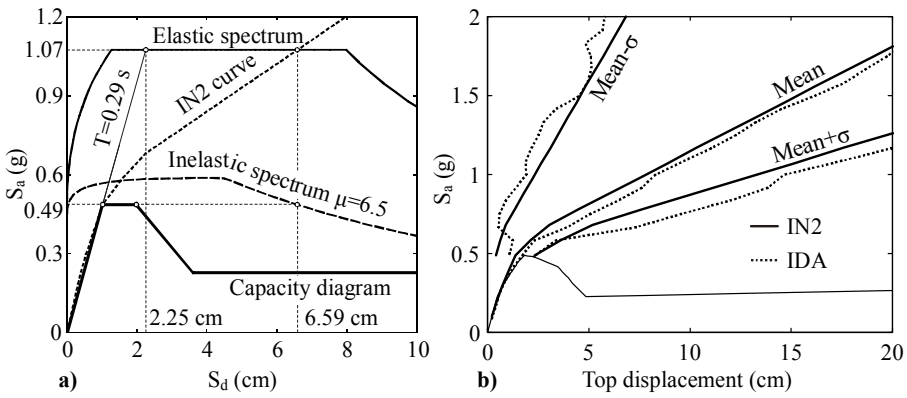

Figure 7. Infilled frame: (a) capacity diagram, demand spectra and IN2 curve (for SDOF system), (b) mean ± σ IDA and IN2 curve.

The IN2 curve can be used in the probabilistic seismic assessment method (Cornell et al. 2002). In such a case, the dispersion has to be known. Dispersion measures for different types of structural systems can be determined by parametric studies and subsequently used as predetermined values in analyses. For example, for infill frames we assumed that the same dispersion as observed for the R-μ-T relation applies also for top displacement.

A four-storey infilled RC frame (Fig.3b), representing an existing building and tested pseudo-dynamically in full-scale in ELSA, will be used for illustration of the N2 method for infilled frames and the IN2 method. Ground motion is defined by an Newmark-Hall type spectrum, which represents the idealized mean spectrum of a set of 20 recorded accelerograms. Pushover curve and the capacity diagram are shown in Figs. 6a and 7a, respectively. The reduction factors, corresponding to the idealized pushover curve and to the applied ground motion, are presented in Fig.6b. Determination of seismic demand for ground motion normalized to PGA = 0.45 g and of a point of the IN2 curve is shown in Fig.7a. In Fig.7b a comparison of the mean IN2 curve with the mean IDA curve, as well as the mean $\pm$ σ curves are presented. Note that displacement of the equivalent SDOF system and top (roof) displacement are plotted on the x-axis in Figs.7a and 7b, respectively. The value of 0.7 was used for the coefficient of variation related to IN2 analysis (as suggested in Dolšek and Fajfar 2004a), and the "exact" coefficient of variation was used in the case of IDA analysis. A fair agreement of results can be observed. Additional results are presented in (Dolšek and Fajfar 2004b).

6. CONCLUSIONS

Simplified non-linear design and assessment methods based on pushover analysis and inelastic spectrum approach represent a rational and effective tool for practical applications. However, the limitations of their applicability should be observed.

REFERENCES

CEN (2003). *Eurocode 8 — Design of structures for earthquake resistance*, Part 1, European standard prEN 1998-1, Stage 49 Draft, October 2003, European Com. for Standardisation, Brussels.

Clough, R. W., J. Penzien (1975). *Dynamics of structures*, 1th edition, McGraw-Hill.

Cornell, C. A., F. Jalayar, R. O. Hamburger, D. A. Foutch. (2002). Probabilistic basis for 2000 SAC Federal Emergency Management Agency Steel Moment Frame Guidelines. *ASCE Journal of Structural Engineering*; 128(4): 526-533.

Dolšek, M., P. Fajfar. (2004a). Inelastic spectra for infilled reinforced concrete frame structures. Submitted to *Earthquake Eng.Struct.Dyn*.

Dolšek, M., P. Fajfar. (2004b). Simplified nonlinear seismic analysis of reinforced concrete infilled frames. Submitted to *Earthquake Eng.Struct.Dyn*.

Dolšek, M., P. Fajfar. (2004c). IN2 — A simple alternative for IDA. *Proc. 13th World Conf. Earthquake Engineering,* Paper No. 3353, Vancouver, Canada.

Fajfar, P. (2000). A nonlinear analysis method for performance-based seismic design. *Earthquake Spectra* 16(3): 573-592.

Fajfar, P. (2002). Structural analysis in earthquake engineering — a breakthrough of simplified non-linear methods. *Proc. 12th European Conf. Earthquake Eng*., London, Keynote lecture, Paper No. 843.

Fajfar, P., P. Gašperšič. (1996). The N2 method for the seismic damage analysis of RC buildings. *Earthquake Eng. Struct. Dyn*. 25: 31-46.

Fajfar P., V. Kilar, D. Marušić, I. Peruš, G. Magliulo. (2002). The extension of the N2 method to asymmetric buildings. *Proc. 4th Forum on Implications of recent earthquakes on seismic risk,* Technical report TIT/EERG 02/1. Tokyo Institute of Technology: 291-308.

Fajfar, P., D. Marušić, I. Peruš. (2004). Influence of ground motion intensity on the inelastic torsional response of asymmetric buildings. *Proc. 13th World Conf. Earthquake Engineering,* Paper No. 3496, Vancouver, Canada.

Freeman, S.A. (1998). Development and use of capacity spectrum method. *Proc. 6th U.S. National Conf. Earthquake Eng*., Seattle.

Vamvatsikos, D., C. A. Cornell. (2002). Incremental Dynamic Analysis*. Earthquake Eng.Struct.Dyn*. 31:491-514.

HORIZONTALLY IRREGULAR STRUCTURES: SOME RECENT DEVELOPMENTS

A. RUTENBERG[1] and W. K. TSO[2]

ABSTRACT

Recent developments in analysis and design techniques for 1-storey and multistorey asymmetric structures, including pushover procedures, are reviewed. The relative paucity of experimental studies characterizing research in the field until recently, and the present welcome activity, are noted. Difficulties in estimating shear demand by either linear models or 1-storey nonlinear ones are illustrated by a case study on a torsionally flexible 10-storey 4-wall system. The need for iteration in applying the static torsional code provisions — resulting from the interdependence of stiffness and strength — motivated the development of alternative design procedures leading to more uniform plan-wise displacement distribution. This approach is presented in some detail.

Keywords: Asymmetric structures; Review; Wall-shear; 1-storey models.

1. INTRODUCTION

Almost fifty years have passed since Rosenblueth (1957) and Housner and Outinen (1958) alerted structural engineers to the problem of possible damage caused by the rotational response of asymmetric structures during earthquakes. Since then, most seismic codes have incorporated some form of guidelines for the horizontal allocation of strength among elements commonly referred to as torsional provisions. With the coming of the computer, an enormous amount of research effort has been devoted to improve the provisions. Developments up to 2001 can be found in several publications (e.g., Rutenberg 1992,Rutenberg and De Stefano 1997**,** Rutenberg 2002). It is only fair to ask whether the current codified provisions are more effective to mitigate torsional damages since those days, and has our predictive ability improved considering also the availability of very powerful computers? The authors have been working in this area over a number of years. This paper is an attempt to answer these questions. In the first part of the paper a short review of the more recent developments is presented. It is followed by some contributions from the authors, and the paper ends

---

[1] *Technion-Israel Institute of Technology, Haifa, Israel; E-mail: avrut@tx.technion.ac.il*

[2] *McMaster University, Hamilton, Ont. Canada; E-mail: tsowk@univmail.cis.mcmaster.ca*

with some thoughts on the challenges still facing engineers when dealing with horizontally irregular structures in seismic zones.

2. RECENT DEVELOPMENTS

With the availability of more powerful computers, an increasing interest in the post-yield behaviour of asymmetric buildings was taking place. While the computation to obtain the seismic responses is relatively straight forward, the ability to translate the observations to design procedures is more problematic. Even in single-storey models (Fig.1), the number of parameters is very larger. In addition to the usual ones such as damping ratio, peak displacement or drift, type of hysteresis model, target ductility demand, there are the strength distribution among the resisting elements.
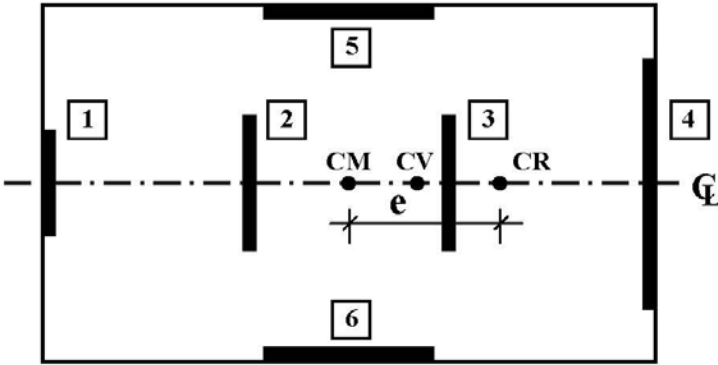
Figure 1. Typical 1-storey model studied by investigators.

While disagreement among researchers due to different definitions of parameters were noted already in the linear range (e.g., the 3 possible and legitimate definitions of the torsional-to-lateral frequency ratio), conflicting conclusions from parametric studies on nonlinear structures have been much more common. Hence it is not surprising that, considering also the complexity of the problem, practitioners were not quick to adopt the emerging recommendations. In the mid 1990s De la Llera and Chopra (1995) brought some order into model characterization by suggesting the use of the base-shear base-torque interaction diagram for this purpose.

One-storey models have been used to study the effect of bidirectional seismic input on asymmetric systems, usually monosymmetric ones. The picture emerging from the studies on the subject is that bidirectional excitation has some effect on the response, but it does not appear substantial (for summary see Rutenberg 2002). It appears that with the advent of efficient, reliable and user-friendly 3-D linear and nonlinear programs the need to extrapolate from unidirectional to bidirectional response will lose its practical importance.

Dutta and Das (2002, 2002b and refs. therein) also used one-storey models to study the effect of *strength deterioration* on the bidirectional response of code-designed asymmetric structures. They concluded that the displacement and ductility demands on the flexible edge as well as on the rigid edge were much larger than those of their symmetric counterparts and of similar models but without strength deterioration. They also observed that the unidirectional input might grossly underestimate the response. These issues deserve further study.

Stathopoulos and Anagnostopoulos (2003) examined critically the use of 1-storey models as proxies for multistorey asymmetric frame structures. These are due to the assumption that plastic hinges form in columns, rather than in beams. For example they found that the simple 1-mass shear-spring (or shear-beam) models commonly used by researchers to assess seismic provisions may not be appropriate, since such models over-predict the flexible edge displacements, as noted earlier by Ghersi et al. (1999).

The easier accessibility of nonlinear 3-D computer programs in the 1990s freed researchers from the need to extrapolate from the 1-storey models. Yet, single mass torsional behaviour continues to attract many researchers, mainly because it is able to provide *qualitative* information on the global behaviour at low computational effort, and even to reveal hitherto unknown phenomena. Indeed, the second part of this paper presents a design procedure based on single mass response.

Most of the interest focused on multistorey frame structures, while several studies on wall-frames were also reported, and will be referred to subsequently. Studies by Duan and Chandler (1993) on multistorey structures modelled as shear beams showed that there could be problems with uncritical extrapolation of 1-storey results. Nassar and Krawinkler (1991) observed that such modelling is likely to be conservative because realistic cases, in which plastic hinges form at beam-ends, usually show smaller ductility demands. Moghadam and Tso (1996) observed that shear beam modelling does not lead to reliable estimates of important design parameters. They also concluded that the seismic provisions could not adequately protect torsionally flexible buildings.

De Stefano et al. (2002) studied the response of a code-designed unidirectionally excited 6-storey frame building. They attributed the excessive ductility demands in unexpected locations to overstrength, and concluded that code-designs, which are calibrated to 1-storey models, may not achieve their goal of bringing the ductility demands in asymmetric structures in line with their symmetric counterparts. This matter should be further explored.

Reports on multistorey asymmetric structures under bi-directional excitation also began to emerge in the late 1990s, along with studies on unidirectionally excited structures. Fajfar and coworkers (e.g., Marusic and Fajfar 1999) compared the response of mass eccentric *perimeter* frame 5-storey models with their torsionally flexible counterparts, i.e., those with lateral load resisting internal frames. They demonstrated that, as in 1-storey frames, increasing the ground motion intensity lowers twist amplification of the torsionally flexible structures. They also suggested

that the SRSS combination of the two separate orthogonal inputs is a conservative estimate of the response. More recently Rutenberg et al. (2002) demonstrated the high torsional stiffness and strength of perimeter frame structures on the SAC 9-storey buildings modelled as mass eccentric structures and excited bidirectionally. They also concluded that corner columns could be quite vulnerable, as noted earlier by, e.g., Cruz and Cominetti (2000). The recent study of Stathopoulos and Anagnostopoulos (2002) on 3 and 5 storey frame structures designed per EC8 concluded that even more caution should be exercised when extrapolating from one-storey models. For example, they found that whereas in some cases code-designs lead to large ductility demands on the stiff side elements, the opposite results were obtained for the corresponding multistorey structure. They also concluded that the amplification of eccentricity as required by SEAOC/UBC has relatively small effect on the response, and hence does not appear to justify the additional computational effort involved. Finally, they found, as also some other researchers did, that code-design did not adequately protect the flexible edge elements. Very recently De la Colina (2003) presented a parameter study on code-designed 5-storey eccentric stiffness shear buildings excited by the two components of the 1940 El Centro record. The results confirm those obtained from 1-storey models, namely that a design eccentricity of 1.5e for elements located on the flexible side of the floor deck and of 0.5e for the rigid side elements recommended by several seismic codes lead to ductility demands lower or equal to those obtained for similar elements in similar but torsionally balanced systems. He also concluded that an eccentricity not lesser than 0.2e for storeys with very small or zero eccentricity should be stipulated in order to avoid excessive ductility demand, again in line with some codes.

The application of pushover analysis to asymmetric structures has become popular since the mid 1990s. However, assigning a shape to the loading vector is a much more difficult problem than for the corresponding 2-D problem, (while the choice of the target displacement is probably not). Several approaches have been proposed. The simplest one is to apply the code loading shape along the mass axis of the building, or at a prescribed offset (the design eccentricity) until the target displacement is reached. Indeed many earlier studies took this approach (see Rutenberg 2002). More recent studies by Fajfar and coworkers (e.g., Fajfar et al. 2002) extended the N2 method to bidirectionally excited multistorey structures by evaluating the performance point separately for each direction and then combining the results by means of the SRSS formula. Again, they concluded that for torsionally stiff structures the approach leads to acceptable results. Ayala and Tavera (2002) propose a pushover procedure in which the shapes of the lateral loads in the two orthogonal directions and of the torques about CM are obtained from 3-D modal analysis using accepted modal combination rules. The resulting 2 base shear and the base torque versus roof displacement/rotation curves are converted into the 1st mode behaviour curves and further transformed into the 1-DOF behaviour curve. Good prediction of the response is shown for the example 8-storey frame building. Chopra and Goel (2003) extended their modal pushover analysis procedure to asymmetric structures.

They tested the procedure on three asymmetric variants of the Los Angeles 9-storey SAC building. The results show similar accuracy as for symmetric buildings. Some problems were noted when strong modal coupling occurs.

Pushover analysis was also applied to asymmetric wall-frame structures with some success by De Stefano and Rutenberg (1998) and Moghadam and Tso (2000). This, however, remains an area in need of further study, since the response is very sensitive to the relative stiffnesses of the walls and frames, and hence extrapolations from either walls or frames are problematic.

Experimental work on the nonlinear response of asymmetric structures, which is needed to provide support for the standard analytical tools, was quite limited in the past. More recently several shaking-table test results have been published by Fardis et al. (1998) and De Stefano et al. (2002), already briefly summarized (Rutenberg 2002). Mola et al. (2004) concluded that codified approaches for assessing the response of horizontally irregular structures, including pushover analyses, "failed to give correct and safe-side estimation of the important features of structural response", including the failure mechanism of the structure. Hence, their findings (also Negro et al. 2004)**,** together with the criticism launched against 1-storey approximations, should be examined very carefully since they all cast very serious doubts about the viability of standard time-honoured procedures.

Passive control is continuing to attract researchers. Several studies have been published during the last two years. Tena-Colunga and Gomez-Soberon (2002) studied the response mass eccentric structure with symmetric base-isolation. Lin and Chopra (2003a, 2003b) presented a design procedure for 1-storey asymmetric structures with nonlinear viscous or viscoelastic dampers. De La Llera and Almazan (2003a, 2003b) studied, the former experimentally, the response of multistorey eccentric structures provided with friction pendulum dampers. Yoshida et al. (2003) presented an experimental verification for design using magnetorheological dampers. Space limitations preclude description of these interesting studies.

3. RECENT STUDIES BY AUTHORS

The nonlinear response of asymmetric multistorey buildings laterally supported by flexural walls has not attracted much research interest because it has been accepted by many that design based on linear analysis would give adequate protection. Results of a recent study on symmetric structural systems comprising walls of different lengths (e.g., Rutenberg et al. 2004) and work in progress on torsionally flexible wall systems show that predicting the peak base shear on the walls can be problematic. This should be of interest since the standard capacity spectrum approach cannot capture this behaviour. Summary of preliminary results is given in section 3.1.

In most studies on asymmetric structures it is assumes that the eccentricity is given, and procedures have been developed to design the structures so that the response would not be larger than that of the corresponding symmetric structure. This was a convenient approach because it assumed that element yield displacements vary with

their assigned strength, without affecting the initially assumed stiffness, a quite unrealistic assumption not only for steel structures but also for reinforced concrete ones. Since in fact stiffness varies with assigned strength the design becomes iterative. However, this interrelation makes it possible to reduce eccentricity by judiciously assigning the reinforcement ratios. Procedures aiming at finding the strength distribution among the lateral force resisting elements that would minimize twist are described in section 3.2.

3.1 Shear Demand on Torsionally Flexible 10-Storey Wall Structure: A Case Study

The studied torsionally flexible mono-symmetric 4-wall 10-storey system is shown schematically in Fig.2. The wall properties are given in Table 1. The stiffness eccentricity = 25.6% of width. Storey weight = 3000kN. This structure was excited by 10 of the 20 SAC 10/50 Los Angeles records with 5% Rayleigh damping in the 1st and 4th modes. Cyclic pushover analyses with inverted triangular loading and with a point load located so as to account for base shear amplification due to higher vibration modes were also carried out. Finally, 1-storey 2-DOF models having the same mass and 1st two natural periods as the full structure were also excited by the same ensemble of records.
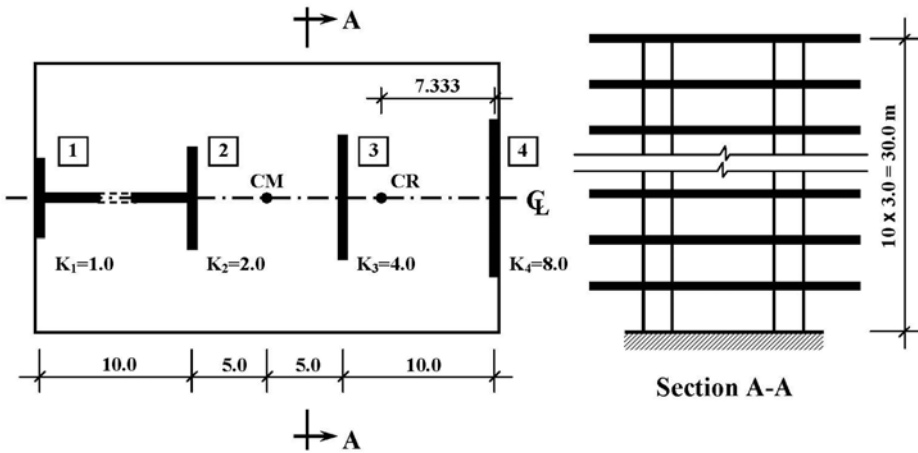

Figure 2. Monosymmetric 10-storey 4-wall model.

Table 1. Properties of the 4 Walls

Wall	EI	I / ΣI	M_y (kN)	$M_y/\Sigma M_y$
1	3.45×10^7	0.0667	15752	0.1097
2	6.90×10^7	0.1333	25008	0.1742
3	13.8×10^7	0.2667	39822	0.2773
4	27.6×10^7	0.5333	63008	0.4388
Σ	51.75×10^7	1.0000	143590	1.0000

The shear demands at the wall bases obtained from the several alternative analyses (mean values for the 10 records), including pushover, are listed in Table 2. Comparing the Ten Storey BH and MH columns it is evident that forcing the hinge to develop solely at base (BH) results in higher shear demands than when hinges are allowed to develop at higher levels (MH). Linear analysis — after division by the strength reduction factor R (≈ 4.2) — underestimates the shear forces on the walls. Cyclic pushover (PO) with inverted triangular loading, including the effects of the UBC modified accidental eccentricity, leads to rather poor approximation since it ignores the effects of higher vibration modes. Pushover analysis, in which the lateral force resultant is located so as to account for higher modes and R (Rutenberg et al. 2004) in an isolated wall — again using the peak values resulting from the factored accidental eccentricity — does improve the wall results appreciably.

Single storey nonlinear results are far off the mark, whereas their linear counterparts are similar to the M-DOF ones. As noted, base shear demand is strongly affected by the higher vibration modes, and is increasing with R, hence 1-storey results cannot predict it. One might be tempted to use the undivided (by R) linear results as a first approximation, but the similarity appears fortuitous.

From the above it appears that the point load Cyclic PO approach deserves further consideration.

Table 2. Comparison of wall shear forces at base (kN)

Wall	Ten Storey BH	Ten Storey MH	Ten Storey Lin/R	Cyclic PO Triang.	Cyclic PO Point	One Storey Nonlin.	One Storey Lin/R
1	4071	3138	947	2212	3339	993	965
2	5836	5654	1224	2982	4923	1578	1266
3	12676	9462	1540	7203	9736	2533	1500
4	9356	6483	1953	3875	7410	3968	2459
BS	10927	10743	4397	3385	19050	9013	4878

3.2 Strength Allocation for Systems with Strength Dependent Stiffness Elements

Most analytical studies in past and current codified torsional provisions are based on the assumption that the stiffness of lateral force resisting elements (LFRE) can be estimated with some degree of accuracy prior to strength allocation, and will not be affected by the subsequent strength allocation process. Using elastic-plastic modelling, the force-displacement relationship of two elements of similar size designed to have different strengths is assumed to take the form as shown in Fig. 3a. Recent studies (Paulay 1997, 2001; Priestley 1998; Priestley and Kowalsky 1998; and Aschheim 2002) have shown that for most ductile LFRE, the stiffness and strength are related. A more realistic representation of the force-displacement relationship for two elements of similar dimensions but different strengths would appear as shown in Fig. 3b.

(a) Strength-Stiffness
Independent Elements

(b) Strength-Stiffness
Dependent Elements
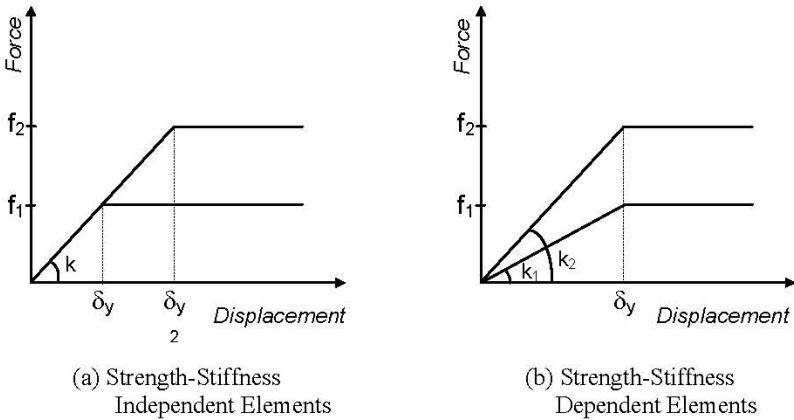
Figure 3: Force-displacement relationships.

An increase of strength will lead to an increase of stiffness, while the yield displacement stays essentially the same. This interdependence between strength and stiffness of LFRE gives rise to a number of issues in the seismic design process. First, the process of strength allocation to LFRE would change both the strength and stiffness distributions of a structure. What would be a desirable strength/stiffness distribution combination to reduce torsional response? Second, contrary to most code procedures, the final stiffness distribution cannot be considered known prior to strength assignment. What strength allocation procedure is available to achieve the desirable strength/stiffness distribution combination target? Finally, how effective are the current torsional provisions for structural systems with LFRE having strength dependent stiffness?

The following is a summary of two studies carried out recently to address these questions in the context of single storey asymmetric structures (Tso and Myslimaj 2003 and Myslimaj and Tso 2004). The studies start with the premise that the yield displacements of LFRE along different column lines can be determined, and hence the yield displacement distribution is known. The asymmetry of such distribution is characterized by the yield displacement centroidal location in relation to center of mass CM, or equivalently, the yield displacement eccentricity (YDE). Using the force-displacement relation as shown in Fig.3b, the stiffness of each individual element is determined once its strength is specified. In terms of distributions, it is shown that the distance D between the center of strength (plastic centroid) CV and the center of rigidity CR is approximately equal to YDE. For design purpose, one can consider the distance D equal to YDE. Another important observation is that the distance D is insensitive to the details of the strength distribution. Therefore, different strength allocation strategies result in pair-wise shift of CV and CR in relation to CM.

The studies showed that in order to reduce torsional responses, a preferred strength allocation strategy is to have both small strength and stiffness eccentricities. This will minimize the occurrence of large torques on the floor deck and reduce its rotation. Such consideration will lead to CR located on one side and CV located on the opposite side of CM, a condition labeled as a "balanced CV-CR location" criterion to reduce torsional response. One can arrive at this balanced CV-CR condition strategy using the following heuristic argument. Subjected to a major pulse from the ground, the elements experience one of the following states. First, they are in the elastic state. Then some elements yield while other remains in the elastic state. Then all of them yield and enter the plastic state. This is followed by the unloading of some elements while other elements remain yielded. Finally, unloading of all elements occurs and all elements are in the "elastic state" again. When all elements are in the elastic state, the resultant of the element resisting forces passes through CR. When all elements are in the plastic state, the resultant of resisting forces passes through CV. To reduce torsional response, one should therefore arrange the strength and stiffness distributions with as small stiffness and strength eccentricities as possible. If both CV and CR were on the same side of CM, the system would have either stiffness or strength eccentricity larger than the YDE, since the distance between CV and CR is equal to the YDE. However, if one adjusts the strength distribution such that CR is, say, on the left and CV on the right of CM, the system would have strength and stiffness eccentricity values lesser than YDE. There is another advantage to arrange CV and CR on opposite sides of CM. With CR located on the left of CM, an anti-clockwise torque will be generated when the elements are in the elastic state. With CV located on the right of CM, a clockwise torque will be generated when the elements are in the yield state. The deck rotations generated by these anti-clockwise and clockwise torques would tend to cancel out, ending in a system with small deck rotation when a system has a balanced CV-CR location.

Two strength allocation procedures are presented to achieve the desired balanced CV-CR location criterion. Both procedures involve steps to create a strength

distribution with a pre-determined CV location. The first procedure has the strength distribution taking the shape of the yield displacement distribution with an adjustment. The adjustment is to allow modification of the CV location desired by the user. It is referred to as a yield displacement distribution based (YDDB) procedure (Tso and Myslimaj, 2003). The second procedure involves the use of static equilibrium analyses to generate the desired strength distribution and is referred to as the static equilibrium analysis based (SEAB) procedure (Myslimaj and Tso, 2005). These procedures lead to different strength distributions in general. Studies showed that the torsional response is sensitive to the CV location, but insensitive to the details of the strength distribution. Therefore, so long as the strength distribution satisfies the balanced CV-CR location criterion, both procedures will give a strength distribution that will lead to small torsional response, as will be demonstrated in the next section.
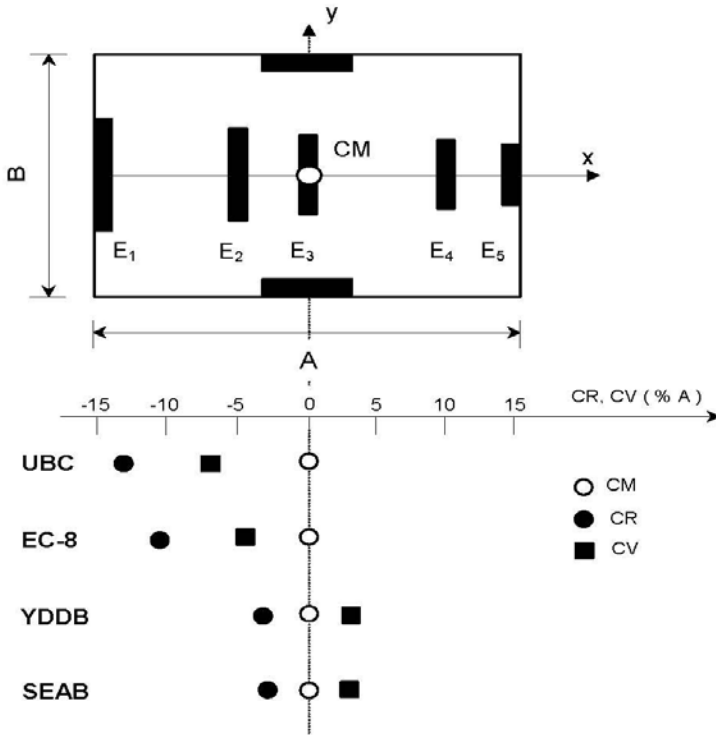

Figure 4. Generic structural model and CV, CR locations of four example structures.

To study the effectiveness of the current torsional provisions, the response of four single storey structures derived from a generic structural model subjected to bi-directional base excitation is compared. The generic model consists of a single

rectangular concrete deck supported by five reinforced concrete flexural wall elements in one direction, and two equal wall elements at the edges in the orthogonal direction, as shown in Fig.4.

The torsional provisions of UBC (Uniform Building Code 1997) and EC-8 (Eurocode 8 2002) are taken as representative of the typical codified torsional provisions. As these two codes stipulate, the design strength for each LFRE is evaluated based on the traditional definition of element stiffness. The effect of cracking is taken into account by using the cracked moment of inertia. However, since the same factor is used to reduce the gross inertia to the cracked moment of inertia, the relative stiffness of the walls remains proportional to the cube of the wall lengths. After the determination of the strength of the individual walls, the actual stiffness used in the dynamic model is determined by dividing the strength by the respective yield displacement. For comparison purpose, two additional structures are created: one with strength allocation following the yield displacement distribution-based procedure (YDDB), and the other following the pseudo-static equilibrium analysis-based procedure (SEAB). For both structures, the strength distribution is adjusted such that they satisfy the balanced CV-CR location criteria, with the strength eccentricity approximately equal to the stiffness eccentricity. The total strength of these two structures is adjusted to that of the UBC structure. The locations of the CV and CR for these four structures are also shown in Fig. 4.
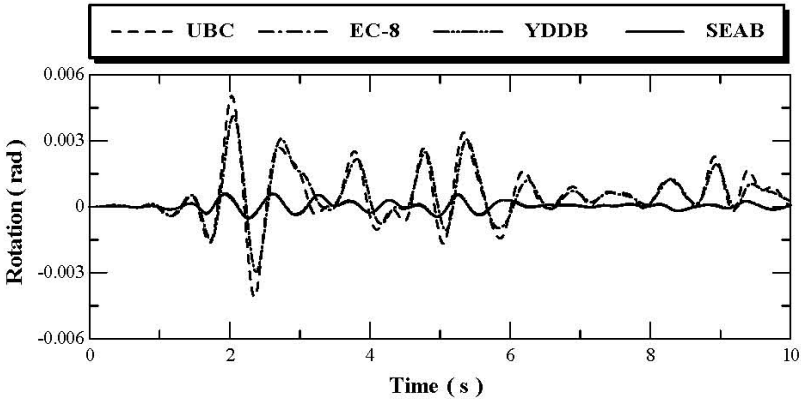
Figure 5. Deck rotation response.

All four structures are subjected to the same bi-directional base excitation consisting of two horizontal components of the 1940 El Centro earthquake ground motions. The deck rotation is used as a direct measure to represent the severity of torsion because a structure with small rotation would be less susceptible to torsional damage. The first ten seconds of rotation time histories for the four models are shown in Fig. 5. Both the UBC and EC8 structures show significant rotation of the deck. The

large rotational response can be explained by noting that both the CR and CV are located on the same left hand side of CM. On the other hand, the two models with strength distributions that satisfied the balanced CV-CR location criteria show similar low rotational response.

4. CONCLUSIONS

Despite of all the codified torsional provisions available, damage caused by excessive rotations has been observed in all recent major earthquakes. One reason may be that some of the damaged buildings were built prior to the adoption of the provisions. It is also possible that some of the damaged buildings were built without attention being paid to the codified provisions. A third possible reason may be that the current provisions are not as effective as we think. Many parametric studies have been carried out for the last two decades to validate the provisions. Most of them were based on models having lateral force resisting elements with independent strength and stiffness properties. However, recent studies suggest that code procedures may not be effective when the interdependence of strength and stiffness in the resisting elements is considered. This issue deserves further investigation.

Extending ideas developed on single storey models to multistorey structures can be problematic. Properties such as strength and stiffness are no longer scalar quantities. It may no longer be possible to use a single value for the plastic centroid or the rigidity center in the most general case of horizontally irregular multistorey structures. There is hope, however, that those concepts can be applied to special classes of multi-storey structure that are vertically regular. To classify multi-storey structures and to extend lessons learned from single mass model studies to special classes of multi-storey structures remains a challenge. At present, simple shortcuts do not appear to be available for predicting the response, particularly the shear demand, of horizontally irregular multistory structures where higher modal contributions become significant.

In this age of performance-based seismic design, it is only fair to ask the following questions. Are we wiser now than in the days when Rosenblueth and Housner warned the profession about the dangers of asymmetry? Do we now have better design guidelines to mitigate torsional damage due to horizontal irregularity? The answer to the first question is a tentative "may be". Regarding the answer to the second question, we believe that the jury is still out.

ACKNOWLEDGEMENT

REFERENCES

Almazan, J. L., and J. C. De La Llera. (2003b). "Accidental torsion due to overturning in normally symmetric structures isolated with FPS". *Earthquake Engineering & Structural Dynamics*, **32**, 919-948.

Aschheim, M.(2002). "Seismic design based on the yield displacement". *Earthquake Spectra*, **18**, 581-600.

Ayala, A. G., and E. A. Tavera. (2002). "A new approach for the evaluation of the seismic performance of asymmetric buildings". 7th US National Conference on Earthquake Engineering, CD ROM Proceedings, Boston.

Chopra, A. K., and R. K. Goel. (2003). A modal pushover analysis procedure to estimate Seismic demand for unsymmetric-plan buildings: Theory and preliminary evaluation". Report UBC/EERC 2003-08, Earthquake Engineering Research Center, University of California, Berkeley.

De la Colina, J. (2003). "Assessment of Design recommendations for torsionally unbalanced multistory buildings". *Earthquake Spectra*, **19**, 47-66.

De la Llera, J. C., and A. K. Chopra. (1995). "Understanding the inelastic seismic behaviour of asymmetric-plan buildings". *Earthquake Engineering & Structural Dynamics*, **24**, 549-572.

De la Llera, J. C., and J. L. Almazan. (2003a). "An experimental study of nominally symmetric and asymmetric structures isolated with FPS". *Earthquake Engineering & Structural Dynamics*, **32**, 891-918.

Cruz, E. F., and S. Cominetti. (2000). "Three-dimensional buildings subjected to bi-directional earthquakes: validity of analysis considering unidirectional earthquakes". 12th World Conference on Earthquake Engineering, CD ROM Proceedings, Upper Hutt.

De Stefano, M., E. M. Marino, and P. P. Rossi. (2002). "The key role of overstrength in the seismic behaviour of multistorey regularly asymmetric buildings". 3rd European Workshop on the Seismic Behaviour of Irregular and Complex Structures, CD ROM Proceedings, Florence.

De Stefano, M., and A. Rutenberg. (1998). "Predicting the dynamic response of asymmetric multistory wall-frame structures by pushover analysis: two case studies". 11th European Conference on Earthquake Engineering, CD ROM Proceedings, Paris.

Duan, X. N., and A. M. Chandler. (1993). "Inelastic seismic response of code-designed multistorey frame buildings with regular asymmetry". *Earthquake Engineering & Structural Dynamics*, **22**, 431-445.

Dutta, S. C., and P. K. Das. (2002). "Inelastic seismic response of code-designed reinforced concrete asymmetric buildings with strength degradation". *Engineering Structures*, **24**, 1295-1314.

Dutta, S. C., and P. K. Das. (2002). "Validity and applicability of two simple hysteretic models to assess progressive seismic damage in R/C asymmetric buildings". *Journal of Sound and Vibration*, **257**, 753-777.

Fajfar, P., G. Magliulo, D. Marusic, and I. Perus. (2002). "Simplified non-linear analysis of asymmetric buildings". 3rd European Workshop on the Seismic Behaviour of Irregular and Complex Structures, CD ROM Proceedings, Florence.

Fardis, M. N., S. N. Boussias, T. B. andPanagiotakos. (1998). "Seismic Response and Design of irregularly infilled R/C structures". 11th European conference on earthquake engineering, CD ROM Proceedings, Paris.

Ghersi, A., E. Marino, P. P. Rossi. (1999). "From one-story to multistory asymmetric systems: Conceptual differences and problems". EAEE Task Group 8: Asymmetric and Irregular Structures. "Irregular Structures", Proceedings of the 2nd Workshop, Vol. 1, Istanbul Technical University.

Housner, G. W., and H. Outinen. (1958). "The effect of torsional oscillations on earthquake stresses" *Bull. Seismological Society of America*, **48**, 221-229.

Lin, W. H., and A. K.Chopra. (2003a). "Asymmetric one-storey elastic systems with non-linear viscous and viscoelastic dampers: Earthquake response". *Earthquake Engineering & Structural Dynamics*, **32**, 555-577.

Lin, W. H., and A. K. Chopra. (2003b). "Asymmetric one-storey elastic systems with non-linear viscous and viscoelastic dampers: Simplified analysis and supplemental damping design". *Earthquake Engineering & Structural Dynamics*, **32**, 579-596.

Marusic, D., and P. Fajfar. (1999). "Nonlinear seismic response of asymmetric steel buildings". EAEE Task Group 8: Asymmetric and Irregular Structures. "Irregular Structures", Proceedings of the 2nd Workshop, Vol. 1, Istanbul Technical University.

Moghadam, A. S., and W. K. Tso. (1996). "Damage assessment of eccentric multistorey buildings using 3-D pushover analysis". 11th World Conference on Earthquake Engineering, CD ROM Proceedings, Acapulco.

Moghadam, A. S., and W. K. Tso. (2000). "Pushover analysis for asymmetric and set-back multi-story buildings". 12th World Conference on Earthquake Engineering, CD ROM Proceedings, Upper Hutt.

Mola, E., P. Negro, and A. V. Pinto. (2004). "Evaluation of current approaches for the analysis and design of multi-storey torsionally unbalanced frames". 13th World Conference on Earthquake Engineering, Vancouver (to be published).

Myslimaj, B., and W. K. Tso. (2005). "A design-oriented approach to strength distribution in structural systems with elements having strength dependent stiffness". *Earthquake Spectra*, (accepted for publication).

Nassar, A. A., and H. Krawinkler. (1991). "Seismic demands for SDOF and MDOF systems". Report 95, John A. Blume Earthquake Engineering Center, Stanford University.

Negro, P., E. Mola, F. J. Molina, G. Magonette, (2004) "Full-Scale Pseudodynamic testing of a torsionally unbalanced three-storey non-seismic RC frame", 13th World Conference on Earthquake Engineering, Vancouver (to be published).

Paulay, T. (1997). "Seismic torsional effects on ductile structural wall systems". *Journal of Earthquake Engineering*, **1**, 721-745.

Paulay, T. (2001). "A re-definition of the stiffness of reinforced concrete elements and its implications in seismic design". *Structural Engineering International*, **1**, 36-41.

Priestley, M. J. N. (1998). "Brief comments on elastic flexibility of reinforced concrete frames and significance to seismic design". *Bulletin of New Zealand Society for Earthquake Engineering*, **31**, 246-259.

Priestley, M. J. N., and M. J. Kowalsky. (1998). "Aspects of drift and ductility capacity of rectangular cantilever structural walls". *Bulletin of New Zealand Society for Earthquake Engineering,* **31**, 73-85.

Rosenblueth, E. (1957). "Considerations on torsion, overturning and drift limitations". Proc. SEAOC Conference 36-38, Coronado.

Rutenberg, A. (1992). "Nonlinear response of asymmetric building structures and seismic codes: a state of the art review". *European Earthquake Engineering,* **2**, 3-19.

Rutenberg, A. (2002). "EAEE Task Group 8: Behaviour of Irregular and Complex Structures: Progress since 1998", 12th European Conference on Earthquake Engineering, CD ROM Proceedings, London.

Rutenberg, A., and M. De Stefano. (1997). "On the seismic performance of yielding asymmetric multistorey buildings: a review and a case study". Seismic Design Methodologies for Next Generation Codes, Proceedings of International Workshop, Bled.

Rutenberg, A., R. Levy, and G. Magliulo. (2002). "Seismic response of asymmetric perimeter frame steel buildings". 12th European Conference on Earthquake Engineering, CD ROM Proceedings, London.

Rutenberg, A., E. Nsieri, and R. Levy. (2004). "Seismic shear forces in cantilever wall systems". 13th World Conference on Earthquake Engineering, Vancouver (to be published).

Stathopoulos, K. G., and S. A. Anagnostopoulos. (2002). "Inelastic earthquake induced torsion in buildings: Results and conclusions from realistic models". 12th European Conference on Earthquake Engineering, CD ROM Proceedings, London.

Stathopoulos, K. G., and S. A. Anagnostopoulos. (2003). "Inelastic earthquake response of single-story asymmetric buildings: An assessment of simplified shear-beam models", *Earthquake Engineering & Structural Dynamics*, **32**, 1813-1831.

Tena-Colunga, A., and L. Gomez-Soberon. (2002). "Torsional Response of base-isolated structures due to asymmetries in the superstructure". *Engineering Structures,* **24**, 1587-1599.

Tso, W. K., and B. Myslimaj. (2003). "A yield displacement distribution-based approach for strength assignment among lateral force resisting elements having strength dependent stiffness". *Earthquake Engineering & Structural Dynamics,* **32,** 2319-2351.

Yoshida, O., S. J. Dyke, L. M. Giacosa, and Truman, K. Z. (2003). "Experimental verification of torsional response control of asymmetric buildings using MR dampers". *Earthquake Engineering & Structural Dynamics*, **32**, 2085-2105.

EFFECTIVE PERIODS OF HIGHLY NONLINEAR STRUCTURES

Hiroshi AKIYAMA[1]

ABSTRACT

The total energy input into a structure exerted by an earthquake is mainly governed by the total mass and the effective period of the structure. The effective periods of elastic structures are their fundamental natural periods. When the structure is plastified, the structure is softened and thus the effective period of structure is elongated by the plastification of structure. The influence of the plastification on the effective period is specified by the type of the restoring force characteristics of the plastified element, the extent of plastification and the pattern of distribution of plastification. In this paper, effective periods are dealt with generally by using various types of restoring force characteristics. Obtained formulae are verified their applicability by direct response analyses.

Keywords: Effective period; Total energy input; Nonlinearity; Plastification.

1. INTRODUCTION

Earthquake resistant design method based on the balance of energy between the total energy input exerted by an earthquake and the energy absorbed by a structure provides a simplest design formulation and most consistent understanding on behavior of a structure up to its collapse state. The most important point is that the total energy input due to an earthquake is a very stable amount governed only by the total mass of the structure and its fundamental natural period and is scarcely influenced by the other structural parameters such as mass distribution, stiffness distribution, and strength distribution. The seismic energy input is absorbed mainly in a form of cumulative plastic strain energy developed in the structural elements. The cumulative plastic strain energy can be called structural damage. Therefore, the seismic design of structures is recognized to be a technique to control the damage distribution in a structure within an allowable limit. The energy spectrum (the relationship between the total energy input and the fundamental natural period of structure) is influenced only by the extent of the nonlinearity of structure. The purely elastic system is characterized by the single natural period and receives the energy only from the single wave component which has the same frequency as that of the structure. On the other hand the nonlinear system is characterized by a set of

[1] *Nihon University, Tokyo, Japan*

instantaneous period of vibration and receives the energy from a set of wave components which correspond to a set of instantaneous period of structure. As a result, the energy spectrum is obtained from the energy spectrum of the purely elastic system through an averaging (smoothing) process. The period which represents a set of instantaneous period is termed to be the effective period. The effective period of the damped elastic system is equal to the natural period, since the instantaneous period spreads around the natural period. The effective period of the inelastic system becomes longer than the initial natural period, since the inelastic system is softened by the plastification. The energy spectrum for design use must reflect the influence of the nonlinearity. The nonlinearity which corresponds to the 10% of the fraction of the critical damping was found to represent the averaging effect met in the practical structures.

Thus, the energy spectrum of the elastic system with 10% of fraction of critical damping is referred to be the energy spectrum for design use. The effective period is influenced by the type of restoring force characteristic and the level of nonlinearity.

In this paper, the effective period is derived theoretically and the effectiveness of the effective period is verified by comparing the result of the direct response analyses and the energy spectra for design use (Akiyama, 1985).

2. ENERGY SPECTRUM

The energy input into a single degree of freedom system subjected to a horizontal ground motion is written as

$$E = -\int_0^{t_0} M\ddot{z}_0 dy \tag{1}$$

where E is the total energy input, M the total mass of the system, $\ddot{z}_0$ the horizontal ground acceleration, y the horizontal displacement of the mass relative to the ground and t_0 the duration time of the ground motion. The energy spectrum is defined by the following functions.

$$E_s(T_e) = \frac{E(T_e)}{M}, \tag{2}$$

$$E_s(T_e) = V_E(T_e) = \sqrt{\frac{2E(T_e)}{M}} \tag{3}$$

where E_s is the energy spectrum and T_e the effective period.

Eq. (2) is the direct expression of the total energy input per unit mass versus the effective period. Eq (3) is the equivalent velocity expression of the direct energy spectrum.

The energy spectrum of the purely elastic system is denoted by $_0E_s$. The energy spectra of the damped elastic system and the inelastic system can be described as follows, based on the energy spectrum of the purely elastic system.
For the damped elastic system,

$$E_s = \frac{\int_{T_0-\Delta T}^{T_0+\Delta T} {_0}E_S(T)dT}{2\Delta T} \tag{4}$$

For the inelastic system,

$$E_s = \frac{\int_{T_0}^{T_0+2\Delta T} {_0}E_S(T)dT}{2\Delta T} \tag{5}$$

In the damped elastic system, the instantaneous period of vibration spreads on the both sides of the natural period, T_0. In the nonlinear system, the instantaneous period spreads on the right hand side of T_0. Let us take up a portion of ${_0}E_s$ (T) which corresponds to $T_1 \leqq T \leqq T_2$. The portion of the energy spectrum, ${_0}E_s(T)$ can be approximated by the linear relationship which connects ${_0}E_s(T_1)$ and ${_0}E_s(T_2)$.

From Eqs. (4) and (5), E_s and T_e are obtained as follows.

$$E_s = \frac{{_0}E_s(T_1) + {_0}E_s(T_2)}{2} , \tag{6}$$

$$T_e = \frac{T_1 + T_2}{2} \tag{7}$$

Eq. (6) implies that the energy spectrum of the nonlinear system is obtained by averaging the energy spectrum of the purely elastic system.

The effective period, T_e is obtained from Eqs. (6) and (7) as follows,
For the damped elastic system,

$$T_e = T_0 \tag{8}$$

For the nonlinear system,

$$T_e = T_0 + T_m \tag{9}$$

where T_m is the longest instantaneous period.

3. EFFECTIVE PERIODS OF SINGLE-MASS SYSTEMS

As is shown by Eq.(9), the effective period of the nonlinear system is obtained by knowing the longest instantaneous period, T_m. T_m can be estimated based on the maximum displacement, δ_m, and the shear stress corresponding to δ_m. In most cases, the monotonic load-deformation curve under the horizontal loading becomes the envelope of the hysteretic load-deformation curve under arbitrarily changing lateral loads. Therefore, the secant modulus which corresponds to the maximum deformation response can be described as follows, referring to the monotonic load deformation curve as shown in Fig.1

$$k_s = \frac{Q_m}{\delta_m} = \frac{q}{1+\bar{\mu}} \cdot k_0 \tag{10}$$

where k_s is the secant modulus which corresponds to Q_m and δ_m, Q_m the shear force under the development of δ_m, $q = Q_m/Q_Y$, Q_Y the yield shear force, $\mu = \delta_m/\delta_Y$-1.0 the maximum plastic deformation ratio, δ_Y the elastic limit deformation, $\bar{\mu}$ the mean

value of the maximum plastic deformation ratios in the positive and negative directions and k_0 the initial elastic slope.
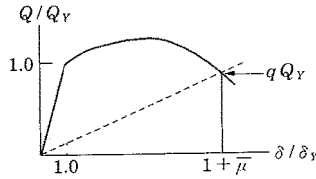

Figure 1. Monotonic load-deformation curve.

The natural period, T_0 in expressed as
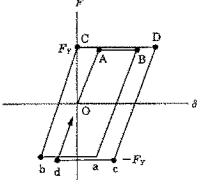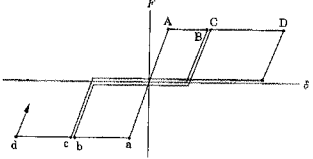
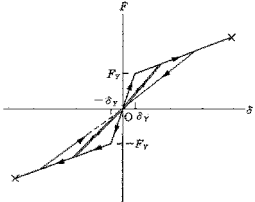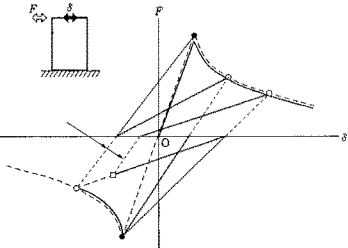$$T_0 = 2\pi \sqrt{\frac{M}{k_0}} \tag{11}$$
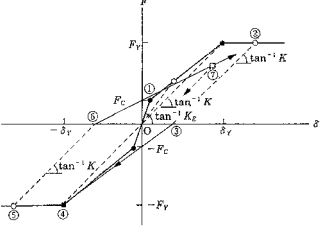
The longest instantaneous period was found to be expressed in terms of the period which is associated with the secant modulus as follows (Akiyama, 1999)

$$T_m = a_T T_s \tag{12}$$

where $T_s = 2\pi \sqrt{\dfrac{M}{k_s}} = T_0 \sqrt{\dfrac{1+\bar{\mu}}{q}}$ is the period associated with k_s, a_T the modification factor and k_s the secant modulus.

The modification factors depends on the restoring force characteristics and are demonstrated in Table 1 for the typical structural Types. The energy spectra of the Hachinohe record in the Tokachi-oki earthquake (1968) are shown in Fig.2. The energy spectra are depicted in the equivalent velocity expression shown by Eq.(3). Three structural types are selected. In Fig. 2(a), the abscissa indicates the natural period, T_0. In Fig.2 (b), the abscissa indicates the effective period, T_e. The solid line indicates the energy spectrum of the damped elastic system with 10% of fraction of the critical damping. The broken line indicates the envelope of the energy spectrum depicted by the solid line. As is indicated by broken line, the energy spectrum is divided into two range ; the shorter period range and longer period range. The individual plot indicates the total energy input which is obtained by the numerical analysis for the single-mass system under the specified condition of the restoring force characteristics and the maximum plastic deformation ratios. In shorter period range, the energy input increases as the T_e increases. As the plastification is deepened. $\bar{\mu}$ increases and T_e is elongated. Therefore, it is natural that the energy input increases as $\bar{\mu}$ increases under the same T_0 as shown in Fig. 2(a). On the other hand, as far as T_e is taken as the abscissa, the dependence of the energy input to $\bar{\mu}$ is dissolved and the energy spectrum of the damped elastic system can be referred to obtain the energy input into highly nonlinear systems (Akiyama, 1999).

Table 1. Values of a_T

restoring force characteristics		a_T
	elastic-perfectly plastic type	$\dfrac{1+\dfrac{\bar{\mu}}{8}}{\sqrt{1+\bar{\mu}}}$
	slip type	$\dfrac{1+\dfrac{2\bar{\mu}}{\pi}}{\sqrt{1+\bar{\mu}}}$
	origin orienting type	1.0
	degrading type (metal shell)	1.0
	degrading type (reinforced concrete)	1.0
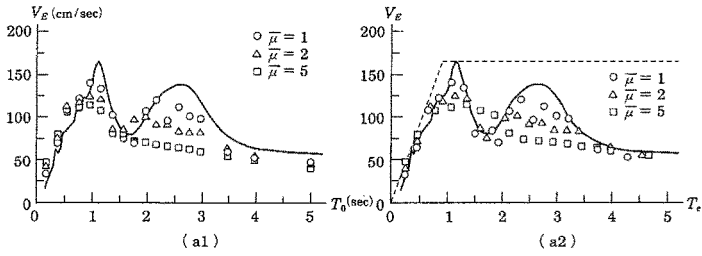
(a) elastic-perfectly plastic type
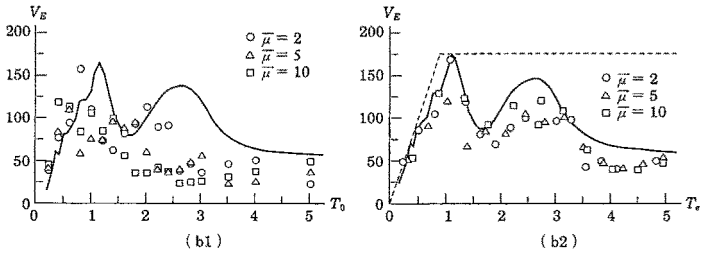
(b) origin pointing type
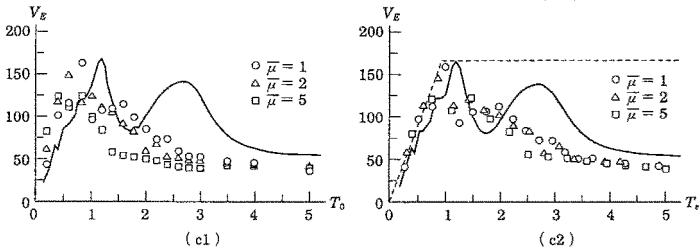
(c) degrading type
(metal shell buckling)

Figure 2. Effective period of one mass system.

4. EFFECTIVE PERIOD OF MULTI-MASS SYSTEMS

The fundamental natural period of the shear type multi-mass systems is formally expressed as follows.

$$T_0 = 2\pi \sqrt{\frac{M}{k_{eq}}} = 2\pi \sqrt{\frac{\kappa_1 M}{k_1}} \tag{13}$$

where M is the total mass of the system, k_{eq} the equivalent spring constant which gives the fundamental natural period the system, k_1 the spring constant of the first story, $\kappa_1 = k_1/k_{eq}$, k_1 is expressed as follows.

$$k_1 = \frac{Q_{Y1}}{\delta_{Y1}} = \frac{\alpha_1 Mg}{\delta_{Y1}} \tag{14}$$

where Q_{Y1} is the yield shear force of the first story, α_1: the yield shear force coefficient of the first story, δ_{Y1}: the elastic limit deformation of the first story, g: the acceleration of gravity. Then, T_0 is written as

$$T_0 = 2\pi \sqrt{\frac{\delta_{Y1} \kappa_1}{\alpha_1 g}} \tag{15}$$

The shear type frames taken in this paper are conditioned to be

$$\delta_Y = \text{const.}, \qquad m_i = \text{const.} \tag{16}$$

where δ_{Yi} is the yield deformation in ith story, m_i the mass of ith story, $(\ )_i$: the quantity in the ith story. In such a system, κ_1 is very closely approximated by

$$H_1 = 0.48 + 0.52N \tag{17}$$

When the type of restoring force characteristics and the maximum deformation ratio ratio, $\bar{\mu}_i$ are same in all stories, the secant modulus, k_{si} is proportional to the initial spring constant, k_i. Therefore, T_s is expressed as follows.

$$T_s = T_0 \sqrt{\frac{1 + \bar{\mu}_i}{q}} \tag{18}$$

Generalizing Eq. (18), T_s for the multi-mass system is obtained as

$$T_s = T_0 \sqrt{\frac{1 + \bar{\mu}}{q}} = 2\pi \sqrt{\frac{\delta_{Y1} \kappa_1 (1 + \bar{\mu})}{q \alpha_1 g}} \tag{19}$$

where $\bar{\mu} = \sum_i \bar{\mu}_i / N$ is the mean value of $\bar{\mu}_i$ and N the number of stories.

In the highly nonlinear system, the total energy input is mainly absorbed in a form of cumulative plastic strain energy, W_p. In multi-story frames, W_p is expressed as

$$W_p = \sum_{i=1}^{N} W_{Pi} \tag{20}$$

where W_{pi} is the cumulative plastic strain energy in ith story. The damage distribution index γ_1 is defined as follows

$$\gamma_1 = \frac{W_P}{W_{P1}} \tag{21}$$

W_{p1} is described as

$$W_{P1} = \frac{Mg^2 T^2}{4\pi^2} \bullet \frac{\alpha_1^2 \bar{\mu}_1 \gamma_1 a}{\kappa_1} \tag{22}$$

where a is the constant peculiar to the type of restoring force characteristics. γ_1 ranges

$$1 \le \gamma_1 \le \sum s_i \; , \; s_i = \left(\frac{\displaystyle\sum_{j=i}^{N} m_j}{M} \right)^2 \cdot \bar{\alpha}_1^2 \cdot \frac{k_1}{k_i} \tag{23}$$

where $\bar{\alpha}_i$ is the optimum yield shear force coefficient which produces the equal distribution of $\bar{\mu}_i$. The upper bound of γ_1 ($=\sum s_i$) is attained in the case where $\bar{\mu}_i$ is equal in all stories. By equating W_p in the case of the evenly distributed damage and that in the case of arbitrarily distributed damage, $\bar{\mu}$ can be related to $\bar{\mu}_i$. W_p is written in two ways.

$$\left. \begin{array}{l} {}_1W_P = \dfrac{Mg^2 T_0^2}{4\pi^2} \cdot \dfrac{\alpha_1^2 \, \bar{\mu} \displaystyle\sum_i s_i a}{\kappa_1} \\[4ex] {}_2W_P = \dfrac{Mg^2 T_0^2}{4\pi^2} \cdot \dfrac{\alpha_1^2 \, \bar{\mu}_1 \, \gamma_1 a}{\kappa_1} \end{array} \right\} \tag{24}$$

The balance of energy results in

$$\frac{\alpha_1^2 \, \bar{\mu}_1 \, \gamma_1 a}{\kappa_1} = \frac{\alpha_1^2 \, \bar{\mu} \displaystyle\sum_i s_i a}{\kappa_1} , \tag{25}$$

$$\bar{\mu} = \frac{r_1 \, \bar{\mu}_1}{\displaystyle\sum_i s_i} \tag{26}$$

5. ILLUSTRATIVE EXAMPLE OF EFFECTIVE PERIOD OF MULTI-MASS SYSTEMS

The general form of shear type multi-mass systems is identified to be the flexible-stiff mixed system as is indicated in Fig.3. The system consists of the flexible element which remains elastic and the stiff element which has a high elastic rigidity and behaves inelastically. The extent of combinations is measured by the participation ratio of the flexible element, f defined by

$$f = \frac{{}_f \bar{Q}_m}{{}_s Q_Y} \tag{27}$$

392

where $_f\bar{Q}_m = k_f \bar{\delta}_m$ is the average maximum stress in the flexible element, $_sQ_Y$ the yield strength of the stiff element, δ_m the average maximum deformation of the positive and negative directions and k_f the spring constant of flexible element.

(a) flexible element　　　**(b) stiff element**　　　**(c) mixed system**
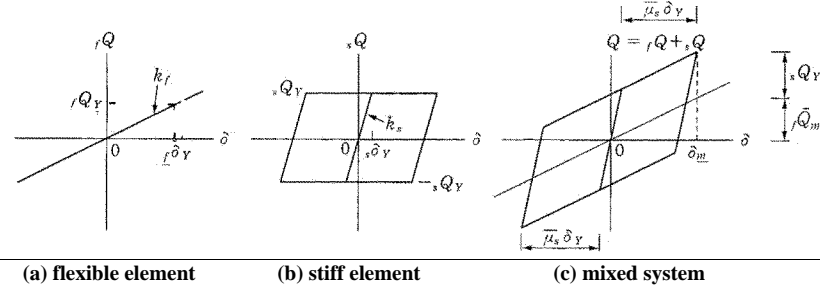
Figure 3. Flexible-stiff mixed system.

Ordinary shear type structures belong to the case of f=0. By adding the flexible element, the structural behavior is highly improved in suppressing the excessive development of the maximum deformation and the damage concentration into a certain story. The effectiveness of the system appears clearly in the following range of f

$$f \geq 0.7 \tag{28}$$

As illustrative examples, ten storied frames of the flexible-stiff mixed type are taken. The restoring force characteristics of the stiff element is of the elastic-perfectly plastic type. The stiffness of the flexible element is defined by the fictitious yield point as follows.

$$k_f = \frac{_fQ_Y}{_f\delta_Y} \tag{29}$$

where $_fQ_Y$=the fictitious yield shear force of the flexible element and $_f\delta_Y$=the fictitious yield deformation of the flexible element. The yield shear force coefficient is defined as follows.

$$\alpha_{fi} = \frac{_fQ_{Yi}}{g\sum_{j=i}^{N} m_j} , \alpha_{si} = \frac{_sQ_{Yi}}{g\sum_{j=i}^{N} m_j} \tag{30}$$

where α_{fi} is the fictitious yield shear coefficient of the flexible element and α_{si}=the yield shear force coefficient of the stiff element. The distribution of α_{fi} and α_{si} is specified to be

$$\frac{\alpha_{fi}}{\alpha_{f1}} = \frac{\alpha_{si}}{\alpha_{s1}} = \bar{\alpha}_i \tag{31}$$

$_f\delta_i$, $_s\delta_i$, and m_i are assumed to be $\dfrac{_f\delta_i}{_f\delta_1} = \dfrac{_s\delta_i}{_s\delta_1} = \dfrac{m_i}{m_1} = \text{const.}$

Referring to Eq. (15), the natural period of the system without the stiff element is obtained as follows

$$_fT_0 = 2\pi\sqrt{\frac{_f\delta_Y\kappa_1}{\alpha_{f1}g}}$$

(32)

The natural period of the system without the flexible element is obtained as

$$_sT_0 = 2\pi\sqrt{\frac{_s\delta_Y\kappa_1}{\alpha_{s1}g}}$$

(33)

Referring to Eq.(12), the maximum instantaneous period of the system without flexible element is obtained as

$$_sT_m = a_{T\,s}T_s =\,_sT_0\left(1 + \frac{_s\bar{\mu}}{8}\right)$$

(34)

where $_sT_s$ is the period of the stiff element associated to the secant modulus and $_s\bar{\mu}$ the value of $\bar{\mu}$ in the stiff element. In deriving Eq.(34), the following values which correspond to the elastic-perfectly plastic system are used.

$$a_T = \frac{1 + \dfrac{\bar{\mu}}{8}}{\sqrt{1 + \bar{\mu}}}, \quad q = 1.0$$

(35)

The effective period of the system without the flexible element is obtained as

$$_sT_e = \frac{_sT_0 +\,_sT_m}{2}$$

(36)

The flexible-stiff mixed structure is a parallel system of the flexible and stiff elements. Then, the effective period of the total system is obtained from

$$\frac{1}{T_e^2} = \frac{1}{_fT_0^2} + \frac{1}{_sT_e^2}$$

(37)

Applying the numerical analyses, $_s\bar{\mu}$ is obtained by the following two ways.

$$_s\bar{\mu} = \sum_{i=1}^{10}\,_s\bar{\mu}_i\,, \quad _s\bar{\mu} = \frac{\gamma_{1\,s}\bar{\mu}_1}{\sum s_i}$$

(38), (39)

$\sum s_i$ is very closely approximated by

$$\sum s_i = 0.36 + 0.64N$$

(40)

The structural system is specified by $_s\delta_Y$, $_f\delta_Y$, α_{s1} and α_{f1}. $_s\bar{\mu}$ obtained by Eq.(38) is shown in Table 2 as $_s\bar{\mu}$.

Table 2. The effective period and V_E

record	$_s\delta_Y$ (°)	$_f\delta_Y$ (°)	α_{s1}	α_{f1}	$_sT_0$ (sec)	$_fT$ (sec)	$_s\bar{\mu}$	$_s\bar{\mu}_1$	$_s\gamma_1$	T_{e1} (sec)	T_{e2} (sec)	V_E (/s)
El CENTRO	0.15	1.5	0.3	0.3	0.338	1.07	0.91	1.33	6.72	0.34	0.35	76.7
	0.15	1.5	0.2	0.2	0.41	1.31	2.25	4.60	5.61	0.44	0.47	99.1
	0.15	1.5	0.1	0.1	0.59	1.85	3.14	4.83	5.47	0.66	0.68	111.8
	0.15	1.5	0.06	0.06	0.75	2.39	4.90	8.00	6.13	0.91	0.99	97.9
	0.15	1.5	0.04	0.04	0.93	2.93	6.94	10.1	5.39	1.21	1.26	87.6
	0.2	1.0	0.1	0.1	0.68	1.51	2.55	3.03	7.05	0.70	0.72	115.3
	0.2	1.0	0.06	0.06	0.87	1.95	3.53	4.60	6.31	0.93	0.96	98.3
	0.5	5.0	0.1	0.1	1.07	3.38	1.83	1.73	11.0	1.12	1.18	95.1
	0.5	5.0	0.06	0.06	1.38	4.36	2.11	2.83	6.25	1.47	1.51	91.5
	0.5	5.0	0.03	0.03	1.95	6.17	2.66	4.81	4.42	2.13	2.18	81.8
	0.5	5.0	0.02	0.02	2.39	7.56	3.66	8.03	3.55	2.74	2.81	72.0
	1.0	5.0	0.02	0.02	3.38	7.56	2.07	2.50	7.07	3.41	3.49	69.7
	1.0	5.0	0.01	0.01	4.78	10.7	2.03	3.37	4.50	4.81	4.95	51.9
HACHINOHE	0.15	1.5	0.2	0.2	0.41	1.31	0.85	1.30	5.98	0.41	0.42	58.4
	0.15	1.5	0.15	0.15	0.48	1.51	2.41	3.87	5.15	0.52	0.53	85.0
	0.15	1.5	0.1	0.1	0.59	1.85	3.99	7.47	5.37	0.68	0.74	103.1
	0.15	1.5	0.06	0.06	0.76	2.39	6.28	8.70	6.06	0.96	1.02	104.1
	0.2	2.0	0.1	0.1	0.68	2.14	3.60	6.33	6.46	0.77	0.86	101.8
	0.2	2.0	0.06	0.06	0.87	2.76	3.82	6.68	4.89	1.00	1.05	100.3
	0.2	2.0	0.04	0.04	1.07	3.38	6.78	8.70	6.18	1.39	1.45	102.2
	0.5	5.0	0.16	0.16	0.85	2.67	1.48	1.73	8.30	0.87	0.81	108.9
	0.5	5.0	0.1	0.1	1.06	3.38	1.64	2.15	6.06	1.11	1.13	114.7
	0.5	5.0	0.06	0.06	1.38	4.37	2.81	3.28	6.18	1.52	1.53	96.2
	0.5	5.0	0.04	0.04	1.69	5.34	3.30	3.64	6.20	1.90	1.90	95.3
	1.0	5.0	0.1	0.1	1.51	3.38	1.14	1.03	7.74	1.45	1.46	90.9
	1.0	5.0	0.06	0.06	1.95	4.37	1.67	1.24	10.6	1.93	1.95	104.5
	1.0	5.0	0.04	0.04	2.39	5.35	1.97	1.69	9.03	2.40	2.43	98.6
	1.0	5.0	0.02	0.02	3.38	7.56	2.23	3.05	7.65	3.55	3.61	80.9
	2.0	5.0	0.02	0.02	4.78	7.56	1.27	0.88	14.80	4.26	4.37	70.0
KOBE	0.15	1.5	0.5	0.5	0.26	0.83	5.27	29.3	1.68	0.32	0.31	204.9
	0.15	1.5	0.3	0.3	0.39	1.07	7.48	9.60	5.61	0.45	0.51	250.7
	0.15	1.5	0.2	0.2	0.41	1.31	15.1	12.9	7.12	0.71	0.65	267.5
	0.25	2.5	0.3	0.3	0.44	1.38	5.27	7.26	5.41	0.54	0.55	233.1
	0.25	2.5	0.2	0.2	0.54	1.69	7.47	7.72	6.76	0.74	0.72	251.8
	0.50	5.0	0.2	0.2	0.41	1.31	15.1	12.9	7.12	0.71	0.66	267.5
	0.5	5.0	0.15	0.15	0.87	2.76	4.41	50.9	5.56	1.08	1.02	219.5
	0.5	5.0	0.1	0.1	1.07	3.38	5.46	7.22	4.85	1.37	1.31	195.6
	0.5	5.0	0.06	0.06	1.38	4.37	4.94	9.24	3.65	1.67	1.67	160.3
	0.5	5.0	0.03	0.03	1.95	6.17	6.79	15.8	2.78	2.53	2.50	123.4
	1.0	5.0	0.2	0.2	1.07	2.39	2.42	2.61	7.23	1.14	1.11	234.4
	1.0	5.0	0.1	0.1	1.51	3.38	2.94	2.87	6.79	1.58	1.58	191.8
	1.0	5.0	0.03	0.03	2.76	6.17	4.17	7.12	3.53	3.03	2.98	126.1
	1.0	5.0	0.015	0.015	3.90	8.73	4.33	9.93	2.75	4.31	4.26	92.8

The effective period obtained by using $_s\bar{\mu}$ in Eq.(38) is T_{e1}. The effective period obtained by using Eq. (39) is T_{e2}. No damping is applied. As is seen in Table 2, T_{e1} and T_{e2} are almost equal. In Fig. 4, V_E-T_e relationship is shown by using T_{e2} as T_e. The value f ranges as follows.

$$0.19 \leq f \leq 1.61, \text{ mean value } f=0.64 \tag{41}$$

The solid lines in Fig. 4 is the energy spectrum of the elastic system with 10% of damping. As is seen in Fig. 4, the input energy of individual systems well corresponds to the solid lines and the effective period shown by Eq.(37) is shown to be adequate in order to estimate the total energy input into the highly nonlinear systems.

(a) El Centro record   (b) Hachinohe record   (c) Kobe record
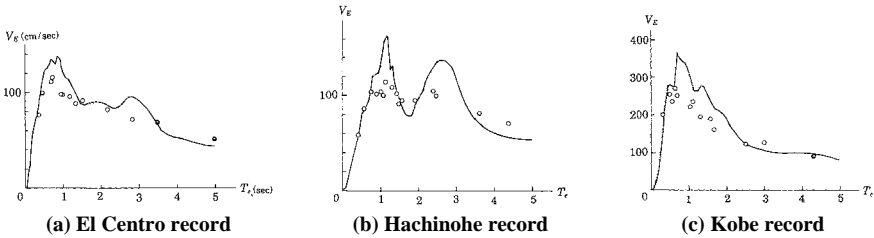
Figure 4. Effective period of multi-mass system.

6. CONCLUSION

The effective period of the highly nonlinear systems is derived by considering the fundamental feature of the energy spectrum. The effective period is the mean value of the fundamental natural period and the instantaneous longest period of the system. The instantaneous longest period is obtained by knowing the averaged maximum deformation of the system. The derived simple formula of the effective period was ascertained its effectiveness by the direct numerical analysis of ten storied shear type frames.

REFERENCES

Akiyama, H. (1985). Earthquake-Resistant Limit-State Design for Buildings, University of Tokyo Press.
Akiyama, H. (1999). Earthquake-Resistant Design Method for Buildings Based on Energy Balance.

BUILDING VULNERABILITY ASSESSMENT USING PUSHOVER METHODS — A TURKISH CASE STUDY

Edmund BOOTH[1], Juliet BIRD[2] and Robin SPENCE[3]

ABSTRACT

Non-linear static pushover analysis forms one key element of current methodologies of performance-based seismic design. It is also central to the estimates of building vulnerability used by the HAZUS earthquake loss methodology. However, despite the theoretical appeal of the methodology, recent comparisons of predictions using HAZUS with damaged recorded in the 1999 Kocaeli earthquake have shown poor agreement, not significantly better than those using intensity based methods. This paper examines further the reasons for this poor correlation, and uses a series of simple Monte Carlo simulations to examine the effect of varying degrees of brittleness and ductility on predicted damage distributions. These Monte Carlo simulations used the capacity spectrum method, and found that in allowing for the randomness of demand and capacity, the degree of brittleness markedly affected damage distributions in a way that appears plausible by comparison with observed data. This dependence on brittleness cannot be directly obtained from the original HAZUS methodology, nor from intensity based methods.

Keywords: Capacity spectrum; Insurance loss; Earthquake loss; HAZUS; Monte Carlo simulation.

1. INTRODUCTION

Predictions of the scale of future losses in earthquakes are vitally important to the insurance industry; *inter alia,* they are needed to set premiums and the size of financial reserves the industry should maintain. In the past, these predictions used empirical data, based on intensity. The methodology introduced by HAZUS (FEMA 1999), using the capacity spectrum method, offered a radical change in approach; the ground motion measure was a response spectrum, and so could be based directly on instrumentally recorded strong motion data, allowing a much more rational approach to the influence of factors such as frequency content and soil conditions on response. Moreover, structural vulnerability was expressed by a capacity curve, which could be directly related to fundamental structural parameters like yield strength, stiffness and ductility in a way that was impossible in an intensity based approach. However, an intensity based approach has its advantages, too. The data are very clearly based on

---

[1] *edmund@booth-seismic.co.uk*   [2] *Imperial College, London*   [3] *CAR Ltd, Cambridge, UK*

real damage data, rather than theoretical predictions; structural calculation of damage has often been notoriously inaccurate. Moreover, when dealing with a very large population of buildings, an intensity based model with few parameters has some appeal over a HAZUS type model with many parameters which may be difficult to estimate on a country wide scale. Also, insurance personnel without a background in structural engineering or engineering seismology tend to prefer the simpler intensity approach to one producing answers from a complex 'black box'.

In 1998, two of the authors were involved in the preparation of seismic loss estimates for the whole of a large industrialized and highly seismic country (Turkey). Despite the reservations noted above, a HAZUS methodology, suitably adapted for local conditions, was adopted (Bommer *et al*., 2002). Early in the project, the devastating Kocaeli and Düzce earthquakes in Western Turkey occurred, creating a large amount of damage data for events which were rich in instrumental recordings, and which affected a large stock of rather uniform recent construction; these events provided an ideal (and rare) opportunity for validation. This paper discusses previous work using these data which suggested that the HAZUS methodology did not (in this case) provide significant predictive advantages over intensity based methods. The paper goes on to describe a Monte Carlo based modification to HAZUS which gives some insights into the reasons for these poor predictions of damage.

2. PREVIOUS VALIDATIONS, USING TURKISH DAMAGE DATA

2.1 Zones Dominated by Ground Shaking Damage

A study by Spence *et al*. (2003) compared predicted damage with that reported by the AIJ (2001) and EEFIT (2003) at three locations in the epicentral area of the Kocaeli earthquake. The ground-shaking demand was defined using smoothed elastic spectra, selected to agree with the recordings from the Kocaeli earthquake, and modified to match local soil conditions; it was also defined in terms of intensity.

The study focused on the predicted performance of reinforced concrete frame buildings, of either 'good' or 'poor' quality, and unreinforced masonry buildings. The estimation of damage using the capacity spectrum approach was based upon the HAZUS methodology (FEMA, 1999), with adaptations for Turkish conditions, while that using intensities employed vulnerability functions derived from damage data from previous Turkish earthquakes; further details are given in Spence *et al*. (2003). The study concluded that neither displacement-based (i.e., HAZUS-based) nor intensity-based approaches showed good agreement with the observed results (Fig. 1).
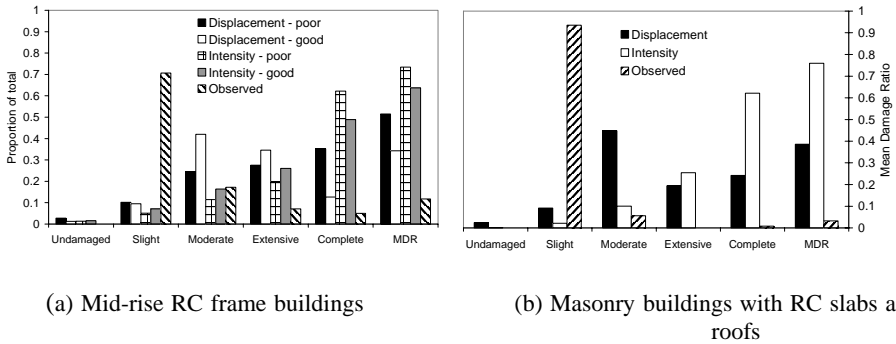
(a) Mid-rise RC frame buildings   (b) Masonry buildings with RC slabs and roofs

Figure 1. Comparison of predictions and observed damage (Spence *et al.,* 2002).

2.2   Zone Including Ground Failure

Subsequently, the above study was extended to consider a region of extensive ground failure (Adapazari), in order to investigate the influence of ground failure on damage distributions (Bird *et al.*, in press). Adapazari was damaged by a combination of ground failure, causing buildings to settle, rotate and slide on their foundations, and ground shaking. In this study, the intensity-based approach was not considered, partly due to the unsuccessful results obtained in the previous work, and additionally because of the inability of intensities to distinguish between the occurrence of ground failure and other damaging hazards such as local amplification due to soft soils. Again the damage estimation was based upon the HAZUS methodology, with some modifications where appropriate for the conditions in Adapazari.   Liquefaction-induced damage was considered in two ways, either by increasing the site category to site class E, or by following the default methodology presented in HAZUS.
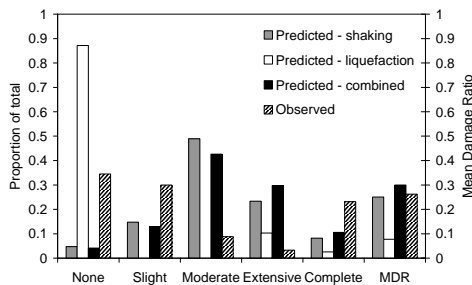

Figure 2. Predicted vs. observed damage to mid-rise RC buildings in Adapazari.

The results suggested that the additional work required to incorporate liquefaction into the damage methodology was not warranted in this case, since there was no obvious improvement in the results compared to those obtained ignoring

liquefaction-induced damage.   This is illustrated in Figure 2, where the third set of predictions shows the combined damage due to liquefaction and ground shaking, following the HAZUS methodology.

Further conclusions from this study were as follows. Existing intensity scales were observed to be lacking in that they do not include ground-failure induced damage such as settlement or rotation of buildings. Without a unified scale for both ground shaking and ground-failure induced damage states, an accurate prediction of damage in liquefied areas will be almost impossible to develop.   The importance of the foundation type on ground-failure induced damage was also noted.   It was suggested that the modelling of liquefaction effects is less significant than the structural model used to determine the ground shaking-induced damage, which should therefore receive (initially at least) the greatest attention.

3. DAMAGE DISTRIBUTIONS

3.1 RMS 'Beskat' Survey

Figure 3 shows the locations of six out of the thirty or so sites where Risk Management Solutions (RMS) Inc conducted a survey of 4 – 7 storey ('beskat') RC buildings (Johnson *et al*., 2000). The surveys were conducted within one week of the Kocaeli earthquake at sites within 10km of the fault. They were therefore all in the very near field of a large event and were conducted within days of its occurrence by a uniform team; moreover, the 6 sites considered in this study had apparently similar, stiff ground conditions. Figure 4 shows the damage distributions recorded; it can be seen that they are very different, and do not seem to be correlated strongly to features such as distance and direction from the source. Without a lot of further information, therefore, it would therefore be impossible to construct a single model that could get even fairly close to all these recorded data. However, at least the capacity spectrum method offers the chance to investigate further what parameters might be important in determining damage distribution, in a way not possible with intensity based measures. This realization informed the further studies reported below.
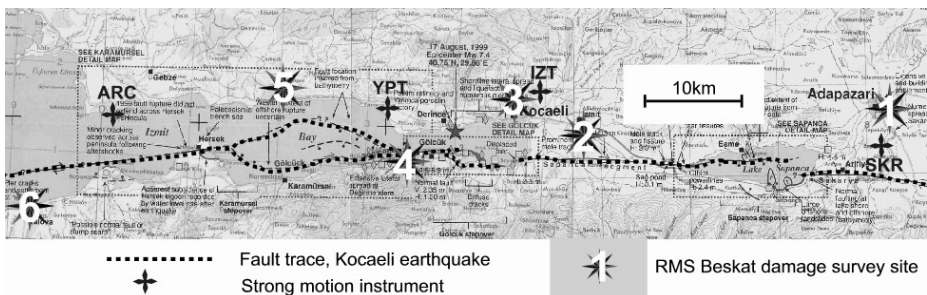

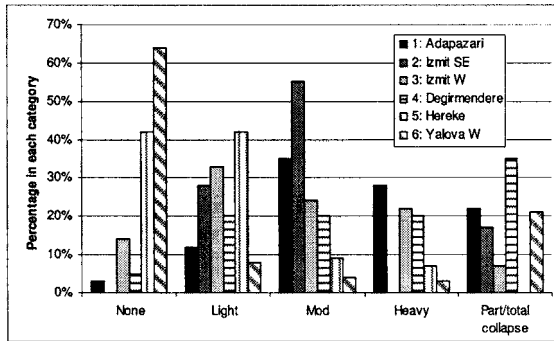**Figure 3. Locations of RMS 'beskat' surveys shown in Figure 4.**

Figure 4. Recorded damage from RMS 'beskat' survey.

3.2 'Type I' and 'Type II' Damage Distributions

The term 'damage distribution' refers to the distribution of the different damage states of *none* through to *complete* for a particular building class. Generally it is assumed that such distributions will have only one peak, with a roughly symmetrical spreads to either side of the peak. HAZUS (FEMA 1999) generally predicts such distributions (termed here 'Type I'), found also in the damage probability matrices used in intensity-based methodologies such as ATC-13 (ATC, 1985). However, a number of damage datasets from the 1999 Kocaeli earthquake collated for this paper display damage distributions that did not follow this trend. Of the ten distributions presented in Figure 5, four have distributions defined here as 'Type II'; they have two peaks, one at *complete* damage, and the other at a lower damage level. The salient features of the sites summarized in Figure 5 and the others considered in this paper, are presented in Table 1; no obvious reasons for the Type II distributions emerge.

One solution for the prediction of these variable distributions, as well as the variability in recorded damage at similar sites noted in the previous section would be to consider the mean damage ratio (MDR) only, and to focus calibration efforts etc. onto this composite parameter, on the basis that the complexity of actual damage distributions cannot be reproduced using simplified methods. Whilst this may be appropriate for some cases, such as those where only the overall loss ratio is of interest, it is not conducive to improving damage estimation approaches and understanding the variables that influence the distribution of earthquake damage. This study therefore devotes itself to improving the understanding of why these different damage distributions occur and thus how to predict them in future earthquakes.

Two causes for 'Type II' damage distributions are now discussed. The first is that they represent damage caused by two independent, superimposed mechanisms.
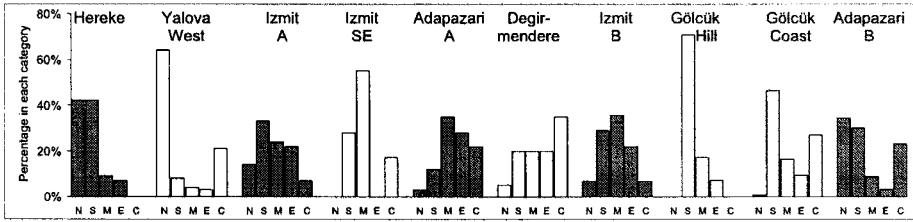
401

Figure 5. Selected damage distributions for mid-rise RC apartment buildings.

Table 1. Characteristics of sites shown in Figure 5

Site	Source	Dist. to fault	Damage distribution	Soils	Ground failure
1: Hereke	RMS	4 km	Type I	Stiff	Unknown
2: Yalova West	RMS	4 km	Type II	Stiff	Minor
3: Izmit A	RMS	7 km	Type I	Stiff	None
4: Izmit SE	RMS	3 km	Type II	Stiff	None
5: Adapazari A	RMS	8 km	Type I	Stiff	Major
6: Degirmendere	RMS	1 km	Type I	Stiff	Moderate
7: Izmit B	CAR	8 km?	Type I	Stiff	None
8: Gölcük Hill	AIJ	2 km	Type I	Stiff	None
9: Gölcük Coast	AIJ	1 km	Type II	Soft	Minor
10: Adapazari B	EERI	4 km	Type II	Soft	None

Superimposition might for example arise in a survey zone which has buildings damaged by both ground shaking and liquefaction. Even within the relatively small zone of central Adapazari, two distinct types of damage were observed, either those with structural damage caused by ground shaking, or those on liquefied soil, which suffered foundation failures, manifested as settlement or tilting of the building, with little or no evidence of damage due to ground shaking in the form of cracks, deformation or partial or complete collapse. Although in many ways this is a plausible explanation for these damage distributions, there are a number of points that do not support it, namely:

- Table 1 shows no clear relationship between the type of damage distributions and the occurrence of extensive ground failure.
- As noted previously, intensity scales used in damage surveys such as these tend not to include liquefaction-related damage. Thus, by strict application of such scales, a building that had suffered major tilting as a result of ground failure, but otherwise remained undamaged structurally, should be classified

as *undamaged*.   Surveyors may make their own subjective decisions that a building that has tilted is damaged beyond repair, but the application described above is the only one that can be interpreted without uncertainty.

- The study by Bird *et al*. (2004) discussed in Section 2.2 attempted to reproduce observed damage by superimposing ground shaking and ground failure damage, but without much success.

Therefore, the superposition of two separate damage distributions cannot entirely explain the Type II damage distributions.

Another possible cause relates to structural ductility.   In stiff and brittle structures, there may be little damage up to the point of effective yield.   However, even small demands beyond this point may lead to a rapid increase in deflections and damage, due to loss of stiffness and strength.   Such structures might therefore be expected to show either low damage or very high damage, with little in-between (e.g. Crowley *et al*. 2004).   The non-ductile concrete frames with rigid, brittle and weak masonry infill found in the Kocaeli region might have had these characteristics, particularly since in many cases open ground floors were present.   A model that gave a damage distribution dependent on ductility as well as yield strength and stiffness might therefore be of value.

Unfortunately, the HAZUS methodology is of no direct help here.   Damage distributions for a given seismic input are based on the expected deflection (the crossing point of demand and capacity spectra), and no account is taken of how far or near that point is from brittle collapse.   The distribution of deflections around that expected point is assumed to be log-normally distributed, based on the central limit theorem and the assumption that both demand (ground motion intensity) and capacity (structural characteristics) are also normally or log-normally distributed.   This latter assumption may be reasonable, but in a highly non-linear brittle system, with a 'cliff-edge' in response around fracture, the assumption that response is also lognormally distributed is unlikely to apply.   To investigate this further, this study developed the model described in the next section.

4. MONTE-CARLO BASED SIMULATIONS FOR THIS STUDY

In order to investigate further the possibility that the 'Type II' damage distributions discussed above were due to a brittle structural response, the HAZUS approach was modified as follows. The capacity spectrum method was still used for determining expected deflection, but the damage distribution was generated from a series of 'Monte Carlo' type simulations, assuming that both the demand (ground) and capacity spectra were lognormally distributed.   Figure 6 shows the idealized capacity spectrum, and Figure 7 shows the ground spectrum, which was a smoothed and simplified version of the SKR stiff soil recording from Kocaeli; Figure 7 also shows spectra recorded at the recording sites shown in Figure 3.
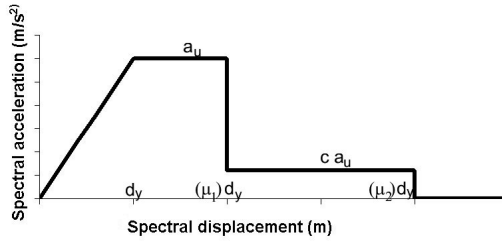
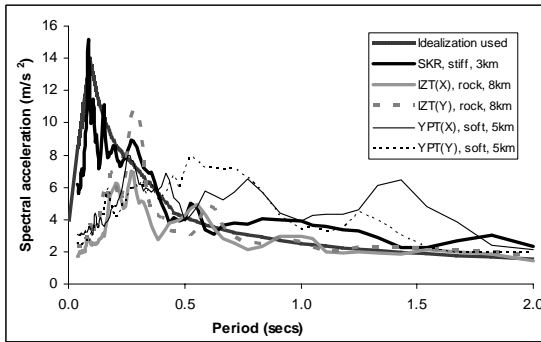**Figure 6. Idealized capacity spectrum assumed for this study.**

Figure 7. Idealized demand spectrum used for study, and Kocaeli spectra.

In Figure 6, a_u and d_y are the spectral acceleration and displacement at yield, and μ_1 and μ_2 are the displacement ductility ratios to first loss of capacity and to fracture; they are assumed to be log-normally distributed random variables with a coefficient of variation β_c. c is the ratio of lower to upper yield plateaux strengths, taken as fixed for a given simulation. The mean 5% damped demand spectrum was taken as the idealized spectrum of figure 7, but this was also treated as log-normally distributed.

Table 2 shows the various cases considered, and Table 3 the adopted parameter values. For the two base cases, called 'brittle' and 'ductile', a_u and d_y were given similar mean values to those used for 4-7 storey RC frames in the TCIP study referred to previously, but with the yield strength a_u increased by about 50% to allow for the effect of masonry infill. The mean values of μ_1, μ_2 and c and also coefficient of variation (β) values were chosen more arbitrarily, but look reasonable, for example in relation to standard values proposed in FEMA 356 or HAZUS. The relationships between peak deflection and damage state shown in Table 4 were also based on HAZUS; note that these values were taken as constant (i.e., not lognormally varying).

Table 2. Cases considered for this study

| CASE	Description
1	Base case: brittle
2	Base case: ductile
3	Base case: brittle + low variability
4	Base case: ductile + high variability
5	CAR Ltd data for Izmit
6	RMS Inc data for Izmit South East

Table 3. Values of parameters for Monte Carlo simulation

CASE (see Table 2)	1	2	3	4	5	6
β_d for demand spectrum	0.5	0.5	0.25	0.9	0.34	0.27
β_c for capacity (a_u, d_y, μ_1, μ_2)	0.5	0.5	0.25	0.9	0.41	0.30
Viscous damping ratio	7%					
κ, reduction factor on hysteretic energy	0.4					
a_u (m/s^2) yield spectral acceln	3	3	3	3	2.5	2.4
d_y (m) yield spectral disp.	0.11	0.11	0.11	0.11	0.11	0.1
μ_1 (ductility to loss of strength)	1.5	2.5	1.5	2.5	2.6	1.42
μ_2 (ductility to fracture)	3	4	3	4	5.2	3.5
c (ratio of yield to residual strength)	0.2	0.4	0.2	0.4	0.55	0.35
T (secs) - struct. period	1.2	1.2	1.2	1.2	1.32	1.28

Table 4. Assumed relationship between deflection and damage state

Damage state	Spectral deflection (mm)	Approx equiv drift	Assumed damage ratio
None	0 - 38	0 – 0.5%	0%
Low	38 – 68	0.5% - 0.9%	2%
Moderate	68 – 126	0.9% - 1.7%	10%
Extensive	126 – 330	1.7% - 4.5%	50%
Complete	>330	>4.5%	100%

Figure 8a shows the predicted distributions for the 'brittle' and 'ductile' base cases; the 'Type II' distribution shape due to the brittle 'cliff-edge' changes to 'Type

I' for the ductile case, as expected. Figure 8b shows that decreasing the variability of the demand and capacity variables changes the brittle structure's distribution to a (more-or-less) 'Type I' one, and Figure 8c shows that an increase in variability has the opposite effect for the ductile structure.
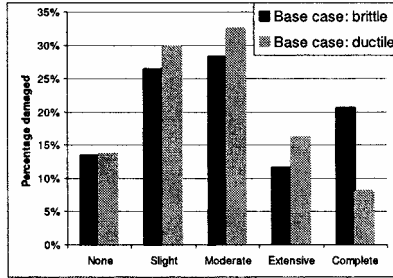
(a) Brittle & ductile base cases: cases 1 & 2
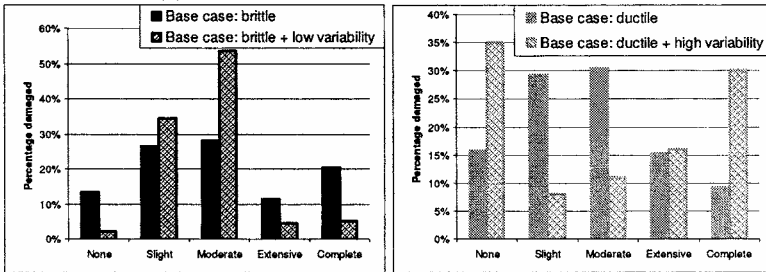
(b) Brittle + low variability: case 3   (c) Ductile plus high variability: case 4

Figure 8. Predicted distributions for 'brittle' and 'ductile' base cases.

Figure 9. Comparison of predictions with HAZUS methodology for base cases.
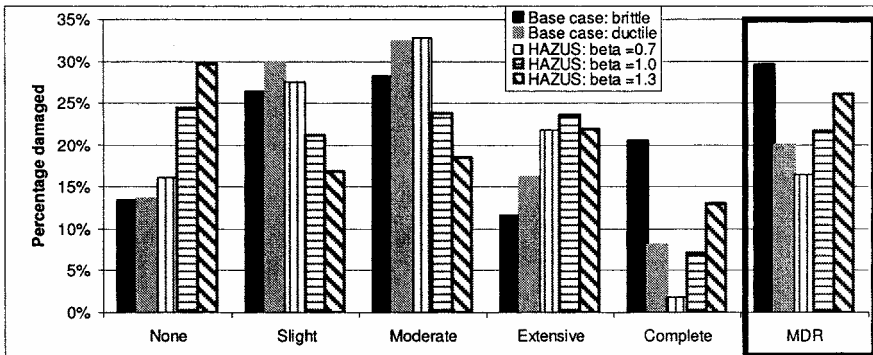
Figure 9 compares the damage predicted by HAZUS for the brittle and ductile base cases with those from the present study. The 'brittle' and 'ductile' structure have the same yield strength and deflection, and the expected deflection is below that corresponding to strength reduction in the brittle structure for the adopted input

spectrum. Hence the expected deflection is the same for both brittle and ductile structures, and the only parameter that HAZUS has available to affect the distribution is the β value, given fixed values of the threshold deflections (Table 4). As the β value changes from 0.7 to 1.3, it can be seen from Fig 4 that the HAZUS distribution shape changes from fully 'Type I' to something approaching 'Type II', although the shape is not as markedly bi-modal as for the brittle base case from this study. The beta value for the HAZUS calculation represents a combination of the effect of ground motion (demand) and structural variabilities (β_d and β_c in Table 3); the combined effect of $\beta_d = \beta_c = 0.5$ (the base case considered here) is broadly equivalent to a combined β of about 1 to 1.3. It may be noted that there appears to be no obvious reason why brittleness and a high value of structural variability should be linked, and the Monte Carlo model used here shows a marked advantage in this respect.

Finally, two actual damage distributions recorded after Kocaeli were chosen (cases 5 & 6 of Tables 2 & 3, but numbered 4 & 7 in Table 1). The parameters available in the model were varied within reasonable bounds to see how closely the model distribution could match the recorded ones. The two right hand columns for cases 5 & 6 in Table 3 show the parameters chosen; the deflection values of Table 4 were assumed to remain applicable. The resulting distributions are shown in Figure 10. They are not of course in any way predictions, but the exercise suggests that reasonable results may be obtained from the model. Whether the building population recorded by CAR Ltd really was so much more ductile than that of the population recorded by RMS Inc. is of course another question.
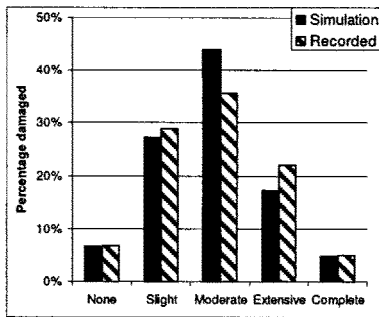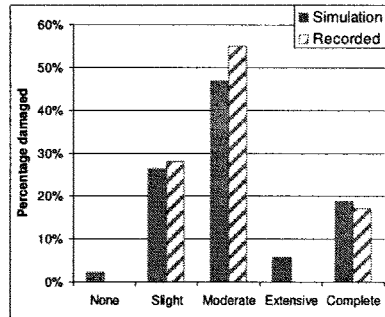
(a) CAR Ltd data for Izmit   (b) RMS Inc data for Izmit South East

Figure 10. Comparison of simulations from this study with Izmit data.

5. CONCLUSIONS

A weakness in the current HAZUS methodology for predicting earthquake losses is that it cannot directly account for the effect of structural brittleness or ductility on damage distributions, and is no better in this respect than intensity based methods.

This study has shown that a modification to HAZUS, using Monte Carlo simulations, redresses this deficiency in HAZUS in a way which (initially at least) appears plausible by reference to observed data from Kocaeli. Further work is needed to develop a viable and reliable tool for predicting losses for the insurance industry, but the approach described here appears a promising one to pursue.

REFERENCES

ATC. (1985). *ATC 13 Earthquake Damage Evaluation Data for California*, Advanced Technology Council.

AIJ. (2001). *Report on Damage Investigation of the 1999 Kocaeli Earthquake in Turkey.* Architectural Institute of Japan.

Bommer, J. et al. (2002). Development of a Turkish Loss Model for Turkish Catastrophe Insurance, *Journal of Seismology*, vol. 6, no. 2, pp. 431-446.

Bird, J. F., J. J. Bommer, J. D. Bray, R. B. Sancio, R. J. S. Spence (2004). Comparing Loss Estimation with Observed Damage in a Zone of Ground Failure: A study of the 1999 Kocaeli Earthquake in Turkey. *submitted to Bull. Earthquake Eng*. March.

Bray, J. D., and J. P. Stewart. (2000). Damage patterns and foundation performance in Adapazari, in Kocaeli, Turkey Earthquake of August 17, 1999 Reconnaissance Report, *Earthquake Spectra*, 16 (Suppl. A), 163-189.

Crowley H., R. Pinho, and J. Bommer. (2004). A Probabilistic Displacement-Based Vulnerability Assessment Procedure for Earthquake Loss Estimation. *Bulletin of Earthquake Engineering* 2(2): in press.

EEFIT. (2003). *The Kocaeli, Turkey earthquake of 17 August 1999. A field report by EEFIT.* D'Ayala, D. and Free, M. (eds.), Earthquake Engineering Field Investigation Team, Institution of Structural Engineers, London.

FEMA. (1999). *HAZUS 99 technical and user manuals.* Federal Emergency Management Agency, Washington, D.C.

FEMA. (2000) *FEMA 356: Prestandard and commentary for the seismic rehabilitation of buildings.* Federal Emergency Management Agency, Washington.

Johnson L. A., A. Coburn, and R. Mohsen. (2000) Damage survey approach to estimating insurance losses. Turkey Earthquake of August 17, 1999 Reconnaissance Report, *Earthquake Spectra*, 16 (Suppl. A), 163-189.

Kircher C., A. Nasser, O. Kustu, and W. Holmes. (1997). Development of building damage functions for loss estimation. *Earthquake Spectra* 13(4) 663-682.

Spence, R. J. et al. (2003). Comparing Loss Estimation with Observed damage: A study of the 1999 Kocaeli Earthquake in Turkey. *Bulletin of Earthquake Engineering*, 1 (1) 83-113.

RELIABILITY OF MULTISTORY BRICK BUILDINGS AT DIFFERENT PERFORMANCE LEVELS

Lingxin ZHANG[1], Jinren JIANG and Jieping LIU

ABSTRACT

This paper analyzes the seismic reliability of multistory brick buildings at different performance levels by the Latin Hypercube Sampling technique and nonlinear seismic time history response analysis. In this analysis, a set of representative multistory dwelling brick buildings needs to be established. The uncertainties of structural parameters and earthquake load are considered. In the end, the seismic reliabilities of multistory brick buildings at three performance levels are given.

Keywords: Performance levels; Reliability; Latin Hypercube Sampling; Nonlinear seismic response; Uncertainty.

1. INTRODUCTION

In this paper, the seismic reliability of multistory brick buildings designed according to the current PRC code is analyzed in detail at different performance levels. The analytical results may lay the foundation of a performance-based seismic design method based on reliability of multistory brick buildings. The seismic reliability is analyzed by the Latin Hypercube Sampling technique and nonlinear seismic time history response analysis. In the analysis, the uncertainties of earthquake load and structural parameters are considered.

2. REPRESENTATIVE MULTISTORY DWELLING BRICK BUILDINGS

In order to evaluate the seismic reliability of multistory brick buildings at different performance levels, a set of representative structures needs to be established according to the Latin Hypercube Sampling technique. Here, we regard multistory dwelling brick buildings as examples. Using typical design parametric values, which are chosen according to the scope of common design parametric values of multistory dwelling brick buildings, four representative multistory dwelling brick buildings, as shown in Table 1, are established by the Latin Hypercube Sampling technique. The

---

thickness of the inner wall is usually 24cm. The grade of mortar is usually M2.5, but can be increased to M5.0 and M10.0 according to the requirement of seismic design. The transversal wall is taken as the load-bearing wall in the four buildings. Combining the four representative brick buildings with design intensities VI, VII, VIII and IX, and considering that the code requirement for intensity IX is a maximum of four-stories, a total of 14 samples of multistory dwelling brick buildings are obtained. The seismic design of these multistory dwelling brick buildings is conducted according to the Chinese "Code for seismic design of buildings" (GBJ11-89).

Table 1. Representative multistory dwelling brick buildings

Design parameters	Buildings			
	1	2	3	4
Story	3	4	5	6
Story height (m)	2.8	2.7	2.8	2.7
Top story height (m)	2.9	2.8	2.8	2.7
Bay (m)	3.3, 3.6	3.3	3.6	3.9
Building width (m)	10.0	10.3	10.3	11.2
Building length (m)	37.2	32.2	34.6	34.6
Outer wall thickness (cm)	37	37	37	37
Roof load (N/m^2)	3310	3310	3310	3310
Floor load (N/m^2)	3790	3790	3790	3790

3. STRUCTURAL MODEL AND UNCERTAINTIES OF ITS PARAMETERS

The brick structure model is a shear stick model. The hysteretic model of a brick wall with and without constructional columns used here is a trilinear model, which is given by referring to a large number of references (Zhang 1998), as shown in Fig.1. The details of the formulas of stiffness and strength in this model are given in Zhang (1998).

The parameters of the structural model include the lumped mass, the viscous damping ratio and the hysteretic model parameters. The lumped mass is usually assumed as deterministic. The viscous damping ratio of brick structures can be expressed as in Zhang (2002):

$$\xi = 0.008 + 0.55A/F \tag{1}$$

where, A is the sum of the horizontal cross-sectional area of transversal walls for each floor. F is the area of structure for each floor.

From Fig.1, we can see that the hysteretic model is characterized by five parameters: the initial stiffness K_0, the hardening stiffness K_1, the softening stiffness K_2, the crack strength Q_c, and the ultimate strength Q_u, which can be determined from experimental data. The relationships between K_2 and K_1, Q_u and Q_c are more or less fixed. And their variability is very small and can be omitted. So only K_0, K_1 and Q_c are treated as independent random variables in this analysis. In terms of K_0 and a strain-hardening ratio α_1, K_1 can be expressed as $K_1 = \alpha_1 K_0$, so α_1 is treated as an independent random variable instead of K_1. Moreover, there is no pinching effect in the inelastic reloading stiffness of the hysteretic model. Variation of the inelastic unloading stiffness has some effect on energy-dissipation under cyclic loadings, but has negligible effect on the maximum deformation of structures. So it is reasonable to assume the unloading stiffness K'_0 as deterministic.

The coefficients of variation of K_0, α_1, Q_c and ξ for the brick wall with and without constructional columns are listed in Table 2, respectively (Zhang 2002).

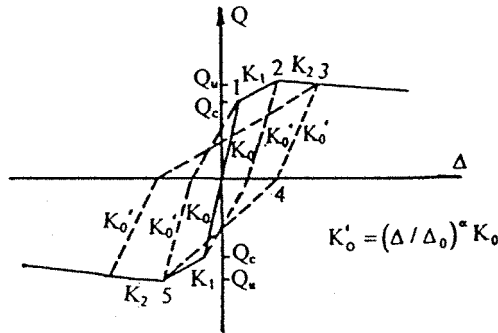**Figure 1. Hysteretic model of brick wall.**

Table 2. Parametric uncertainties of structural model

Coefficient of variation of model parameters	β_{K_o}	β_{α_1}	β_{Q_c}	β_ξ
Brick wall without constructional columns	0.30	0.33	0.30	0.30
Brick wall with constructional columns	0.30	0.42	0.20	0.30

4. EARTHQUAKE GROUND MOTION INPUT AND UNCERTAINTIES OF ITS PARAMETERS

The earthquake ground motion input used in this analysis is the artificial ground motion (Jiang 1984). The earthquake acceleration time history is expressed as:

$$a(t) = \psi(t)a_s(t) \tag{2}$$

where $a_s(t)$ is a stationary Gaussian process with zero mean value and $\psi(t)$ is an envelope function describing the nonstationary process.

$$\psi^2(t) = \begin{cases} (t/t_1)^2 & \text{when } t < t_1 \\ 1 & \text{when } t_1 \leq t \leq t_2 \\ e^{-c(t-t_2)} & \text{when } t > t_2 \end{cases} \tag{3}$$

where c is an attenuation constant.

$$a_s(t) = \sqrt{2} \sum_{k=1}^{N-1} \sqrt{G(\omega_k)\Delta\omega} \ \cos(\omega_k t - \phi_k) \tag{4}$$

where ϕ_k are random phase angles of uniform distribution and are independent of each other during $(0, 2\pi)$. $G(\omega_k)$ is a density function of the power spectrum, and is obtained by transformation of the mean response spectrum $R(\omega, \xi)$ with the power spectrum $G(\omega)$.

The acceleration time history a(t) is normalized using its maximum amplitude a_{max}. The normalized nonstationary acceleration time history is as follows:

$$a_m(t) = \frac{\psi(t)a_s(t)}{a_{max}} \tag{5}$$

So, the nonstationary acceleration time history is:

$$a_g(t) = A_p a_m(t) \tag{6}$$

where, A_p is a given peak ground acceleration.

The artificial wave as mentioned above is obtained by transforming the mean response spectrum into the power spectrum. So the parameters of the earthquake model include the mean response spectrum, the duration of earthquake ground motion and the damping ratio. We take the standard response spectrum in the Chinese "Code for seismic design of buildings" (GBJ11-89) as the mean response spectrum. The former is obtained by simply averaging a large number of strong earthquake

acceleration response spectra and smoothing them. The coefficient of variation of the normalized mean response spectrum changes with period. But for general site and the range of period of multistory dwelling brick buildings, it can be taken as $\beta_R = 0.26$ according to Jiang (1995). The duration of strong motion is taken as the 1/2 peak acceleration duration τ. By utilizing 24 strong earthquake records longer than 2.75s from Jiang (1995), we obtain that the mean value is 8.25s, and the coefficient of variation $\beta_\tau = 0.678$. The standard response spectrum in the code is the one with the damping ratio of 0.05. When the structural damping ratio isn't 0.05, the response spectrum is revised by the damping revising coefficient formula specified in the Chinese "Design code for antiseismic of special structures" (GB50191-93). The coefficient of variation of the damping ratio is already given above. In the reliability analysis, the peak ground acceleration is a given independent variable, so it should be regarded as deterministic.

5. SEISMIC RELIABILITY ANALYSIS OF MULTISTORY DWELLING BRICK BUILDINGS

5.1   The Earthquake Load-Structure System

In order to analyze the seismic reliability of multistory dwelling brick buildings at different performance levels, the Latin Hypercube Sampling technique is utilized to establish the structure model assembly and the earthquake load assembly, and then match them to obtain the earthquake load-structure system. In the analysis, four parameters describing the structural model and four parameters describing the earthquake model are considered. The uncertainties of each parameter are expressed in terms of three representative values, i.e., mean, mean minus and plus one standard deviation. So, for the ensemble of structural models, from the combinations of three representative values of the four parameters, a total of 81 structural models can be established. For the ensemble of earthquake time histories, from the combinations of three representative values of response spectrum and damping ratio, nine response spectra are obtained. For each response spectrum, three stationary time histories are generated. Thus, 27 stationary time histories are produced. It is noted that 27 different sets of random phase angles are used to generate these time histories. And then three envelope functions represented by strong motion duration are applied to each stationary time history to generate three normalized nonstationary time histories. Three strong motion durations are taken as its mean, mean minus and plus 0.8 times standard deviation (Zhang 2002). Thus, a total of 81 normalized earthquake acceleration time histories are generated. Finally, these earthquake time histories are matched to the structural models so that the earthquake load-structure system with 81 samples is constructed.

5.2   Performance Levels and Limit States of Structure

The performance objective given by the Chinese "Code for seismic design of buildings" (GBJ11-89) is as follows. For frequently occurring earthquakes of intensity lower than the seismic strengthening intensity of the region, buildings designed according to the code shall not be damaged and/or shall be able to be in service; for occasionally occurring earthquakes of intensity corresponding to the seismic strengthening intensity of the region, buildings may be damaged but should be restorable to service with minor repairs; for rarely occurring earthquakes of intensity higher than the seismic strengthening intensity of the region, buildings shall not collapse or incur severe life-threatening damage. So, on the basis of the seismic strengthening objective, three performance levels are specified: for frequently occurring, occasionally occurring and rarely occurring earthquakes, which are the so-called "no damage during frequently occurring earthquakes, repairable during occasionally occurring earthquakes, and no collapse during rarely occurring earthquakes".

In order to conduct reliability analysis, the limit states of a structure need to be given. Usually, five limit states are considered: representing initial cracking damage, slight damage, moderate damage, severe damage and collapse of the structure. We can see from the definition of three performance levels as mentioned above that the first one corresponds to the initial cracking damage; the second one corresponds to slight to moderate damage; the third one corresponds to severe damage.

In this analysis, the limit state of a structure is defined in terms of the structural ductility factor. For each limit state, a corresponding capacity in terms of the ductility factor can be established. The ductility factor of the brick wall is defined as the ratio of the maximum deformation to the cracking deformation. The structural capacity can be usually modeled by a lognormal distribution. According to Zhang (2002), on the basis of the cracking features of walls in each hysteretic skeleton curve stage and compared with the true earthquake damage degree of buildings, the median $\widetilde{\mu}_R$ and logarithmic standard deviation σ_R can be obtained, as shown in Table 3.

Table 3. Ductility factor capacity

Limit states	Brick wall without constructional column		Brick wall with constructional column	
	$\widetilde{\mu}_R$	σ_R	$\widetilde{\mu}_R$	σ_R
Initial cracking damage	1.0	0.3	1.0	0.3
Severe damage	1.6	0.3	2.6	0.3
Collapse	2.6	0.3	4.8	0.3

The collapse capacities of the brick wall with and without constructional columns are taken as 90% and 85% of ultimate strength, respectively. The capacity for the severe damage is related to the ultimate strength. The capacity for the initial cracking damage is related to the cracking strength. The capacities for slight damage and moderate damage are taken as the values at 1/5 and 3/5 points between the capacities for the initial cracking damage and severe damage, respectively. The median and logarithmic standard deviation of story capacity of the brick buildings are obtained by composing the mean and standard deviation of the brick wall with and without constructional columns according to their cross section ratio.

5.3 Probabilistic Response of Earthquake Load-Structure System

The hysteretic model used in nonlinear seismic response analysis includes a negative stiffness branch. In order to avoid the probable unstable phenomenon in the iteration method and probable non-definite abnormal matrix in the variable stiffness matrix method during dealing with the negative stiffness, we use the method of nonlinear dynamic response analysis based on pattern of self-equilibrating stresses (Zhang 1998, Zhang 1997b) to analyze the response of multistory brick buildings.

For each earthquake load-structure system, the nonlinear seismic response analysis is carried out. The i-th story ductility ratio is:

$$\mu_i = \frac{U_{max,i}}{U_{c,i}} \tag{7}$$

where $U_{max,i}$ is the maximum absolute inter-story deformation of the i-th story and $U_{c,i}$ is the cracking deformation of the i-th story.

For the results of 81 samples, statistical analysis is utilized to determine mean, standard deviation and distribution function of the maximum response. According to Zhang (2002), the maximum structural response can be modeled by a lognormal distribution.

5.4 Reliability Analysis

The structural seismic reliability analysis is used to determine the limit state probability PF with respect to a particular limit state during the structure's service life. It can be expressed as:

$$PF = \sum_{j=6}^{10} \lambda_{I_j} \cdot P_f(I_j) \tag{8}$$

where j=6, 7, 8, 9, 10, is the number of intensity. The structural reliability index with respect to a particular limit state is:

$$\beta = -\Phi^{-1}(PF) \tag{9}$$

where λ_{I_j} is the occurrence rate of an earthquake with intensity I_j during the structural service life. For a given earthquake hazard curve $F_I(I_j)$, it can be written as:

$$\lambda_{I_j} = F_I(I_j) - F_I(I_j + 1) \tag{10}$$

$P_f(I_j)$ is the conditional limit state probability with respect to a particular limit state for a given intensity I_j. The i-th story conditional limit state probability of multistory brick buildings with respect to a particular limit state is defined as the conditional probability that structural response E_i exceeds the structural capacity R_i, which can be written as:

$$P_{f_i}(I_j) = P_{ri}(R_i \le E_i \mid I_j) = \int_0^\infty \left[1 - F_{E_{ji}}(r)\right] f_{R_{ji}}(r)dr \tag{11}$$

where, $F_{E_{ji}}(\bullet)$ is the cumulative probability distribution of E_i and $f_{R_{ji}}(\bullet)$ is the probability density function of R_i for a given intensity I_j. The limit state probability of the entire structure can be taken as:

$$P_f(I_j) = \max(P_{f_i}(I_j)) \tag{12}$$

For the case of both the maximum structural response and deformation capacity conforming to a lognormal distribution, the i-th story limit state probability of structures, equation (11) can be written as:

$$P_{f_i} = \Phi\left[\frac{-\ln(\widetilde{\mu}_{R_i}/\widetilde{\mu}_{E_i})}{(\sigma_{R_i}^2 + \sigma_{E_i}^2)^{1/2}}\right] \tag{13}$$

where, $\widetilde{\mu}_{R_i}$ and $\sigma_{R_i}^2$ are the median and the logarithmic variance of R_i, respectively. $\widetilde{\mu}_{E_i}$ and $\sigma_{E_i}^2$ are the median and the logarithmic variance of E_i, respectively.

Firstly, the statistics of the ductility factor and the corresponding deformation capacity of 14 multistory dwelling brick buildings are calculated. And then the conditional limit state probabilities of 14 multistory dwelling brick buildings for a given intensity are obtained according to the above equation. Finally, the seismic reliabilities of 14 buildings designed for various intensities are obtained by convolution of the conditional limit state probabilities and the earthquake risk curves.

5.5   Reliability of Multistory Brick Buildings at Different Performance Levels

In this paper, the multistory dwelling brick buildings analyzed are assumed to be located in Tianjing and Beijing. Their basic intensities are VII and VIII, respectively, and for their earthquake hazard curves refer to Tao (2000). The basic intensity is taken as the seismic strengthening intensity.

In the analysis, the peak ground accelerations with respect to various intensities are taken as 0.05g, 0.10g, 0.20g, 0.40g and 0.70g for intensity VI, VII, VIII, IX, and X, respectively.

Figs. 2 and 3 show the seismic reliability indexes of four multistory brick buildings designed for intensity VI, VII, VIII and IX in region of intensity VII (Tianjing) and VIII (Beijing) at three performance levels, respectively. The seismic reliability index at the second performance level is taken as the average of those for slight damage and moderate damage. Tables 4 and 5 list the seismic reliability indexes of four multistory brick buildings designed for the basic intensity in region of intensity VII (Tianjing) and VIII (Beijing) at three performance levels, respectively. The averages in the table and figure are the ones of the seismic reliability indexes of three-story, four-story, five-story and six-story brick buildings for the multistory brick building designed for intensity VI, VII and VIII, and the ones of the seismic reliability indexes of three-story and four-story brick buildings for the multistory brick buildings designed for intensity IX. These averages represent the seismic reliability of these kinds of multistory brick buildings.

From Figs. 2 and 3, we can see the dispersion of the seismic reliability indexes of various story brick buildings and the averages. For the buildings designed for intensity VI, the index is lower than the average for a five-story building at three performance levels, and higher than the average for a six-story building at the second and third performance levels. This is mainly because constructional columns are installed rarely in five-story buildings and more frequently in six-story buildings. For buildings designed for intensity VII, the indexes of various story buildings are near the average at the first performance level. The index is near the average for a six-story building, much higher than the average for a five-story building, and lower than the average for three-story and four-story buildings at the second and third performance levels. The reason for the higher index of a five-story building is that the number of constructional columns in a five-story building is increased compared with the number used in buildings with fewer stories. For buildings designed for intensity VIII, the index is much higher than the average for a six-story building, and lower than the average for other buildings at the second and third performance levels. The reason for the higher index of the six-story building is that a six-story building is installed with the same number of constructional columns as a five-story building, but the grade of mortar is higher than that in a five-story building. For buildings designed for intensity IX, because the number of constructional columns installed in three-story and four-story buildings is the same but the grade of mortar in a four-story building is much higher than that of a three-story building, there are many differences between the indexes of three-story and four-story buildings. The index is higher than the average for the four-story building, and lower than the average for the three-story building at the three performance levels. For three performance levels, the indexes of the six-story building designed for intensity VI and VII are close. The index of a four-story building designed for intensity VI is higher than a building designed for intensity VII because the grade of mortar is much higher and the constructional columns installed are more for buildings designed for intensity VII than VI. The index of the five-story building designed for intensity VII is much higher than the building designed for

intensity VI because the number of constructional columns is increased significantly for buildings designed for intensity VII than VI.

Figure 2. Seismic reliability indexes of multistory brick buildings designed for various intensities in region of intensity VII at three performance levels.
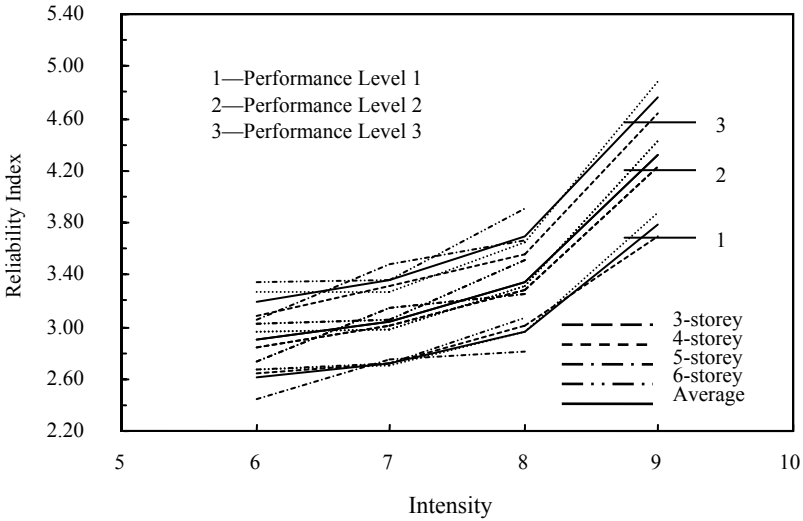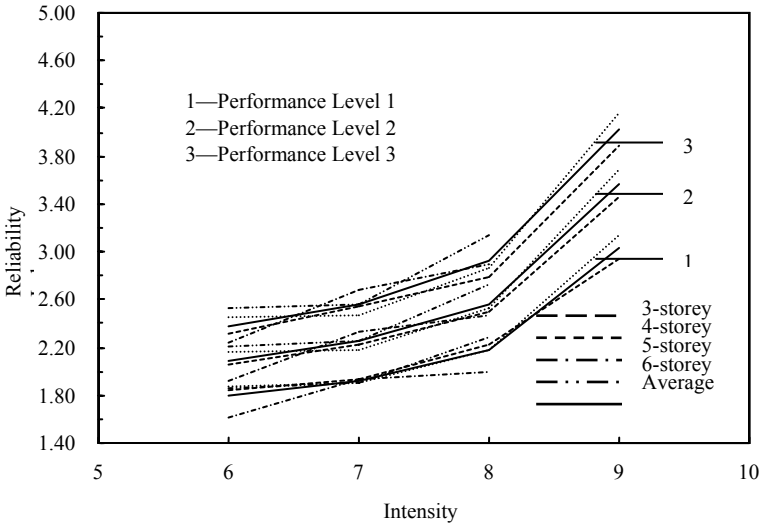

Figure 3. Seismic reliability indexes of multistory brick buildings designed for various intensities in region of intensity VIII at three performance levels.

Table 4. Seismic reliability indexes of multistory brick buildings designed for the basic intensity in region of intensity VII at three performance levels

Story Performance levels	Three-story	Four-story	Five-story	Six-story	Average
The first performance level	2.72	2.71	2.75	2.72	2.72
The second performance level	3.00	2.98	3.14	3.06	3.05
The third performance level	3.31	3.26	3.48	3.36	3.35

Table 5. Seismic reliability indexes of multistory brick buildings designed for the basic intensity in region of intensity VIII at three performance levels

Story Performance levels	Three-story	Four-story	Five-story	Six-story	Average
The first performance level	2.23	2.18	2.00	2.28	2.17
The second performance level	2.50	2.53	2.46	2.72	2.55
The third performance level	2.79	2.87	2.89	3.14	2.92

Tables 4 and 5 show that the seismic reliability indexes of multistory brick buildings designed for intensity VII in region of intensity VII are larger than those designed for intensity VIII in region of intensity VIII. This illustrates that the true reliability indexes of multistory brick buildings designed according to the current code in various region are different. Thus the goal of equal seismic safety fails to come true.

6. CONCLUSIONS

This paper presents the seismic reliability indexes of four multistory brick buildings in given regions of intensity VII and VIII at different performance levels by the Latin Hypercube Sampling technique and nonlinear seismic time history response analysis. The results illustrate that there are unbalanced reliability indexes of multistory brick buildings designed according to the current code in different regions. Thus the goal of equal seismic safety fails to come true.

In the current code, the seismic constructional columns of multistory brick buildings are treated as details of seismic design and installed according to experience

and thus are not considered in seismic analysis. The analytical results reveal that different grade of mortar and constructional columns of various story brick buildings designed for various intensities cause the unbalanced seismic reliability indexes. These results provide the basis for a performance-based seismic design method based on reliability of multistory brick buildings.

REFERENCES

Hwang, H.M. and Jing-Wen Jaw. (1990). Probabilistic Damage Analysis of Structures. *J. Struct. Engrg.* 116(7).

Zhang Ling-xin, Jin-ren Jiang and Jie-ping Liu. (2002). Seismic Vulnerability Analysis of Multistory Dwelling Brick Buildings. *Earthquake Engineering and Engineering Vibration.* 22(1): 49-55. (In Chinese).

Zhang Lingxin and Jinren Jiang. (1997a). Latin Hypercube Sampling and Its Application to Structural Reliability Analysis. *World Information on Earthquake Engineering.* 13(4): 1-6. (In Chinese).

National Standard of the People's Republic of China: Code for seismic design of buildings (GBJ11-89), Architectural Industry Press of China. (In Chinese).

Zhang Lingxin and Jinren Jiang. (1998). Nonlinear Seismic Response Analysis of Multistory Brick Buildings. *Proceedings of the 5th National Conference on Earthquake Engineering, Beijing*, 418-423. (In Chinese).

Zhang Lingxin and Jinren Jiang. (1997b). Method of Elasto-plastic Dynamic Response Analysis Based on Pattern of Self-equilibrating Stresses. *Earthquake Engineering and Engineering Vibration.* 17(4): 9-17. (In Chinese).

Jiang Jinren and Feng Hong. (1984). Conversion Between Power Spectrum and Response Spectrum and Artificial Earthquakes. *Earthquake Engineering and Engineering Vibration.* 43: 1-11. (In Chinese).

Jiang Jinren, Qinnian Lu and Jingjiang Sun. (1995). Statistical Characteristics of Strong Ground Motion Specified by Response Spectrum and Power Spectral Density Function. *Earthquake Research in China.* 9(4): 387-402. *Allerton Press, Inc. / New York.*

National Standard of the People's Republic of China: Design code for antiseismic of special structures (GB50191-93), Project Press of China. (In Chinese).

EVALUATION OF INELASTIC DISPLACEMENTS IN DETERIORATING SYSTEMS USING AN ENERGY-BASED APPROACH

Haluk SUCUOĞLU[1] and M. Altug ERBERIK[1]

ABSTRACT

Seismic performance of deteriorating systems is investigated by employing an energy-based approach. Low-cycle fatigue principle forms the basis of the analytical hysteresis model, which is based on two deterioration parameters. These parameters are calibrated by using experimental data in the literature obtained from reinforced concrete specimens subjected to constant and variable amplitude displacement cycles. The effect of stiffness and strength deterioration is studied by evaluating the ratio of the maximum inelastic displacements of deteriorating and non-deteriorating (elasto-plastic) systems (C_2 coefficient), calculated under 40 ground motion components recorded on stiff and soft sites. The results revealed that C_2 is independent from the yield strength and ductility characteristics, whereas it is strongly influenced from the level of deterioration and the site class. The values proposed in FEMA-356 capture the calculated trends in general, however they require better tuning with a more comprehensive classification of deteriorating systems by focussing on the characteristics of existing vulnerable buildings.

Keywords: C_2 coefficient; Strength deterioration; Energy-based hysteresis; Low-cycle fatigue; Inelastic displacement.

INTRODUCTION

Deterioration in the mechanical properties of concrete, steel and masonry structures are observed usually under repeated cyclic loading in the inelastic range due to low cycle fatigue. When these types of structures are subjected to strong ground motions, deteriorations in the stiffness and strength lead to larger displacements hence increased damage. Maximum inelastic displacements of equivalent SDOF systems can be approximated from the maximum displacements of the associated elastic SDOF systems either by using equivalent linearization, or by applying a set of displacement modification coefficients (Miranda and Ruiz-Garcia, 2002). This study focuses on the displacement coefficient that represents the effect of stiffness and strength deterioration on the inelastic displacement response, with reference to the inelastic response of a non-deteriorating elasto-plastic system.

[1] *Department of Civil Engineering, Middle East Technical University, Ankara 06531, Turkey*

The values of the displacement modification coefficients have been proposed first in the NEHRP Guidelines for Seismic Rehabilitation (Federal Emergency Management Agency, 1997) for different building framings systems and performance levels. The first coefficient C_1 is the spectral ratio of maximum inelastic to elastic displacements where the inelastic system exhibits negligible deterioration in stiffness and strength. Such an ideal inelastic performance may be displayed by new buildings designed and detailed to satisfy the requirements of modern seismic design codes. This coefficient is later studied extensively by Miranda (2000) for ground motions recorded on different soil conditions, and for several ductility factors. The second coefficient C_2 is the spectral ratio of the maximum inelastic displacements of deteriorating and non-deteriorating (elasto-plastic) systems. Existing structures that do not conform with modern code requirements usually exhibit significant deterioration under strong seismic excitation, therefore their maximum displacement responses are controlled more with the C_2 coefficient rather than the C_1 coefficient. Song and Pincheira (2000) and Gupta and Kunnath (1998) studied the influence of different hysteresis parameters on C_2. One problem that arises in their evaluation of C_2 is that the hysteresis models developed for representing the deteriorating systems depend on too many parameters, most of which are difficult to calibrate with experimental data. Miranda et al. (2002) evaluated the C_2 coefficient proposed in FEMA356 (Federal Emergency Management Agency, 2000) by employing a stiffness degrading model for representing the deteriorating systems. This is a limited evaluation however since stiffness degrading model is only suitable for a Type 2 Structure described in FEMA where C_2 is equal to unity.

An energy-based model is developed in this study that accounts for both the stiffness and strength deterioration (Sucuoğlu and Erberik, 2004). The model has been calibrated by using the results of experimental studies on concrete members subjected to constant and variable amplitude cyclic displacements. Then the C_2 coefficient is evaluated for different levels of deterioration under ground motions classified with respect to the site conditions.

ENERGY-BASED DETERIORATION IN STRUCTURAL SYSTEMS

Structural systems can be classified into two groups according to the behavior they exhibit when they are subjected to cyclic loading in the inelastic response range: (a) Non-deteriorating systems, (b) Deteriorating systems. Non-deteriorating systems exhibit no or very little strength loss under cyclic loading. Systems with stiffness deterioration are also included in this group. Such structures display stable hysteresis loops with constant energy dissipation in each constant-amplitude cycle. However deteriorating systems cannot maintain stable energy dissipation under cyclic loading and dissipated energy reduces with increasing number of cycles. Therefore cyclic energy dissipation capacity can be employed as a convenient measure in differentiating between non-deteriorating and deteriorating systems.

In this study, a two parameter low-cycle fatigue model is used to quantify the deterioration characteristics of structural systems (Erberik and Sucuoğlu, 2004; Sucuoğlu and Erberik, 2004). The relationship between the energy dissipation capacity per cycle (normalized with respect to the energy dissipated at the first cycle) and the number of constant amplitude cycles is defined in the form of an exponential function

$$\overline{E}_{h,n} = \alpha + (1-\alpha)\,e^{\beta\,(1-n)} \tag{1}$$

Here, $\overline{E}_{h,n}$ is the normalized dissipated energy at cycle n, α and β are the two fatigue parameters. The first parameter α is related to the ultimate level of deterioration at large values of n and the second parameter β is related to the rate of deterioration. A system with $\alpha = 0$ loses all of its energy dissipation capacity as $n \to \infty$ whereas a system with $\alpha = 1$ always retains its initial energy dissipation capacity (curve-A in Figure 1). An elastic-perfectly plastic system is an example of a non-deteriorating system, with $\alpha = 1$. The second parameter β has a wider range between 0 and ∞, and it represents the rate of loss in cyclic energy dissipation capacity. In the limit, $\beta = 0$ means no deterioration whereas $\beta = \infty$ defines a system which loses all of its energy dissipation capacity after completing the first cycle (curve-C in Figure 1). Curve-B in Figure 1 shows a typical system with realistic fatigue parameters having values between the upper and lower limits.
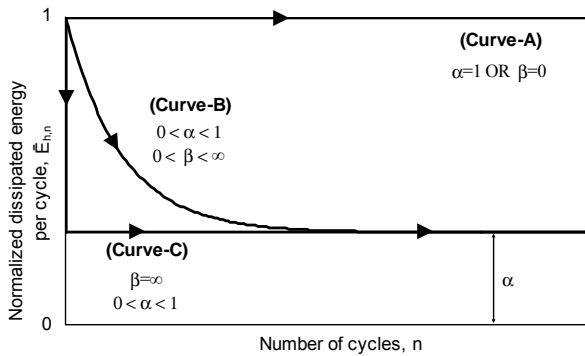

Figure 1. Energy-based fatigue model with two parameters (α, β).

Experimental results obtained from different reinforced concrete specimens are employed in order to calibrate the low-cycle fatigue parameters and to relate them to the general behavior of structural systems under cyclic excitations. The experimental data used is listed in Table 1 with the characteristic properties of each specimen. Code name of the specimens also indicate the researchers: WS (Wight and Sözen, 1973), SO (Saatçioğlu and Özcebe, 1989), PJ (Pujol, 2002), ES (Erberik and Sucuoğlu, 2004). The third column shows the pattern employed in the cyclic loading history:

constant amplitude loading (CA) or variable amplitude loading (VA). The following columns are the compressive strength of concrete (f_c), axial load level (N/f_cA_g), longitudinal reinforcement ratio (ρ_l) and transverse reinforcement ratio (ρ_t) and the low-cycle fatigue parameters α and β calibrated for each specimen in the list. For variable amplitude (VA) cyclic test data, an inverse solution procedure is employed to estimate the model parameters. This is achieved by employing a least square fit on the experimental cumulative dissipated energy versus the number of cycles.

Table 1. Properties of R/C beam column specimens under cyclic loading

No	Code Name	LH	f_c (MPa)	N/f_cA_g	ρ_l (%)	ρ_t (%)	α	β	Class
1	WS1	VA	34.7	0.117	2.4	0.3	0.25	0.50	SV
2	WS2	VA	34.7	0.117	2.4	0.3	0.30	0.30	SV
3	WS3	VA	26.1	0.147	2.4	0.5	0.55	0.60	MD
4	WS4	CA	33.5	0.115	2.4	1.5	0.85	0.20	SL
5	WS5	CA	33.5	0.115	2.4	1.5	0.90	0.30	SL
6	WS6	VA	33.6	0.071	2.4	0.3	0.60	1.20	MD
7	SO1	VA	43.6	0	3.2	0.9	0.25	0.60	SV
8	SO2	VA	34.8	0.141	3.2	1.7	0.60	0.40	MD
9	SO3	VA	32.0	0.153	3.2	2.5	0.80	0.60	SL
10	SO4	VA	37.3	0.131	3.2	2.0	0.95	0.30	SL
11	SO5	VA	39.0	0.126	3.2	2.0	0.95	0.40	SL
12	ES1	CA	20.6	0	1.3	0.8	0.16	0.75	SV
13	ES2	CA	21.2	0	1.3	0.8	0.26	1.16	SV
14	ES3	CA	20.6	0	1.3	0.8	0.23	0.81	SV
15	ES4	VA	20.6	0	1.3	0.8	0.15	0.80	SV
16	ES5	VA	21.2	0	1.3	0.8	0.30	0.90	SV
17	ES6	VA	21.2	0	1.3	0.8	0.15	0.50	SV
18	PJ1	VA	33.7	0.085	2.5	0.6	0.50	0.20	MD
19	PJ2	CA	29.9	0.096	2.5	0.6	0.45	0.30	MD
20	PJ3	CA	27.4	0.104	2.5	0.6	0.55	0.20	MD
21	PJ4	CA	36.4	0.158	2.5	0.6	0.65	0.30	MD
22	PJ5	VA	34.9	0.082	2.5	0.6	0.60	0.20	MD

In the last column of the table, the specimens are classified according to their estimated low cycle fatigue parameters. The abbreviation "SL" denotes theoretically a non-deteriorating, or in practice a slightly deteriorating system with α parameter closer to unity and β parameter closer to zero. Examples of this sort of behavior belong to test specimens WS4-5, SO3-5. For these specimens, parameter α ranges between 0.80-0.95 and parameter β ranges between 0.2-0.6. The force-displacement relationship for SO4 is shown in Figure 2.a. It represents a desired seismic behavior with stable loops and with little stiffness and strength deterioration.

Examples of moderate deterioration (MD) behavior belong to test specimens WS3, WS6, SO2 and PJ1-5 with parameter α ranging between 0.45-0.65 and parameter β ranging between 0.2-1.2. The observed behavior for "MD" type of structural members is gradual deterioration in strength with increasing cycle number, and slight pinching. However the specimen can still dissipate a considerable amount of energy after a significant number of cycles. Such a behavior is presented in Figure 2.b for the specimen WS6.
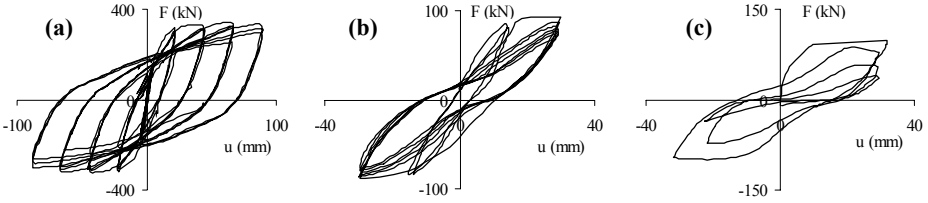

Figure 2. Force-displacement relationships for specimens (a) SO4, (b) WS6, (c) WS1.

Severely deteriorating (SV) structural members include test specimens WS1-2, SO1 and ES1-6. These specimens either have plain longitudinal bars, or low confinement ratio. When plain bars are used as longitudinal reinforcement, excessive bar slip occurs even in the early stages of displacement reversals leading to pinching and strength deterioration, which reduces the energy dissipation capacity significantly. The curves given in Figure 2.c for specimen WS1 validate this behavior.

For seismic performance evaluation of deteriorating structures, three different classes of structural systems are defined based on the experimental database. These classes are defined as slightly deteriorating (SL) systems, moderately deteriorating (MD) systems and severely deteriorating (SV) systems; a different pair of low cycle fatigue parameters (α, β) is assigned to each class. For SL systems, α=0.9 and β=0.3 are assigned as the low cycle fatigue parameters. Considering the experimental results, the values of the parameters α and β for MD systems are taken as 0.6 and 0.5 respectively. Finally the low-cycle fatigue parameters for SV systems are taken as α=0.3 and β=0.7, respectively.

Figure 3 presents the normalized dissipated energy per cycle ($\bar{E}_{h,n}$) versus cycle number (n) relationship for each specimen in Table 1, obtained by substituting α and β parameters into Equation 1. Three different levels of performance can be clearly distinguished from the grouping of the curves, each group corresponding to a class of structural system defined as SL, MD or SV. The sensitivity of the parameter α, which describes the ultimate level of deterioration in the energy dissipation capacity, to several structural characteristics has been evaluated by employing the experimental data base summarized in Table 1. It is observed that three fundamental characteristics of concrete members have a significant influence on the level of strength

deterioration. These are the type of reinforcing bars (plain or deformed), compressive strength of concrete, and the transverse reinforcement ratio (confinement).
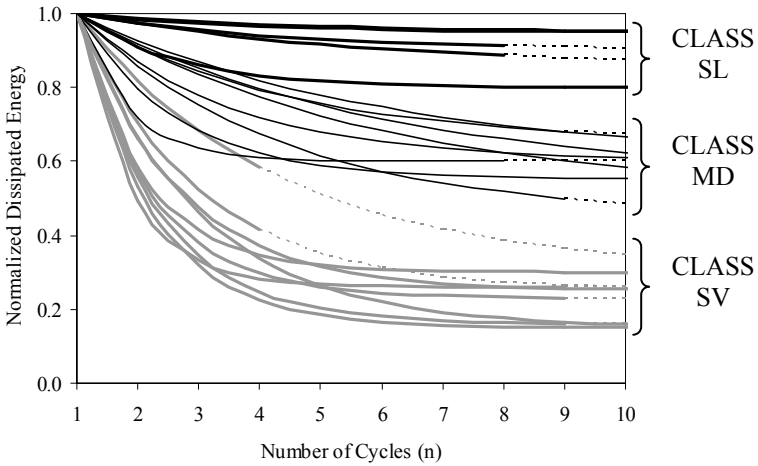

Figure 3. Variation of normalized dissipated energy ($\bar{E}_{h,n}$) per cycle vs. the number of cycles (n) for each specimen in Table 1.

Concrete strength, type of reinforcing bars and the amount of confinement implemented in construction are easily identifiable parameters for an existing building. A decision chart indicating the level of deterioration can be designed based on the range of values for these three parameters. Table 2 presents the proposed decisions for slight, moderate and severe levels of deterioration. The values on the left in each cell are for deformed bars, and those in parentheses are for plain bars. The levels printed in bold are the ones conforming to the experimental results of Table 1.

Table 2. Decision chart for the levels of strength deterioration

Concrete Strength (MPa)	Confinement Ratio (%)		
	≤ 0.5	$0.5 - 1.0$	≥ 1.0
≤ 15	SV (SV)	MD (SV)	NA
15-25	SV (SV)	**MD (SV)**	SL (MD)
≥ 25	**MD** (NA)	**MD** (MD)	**SL** (MD)

NA: Not applicable in practice

SENSITIVITY OF INELASTIC AND RESIDUAL DISPLACEMENTS TO DETERIORATION LEVEL

The influence of the level of deterioration on inelastic and residual displacements is demonstrated by calculating the displacement time histories of a SDOF system that

represents moderate height buildings, designed for a base shear coefficient of 20 percent. Elastic displacements are also calculated for comparison. It is notable to observe in Figure 4 that even slight deterioration has a major influence on inelastic displacements. Moreover, the residual displacements, which are consistent indicators of permanent damage at the end of ground excitation, accumulate to values exceeding the peak displacement of elastic system. When the level of deterioration is severe, both maximum and residual displacements reach values twice as much as those for the slight and moderate deterioration levels. A severely deteriorating system here represents majority of existing buildings constructed with plain reinforcing bars and lacking confinement at the critical sections.
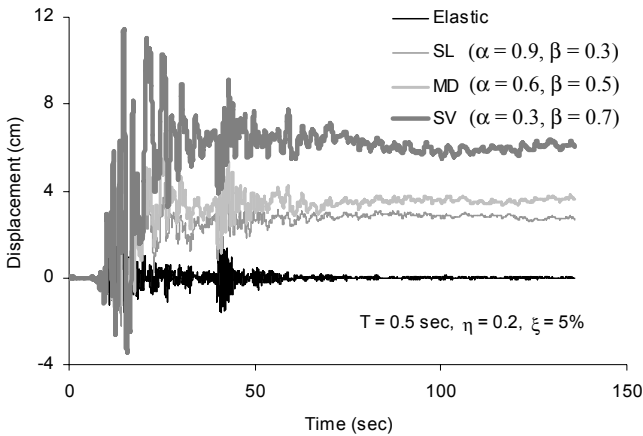

Figure 4. Displacement responses of a SDOF system with three levels of performance subjected to Marmara 1999 Earthquake, YPT Record, NS Component (also compared with the elastic response).

ENERGY BASED HYSTERESIS MODEL FOR DETERIORATING SYSTEMS

A simple piece-wise linear hysteresis model is developed for representing the force-deformation response of deteriorating SDOF systems. It operates on a bilinear skeleton curve and based primarily on the stiffness degrading model (Clough, 1966), extended with an energy-based memory for simulating strength deterioration. The energy-based fatigue model given in Equation 1 is employed for calculating the reduction in the energy dissipation capacity under repeated inelastic displacement cycles. Once the reduced energy dissipation capacity at an equivalent cycle number is predicted by the model, the force-displacement path is determined by reducing the strength capacity of the deteriorating system accordingly. Pinching is not considered explicitly in the generated force-deformation reloading paths, however loss of energy dissipation capacity due to pinching, or anchorage slip in reinforced concrete

members, is the main feature of the model. A sketch of the model is given in Figure 5. The governing rules and details of the hysteresis model can be found in Sucuoğlu and Erberik (2004).

Figure 6 demonstrates that the hysteresis model simulates the observed energy dissipation reasonably well for the test specimen PJ2 under constant amplitude cyclic loading, although the parameter estimation is based on cumulative dissipated energy variation. In figure, the comparison of the experimental and analytical force-displacement curves is given on the left and the comparison of the experimental and predicted normalized dissipated energy per cycle ($\bar{E}_{h,n}$) vs. the cycle number relationship is given on the right. The same model can also predict energy dissipation characteristics under variable amplitude loading as shown in Figure 7 for the specimen ES4. Cumulative dissipated energy per half-cycle (ΣE_h) vs. half-cycle number relationship for ES4 is used for comparison since variable amplitude is not symmetric and amplitude of loading changes per half-cycle.
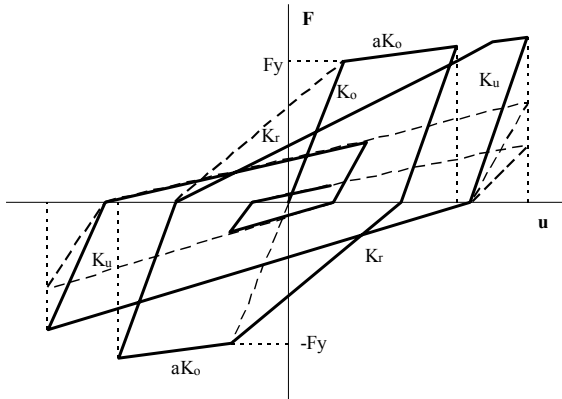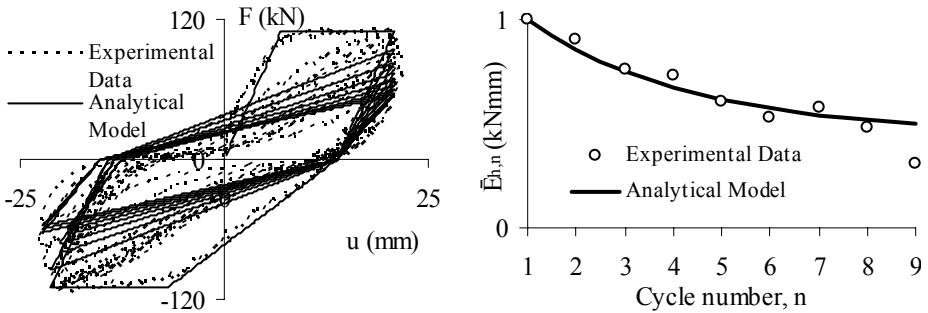

Figure 5. Energy-based hysteresis model.

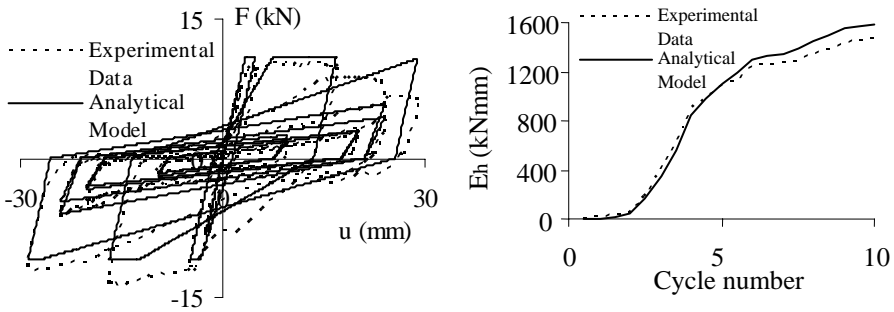**Figure 6. Comparison of experimental data and analytical model for PJ1.**

428

Figure 7. Comparison of experimental data and analytical model for ES4.

STRONG GROUND MOTIONS

A set of 40 strong motion records are selected from 14 different earthquakes. The dates and magnitudes of the earthquakes are Tokachi Oki 1968 (8.2), Chi-Chi 1999 (7.6), Kocaeli 1999 (7.4), Miyagi Oki 1978(7.4), Kern County 1952 (7.4), Kobe 1995 (6.9), Loma Prieta 1989 (6.9), Erzincan 1992 (6.9), Gazli 1976 (6.8), Spitak 1988 (6.8), San Fernando 1971 (6.7), Imperial Valley 1979 (6.5), Irpinia 1980 (6.5) and Whittier Narrows 1987 (6.0).

These 40 ground motion components are grouped with respect to the site conditions as stiff (NEHRP B, C) and soft (NEHRP D, E). There are 20 ground motion components in each group. The mean elastic acceleration and displacement response spectra of each group are shown in Figures 8.a and 8.b, respectively, for 5% damping. It is observed that the intensity levels of the two groups are similar in short and medium period ranges, however ground motions recorded on soft soil sites exhibit larger intensities than those on stiff sites at periods longer than 0.8 seconds. The results presented in the following section are arranged for considering the influence of site characteristics on inelastic displacements of deteriorating systems.
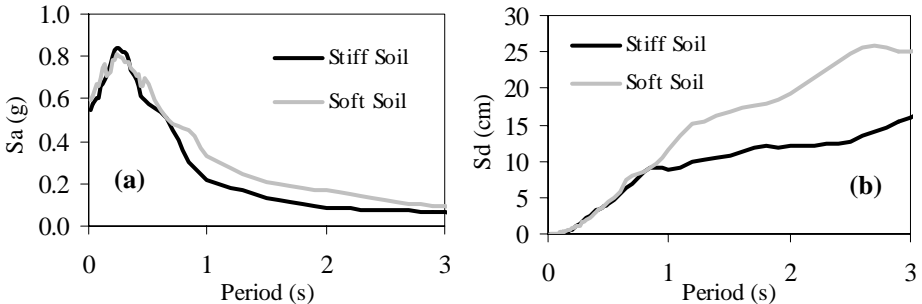

Figure 8. Mean elastic acceleration and displacement spectra for each group.

RESULTS, DISCUSSIONS AND CONCLUSIONS

The results are obtained for different normalized yield strength parameters C_y, which is described as the ratio of yield strength to the total weight mg. Four different C_y values are considered: 0.1, 0.2, 0.3 and 0.4. The mean spectral distributions of the C_2 coefficient are then classified for the stiff and soft soil sites, and for slightly (SL), moderately (MD) and severely (SV) deteriorating systems separately, resulting in six combinations. These spectral relations are shown in Figures 9.a-f. In all presented results, the C_2 coefficient are defined as the mean ratios of the maximum inelastic displacements of deteriorating to non-deteriorating (elasto-plastic) systems. Mean values are calculated over the dynamic responses to 20 ground motions.

A general observation can be easily made on the effect of normalized yield strength C_y from the set of six spectral graphics in Figures 9. There is no consistent trend in the variation of C_2 with C_y. This is somewhat expected because both the numerator and the denominator of C_2 are equally influenced by the yield strength Cy. Therefore C_2 can be evaluated independent from the yield strength, accordingly independent from the ductility ratio. The definition of C_2 in FEMA 356 (2000) is consistent with these observations.

The slightly deteriorating systems (SL) defined herein are equivalent to Type-2 frames in FEMA 356, where C_2 is assigned a constant value of unity. Figure 11.a reveals that this is reasonable for stiff sites, however Figure 11.b does not confirm this assumption for soft sites. An inverse exponential variation of C_2 from 1.5-2.0 at short periods, to 1.0 at periods in the vicinity of the site period T_s is clearly observed from Figure 9.b.

Moderately and severely deteriorating systems (MD and SV) defined in accordance with Figure 3 are classified as Frame Type-1 in FEMA 356, without further distinction. The spectral distributions of the C_2 coefficient for these systems are shown separately in Figures 9.c-f, along with the values proposed in FEMA-356 T_s is taken as 0.5 second for stiff sites (NEHRP B, C), and 0.8 second for soft sites (NEHRP D, E), respectively, in constructing the FEMA curves.

Before comparing the values proposed by FEMA with the calculated values, three different C_2 levels described in FEMA for immediate occupancy, life safety and collapse prevention performances deserves critical attention. A target displacement has to be related to the return period of the seismic hazard in a probabilistic assessment, whereas the performance limit states are for controlling the acceptance of member performances when the system attains the target displacement. Three different levels for C_2, and accordingly for the target displacement is confusing and not practical in implementation.

It can be observed from Figures 9.c-f that as deterioration level increases from moderate to severe, C_2 displays an increasing trend over the entire period range. This is valid for both stiff and soft sites respectively. Further, mean C_2 approaches unity at longer periods. The period where C_2 reaches unity is somewhat closer to T_s for MD systems whereas it is longer for the SV systems.
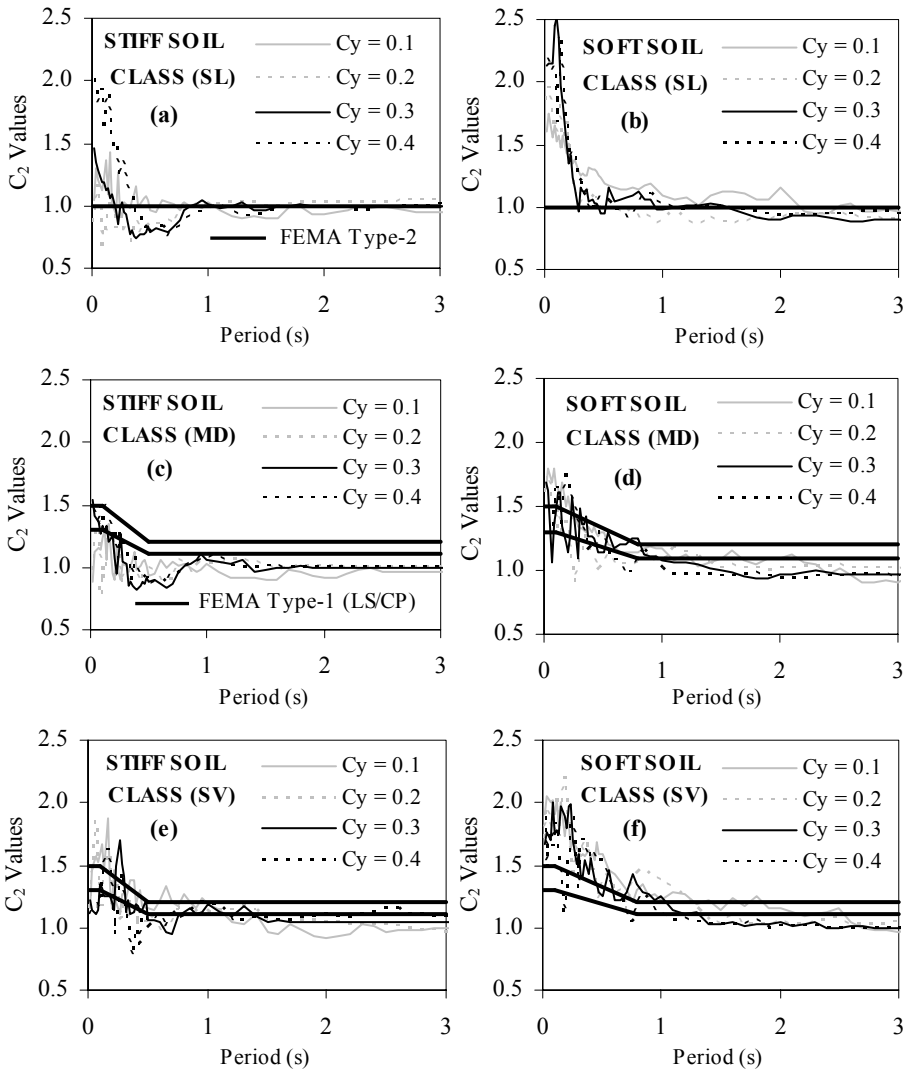
Figure 9. Comparison of mean deformation ratio of deteriorating systems (SL, MD, SV) to elasto-plastic systems with C_2 coefficient for stiff and soft soil conditions.

FEMA curves overestimate the calculated values generally along the long period range for MD and SV systems on both stiff and soft sites. Along the short and moderate period ranges ($T<T_s$), they overestimate the C_2 values for MD systems on stiff sites and reasonably estimate them on soft sites. The reverse is true for the SV

systems, where FEMA estimations are reasonable on stiff sites but unconservative on soft sites in the period range T<Ts.

REFERENCES

Clough, R. W., S. B. Johnston. (1966). Effect of stiffness degradation on earthquake ductility requirements. *Proceedings, 2ⁿᵈ Japan National Conference on Earthquake Engineering*: 227-232.

Erberik, M. A., H. Sucuoğlu. (2004). Seismic energy dissipation in deteriorating systems through low-cycle fatigue. *Earthquake Engineering and Structural Dynamics* 33: 49-67.

Federal Emergency Management Agency. (1997). *NEHRP Guidelines for the Seismic Rehabilitation of Buildings: FEMA 273 (Guidelines) and 274 (Commentary).* Washington, DC.

Federal Emergency Management Agency. (2000). *Prestandard and Commentary for the Seismic Rehabilitation of Buildings: FEMA 356.* Washington, DC.

Gupta, B., S. K. Kunnath (1998). Effect of hysteresis model parameters on inelastic seismic demands. *Proceedings, 6ᵗʰ US National Conference on Earthquake Engineering*, Washington, DC.

Miranda, E. (2000). Inelastic displacement ratios for structures on firm sites. *Journal of Structural Engineering* 126: 1150-1159.

Miranda, E., D. S. Akkar. (2002). Evaluation of approximate methods to estimate target displacements in nonlinear static procedures. *The 4ᵗʰ U.S.-Japan Workshop on Performance-Based Earthquake Engineering Methodology for R/C Building Structures*. Toba, Japan.

Miranda, E., J. Ruiz-Garcia. (2000). Evaluation of approximate method to estimate maximum inelastic displacement demands. *Earthquake Engineering and Structural Dynamics* 31: 539-560.

Pujol, S. (2002). Drift capacity of reinforced concrete columns subjected to displacement reversals. *Ph.D. Thesis*, Purdue University, IN.

Saatçioğlu, M., G. Özcebe. (1989). Response of reinforced concrete columns to simulated seismic loading. *ACI Structural Journal,* January - February: 3-12.

Song, J-K, J. A. Pincheira. (2000). Spectral displacement demands of stiffness and strength degrading systems. *Earthquake Spectra* 16: 817-851.

Sucuoğlu, H., M. A. Erberik. (2004). Energy-based hysteresis and damage models for deteriorating systems. *Earthquake Engineering and Structural Dynamics* 33: 69-88.

Wight, J. K., M. A. Sözen. (1973). Shear strength decay in reinforced concrete columns subjected to large deflection reversals. *Structural Research Series No. 403, Civil Engineering Studies*, University of Illinois, Urbana-Champaign, IL.

REINFORCED CONCRETE STRUCTURAL WALLS AS SOLUTION TO RETROFIT A R/C FRAME

Patricio BONELLI[1], Rubén BOROSCHEK[2]

ABSTRACT

A retrofitting methodology applied to a six-story R/C frame building is described. The original building is a typical limited ductility design moment resistant frame of the seventies, i.e., with insufficient splice length for longitudinal reinforcement, insufficient amount of ties in columns and no reinforcement in joints. A previous vulnerability study showed that the structure could have a brittle failure. The frame could be reinforced jacketing all the columns and reinforcing all the external joints, but large drifts could make the building loose its functionality under an expected earthquake in the area.

Adding reinforced concrete walls in facades and at interior frames was selected as the final solution after a cost-benefit analysis, since lateral displacements can be reduced as stiffness increases, decreasing ductility demands in joints and shear stresses in beams and columns, so that the frames mainly acted as gravitational systems. Acceptance criteria for the retrofit are based on functional restrictions and drift control.

Keywords: Retrofitting; Structural walls; Brittle frames; Shear demands; Non-linear analysis; and Column jacketing.

1. INTRODUCTION

Different modes of failure have occurred in earthquakes in the 1970's type of reinforced concrete frames. Typically they are: shear failure in columns and joints, sliding of longitudinal reinforcement due to insufficient splice development and local buckling in longitudinal reinforcement in columns. In Chile there are a few reinforced concrete frame buildings that could show this behaviour.

This paper presents a procedure applied to an existing building to detect possible modes of failure and retrofit alternatives using Performance Based Seismic Design.

[1] *Departamento de Obras Civiles, Universidad Técnica Federico Santa María, Casilla 110 V, Valparaíso, Chile, Fax: +56-32-654115, Email: patricio.bonelli@usm.cl*

[2] *Civil Engineering Department, Faculty of Physical and Mathematical Sciences, University of Chile, Blanco Encalada 2002, Santiago, Chile, Email: rborosch@ing.uchile.cl*

The case study is a Hospital in the North of Chile. The structure is a reinforced concrete frame building, designed in the seventies, that is vulnerable to brittle shear failure in columns at very low lateral displacements demands.

2. CASE STUDY

A typical plan view and longitudinal elevation of one of the buildings are shown in figure 1. A cross section of a column is shown in figure 2. Table 1 shows the dimensions of the cross section and the amount of reinforcement in the columns.

The Magnitude Mw = 8.4, 2001 Earthquake in the South of Peru caused important non-structural damages in the building, loosing its functionality, but with minor structural damages. Surgery rooms and in general partition walls suffered moderate and severe cracking. In this case it was considered that operation rooms could not be used if their walls were cracked. This fact showed the need to apply performance-based design criteria in the design and retrofitting of hospitals, as it is not enough to ensure the structural integrity, but to allow the functionality protection of the system. The Hospital was evacuated due to the pressure of the personnel that was worried about visible damage and loose of functionality. Patients were moved to an old 1940's two-story confined masonry building next to the Hospital that suffered no damage.

3. SHEAR STRENGTH AND SHEAR DEMANDS OF EXISTING COLUMNS

Existing columns have double 10-millimeter diameter ties spaced every 20 centimetres. Interior ties have been placed alternating its direction. Thus if shear forces produced a crack with an inclination of 30 degrees, the arrangement of the reinforcement allows only two 10-mm diameter to resist the shear forces, as shown in figure 2 for a column of the second floor. Severe corrosion of the transverse reinforcement at base columns was observed during an inspection of the building. For this reason in the analysis it was considered that the shear strength of the main element is due only to the contribution of the concrete. Also the number and disposition of existing ties did not comply with modern ACI 318 codes.
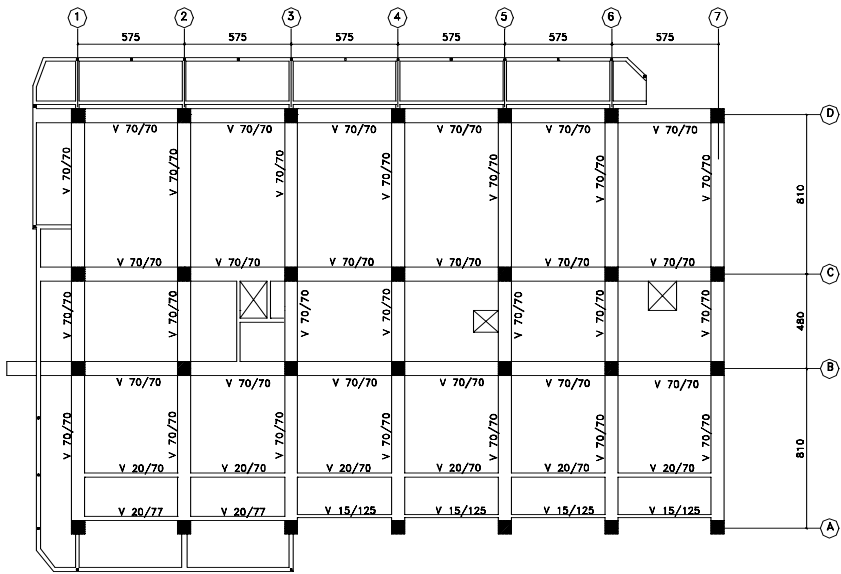
(a) Plan view
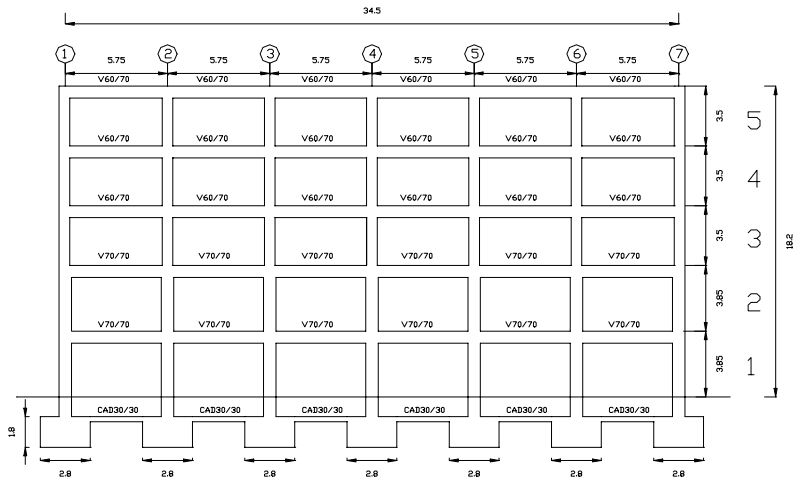
(b) Elevation

Figure 1. Plan view and longitudinal elevation.

435

Table 1. Dimensions and amount of reinforcement of columns

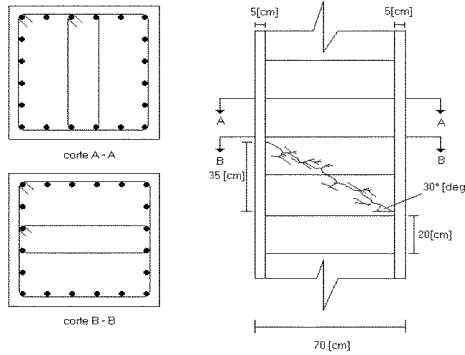| Floor	Dimension [cm]	Longitudinal reinforcement	Transversal reinforcement
1	70x70	36φ26	2Eφ10@20
2	70x70	20φ26	2Eφ10@20
3	60x60	28φ26	2Eφ10@20
4	60x60	20φ26	2Eφ10@20
5	60x60	16φ26	2Eφ 8@20

Figure 2. Cross section of the columns and arrangement of ties.

4.   SHEAR DEMAND CALCULATED WITH EARTHQUAKE RECORDS, BY NON-LINEAR ANALYSIS

4.1   Time History Analysis

In this study, two Chilean March 3, 1985 earthquake records, Viña del Mar (0.35 g) and Llolleo (0.67 g) were chosen to estimate the possible demands. The fault mechanism of the expected seismic action at the site and its epicentral distance are similar to the ones that generated the selected records. In the vulnerability study of the building, a maximum acceleration of 0.55 g was estimated [1]. This value was used to scaled Viña del Mar S20W records to 055g. In the analysis, because the columns of

the existing building have a low shear resistance and they could suffer brittle failure, a 2% damping ratio was considered.

Figure 3 shows the maximum bending moment and shear forces calculated with Llolleo N10E and Viña del Mar S20W scaled to 0.55g records. If columns had had larger shear strength, the bending moments drawn in figure 3 would have been reached, yielding some columns in the base of the third and fourth floors. Envelopes of shear calculated for a 5% damping ratio were very similar to the ones calculated with a 2% damping.

Llolleo   Viña del Mar
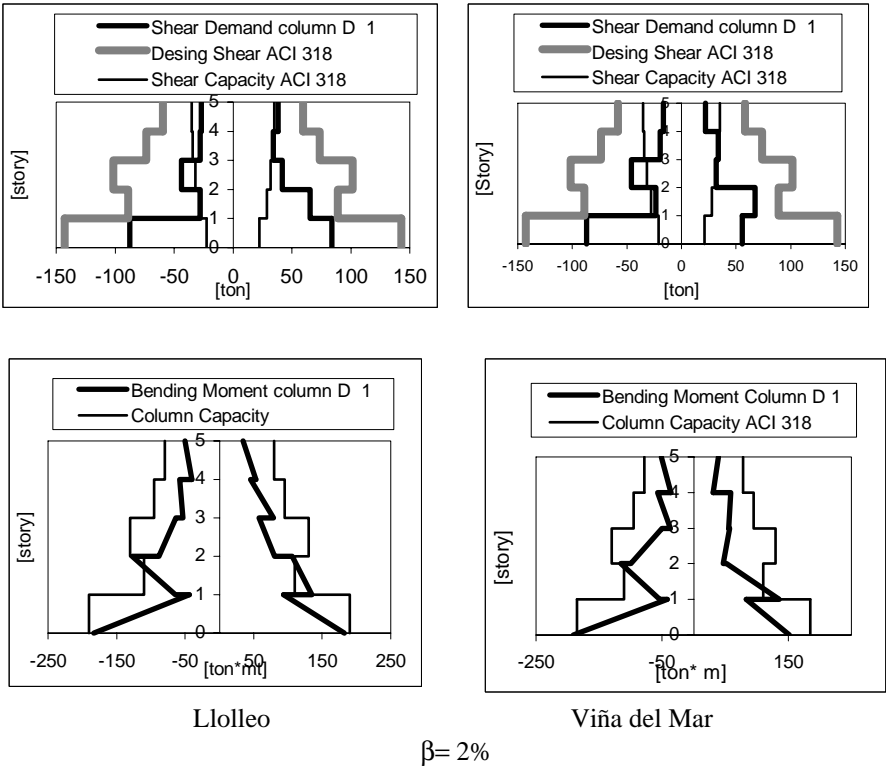
β= 2%

Figure 3. Shear and bending moment envelopes.

4.2   Incremental Analysis

Base shear versus roof displacement for the longitudinal direction of the building, calculated from applied uniform and inverted triangular distributed loads are shown in figure 4. Additional marks are included in the figure to show the maximum displacement demands for the records, calculated with a non-linear dynamic analysis, and the results of an elastic linear analysis with the elastic spectrum of the Chilean Code.
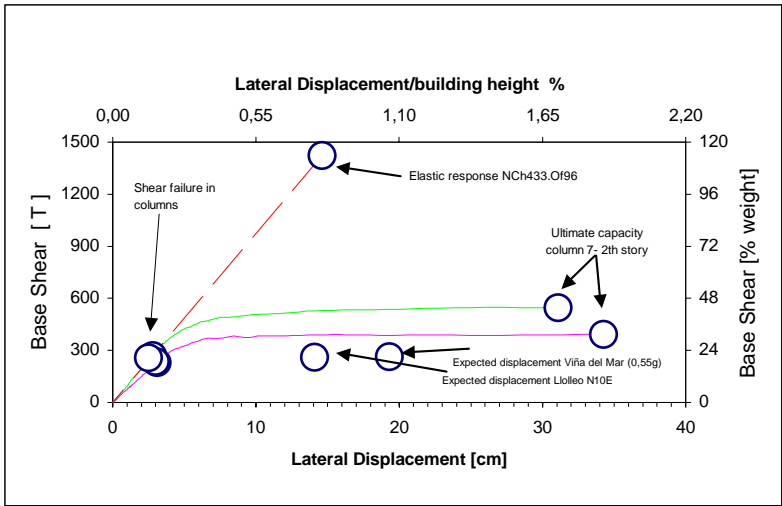

Figure 4. Basal shear vs. displacement of the roof.

5. SHEAR STRENGTH IN COLUMNS

Only the concrete contribution, Vc, to shear resistance of columns was considered in the analysis. Since shear resistance depends on axial forces, their magnitude was obtained from the Llolleo record response, considering 2% of damping ratio. With these values available, shear resistance varies between 43 [tons] and 22 [tons]. The available shear resistance of the existing columns, calculated with ACI 318-99, does not allow the columns to reach their flexural capacities.

Since ACI 318 is conservative, to estimate the shear in columns that do not suffer tension axial forces, the internal column shear resistance was also calculated with expressions obtained experimentally by Ang, Priestley and Paulay [2],[3]. In this case the contribution of the concrete to the strength of the shear can be estimated as:

$$V_c = 0.37 \cdot \alpha \cdot \left(1 + \frac{3P}{f'_c \cdot A_g}\right) \cdot \sqrt{f'} \cdot A_g \qquad [MPA]$$

Eq.(1)

where:

$$\alpha = \frac{2}{\left(M/(V \cdot D)\right)} \geq 1$$

Eq.(2)

P is the axial compression force, Ag the gross area, Ag the effective area (0,8·Ag), M the moment, V the shear and D the diameter of the confined concrete area.

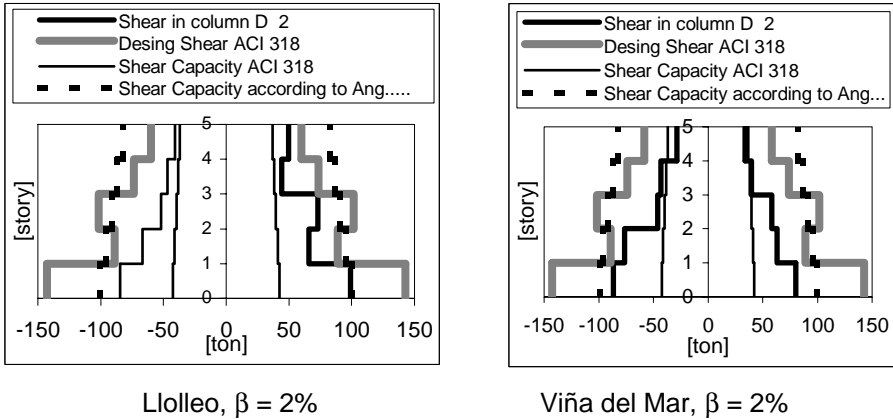Llolleo, β = 2%   Viña del Mar, β = 2%

Figure 5. Shear capacity and shear demands in columns.

Column shear capacity of existing columns is compared in figure 5 to the shear demands of the considered records.

The exterior columns, which could be in tension during an earthquake, would have less shear resistance than the interior ones, which remain under compression during the whole response. The record of Viña del Mar S20W scaled to 0.55g has a displacement demand on the structure of 14.1cm (0.8% of height). If columns at the perimeter are not reinforced with jackets, they could resist the earthquake without a shear failure only for displacements below 2.5 [cm]. Therefore, all exterior columns of the building and in all floors must be reinforced.

An option to meet the required shear strength, as indicated in ACI 318 -Chapter 21, would be to add jackets to the columns with reinforced concrete, steel plates or carbon fibers.

When adding jackets to columns, the building could sustain lateral displacements as large as 31.1 [cm] (1.71% of height), enough to withstand all the considered demands satisfactorily[4]. .

This type of analysis helps to decide if reinforcement of a building is mandatory and provides a criterion to decide whether to evacuate or not the building if a severe seismic action is expected. In this case, the probability to have a shear failure in columns is very high.

When reinforced concrete jackets are used, the requirements are met with single 16 mm diameter ties every 6 cm (E Φ16@6) in plastic hinges zones and every 9 cm (E Φ16@9) in the rest of the column. Use of carbon fibers was evaluated but discarded because their cost was four times the cost of the other solutions.

6. WALLS AS AN ALTERNATIVE SOLUTION

Jacketing columns and reinforcing joints could be a reasonable solution to maintain the structure safe, but to avoid non structural element damage and assure functionality of the building it is wise to decrease drift demands and also to provide a corresponding seismic design to non-structural elements. Displacement demands can be decreased considerably, isolating the building at the base or increasing the stiffness of the building with structural wall or braces. Several options were examined and only one of the selected options is shown in Figure 6. It consists on adding reinforced concrete walls of 30 cm thickness in direction X and 40 cm in direction Y. This solution has been suggested because similar buildings that have this structural system had a satisfactory response in previous Chilean earthquakes. The use of structural walls in facades as retrofit strategies has several advantages: it lowers the cost of the final building because additional architectural facades are reduced because they are transformed into structural elements. The long length of these walls permits control of overturning moments, in this case if the walls are supported on a grade beam that connects existing footings, no additional foundations are needed. Concentrating the retrofitting elements on the perimeter of the building reduces functional interference.

The analysis of this solution was made with the Viña del Mar record scaled to 0.55g, for a damping ratio of 3%, because wall and beam cracks are expected, assuming that the columns will remain with minor cracking.

Figure 7 shows the required shear strength and the demands of the bending moment in an external column. Even though in direction X the proposed wall density is different than that the one used in direction Y, results were very similar.
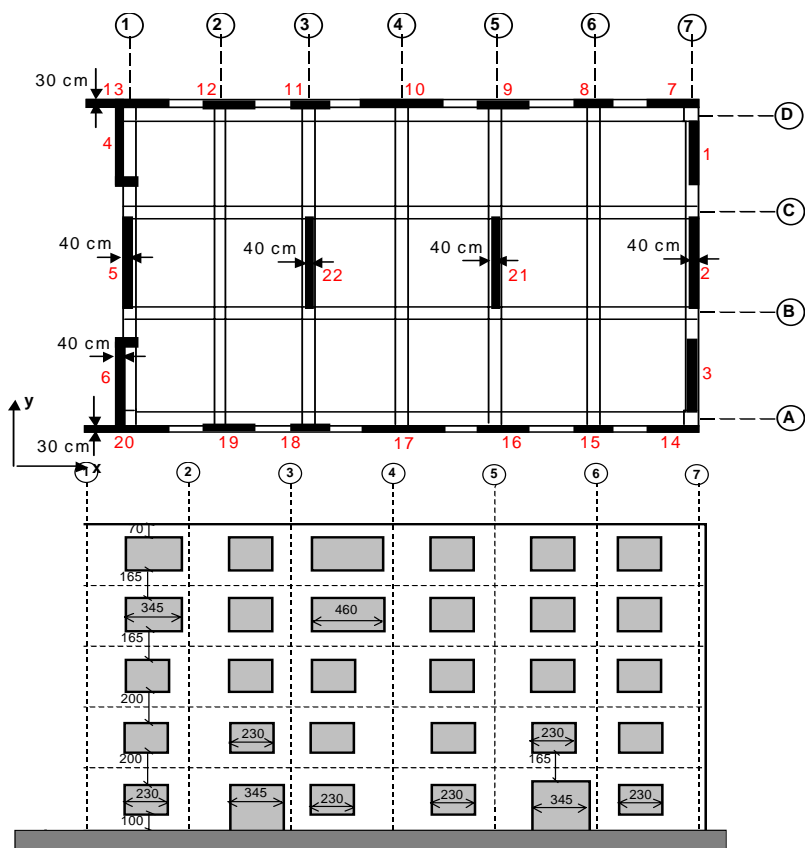
Figure 6. Plan view and elevation.
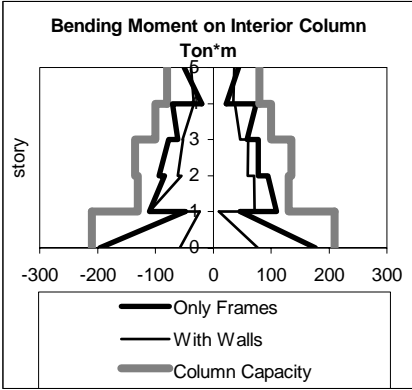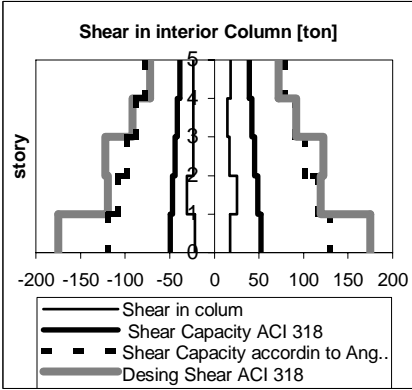
Figure 7. Shear and bending moment demands and lateral displacement envelopes.

Figure 8 compares the lateral displacement envelopes at the original frame building with the retrofitted structure. The abrupt change in stiffness and strength at columns at the first floor produces the observed reduction in drift at first level. Walls reduce overall displacement and change the deformed shape decreasing shear demands in every element and joint.
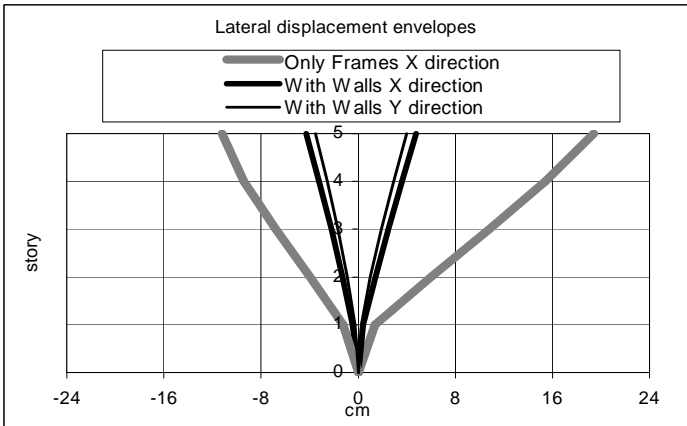
Figure 8. Lateral displacement envelopes.

442

7. CONCLUSIONS

In the analysed frame building, a shear failure in columns could occur for very small deformations. When structural walls are included, the demands of the displacements are drastically reduced, and the alteration of the deformed shape decreases the strength demands in the elements of the frames. The analysed building reaches expected lateral deformations before critical beam sections yield. Nevertheless, the increase in accelerations due to the increase in stiffness must be taken into account in the design of non-structural elements.

REFERENCES

1. Boroschek, R. 2000. "Estudio de la Vulnerabilidad sísmica del Hospital Juan Noe Crevani de Arica: Un modelo". Fundación para la Transferencia Tecnológica Universidad de Chile. Santiago de Chile, Julio.
2. Priestley, M. J. Nigel, Yan Xiao and Ravindra Verma. 1994. "Steel Jacket Retrofitting of Reinforced Concrete Bridge Columns for Enhanced Shear Strength — Part 2: Test Results and Comparison with Theory". ACI Structural Journal, V.91,No.5, September-October, pp.537-551.
3. Priestley, M. J. Nigel, Frieder Seible, Yan Xiao and Ravindra Verma. 1994. "Steel Jacket Retrofitting of Reinforced Concrete Bridge Columns for Enhanced Shear Strength — Part 1: Theoretical Considerations and Testing Design". ACI Structural Journal, V.91,No.4, July-August, pp.394-405.
4. Aboutaha, Riyad S., Michael D. Engelhardt, James O. Jirsa and Michael E. Kreger. 1999. "Experimental Investigation of Seismic Repair of Lap Splice Failures in Damaged Concrete Columns". ACI Structural Journal, V.96, March-April, pp.297-306.

PERFORMANCE-BASED SEISMIC ASSESSMENT OF TWO PRECAST CONCRETE HYBRID FRAME BUILDINGS

Sri SRITHARAN[1] and Ataur RAHMAN[2]

ABSTRACT

The application of precast concrete hybrid frames has gained popularity in high seismic regions due to their unique features, which include minimum structural damage when subjected to earthquake loading and the re-centering capability. The hybrid frame that utilizes a combination of mild steel reinforcement and unbonded prestressing to connect precast beams and columns has been implemented in a few structures in high seismic regions of the United States. This frame was also one of the four jointed frames included in a large-scale five-story building test conducted as part of the PRESSS (PREcast Seismic Structural System) program. The use of mild steel and prestressing steel at the connections reduces the hysteresis energy dissipating ability of the frame when compared to an equivalent monolithic concrete frame. Utilizing the test results obtained from the PRESSS building to validate the analytical models and defining acceptance criteria based on transient and residual inter-story frame drifts, this paper presents a multiple-level performance-based assessment of two five-story precast hybrid frame buildings. Based on the prototype building from the PRESSS program, the analytical investigation was conducted at a 60 percent scale so that a direct comparison between the analytical results and PRESSS test data would be possible.

Keywords: Precast; Concrete; Hybrid frame; Performance-based; Seismic; Assessment.

1. INTRODUCTION

1.1   Framing Concept

The hybrid framing concept is used to establish moment-resisting frames from single-bay precast concrete beams and multi-story high precast concrete columns. Figure 1 shows typical details of a hybrid frame, in which the beams and column are connected using unbonded post-tensioning tendons and mild steel reinforcement across the precast interfaces at the mid-height and closer to the top and bottom surfaces of the beams, respectively. Prior to post-tensioning, the interfaces and ducts housing the

---

[1]*Assistant Professor, Department of Civil, Construction and Environmental Engineering, Iowa State University, Ames, IA 50011, USA*

[2]*Graduate Research Assistant, Department of Civil, Construction and Environmental Engineering, Iowa State University, Ames, IA 50011, USA*

mild steel reinforcement are filled with non-shrink cementituous fiber grout. The grout at the interfaces ensures continuity between precast members while grouting the ducts enables the reinforcement to contribute to the stiffness and strength of the hybrid frames. The mild steel reinforcing bars are debonded over a short length near the interfaces to control the inelastic strain accumulation and avoid premature fracture of the reinforcement. A friction mechanism is relied upon for shear transfer across the precast connection interface.

The hybrid frame concept has been studied over the past decade, which included experimental verification using component (Stone et al. 1995; Stanton et al. 1997) and structure level testing (Priestley et al. 1999; Sritharan 2002). More recently, the hybrid frame has been implemented in a few buildings including a 38-story apartment complex in San Francisco, California (Englekirk 2002).
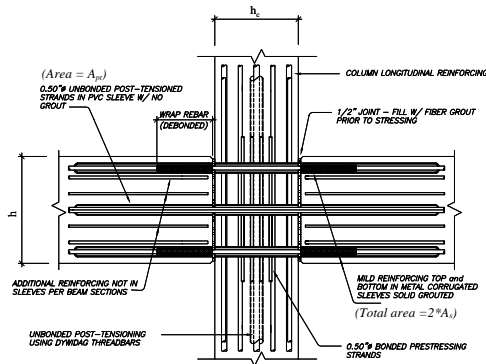

Figure 1. The connection details of a precast hybrid frame.

1.2   Benefits

The use of unbonded steel reinforcement at the precast connections causes flexural cracks to concentrate at the beam ends. Consequently, the beams will undergo minimal structural damage when the hybrid frame is subjected to inelastic lateral deformations. An added benefit of reducing the beam damage is that the frame elongation resulting from the formation of plastic hinges at the beam ends will be smaller than that expected in a monolithic concrete frame. Nonlinear elastic response from the unbonded post-tensioning tendons and hysteretic behavior from the mild steel reinforcement will enable the hybrid frames to dissipate energy and minimize residual displacements. The reduced residual displacements will also make these frames less sensitive to P-Δ effects. The post-tensioning tendons that run across the column width reduce the principal tensile stresses in the beam-to-column joints. The reduction to the principal tensile stress suggests that the amount of joint shear reinforcement could be reduced when compared to the joints in equivalent conventional concrete frames.

2. HYBRID FRAME BUILDINGS

Two precast hybrid frame buildings were chosen for the analytical investigation reported in this paper. Developed from the prototype building shown in Figure 2, these hybrid frame buildings represented the prototype building at 60 percent scale. Furthermore, only two of the four bays in the prototype seismic frames were modeled in the hybrid frame buildings. These modifications were consistent with the procedures used to create the PRESSS test building that was subjected to rigorous seismic testing (Nakaki et al. 1999; Priestley et al. 1999; Sritharan 2002). Including the hybrid details in the lower three floors of a seismic frame, the PRESSS building was designed with four different precast frame connections.

A typical floor plan and an elevation view of a typical seismic frame in the hybrid frame buildings are shown in Figure 3. As seen in the plan view, these buildings consisted of two identical seismic frames in one direction and a precast wall system in the orthogonal direction as the primary lateral load resisting systems. The analytical investigation was performed for these buildings in the frame direction of response.
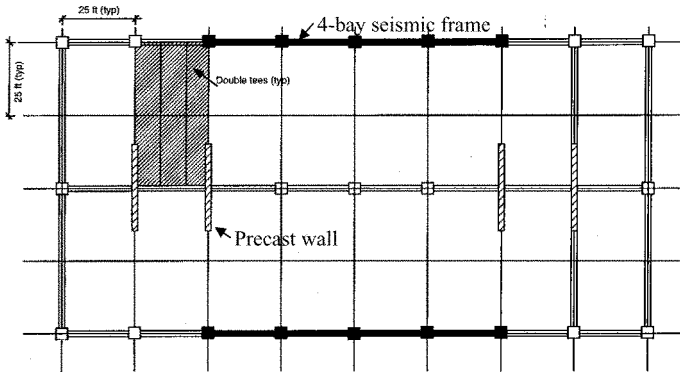
Figure 2. Plan view of the precast concrete prototype building.

The first hybrid frame building, referred to as HFB1, was dimensioned and detailed using a direct-displacement based design (DBD) method that was adopted in the design of the PRESSS building (Priestley 2002). As a result, the dimensions of the precast beams and columns and the hybrid frame connection details in the lower three floors in HFB1 were identical to those used in the PRESSS test building. The second building, referred to as HFB2, was established using a force-based design method (FBD) in accordance with UBC 97 (1997). The design base shear of HFB1 was 132 kips, which was 40 percent lower than the base shear of 220 kips obtained for HFB2. Hence, HFB1 and HFB2 were considered as two contrasting solutions for the design of the prototype building shown in Figure 1. Table 1 and Table 2 summarize the member dimensions and connection details derived for the hybrid frame buildings as

well as the material properties. The specified properties were used for the design and analysis of the two buildings, except for the model validation part of the study which was based on the measured material properties from the PRESSS building. The beams and columns in HFB1 and HFB2 were dimensioned to experience similar maximum shear stresses in the interior beam-to-column joints. As with the PRESSS building, the two hybrid buildings were designed with steel plate connections between the floors and seismic frames and hybrid connections between the columns and footings.

Table 1. A summary of member dimensions and material properties

Parameter	HFB1 (DBD)	HFB2 (FBD)
Column (width x depth)	18 in. x 18 in.	20 in. x 20 in.
Beam (width x depth)	14 in. x 23 in.	16 in. x 27 in.
Unconfined concrete strength, f'_c	8.8 ksi[*] (5 ksi[†])	5 ksi[†]
Mild steel reinforcement		
Yield strength, f_{sy}	60 ksi[†] (68 ksi[*])	60 ksi[†]
Ultimate strength, f_{su}	98 ksi[*]	98 ksi[*]
Post-tensioning tendon		
Yield strength, f_{py}	255 ksi[*]	255 ksi[*]
Initial stress after losses, f_{pi}	119 ksi[†]	119 ksi[†]
Grout strength	10 ksi[†] (9.3 ksi[*])	10 ksi[†]

[†]specified properties in design; [*]measured properties.

Table 2. A summary of hybrid frame connection details

Location	HFB1 (DBD)		HFB2 (FBD)	
	A_s (in[2])	A_{pt} (in[2])	A_s (in[2])	A_{pt} (in[2])
Floor 1	0.88	0.918	1.24	1.071
Floor 2	0.62	0.765	0.93	0.918
Floor 3	0.62	0.765	0.88	0.918
Floor 4	0.54	0.531	0.62	0.612
Floor 5	0.54	0.531	0.62	0.612
Column base	Exterior: 0.88 Interior: 0.88	Exterior: 2.50 Interior: 2.50	Exterior:1.24 Interior: 1.24	Exterior: 2.50 Interior: 2.50

3. ANALYTICAL MODELS

For the analysis of both buildings, 2-D models were developed using the computer program RUAUMOKO (Carr 2002) and only one seismic frame was included in each model. In series with the seismic frame, a pin-based fictitious column was also modeled. By lumping the seismic mass at the floor levels of the fictitious column and modeling the floor connections with spring elements between the column and seismic
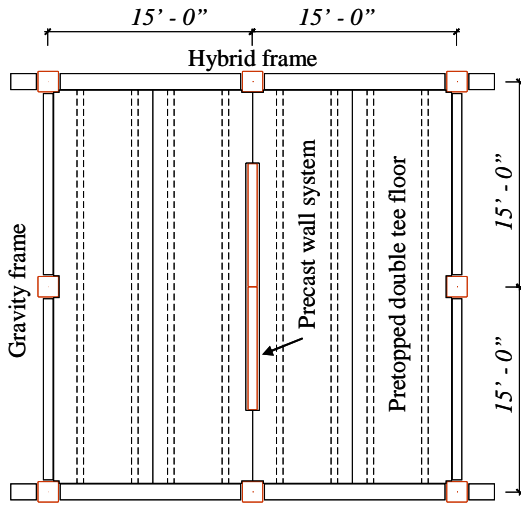
(a) Plan view
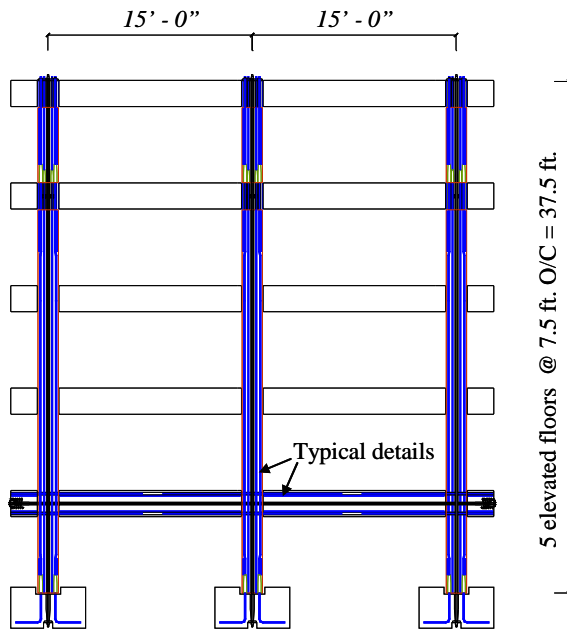
(b) Elevation view

Figure 3. General layout of the hybrid frame buildings.

frame, the influence of the floor connections was included in the analyses. However, the lateral load resistance from the gravity columns and out-of-plane bending of the precast wall system was neglected.

As demonstrated elsewhere (Pampanin et al. 2000), the beams and columns in the RUAUMOKO models were represented with the beam-column elements while two rotational springs per nodal location modeled the hybrid connections at the beam-to-column and column-to-footing interfaces. The use of two springs to model each hybrid connection was to represent the moment contributions of the mild steel reinforcement and prestressing steel separately. The moment–rotation response envelopes of the springs were derived using the modified PRESSS analysis procedure reported by Celik and Sritharan (2004). The modified Takeda hysteresis and bi-linear elastic models were used to define the cyclic behavior of the springs representing the mild steel reinforcement and post-tensioning tendons, respectively. The combination of using two cyclic models for the precast connections enabled the hysteretic energy dissipation and re-centering capability of the hybrid frames to be characterized satisfactorily. To account for the influence of flexural cracking, the moment of inertia for the beam-column elements was taken as a fraction of that corresponded to the uncracked concrete gross section (I_g). Based on the test observations reported for the PRESSS building (Priestley et al. 1999), $0.6I_g$, I_g, and $0.5I_g$ were used for the columns in the first story, all other columns, and beams, respectively.

4. ASSESSMENT PROCEDURE

Seismic performance of the two hybrid frame buildings was assessed using a multiple-level performance objective that enabled examination of damage states under four levels of earthquake ground motion. Consistent with the Appendices G and I of the SEAOC Blue Book (Seismology Committee 1999), the four earthquake levels were identified as EQ-1, EQ-II, EQ-III and EQ-IV (see Figure 4), which respectively corresponded to 33%, 50%, 100% and 150% of a design level earthquake.

Using the strong segments of recorded input motions from small to large earthquakes, earthquake ground motions compatible with the EQ-1, EQ-II, EQ-III and EQ-IV spectra shown in Figure 4 were previously developed (Sritharan et al. 1999). These motions, as a continuous sequence as shown in Figure 5, were essentially used in the performance assessment of the hybrid frame buildings. A sufficient number of time steps with zero accelerations was included in the input sequence shown in Figure 5 to examine the free vibration response of the buildings at the end of each earthquake segment. Because the hybrid buildings were dimensioned at 60 percent scale, the time step and accelerations were multiplied by 0.6 and 1.67, respectively, during the dynamic analyses.

Based on the performance-based seismic design concept presented in the SEAOC Blue Book, the minimum requirements chosen for the precast hybrid frame buildings were fully operational, operational, life safety and near collapse performances when subjected to EQ-I, EQ-II, EQ-III and EQ-VI, respectively. The maximum transient

and maximum residual inter-story frame drifts were used to define the acceptance criteria in this study. The following drift limits were used as acceptable limits for the four performance levels: maximum transient drifts of 0.5% (EQ-I), 1.5% (EQ-II), 2.5% (EQ-III) and 3.8% (EQ-IV); and maximum residual drifts of 0.1% (EQ-I), 0.3% (EQ-II), 0.5% (EQ-III) and 0.75% (EQ-IV). These limits were chosen based on the guidance given in the Blue Book and considering the re-centering nature of the hybrid frames. Although it is unnecessary to set a stringent residual drift limit for the near collapse performance, the selected residual drift limits were 20% of the maximum transient drifts for all earthquake levels.
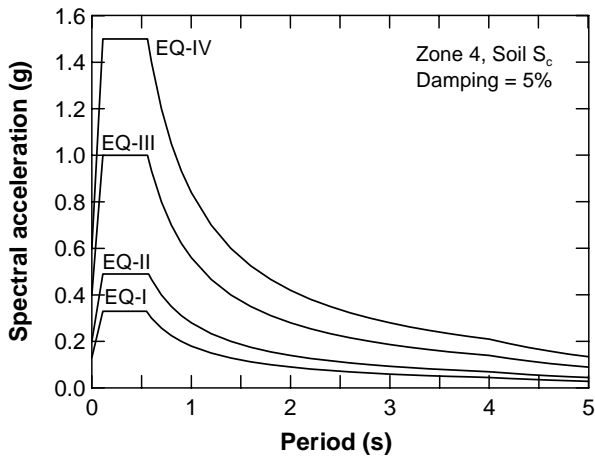
Figure 4. Multiple-level acceleration response spectra.
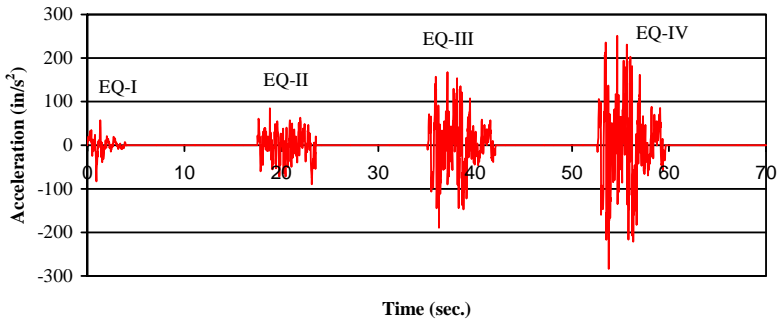
Figure 5. Earthquake input motions.

5. RESULTS

By comparing the analysis results from the frame model developed for HFB1 with pseudodynamic test data obtained for the PRESSS building, the modeling procedure described above was validated. By adopting the input motions and the mass and viscous damping parameters from the PRESSS building test, Figure 6 compares the measured lateral displacement at the third floor of the hybrid frame and base moment of this frame in the PRESSS building with those obtained analytically from the HFB1 model. It is noted that the pseudodynamic testing of the PRESSS building was conducted using 0.5EQ-I, EQ-I, EQ-II and a modified form of EQ-III (EQ-III-M). A good agreement seen between the experimental and analytical results in Figure 6 confirmed that the procedure used for establishing the HFB1 and HFB2 models was adequate.

(a) Lateral displacement

(b) Base moment

Figure 6. Comparison between the HFB1 results and PRESSS test data.

452

As the first step in understanding their lateral load behavior, both hybrid building models were subjected to pushover analyses. Figure 7 compares the base shear-lateral displacement responses, in which the increased stiffness and strength of HFB2 are apparent. Another interesting observation is that both bui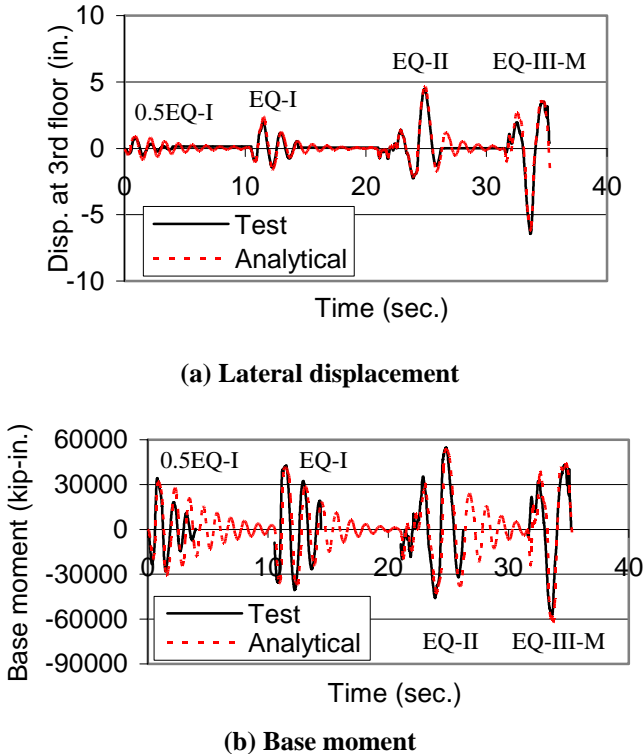ldings had yield displacements of about 1.5 inches despite using different methods to deign the hybrid buildings. Due to the increased stiffness, the first mode of the HFB2 was 0.21 seconds less than the fundamental period of 0.99 seconds for HFB1.
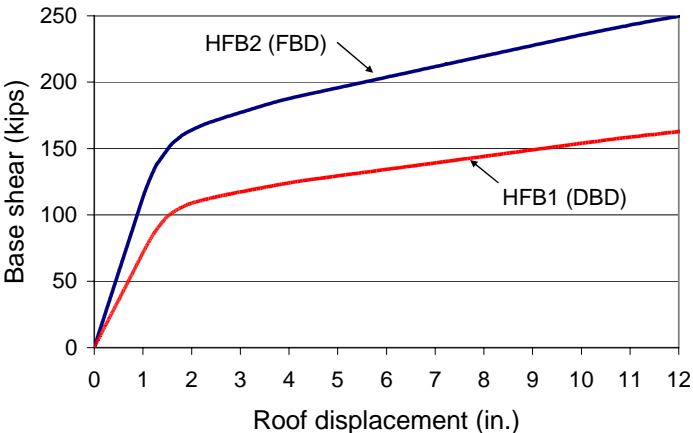
Figure 7. Pushover analysis results from HFB1 and HFB2 models.

When the HFB1 and HFB2 models were subjected to 0.5EQ-1 and the earthquake input sequence shown in Figure 5, the maximum average inter-story drifts and base moment resistance shown in Figures 8 and 9 were obtained. As seen in Figure 8, the residual drifts calculated for both buildings at the end of each earthquake segment were negligibly small and satisfied the acceptance criteria. Table 3 lists the maximum transient inter-story drifts obtained during the analyses of the buildings, which confirmed that the inter-story drifts of both buildings were below the acceptable transient drift limits for the EQ-II, EQ-III and EQ-IV input motions. For EQ-1, the calculated maximum transient drifts exceeded the acceptable drift for both buildings, which should not be of a concern for three reasons. First, the cracked section properties selected for the beam-column members in the buildings were more representative for seismic assessment at EQ-II or greater intensity. Next, the analyses are based on specified rather than probable material properties, and finally, it has been suggested that the spectral ordinates of EQ-I spectrum in the SEAOC Blue Book may be too large (Performance-Based Seismic Engineering Ad Hoc Subcommittee 2003). Therefore, it is concluded that both HFB1 and HFB2 are acceptable solutions for the design of the prototype building despite the design base shear force of HFB1 being 40% less than that obtained for HFB2.

Generally, the response of HFB2 was expected to provide larger moment resistance and lower inter-story drifts, which can be seen in Figures 8 and 9 for the input motions corresponding to EQ-I through EQ-III. At EQ-IV, the maximum inter-story and maximum average frame drifts obtained for HFB2 were greater or equal to those obtained for HFB1 (see Table 3 and Figure 8), emphasizing the dependency of the building responses on the frequency contents of the input earthquakes. When compared to the response at the lower intensity motions, the maximum transient drift of HFB1 appears to be small at EQ-IV and was found to be influenced by a large displacement excursion in the opposite direction response immediately prior to experiencing the maximum inter-story drift. It is expected that HFB2 will generally produce smaller drifts than HFB1 for other EQ-IV level motions, which will be investigated as part of an ongoing study.
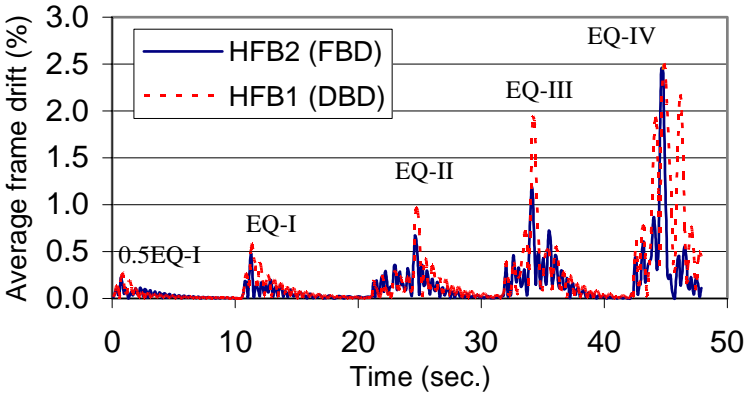

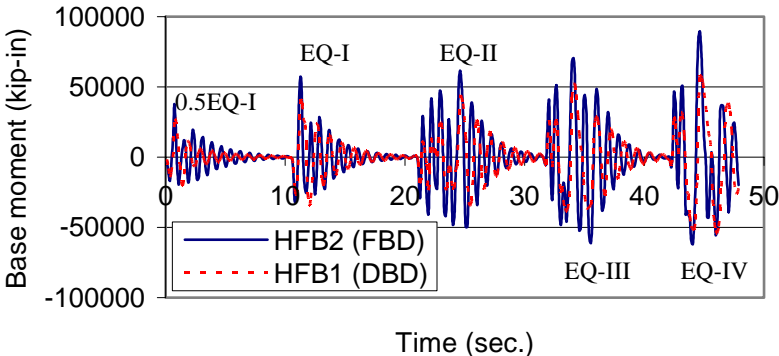**Figure 8. Absolute values of the average lateral inter-story frame drifts.**

Figure 9. Base moment calculated for the two hybrid frame buildings.

454

Table 3. Comparison of calculated maximum transient inter-story drifts with acceptable limits

Earthquake level	EQ-I	EQ-II	EQ-III	EQ-IV
Acceptable limit (%)	0.5	1.5	2.5	3.8
HFB1 (DBD) (%)	0.75	1.29	2.16	2.85
HFB2 (FBD) (%)	0.56	0.99	1.73	3.00

6. CONCLUSIONS

Seismic performances of two hybrid frame buildings representing a 5-story prototype building were analytically studied in this paper. The first building was based on a direct-displacement based design while the second building was established from a force-based design method. Consequently, the design base shear of the first building was 40% lower than that of the second building and thus the strength and stiffness of the two buildings were significantly different.

Following validation of the analytical modeling procedure, both buildings were subjected to short segments of earthquake input motions which were compatible with response spectra corresponding to four levels of earthquake intensities. Using the analysis results, the following conclusions have been drawn:

1. The force-based design described in design codes for monolithic concrete special moment frames and the direct-displacement design described in Reference (Priestley 2002) are acceptable procedures for the design of the prototype five-story precast hybrid frame building. Because of significantly lower design base shear, the DBD solution is expected to be more economical.

2. The response of both buildings satisfied the transient and residual average inter-story drift limits imposed for different performance limit states. Consequently, both the FBD and DBD methods are expected to provide low-rise precast buildings with acceptable performances under the four levels of input motions.

3. The combination of hysteretic energy dissipation and re-centering capabilities of the hybrid connections produced negligible residual drifts for all earthquake levels. Hence, by controlling the inelastic strain in the post-tensioning steel and introducing a procedure to replace the mild steel reinforcement when required, hybrid frame buildings may be designed to achieve a higher level of seismic performance than that considered in this study.

4. Although lower drifts were generally obtained for the stiffer building that was designed using a higher base shear, this trend did not hold for the input motion corresponding to EQ-IV, which represented an event at 150% of a design level earthquake.

The response of the buildings are further examined in an ongoing study at Iowa State University by subjecting them to different input motions and characterizing their

responses using additional parameters such as accumulated plastic rotations and floor accelerations.

REFERENCES

Carr. A. J. (2003). RUAUMOKO - Inelastic Dynamic Analysis Program. University of Canterbury, Christchurch, New Zealand.

Celik, O., and S. Sritharan. (2004). An Evaluation of Seismic Design Guidelines Proposed for Precast Concrete Hybrid Frame Systems. ISU-ERI-Ames Report ERI-04425, Iowa State University, Ames, Iowa.

Englekirk, R. E. (2002). Design-Construction of The Paramount – A 39-story Precast Prestressed Concrete Apartment Building. *PCI Journal* 47(4):56-71.

Nakaki, S. D., J. F. Stanton, and S. Sritharan. (1999). An Overview of the PRESSS Five-story Precast Test Building. *PCI Journal* 44(2), 26-39.

Pampanin, S., M. J. N. Priestley, and S. Sritharan. (2001). Analytical Modeling of Seismic Behavior of Precast Concrete Ductile Frame Connection. *Journal of Earthquake Engineering* 5(3):329-367.

Performance-Based Seismic Engineering Ad Hoc Subcommittee. (2003). Appendix I — Performance Based Seismic Engineering, Revised Interim Guidelines. Structural Engineers Association of California (SEAOC), California.

Priestley, M. J. N. (2002). Direct Displacement-Based Design of Precast/Prestressed Concrete Buildings. *PCI Journal* 41(2):67-79.

Priestley, M. J. N., S. Sritharan, J. R. Conley, and S. Pampanin. (1999). Preliminary Results and Conclusions from the PRESSS Five-Story Precast Concrete Test Building. *PCI Journal* 44(6):42-67.

Seismology Committee. (1999). *Recommended Lateral Force Requirements and Commentary*. Structural Engineers Association of California (SEAOC), California.

Sritharan S. (2002). Performance of Four Jointed Precast Frame Systems under Simulated Seismic Loading. *Proceedings of the Seventh National Conference on Earthquake Engineering*, Paper No. 480, Boston.

Sritharan, S., A. Igarashi, M. J. N. Priestley, and F. Seible. (1999). Test Design of the PRESSS Five-Story Precast Concrete Building. *Proceedings of the 68th SEAOC Annual Convention* 255–261, Santa Barbara, California.

Stanton, J. F., W. C. Stone, and G. S. Cheok. (1997). A Hybrid Reinforced Precast Frame for Seismic Regions. *PCI Journal* 42(2):20-32.

Stone, W. C., G. S. Cheok, and J. F. Stanton. (1995). Performance of Hybrid Moment-Resisting Precast Beam-Column Concrete Connections Subjected Cyclic Loading. *ACI Structural Journal* 91(2):229-249.

Uniform Building Code (UBC). (1997). International Conference of Building Officials, Whittier, California.

NEW MODEL FOR PERFORMANCE BASED DESIGN OF RC KNEE JOINT

Hitoshi SHIOHARA[1] and Yongwoo Shin[2]

ABSTRACT

This paper presents an application of the new theory of quadruple flexural resistance developed by the author for the performance evaluation of R/C knee joints. Ultimate capacity as well as failure type are predictable by the model, if the dimension, geometry and material properties are given. The quadruple flexural resistance considers that joint panel consists of triangular segments divided by four diagonal flexural critical sections in beam-column joints. The model uses equilibrium equations to relate magnitude of applied load such as column shear, beam shear and axial force in column, to the magnitude of stress resultants on the critical sections. Failure criteria of concrete, steel, bond and anchorage are combined to predict the strength and failure type. While the model is applicable to beam-column joints with different configuration, including interior, exterior as well as knee joint, this paper focuses on correlation studies using test data of knee joints.

Keywords: Analytical model; Knee joint; Strength; Failure mode; Beam-column joint.

1.   INTRODUCTION

The evaluation of stiffness, strength, damage and ductility of beam-column joints is an indispensable for performance based earthquake resistant design of reinforced concrete (RC) moment-resisting frames. Recent design recommendations in codes provide upper limit for joint shear stress to preclude shear failure of beam-column joint based on tests. Figure 1 compares configuration factors for joint shear capacity for US (ACI352 2002) and Japan (AIJ 1999). Design recommendations in the US and Japan recognize that the joint shear capacity is significantly affected for different geometry, whereas New Zealand code does not request such reduction of joint shear strength. The value of configuration factors are such different in different countries, because the adopted reduction factors are empirical in general and no theory or mathematical models are available.

---

1. *Associate Professor, Dept. of Architecture, Graduate School of Engineering, University of Tokyo, Tokyo 113-8656, Japan. Email: shiohara@arch.t.u-tokyo.ac.jp*

2. *Graduate Student, Dept. of Architecture, Graduate School of Engineering, University of Tokyo, Tokyo 113-8656, Japan. Email: shin@rcs.arch.t.u-tokyo.ac.jp*

loading direction	joint shear capacity (in MPa)	knee joint	exterior	interior	3D interior
ACI 352 type I (2002)	$0.083\gamma\sqrt{f'_c}\,A_j$	$\gamma = 12$ 0.6	$\gamma = 15$ 0.75	$\gamma = 20$ 1.0	$\gamma = 24$ 1.33
AIJ Guidelines (1999)	$\kappa\phi \times 0.8 f_c^{0.7} A_j$	$k = 0.4$ $\phi = 0.85$ 0.40	$k = 0.7$ $\phi = 0.85$ 0.70	$k = 1.0$ $\phi = 0.85$ 1.0	$k = 1.0$ $\phi = 1.0$ 1.18

Figure 1. Comparison of configuration factors for joint shear design.

Recently a novel model was proposed by the author (Shiohara 2001, 2002a, 2002b, 2003, 2004). The model is much simpler than the FEM, but is comprehensive enough and unified in which joint shear failure for all types of beam-column joints with different configurations is intrinsically incorporated (Shiohara 2004). This theory require no empirical assumptions accounting the difference in strength and type of failure, despite of various geometry of beam-column joints. This paper reports a correlation study with theoretical prediction by the model and in particular, test results of knee joints.

2. QUADRUPLE FLEXURAL RESISTANCE AND MODELING

2.1 Behavior of Quadruple Flexural Resistance

The new behavior model for shear failure of interior beam-column joints as well as knee joints are depicted in Fig. 2. In tests, two diagonal opening of cracks usually becomes dominant. So in this model, shear deformation of the joint panel is assumed primarily due to the rotation of the four triangular concrete segments and the opening of the cracks. Thus rotational movements of the segments are caused by uneven opening of the diagonal cracks like flexural cracks at the diagonal boundaries of the segments. When moment is applied to the segments from adjacent beams and columns, rotation of the segments occur as shown in Figs. 1(b) and 1(c) for knee joint under closing and opening loads respectively. Because four sets of flexural resisting action are identified in the moment resistance of the beam-column joints in this mode, it is named quadruple flexural resistance.

2.2 J (Joint) Mode and B (Beam) Mode

Beam-column joints need to be designed such that the contribution of shear deformation in the joint in total story should be minimized by achieving desirable hierarchy of
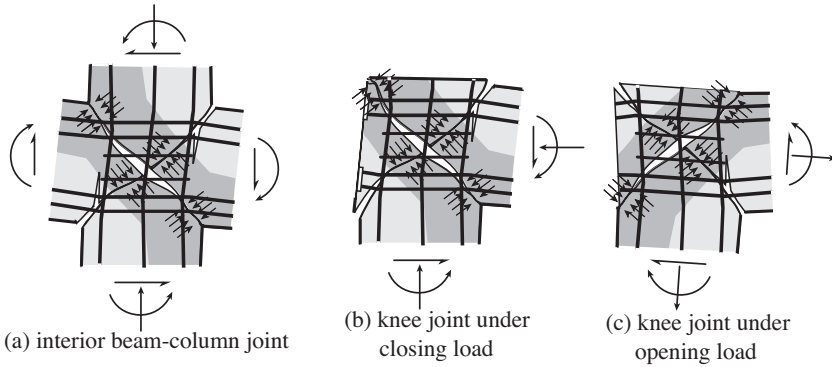
(a) interior beam-column joint   (b) knee joint under closing load   (c) knee joint under opening load

Figure 2. Behavior model for joint shear failure.

the strength, although the quadruple flexural resistance has an essential role to define the joint shear behavior. So it is not enough to predict joint shear strength considering the quadruple flexural resistance, but it is necessary to control the contribution of shear deformation occupied in story drift. Thus, the quadruple flexural resistance was evolved into a more comprehensive and mathematical model (Shiohara 2004). The model considers two sets of critical sections associated with two independent deformation modes, called J-mode and B-mode. J-mode is equivalent to the quadruple flexural resistance and featured by the diagonal crack as shown in the Fig. 2. This action causes observed joint shear deformation. So this type of resistance and relevant deformation is hereafter called J (joint)-mode. If the J-mode deformation becomes too excessive, concrete will crush adjacent to the crossing point of diagonal cracks and cover concrete will spall off. Whereas, B-mode is featured by the cracks along the face of column or beam as contrasted with J-mode in Fig. 3. The increase of section curvature due to B-mode deformation primarily causes cord rotation of beam or column.The objective of the introduction of the two modes is to obtain two joint shear strengths calculated from both J-mode and B-mode. The two modes of J-mode and B-mode usually give different strength reflecting a difference in critical sections. The smaller value of the strengths gives the real strength and its mode becomes dominant. Thus prediction of dominant deformation mode is feasible by comparing the two strengths.

Hence the analytical methods to calculate the strength of the both modes are necessary. The method of calculation of the strengths for J-mode and B-mode is very similar to the classical flexural theory where each section curvature causes moment resistance by a pair of force resultants in tension and compression arising in reinforcing bars and concrete.
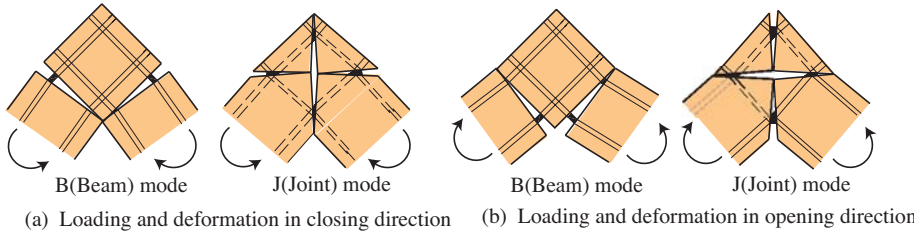
B(Beam) mode	J(Joint) mode	B(Beam) mode	J(Joint) mode
(a) Loading and deformation in closing direction		(b) Loading and deformation in opening direction	

Figure 3. B(Beam)-mode and J(Joint)-mode for knee joints.

.

3. APPLICATION TO KNEE JOINT

To demonstrate how the theory works for the prediction of the strength and type of failure, an example of application to a very simple R/C knee joint is examined. Due to the limit of the space, the procedure of analysis is briefly introduced here. Detailed explanation is available in the reference (Shin and Shiohara 2004).

3.1 Geometry and Notations

Figure 4 shows the geometry of the symmetric knee joint. To simplify the solution, the substructure are assumed symmetric and the joint panel is square of D. The thickness of column and joint are assumed to be t. The distance between the center of the joint panel to the contra flexural points in the beam or column is L. External loads are applied at the contra flexural points in the direction of straight line connecting the two contra flexural points. As a result, column shear V and column axial force N (=V) acts on the contra flexural points on the column.

3.2 Notations for Internal Forces

Figures. 4(d) to 4(g) show the notations defining the set of internal forces at the critical sections for the J-mode of knee joints under loading in closing direction and opening direction respectively. The notations T_1, T_2, T_3, and T_4 represent the resultant tensile forces in longitudinal bars, while C_1 C_2 and C_3 represent the resultant compressive forces on the concrete boundaries when it subjected to closing force, and C_4 C_5 and C_6 represent the resultant compressive forces in concrete when it is subject to load in opening direction. The values of C_1 and C_2 equal to the x component of compressive resultant in concrete. So the direction of concrete principle stress is normal to the critical section. The forces T_2, and T_3 are common variables for both B-mode and J-mode. All of the compressive stress in concrete on the critical section is assumed to be

460

(a) boundary conditions   (b) geometries (type I)   (c) geometries (type II)

(with idealization of stress blocks)

(d) J-mode (closing directional loading)   (e) B-mode (closing directional loading)

(with idealization of stress blocks)

(f) J-mode (opening directional loading)   (g) B-mode (closing directional loading)
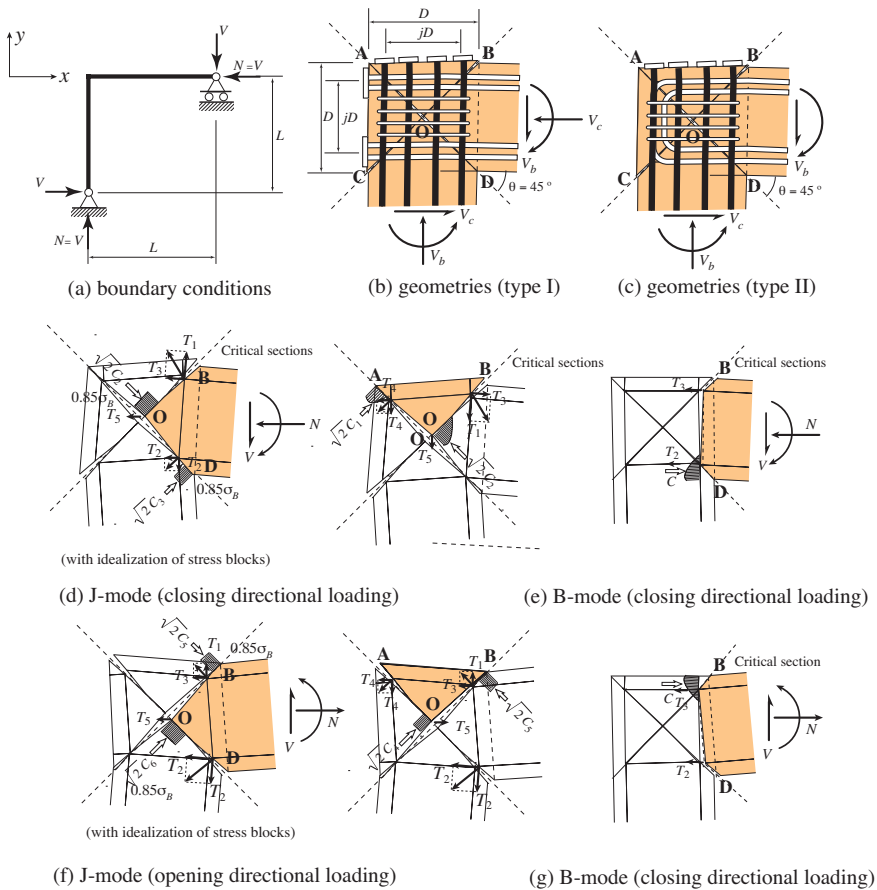
Figure 4. Model for knee joints loaded to closing and opening direction.

normal to the critical section and distribution is assumed to be rectangular stress block with compressive stress of σ_c ($=0.85\,\sigma_B$: concrete compressive strength). The notation T_5 represents the resultant force in joint shear reinforcements distributed in beam-column joint in vertical and horizontal direction, which confines the joint core. In this paper, horizontal and vertical resultant forces are assumed not to damage to the geometrical symmetry. The distance of tensile and compressive longitudinal bars is assumed to be jD. Solution for general case is more complicated where knee joint is non symmetric and not shown here.

3.3 Equilibrium Equations

Equilibrium should be satisfied. Equilibrium equations are established for each free body for horizontal and vertical directional forces as well as moment for J-mode. Equilibrium equations are established for axial force and moment for B-mode. Compatibility condition may not be necessarily satisfied.

3.3.1 J-mode

By considering the symmetry of the free body, six equilibrium equations are necessary to define the equilibrium of the knee joint. However number of independent equilibrium equations is five for each case (a) under closing moment shown in Fig. 4(d), and (b) under opening moment shown in Fig. 4(f). In the case under closing moment, the independent equilibrium equations are from Eqns. (1) to (5),

$$-T_2 - T_3 + C_2 + C_3 - T_5 - N = 0 \quad \text{(segment } \mathbf{BOD}\text{: } x\text{-direction)} \tag{1}$$

$$-T_1 - T_4 + C_1 + C_2 - T_5 = 0 \quad \text{(segment } \mathbf{AOB}\text{: } y\text{-direction)} \tag{2}$$

$$T_1 - T_2 - C_2 + C_3 - V = 0 \quad \text{(segment } \mathbf{BOD}\text{: } y\text{-direction)} \tag{3}$$

$$\frac{1}{2}jD(2T_4 - T_1 - T_3) + \frac{C_2^2}{t\sigma_c} - C_1\left(D - \frac{C_1}{t\sigma_c}\right) = 0 \quad \text{(segment } \mathbf{AOB}\text{: moment)} \tag{4}$$

$$\frac{1}{2}jD(T_1 - 2T_2 + T_3) - \frac{C_2^2}{t\sigma_c} + C_3\left(D - \frac{C_3}{t\sigma_c}\right) - LV = 0 \quad \text{(segment } \mathbf{BOD}\text{: moment)} \tag{5}$$

whereas, for the case under opening moment, equilibrium equations are Eqns. (6) to (10).

$$-T_2 - T_3 + C_5 + C_6 - T_5 + N = 0 \quad \text{(free body } \mathbf{BOD}\text{: } x\text{-direction)} \tag{6}$$

$$-T_1 - T_4 + C_4 + C_5 - T_5 = 0 \quad \text{(free body } \mathbf{AOB}\text{: } y\text{-direction)} \tag{7}$$

$$T_1 - T_2 - C_5 + C_6 + V = 0 \quad \text{(free body } \mathbf{BOD}\text{: } y\text{-direction)} \tag{8}$$

$$\frac{1}{2}jD(2T_4 - T_1 - T_3) - \frac{C_4^2}{t\sigma_c} + C_5\left(D - \frac{C_5}{t\sigma_c}\right) = 0 \quad \text{(free body } \mathbf{AOB}\text{: moment)} \tag{9}$$

$$\frac{1}{2}jD(T_1 - 2T_2 + T_3) + \frac{C_6^2}{t\sigma_c} - C_5\left(D - \frac{C_5}{t\sigma_c}\right) + LV = 0 \quad \text{(free body } \mathbf{BOD}\text{: moment)} \tag{10}$$

3.3.2 B-mode

The equilibrium condition for the free body for B-mode are given by Eq. (11) for horizontal direction and moment around the center of the beam-column joint by Eq. (12), where sign (±) stand for (-) for closing and (+) for opening respectively.

$$- T_2 - T_3 + C \pm N = 0 \quad \text{(free body } \mathbf{BD}: x\text{-direction)} \tag{11}$$

$$\frac{1}{2}jD(T_2 - T_3) + \frac{C}{2}\left(D - \frac{C}{b_c\sigma_c}\right) \pm LV = 0 \quad \text{(free body } \mathbf{BD}: \text{moment)} \tag{12}$$

3.4   Failure Criteria of Materials

3.4.1 Concrete

It is assumed that diagonal cracks transfers no tensile force across the crack. Resultant forces in compression are transferred by compressive reinforcement and/or across concrete cracks. In J-mode, each direction of principle stress on the critical section is assumed parallel to the diagonal direction of the joint panel. On the critical sections, distribution of the concrete stress is assumed as a rectangular stress block, where the concrete stress is σ_c and 85% of concrete compressive strength σ_B, typical value for flexural analysis.

3.4.2 Reinforcing Steel

Tensile force is transmitted by the longitudinal bars. Thus it is assumed that they do not exceed the yielding force. The typical restrictive conditions are given by Eq. (13).

$$T_3 \leq \Sigma a_t f_y \tag{13}$$

where, Σa_t: total cross section area of tensile reinforcements, and f_y: tensile yield point of longitudinal reinforcement. Joint shear reinforcing bars are assumed that they are concentrated at the mid-height of the joint and always equal to the yielding force and given by Eq. (14),

$$T_5 = p_w b_c (jD) f_{sy} \tag{14}$$

where, p_w: joint shear reinforcement ratio, f_{sy}: tensile yield point of joint reinforcement.
        In the analysis below, longitudinal bars in beam and columns are assumed perfectly anchored for the simplicity.

3.5 Ultimate Strength

Under closing moment, the value of T_1, T_2; the resultant forces in longitudinal bars in compression are assumed to be zero. Then, five unknown variables V, T_4, C_1, C_2, and C_3 are determined as a function of T_3 by solving the simultaneous equations from (1)
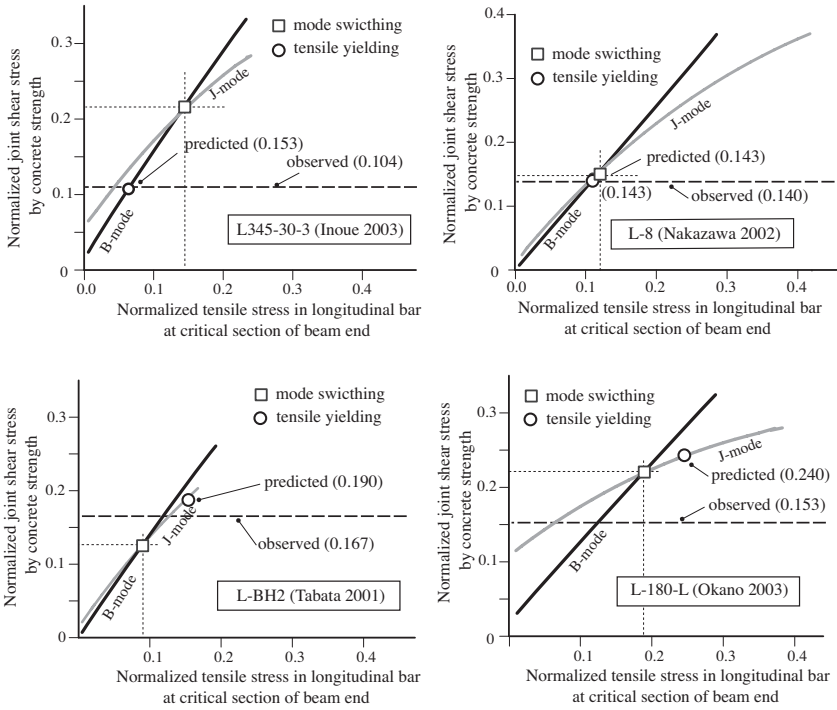
Figure 5. Comparison of prediction and test result.

to (5). Under opening forces, the values of C_4, C_5; the resultant forces in concrete is assumed to be zero. As a result, five unknown variables V, T_4, T_1, T_3, C_6 are obtained as functions of T_2 by solving the simultaneous equations from (6) to (10). In both cases, the force T_5, confinement due to horizontal and vertical joint reinforcement are assumed to be equal to the yield stress.

By substituting the yielding force of reinforcing bar in to T_3, beam shear of J-mode is obtained as $V_{\text{J-mode}}$. The moment capacity of J-mode is hereafter defined as $M_j = L \times V_{\text{J-mode}}$. By substitute the value T_3 and T_2 into Eqs. (11) and (12), considering $N=V$, beam shear of B-mode is obtained as $V_{\text{B-mode}}$. The moment capacity of B-mode is hereafter defined as $M_b = L \times V_{\text{B-mode}}$. The predicted strength M_{uj} of beam-column joint is obtained as the smaller one of J-mode and B-mode, as follows,

$$M_{uj} = \min\{M_j, \ M_b\} \tag{15}$$

3.6 Failure Mode

Based on the calculated hierarchy of the strengths of J-mode and B-mode, type of failure mode of **J**, or **B** is determined by applying rules given in Table 1.

Table 1. Prediction of failure mode of knee joint

Failure type	Condition	Explanation
J	$M_j < M_b$	Joint shear failure
B	$M_j > M_b$	Beam yielding

4. CORRELATION STUDY

Figure 5 shows the result of calculating for four specimens from references which show typical types of failure, **B**: beam yielding, **J**: joint shear failure or **T**: premature anchorage failure. To apply the theory the following rules were used. If the column has larger capacity than beam, column reinforcing detail is neglected in estimating the strength of knee joint. If the amount of joint shear reinforcement in vertical and horizontal direction is different, average value was used to estimate the T_5. The column longitudinal bars in mid-layer is included as vertical joint shear reinforcement. If length of column and beam is different, averaged length is used.

Specimen L345-30-3 (Inoue et al.2003) shown in Fig. 5(a) exhibited joint beam yielding failure (**B**). The predicted maximum moment is very closed to the observed value. The specimen L-8 (Nakamura et al. 2003) in Fig. 5(b) showed yielding of longitudinal bar as well as joint shear failure accompanied with strength degradation. The calculated and observed strength show good agreement.

Figure 5(c) shows specimen L-BH2 (Tabata 2001) which exhibited joint shear failure (**J**). The J-mode strength at beam bar yielding is smaller than that of B-mode, hence the predicted failure mode was **J**. Figure 5(d) shows the specimen L-180-L (Okano 2003) in which premature anchorage failure (**T**) of beam bars in outside face occurred under closing loading. The observed strength is much smaller than predicted. This is because the analyses here assume perfect anchorage. So it is necessary to incorporate the failure criteria of anchorage failure to enhance the accuracy of the model taking into account the anchorage detailing in beam-column joint.

4.1 Correlation Study with Inventory of Knee Joint Tests

Table 2 compares the calculated strength, failure mode with observed ones. All the specimens in the list have aspect ratio of unity. The observed failure modes were based on description in reference. If the information was not reported, the failure mode was determined by considering the failure pattern and hysteresis loops.
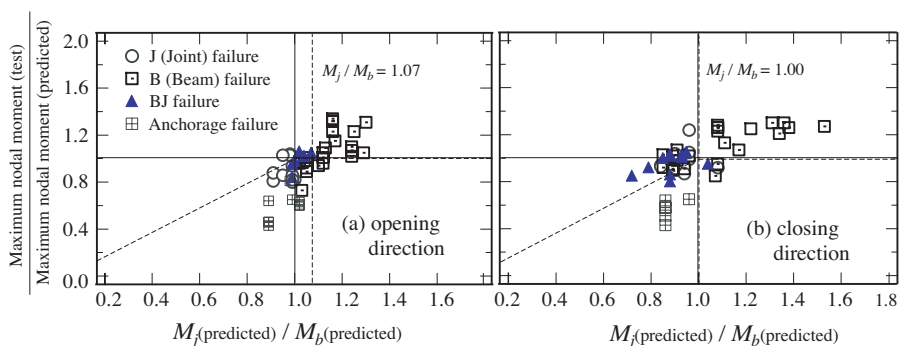
Figure 6. Correlation of strength and failure mode.

The average of the ratio of observed strength to predicted one is 1.01 for closing loading and 1.04 for opening loading respectively. It shows good correlation. It should be noted, test results shows that the strength under closing load is always larger than that under opening loading. The model account for this tendency correctly for the inventory data, which includes specimens with joint failure and beam failure.

In Fig. 6, the fifty one specimens are plotted to compare the observed and calculated results listed in Table 2. Horizontal axis shows the ratio of M_j/M_b. Vertical axis shows the observed strength normalized by M_b. The predicted strength by the model show good correlation with test result, except the specimens which exhibited premature anchorage failure in the tests.

It is also observed that all the specimens which exhibited beam yielding failure in tests, have value of M_j/M_b larger than 1.07 for opening and 1.00 for closing except two specimens. Hence, the ratio of M_j/M_b is good index to predict the failure mode of knee joint if the longitudinal bars in beams and column are satisfactory anchored in knee joint. The value of M_j/M_b of 1.0 may be good criteria for discriminate joint shear failure from beam yielding failure.

5. CONCLUDING REMARKS

A new theory of Quadruple flexural resistance in reinforced concrete monolithic beam-column joint was applied to knee joints. Although the theory is based on a simple concept, it has an potential to predict both strength and failure type, reflecting essential critical parameters affecting the behavior of beam-column joints. The model contains no empirical factors accounting the difference between interior, exterior or knee joint like a configuration factors adopted in current design codes. It is demonstrated that the quadruple flexural resistance is applicable to knee joint. The calculated value of joint capacity and predicted failure mode agree well with wide variety of specimens in inventory of tests data of knee joint.

Table 2. Comparison of prediction and test results

Name of Specimen	Closing					Opening					Reference
	Observed		Predicted			Observed		Predicted			
	M_{test} k•Nm	Fail. mode	M_{calc} k•Nm	$\dfrac{M_{test}}{M_{calc}}$	M_f/M_b	M_{test} k•Nm	Fail. mode	M_{calc} k•Nm	$\dfrac{M_{test}}{M_{calc}}$	M_f/M_b	
L-BH1	202	J	248	0.81	0.91(J)	145	J	154	0.94	0.84(J)	Tabata
L-BH2	218	J	248	0.88	0.91(J)	144	J	154	0.93	0.84(J)	(2001)
L-BU	285	J	272	1.04	0.98(J)	171	J	172	0.99	0.96(J)	
L-BP	221	T	272	0.81	0.98(J)	181	J	172	1.05	0.96(J)	
L-PP	279	J	272	1.03	0.98(J)	214	J	172	1.24	0.96(J)	
Mazzoni 1	105	(J)*1	122	0.86	0.95(J)	55	(T)	85	0.64	0.86(J)	Mazzoni
Mazzoni 2	106	(J)	130	0.82	1.00(B)	61	(T)	94	0.65	0.96(J)	(1991)
Mazzoni r	132	(B)	131	1.01	1.05(B)	114a	(B)	111a*2	1.02	0.96(J)	
LP15-1	125	(J)	145	0.86	0.99(J)	89	B	98	0.90	0.89(J)	Aota
LP15-2	115	(J)	145	0.80	0.99(J)	89	B	98	0.91	0.89(J)	(2001)
LP15-3	118	(J)	145	0.82	0.99(J)	88	B	98	0.90	0.89(J)	
LP18-1	136	(J)	145	0.94	0.99(J)	100	B	98	1.02	0.89(J)	
LP18-2	117	(J)	122	0.96	1.02(B)	83	B	84	0.98	0.91(J)	
LP18-3	75	T	122	0.61	1.02(B)	90	B	84	1.07	0.91(J)	
LP16-4	185	J	180	1.03	0.96(J)	126	B	123	1.03	0.85(J)	
LP20-5	122	B	116	1.05	1.12(B)	79	B	83	0.95	1.08(B)	
Knee J1	41	(B)	42	0.97	1.02(B)	33	(J)	33	1.02	0.90(J)	Megget
Knee J2	40	(B)	42	0.96	1.02(B)	34	(J)	33	1.04	0.90(J)	(1998)
Knee J3	49	(B)	51	0.96	1.12(B)	41	(B)	43	0.95	1.04(B)	
Knee J4	48	(B)	51	0.94	1.10(B)	31	(B)	29	1.07	1.17(B)	
Knee J6	51	(B)	50	1.01	1.12(B)	34a	(B)	40a	0.85	1.07(B)	
Knee J7	73	(B)	81	0.89	1.05(B)	60	(J)	66	0.92	0.94(J)	
Knee J9	47	(B)	52	0.92	1.05(B)	34a	(J)	39a	0.87	0.94(J)	
Knee J10	50	(B)	52	0.98	1.04(B)	35a	(B)	39a	0.91	0.94(J)	
Knee J14	55	(B)	51	1.09	1.13(B)	37a	(J)	40a	0.92	1.08(B)	
L-1	213	B	159	1.34	1.16(B)	128	B	102	1.26	1.08(B)	Nakazawa
L-2	234	B	190	1.23	1.25(B)	146	B	117	1.25	1.22(B)	(2002)
L-3	125	B	109	1.15	1.17(B)	78	B	69	1.13	1.11(B)	
L-4	213	B	162	1.31	1.30(B)	127	B	98	1.30	1.31(B)	
L-5	195	B	159	1.23	1.16(B)	128	B	102	1.26	1.08(B)	
L-6	209	B	159	1.32	1.16(B)	125	B	102	1.23	1.08(B)	
L-7	209	B	159	1.32	1.16(B)	130	B	102	1.28	1.08(B)	
L-8	388	BJ	394	0.98	1.00(B)	233	BJ	232	1.00	0.85(J)	
L-9	422	BJ	400	1.05	1.07(B)	266	BJ	254	1.05	0.95(J)	
L-10	408	BJ	399	1.02	1.04(B)	253	BJ	249	1.01	0.93(J)	
L-11	407	BJ	399	1.02	1.04(B)	256	BJ	249	1.03	0.93(J)	
L-1	68	BJ	82	0.84	0.99(J)	48	BJ	55	0.86	0.88(J)	Cui
L-2	53	T	82	0.65	0.99(J)	44	BJ	55	0.79	0.88(J)	(2003)
L-3	77	BJ	82	0.95	0.99(J)	57	BJ	55	1.03	0.88(J)	
L-4	49	T	85	0.58	1.02(B)	57	BJ	55	1.02	0.88(J)	
L-5	52	T	85	0.61	1.02(B)	70a	BJ	76a	0.92	0.79(J)	
L-6	87	BJ	85	1.03	1.02(B)	78a	BJ	93a	0.85	0.72(J)	
L345-30-3	180	B	171	1.05	1.29(B)	117	B	92	1.27	1.53(B)	Inoue
L345-30-3w	180	B	168	1.07	1.24(B)	120	B	95	1.26	1.38(B)	(2003)
L345-60-4	247	B	224	1.10	1.24(B)	164	B	126	1.30	1.36(B)	
L490-60-3	233	B	228	1.02	1.24(B)	156	B	129	1.21	1.34(B)	
L-180-S	33	T	71	0.46	0.89(J)	30	T	51	0.58	0.86(J)	Okano
L-180-L	46	T	71	0.64	0.89(J)	29	T	51	0.58	0.86(J)	(2003)
LP-180-S	33	T	71	0.46	0.89(J)	26	T	51	0.50	0.86(J)	
L-90-S	31	T	71	0.43	0.89(J)	22	T	51	0.43	0.86(J)	
OT36B-T	194	B	264	0.73	1.03(B)	145	B	158	0.92	0.85(J)	Nakamura (2003)

*1 Observed failure mode were classified into J (joint shear failure), B(beam yielding failure) BJ (combination of B and J) or T (preamature anchorage failure) based on the decription in each report, while the notation in (parensis) means the observed failure mode is not clearly described in the report and determined by the author based on failure pattern and its load-deflection relation.

*2 Specimens with notation [a] contains inclined bar in reentrant corner, the tensile capacity of the inclined bar were added to the estimated tensile capacity of longitudinal bars.

REFERENCES

ACI-ASCE Committee 352R-02. (2002). *Recommendations for design of beam-column joints in monolithic R.C. structures*. 37pp.

Aota K., T. Watanabe, T. Naruse and T. Morimoto. (2001). Study on Plate Anchorage in the Joint of the Highest Story. *Proc. of Japan Concrete Institute*, **23-3**, 391-396 (in Japanese)

Architectural Institute of Japan (AIJ). (1999). *Design Guideline for Earthquake Resistant Reinforced Concrete buildings Based on Inelastic Displacement Concept*. Tokyo, Japan. (in Japanese).

Cui Jianyu, S. Fujii, M. Nishiyama and F. Watanabe. (2003). Modeling of Load-Resistance Mechanism on Corner Joints, *Journal of Structural and Construction Engineering AIJ*, **567**, 101-109. (in Japanese).

Inoue T., K. Masuo and N. Okamura. (2003). Ultimate Strength and Ductility of L Shaped and T Shaped R/C Frames Using Mechanical Anchorages. *Proc. of JCI*, **25-2**, 499-504. (in Japanese).

Mayfield B., Fung-Knew Kong, A. Bennison and Julian C.D. Twiston Davies. (1971). Corner Joint Details in Structural Lightweight Concrete. *ACI Journal*, **68**(5), 366-372.

Mazzoni, S. et al. (1991). Cyclic response of RC beam-column knee joints test and retrofit, *Report No.UCB/EERC-91/14*, EERC and Dept. of Civil Engineering, Berkeley, California, 18pp.

Megget, Leslie M. (1988). The Seismic Behavior of Small Reinforced Concrete Beam-Column Knee Joints, *Bulletin NZNSEE*, **31**(4), 215−245.

Nakamura K., T. Kishimoto, Y. Ishiwata and S. Hattori. (2003). Experimental Study on L-Shaped Beam-Column Joint of Mechanical Anchorage using Circular Anchor Plate. *Proc. of JCI*, **25-2**, 925-930. (in Japanese).

Nakazawa H., N. Sakaguchi and M. Asai. Experiments on the structural capacity of reinforced beam-column joints using mechanical reinforcement. *Proc. of JCI*, **24-2**, 847-852. (in Japanese).

Okano H., T. Mukai and S. Nomura. (2003). Experimental Study on Behavior and Rehabilitation of R/C Beam-Column L-Joint. *Proc. of JCI*, **25**, 475-480. (in Japanese).

Shin, Yong-Woo, and H. Shiohara. (2004). Analysis on Ultimate Shear Strength of Reinforced Concrete Knee joints. *Journal of Structural Engineering*, AIJ, **50B**, 87−96. (in Japanese)

Shiohara, H. (2001). New Model for Shear Failure of RC Interior Beam-Column Connections. *ASCE Structural Journal*, **127**(2), 152-160.

Shiohara, H. (2002a). Effects of Interaction between Joint Shear and Anchorage Force within R/C beam-column Joints on their Strength and Failure Modes. *Proceedings 7NCEE*, July 21-25, 2002, Boston, Massachusetts.

Shiohara, H. (2002b). New Model for Joint Shear Failure of R/C Exterior Beam-column Joints. *Proceedings of U.S.-Japan Workshop on PBEE for RC Structures*, October 2002, Toba, Mie, Japan.

Shiohara, H., and Yongwoo Shin. (2003). New Model for Joint Shear Failure of R/C Knee Joints. *Proc. of the 5th U.S.-Japan Workshop on PBEE for Reinforced Concrete Structures*, September 2003, Hakone, Kanagawa, Japan.

Shiohara, H. (2004). Quadruple Flexural Resistance in R/C Beam-column Joints. *Proc. 13WCEE*, Vancouver, B. C., Canada, August 1-6, 2004 (to be published).

Tabata T., and N. Nishihara. (2001). Shear and Anchorage Capacity of Exterior, T-shaped and L-shaped beam-column-joint in RC frame. *Proc. of JCI*, **23**, 373-378. (in Japanese).

EARTHQUAKE ACTIONS IN SEISMIC CODES: CAN CURRENT APPROACHES MEET THE NEEDS OF PBSD?

Julian J. BOMMER[*]

ABSTRACT

The successful implementation of performance-based seismic design (PBSD) will require its incorporation into seismic design codes in order to achieve application to all new constructions and possibly also to existing buildings. Since PBSD has the objective of limiting structural and non-structural damage under different levels of earthquake loading, the requirements for the specification of design seismic actions inevitably exceed the current approach embodied in nearly all design codes of an acceleration spectrum that approximates the uniform hazard spectrum for a return period of 475 years, modified to account for energy dissipation through inelastic deformations. PBSD will require multiple levels of loading to be specified in codes and since the correlation between spectral acceleration and structural damage is poor the ground motions will need to be represented in alternative formats, primarily displacements. Current code formats could be adapted to meet the needs of PBSD but the presentation of the seismic actions in this way could become rather cumbersome. At the same time, the introduction of PBSD should be taken as an opportunity to review and improve the way in which earthquake ground shaking is characterized for design. Considering the requirements of PBSD and the shortcomings in current code specifications, alternative formats for presenting seismic actions are proposed.

Keywords: Seismic design codes; Earthquake actions; Performance-based seismic design.

1. INTRODUCTION

Performance-based seismic design (PBSD) is essentially the formalization of often cited objectives of designing structures to withstand minor or frequent earthquake shaking without damage, moderate levels of shaking with only non-structural damage and severe shaking without collapse and a threat to life safety (ATC, 1978). In the Vision 2000 document (SEAOC, 1995) this is elegantly stated as the "*coupling of expected performance level with expected levels of seismic ground motions*". Two requirements regarding the representation of earthquake actions for PBSD are then immediately apparent: several levels of seismic shaking must be specified and the

---

[*] *Civil & Environ. Engineering, Imperial College London, SW7 2AZ, UK. Email:*
  j.bommer@imperial.ac.uk

ground motion must be given in a form that has a direct correlation with the behaviour of real structures, particularly in terms of the capacity to cause damage. This leads to the question of whether current code formats for representing earthquake actions can be directly adapted to the requirements of PBSD.

The paper begins with a critical review of design code specifications of seismic actions, highlighting shortcomings even with regards to current design practice. The third section of the paper then briefly summarizes the requirements of PBSD in terms of earthquake actions. The fourth section then discusses possibilities for extending current code formats to cover the needs of PBSD and also explores alternative formats that could be used, both to address weaknesses in current approaches and to meet PBSD requirements.

2. EARTHQUAKE ACTIONS IN CURRENT SEISMIC CODES

Most earthquake-resistant design of structures is carried out by engineers without specialist training in earthquake engineering by following the specifications and guidelines of design codes. To enable this, the codes must provide, in a simplified and accessible manner, the nature of the ground shaking to be considered, the way the response of the structure to this shaking can be calculated, and the stress and/or deformation criteria that the structure is required to meet under the specified actions. In the following sections, the way in which ground motions are specified for design in current codes — including a few recent innovations — are briefly reviewed.

2.1   Design Levels of Motion

The first seismic design regulations to be based on a probabilistic seismic hazard map appeared in ATC 3-06 (ATC, 1978). The hazard map for the USA, showing PGA values with a return period of 475 years, was taken from Algermissen and Perkins (1976). The return period of 475 years was the result of selecting 50 years as the exposure period, although it was acknowledged that "*the use of a 50-year interval to characterize the probability is a rather arbitrary convenience, and does not imply that all buildings are thought to have a design life of 50 years*" (ATC, 1978). Algermissen and Perkins (1978) stated that "*for structures which should remain operable after large, damaging earthquakes, the 10 percent exceedance probability in 50 years seems reasonable*", although the choice of 10% was adopted on the rather arbitrary basis of being a significance level often taken by statisticians "*to be meaningful*" (Perkins, 2004). A very interesting observation made in ATC 3-06 is that it was not decided *a priori* to base the design seismic actions on the selected 475-year return period: a map of effective peak acceleration was drafted for ATC 3-06 — "*literally having been drawn by a committee*" (ATC, 1978) — and was found to be consistent with the 475-year PGA map of Algermissen and Perkins (1976). On this basis the 10% in 50 year map was adopted in ATC 30-6 and subsequently in the 1988 edition of UBC. The extensive commentary in ATC 3-06 provides a rational and honest

examination of the risk implications of basing structural design on the ground motions with a return period of 475 years, although the estimates of losses are based entirely on expert judgment rather than modeling, and the tone is very much one of assessing and judging the chosen design basis as being reasonable and at least as stringent as the design basis in use at the time.

The formulation and arguments presented in ATC 3-06 represented an important landmark and are laudable when viewed in a historical context. With time, however, the issues have been re-visited and examined in the light of improved understanding of seismic hazard and the relationships between ground-motion intensities and structural damage. These considerations have led to the adoption of 2% in 50 years — a return period of 2,475 years, considered to be more closely related with the probability of structural collapse — as the design level of hazard in the 1997 NEHRP guidelines and in IBC 2000 (Leyendecker *et al.*, 2000) as well as in the 2005 edition of the Canadian seismic code (Heidebrecht, 2003). However, the seismic design codes of nearly every other country in the world, regardless of differences with the USA in terms of seismicity and construction practices, have adopted — generally without any clear risk-based rationale — the 475-year return period as the basis for the ground motions considered in design. A notable exception to this is the 1986 Costa Rican code, which provides maps of PGA for return periods of 50, 100, 500 and 1,000 years and allows the designer to calculate the appropriate return period explicitly considering the importance, the design life and the ductility of the structure. Although most codes are based on a single hazard map, such performance-based considerations are actually present in most codes through the use of importance factors that increase the spectral ordinates for structures required to perform above simple life-safety criteria under the 475-year ground motions. The factors essentially result in safety-important structures being designed for longer return-period ground-motions. The shortcomings of this approach are obvious: firstly, it assumes that the variation of ground-motion amplitude with return period is constant throughout the country covered by the code, and secondly, it assumes that designing for life-safety under ground shaking with a longer return period will ensure that the structure remains operational under the 475-year return period.

2.2   Design Response Spectra

2.2.1 *Horizontal Spectral Shapes*

In the majority of current seismic design codes around the world the elastic response spectrum of acceleration is constructed by anchoring a spectral shape defined for each site class to the design peak ground acceleration (PGA). Apart from the lack of geophysical or engineering significance of PGA, this approach has the significant drawback that the shape of the response spectrum changes only with the site class, even though it is well established that the spectral shape is strongly influenced by earthquake magnitude and, to a much lesser extent, by source-to-site distance. As a result, the spectrum will often not be of uniform hazard (McGuire, 1977). The

approximation to the uniform hazard spectrum (UHS) is improved by using two independent parameters to build the spectrum: examples includes the use of two hazard maps, one for an acceleration-related parameter and the other a velocity-related parameter, as in the 1984 Colombian code and the 1990 Canadian code. In IBC 2000, the UHS is constructed using the NEHRP approach of maps of spectral acceleration at 0.2 and 1.0 second. A less elegant — and indeed less effective — approach has been adopted in EC8 (CEN, 2003), prompted by resistance to facing engineers with a second ground-motion parameter: two spectral shapes are presented, one for regions only affected by earthquakes of magnitude $M_s < 5.5$ and the other for regions affected by larger events, and each country will adopt the more appropriate shape in its National Application Document.

For regions affected by significantly different sources of seismicity, such as major subduction zones and moderate magnitude crustal earthquakes, the variation of the bedrock spectral shape across a country may be pronounced. In the 1994 Spanish code, the variation is included via a coefficient K — mapped as contours on top of the basic zonation map — that represents the degree of influence of large offshore earthquakes and raises the long-period spectral ordinates accordingly. Neighbouring Portugal adopts a more radical approach, defining two separate spectra — one for local events and one for large, distant earthquakes — each of which must be considered separately in design. The 1989 Chinese code also defines separate spectral shapes for near-field and far-field earthquakes. EC8 also envisages such a possibility: "*When the earthquakes affecting a site are generated by widely differing sources, the possibility of using more than one shape of spectra should be contemplated to adequately represent the design seismic action. In such circumstances, different values of PGA will normally be required for each type of spectrum and earthquake*" (CEN, 2003).

Another shortcoming with the acceleration spectra specified in most current seismic codes is that they cannot be converted to displacement spectra because this results in excessively large long-period ordinates due to the absence of a branch in which the ordinates decay as $1/T^2$. A notable exception to this is EC8 in which the acceleration spectrum is specified to be compatible with the displacement spectrum, following the proposal of Bommer *et al*. (2000). The 2003 NEHRP guidelines also include a transition to constant displacement ordinates, although at much longer periods (ranging from 4 to 16 seconds, depending on the modal earthquake magnitude obtained from disaggregation) than the 2.0 s adopted in EC8.

2.2.2 Vertical Spectral Shapes

The importance of the vertical component of the ground motion in terms of structural damage is a subject of ongoing debate; many current codes do not consider vertical ground acceleration at all and those that do simply specify the vertical acceleration spectrum to be equal to ½ or ⅔ of the horizontal spectrum. An exception to this is the current version of EC8 (CEN, 2003), in which the vertical spectrum, based on the work of Elnashai (1997), is specified independently from the horizontal spectrum.

Bozorgnia and Campbell (2004) find that the ratio of vertical-to-horizontal spectral ordinates is strongly dependent on period and on source-to-site distance, as indicated in Figure 1, where the simplified ratio they propose is compared with the V/H ratio of the Type 1 spectrum in EC8. The comparison suggests that in the relevant period range the EC8 vertical spectrum is likely to be conservative except for sites close to the source of earthquakes.
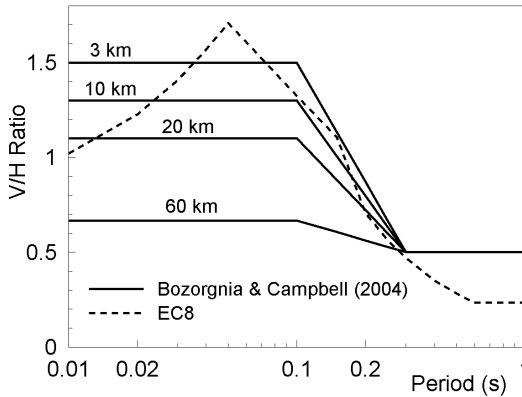

Figure 1. Vertical-to-horizontal spectral ratios for NEHRP Class D site from EC8 Type 1 spectrum (dashed line) and from Bozorgnia and Campbell (2004).

The curves in Figure 1 support the definition of the vertical spectrum independently from the horizontal spectrum because their shapes are clearly different (hence the variation of the V/H ratio with period) and their amplitudes display very different variation with distance from the earthquake source.

2.2.3 Site Amplification Effects

During recent years there has been a tendency to move from two or three site classes to four or five, as embodied now in the NEHRP guidelines. The most significant advance was the definition in UBC 1997 (based on NEHRP) of spectral amplification factors at short and intermediate periods simultaneously in terms of site class and the spectral accelerations at rock sites, thus modeling the non-linear response of soils (Dobry *et al*., 2000). The NEHRP site classes, like those adopted in EC8 (e.g., Rey *et al*., 2002), are based on the average shear-wave velocity over the uppermost 30 m, a depth related to the cost of drilling boreholes rather than of any geophysical significance: it has been pointed out that for long-period ground motions, the wavelengths are such that the shaking is not strongly influenced by the properties of the uppermost 30 m (e.g., Gregor and Bolt, 1997). This has led to some ground-motion prediction equations including the depth to basement rock as an explanatory variable, which "*boosts long period motions*" (Spudich, 1999).

2.2.4 Spectral Modification Factors

In all seismic design codes, the elastic response spectrum of acceleration is reduced by a factor that accounts for, amongst several other features, the dissipation of seismic energy through inelastic deformations in the structure. The reduction factors are defined in terms of the structural system and the construction material; some codes, amongst them EC8, also define the factors as a function of period.
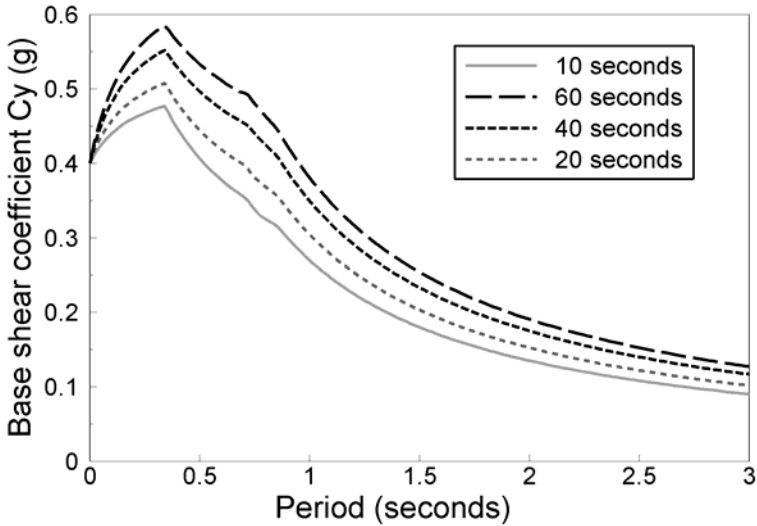

Figure 2. Design acceleration spectra (for ductility demand of 4 in reinforced concrete) as function of the significant duration (5–95% Arias intensity) as proposed by Chai and Fajfar (2000).

In all current codes, however, the reduction of spectral ordinates is independent of the nature of the expected ground motion. Chai and Fajfar (2000) propose a procedure for generating inelastic acceleration spectra that accounts for the increased number of cycles into the inelastic range experienced by yielding structures subjected to large magnitude earthquakes producing ground motions of long duration (Figure 2).

2.3   Acceleration Time Histories

There are cases when accelerograms are required for dynamic analysis; if one accepts the premise that records should be selected from magnitude-distance pairs consistent with the seismic hazard, the guidelines provided in current codes are generally deficient in this respect because dominant magnitude-distance scenarios are not identified (Bommer and Ruggeri, 2002). Shome *et al.* (1998) assert that provided records are scaled to the correct spectral acceleration at the fundamental period of the

structure, the results of inelastic structural analyses are insensitive to the magnitude-distance pairs corresponding to the records. This assertion effectively circumvents the shortcoming in current code specifications of accelerograms, but the results of Shome *et al.* (1998) are not conclusive regarding the influence of magnitude (due to the type of structure and the damage measure employed), and therefore duration, on inelastic structural demand and there is still a good case to be made for selecting records from earthquakes of appropriate magnitude (e.g., Bommer and Acevedo, 2004).

3. EARTHQUAKE ACTIONS FOR PBSD

The two most significant changes in the specification of earthquake actions for design for PBSD as compared with current code-based design are the requirement to define several different levels of ground shaking and to present the ground motion in terms of parameters that are more closely related to structural demand than maximum peaks of transient accelerations.

3.1 Multiple Levels of Earthquake Shaking

All formulations for PBSD presented to date assume that the different design levels considered will be determined from probabilistic seismic hazard assessment (PSHA) and a series of selected return periods (e.g., Stewart *et al.*, 2002). Although PBSD may ultimately aim to provide a check on performance over the full range of hazard, in most code applications this is likely to be approximated by a few pairs of load levels and performance targets. In the now famous matrix of design levels and performance levels presented in Vision 2000 (SEAOC, 1995) — which renders the importance factors defined in current codes redundant — the return periods specified (without explanation or commentary) for design ground motions are 43, 72, 475 and 970 years, which correspond to exceedance probabilities of 69, 50, 10 and 5% during an exposure period of 50 years. Clearly there remains a great deal of work to be done to arrive at robust selections of design levels (the IBC 2000 design level already exceeds the most severe loading case envisaged in the SEAOC proposals). One possible solution is the calibration of the pairs of design and performance levels through iterative earthquake loss modeling facilitated by computationally efficient and mechanically-based techniques (Pinho, 2004).

3.2 Format for Earthquake Actions

The inadequacy of current forced-based approaches to seismic design is widely acknowledged. Whilst it is possible that future codes may adopt energy-based approaches, these have not yet been formulated in a sufficiently simple fashion. At the same time a very convincing case has been made for displacement-based approaches (Priestley, 2000) to form the basis of PBSD. Direct displacement-based design, using the substitute structure concept, leads to two new requirements in terms of seismic

actions: response spectral ordinates at long periods and spectral ordinates at multiple levels of damping. The displacement spectra for higher damping values would usually be derived from the spectrum constructed for the nominal 5% of critical damping; recent work has indicated that the reduction of the spectral ordinates with increasing damping increases with earthquake magnitude (Figure 3) and hence with the duration of the ground shaking (Bommer and Mendis, 2004).
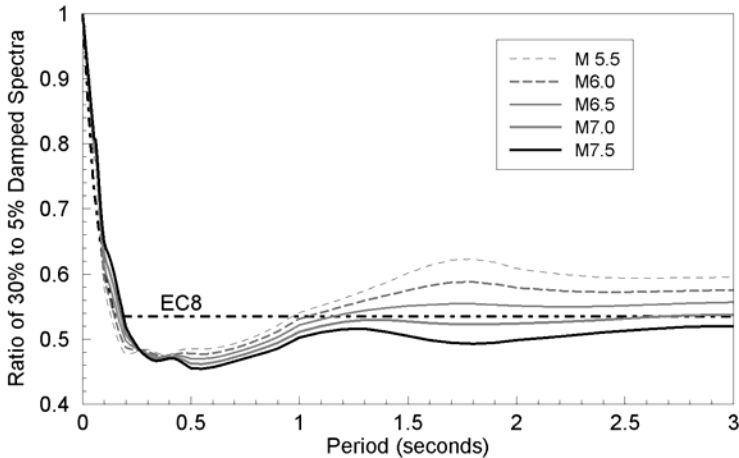

Figure 3. Variation of spectral scaling with damping for different magnitudes inferred for rock sites at 10 km from earthquakes of different magnitudes. Also shown are the scaling factors from EC8.

The variation of the spectral scaling factors indicated in Figure 3 is appreciable at certain response periods and this suggests that the use of scaling factors that are independent of the nature of the ground motion to adjust the 5% damped spectrum for higher levels of damping may be an oversimplification.

4. EARTHQUAKE ACTIONS IN PBSD CODES

4.1 Extrapolation of Current Code Formats

Somerville (1996) points out that seismic hazard curves are ideally suited to PBSD "*because they specify the ground motions that are expected to occur for a range of different annual probabilities (or return periods) that correspond to different performance objectives*". If it were found that the hazard curves for a given ground-motion parameter were of the same shape at all sites in a country, then it would be sufficient to provide 475-year maps of the selected ground-motion parameters and an equation to scale these amplitudes to other return periods. Since the shape of the

hazard curves will often vary throughout a country, advantage can be taken of the approximately linear relationship (over the range of return periods of usual engineering interest) between the logarithms of exceedance frequency and of the ground-motion parameter to determine two coefficients that relate them; from maps of these two coefficients the value of the ground-motion parameter can be determined for any return period (Grases *et al.*, 1992). This elegant approach would allow current code approaches such as that in IBC 2000 to cover all return periods of interest with just four hazard maps: two for the short-period spectral acceleration and two for the 1.0-second ordinate.

For PBSD, assuming that it will involved displacement-based design, the definition of long-period spectral ordinates will require at least a third parameter to be mapped: one option is the corner period that defines the constant displacement plateau mapped in the 2003 NEHRP guidelines; another is that proposed by Bommer *et al.* (2000) of mapping PGA, PGV and PGD and then defining the corner periods from the ratios of these parameters. Using the method of Grases *et al.* (1992) this leads to six maps, whereas if four return periods are to be considered — as recommended in Vision 2000 — and mapped individually, then the code would include 12 separate maps, which starts to be cumbersome (although this could be overcome by embedding the maps within a GIS provided on CD-ROM with the code). The situation becomes more complicated if maps for other parameters, such as independently defined vertical motions and strong-motion duration, are also needed.

4.2 Disaggregated Seismic Hazard

Disaggregation of seismic hazard (e.g., McGuire, 1995; Bazzurro and Cornell, 1999) allows the contributions made to the hazard at a site by different magnitude-distance pairs to be identified. In the USA there is the unique situation wherein the US Geological Survey operates a web site that allows users to enter the coordinates of the site and obtain disaggregations of the hazard at selected response and return periods; since the hazard maps and UHS in the seismic design codes are very closely related to the national hazard maps of the USGS, this effectively allows users of the code to identify hazard-consistent scenarios. Such a facility offers many advantages, not least of which is it enables selection of appropriate acceleration time-histories when these are required for design (Bommer and Acevedo, 2004). The controlling magnitude-distance pairs identified for horizontal spectral ordinates at the structural period of interest and for the selected return period can be used to estimate other parameters such as the vertical spectral ordinates and the strong-motion duration. This approach is preferable to producing separate maps for these other parameters since the horizontal and vertical spectral accelerations and the strong-motion duration, for a given return period, will often be controlled by different earthquake scenarios. This would imply that the motions were not compatible hence the use of multiple maps could result in the elastic spectral ordinates controlled by one source of seismicity being reduced by a duration-related ductility or damping factor controlled by another.

5. DISCUSSION AND CONCLUSION

From the preceding discussion it is clear that the basic information required for all representations of the earthquake ground-motions to be considered in design is the magnitude and distance of the dominant earthquake scenario. For most current design codes, however, there is no facility for performing disaggregation and the controlling earthquake scenarios are effectively invisible to the design engineer. Providing insight into dominant earthquake scenarios not only enables comprehensive definition of the ground motions but can also facilitate communication regarding seismic risk (Merovich, 1995).

Clearly there is much to be gained by providing some information regarding the disaggregated hazard in addition to the hazard maps in a code. There is, however, another possibility, which is to substitute the maps of ground-motion parameters for a given return period with maps of the magnitude and distance pairs that dominate the hazard at a given return period for each ground-motion parameter (e.g., Harmsen *et al*., 1999). There is also the possibility to go one step further and present maps of M-D pairs corresponding to the dominant source for each site, or if the hazard is affected by two different types of source, by a pairs of maps for each source (Bommer, 2000). The third element of the disaggregated hazard, the number (ε) of standard deviations away from the logarithmic mean, needs to be accommodated in the calculation of the resulting ground motions. There is no way to prescribe a procedure for drafting such maps, since they would need to be adapted to the characteristics of the seismicity of each region; Bommer and White (2001) present an illustrative application for Central America. These maps are not unlike the scenario ground motion maps proposed by Anderson (1997) but rather than presenting a single ground-motion parameter on each map, two maps (one of magnitudes, one of distances) provide the information required to determine all the required features of the design ground motions. At this point it is important to make a clarification: to represent the hazard from a given seismic source by a single M-D pair, coupled with a constant value of ε, is an approximation, since the hazard at different response periods will be dominated by different M-D combinations and different degrees of aleatory variability. The acceptability of this approximation, however, needs to be assessed not in absolute terms but in comparison with the much cruder approximations made in current code formats for expressing earthquake actions for design.

A key element in improving code representations of seismic actions is discarding the UHS concept — which many consider appropriate because of the inherent problems that it presents for any representation of earthquake actions beyond the spectral response at the structure's fundamental period of vibration — and also dropping the insistence on the total probability theorem (which the codes of Portugal and China have already done). This does not imply, however, total abandonment of probability: adjustments to the design return periods on each map can take account of the reduction of exceedance frequencies caused by separating seismic sources. Given the rather arbitrary basis of the return periods currently used in design codes, and the

large uncertainties associated with calculating the ground motions at the selected exceedance frequencies (and the approximation that inevitably results from presenting the continuous variations of hazard in discrete intervals of ground motion), it does not seem reasonable to oppose a change to the format of seismic codes on the basis of preserving nominal adherence to the total probability theorem.

The task of drafting seismic design codes for PBSD should be treated as an opportunity to consider afresh — and improve — the ways in which design earthquake actions are presented, without being constrained by the concepts and conventions that have led to the current state-of-the-practice embodied in today's seismic codes.

REFERENCES

Algermissen, S. T., and D. M. Perkins (1976). A probabilistic estimate of maximum accelerations in rock in the contiguous United States. *USGS OFR* 76-*416*.

Anderson, J. G. (1997). Benefits of scenario ground motion maps. *Engineering Geology* 48: 43-57.

ATC (1978). Tentative provisions for the development of seismic regulations for buildings. *ATC 3-06,* Applied Technology Council.

Bazzurro, P., and C. A. Cornell (1999). Disaggregation of seismic hazard. *Bull. Seis. Soc. Am.* 89: 501-520.

Bommer, J. J. (2000). Seismic zonation for comprehensive definition of earthquake actions. *Proceedings 6th Int. Conf. Seismic Zonation*, Palm Springs, CA.

Bommer, J. J., and A. B. Acevedo (2004). The use of real earthquake accelerograms as input to dynamic analysis. *Jrnl. Earthqu. Eng.* 8(special issue 1): *in press*.

Bommer, J. J., and R. Mendis (2004). Scaling of spectral displacement ordinates with damping ratios. *Earthquake Engineering & Structural Dynamics: in press.*

Bommer, J. J., and C. Ruggeri (2002). The specification of acceleration time-histories in seismic design codes. *European Earthquake Engineering* 16(1): 3-17.

Bommer, J. J., and N. White (2001). Una propuesta para un método alternativo de zonificación sísmica en los países de Ibero-América. *Proceedings 2nd Ibero-American Conference on Earthquake Engineering*, Madrid.

Bommer, J. J., A. S. Elnashai and A. G. Weir (2000). Compatible acceleration and displacement spectra for seismic design codes. *Proc. 12WCEE*, Paper no. 207.

Bozorgnia, Y., and K. W. Campbell (2004). The vertical-to-horizontal spectral ratio and tentative procedures for developing simplified V/H and vertical design spectra. *Jrnl Earthqu. Eng.* 8(2): 175-207.

CEN (2003). *Eurocode 8: Design of structures for earthquake resistant, Part 1: (Stage 49Draft), prEN 1998-1.* Comité Européen de Normalisation, Brussels.

Chai, Y. H., and P. Fajfar (2000). A procedure for estimating input energy spectra for seismic design. *Jrnl Earthqu. Eng*. 4(4): 539-561.

Dobry, R., R. D. Borcherdt, C. B. Crouse, I. M. Idriss, W. B. Joyner, G. R. Martin, M. S. Power, E. E. Rinnie and R. B. Seed (2000). New site coefficients and site

classification system used in recent building seismic code provisions. *Earthqu. Sp*. 16(1): 41-67.

Elnashai, A. S. (1997). Seismic design with vertical earthquake motion. *In*: Seismic Design Methodologies for the Next Generation of Codes, Fajfar & Krawinkler (*eds.*), Balkema, 91-100.

Grases, J., G. Cascante and E. Gajardo (1992). Earthquake hazard mapping for seismic design: a new approach. *Proc. 10WCEE*, 1: 5777-5782.

Gregor, N. J., and B. A. Bolt (1997). Peak strong motion attenuation relations for horizontal and vertical ground displacements. *Jrnl Earthqu. Eng*. 1(2): 275-292.

Harmsen, S. D., D. Perkins and A. Frankel (1999). Deaggregation of probabilistic ground motions in Central and Eastern United States. *Bull. Seis. Soc. Am* 89: 1-13

Heidebrecht, A. C. (2003). Seismic design implications of revisions to the national building code of Canada. *Proceedings Pacific Conf. Earthqu. Eng*., Paper no. 148.

Leyendecker, E. V., R. J. Hunt, A. D. Frankel and K. S. Rukstales (2000). Development of maximum considered earthquake ground motion maps. *Earthqu. Sp*. 16: 21-40.

McGuire, R. K. (1977). Seismic design spectra and mapping procedures using hazard analysis based directly on oscillator response. *Earthqu. Eng. Str. Dyn*. 5: 211-234.

McGuire, R. K. (1995). Probabilistic seismic hazard analysis and design earthquakes: closing the loop. *Bull. Seis. Soc. Am*. 85: 1275-1284.

Merovich, A. T. (1999). Future characterizations of ground motion for design (an engineer's perspective). *ATC 35-3*, Applied Technology Council, 9-20.

Perkins, D. M. (2004). Written communication (email) to Dr Dario Slejko, Trieste.

Pinho, R. (2004). Performance- and displacement-based earthquake loss estimation of urban areas. *This volume*.

Priestley, M. J. N. (2000). Performance based seismic design. *Proc. 12WCEE*, Paper no. 2831.

Rey, J., E. Faccioli and J. J. Bommer (2002). Derivation of design soil coefficients (S) and response spectral shapes for Eurocode 8 using the European Strong-Motion Database. *Journal of Seismology* 6: 547-555.

SEAOC (1995). *Vision 2000: Performance based seismic engineering of buildings*. Structural Engineers Association of California, Sacramento CA.

Shome, N., C. A. Cornell, P. Bazzurro and J. E. Carballo (1998). Earthquakes, records and nonlinear responses. *Earthqu. Sp.* 14(3): 469-500.

Somerville, P. (1996). Ground motion prediction for performance based seismic engineering. *Proc. 65th SEAOC Convention*, Maui, Hawaii.

Spudich, P. (1999). What seismology may be able to bring to future codes (a seismologist's perspective). *ATC 35-3*, Applied Technology Council, 21-33.

Stewart, J. P., S-J. Chiou, J. D. Bray, R. W. Graves, P. G. Somerville and N. A. Abrahamson (2002). Ground motion evaluation procedures for performance-based design. *Soil Dyn. Earthqu. Eng*. 22: 765-772.

A PRAGMATIC APPROACH FOR PERFORMANCE-BASED SEISMIC DESIGN

Mark ASCHHEIM[1]

ABSTRACT

A practical design approach that achieves a subset of the potential goals of performance-based earthquake engineering is described. The design approach integrates a number of recent developments and interprets fundamental observations from non-traditional perspectives. The shift in perspective—from a focus on period of vibration to a focus on yield displacement—allows simple and direct approaches to be used to limit peak displacement and system ductility demands to acceptable values. A required base shear strength is determined for use in preliminary design, maintaining consistency with current design practice. Nonlinear dynamic analyses are used for performance assessment and refinement of the design.

Keywords: Displacement-based design procedures; Yield displacement.

1. INTRODUCTION

The need to limit damage in moderate earthquakes has motivated research in performance-based earthquake engineering (PBEE) for over a decade. Substantial progress continues to be made in simulation capabilities, modeling of component response, and refinement of performance specifications. Multiple performance objectives (e.g., SEAOC, 1995) are routinely contemplated and the feasibility of displacement-based design approaches (e.g., Moehle, 1992) is accepted. However, current practice is far from achieving the potential of PBEE. A simple procedure is presented herein that addresses a subset of the response parameters of interest. The approach is effective for limiting roof drift and system ductility to arbitrary limits associated with one or multiple performance objectives (e.g., Sullivan et al., 2003) and produces a base shear for use in design, maintaining consistency with current design practice. The focus is on the lateral response of regular multistory buildings that can be represented by planar (2D) elements, that are not sensitive to P-Delta effects, and which are being designed at displacements well below their collapse values.

[1] Associate Professor, Department of Civil Engineering, Santa Clara University, 500 El Camino Real, Santa Clara, CA 95050; maschheim@scu.edu

2. SYSTEM SELECTION AND PRELIMINARY DESIGN

A design must be developed in order for its performance to be assessed analytically. This section describes relatively simple techniques that can be used in system selection, schematic design, and for the design of the members in the preliminary design of the selected system. The design relies on the use of an "equivalent" SDOF system to establish the base shear strength required to limit roof drift and system ductility demands to desired values. Roof drift is related to nonstructural damage and system ductility is related to structural damage.

2.1   Modal Property Estimates

Modal properties such as the first mode participation factor (Γ_1) and the modal mass coefficient (α_1) depend on the relative distribution of stiffness and mass rather than their absolute values, and therefore can be estimated prior to the detailed design of the structure. Estimates of adequate precision may be made on the basis of assumed mode shapes and mass distributions, or using simplified models as described by Miranda (1997). The values of Table 1 are based on the deflected shapes of Figure 1 and assume the floor masses to be uniform and the roof mass to be 80% of the floor mass. Somewhat similar values (or their inverses) are reported in Appendix I of the 1999 *Blue Book* (SEAOC, 1999).

Table 1. Modal property estimates

Number of Stories	Moment-Resistant Frames		Dual Shear Wall-Moment Frame Systems		Slender Cantilevered Shear Walls and Braced Frames	
	Γ_1	α_1	Γ_1	α_1	Γ_1	α_1
1	1.00	1.00	1.00	1.00	1.00	1.00
2	1.21	0.94	1.24	0.89	1.24	0.76
3	1.27	0.90	1.33	0.85	1.35	0.70
4	1.30	0.87	1.37	0.83	1.42	0.68
5	1.32	0.86	1.40	0.82	1.46	0.66
10	1.35	0.82	1.45	0.79	1.54	0.63
15	1.37	0.81	1.47	0.77	1.57	0.62
20	1.37	0.80	1.48	0.77	1.59	0.62

2.2   Yield Displacement Estimates

The yield displacements of structures in first-mode pushover analyses often can be estimated as a fixed percentage of the height of the structure, for a given structural system and material (e.g., Aschheim, 2002). Furthermore, the yield displacement is stable even as the lateral strength of the system is changed, in many design contexts. This is illustrated in Figure 2 for two four-story moment resistant frames. In contrast,
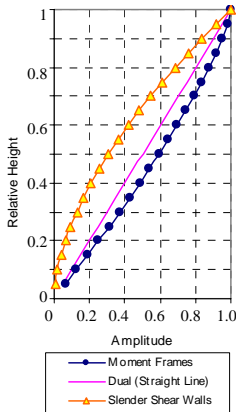
Figure 1. Deflected shapes used for determining values of Γ_1 and α_1 in Table 1.
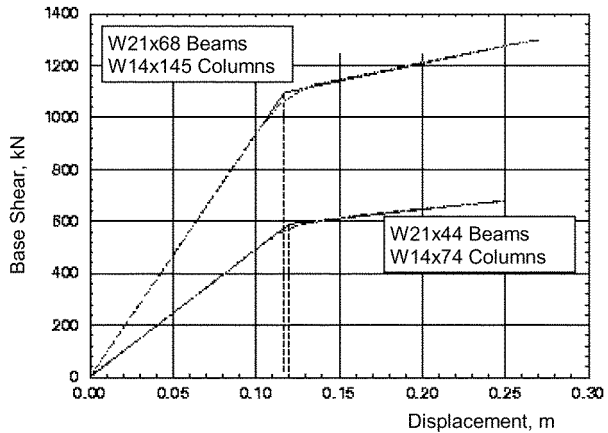
Figure 2. The stability of the yield displacement with changes in lateral strength. The capacity curves were obtained for two four-story moment-resistant steel frames in which beam and column depths remained constant and section weights were varied.

the fundamental period of vibration is recognized to be affected by the lateral strength (e.g., Priestley, 2000) and the number of stories. Because the yield displacement is relatively stable, it is a more robust parameter to use for preliminary design.

The displacement of the roof at yield may be estimated based on experience, simple formulae, or a previous nonlinear static analysis. For example, the yield displacement of steel moment-resistant frames often is 1 to 1.2% of the height of the frame. Estimates of the yield displacement of other systems are available; for example, Pinho (2004) provides estimates of the yield displacement of reinforced concrete moment resistant frames.

2.3   Inelastic Response Spectra

Estimates of the inelastic response of the "equivalent" SDOF (ESDOF) systems are required. The graphic depiction of inelastic demands and the underlying relationships used to estimate these demands, given the elastic ordinates, are discussed below.

The expected peak displacement response of inelastic systems can be estimated on the basis of elastic response spectra using equivalent linearization and displacement modification approaches. Equivalent linearization (e.g., the Capacity Spectrum Method) estimates the peak response on the basis of a linear elastic system having increased damping and reduced stiffness. Displacement modification considers the strength reduction (R) factor and period (T) to estimate the peak displacement in relation to the response of an elastic system having the same period
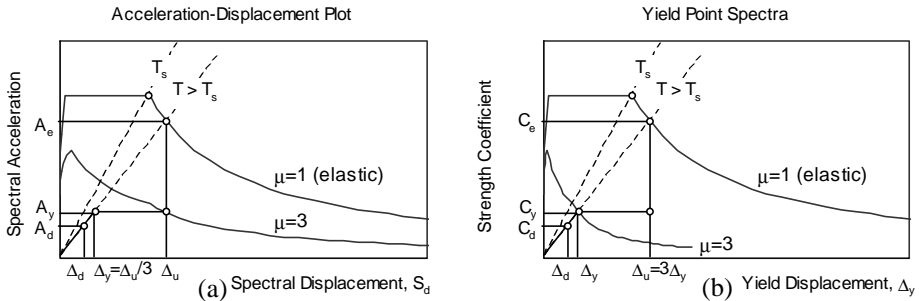
483

Figure 3. (a) ADRS format and (b) YPS format for response spectra, for μ=3.

and viscous damping. Both approaches require calibration to the response of inelastic SDOF oscillators. While either approach may be used, it is often easier to develop inelastic response spectra using displacement modification. Users of these approaches should be aware of the large inherent variability in response amplitudes.

Displacement modification relationships typically are derived on the basis of analyses in which oscillator strengths are adjusted to achieve constant ductility (μ) values or are determined using constant strength ratios (R factors). Regression of the response data leads to R-μ-T or R-C_1-T relationships. Either form may be used, as $C_1 = \Delta_u/S_d$ and $\mu = \Delta_u/\Delta_y = (\Delta_u/S_d)(S_d/\Delta_y) = C_1 R$, where Δ_u= peak displacement, Δ_y= yield displacement, and S_d= spectral displacement (of the linear oscillator).

Of particular relevance to design is the strength resulting in an expected ductility (or displacement) demand equal to a desired value. This is determined directly in studies in which constant R factors are used and the resulting displacement or ductility demands are regressed. R-μ-T relationships, when derived on the basis of constant ductility responses, represent the mean of the R values associated with a given ductility response. Oscillator strengths (V_y), however, are determined using the inverse of R (since $V_y = S_a \cdot m/R$) and the mean of the $1/R$ values differs from the mean of the R values. Furthermore, slight nonlinearity in the R-μ relationship indicates that the expected ductility will tend to exceed the value of constant ductility that was used to determine the R factor. Although the differences are small, it is preferable to use relationships derived on the basis of constant R values.

Distinct from the relationship used to estimate inelastic response is the graphical depiction of inelastic demands. The Capacity Spectrum Method (e.g., ATC-40, 1996) provides engineers with an intuitive and easily visualized means for understanding the relationship between structural properties (initial stiffness and strength) and peak displacement. This graphical format was retained in the improvements suggested by Fajfar (1999) and Chopra and Goel (1999). A similar visualization is available with the Yield Point Spectra (YPS) format, which plots curves of constant ductility demand on the axes of yield displacement and yield strength coefficient. Figure 3 compares these formats for oscillators having μ=3.
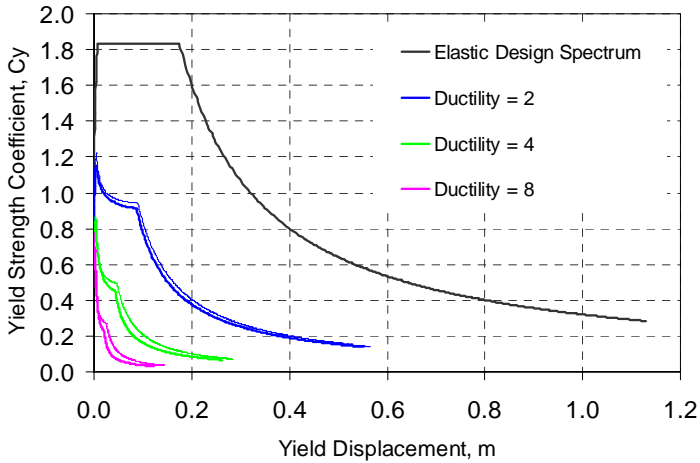
Figure 4. Yield Point Spectra: determined using Nassar and Krawinkler R-μ-T relationship (thick lines) and using ATC-55 R-C_1-T relationship (thin lines).

The author has a clear preference for the YPS format, primarily because this format uncouples the degree of inelastic response (associated with the hazard) from the properties of the structure (represented by the yield point). This uncoupling makes it easy to identify the domain of yield points that satisfies a given performance objective (termed an Admissible Design Region) and to identify the yield strength required to satisfy multiple performance objectives (Aschheim and Black, 2000).

Other advantages to the YPS format are: (1) YPS can be developed for arbitrary hysteretic relationships. (2) For design or evaluation, one can focus on the yield point, without concern for how the post-yield stiffness affects the intersection with the ADRS curves. (3) Peak response can be estimated by interpolating between the constant ductility curves, without iteration. (4) The YPS plots for individual ground motions are clear and easily read, but the same data plotted as a function of peak displacement can be difficult to make sense of. (5) P-Delta effects can be represented in YPS format (Aschheim and Hernández-Montes, 2003).

Figure 4 presents YPS determined by applying R-μ-T and R-C_1-T relationships to the NEHRP design spectra (2/3 of the MCE) for Site Class C conditions in Berkeley, California. The constant ductility curves were determined for ductilities of 2, 4, and 8. Shown by thick lines are results obtained using the R-μ-T relationship determined by Nassar and Krawinkler (1991) for bilinear oscillators having a post-yield stiffness equal to 2% of the initial stiffness. Shown by thin lines are results obtained using an R-C_1-T relationship that was developed for the ATC-55 project using the constant R factor approach, given by

$$C_1 = 1 + \frac{R-1}{90T^2}$$ (1)

where R = the ratio of the strength required for elastic response and the yield strength of an oscillator having an identical initial period, T. In general, the two relationships are seen to produce consistent results. However, the R-C_1-T approach results in somewhat higher design strengths for intermediate period oscillators having relatively large ductility demands.

2.4 Performance Limits

Discrete performance objectives, consisting of the pairing of performance limits and hazard levels, may be considered. The performance limits are interpreted in terms relevant to the response of the ESDOF system:

- The peak displacement limit of the ESDOF system is equal to Δ_u/Γ_1, where Δ_u= the roof drift limit.
- The displacement ductility limit of the ESDOF system is equal to the system ductility limit.

Note that peak dynamic interstory drifts can be related to peak roof drifts (e.g., Ghoborah, 2004), and that simple analytical expressions can relate code limits on story drift to roof drift limits.

2.5 Required Strength Determination

If an estimate of the roof displacement at yield is available, then the required strength can be determined using the procedure described in this section. For other cases, Admissible Design Regions may be used to identify a continuum of yield points that satisfy one or more performance objectives (Aschheim and Black, 2000).

Using standard approaches such as those described in ATC-40 (1996), the yield displacement of the ESDOF oscillator, Δ_y^*, is given by

$$\Delta_y^* = \Delta_y / \Gamma_1 \qquad (2)$$

YPS are used to determine the required yield strength coefficient of the ESDOF oscillator, C_y^*, from which the base shear coefficient (at yield) of the MDOF system is determined as

$$C_y = C_y^* \alpha_1 \qquad (3)$$

The base shear strength (at yield) of the MDOF system is given by $V_y = C_y W$. The fundamental period of the MDOF system matches that of the ESDOF system, given by

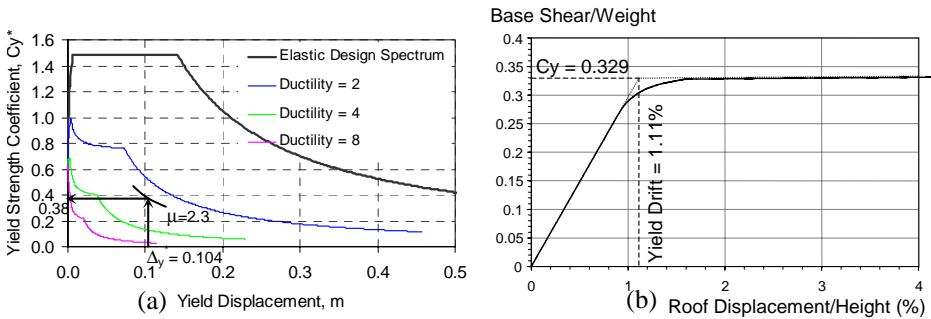$$T = 2\pi \sqrt{\frac{\Delta_y^*}{C_y^* g}}, \qquad (4)$$

Figure 5. (a) YPS for design of 3-story frame, and (b) capacity curve obtained from pushover analysis.

where g= the acceleration of gravity. (If the capacity curve exhibits early softening, formulas such as those in ATC-40 can be used to relate the initial and effective periods of vibration.)

As an example, the design of steel moment-resistant frames is typically controlled by drift. Suppose that the roof drift of a 3-story frame is to be limited to 2.5% of the building height and that story heights are 4 m. Assuming that the roof drift at yield is 1.1% of the height, the system displacement ductility limit is $\mu = 2.5/1.1 = 2.3$. The roof drift at yield is estimated to be $\Delta_y = (1.1\%)(4 \text{ m})(3) = 0.132$ m. The ESDOF yield displacement is estimated to be $\Delta_y^* = 0.132/1.27 = 0.104$ m, based on an estimate of Γ_1 from Table 1.

Using the YPS of Figure 5a, the required yield strength coefficient, C_y^*, is 0.38. The corresponding base shear coefficient (at yield) is $C_y = 0.38(0.90) = 0.34$, based on an estimate of α_1 from Table 1. The corresponding period, T, is 1.05 s according to Equation (4).

A design nominally satisfying these requirements is the 3-story moment-resistant frame designed for Los Angeles in the SAC steel project. The capacity curve for this frame, corresponding to the "M1" model in which beam-column elements extend between nodes located at the intersections of member centerlines, is given in Figure 5b. The base shear coefficient is 0.329 and fundamental period is 1.01 sec, making the frame slightly stiffer than is needed on the basis of the estimated properties. The actual values of Γ_1 and α_1 (1.27 and 0.83, respectively) can be used to refine the yield displacement estimate to $\Delta_y^* = (1.11\%)(4 \text{ m})(3)/1.27 = 0.104$ m and the required base shear coefficient to $0.38(0.83) = 0.32$. The actual base shear coefficient slightly exceeds the required base shear coefficient, resulting in a slightly lower period of vibration and a smaller displacement ductility demand, indicating acceptable performance. Further refinement of the design is not warranted at this stage.

The preceding illustrates that in a single step the strength can be selected to satisfy limits on roof drift and system ductility. This is simpler than other proposals for performance-based design and current design procedures, which often require several design cycles to satisfy code drift limits. This simplicity is possible when
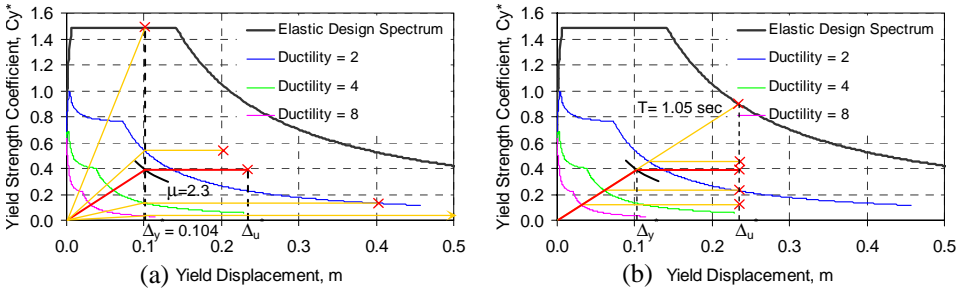
Figure 6. The influence of strength on peak displacement response (indicated by an "x") for (a) a given yield displacement, and (b) a given period.

demands are represented using YPS and design is based on an estimate of the yield displacement. As indicated by Equation (4), the period is a consequence of the strength required to satisfy the performance specification. Figure 2 illustrates that the yield displacement typically is independent of the strength provided. Therefore, had a different roof drift limit, a different hazard level, or a number of performance objectives been considered, the required base shear strength would have differed, but the associated yield displacement would have remained constant or nearly so.

More generally, the influence of lateral strength on peak displacement response is illustrated in Figure 6. Given a yield displacement estimate, one simply selects the strength that results in acceptable displacement and ductility demands (Figure 6a). In contrast, if the period is presumed to be known, the influence of strength on displacement is as illustrated in Figure 6b. In this case, the equal displacement rule applies, indicating that strength affects displacement ductility demands but not peak displacement. Consequently, proposals for design that use period as a fundamental design parameter must assume the period is unknown and can be varied (in conjunction with strength) to achieve the desired performance. In reality, a continuum of yield points exist that will satisfy the performance objective. The engineer, however, generally does not have the latitude to provide the strength and stiffness associated with a particular yield point, selected arbitrarily from the continuum that satisfies the performance objective. Thus, proposals that use period as a fundamental design parameter inevitably will be iterative, as infeasible yield points are tried and discarded in the search for an acceptable design. The stability of the yield displacement is exploited here to reduce or eliminate the need for iteration in design.

The base shear strength required of alternative structural systems may be evaluated in this fashion to determine the system best-suited to any particular application. Once the best-suited system has been identified, member depths and spans can be adjusted (within architectural constraints) to modify the yield displacement in order to reduce the required base shear strength (and cost).

2.6   Preliminary Design

In the preceding section, an estimate of the yield displacement was used to determine the required base shear strength coefficient, C_y, and corresponding period, T. Once determined, it will often be convenient to use C_y and T (rather than C_y and Δ_y) for the preliminary design of the structure, thereby allowing conventional (elastic) structural analysis software packages to be used for design as is currently done in practice. Required member strengths can be determined by a simple rigid-plastic mechanism analysis or using conventional design analyses in conjunction with an assumed overstrength factor. As the mathematical model of the structure is developed, the actual period of vibration, modal mass coefficient, and modal participation factor can be determined for the fundamental mode of response.

A comparison of the fundamental period of the preliminary design and the period of the ESDOF system provides a quick check on the validity of the assumptions used in preliminary design. Differences in these periods indicate potentially incorrect assumptions regarding the estimated yield displacement and estimated modal parameters. If significant differences exist, the actual period, design strength, and modal mass coefficient may be used to determine a new ESDOF yield point (using Equations (2) and (3) to determine the parameters C_y^* and Δ_y^*). This yield point may be found to have acceptable performance (i.e., if it is within the Admissible Design Region); if unacceptable performance is identified, a new ESDOF yield strength can be identified for the revised yield displacement, and member strengths then may be increased in proportion to the increase in base shear coefficient. The need for further iteration on the preliminary design would not be anticipated if member dimensions, span lengths, and material properties are kept approximately the same.

Although the design approach is based on the use of ESDOF systems and nonlinear static (pushover) analysis, a nonlinear model of the structure is not required for preliminary design. Strength may be assessed by means of a mechanism analysis or by using approximate overstrength factors. However, nonlinear static analyses can aid in understanding the behavior of the structure (e.g., Krawinkler and Seneviratna, 1998), and once developed, the model used for the nonlinear static analysis may be useful for dynamic analyses as described in the next section.

3. DESIGN REFINEMENT AND PERFORMANCE ASSESSMENT

The preliminary design was determined to limit peak roof drifts and system ductilities for a mechanism involving primarily first mode deformations. MDOF effects (associated with higher mode contributions) can significantly affect interstory drifts, story shears, and many other response quantities. For many structures, MDOF effects should be addressed to establish: (1) that the intended inelastic mechanism develops, (2) statistical distributions of performance parameters (e.g., interstory drifts and deformation demands in inelastic components), and (3) the forces that must be
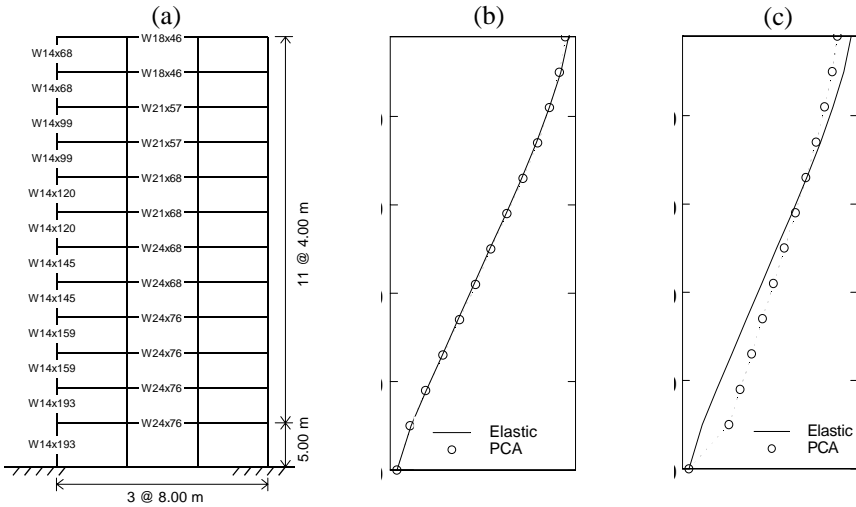
Figure 7. PCA and elastic mode shapes computed for a 12-story steel moment frame (a) under a beam-hinging mechanism (b) and a weak-story mechanism (c).

sustained (in force-controlled components) to enable the development of the intended mechanism.

Many approximate techniques for accounting for MDOF effects in inelastic systems have been suggested, but experience within the ATC-55 project suggests these techniques are not universally applicable. One promising technique identified within the ATC-55 project is the Scaled Nonlinear Dynamic Procedure, so named because ground motion records are scaled so that the peak roof displacement matches the estimate made on the basis of the ESDOF system. It is suggested that this technique can be used to determine statistical distributions of performance parameters and to determine the strengths that must be provided to force-controlled components. Further information on this procedure can be found in Aschheim et. al (2004).

Finally, a characterization of the predominant mode and an assessment of the predominant mechanism can be made using a technique of multivariate statistics known as Principal Components Analysis (PCA). When applied to the displacement response data of an elastic dynamic system, the principal components coincide with or are related to the elastic mode shapes, depending on the mass distribution. PCA may be applied to data obtained from systems responding inelastically, to identify the predominant "modes" of such systems. Figure 6 illustrates the first PCA mode shapes and elastic mode shapes for a 12-story steel moment-resistant frame having a uniform distribution of mass. The first PCA mode shape nearly coincides with the elastic mode shape when a beam-hinging mechanism develops (Figure 7b). The development of a weak-story mechanism after the lowest-story columns were numerically weakened is easily identified in the PCA mode shape of Figure 7c. Further information can be found in (Aschheim, Black, and Cuesta, 2002).

4. CONCLUSIONS

In the space available, a simple and effective design procedure was outlined that explicitly addresses roof drift, system ductility, and the influence of MDOF effects (higher mode effects). The design procedure uses an estimate of the yield displacement as a primary design parameter. Yield Point Spectra are used to determine the required lateral strength. The fundamental period of vibration of the structure is observed to be a consequence of the strength provided to satisfy the performance objectives, rather than being an independent parameter whose value is estimated at the start of the design, as is done in conventional design procedures. The basic elements of the design approach are described herein; examples provided in the references suggest the robustness of the basic assumptions and procedures.

The design procedure was developed on the basis of planar systems and involved simplifying assumptions. Various modifications can be considered. For example, corrections could be introduced to account for tendency of ESDOF systems to overestimate the roof displacement of inelastic systems (e.g., Chopra et al., 2003). However, the slight conservatism that results from neglecting this effect is considered advantageous at this time. Similarly, the Yield Point Spectra format may be used to plot curves of other performance parameters (e.g., hysteretic energy dissipation or residual displacement ductility). However, ductility is directly related to the roof displacement, and other parameters can be correlated to ductility (e.g., Farrow and Kurama, 2003). Similarly, the design procedure is intended for structures that do not develop plan torsion. Extensions to consider torsionally-irregular structures can be considered at an appropriate time. Finally, the validity of the design procedure depends on the accuracy with which the structure is modeled. Assumptions regarding the strength, stiffness, and hysteretic characteristics of the lateral-force-resisting and gravity-load carrying structural components as well as the possible participation of so-called "non-structural" components can be significant, regardless of the method used for design.

REFERENCES

Aschheim, M., E. Black (2000). Yield Point Spectra for seismic design and rehabilitation, *Earthquake Spectra*, 16(2):317-335.

Aschheim, M. A. (2002). Seismic design based on the yield displacement, *Earthquake Spectra*, 18(4):581-600.

Aschheim, M. A., E. F. Black, I. Cuesta (2002). Theory of principal components analysis and applications to multistory frame buildings responding to seismic excitation, *Engineering Structures*, 24(8):1091-1103.

Aschheim, M., E. Hernández Montes (2003). The representation of P-Δ effects using Yield Point Spectra, *Engineering Structures*, 25:1387-1396.

Aschheim, M., T. Tjhin, C. Comartin, R. Hamburger, M. Inel (2004). The Scaled Nonlinear Dynamic Procedure, *ASCE Structures Congress*, May 22-26.

ATC-40 (1996). *Seismic Evaluation and Retrofit of Concrete Buildings*, Report No. SSC 96-01, Seismic Safety Commission, State of California.

Chopra, A. K., R. K. Goel (1999). Capacity-demand-diagram methods based on inelastic design spectrum, *Earthquake Spectra*, 15(4):637-656.

Chopra, A. K., R. K. Goel, C. Chintanapakdee (2003). Statistics of single-degree-of-freedom estimate of displacement for pushover analysis of buildings, *Journal of Structural Engineering*, 129(4):459-469.

Fajfar, P. (1999). Capacity spectrum method based on inelastic demand spectra, *Earthquake Engineering & Structural Dynamics*, 28(9):979-993.

Farrow, K. T., Y. C. Kurama (2003) SDOF demand index relationships for performance-based seismic design, *Earthquake Spectra* 19:799.

Ghobarah, A. (2004). On drift limits associated with different damage levels, *International Workshop on Performance-Based Seismic Design*, Bled, Slovenia, June 28 – July 1, 2004.

Krawinkler, H., G. D. P. K. Seneviratna (1998). Pros and cons of a pushover analysis of seismic performance evaluation, *Engineering Structures*. 20(4-6):452-464.

Miranda, E. (1997). Estimation of maximum interstory drift demands in displacement-based design, Seismic Design Methodologies for the Next Generation of Codes, Proceedings of the International Workshop, Bled, Slovenia, 24-27 June, 253-264.

Moehle, J. P. (1992). Displacement-based design of RC structures subjected to earthquakes, *Earthquake Spectra*, 8(3):403-428.

Nassar, A. A., H. Krawinkler (1991). *Seismic Demands for SDOF and MDOF Systems*, John A. Blume Earthquake Engineering Center, Stanford University.

Pinho, R. (2004). Performance and displacement-based earthquake loss estimation of urban areas, *International Workshop on Performance-Based Seismic Design*, Bled, Slovenia, June 28 – July 1, 2004.

Priestley, M. J. N. (2000). Performance-based seismic design, *12th World Conference on Earthquake Engineering*.

SEAOC (1995). *Vision 2000*, Structural Engineers Association of California, Sacramento, CA.

SEAOC (1999). *Recommended Lateral Force Requirements and Commentary*, Structural Engineers Association of California, Sacramento, CA.

Sullivan, T. J., G. M. Calvi, M. J. N. Priestley, M. J. Kowalsky (2003). The limitations and performances of different displacement based design methods, *Journal of Earthquake Engineering*, 7:201-241.

EXAMINATION OF THE EQUIVALENT VISCOUS DAMPING APPROACH

Hazim DWAIRI[1] and Mervyn KOWALSKY[2]

ABSTRACT

This paper aims to investigate the accuracy and potential problems associated with the equivalent viscous damping concept as applied to direct displacement-based seismic design, and to suggest a recommendation to modify Jacobsen's approach that is based on level of ductility and hysteretic model used. The parameters considered include: Earthquake time-history and hysteretic models ranging from origin centered systems to Takeda-type response systems. Results of the research indicate that the fundamental period of the ground motion is a critical variable in assessing the accuracy of the equivalent viscous damping concept. In general, results from non-linear analysis conducted with regular sinusoidal events is excellent, which is expected given the assumptions of sinusoidal response in Jacobsen's approach, however, results from real time histories indicate more scatter. In this paper, results for two hysteretic models based on 100 earthquake records and 125,000 inelastic time-history analyses indicate that Jacobsen's approach overestimates damping which requires a reduction factor that will be introduced in a future study for 4 hysteretic models and based on 280,000 inelastic time-history analyses.

Keywords: Equivalent damping; Jacobsen's approach; Displacement-based design.

1. INTRODUCTION

1.1   Direct Displacement-Based Design

In the Direct Displacement-Based Design (DDBD) approach, a structure is designed such that a predefined displacement limit is achieved when the structure is subjected to a predefined earthquake that is consistent with that assumed for the design. The design procedure utilizes Jacobsen's approach [1] for equivalent viscous damping and the Gulkan and Sozen [2] substitute structure concept to approximate the displacement of an inelastic system with equivalent elastic system. The DDBD approach focuses the design directly on displacement demand which is more attractive than strength as a damage measure. Due to the fact that structures in seismic regions are designed to respond in-elastically and the design procedure needs to be

---

[1] *Ph.D. Student.* [2] *Assistant Professor.*
Department of Civil Engineering, North Carolina State University, Campus Box 7908, Raleigh, NC 27695

simple, methods of approximating maximum displacements of inelastic system gain primary importance in DDBD.

One of the methods used to determine the maximum displacement of a non-linear system is the inelastic response spectrum, where an exact spectrum could be obtained for a SDOF system with a selected period and hysteretic rule. Unfortunately, the resulting R-μ-T relationships vary also as a function of earthquake and soil type. The other method being used involves representing the nonlinear system by an equivalent elastic system with effective stiffness and equivalent viscous damping. The advantage of this method lies in its simplicity and ability of using the more familiar elastic response spectrum.

1.2   Equivalent Viscous Damping Approach

The Equivalent viscous damping concept was first introduced by Jacobsen in 1930 [1]. In his paper, Jacobsen approximated the steady state solution of a nonlinear SDOF system by equating the energy dissipated by that system to the energy dissipated by one cycle of sinusoidal response of a linear system with equivalent viscous damping. He also pointed out the arbitrariness in choosing the one cycle criterion and that it is not better than the other criterion of equivalent time-average of damping force, although he noted it was superior at or near resonance. In 1974, Gulkan and Sozen [2] introduced the definition of substitute damping, utilizing the earthquake time-history and the response time-history of SDOF frames. In their research, they computed the substitute viscous damping by equating the energy input into the system to the energy dissipated by an imaginary viscous damper over the period of excitation. Gulkan and Sozen compared the results of their approach with experimental results and with Jacobsen's approach, and found them to be in good agreement. It should be noted that the Gulkan and Sozen approach requires prior knowledge of the system response which is not available at the design stage, while Jacobsen's approach requires no such knowledge and as a result is more appealing for design procedures.

In 1976, Shibata and Sozen [3] introduced the definition of a substitute structure to determine the seismic design forces for a given structure and earthquake intensity. They characterized the substitute structure by the substitute damping and effective, or secant stiffness to maximum response. This is the slope of the line that connects the origin to the maximum displacement in a hysteretic model. Utilizing the definition of effective stiffness, and applying it to the bilinear hysteretic model in figure 1 leads to the following relation between initial and effective stiffness:

$$K_0 = \frac{\mu}{r\mu - r + 1} K_{eff} \tag{1}$$

In 1995, Kowalsky et al. [4] applied Jacobsen's approach to the Takeda hysteretic model [5]; by utilizing the same formulation and applying it to the bilinear hysteretic model shown in figure 1, i.e., equating the energy dissipated by one cycle

of the bilinear model with the energy dissipated by one cycle of sinusoidal response of a spring-dashpot-mass system at resonance, with spring constant K_{eff} yields:

$$\xi_{hyst} = \frac{2}{\pi} R_{LA} \tag{2}$$

$$R_{LA} = \frac{A_1}{A_2} = \frac{(\mu - 1)(1 - r)}{\mu(1 + r\mu - r)} \tag{3}$$

In Eq.(3), A_1 is the area of the nonlinear hysteretic loop, A_2 is the area of the rigid perfectly plastic loop that passes through the maximum displacement, and μ is the displacement ductility.
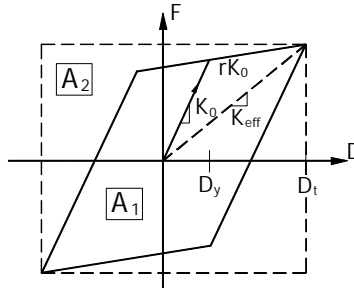
Figure 1. Jacobsen's equivalent damping approach.

2. BACKGROUND OF DIRECT DISPLACEMENT-BASED DESIGN

As discussed earlier, the fundamental goal of the direct displacement-based design is to obtain a structure which will reach a predefined target displacement when the structure is subjected to an earthquake consistent with the design level event. DDBD is a response spectrum-based design procedure in which the substitute structure methodology, developed by Gulkan and Sozen [2] and expanded to multi-degree-of freedom structure by Shibata and Sozen [3], is utilized to model an inelastic system with equivalent elastic properties as shown in figure 1.

After general parameters such as column height and mass being established, the following steps could be followed to obtain the design forces:

1. **Obtain a target displacement (D_t):** In the case of a single column bridge, the target displacement can be obtained from the drift ratio or strain criterion that defines the desired level of performance of the column.

2. **Estimate level of equivalent viscous damping (ξ_{eq}):** Using the chosen target displacement and an estimated yield displacement based on the column section and yield curvature, the ductility level is calculated in accordance with Eq.(4). The ductility versus hysteretic damping relationship is obtained utilizing Jacobsen's approach with a convenient assumed hysteretic model. An additional 0%-5% viscous damping could be added to obtain the level of equivalent viscous damping. An example of the ductility versus equivalent damping relation is

shown in figure 2; for instance, a ductility of 2.1 and the Takeda smallest loop hysteretic model yield a 10% hysteretic damping.
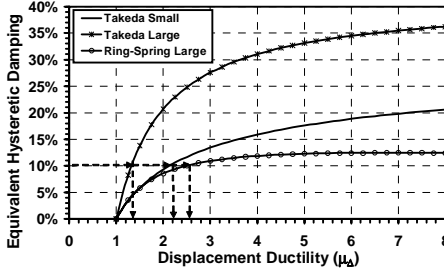
$$\mu_\Delta = D_t/D_y \tag{4}$$

Figure 2. Hysteretic damping versus ductility for modified Takeda and Ring-Spring models.

3. **Determine effective period of the structure (T_{eff}):** utilizing the target displacement, level of equivalent viscous damping and elastic response spectra for the chosen seismic demand, the equivalent period of the structure could be determined as shown in figure 3. For a design displacement of 0.375m and 10% level of damping, the equivalent period is estimated to be 2.1 seconds.

4. **Evaluate effective stiffness (K_{eff}) and design base shear (V_B):** using the equivalent period and the structure mass, the equivalent stiffness could be easily calculated as given by Eq.(5). Compute the base shear by multiplying the equivalent stiffness by the target design displacement (D_t).

$$K_{eff} = 4\pi^2 \frac{M}{T_{eff}^2} \tag{5}$$

5. **Design the structure:** and check for the assumed or estimated yield displacement, if it changes significantly, repeat the previous steps until convergence is achieved.
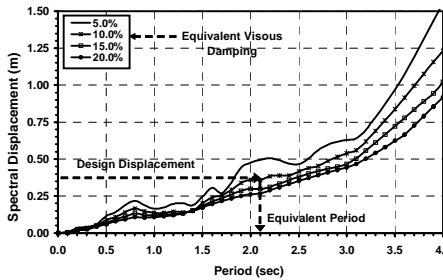

Figure 3. Obtaining effective period for direct displacement-based design.

3. STUDY PARAMETERS AND ASSESSMENT ALGORITHM

In this paper, an assessment algorithm has been used to investigate the accuracy of the equivalent viscous damping approach (Kowalsky's formulation of Jacobsen's approach [5]) as it's been used in direct displacement-based seismic design (DDBD). Jacobsen's approach was tested first for a sinusoidal earthquake to eliminate the main assumption in his approach. Then it was tested for real earthquake records, and finally a comprehensive evaluation of the approach was carried out utilizing a large number of earthquake records.

3.1 Study Parameters

In this study, The Takeda hysteretic model [5] and Ring-Spring hysteretic model [6] were considered as shown in figure 4. An expression between displacement ductility and hysteretic damping could be obtained by applying Jacobsen's approach to both models. The expression given by equations 6-8 is for the Takeda model, where μ is the displacement ductility, α is the unloading stiffness and γ is the reloading stiffness.

Two extreme cases were selected for the Takeda model: the smallest and largest loop possible by changing α and β values. For the Ring-Spring model only the largest possible loop was considered and the equivalent viscous damping expression is not shown due to size limitations.

$$\xi_{hyst} = \frac{2}{\pi} R_{LA} \tag{6}$$

$$R_{LA} = 1 - \frac{3}{4}\mu^{\alpha-1}\gamma - \frac{1}{4}\left[(r\beta\mu/\gamma)(1-1/\mu)+1\right]\left[2-\beta(1-1/\mu)-\mu^{\alpha-1}\gamma\right]-$$
$$\frac{1}{4}\left[(r\beta^2\mu/\gamma)(1-1/\mu)^2\right] \tag{7}$$

$$\gamma = r\mu - r + 1 \tag{8}$$
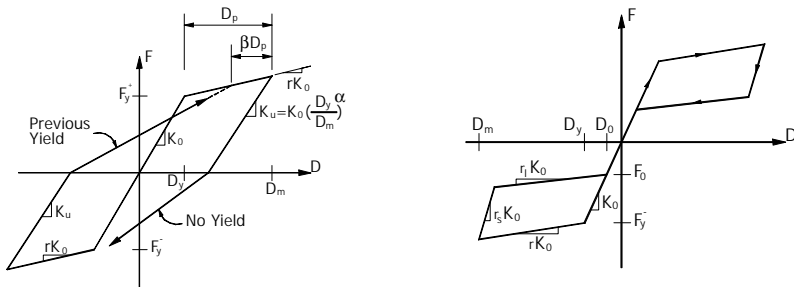
(a) Modified Takeda hysteretic model   (b) Ring-Spring hysteretic model

Figure 4. Hysteretic models considered. (a) modified Takeda hysteretic model. (b) Ring-Spring hysteretic model.

Figure 2, shows a plot of the relationship between displacement ductility and hysteretic damping for the two extreme cases of Takeda's model and the Ring-Spring model. For the Takeda model, the maximum hysteretic damping produced by the largest loop is 41% and by the smallest is 32%, at impractical levels of ductility, while the largest damping level could be achieved by the Ring-Spring models is 12%. So in this study the hysteretic damping considered, ranges between 2% and 30%.

3.2   Assessment Algorithm

The equivalent viscous damping is an important component of DDBD as it represents the non-linear response of the hysteretic system with the effective stiffness. The following algorithm has been used to investigate the accuracy of those relationships as they were used in the direct displacement-based seismic design.

1. Select earthquake time history and generate elastic response spectrum for different levels of damping. Each point maybe assumed to represent a SDOF equivalent oscillator with equivalent parameters, namely: design displacement, equivalent period and equivalent viscous damping, as shown in figure 3.

2. Select a hysteretic model, and formulate the relationship between ductility and equivalent viscous damping. Using the damping value from point one, the level of ductility in the system could be determined as shown in figure 2. For each level of hysteretic damping there are three values of ductility based on the modified Takeda and Ring-Spring hysteretic models.

3. Using the design displacement, ductility and equivalent period, define the inelastic SDOF structure by calculating, the initial stiffness and the yield moment of that structure.

4. Conduct inelastic time history analysis for the nonlinear structure and compare the maximum resulted displacement with the design displacement selected in point 1.

4. ANALYSIS RESULTS AND DISCUSSION

The major assumptions made by Jacobsen were (1) assuming a steady state response (sinusoidal) and, (2) the arbitrary choice of the one cycle criterion where Jacobsen utilizes only one cycle of the response to estimate the equivalent viscous damping. Those two assumptions play a major rule in the accuracy of the method especially if applied to real earthquake records. For instance, in a real earthquake response there is a good possibility that the maximum response will occur before the transient response damps and the system reaches a steady state response. In a fling type event, where the structure could be pushed immediately into the inelastic range forming one large loop, it seems reasonable to adopt the one cycle criterion, but what if the structure was pushed gradually into the inelastic range? In order to answer those questions, it was

decided to investigate the accuracy of Jacobsen's approach for different types of ground motions.

In this paper, all the analyses were conducted assuming 2% viscous damping and different levels of hysteretic damping. The main focus of the analysis was to compare the chosen design displacement with the actual time history displacement and to use the ratio of both displacements as an estimate of the accuracy of Jacobsen's approach. In the following sections, a discussion of the results from the assessment of the equivalent viscous damping approach for various types of earthquakes is presented.

4.1 Sinusoidal Earthquake Results

Since Jacobsen assumed a sinusoidal response in his formulation of the equivalent viscous damping, a number of sine waves were chosen to test the accuracy of the procedure based on the previous algorithm. Only the results of one sine wave with circular frequency of 10 Hz is shown in figure 5. Elastic response spectra were generated for different viscous damping values ranging between 4% and 32%; assuming in the analysis 2% viscous damping and the remainder as hysteretic damping. Figure 5 shows the ratio of the inelastic time history analysis displacement to the design displacement (i.e., inelastic oscillator to equivalent elastic oscillator displacement) versus equivalent period as a function of damping for the Takeda small and large loop models and the Ring-Spring model. The dashed vertical line at a period of 0.62 seconds represents the period of the sinusoidal earthquake, and it is clear that it forms a turning point in the results. For periods less than the earthquake fundamental period the design is conservative (i.e., overestimating the actual displacement) while for greater periods, the design generally underestimates the actual displacement. The same behavior was noticed for different sinusoidal earthquakes with different fundamental periods. Clearly Jacobsen's approach fails to estimate the maximum displacements for periods less than the earthquake period and high levels of damping.

The difference between the largest and smallest loop models is that the latter predicts less hysteretic damping for the same level of ductility. From figure 6, it's clear that the largest loop model overestimates the damping, which underestimates the displacements and yields more unconservative designs than the smallest loop model. Similarly, Ring-Spring model predicts the lowest damping for the same ductility which resulted in better ratios than both Takeda models.

To further investigate this behavior, the displacement time histories for the nonlinear and the equivalent linear oscillator were plotted as shown in figure 6. In addition, the hysteretic behavior for the nonlinear oscillator was also plotted with the linear response of the equivalent oscillator. Three oscillators were chosen to represent the results with ratios less than, equal to and greater than one. Each oscillator has a different fundamental period, effective and initial stiffness, ductility and equivalent viscous damping. It was concluded that for the cases with a ratio less than one, as shown in figure 6a, the displacements were overestimated because the nonlinear

oscillator didn't respond in-elastically; instead it remained linear in most of the cases or did not go far into the inelastic range in other cases.
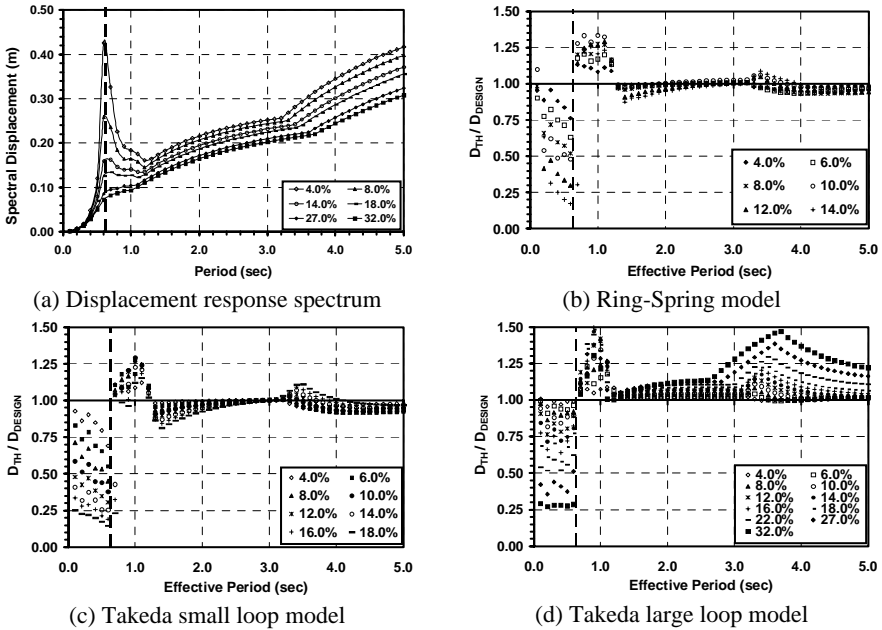

(a) Displacement response spectrum

(b) Ring-Spring model

(c) Takeda small loop model

(d) Takeda large loop model

Figure 5. Time-history to design displacement ratio for sinusoidal earthquake ($\omega = 10$ Hz).

In the case where the ratio is nearly one, there was good agreement between the nonlinear and linear oscillator displacement time histories, the loops were developed gradually with sufficient amount of ductility into the system as shown in figure 6b.

After investigating some of the cases where the displacements were underestimated (i.e., ratio greater than one), the hysteretic loops show a shift in the vibrating position of the nonlinear oscillator; this behavior is shown in figure 6c. This behavior is attributed to a large pulse that pushes the structure into the inelastic range and as a result, when it starts to unload, it vibrates around a new position which causes the shift in the loops as shown.

4.2   Typical Real Earthquake Results

Since real earthquake records are unlikely to have a specific frequency, but rather a range of frequencies, the sudden change in the results seen in figures 5 will be less apparent. Due to an expected increase in the scatter and to show a sample of real earthquakes results, two typical real earthquake records with different characteristics were selected: (1) Northridge 1994, and (2) Kobe 1995.
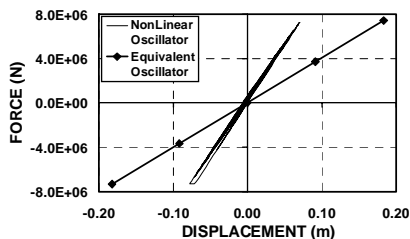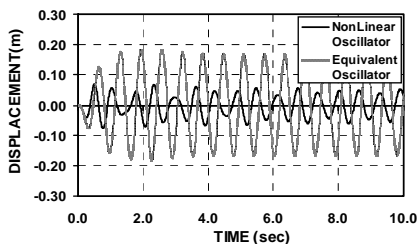
(a) Displacement Time-History and Hysteretic Behavior for Oscillator 1 (Teq=0.7 sec)
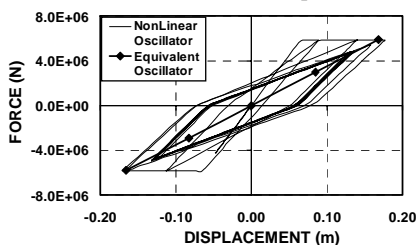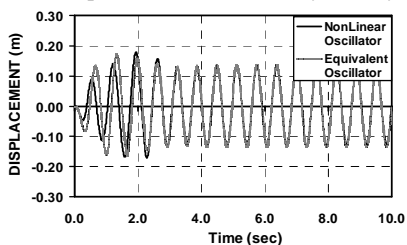
(b) Displacement Time-History and Hysteretic Behavior for Oscillator 2 (Teq=0.75 sec)
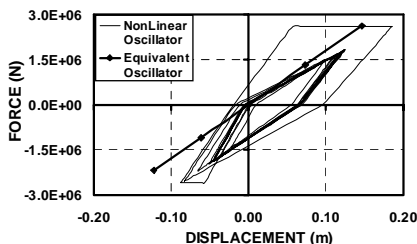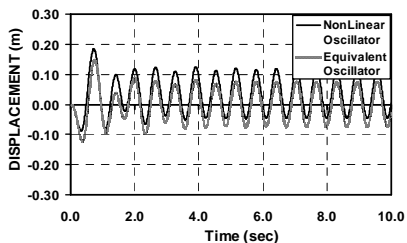
(c) Displacement Time-History and Hysteretic Behavior for Oscillator 3 (Teq=1.05 sec)

Figure 6. Nonlinear and equivalent oscillators displacement time-history and hysteretic behavior for the Takeda small loop model, sinusoidal earthquake and 12% hysteretic damping.

The ratio of inelastic time-history analysis displacement to design displacement (i.e., inelastic oscillator to equivalent elastic oscillator displacement) is shown in figures 7 and 8. The Takeda small and large loop models and Ring-Spring model were considered for various levels of damping.

The results from the two records show wider scatter than the sinusoidal earthquake, as expected, and varies between conservative and unconservative. For both records a wider scatter is noticed in the short period region where the oscillators vibrate about their fundamental frequency, while less scatter is noticed in the long period region where oscillators vibrate about the loading function frequency. The two records clearly have distinctly different response spectrums; both have a flat portion or humps, depending on the level of damping. By comparing the results of both

records, Jacbson's approach is not only sensitive to the earthquake characteristics but also to the oscillator fundamental period and level of ductility. Clearly the best way to quantify the scatter, in order to introduce any modification, will be through obtaining a large number of such results and utilizing a simple statistical analysis.
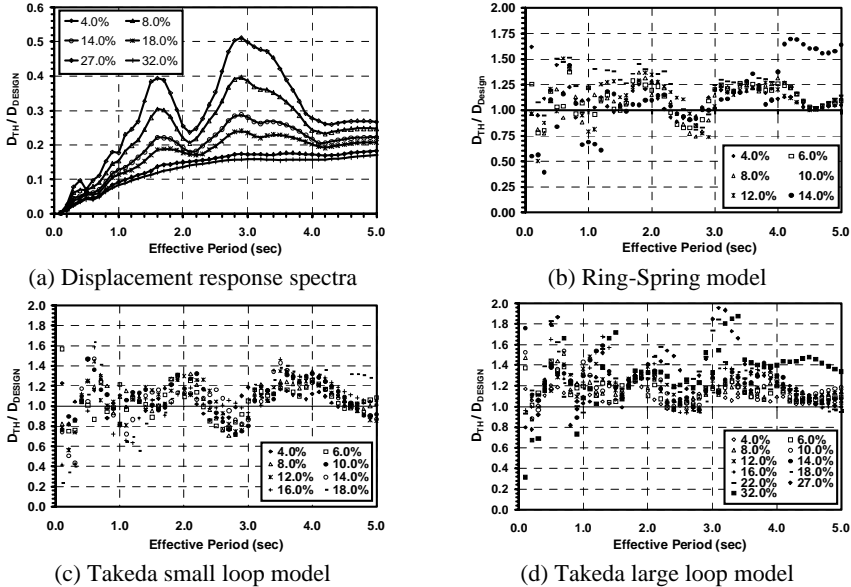

(a) Displacement response spectra

(b) Ring-Spring model

(c) Takeda small loop model

(d) Takeda large loop model

Figure 7. Time history to design displacement ratio for the Northridge earthquake, 1994.

4.3 Comprehensive Evaluation of the Equivalent Damping Approach

Given the variation of the results for real earthquakes and due to the significance of Jacobsen's approach in the direct displacement-based design, it was decided to evaluate the equivalent viscous damping approach for a large number of real earthquake records. In this study 100 earthquake records were selected, in order to evaluate the accuracy of the approach and to obtain more reliable and simple statistical data. The 100 records were collected and categorized based on the soil type, namely: B, C, D, E and NF by Miranda [9]. The previously discussed assessment algorithm was carried out for each one of the records, assuming the Takeda small and large loop models in addition to Ring-Spring hysteretic model. 50 oscillators were used with fundamental periods range from 0.1 to 5.0 seconds, for various levels of equivalent viscous damping. Each oscillator was assumed to be designed according to the DDBD approach, the nonlinear oscillator was identified and inelastic time-history analysis was carried out to determine its actual maximum displacement. The total number of inelastic time-history analysis conducted in this part of the study is 125,000.

The results for all 100 earthquake records were averaged and plotted as a function of equivalent damping against oscillator periods as shown in figures 8 and 9. The coefficient of variation of the average values, which represents the scatter of the data around its average, is also shown in the same figures.

On average, the hysteretic models which predict less damping have better results, which suggest that all over Jacobsen's approach overestimates damping and consequently underestimates actual displacements. It worth mentioning that by averaging the results, the effect of earthquake characteristics has been eliminated since the ratios are about the same for all oscillators. The coefficients of variation are bounded between 10% and 30% except for short periods, which is fairly good considering the large number of earthquakes considered.
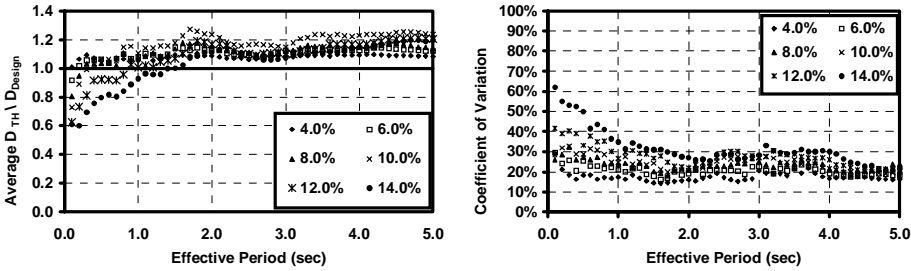
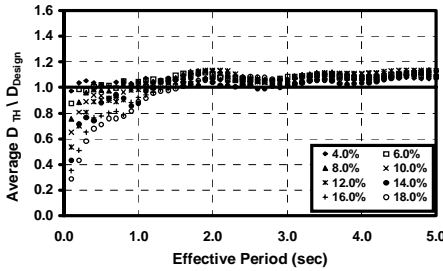(a) Average D_{TH}/D_{Design} for Takeda small loop   (b) CoV for Takeda small loop

Figure 8. Average time-history to design displacement ratios for Ring-Spring hysteretic model and 100 earthquake records.

5. CONCLUSIONS

Since the major assumption in Jacobsen's approach is a sinusoidal response, the approach was tested with a sinusoidal earthquake; the results indicated, as expected, that the approach works very well, however, it overestimates the displacements for periods less than the sine wave fundamental period. In some cases the approach underestimates the displacements not only due to overestimating damping but also due to the shift in the hysteretic loops because the oscillator starts vibrating around a new equilibrium position. A wider scatter is clearly noticed for real earthquake records, which varies based on the earthquake characteristics, oscillator fundamental period and level of ductility.

The results for 100 earthquake records indicate that Jacobsen's approach, on average, overestimates damping and consequently underestimates the actual displacements which suggest that a reduction factor is needed. As a part of future work, a reduction factors will be obtained based on hysteretic model and level of ductility.
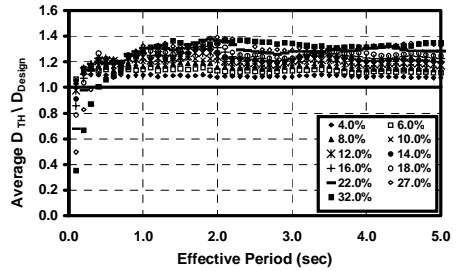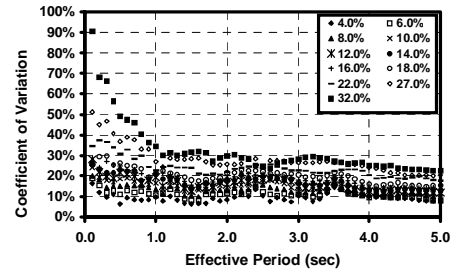
(a) Average D_{TH}/D_{Design} for Takeda small loop   (b) Average D_{TH}/D_{Design} for Takeda large loop
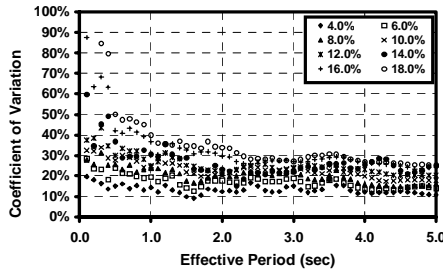
(c) CoV for Takeda small loop   (d) CoV for Takeda large loop

Figure 9. Average time-history to design displacement ratios for Takeda hysteretic model and 100 earthquake records.

REFERENCES

Jacobsen, L. S. (1930). Steady Forced Vibrations as Influenced by Damping. *ASME Transactions* 1930, 52(1): 169-181.

Gulkan, P., and M. Sozen. (1974). Inelastic Response of Reinforced Concrete Structures to Earthquake Motion. *ACI Journal* 71: 604-610.

Shibata, A., and M. Cozen. (1976). Substitute Structure Method for Seismic Design in R/C. *Journal of the Structural Division, ASCE* 102(ST1): 1-18.

Kowalsky, M. J., M. J. N. Priestley, and G. A. McRae. (1995). Displacement Based Design of RC Bridge Columns in Seismic Regions. *Earthquake Engineering and Structural Dynamics* 24(12): 1623-1643.

Takeda, T., M. Sozen, and N. Nielsen. (1970). Reinforced Concrete Response to Simulated Earthquakes. *Journal of the Structural Division, ASCE* 96(12): 2557-2573.

Hill, K. E. (1968). Dynamic Properties of Ring Springs for Use as Seismic Energy Dissipaters. *Proceedings of NZSEE Technical Conference*, Norway.

Miranda, E. (2003). Personal correspondence. *Department of Civil and Environmental Engineering, Stanford University, CA.*

CONTRASTING PERFORMANCE-BASED DESIGN WITH PERFORMANCE ASSESSMENT

Helmut KRAWINKLER[1], Farzin ZAREIAN[1], Ricardo A. MEDINA[2], and Luis IBARRA[3]

ABSTRACT

Performance <u>assessment</u> implies that the structural, nonstructural, and content systems are given and that decision variables, *DVs*, (e.g., expected annual losses, mean annual frequency of collapse) are computed and compared to specified performance targets. Performance-based <u>design</u> (PBD) is different by virtue of the fact that the building and its components and systems first have to be created. Good designs are based on concepts that incorporate performance targets up front in the conceptual design process, so that subsequent performance assessment becomes more of a verification process of an efficient design rather than a design improvement process that may require radical changes of the initial design concept. In short, the design approach could consist of (a) specifying desired performance targets (e.g., tolerable probability of collapse, acceptable dollar losses) and associated seismic hazards, and (b) inverting the performance assessment process, i.e., deriving parameters for design decisions, given the seismic hazard and targeted values of *DVs* (rather than computing *DVs*, given the seismic hazard and a designed structure). This paper illustrates basic concepts on which PBD can be based and contrasts PBD with performance assessment.

Keywords: Performance-based design; Conceptual design; Performance assessment; Collapse; Losses.

1. INTRODUCTION

Performance assessment, as developed in recent PEER research, implies that for a given system so called decision variables, *DVs*, are determined whose values should fulfill specified performance targets (Cornell 2000, Krawinkler 2004, Deierlein 2004). For life safety/collapse performance, the process of determining *DVs* is illustrated in the left half of Figure 1, with the information flowing from right to left, as indicated by the light horizontal arrow lines and as summarized here: intensity measures, *IMs*, (e.g., spectral acceleration at the first mode period, $S_a(T_1)$), are determined from hazard analysis; relevant engineering demand parameters, *EDPs*, (e.g., story drifts)

---

[1] *Dept. of Civil and Environmental Engineering, Stanford University, Stanford, CA, 94305-4020, USA*
[2] *Dept. of Civil and Environmental Engineering, University of Maryland, College Park, MD 20742, USA*
[3] *Southwest Research Institute, CNWRA, San Antonio, TX 78238, USA*

are predicted from structural analysis for given values of *IMs* (and representative ground motions); local collapse fragility curves (e.g., for floor slabs that may drop because of shear failure at column-to-slab connection) and global collapse fragility curves of the type shown in Figure 6 are used to predict local and global collapse probabilities; and as a last (and not yet fully resolved) step, predictions are made of the number of lives lost and the number of injuries. Similarly, for performance associated with losses and downtime, the process of determining *DVs* is illustrated in the right half of Figure 1, again with the information flowing from right to left.
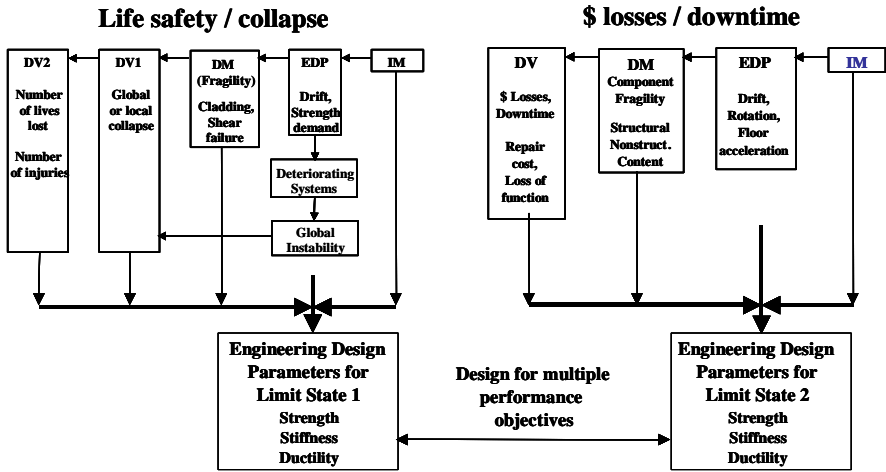

Figure 1. Design for multiple performance objectives (Krawinkler 2004).

The mathematical formulation for evaluating decision variables and providing decision support to the owner/user, considering uncertainties inherent in all parts of the process, is provided by the PEER framework equation expressed as follows:

$$\lambda(DV) = \iiint G\langle DV \mid DM \rangle \, dG\langle DM \mid EDP \rangle \, dG\langle EDP \mid IM \rangle \, d\lambda(IM) \qquad (1)$$

Design is different from performance assessment, simply by virtue of the fact that the building and its structural components and system first have to be created. One can view design as an iterative assessment process that starts with a judgmental conceptual design for which performance assessment is carried out, and the design is improved (tuned) in successive iterations until the performance targets are met. This design process is an option, but not a very attractive one. A poor initial conceptual design may be tuned to an extent that it fulfills the performance targets, but it likely will not become a good design. Good designs are based on concepts that incorporate performance targets up front in the conceptual design process, so that subsequent performance assessment becomes more of a verification process of an efficient design rather than a design improvement process that may require radical changes.

Conceptual design is greatly facilitated by focusing on discrete performance targets associated with discrete hazard levels — similar to the way it is being practiced in most of the performance-based guidelines presently in use. In the conceptual design phase, engineers are used (and likely will be so for many years to come) to select and rough-proportion structural systems for strength, stiffness (drift limitations), ductility, and perhaps energy dissipation and floor accelerations. The art of engineering, which should be practiced in this phase, is to use global information on important performance targets in order to come up with a structural system that fulfills specified performance objectives in the most effective manner. This implies exploration of alternatives, which may be utilizing different structural materials and systems or advanced technologies such as base isolation or internal energy dissipation devices.

The challenge is to provide the designer with a small set of most relevant criteria on important *EDPs* on which good conceptual design can be based. In concept, this means reversing the information flow discussed before for performance assessment, and working towards quantification of relevant *EDPs*, given that desired performance can be expressed in terms of targeted *DV* values at discrete performance levels. This reversal of information flow is indicated in Figure 1 with vertical arrow lines that flow into two horizontal arrow lines and merge at the *EDP* level, which then contains limit values of relevant *EDPs* (strength, stiffness, ductility, floor acceleration, etc.) that drive design decisions.

Given *EDP* limits and associated *IM* hazards for various performance levels, such as the two illustrated in Figure 1, conceptual design for multiple performance objectives can be performed. In general, performance should be concerned with structural and nonstructural systems as well as building contents. There is no single design parameter that will control all performance goals at all performance levels. For instance, nonstructural damage is controlled often by interstory drift limitations, which demand large stiffness. Content damage, on the other hand, is mostly proportional to floor accelerations, which can be limited by reducing the stiffness and/or strength of the structure. At the other extreme, life safety and collapse prevention are controlled by the inelastic deformation and energy dissipation capacities of ductile elements and the strength capacity of brittle ones.

This discussion indicates that different performance objectives may impose conflicting demands on strength and stiffness, and that seismic design is likely to become an iterative process in which different performance criteria may lead to trade-offs between strength and stiffness requirements, but in which no compromise can be made on issues of life safety and collapse prevention. This iterative process can be accomplished in two phases; a conceptual design phase in which one or more effective structural systems are explored and rough-sized, and a performance assessment phase in which performance of the structural, nonstructural, and content systems is evaluated and final design decisions and modifications are made.

This paper is concerned with the conceptual design phase. Two challenges need to be addressed in the context of performance-based conceptual design. One is to

develop data on *EDP* limits associated with specific performance targets. Once such *EDP* limits have been established, together with *IMs* that represent discrete hazard levels for which the *EDP* limits apply, the challenge is to device structural systems that efficiently accommodate these *EDP* limits. This paper is concerned with these two challenges.

2. PERFORMANCE TARGETS AND HOW TO EXPRESS THEM

It is widely accepted that earthquake design decisions should be based on the three Ds, i.e., death, dollars, and downtime. Unfortunately, there are many variations to this simple phrase. For one, we have not yet succeeded in quantifying death, or more appropriately, casualties. Thus, in the following discussion we will stop short and replace casualties (life safety) with collapse. Furthermore, we still have only vague insight into downtime and the quantification of associated losses, which may affect not only the owner but may have more global consequences. Therefore, also downtime is not discussed explicitly here, although it can be incorporated into the loss-*EDP* relationships discussed in the next section.

2.1 Loss or Function Controlled Performance Targets

The following is an attempt to illustrate how performance targets can be quantified, based on the existence of three subsystems in a building, a structural system (*SS*), a nonstructural drift sensitive system (*NSDSS*), and a nonstructural and content system that is sensitive to floor acceleration (*NSASS*). It is assumed that the *NSDSS* and *NSASS* subsystems are known and can be quantified before structural design decisions have to be made. The SS system is design dependent, but it usually is a relatively small contributor to total investment [in a loss estimation study on a Californian hotel building the *SS* contributed less than 20% to the total investment (Miranda 2004)].

The objective is to establish a relationship between a loss parameter and a "most relevant" engineering demand parameter (*EDP*), so that the latter can be used by the engineer to guide design decisions. The *EDP* has to be well correlated with losses in all components of the subsystem, and it has to be well correlated with global structural response in order to permit deduction of global design decisions.

One way of expressing desired performance is by specifying acceptable losses in earthquakes associated with specific hazard levels, such as 50/50 and 10/50 hazards. Implementing such a performance target implies the ability to compute component losses as a function of a relevant *EDP* and summing the losses over all components in the building, resulting in loss-*EDP* relationships for selected subsystems. Story drift and floor acceleration are examples of relevant *EDPs*. The process of computing loss-*EDP* relationships requires the following ingredients and steps:

1. The availability of a set of fragility curves for each component of the subsystem, which define, as a function of the *EDP*, the probability of being in, or exceeding, specific damage states requiring specific repair actions.

2. The availability of cost-of-repair functions for each damage state.
3. The ability to integrate fragility and cost-of-repair functions for each component. In the context of conceptual design it appears quite acceptable to use expected costs of repair for each damage state ($E[L_j | DM=dm_i]$) and compute only expected loss as a function of *EDP*, i.e.,

$$E[\,L_j\,/\,EDP_j = edp\,] = \sum_{i=1}^{m} E[\,L_j\,/\,DM = dm_i\,]\,P(\,DM = dm_i\,/\,EDP_j = edp\,) \qquad (2)$$

The result is an expected loss-*EDP* relationship for the specific component.
4. The summation of expected losses (as a function of *EDP*) over all the components of the subsystem that is expected to govern the loss at the hazard levels of interest. The result will be a single expected loss-*EDP* relationship for this subsystem. The same process can be carried out for all three subsystems, which will provide information on the contribution of the individual subsystems to the total loss, given a value of *EDP*.

This process is straight forward, in concept, and is the most effective way to perform PBD. But at this time it is most difficult or impossible to implement, simply because of the lack of data. Expected loss-*EDP* relationship for the subsystem that governs losses are not available at this time, but we have to raise the issue so that, hopefully, such relationships will be developed in the future. The added difficulty is that these relationships do not yet account for downtime losses. Incorporation of such losses is an additional challenge for the future.

Collapse also is a contributor to direct losses. In fact, it may be a major contributor for "non-conforming" structures (e.g., older RC frame structures, see Miranda 2004). But for "conforming" structures (i.e., structures designed according to modern standards) most of the losses come from relatively moderate but frequent events, rather than from complete or partial collapse. Thus, the cost of collapse is not considered in the expected loss-*EDP* relationships, and collapse is treated as a separate performance level.

2.2   Collapse Performance Targets

In most codes and guidelines, it is assumed that adequate collapse safety (and life safety) is provided by limiting the maximum story drift at the design earthquake level to a specific value (e.g., a drift limit of 0.02 at the 10/50 hazard level). The drift at this hazard level is estimated from either an elastic analysis or an inelastic time history analysis. But the latter usually is executed with the use of component hysteresis models that do not account for strength and stiffness deterioration. Thus, these *EDP* predictions cannot be used as indicators of actual collapse. With the advent of deterioration models that do account for important aspects of deterioration it is becoming possible to trace the response of structures to collapse (e.g., Ibarra 2003) and to be specific about a collapse performance target. Such a target could be expressed as a tolerable probability of collapse (say, 10%) at the 2/50 hazard level, or

more general, as a tolerable mean annual frequency of collapse. Both options are pursued in Section 3.2.

3. DECISION SUPPORT IN CONCEPTUAL DESIGN

In the up-front conceptual design process, decisions have to be made on the type of structural system and its global strength, stiffness, and ductility properties. In the following discussion general comments are made on design decisions based on the performance targets summarized in the previous section, with implementations illustrated for moment resisting frames, simply because many "design decision aids" have been developed for such frames. The development of similar design decision aids for wall structures is in progress.

3.1 Design Decisions Derived from Loss-Based Performance Targets

The conceptual process of making design decisions based on acceptable dollar losses, is illustrated in Figure 2. The lower portion illustrates the expected loss-*EDP* relationship for the dominant subsystem (e.g., *NSDSS*). The left upper portion shows the mean S_a hazard curve for the specific site, for the estimated first mode period of the structure. The right upper portion shows mean S_a-*EDP* relationships for several design alternatives. The process is to enter the lower graph with a value of acceptable loss and obtain the associated *EDP*, and to enter the left upper portion with the hazard level at which the loss is acceptable and obtain the associated S_a. The intersection of the S_a value and the *EDP* value in the design alternatives graph can be viewed as a "design target". All system solutions that intersect the S_a line to the left of the design point are "feasible" solutions, i.e., the associated expected losses are smaller than the target acceptable loss. The "best" solution will depend on many considerations, some of them being discussed in the example given in Section 3.1.1.
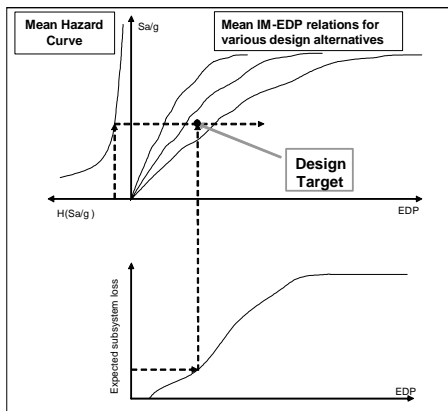

Figure 2. Designing for acceptable monetary loss (or for targeted EDP).

There are many questions to be answered, with a few of them addressed in general next, and a few more addressed specifically in the subsequent example.

What is an appropriate EDP? The choice of the *EDP* is driven by the sensitivity of the loss to variation in a basic design parameter. As discussed in Section 2.1, for the *NSDSS* subsystem, story drift is an appropriate choice. The best choice is believed to be the average of the maximum drifts in each story, which is a measure of the "expected" maximum drift. It is larger than the global drift, because maximum story drifts occur at different times (Medina 2003).

What are the S_a-EDP curves for design alternatives? They are relationships, for a specific design solution, between the mean value of a relevant *EDPs* and an appropriate intensity measure, *IM*. Customarily, the spectral acceleration at the first mode period of the structure is selected as an *IM*. The curves represent mean IDA (incremental dynamic analysis) curves obtained by subjecting design alternatives to a statistically representative set of ground motions. The design variables could be base shear strength V_y, stiffness or strength variation over the height, or first mode period (if *T* is varied, the hazard curve changes accordingly). For regular frame structures many such S_a-EDP curves are documented in Medina (2003), and more are under development. Similar curves are being developed for wall structures.

Why bother with MDOF S_a-EDP curves rather than use approximate SDOF representations? In the writers' opinion the usefulness of SDOF representations in seismic design is overestimated. Their use invites approximations that are justified in some cases but not in others. Why not avoid their use if appropriate MDOF information is available? This, in fact, is a necessity when the *EDP* is floor acceleration, which is an *EDP* that correlates poorly with any SDOF parameter.

3.1.1 Example of Design for Acceptable Losses

An example of design decisions based on acceptable losses is illustrated in Figure 3. The example addresses a 9-story frame structure, located in Southern California at a site for which the spectral acceleration hazard curves for the periods of 0.9 sec. and 1.8 sec. are as shown in the upper left portion of the figure. The expected loss-*EDP* curves for the three subsystems are as shown in the lower portion. The *NSDSS* and *SS* subsystems account for 60% and 20% of the replacement cost, respectively, and the *NSASS* subsystem accounts for the remaining 20%. The *EDP* is the average of the maximum interstory drifts (*IDR*) for the *SS* and *NSDSS* subsystems, and the average of maximum floor accelerations (*FA*) for the *NSASS* subsystem. At this time there is little hard data behind these loss-*EDP* curves; they are based on judgment.

Based on relative value of the subsystems, in this example "designing for acceptable losses" needs to focus on the *NSDSS* subsystem. An owner could target acceptable losses in the *NSDSS* subsystem of 5% of total replacement cost at the 50/50 hazard level. Thus, design targets are created by entering the figure with the *EDP* associated with the expected loss of 5% and with the 50/50 mean S_a hazards for appropriate periods. For illustration, periods of 0.9 sec. and 1.8 sec. are selected. The upper right portion of the figure contains mean S_a-EDP curves for various design

solutions (obtained from statistical studies reported in Medina 2003). From the middle graph it is evident that any solution with $T_1 = 1.8$ sec. would cause losses at the 50/50 hazard level that by far exceed the acceptable losses. In fact, the three $T_1 = 0.9$ sec. design solutions barely meet the loss target, i.e. solutions with $T_1 > 0.9$ sec. are discarded. In the three presented $T_1 = 0.9$ solutions the base shear strength coefficient $\gamma = V_y/W$ is varied from 0.3 to 0.2 and 0.1. [The fact that the three solutions overlap for a large range is a consequence of adherence to the equal displacement rule.] Only the $\gamma = 0.3$ solution is attractive because for solutions with smaller γ values the ratio $[S_a(T_1)/g]/\gamma$ is much smaller than 1.0 ($S_a(T_1)/g$ is close to 0.3 at the 50/50 hazard level), which indicates considerable inelastic response of the *SS* system at the 50/50 hazard level. This would move the *SS* loss curve far to left, make it steeper, and make the *SS* losses unacceptable.
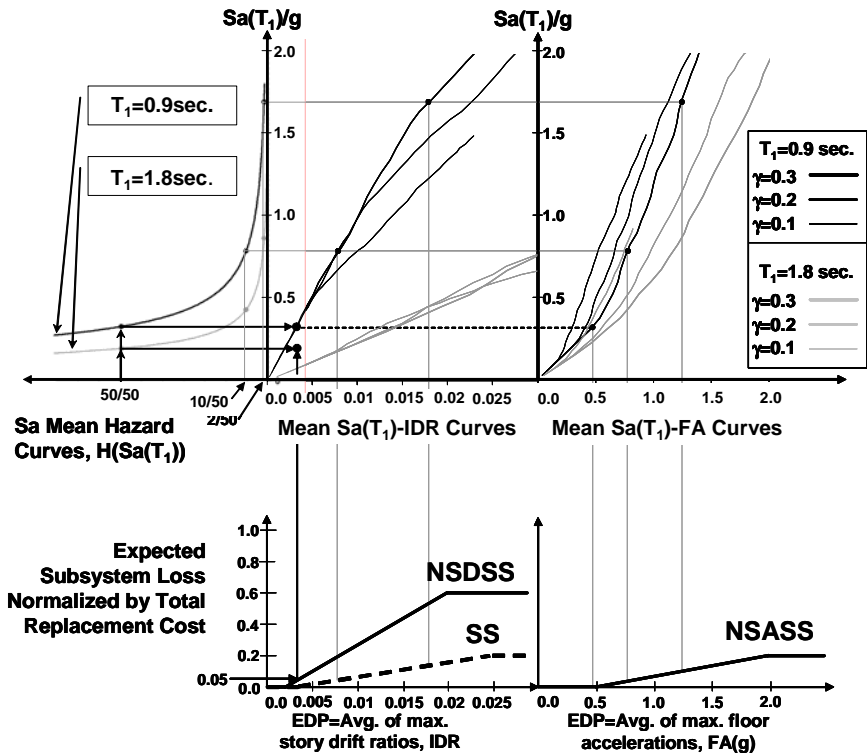

Figure 3. Example of design decision support based on targeted acceptable losses.

The merits of the $T_1 = 0.9$ and $\gamma = 0.3$ solution can be assessed further by inspecting the expected *SS* and *NSDSS* losses at other hazard levels, such as the 10/50 and 2/50 levels, as illustrated in Figure 3. The upper right graph can be utilized to

512

assess expected *NSASS* losses. For the case illustrated, these losses are relatively small. But the picture could change radically if the building were a museum, in which case the *NSASS* expected loss-*EDP* curve likely will be much steeper and may be the dominant contributor to total losses. In this case, longer period structures and weaker structures (smaller base shear strength) become more attractive.

This example serves to illustrate the evaluation of design options based on expected losses, and the kinds of trade-offs that can be made between strength and stiffness based on the relative contributions of the subsystems to the total losses.

3.2   Design Decisions Based on Collapse Performance Targets

Providing collapse safety implies adherence to capacity design concepts, and it implies design for ductility. The latter is implicitly considered in present design approaches with the judgmental response modification (R) factor or behavior (q) factor. These factors are tied to component detailing (ductility) requirements, and in the design process they are used to reduce the strength design level to a fraction of the elastic demand associated with the spectral acceleration at the first mode period.

Research has been performed recently on the "collapse capacity" of moment resisting frames, utilizing component hysteresis models that account for strength deterioration in the backbone curve (see Figure 4) and for cyclic deterioration in strength and stiffness (Ibarra 2003). The collapse capacity is defined as that value of the "relative intensity", $[S_a(T_1)/g]/\gamma$, at which dynamic instability occurs in a sideways mode due to deterioration and P-Δ effects. It is noted that $[S_a(T_1)/g]/\gamma$ is equivalent to the ductility dependent strength reduction factor R_μ. Collapse fragility curves of the type shown in Figure 5 have been derived for regular frames subjected to a set of 40 ground motions (Ibarra 2003). It has been concluded that the collapse capacity depends primarily on the component ductility capacity δ_c/δ_y, the post capping stiffness ratio α_c (see Figure 4), and the cyclic deterioration parameter $\gamma_{s,c,k,a}$. These parameters, together with the fundamental period T_1 and the base shear strength parameter $\gamma = V_y/W$, control the design for collapse safety.
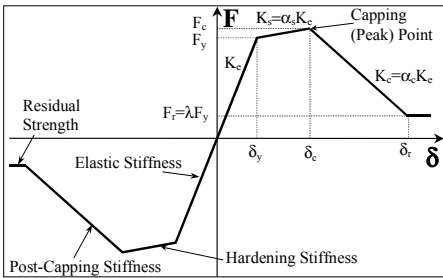

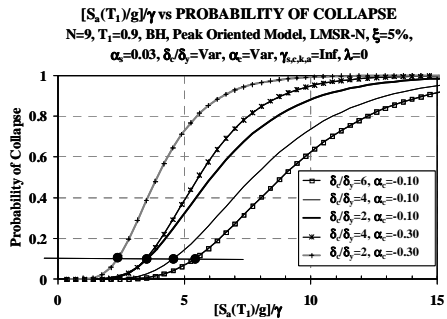| Figure 4. Backbone curve for deteriorating hysteretic models. | Figure 5. Collapse fragility curves for 9-story frame structures with $T_1 = 0.9$ s. |

3.2.1 Design for Tolerable Probability of Collapse at a Specific Hazard Level

Desired performance at the collapse prevention level could be expressed in terms of a tolerable probability of collapse at a specified hazard level, as for instance, a tolerable probability of collapse of 0.1 at the 2/50 hazard level. For a 9-story frame structure with $T_1 = 0.9$ sec. the corresponding $([S_a(T_1)/g]/\gamma$ values (R_μ values) for several combinations of system parameters are presented in the collapse fragility curves shown in Figure 5. More general design aids are collapse capacity spectra of the type shown in Figure 6, which show the effect of component ductility capacity on the collapse capacity (the R_μ value causing collapse), for a 10% and 50% probability of non-exceedance, and assuming $\alpha_c = -0.1$ and no cyclic deterioration ($\gamma_{s,c,k,a} = \infty$). [Note that the R_μ value causing collapse is strongly period dependent and decreases to a low value for long period structures because of P-delta effects.]
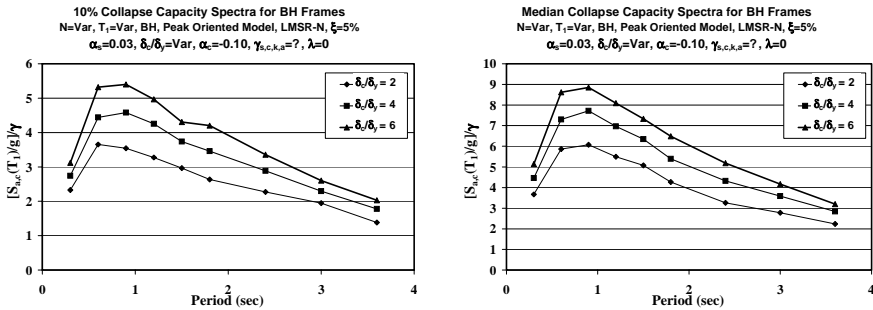

Figure 6. Collapse capacity spectra for frames with plastic hinges at beam ends (strong-column designs); (a) 10% probability of non-exceedance, (b) median.

For a tolerable probability of collapse of 10% in a 2/50 event, data of the type shown in Figure 6(a) provides the necessary design decision support (similar spectra are available for other combinations of system parameters). For instance, if T_1 is selected as 0.9 sec. and the component ductility capacity is 4.0, the R_μ is 4.6, which for the 2/50 hazard of the example problem of Section 3.1.1 results in a required base shear strength coefficient of $\gamma = 1.7/4.6 = 0.37$. This is larger than estimated from the design for acceptable direct losses. Thus, collapse prevention would control the required strength, unless a larger ductility capacity (better detailing) is utilized or a more flexible structure is used. For instance, for $T_1 = 0.9$ sec. and $\delta_c/\delta_y = 6$, the R_μ is 5.4, which would result in $\gamma = 1.7/5.4 = 0.31$. Alternatively, a more flexible structure could be selected (albeit this would be a poor solution based on monetary losses, see Figure 3). For $T_1 = 1.8$ sec. and $\delta_c/\delta_y = 4$, the R_μ is 3.5, which for the 2/50 S_a value of 0.86g at 1.8 sec. results in a required base shear strength coefficient of $\gamma = 0.86/3.5 = 0.25$. These are the kind of trade-offs that can be evaluated through the use of collapse capacity spectra, presuming that a tolerable probability of collapse is specified at a specific hazard level.

3.2.2 Design for Tolerable Mean Annual Frequency of Collapse

A different way to express desired collapse performance is to target a tolerable mean annual frequency (MAF) of collapse, λ_{Coll}. This performance target is more general (it permits the estimation of the probability of collapse over an expected life time), but it is more difficult to implement because the "accurate" computation of a MAF requires integration over the S_a hazard curve. An approximate implementation is possible by means of the simplified closed form expression proposed by Cornell (Cornell 1996), which estimates the MAF of collapse as follows:

$$\lambda_{Coll} = \int_{S_a} F_{C/S_a}(c/s_a)/d\lambda_{S_a}(s_a)/ = \lambda_{S_a}(\eta_C)\,exp(\frac{1}{2}k^2\beta_{RC}^2) \qquad (3)$$

The simplified expression on the right-hand side contains the MAF of the spectral acceleration associated with the median collapse capacity, $\lambda_{Sa}(\eta_C)$, and a term that accounts, in an approximate manner, for the uncertainties inherent in the computation of the collapse capacity. This term contains the slope of the hazard curve at the referenced spectral acceleration value, k, and the dispersion(s) in the collapse fragility curve, β (the σ of the log of the data if a log-normal distribution is assumed for the probability of collapse given the spectral acceleration). In the example illustrated here only record-to-record (RTR) variability if considered, which is explicitly contained in the fragility curves shown in Figure 5 (these fragility curves are obtained by using an "expected" structural model subjected to 40 ground motions). Thus, the term β_{RC} in equation (3) expresses the effect of RTR variability only ("Randomness in collapse Capacity"), and is found to be on the order of 0.4 to 0.5 (except for long period structures for which it is smaller because of the dominance of P-delta effects).

As an example, let us target a tolerable annual frequency of collapse of 0.0002 (i.e., a tolerable probability of collapse of approximately 0.0002x50 = 0.01 in a 50 year life). This criterion could be used, together with median collapse capacity spectra of the type shown in Figure 6(b), to arrive at effective design solutions. Again using the example of a 9-story frame structure, the following design alternatives could be explored. If a period of 0.9 sec. and a component ductility capacity of $\delta_c/\delta_y = 4$ are assumed, then the median $[S_a(T_1)/g]/\gamma$ value from Figure 6(b) is 7.7. For the site specific hazard curve of the previously illustrated example the slope of the S_a hazard curve in the neighborhood of a MAF of 0.0001 to 0.0004 is about 2.2, and the β_{RC} value is about 0.4 (from collapse fragility analyses, Ibarra 2003). Thus, from equation (3), the MAF of the S_a associated with the median collapse capacity, $\lambda_{Sa}(\eta_C)$, is equal to $0.0002/exp(0.5 \times 2.2^2 \times 0.4^2) = 0.000136$. From the S_a hazard curve for the site of the example problem, the corresponding S_a is 2.8g, and the corresponding γ value is $2.8/7.7 = 0.36$. Again, this is a larger value than that based on loss-controlled performance targets. Alternatives are to increase the component ductility capacity (if it is increased from 4 to 6, $[S_a(T_1)/g]/\gamma$ is 8.9, and for the same $\lambda_{Sa}(\eta_C)$ of 0.000136 the γ value becomes $2.8/8.9 = 0.31$), or to increase the structure period. If, for

instance, T_1 is 1.8 sec., the $[S_a(T_1)/g]/\gamma$ value from Figure 6(b) is 5.4 (for $\delta_c/\delta_y = 4$), and, using the site specific k value of 2.4 for the T = 1.8 sec. hazard curve, $\lambda_{Sa}(\eta_C)$ becomes 0.000126, the S_a value for this MAF is 1.4g, and the base shear strength parameter γ becomes 1.4/5.4 = 0.26.

4. CONCLUSIONS

Conceptual PBD implies a decision process that leads to the selection of one or several effective design alternatives based on performance targets for acceptable losses and a tolerable probability of collapse. In this context, two challenges have to be addressed. One is to develop data on *EDP* limits associated with these performance targets. The other is to select structural systems that efficiently accommodate these *EDP* limits. This necessitates the development of MDOF "design decision aids" that facilitate the design decision process, or of global criteria that can be translated into strength and stiffness requirements. This paper proposes a process to accomplish effective PBD and illustrates how these two challenges can be met.

ACKNOWLEDGEMENTS

REFERENCES

Cornell, C. A. (1996). Calculating building seismic performance reliability; a basis for multi-level design norms. *Proc. 11ᵗʰ WCEE*, Acapulco, Mexico.

Cornell, A., and H. Krawinkler. (2000). Progress and challenges in seismic performance assessment. *PEER News*, April 2000.

Deierlein, G. (2004). Overview of a comprehensive framework for earthquake performance assessment. *Bled-04 proceedings*.

Ibarra, L. (2003). Global collapse of frame structures under seismic excitations. *PhD. Dissertation* Department of Civil Engineering, Stanford University, Stanford, CA.

Krawinkler, H., and E. Miranda. (2004). Performance-based earthquake engineering. Chapter 9 of *Earthquake Engineering: from engineering seismology to performance-based engineering*, CRC Press, 2004.

Medina, R. A., and H. Krawinkler. (2003). Seismic demands for nondeteriorating frame structures and their dependence on ground motions. *John A. Blume Earthquake Engineering Center Report No. 144*, Dept of Civil Eng'ng., Stanford U.

Miranda, E., H. Aslani, and S. Taghavi. (2004). Assessment of seismic performance in terms of economic losses. *Bled-04 Proceedings*.

THE PERFORMANCE REQUIREMENTS IN JAPANESE BUILDING CODE

Shunsuke OTANI[1]

ABSTRACT

The concept and application of performance based design and engineering is influenced by the social and technical environments in which engineers and researchers live in. The performance objectives in Japan are "no serviceability problems from normal loading conditions, no structural damage under more frequent snow, wind and earthquake events and no loss of human lives under very rare snow, wind and earthquake events." "No serviceability and structural damage" is examined by the traditional allowable stress design procedure, while "no loss of human lives" is examined either by (a) examining the minimum resistance of a structure at the formation of collapse mechanisms and the deformation limit of yielding members in the mechanism or (b) the capacity-demand spectrum procedure.

Keywords: National building code; Performance objectives; Code requirements; Design; Construction; Inspection.

1.   INTRODUCTION

Hammurabi, the ruler of Babylon (1795-1750 BC), wrote the oldest world-known code of law, in which he referred to building construction in six paragraphs; the three paragraphs are quoted below after the translation by L.W. King in 1910.

> Paragraph 228: "If a builder build a house for some one and complete it, he shall give him a fee of two shekels in money for each sar of surface."

> Paragraph 229: "If a builder build a house for some one, and does not construct it properly, and the house which he built fall in and kill its owner, then that builder shall be put to death."

> Paragraph 232: "If it ruin goods, he shall make compensation for all that has been ruined, and inasmuch as he did not construct properly this house which he built and it fell, he shall re-erect the house from his own means."

These paragraphs state that a proper fee should be paid for construction work and, in return, that the constructor (engineer) should be responsible for the safety of occupants and the protection of contents. The code of Hammurabi specified the safety and serviceability performance, but no loading conditions were defined.

---

[1] *Chiba University,Chiba, Japan*

A developed nation generally establishes a building code of the nation, to which all design and construction should conform. The scope of the building code varies from a nation to another. The code should include the minimum statements about the following structural design and construction issues; (a) code enforcement in design and construction, (b) structural performance under normal loading as well as extreme events, (c) specifications for materials and construction and (d) inspection during and after construction.

It should be noted that the building code normally outlines the minimum performance requirements for the society. The minimum performance (acceptable damage) of buildings varies from a country to another because each country has different levels of (a) seismic risk, (b) hazard tolerance, (c) economic background, (d) social acceptance of damage, (e) technical development, and construction practice. Even in a country, the performance level of a building, above the code specified minimum, should be selected by the owner after the engineer provides information about the building performance to the building owner.

This paper introduces the system of building codes in Japan and the performance objectives outlined in the Building Standard Law. The building codes of Japan consist of (a) Building Standard Law (national law), (b) Building Standard Law Enforcement Order (cabinet order), (c) Notification of Ministry of Land, Infrastructures and Transport (previously Ministry of Construction), and (d) By-laws of municipal governments.

2. BUILDING STANDARD LAW

The Building Standard Law of Japan was proclaimed as a national law in May 1950, and has been revised from time to time to meet the change in demand of the society. The objectives were to "safeguard the life, health, and property of people by providing minimum standards concerning the site, structure, equipment, and use of buildings, and thereby to contribute to the furtherance of the public welfare." It should be noted that the law sets up the minimum standards necessary for the life, health, and property of people.

The framework of Building Standard Law was significantly revised in 1998, e.g.,
(1) Introducing performance-based regulations wherever feasible,
(2) Allowing private agencies to execute the building confirmation and construction inspection works during and after the construction,
(3) Deregulating urban land use, and
(4) Allowing public access to design and inspection documents.

The performance-based requirements in building codes are generally encouraged in recent years with the expectation to expand the scope of structural design, especially for the application of new materials, construction technology and structural systems. It is further expected to remove international trade barriers in the design and construction markets and to encourage the engineer to develop and apply new construction technology and engineering.

2.1 Law Enforcement and Inspection

The Building Standard Law is a national law which must be conformed to in selecting the site, in designing and constructing a building and equipment, and in the use of building. When a new construction or a major repair or remodeling of the building is planned, the building owner must submit an application for confirmation to the building official that the design and construction conforms to the provisions of laws concerning the site, structure, and building equipment prior to the construction work. This requirement made the code prescriptive because building officials must be able to judge the legal conformity of the design work to the regulations.

Upon the completion of the construction, the building official or his designated person must inspect the construction for the conformance of the building requirements. If the construction site or building violates the legal requirements, the chief of a municipality may order the suspension of construction, the demolition, removal, or correction of the building, or the prohibition of the building occupancy and use. The 1998 revision allowed a designated private agency to review the confirmation application and inspect the construction after completion.

2.2 Structural Requirements

The structural requirements in the law are that "the building shall be constructed safe against dead and live loads, snow loads, wind forces, soil and water pressures, and earthquake and other vibration forces and impacts," and also the structure shall satisfy the following requirements:
  (1) The structural calculation outlined by cabinet order, Building Standard Law Enforcement Order, and
  (2) The technical standards set forth by the Minister of Construction.

2.3 Materials

The quality of construction materials shall satisfy the Japanese Industrial Standards or the Japan Agricultural and Forestry Standards or the technical standards, fire resistance and health, set forth by the Minister of Construction.

3. BUILDING STANDARD LAW ENFORCEMENT ORDER

The Building Standard Law Enforcement Order is issued by the Cabinet to outline technical requirements for the law. The construction and structural calculation requirements are specified in Chapter 3 "Structural Strength." The technical standards about structures, referred in Article 20 of the law, are outlined in Sections 1 to 7 below.

Section 1: General Provisions,
Section 2: Structural Members and others,

Section 3: Timber Construction,

Section 4: Masonry Construction and Reinforced Concrete Block Construction,

Section 5: Steel Construction,

Section 6: Reinforced Concrete Construction and Steel Reinforced Concrete Construction, and

Section 7: Plain Concrete Construction and Other Construction.

These sections specify mandatory requirements associated with (a) basis of structural calculations, (b) quality of construction materials, (c) durability of structural members, (d) workmanship during construction and (e) safety against fire.

3.1 Technical Standards about Structures

A structure shall satisfy one of the following three structural requirements:

(1) The safety of a structure, after satisfying the requirements of Sections 1 through 7, shall conform to the allowable strength calculation or by the structural calculation, which safety level is equivalent to the allowable stress calculation, set forth by the Minister of Land, Infrastructure and Transport (hereafter abbreviated as "MOLIT," the Ministry of Construction was reorganized to MOLIT in 2001). The durability provisions cannot be replaced by structural calculation about performance.

(2) The safety of a structure, after satisfying the durability related provisions, shall conform to either by the ultimate strength calculation or the structural calculation set forth by MOLIT as a procedure deemed to ensure a safety level of a building equivalent or superior to the ultimate strength calculation.

(3) The structural method, after satisfying the durability related provisions, shall be specially approved by MOLIT as the structure which safety is confirmed by the structural calculation (response history calculation) set forth by MOLIT.

3.2 Example: Technical Requirements for Concrete Construction

An example of the technical requirements is introduced here for reinforced concrete construction. Most requirements are performance-based, but some are specification-type in which numbers or values or shapes are specified.

Materials for concrete: Materials for the reinforced concrete construction are specified in performance format as follows:

(1) Aggregate, water and admixture shall be free from acids, salts, organic matter or particles of mud liable to cause rusting of steel or detrimental to the normal process of setting and hardening of concrete;

(2) Aggregate shall be of such size that it can pass easily between reinforcing bars and between reinforcing bars and formwork;

(3) Aggregate shall have appropriate grading and grain shape and give necessary strength, durability and fire resistance to the concrete.

Splices and development of reinforcing bars: The ends of reinforcing bars shall be anchored by bend to prevent the bars from slipping out of concrete, but the hook may be omitted in exterior ends of columns and beams and in chimneys. Longitudinal bars shall be joined at a part of structural members where tensile force is least. When the longitudinal bars are spliced at a point where tensile force is not least, the splice length shall be not less than 40 times the bar diameter. Tension reinforcing bars in beams shall have a development length of not less than 40 times the bar diameter. The lap splice length and development length shall be not less than 50 times the bar diameter if used with light weight aggregate concrete. The provisions, herein, shall not apply if the safety is confirmed by the structural calculation outlined by the Minister of Construction.

Strength of concrete: The compressive strength of concrete at the age of 28 days shall be 12 N/mm^2 (9 N/mm^2 in the case of the light weight aggregate concrete) or larger, and also shall satisfy the specified design strength of concrete established by the Minister of Construction. The strength of concrete shall be determined by a test specified by the Minister of Construction. Mixture of concrete shall be determined so that the product will be uniform and compact and have necessary strength.

Curing of concrete: Concrete shall be cured under the temperature of concrete at not less than 2 degrees C over 5 days after the concrete is poured, and due care shall be taken for dry-out or vibration that might prevent the concrete from setting and hardening. This shall not apply in cases where special measures are taken for facilitating the setting and hardening of the concrete.

Removal of forms and supports: Forms and supports for structural members shall not be removed until the concrete attains strength sufficient to prevent large deformation, cracks or other damage due to dead load and other forces during construction work. Necessary technical standards with respect to the removal of forms and supports described in the preceding paragraph shall be established by the Minister of Construction.

Structures of columns: Columns constituting principal parts necessary for structural strength shall satisfy the following:

(1) Longitudinal reinforcement of a column shall consist of four or more reinforcing bars and be firmly fastened to hoops;
(2) Diameter of hoops shall be 6 mm or larger, and the interval shall be 150 mm or less (100 mm or less within the range of twice the smallest width of a column immediately above the floor slab and below the girder) and 15 times or less of the bar diameter;
(3) Lateral reinforcement ratio shall be 0.2% or larger;
(4) Smallest width of a column shall be 1/15 or more of the distance between its supports; and
(5) Gross longitudinal ratio of column longitudinal reinforcement shall be 0.8% or more.

Provisions (2) through (5) shall not apply if structural safety is confirmed by the structural calculation outlined by the Minister of Construction.

Construction of floor slabs: Floor slabs shall be constructed to satisfy the following:

(1) Thickness of floor slabs shall be 80 mm or more and 1/40 or more of the effective span in the direction of the shorter side,

(2) Spacing between tension reinforcing bars at maximum bending moment shall be 200 mm or less in the direction of the shorter side and 300 mm or less in the direction of the longer side, and also 3 times or less of he thickness of the floor slabs.

The above provisions (1) and (2) shall not apply if the vibration and deformation is examined by structural calculation in the Ultimate Strength Calculation outlined in the Building Standard Law Enforcement Order.

Precast concrete slabs shall meet the following additional requirements:

(1) Connections with surrounding beams shall be able to transfer the existing stress;

(2) Where two or more members are used, those members shall be firmly tied to each other. Provided, that this shall not apply in cases where structural safety has been confirmed through structural calculation or experimentation.

The provisions (1) and (2) shall not apply if the vibration and deformation is examined by structural calculation in the Ultimate Strength Calculation outlined in the Building Standard Law Enforcement Order.

Construction of girders: Girders shall be provided with longitudinal reinforcement at the top and bottom, and shall have stirrups at intervals not exceeding 3/4 of the girder depth.

Bearing walls: Bearing walls shall be constructed to satisfy the followings: (1) thickness shall be 120 mm or more; (2) periphery of an opening of bearing walls shall be reinforced with reinforcing bars of diameter of 12 mm or more; (3) bearing walls shall be provided with horizontal and vertical reinforcing bars of diameter of 9 mm or more at an interval of 300 mm or less (450 mm or less in the case of double reinforcement) unless the structural safety is confirmed by the structural calculation outlined by the Minister of Construction. The interval may be extended up to 350 mm (500 mm in the case of double reinforcement) for single-story buildings; (4) connection with surrounding columns and beams shall be able to transfers the existing stress at the parts. Bearing walls of box frame construction shall meet the additional following requirements: (1) width of bearing walls shall be 450 mm or more; (2) edge and corner of a bearing wall shall be reinforced by reinforcing bars of diameter of 12 mm or more; (3) bearing walls shall be firmly tied at the top and the bottom to wall girders (continuous foundation or foundation girders in the case of the bottom of a bearing wall on the lowest floor) of width not less than the thickness of the bearing wall, and to transfer the existing stress at the connection.

Thickness of concrete cover for embedded bars: The thickness of concrete cover for embedded bars shall be 20 mm or more for walls other than bearing walls or floor slabs, 30 mm or more for bearing walls, columns or beams, 40 mm or more for walls, columns, floors or beams which come directory in contact with the soil as well

as for the rising part of continuous foundation, and 60 mm or more for foundation (excluding the rising part of continuous foundation).

3.3 Durability Provisions

The requirements, which cannot be replaced by the examination of structural performance through structural calculation, are called "durability related provisions". The durability provisions specify (a) principle of structural design, (b) quality of materials to be used in construction, (c) durability of structural members, (d) special care to be exercised during construction work, and (e) safety requirements during fire. The durability provisions are listed below.

Fundamental principles of structural design: In planning the structural design of buildings, structural members shall be arranged effectively for the use, scale and structural features so that the structure is safe against dead load, live load, snow load, wind pressure, ground pressure and water pressure as well as earthquakes or other vibration or shock acting upon the building. Principal parts necessary for structural strength shall be arranged in balance so as to resist any horizontal forces acting upon the building. Principal parts of a building necessary for structural strength shall be designed to have rigidity enough to prevent distortion or vibration affecting the use of the building and ductility to prevent sudden destruction.

Durability of structural members: The structural members which are particularly liable to corrosion, deterioration or abrasion shall be made of materials which resist corrosion, deterioration or abrasion or which are provided with effective measure s for preventing rust, deterioration or abrasion.

Foundations: Foundation of building shall transfer the vertical loads and external forces acting upon the building to the ground and be structurally safe against settling or distortion of the ground. Foundation piles to be driven by percussion, pressure or vibration shall be structurally safe against the percussion or other external force applied to drive them in. If wood piles are used for the foundation of buildings, they shall be driven down below the normal water level.

Anchoring of **roofing materials**: Roofing materials, interior finishing materials, exterior finishing materials, curtain walls and other similar parts fixed outside the building, shall be fixed to the structure so as not to fall under wind pressure, earthquakes or other vibration or shock.

For reinforced concrete construction, specification requirements for (a) materials for concrete, (b) strength of concrete, (c) curing of concrete, (d) thickness of concrete cover for embedded bars are designated as a part of durability provisions.

3.4 Structural Calculation

Building Standard Law Enforcement Order was revised in 2000 to enforce the 1998 revision of the law. Significant revisions were made toward performance-based requirements in the area of fire protection and evacuation. However, relatively small

revisions were made in structural design requirements because the structural design regulations were already in a performance-based format. The capacity-demand spectrum method was introduced in seismic design in the 2000 revision.

Structural calculation methods are outlined in Section 8: Structural Calculation. Structural calculation for buildings, less than 60 m in height, shall follow either (a) the allowable stress calculation (old procedure) or (b) the ultimate strength calculation (new procedure) or (c) the structural calculation set forth by MOLIT to produce structures as safe as the allowable stress calculation or the ultimate strength calculation.

Three performance objectives are defined for the evaluation and verification of performance (response) under (a) gravity loads, (b) snow loads, (c) wind pressures, and (d) earthquake forces; i.e.,

(1) Maintenance of building serviceability under permanent loading conditions (dead and live loads),

(2) Prevention of structural damage under frequent loading conditions (snow, wind and earthquake events corresponding to a return period of approximately 50 years), and

(3) Protection of occupants' life under extraordinary loading conditions (snow, wind and earthquake events corresponding to a return period of approximately 500 years.

The types and amplitudes of loads and external forces, the allowable stress and the nominal strength of materials are outlined in the law enforcement order.

3.5 Allowable Stress Calculation

The allowable stress calculation is briefly introduced in this section.

The stress in any part of structural members under the combination of dead and live loads (long term loads) shall be less than the allowable stress of construction materials set forth for long-term loading. The allowable stresses for the long term loading are specified much lower than the elastic limit or creep limit of materials; e.g., allowable compressive stress of concrete is one-third of the nominal compressive strength, allowable shear stress is one-thirtieth of the nominal compressive strength, and allowable tensile stress of reinforcing bars is two-thirds of the nominal yield stress. The unit weight of materials for the evaluation of dead loads and the unit weight associated with room use for the evaluation of live loads are specified. The serviceability of the building shall not be impaired by the deformation and vibration caused by the long term loads, the serviceability should be examined by the structural calculation set forth by MOLIT Notification 1459.

The stress in any part of structural members under the combination of (a) dead, live and snow loads (b) dead, live loads and wind forces, and (c) dead, live and earthquake forces shall be less than the allowable stress of construction materials set forth for short term loading. The allowable stresses for the short term loading are specified lower than or equal to the elastic limit of materials; e.g., allowable

compressive stress of concrete is two-thirds of the nominal compressive strength, allowable shear stress of concrete is one-twentieth of the nominal compressive strength, and allowable tensile stress of reinforcing bars is the nominal yield stress. The design snow depth is specified by MOLIT Notification 1455. The method to evaluate design wind forces is specified, and the parameters to define the wind pressure are specified by MOLIT Notification 1454. The method to evaluate design earthquake forces is specified, and seismic zone factor is specified by MOLIT Notification 1918. The amplitude of snow loads, wind forces and earthquake forces used here may be expected once in fifty years. The safety of roofing materials under design wind pressure shall be examined by the calculation method set forth by MOLIT Notification 1458. The story drift under design earthquake forces shall be less than 1/200 of the story height, but the value may be relaxed to 1/120 if the performance of the building is shown to be acceptable. For buildings less than 31 m in height, the eccentricity in plan and stiffness distribution along the building height shall satisfy limiting values and the structural calculation, set forth by MOLIT shall be carried out. For buildings taller than 31 m, the ultimate story resistance at the formation of collapse mechanism under lateral loading shall be larger than the required value, which takes in account (a) eccentricity in plan and stiffness distribution along the building height, and (b) deformation capacity of yielding members.

3.6   Ultimate Strength Calculation

The allowable stress calculation for the combination of dead and live loads using the allowable stress of materials for long term loading and the allowable stress calculation for the combination of (a) dead, live and snow loads, and (b) dead and live loads and wind forces using the allowable stress of materials for short term loading shall be carried out. The amplitude of snow loads and wind forces used here may correspond to the values expected once in 50 years.

The forces in any structural members shall not exceed the ultimate strength calculated using the ultimate strength of materials under the combination of (a) dead and live loads and 1.4 times the snow load at the construction site, and (b) dead and live loads and 1.6 times the wind force at the construction site. The amplitude of the amplified snow load and wind force used here may correspond to the values be expected once in 500 years.

The design earthquake motion is defined by the response spectrum of 0.05 damping factor specified at engineering bed rock (soil layer whose shear wave velocity is approximately 400 m/sec and above), and the response spectrum of ground motion at the base of the structure shall be calculated taking into consideration the amplification by surface geology. The intensity of ground motion at the engineering bedrocks is specified for two levels; one corresponding to a rare event of once in 50 years, and the other corresponding to an extraordinary rare event of once in 500 years. The intensity level of the former earthquake motion is one-fifth of the latter

earthquake motion. The story drift under the rare earthquake motion shall be less than 1/200 of the story height (or 1/120 of the story height if the performance of the building is shown to be acceptable) and the stress in any part of structural members and foundation shall be less than the allowable stress of materials for short term loading. The maximum story shear under the extraordinary rare earthquake motion shall be less than the ultimate lateral resistance of the story. The performance of the structure shall be examined by the demand-capacity spectrum procedure.

4. NOTIFICATIONS OF MINISTRY OF LAND, INFRASTRUCTURE AND TRANSPORT

Numerous notifications have been issued by MOLIT to outline the detailed technical requirements or to specify the calculation methods stated in the Building Standard Law Enforcement Order; for example:

- Notification 1918 of year 1987: Specification of seismic zone factor Z of regions, calculation of dynamic characteristic factor R_t and story shear distribution factor A_i.
- Notification 1454 of year 2000: Calculation of values E (environmental factor to influence wind velocity) and V_o (design wind velocity of regions) and wind force coefficient.
- Notification 1457 of year 2000: Calculation of parameters necessary for the ultimate strength calculation (Demand- and capacity-spectra procedure).
- Notification 1458 of year 2000: Structural calculation for the safety of roofing elements, exterior finishing elements and exterior curtain walls under wind pressure.
- Notification 1459 of year 2000: Criteria to judge interference of serviceability of buildings in structural calculation.
- Notification 1461 of year 2000: Structural calculation to examine the safety of high-rise buildings taller than 60 m.

5. PERFORMANCE REQUIREMENTS FOR HIGH-RISE BUILDINGS

The law enforcement order requires that the structural design and construction of high-rise buildings, taller than 60 m, shall satisfy the durability related provisions, and shall be approved by MOLIT to be structurally safe based on the calculation procedure outlined by MOLIT. The law enforcement order also requires that the structural calculation of high-rise buildings shall follow the calculation procedure, outlined by MOLIT, which can verify the structural safety of the building by evaluating the local action and deformation of the structure continuously taking into consideration the construction methods and dynamic characteristics of the structure.

MOLIT Notification No. 1461 outlines the structural calculation for high-rise buildings. The notification is written in a performance-based format consisting of eight articles:

Article 1: No structural members shall be damaged under the dead and live loads representing actual conditions, and other loads and forces acting on all parts of the building.

Article 2: Following structural calculation shall be made for snow loads on the building. The snow load can be reduced for the structure where the snow melting devices are installed or special measures are taken to reduce snow loads.

(a) Snow load shall be determined in accordance with the law enforcement order. If an expected value associated with a 50-year return period is assessed for the construction site by special study or investigation, the assessed value can be used.

(b) No structural members shall be damaged under snow load defined in (a).

(c) The structure shall not collapse under the snow load equal to 1.4 times the value defined in (a).

Article 3: Following structural calculation shall be made for wind forces acting on the building. The effect of vibration normal to the wind direction in the horizontal plane and torsional vibration on structural response, and the effect of vertical vibration on the roof elements shall be appropriately taken into consideration in the structural calculation.

(a) No structural members shall be damaged under rare strong winds which produce a wind velocity equal to or higher than the average wind velocity at 10 m above ground level taking into consideration ground roughness defined by the law enforcement order. This requirement does not apply to vibration control devices whose fatigue, hysteresis and damping characteristics have been established to be effective during extremely rare winds and earthquake motions.

(b) The structure shall not collapse by extremely rare strong winds which produce an average wind velocity 1.25 times the value defined in (a) at 10 m above ground level.

Article 4: Following structural calculation shall be made for earthquake forces acting on the building. The effect of vertical ground motion considering the size and configuration of the building, the effect of ground motion normal to the principal ground motion concerned, the effect of phase difference of ground motion, and the effect of vertical loads under horizontal sway shall be appropriately taken into consideration in the structural calculation.

(a) The ground motion acting on structures in the horizontal direction is defined in parts (1) to (4) below. If the ground motion is determined taking into consideration the effect of faults in the vicinity of the construction site, the effect of epicentral distance and other characteristics of seismic motions and the influence on structural response, the followings may not be satisfied.

527

(1) Acceleration response spectrum at 5 % damping factor of the ground motion on the open engineering bedrock (a soil layer located below the structure with sufficient thickness and rigidity having a shear wave velocity larger than 400 m/sec, free from the effect of surface soil layers above) shall satisfy the values given in Table 1, and the amplification of ground motion by surface geology should be considered in defining the design ground motion.

Table 1. Design acceleration spectrum at open engineering bedrock

Period, sec	Acceleration response spectral value, m/sec^2	
	Rare earthquake ground motion	Extremely rare earthquake ground motion
$T<0.16$	$(0.64+6T)Z$	Five times the acceleration response values defined for the rare earthquake ground motion
$0.16<T<0.64$	$1.6Z$	
$0.64<T$	$(1.024/T)Z$	
T: period of structure, sec. Z: seismic zone factor.		

(2) The duration of motion shall be longer than 60 sec.
(3) The earthquake ground motion (acceleration, velocity or displacement or their combination) shall be digitally defined at appropriate time intervals.
(4) The number of ground motions shall be large enough to verify the safety of the structure under the effect of earthquake motion.
(b) Structural members shall be examined not to be damaged under the rare earthquake ground motions defined in (a) using the equation of motion. Structural vibration control members are exempted from this requirement.
(c) The structure shall be examined not to collapse under the extremely rare earthquake ground motions defined in (a) using the equation of motion.

Article 5: Loads and forces defined in Article 1 shall be used in the structural calculation specified in Articles 2 through 4.

Article 6: The deformation and vibration of structural members under loads and forces defined in Article 1 shall not interfere with the use of the building.

Article 7: Roofing elements, exterior finishing materials and exterior curtain walls shall be structurally safe under the wind forces, earthquake forces and other impact forces.

Article 8: In a building located within a land failure warning zone, exterior walls shall not fail under the forces caused by the land failure of slope considering the types of natural hazards. The loads and forces defined in Article 1 shall be considered in the examination.

It should not noted that no specific material properties, structural dimensions, calculation methods are specified. The appropriateness of structural calculation and verification of structural performance used in design calculation should be examined by specialists who have sufficient knowledge and experience in assessing earthquake ground motion, dynamic analysis, structural analysis and the behavior of structural members before the approval by MOLIT.

AUTHOR INDEX

PEER REPORTS

PEER reports are available from the National Information Service for Earthquake Engineering (NISEE). To order PEER reports, please contact the Pacific Earthquake Engineering Research Center, 1301 South 46th Street, Richmond, California 94804-4698. Tel.: (510) 231-9468; Fax: (510) 231-9461.

PEER 2004/05 *Performance-Based Seismic Design Concepts and Implementation: Proceedings of an International Workshop.* Peter Fajfar and Helmut Krawinkler, editors. September 2004.

PEER 2004/02 *Analytical Investigations of New Methods for Reducing Residual Displacements of Reinforced Concrete Bridge Columns.* Junichi Sakai and Stephen A. Mahin. August 2004.

PEER 2004/01 *Seismic Performance of Masonry Buildings and Design Implications.* Kerri Anne Taeko Tokoro, James C. Anderson, and Vitelmo V. Bertero. February 2004.

PEER 2003/18 *Performance Models for Flexural Damage in Reinforced Concrete Columns.* Michael Berry and Marc Eberhard. August 2003.

PEER 2003/16 *Seismic Demands for Performance-Based Design of Bridges.* Kevin Mackie and Božidar Stojadinovic. August 2003.

PEER 2003/15 *Seismic Demands for Nondeteriorating Frame Structures and Their Dependence on Ground Motions.* Ricardo Antonio Medina and Helmut Krawinkler. May 2004.

PEER 2003/14 *Finite Element Reliability and Sensitivity Methods for Performance-Based Earthquake Engineering.* Terje Haukaas and Armen Der Kiureghian. April 2004.

PEER 2003/13 *Effects of Connection Hysteretic Degradation on the Seismic Behavior of Steel Moment-Resisting Frames.* Janise E. Rodgers and Stephen A. Mahin. March 2004.

PEER 2003/12 *Implementation Manual for the Seismic Protection of Laboratory Contents: Format and Case Studies.* William T. Holmes and Mary C. Comerio. October 2003.

PEER 2003/11 *Fifth U.S.-Japan Workshop on Performance-Based Earthquake Engineering Methodology for Reinforced Concrete Building Structures.* February 2004.

PEER 2003/10 *A Beam-Column Joint Model for Simulating the Earthquake Response of Reinforced Concrete Frames.* Laura N. Lowes, Nilanjan Mitra, and Arash Altoontash. February 2004.

PEER 2003/09 *Sequencing Repairs after an Earthquake: An Economic Approach.* Marco Casari and Simon J. Wilkie. April 2004.

PEER 2003/08 *A Technical Framework for Probability-Based Demand and Capacity Factor Design (DCFD) Seismic Formats.* Fatemeh Jalayer and C. Allin Cornell. November 2003.

PEER 2003/07 *Uncertainty Specification and Propagation for Loss Estimation Using FOSM Methods.* Jack W. Baker and C. Allin Cornell. September 2003.

PEER 2003/06 *Performance of Circular Reinforced Concrete Bridge Columns under Bidirectional Earthquake Loading.* Mahmoud M. Hachem, Stephen A. Mahin, and Jack P. Moehle. February 2003.

PEER 2003/05 *Response Assessment for Building-Specific Loss Estimation.* Eduardo Miranda and Shahram Taghavi. September 2003.

PEER 2003/04 *Experimental Assessment of Columns with Short Lap Splices Subjected to Cyclic Loads.* Murat Melek, John W. Wallace, and Joel Conte. April 2003.

PEER 2003/03 *Probabilistic Response Assessment for Building-Specific Loss Estimation.* Eduardo Miranda and Hesameddin Aslani. September 2003.

PEER 2003/02 *Software Framework for Collaborative Development of Nonlinear Dynamic Analysis Program.* Jun Peng and Kincho H. Law. September 2003.

PEER 2003/01 *Shake Table Tests and Analytical Studies on the Gravity Load Collapse of Reinforced Concrete Frames.* Kenneth John Elwood and Jack P. Moehle. November 2003.

PEER 2002/24 *Performance of Beam to Column Bridge Joints Subjected to a Large Velocity Pulse.* Natalie Gibson, André Filiatrault, and Scott A. Ashford. April 2002.

PEER 2002/23 *Effects of Large Velocity Pulses on Reinforced Concrete Bridge Columns.* Greg L. Orozco and Scott A. Ashford. April 2002.

PEER 2002/22 *Characterization of Large Velocity Pulses for Laboratory Testing.* Kenneth E. Cox and Scott A. Ashford. April 2002.

PEER 2002/21 *Fourth U.S.-Japan Workshop on Performance-Based Earthquake Engineering Methodology for Reinforced Concrete Building Structures.* December 2002.

PEER 2002/20 *Barriers to Adoption and Implementation of PBEE Innovations.* Peter J. May. August 2002.

PEER 2002/19 *Economic-Engineered Integrated Models for Earthquakes: Socioeconomic Impacts.* Peter Gordon, James E. Moore II, and Harry W. Richardson. July 2002.

PEER 2002/18 *Assessment of Reinforced Concrete Building Exterior Joints with Substandard Details.* Chris P. Pantelides, Jon Hansen, Justin Nadauld, and Lawrence D. Reaveley. May 2002.

PEER 2002/17 *Structural Characterization and Seismic Response Analysis of a Highway Overcrossing Equipped with Elastomeric Bearings and Fluid Dampers: A Case Study.* Nicos Makris and Jian Zhang. November 2002.

PEER 2002/16 *Estimation of Uncertainty in Geotechnical Properties for Performance-Based Earthquake Engineering.* Allen L. Jones, Steven L. Kramer, and Pedro Arduino. December 2002.

PEER 2002/15 *Seismic Behavior of Bridge Columns Subjected to Various Loading Patterns.* Asadollah Esmaeily-Gh. and Yan Xiao. December 2002.

PEER 2002/14 *Inelastic Seismic Response of Extended Pile Shaft Supported Bridge Structures.* T. C. Hutchinson, R. W. Boulanger, Y. H. Chai, and I. M. Idriss. December 2002.

PEER 2002/13 *Probabilistic Models and Fragility Estimates for Bridge Components and Systems.* Paolo Gardoni, Armen Der Kiureghian, and Khalid M. Mosalam. June 2002.

PEER 2002/12 *Effects of Fault Dip and Slip Rake on Near-Source Ground Motions: Why Chi-Chi Was a Relatively Mild M7.6 Earthquake.* Brad T. Aagaard, John F. Hall, and Thomas H. Heaton. December 2002.

PEER 2002/11 *Analytical and Experimental Study of Fiber-Reinforced Strip Isolators.* James M. Kelly and Shakhzod M. Takhirov. September 2002.

PEER 2002/10 *Centrifuge Modeling of Settlement and Lateral Spreading with Comparisons to Numerical Analyses.* Sivapalan Gajan and Bruce L. Kutter. January 2003.

PEER 2002/09 *Documentation and Analysis of Field Case Histories of Seismic Compression during the 1994 Northridge, California, Earthquake.* Jonathan P. Stewart, Patrick M. Smith, Daniel H. Whang, and Jonathan D. Bray. October 2002.

PEER 2002/08 *Component Testing, Stability Analysis and Characterization of Buckling-Restrained Unbonded Braces^{TM}.* Cameron Black, Nicos Makris, and Ian Aiken. September 2002.

PEER 2002/07 *Seismic Performance of Pile-Wharf Connections.* Charles W. Roeder, Robert Graff, Jennifer Soderstrom, and Jun Han Yoo. December 2001.

PEER 2002/06 *The Use of Benefit-Cost Analysis for Evaluation of Performance-Based Earthquake Engineering Decisions.* Richard O. Zerbe and Anthony Falit-Baiamonte. September 2001.

PEER 2002/05 *Guidelines, Specifications, and Seismic Performance Characterization of Nonstructural Building Components and Equipment.* André Filiatrault, Constantin Christopoulos, and Christopher Stearns. September 2001.

PEER 2002/04 *Consortium of Organizations for Strong-Motion Observation Systems and the Pacific Earthquake Engineering Research Center Lifelines Program: Invited Workshop on Archiving and Web Dissemination of Geotechnical Data, 4–5 October 2001.* September 2002.

PEER 2002/03 *Investigation of Sensitivity of Building Loss Estimates to Major Uncertain Variables for the Van Nuys Testbed.* Keith A. Porter, James L. Beck, and Rustem V. Shaikhutdinov. August 2002.

PEER 2002/02 *The Third U.S.-Japan Workshop on Performance-Based Earthquake Engineering Methodology for Reinforced Concrete Building Structures.* July 2002.

PEER 2002/01 *Nonstructural Loss Estimation: The UC Berkeley Case Study.* Mary C. Comerio and John C. Stallmeyer. December 2001.

PEER 2001/16 *Statistics of SDF-System Estimate of Roof Displacement for Pushover Analysis of Buildings.* Anil K. Chopra, Rakesh K. Goel, and Chatpan Chintanapakdee. December 2001.

PEER 2001/15 *Damage to Bridges during the 2001 Nisqually Earthquake.* R. Tyler Ranf, Marc O. Eberhard, and Michael P. Berry. November 2001.

PEER 2001/14 *Rocking Response of Equipment Anchored to a Base Foundation.* Nicos Makris and Cameron J. Black. September 2001.

PEER 2001/13   *Modeling Soil Liquefaction Hazards for Performance-Based Earthquake Engineering.* Steven L. Kramer and Ahmed-W. Elgamal. February 2001.

PEER 2001/12   *Development of Geotechnical Capabilities in OpenSees.* Boris Jeremic. September 2001.

PEER 2001/11   *Analytical and Experimental Study of Fiber-Reinforced Elastomeric Isolators.* James M. Kelly and Shakhzod M. Takhirov. September 2001.

PEER 2001/10   *Amplification Factors for Spectral Acceleration in Active Regions.* Jonathan P. Stewart, Andrew H. Liu, Yoojoong Choi, and Mehmet B. Baturay. December 2001.

PEER 2001/09   *Ground Motion Evaluation Procedures for Performance-Based Design.* Jonathan P. Stewart, Shyh-Jeng Chiou, Jonathan D. Bray, Robert W. Graves, Paul G. Somerville, and Norman A. Abrahamson. September 2001.

PEER 2001/08   *Experimental and Computational Evaluation of Reinforced Concrete Bridge Beam-Column Connections for Seismic Performance.* Clay J. Naito, Jack P. Moehle, and Khalid M. Mosalam. November 2001.

PEER 2001/07   *The Rocking Spectrum and the Shortcomings of Design Guidelines.* Nicos Makris and Dimitrios Konstantinidis. August 2001.

PEER 2001/06   *Development of an Electrical Substation Equipment Performance Database for Evaluation of Equipment Fragilities.* Thalia Anagnos. April 1999.

PEER 2001/05   *Stiffness Analysis of Fiber-Reinforced Elastomeric Isolators.* Hsiang-Chuan Tsai and James M. Kelly. May 2001.

PEER 2001/04   *Organizational and Societal Considerations for Performance-Based Earthquake Engineering.* Peter J. May. April 2001.

PEER 2001/03   *A Modal Pushover Analysis Procedure to Estimate Seismic Demands for Buildings: Theory and Preliminary Evaluation.* Anil K. Chopra and Rakesh K. Goel. January 2001.

PEER 2001/02   *Seismic Response Analysis of Highway Overcrossings Including Soil-Structure Interaction.* Jian Zhang and Nicos Makris. March 2001.

PEER 2001/01   *Experimental Study of Large Seismic Steel Beam-to-Column Connections.* Egor P. Popov and Shakhzod M. Takhirov. November 2000.

PEER 2000/10   *The Second U.S.-Japan Workshop on Performance-Based Earthquake Engineering Methodology for Reinforced Concrete Building Structures.* March 2000.

PEER 2000/09   *Structural Engineering Reconnaissance of the August 17, 1999 Earthquake: Kocaeli (Izmit), Turkey.* Halil Sezen, Kenneth J. Elwood, Andrew S. Whittaker, Khalid Mosalam, John J. Wallace, and John F. Stanton. December 2000.

PEER 2000/08   *Behavior of Reinforced Concrete Bridge Columns Having Varying Aspect Ratios and Varying Lengths of Confinement.* Anthony J. Calderone, Dawn E. Lehman, and Jack P. Moehle. January 2001.

PEER 2000/07   *Cover-Plate and Flange-Plate Reinforced Steel Moment-Resisting Connections.* Taejin Kim, Andrew S. Whittaker, Amir S. Gilani, Vitelmo V. Bertero, and Shakhzod M. Takhirov. September 2000.

PEER 2000/06 *Seismic Evaluation and Analysis of 230-kV Disconnect Switches.* Amir S. J. Gilani, Andrew S. Whittaker, Gregory L. Fenves, Chun-Hao Chen, Henry Ho, and Eric Fujisaki. July 2000.

PEER 2000/05 *Performance-Based Evaluation of Exterior Reinforced Concrete Building Joints for Seismic Excitation.* Chandra Clyde, Chris P. Pantelides, and Lawrence D. Reaveley. July 2000.

PEER 2000/04 *An Evaluation of Seismic Energy Demand: An Attenuation Approach.* Chung-Che Chou and Chia-Ming Uang. July 1999.

PEER 2000/03 *Framing Earthquake Retrofitting Decisions: The Case of Hillside Homes in Los Angeles.* Detlof von Winterfeldt, Nels Roselund, and Alicia Kitsuse. March 2000.

PEER 2000/02 *U.S.-Japan Workshop on the Effects of Near-Field Earthquake Shaking.* Andrew Whittaker, ed. July 2000.

PEER 2000/01 *Further Studies on Seismic Interaction in Interconnected Electrical Substation Equipment.* Armen Der Kiureghian, Kee-Jeung Hong, and Jerome L. Sackman. November 1999.

PEER 1999/14 *Seismic Evaluation and Retrofit of 230-kV Porcelain Transformer Bushings.* Amir S. Gilani, Andrew S. Whittaker, Gregory L. Fenves, and Eric Fujisaki. December 1999.

PEER 1999/13 *Building Vulnerability Studies: Modeling and Evaluation of Tilt-up and Steel Reinforced Concrete Buildings.* John W. Wallace, Jonathan P. Stewart, and Andrew S. Whittaker, editors. December 1999.

PEER 1999/12 *Rehabilitation of Nonductile RC Frame Building Using Encasement Plates and Energy-Dissipating Devices.* Mehrdad Sasani, Vitelmo V. Bertero, James C. Anderson. December 1999.

PEER 1999/11 *Performance Evaluation Database for Concrete Bridge Components and Systems under Simulated Seismic Loads.* Yael D. Hose and Frieder Seible. November 1999.

PEER 1999/10 *U.S.-Japan Workshop on Performance-Based Earthquake Engineering Methodology for Reinforced Concrete Building Structures.* December 1999.

PEER 1999/09 *Performance Improvement of Long Period Building Structures Subjected to Severe Pulse-Type Ground Motions.* James C. Anderson, Vitelmo V. Bertero, and Raul Bertero. October 1999.

PEER 1999/08 *Envelopes for Seismic Response Vectors.* Charles Menun and Armen Der Kiureghian. July 1999.

PEER 1999/07 *Documentation of Strengths and Weaknesses of Current Computer Analysis Methods for Seismic Performance of Reinforced Concrete Members.* William F. Cofer. November 1999.

PEER 1999/06 *Rocking Response and Overturning of Anchored Equipment under Seismic Excitations.* Nicos Makris and Jian Zhang. November 1999.

PEER 1999/05 *Seismic Evaluation of 550 kV Porcelain Transformer Bushings.* Amir S. Gilani, Andrew S. Whittaker, Gregory L. Fenves, and Eric Fujisaki. October 1999.

PEER 1999/04 *Adoption and Enforcement of Earthquake Risk-Reduction Measures.* Peter J. May, Raymond J. Burby, T. Jens Feeley, and Robert Wood.

PEER 1999/03 *Task 3 Characterization of Site Response General Site Categories.* Adrian Rodriguez-Marek, Jonathan D. Bray, and Norman Abrahamson. February 1999.

PEER 1999/02 *Capacity-Demand-Diagram Methods for Estimating Seismic Deformation of Inelastic Structures: SDF Systems.* Anil K. Chopra and Rakesh Goel. April 1999.

PEER 1999/01 *Interaction in Interconnected Electrical Substation Equipment Subjected to Earthquake Ground Motions.* Armen Der Kiureghian, Jerome L. Sackman, and Kee-Jeung Hong. February 1999.

PEER 1998/08 *Behavior and Failure Analysis of a Multiple-Frame Highway Bridge in the 1994 Northridge Earthquake.* Gregory L. Fenves and Michael Ellery. December 1998.

PEER 1998/07 *Empirical Evaluation of Inertial Soil-Structure Interaction Effects.* Jonathan P. Stewart, Raymond B. Seed, and Gregory L. Fenves. November 1998.

PEER 1998/06 *Effect of Damping Mechanisms on the Response of Seismic Isolated Structures.* Nicos Makris and Shih-Po Chang. November 1998.

PEER 1998/05 *Rocking Response and Overturning of Equipment under Horizontal Pulse-Type Motions.* Nicos Makris and Yiannis Roussos. October 1998.

PEER 1998/04 *Pacific Earthquake Engineering Research Invitational Workshop Proceedings, May 14–15, 1998: Defining the Links between Planning, Policy Analysis, Economics and Earthquake Engineering.* Mary Comerio and Peter Gordon. September 1998.

PEER 1998/03 *Repair/Upgrade Procedures for Welded Beam to Column Connections.* James C. Anderson and Xiaojing Duan. May 1998.

PEER 1998/02 *Seismic Evaluation of 196 kV Porcelain Transformer Bushings.* Amir S. Gilani, Juan W. Chavez, Gregory L. Fenves, and Andrew S. Whittaker. May 1998.

PEER 1998/01 *Seismic Performance of Well-Confined Concrete Bridge Columns.* Dawn E. Lehman and Jack P. Moehle. December 2000.